AFAPL TR 68-17

3rd

AEROSPACE

expandable and modular

STRUCTURES CONFERENCE

May 16-18, 1967

NOTICES

When Government drawings, specifications, or other data are used for any purpose other than in connection with a definitely related Government procurement operation, the United States Government thereby incurs no responsibility nor any obligation whatsoever; and the fact that the Government may have formulated, furnished, or in any way supplied the said drawings, specifications, or other data, is not to be regarded by implication or otherwise as in any manner licensing the holder or any other person or corporation, or conveying any rights or permission to manufacture, use, or sell any patented invention that may in any way be related thereto.

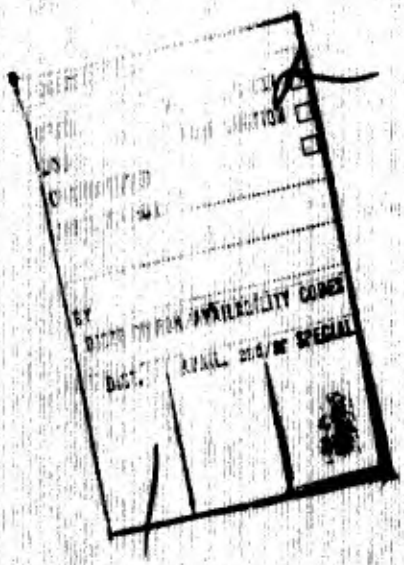

Copies of this report should not be returned to the Air Force Aero Propulsion Laboratory unless return is required by security considerations, contractual obligations, or notice on a specific document.

700 - April 1968 - CO455 - 30-628

BLANK PAGE

TRANSACTIONS

THIRD AEROSPACE

EXPANDABLE AND MODULAR

STRUCTURES CONFERENCE

Carillon Hotel
Miami Beach, Florida
May 16-18, 1967

Sponsored By:

AIR FORCE AERO PROPULSION LABORATORY
(SPACE TECHNOLOGY BRANCH)
WRIGHT PATTERSON AIR FORCE BASE, DAYTON OHIO

In Cooperation With:

GOODYEAR AEROSPACE CORPORATION

LOCKHEED MISSILE AND SPACE COMPANY

G. T. SCHJELDAHL COMPANY

SPACE GENERAL CORPORATION

Luncheon Speaker
HAROLD K. KELLY
Brigadier General, USAF
Headquarters, TAC

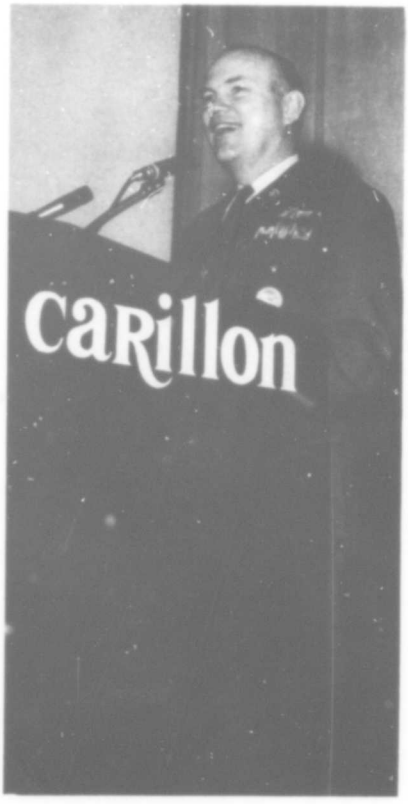

Keynoter
RAYMOND A. GILBERT
Brigadier General, USAF
Headquarters, AFSC

Underwater Neutral Bouyancy Demonstration
DANIEL SEGER
Captain, USAF
Air Force Aero Propulsion Laboratory

Conference Chairman
FRED W. FORBES
Branch Chief
Air Force Aero Propulsion Laboratory

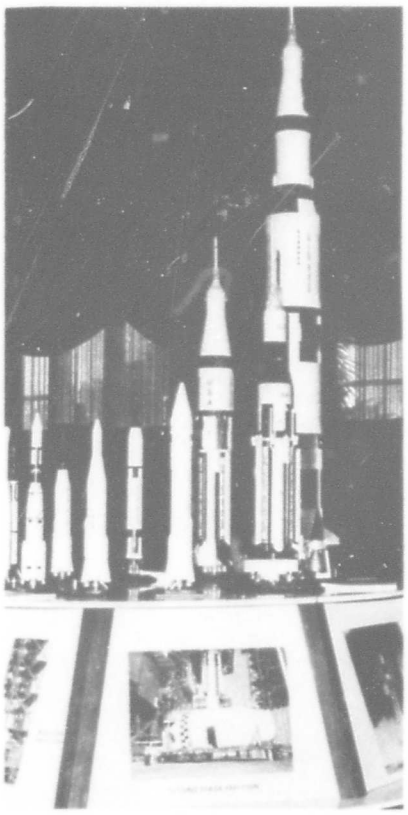

NASA Exhibit

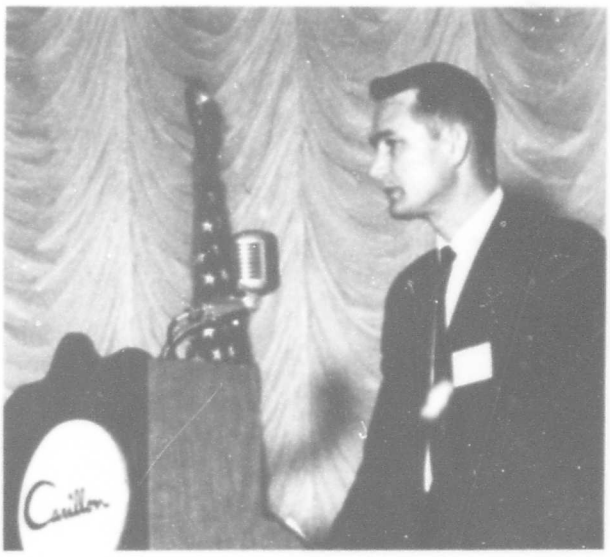

Luncheon Speaker
JOHN PRICE
NASA-Marshall Space Flight Center

Banquet Speaker
DR. EUGENE KONECCI
University of Texas

Contractor Exhibit

Session VI Chairman
EDDIE J. BROUSSARD, JR., Colonel, USAF
and
JAMES A. McMILLAN, Major, USAF
Support Technology Division AFAPL

Session IV Chairman
RAYMOND A. YERG
Colonel, USAF; MCUSAF Commander
Aerospace Medical Research Laboratories

Welcoming Remarks
RICHARD T. HEMSLEY
Colonel, USAF
Director Air Force Aero Propulsion Laboratory

Session Chairman
DR. MICHAEL I. YARYMOVYCH
Technical Director
MOL Program, USAF

Speaker
L. JURICH
Goodyear Aerospace Corporation

Speaker
J. GATES
NASA - Goddard Space Flight Center

Underwater Neutral Bouyancy Demonstration
GARY REID
Captain, USAF
Aerospace Medical Research Laboratories

Session I Chairman
WILBUR A. BALLENTINE
Colonel, USAF
Commander Det. 2 Space Systems Division

Speaker
R. FRENCH
Goodyear Aerospace Corporation

Speaker
J. M. JERKE
NASA-Langley Research Center

FOREWORD

The Aerospace Expandable and Modular Structures Conference serves as a forum in which leading authorities in structures technology advance new ideas and techniques for critical discussion. The objectives of the conference are (1) to present current research and development contributions in the fields of expandable and modular structures and (2), through the exchange and evaluation of the most advanced concepts, to stimulate further advances in structures technology. By publishing the transactions of this conference, the Air Force Aero Propulsion Laboratory hopes to further promote these objectives.

Herbert A. Lyon
Colonel, USAF
Director,
Air Force Aero
Propulsion Laboratory

ABSTRACT

This report contains a presentation of technical contributions summarizing the status of current and significant research in the fields of expandable and modular structures. The report is based upon the discussions at the Third Aerospace and Modular Structures Conference held May 16-18 at the CARILLON HOTEL, Miami Beach, Florida. The conference transactions have been arranged in the order of presentation during the six sessions of the conference.

BLANK PAGE

CONFERENCE COMMITTEE

Fred W. Forbes, Chairman
Air Force Aero Propulsion Laboratory

Members:

James E. Crawford
Space General Corporation

Robert T. Madden
Goodyear Aerospace Corporation

Richard J. Slater
G. T. Schjeldahl Company

Charles Dusheck
Lockheed Missile and Space Company

ACKNOWLEDGMENTS

The Conference Committee would like particularly to acknowledge the efforts of the following Air Force Aero Propulsion Laboratory personnel who have made major contributions in planning and arranging the program requirements:

Captain John B. Catiller
Robert P. Huie
Steven D. Shook
Captain Anthony J. Zappanti
Adam W. Cormier
James F. Brophy

In addition, thanks go to Captain Dan R. Seger and Captain Gary B. Reid for setting up and carrying through the Underwater Neutral Buoyancy Demonstration on Airlock/Astronaut Capability.

A special acknowledgment should be noted for the services rendered by Mr. Allen J. Cannon and Mrs. Frances R. Dempsey of the Research and Technology Division for their special efforts to assure that hotel arrangements and associated provisions for conference attendees were made to provide an environment wherein the accent on technical interchange can be mutually beneficial to the Air Force, NASA, and the Aerospace Industry.

SESSION CHAIRMEN

SESSION I

Col Wilbur A. Ballentine
USAF Space Systems Division Det. 2

SESSION II

Dr Michael I. Yarymovych
Technical Director, MOL Program, USAF

SESSION III

Norman J. Mayer
Headquarters NASA-OART

SESSION IV

Col Raymond A. Yerg
MCUSAF Commander
Aerospace Medical Research Laboratories

SESSION V

Leonard J. Carter, Secretary
British Interplanetary Society

SESSION VI

Col Eddie J. Broussard Jr,USAF
Director of Engineering Plans (TAC-DEPL)

KEYNOTE ADDRESS

EXPANDABLE AND MODULAR STRUCTURES TECHNOLOGY

Brig Gen R. A. Gilbert
Director of Laboratories
Air Force Systems Command

Colonel Hemsley, distinguished guests, ladies and gentlemen.

I welcome the opportunity to participate with you in this Third Aerospace Expandable and Modular Structures Conference. I believe the technical advances that have been and are being made in expandable and modular structures technology, for which you have been responsible, are a stimulating example of the benefits to be gained through the combined efforts of the Air Force and its laboratories, other service agencies, NASA and industry in a technology area of mutual interest and payoff.

One has only to look over the program we shall cover during the next three days to understand the broad applications and the potential payoffs of expandable structure technology in such vital areas a future space systems, advanced aeronautical systems, and capability to wage limited war, with special attention to the needs in Vietnam.

The expandable and modular structure work in space structures, expandable airlocks, space escape and re-entry vehicles, solar energy concentrators, and antennas - coupled with supporting zero-g and vacuum testing techniques - are excellent examples of where our exploratory development or, if you will, applied research programs are providing the technological building blocks for our operational space systems of the future.

We will hear more this morning about the modular assembled antenna experiment work which is being performed in-house by the Air Force Aero-Propulsion Laboratory and the Aerospace Medical Research Laboratory. This effort will culminate in an orbital flight test of Man's ability to assemble a large, complex,accurately-contoured structure. One of the important goals of this work is to provide flight data which will enable us to calibrate ground-based

simulation techniques. This could lead to significantly reduced flight-test requirements and development costs. This is an excellent example of the in-house capabilities of our Air Force Laboratories.

Our future space systems will obviously include structures with large volumes when deployed in space. On the other hand, the available payload launch volumes will usually be relatively small in the foreseeable future. To meet these constraints, expandable and modular structures are highly attractive for such space applications as expandable airlocks, crew quarters, data return packages, and space-escape techniques. Our banquet speaker, Dr. Eugene Konecci, will speak on the subject of space rescue.

An excellent example of NASA and Air Force cooperation in an area of mutual payoff is the joint participation of NASA Langley Research Center and of our AF Laboratories in an Expandable Airlock Experiment which is scheduled for flight test aboard NASA's Saturn IV-B Orbital Workshop. This experiment will be the first U.S. manned flight demonstration of an expandable structure. Our luncheon speaker today, Dr. John Price of NASA Marshall Space Flight Center, will discuss the Saturn IV-B Workshop and Experiments.

We all recognize the involvement of the U.S. in Southeast Asia. I'm particularly pleased, therefore, to note that expandable and modular structure efforts are being directed toward the solving of Vietnam problems.

This conference will highlight examples of expandable and modular structure technology applied to limited war capabilities and aeronautical systems. In fact, the entire session Thursday afternoon will be devoted to limited war applications.

The Air Force Aero-Propulsion Laboratory's portable shelter developments and rapid site construction techniques are dynamic examples of technology which we have tested in Vietnam and have proven feasible. Lightweight, economical personnel shelters easily packageable for air transport and rapid assembly have successfully met the test of Vietnam deployment and operational use. Additionally, we have successfully tested rapid site-construction techniques such as sprayable plastic floors for portable shelters, helicopter pads and parking areas in Vietnam.

The Compound Curvature Airmat developed by the Air Force Materials Laboratory will provide inflatable structures with complex geometries. The concept is being incorporated in the F-111 wing-fuselage fairing design and is being evaluated for use in the design of F-111 wing fuel tanks. Another aircraft application is expendable wing tanks. We are currently evaluating two types of plastic expendable wing tanks for aircraft in Vietnam. We hope to provide expandable fuel tanks which are easier to handle and cheaper to produce than current aluminum tanks.

A by-product of expandable structures technology has been the development, by the Air Force Weapons Laboratory, of a protective shelter for fighter aircraft. This shelter is currently scheduled for a live weapons test at Eglin with a follow-on Air Force operational use in Vietnam.

Speaking from the user's point of view, Brigadier General Harold K. Kelley the Civil Engineer of the Tactical Air Command will discuss TAC's needs.

I will leave to the experts who will follow me on this podium the detailed discussions of the substantial technical progress you have made since our 2nd Conference. It is exciting to see this technology move from chemical formulations in the laboratory to full-scale prototypes. With the recent substantive progress in such key-material properties as basic strength, shelf life, rigidization times, environmental compatibility, and advancements in fabrication techniques, we can expect to experience an increasing application of this technology to equipment in our operational inventory.

Thank you.

TABLE OF CONTENTS

TABLE OF CONTENTS

SESSION I

A PROPOSED MODULAR ASSEMBLED ANTENNA EXPERIMENT FOR THE SIVB WORKSHOP

Fred W. Forbes*
Robert P. Huie*
Steven D. Shook*
James E. Crawford**
Earl G. Blackwell**
Gary B. Reid, Capt, USAF***

INTRODUCTION

PURPOSE - The purpose of this paper is to discuss an experiment being planned pertaining to the manual assembly of an antenna structure in space.

SCOPE - This paper will present a concise summary of the background technology leading up to the planning of this proposed experiment, the objectives of the experiment, a discussion of the design parameters, the design, hardware status, and human factor aspects of the program.

BACKGROUND - During the next decade, more ambitious space programs will be undertaken which will undoubtedly make extensive utilization of large space structures for application to communication antennas, radio telescopes, space stations, and astronomical telescopes. The Air Force Aero Propulsion Laboratory and other Government agencies have for the past decade been pursuing technology programs which will hopefully satisfy these future needs. Generally speaking, the approach to orbiting large structures in space falls into one of the three concepts: (1) Expandable Structures, (2) Modular Assembled Structures, or (3) One Piece Structures.

The expandable structures concept can of course be subdivided into more descriptive categories such as inflatables, chemically rigidized, elastic recovery concepts, and mechanically deployed concepts. Basically these approaches do not rely on, or in general, require a mans participation in the deployment; however, man would provide a valuable back-up in case of a sub-system malfunction or perhaps in the fine tuning or alignment of a large antenna. NASA Echo Satellites, shown in fiqure 1, are an outstanding example of the technological capabilities of inflatable structures. While the Pegasus Satellite, shown in fiqure 2, with a 96 foot wing span is an excellent example of what can be done with mechanically deployed satellite concepts. The Air Force Aero Propulsion Laboratory has had an extensive program in chemically rigidized structures for such applications as space stations, solar collectors, and antennas.

* AF Aero Propulsion Laboratory
** Space General Corporation
*** Aerospace Medical Research Laboratory

These structures are shown in figures 3 and 4. Extensive ground tests, and demonstrations have been made in this area. Space experiments such as the D-021 "Expandable Airlock" and D-022 "Expandable Re-entry Vehicles" plus future experiments will provide a firm foundation for aerospace designers considerations.

Finally, the Air Force and NASA has been conducting technology programs in the manual assembly area; however, until recently this area could not advance as rapadily as desired because invariably these assembly concepts require extensive zero "G" simulation and space flight to truly determine the feasibility of the concepts. To date, only simulated zero "G" via the Keplerian trajectory using a modern aircraft and underwater neutral buoyancy tests, appear to be a reasonable facsimile for zero "G". The aircraft has three drawbacks: (1) The aircraft zero "G" time is usually limited to a maximum of 30 seconds, (2) The size of the structural concept is limited because of aircraft cabin size, and (3) The aircraft suited for zero "G" simulation have limited availability. Although neutral buoyancy testing has been in existence for several years, it has not been until recently that the techniques for underwater testing of human performance have been truly perfected. Finally, a cross validation of aircraft and neutral buoyancy testing has not yet been made with actual zero "G" encountered in space flights.

Recent flights, such as Gemini 12, have raised the over-all confidence level of work in space and neutral buoyancy testing for zero "G" simulation, and in fact, have demonstrated that man properly restrained with proper work-rest cycles can accomplish discrete tasks which pertain to the assembly and service of large structures.

Today and probably for the near future, a divergence of opinion exists between engineers concerning whether expandable or assembled structures are optimum for space applications. Most likely, as for all competitive technologies, both will find useful applications.

The Space General Corporation, under the direction of the Aero Propulsion Laboratory, developed a breadboard concept for a modular assembled antenna, which was subsequently fabricated and tested in neutral buoyancy tests at the General Electric underwater facility, and the Air Force Aerospace Medical Research Laboratory's underwater facility. This antenna structural concept included a latch and catch system, panel geometry, hub and boom, and work site.

With this background, one can see that the time has come to conduct a basic space experiment on the assembly of a structure. The parabolic dish or antenna was selected because it is one of the needed applications for large structures, and because it imposed an accuracy requirement not associated with other space applications.

BLANK PAGE

Consequently, a space experiment is being defined, designed, fabricated, and qualification tested for submission to orbital flight tests and evaluation. The following is a technical discussion of this experiment:

TECHNICAL DISCUSSION

OBJECTIVES - The objectives of the proposed space experiments are: (1) Demonstrate the technical feasibility of in-orbit assembly of structures, particularly an antenna or solar collector. (2) Cross-validates zero "g" simulation techniques including underwater neutral buoyancy and zero gravity aircraft, especially with respect to assembly. (3) Begin the determination of the relative contributions of manned assembly versus automatic deployed structure. (4) Obtain assembly data pertaining to antennas which can be extrapolated to larger structures. (5) Obtain biomedical data on the assembly task by a suited subject in a pressurized and unpressurized mode.

EXPERIMENT CONCEPT SELECTION

This experiment is based on the general concept previously designed by the Space General Corporation under Air Force Aero Propulsion Laboratory direction; however, a considerable number of improvements have been made in the general concept. Before discussing the rationals for selecting this approach for a proposed experiment, a discussion of the Space General breadboard antenna concept is warranted. A 10 foot diameter parabolic dish configuration was selected for "breadboard" work because packaging or stacking volume would be minimized, scalable assembly operation would be simulated, and it is a size that easily lends itself to underwater testing, possible aircraft tests, and more important, space flight tests. (See Figure 5) In addition, 10 foot diameter expandable parabolic dishes have been used as a type of standard specimen size in other expandable structure programs sponsored by the Aero Propulsion Laboratory.

It was determined that scalability could be simulated by employing two rings of panels, as larger structures could be assembled by simply adding more rings of modules. (See Figure 6) These panels are somewhat smaller than could probably be handled by the astronaut. In order that stacking volume be minimized, all panels are nearly equal in length and width so that, when nested, a minimum-sized single canister could be utilized. By varying hub size, panel width, and number of panels per ring, a number of configurations can be established. The configuration selected consists of a 14 inch diameter hub with eight panels in the inner ring and 16 panels in the outer ring. The panel envelope is approximately 27 X 28 inches. Addition of the tapered wedge joints increases the envelope to approximately 28 X 29 inches.

The basic module material selected was an aluminum honeycomb sandwich structure which is pre-fabricated into high precision compound curvature surfaces. Each panel contains a latch on the end and two latches on each side. The outer end of the inner panels contain two latches, one for each of the two outer panels which mate with it.

The location of the side latches are equally spaced radially, establishing essentially four rings of latches. Panel configuration is shown in figure 16. Various panel interconnecting joint designs were considered. The tapered tongue and groove type joint was selected as the best candidate for more detailed study. This concept employed a flat leaf spring on the female member which would snap into a groove on the male member when fully engaged. (As shown in figure 7) The fundamental requirement for any precision joint to repeat original assembly accuracies is for a known pre-load to be applied. To achieve this, various means for obtaining a pre-loaded joint were examined. The addition of cam type mechanisms to tighten the design and required that the astronaut reach out and operate each tightening mechanism, once a panel had been inserted into the assembly, which complicated the assembly task. The initial concept did provide the required pre-load, with mechanical and task simplicity but necessitated that the astronaut supply the two or three pound insertion force until the spring clips snapped into position.

A full-scale mock-up was built for a neutral buoyancy task evaluation of the assembly tasks. (See Figures 5 & 6) The General Electric Company, Space Systems Division at Valley Forge, Pennsylvania, under contract to Space General Corporation, conducted neutral buoyancy tests. Fabrication of the contoured panels employed a polypropylene sheet material with a specific gravity of approximately 0.90. The addition of the aluminum interconnection joints gave the panel assembly almost perfect neutral buoyancy in the Aquarama test facility salt water. Large cutouts were made in the panels to reduce the drag of the module during translation through the water. The modular parabola is assembled onto a 14 inch diameter hub affixed to a ten foot aluminum boom, which could be adjusted in attitude by a pivot at each end. The work station provides the restraint for reacting body movements and assembly forces, in addition to a support for a panel canister, and station.

The assembly task consisted of the subject assuming his position at the work station, adjusting the boom to within reach, extracting the panels from the canister, and inserting the modular panels into the mating joints provided peripherally about the hub. The hub is rotated, after each panel has been inserted, to a new position to receive the next panel.

The panel insertion is accomplished by simultaneously engaging the three tapered wedge joint members into the female members on the hub and previously installed panel, until the tapered wedges are aligned and fully engaged.

A low additional force preloads the joints and allows the spring clip on the wedges to snap into the slots on the male receiving portion of the latch, securing the panel in place. This procedure, while appearing a bit difficult at first, was accomplished quite easily by the pressure-suited test subject in less time than was anticipated. After the eight panels of the inner annulus are installed, the boom and hub angles are re-adjusted for the second ring of panels. The installation procedure for the outer annular modules is identical to the previous annulus until the parabola assembly is complete.

The twenty four panels are stacked sequentially in the canister and are removed in order of assembly. A small bar provided with an elastic bungee is used across the top of the open canister to prevent the stowed panels from drifting away when unattended.

Two underwater assembly trials were made by the General Electric test engineer for training purposes. The assembly required little effort, and the psychomotor control requirements were less than anticipated. It was noted that if movements were slow and deliberate, the presence of the water drag became secondary and the test engineer operated in an environment approximating total weightlessness.

This general concept was selected for the definition of a manned space experiment because of the following rationale:

a. The structural contour accuracy of each rigid module can be closely controlled and tested in the laboratory before launch. This accuracy can also approach the test tooling state-of-the-art fabrication tolerances.

b. No exotic technological development is required.

c. The manual assembly task can be accomplished within the anthropometric and metabolic restraints imposed by a pressure-suited astronaut in zero "g".

d. The design concept incorporates scalability for larger structures.

e. A damaged module or section may be replaced, thereby maintaining operational integrity of the structure.

These many advantages in reality become requirements for many structural applications for manned assembly.

AIR FORCE EVALUATION OF BREADBOARD CONCEPT

The early "breadboard" antenna concept was evaluated by the Air Force Aero Propulsion Laboratory and Air Force Aerospace Medical Research Laboratory to determine what modifications would be necessary to provide space flight experiment hardware. This evaluation is shown in figures 9, 10, 11, and 12. These tests were executed by the authors of this paper and in particular, Captain Gary Reid, AMRL, and Captain Daniel R. Seger, AFAPL. These tests were conducted in-house at Wright-Patterson AFB and are described below:

a. The assembly procedure proceeded smoothly; however, the disassembly sequence disclosed that the latches in breadboard configuration were extremely difficult to release. The basic conclusions of these Air Force tests were:

(1) Latches are basically good but must be redesigned for ease of disassembly.

(2) The rotation method of the antenna/dish should be studied.

(3) The restraint system was good but to assure selection of the most functional design, the astronaut foot restraint system developed for the Gemini program, should also be evaluated for this experiment.

(4) The packing container for the antenna panels was adequate for the mock-up model but the actual parabolic panels would require a redesigned container.

(5) The worksite, boom, and hub must be redesigned for easy assembly in space and must have the capability to be repackaged in a small storage volume.

EXPERIMENT DESCRIPTION

Concurrently and subsequent to the Air Force evaluation, an experiment was defined in order to satisfy the previously stated experiment objectives. A major constraint that has been self-imposed in the definition of the experiment was to define an experiment that had growth potential for future flights both in task complexity, mission scope, and structural size, while providing initial experiment of minimal weight, approximately 100 lbs, and volume of 12 cubic feet or less.

The basic experiment concept that is being studied, is to assemble a 10 foot diameter modular antenna structure inside the SIVB Orbital Workshop Hydrogen Tank utilizing a basic knee bar toe block restraint system for an astronaut work site. These assembly tests will determine bio-medical data, work forces, and work complexity. In addition, identical data will be taken in neutral buoyancy tests and aircraft zero "G" simulation tests to provide cross-validation data. Finally, the antenna will be disassembled and assembled utilizing other NASA and Air Force on-board astronaut restraint systems and possibly even an on-board maneuvering unit. Tests of assembly and disassembly will be conducted with unpressurized and pressurized space suited subject. The SIVB Workshop has been selected as a baseline type vehicle because of its long mission and early flight dates. Conducting the experiment inside the hydrogen tank will still provide the zero "G" environment and its internal size will still permit erection of a 10 foot diameter antenna. The antenna structure would not be made to function for the initial experiments; however, later flight experiments are being considered with functioning antennas. Finally, this experiment will be defined as a basically in-house experiment to be conducted jointly by AF Aero Propulsion Laboratory and AF Medical Research Laboratories.

HARDWARE DESIGN

After review of the experiment objectives, and the Air Force in-house test results of the "breadboard" modular antenna, it was determined what changes or modifications would be required to provide space flight experiment hardware that could be fabricated in-house. This review indicated that a modification of the latches was required to facilitate disassembly of the structure, to modify the hub to use a friction clutch rotation mechanism because of human engineering considerations and engineering simplifications, and to use a telescoping boom to provide a minimum packaging volume. The canister design, of course, must be completely redefined, and the worksite must be refined and modified. The following is a discussion of the status of each of these items:

LATCHES - The original latch concept, tongue and groove secured by a spring metal clip (Shown in figure 7) was satisfactory, as far as, assembling the modular structure; however, it required either a "finger nail" tool or extra tool to release or raise the spring clip. A release mechanism was finally developed utilizing a sliding teflon button which is in contact with an inclined plane machined into the surface of the latch. (This is shown in figure13) This button when moved forward, raises the spring metal retaining clip and concurrently releases the latch. (Shown in figure 14 & 15) Additionally, it has been determined that the basic aluminum tongue and groove latch components shall be cast for the mass production in order to reduce machinery times.

PANEL GEOMETRY - The panel geometry of the modular antenna was changed from a 45° rim angle, which has been used as a general standard for solar concentrator work, to a focal length/diameter ratio of 0.5, which is the range of standard dish antennas. (See figure 16) In addition, some refinement of the latch location geometry on the panels was also made to facilitate assembly and disassembly.

PANEL MATERIAL - A 0.005 inch thick aluminum 5052 H25 panel facings were selected for flight hardware in order to reduce material delivery time and make the panels more durable. A standard type 3.1-1/8 inch cell, .0007 inch perforated aluminum honeycomb was used at 0.44 inch thickness. The over-all surfaces accuracy of this panel will be in the range of -0.010 inch or better. FM 1000 adhesive, a heat activated adhesive, is being used for bonding the panels together with a bonding pressure of approximately 8 psi at a temperature of 350°F for 1 hour. Fabrication of prototype sections has already been initiated and completed with successful results. (The panel materials are shown in figure 17)

HUB - The Space General hub used a spring loaded pin release (shown in figure 17), to allow the test subject to move it from one position to another. (See figure 11) This pin release was activated by a cable attached to the worksite and pulled by the test subject.

During underwater test, the subject found the cable awkward to operate and since it is not desirable for the test subject to be required to connect a cable release during the test in orbit, this design was eliminated in favor of a simple friction clutch hub.

TELESCOPING BOOM - A two sectioned aluminum telescoping boom assembly is being designed for flight hardware. This boom will be made from .040 aluminum tubing of 2024 H19 alloy. A set of strain gauges will be installed at the lower part of the boom in order to determine the approximate loads applied by the astronauts during the assembly of structure. The canister and worksite are presently in the preliminary design phase. It is planned that the packaged experiment containers will be stowed in the Modular Docking Adapter and each container must not exceed 20" x 30" x 40" in size. It was initially planned that the total experiment hardware be packaged in one container. However, it appears that it will be necessary to use two containers, one approximately 20" x 30" x 30" and the other 10" x 10" x 40". The worksite, boom, and attachment system will be placed in one container and the antenna panels and hub in the other. The rectangular containers will be constructed of perforated aluminum honeycomb similar to that used to construct the antenna panels. The top portion of one container will be inverted and used as an attachment platform for the boom and hub. The bottom portion of the container will be anchored to the attachment rails in the SIVB tank and the knee bar and toe block restraint system, which will be hinged to the container, will be raised into place. The antenna panels will be stowed in the second container. This container, when opened, will be secured to the worksite and hold the panels during the assembly and disassembly procedure.

DETAILED EXPERIMENT PROCEDURE

After preliminary design of the proposed experiment hardware, a more detailed task analysis has been made of the Modular Antenna experiment. A summary of this task analysis is provided below:

(1) Retrieval and erection of experiment hardware.

a. Two (2) crewmen, both suited and unpressurized will remove stowed antenna from Multiple Docking Antenna (MDA).

b. Number one (1) crewman (CM1) and Number two (2) crewman (CM2) will unpackage antenna and attach restraint system and panel container.

c. Both crewmen will attach the boom to SIVB tank.

d. Both crewmen attach the rotary hub.

e. Both crewmen rest.

(2) Experiment Assembly

a. CM2 pressurizes his suit and attaches himself to restraint system.

b. CM1 remains unpressurized to act as a safety moniter. He also assists in photographic coverage.

c. CM2 retrieves panel no. 1 from panel container and affixes it to the hub.

d. CM2 rotates hub, retrieves panel no. 2 and installs it to the hub and panel no. 1.

e. This procedure is continued until all 8 panels of the inner annulus are installed.

f. CM2 dismounts worksite and proceeds to boom attachment point.

g. CM2 resets the boom and hub angle to achieve proper position for the installation of the outer annulus.

h. CM2 remounts worksite, attaches himself to the restraint system and continues assembly process for panels 9 through 24.

i. Upon completion of assembly process, the antenna is inspected, photographed and germane comments recorded.

j. On future assembly of a working antenna, a tension cable, to preload the joints, will be installed and tightened to assure contour accuracy of the antenna.

(3) Experiment Disassembly

a. CM2 remounts worksite while CMI proceeds to antenna worksite.

b. CM2 removes panels 24 and 23 and stores themin the experiment packing container.

c. CM2 depressurizes suit.

d. CMI detaches panels and hands them to CM2 who stores them in the experiment packing container.

e. Upon storing no. 1 panel, CM2 dismounts the worksite.

This fulfills one complete assembly-disassembly cycle. It should be noted that the total assembly and disassembly procedure can be conducted from one stationary restrain point.

DATA ACQUISITION AND REDUCTION

Bio-medical data, tape recordings of the astronaut's comments, strain gauge and photographic coverage will be used to evaluate the over-all success of the experiment.

Bio-medical data will be that normally taken by NASA, heart rate, respiration rate, and body temperature. The astronaut's comments during the actual experiment will also be valuable especially when matched with photographic coverages.

The strain gauges to be mounted on the boom will be calibrated on the ground to determine what forces are actually being applied to the structure during assembly or disassembly. The strain gauge reading will be correlated with the photographic coverage to determine the approximate angle of the force.

The photographic coverage will also be an invaluable aid in determining the over-all success of the experiment.

This same type of data will be taken during ground zero "g" simulation tests and correlated against the space experiment data. This should provide an excellent cross-correlation between simulated zero "g" tasks and actual zero "g" tests.

FUTURE POTENTIAL

After successful completion of the proposed experiment, the next logical step would be another space experiment in which the structure would be assembled EVA. This step would most likely transform the mockup into a functioning RF antenna in the 200-500 megahertz range. In this structure the panels will be constructed of RF reflector screen with aluminum honeycomb edge strip for structural integrity.

Since one of the major advantages of this type of structure is its scalability or growth potential, the next logical step would be the fabrication of a 50 to 100 foot diameter antenna. In its present size (10' diameter) the package and antenna accessories make up a major percentage of the total experiment weight. When the antenna is scaled up to a larger size, the weight of the packaging and accessories remain the same or increases only slightly, thus becoming only a small percentage of the total weight. In large antennas or structures, the weight per square foot can also be reduced. By using lightweight metals and plastics the weight of the dish can be reduced from 1 pound per square foot for the present experiment to .1 to .2 pounds per square foot for a 100 foot antenna. Erection time per square foot of surface can also be reduced for larger antennas by incorporating larger modular pieces in the design. In large structures, the disassembly requirements will most likely be negated, therefore greatly simplifying the latch design.

This type of structure can also be used for large space stations. Modules with their equipment pre-installed could be separately orbited and linked in space to form a large structure. Expandable materials would most likely be used to link modules together thus forming habitable experimental facilities and crew quarters.

CONCLUSION

1. The preliminary design for a modular antenna developed by the Space General Corporation under Aero Propulsion Laboratory directions merits further development.

2. A space experiment on modular assembly is a needed and logical step in modular structures technology.

3. This experiment will determine the feasibility of manned assembled modular structures.

REFERENCES

1. Gemini Program Mission Report XII, Gemini Mission Evaluation Team January 1967 MSC-G-P-67-1 Manned Spacecraft Center National Aeronautics and Space Administration Houston, Texas.
(CONFIDENTIAL)

2. Crawford, J. E. and E. G. Blackwell
Project AHT, AFAPL-TR-67-30
Air Force Aero Propulsion Laboratory
January 1967.

3. Space Technology Branch Preliminary Definitive Experiment
Plan for Modular Antenna for Assembly
April 1967.

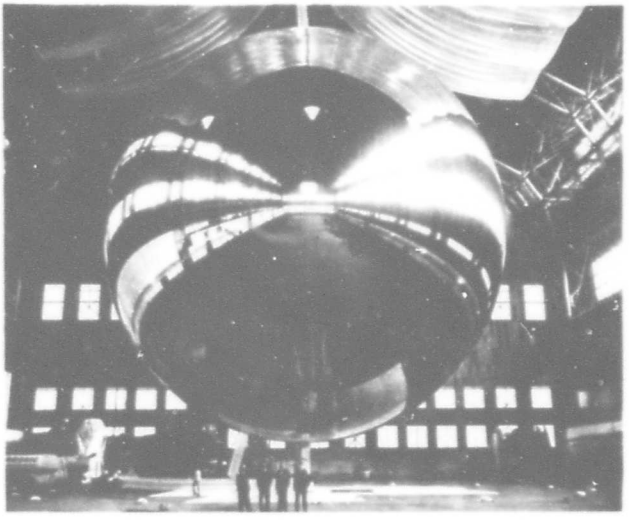

Figure 1

ECHO INFLATABLE STRUCTURE

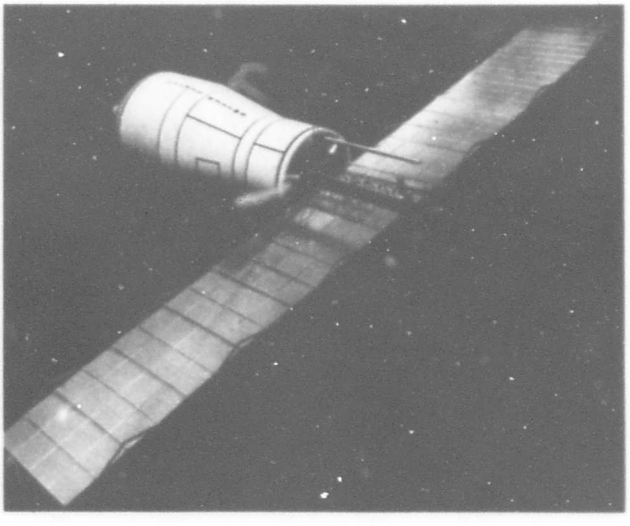

Figure 2

PEGASUS MECHANICAL DEPLOYED STRUCTURE

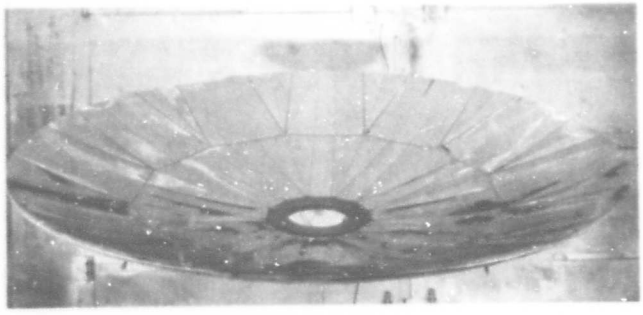

Figure 3

CHEMICAL RIGIDIZED SOLAR COLLECTOR

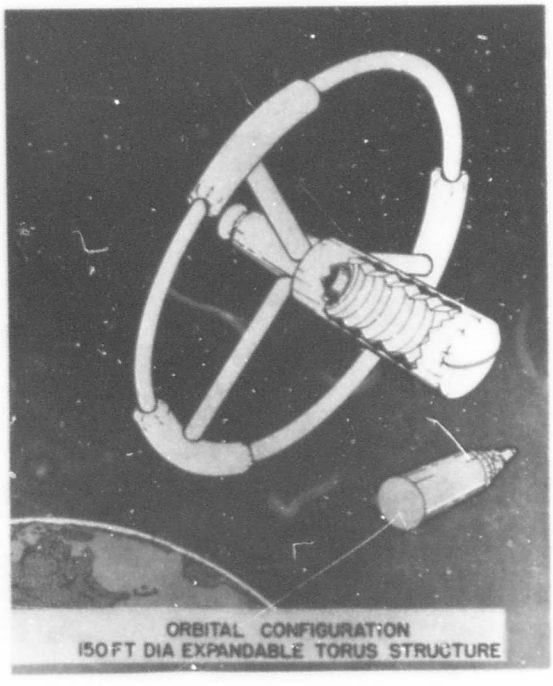

Figure 4

ELASTIC RECOVERY STRUCTURE

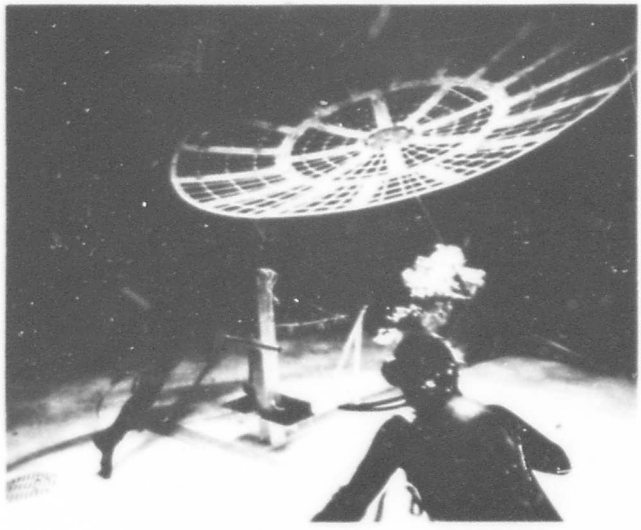

Figure 5

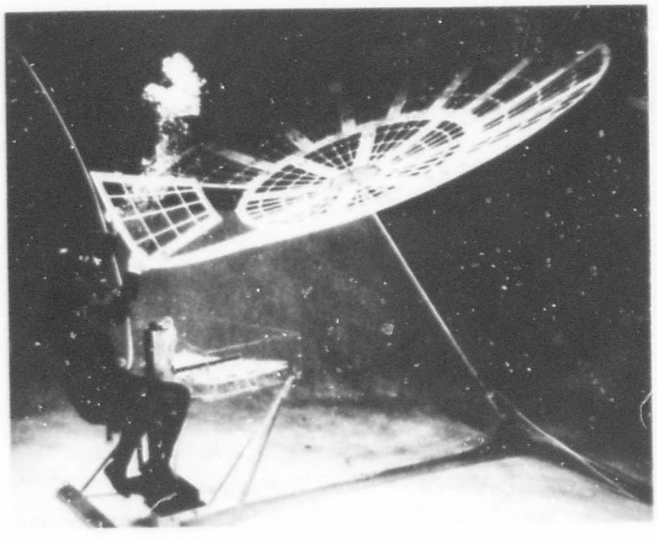

Figure 6

UNDERWATER ASSEMBLY OF BREADBOARD MOCK-UP

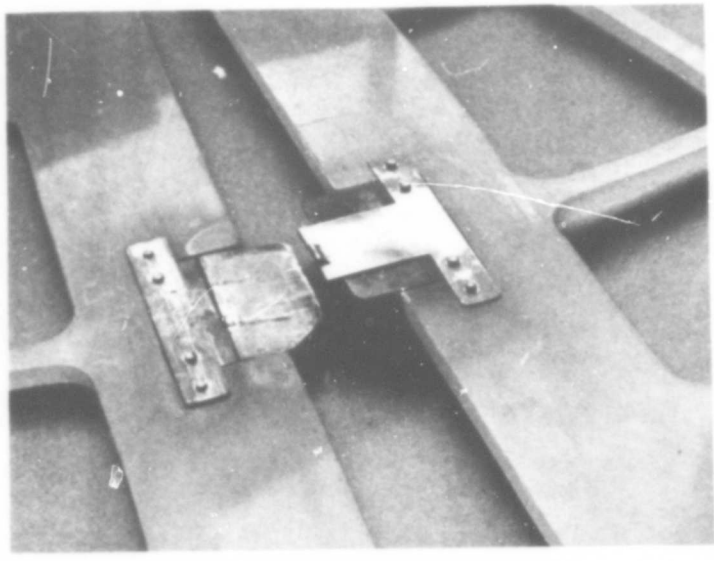

Figure 7

ORGINAL PANEL JOINT UNASSEMBLED

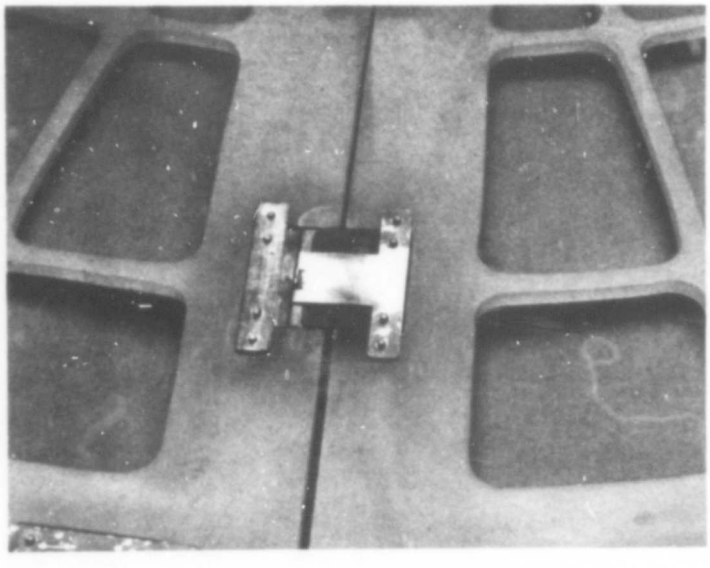

Figure 8

ORIGINAL PANEL JOINT ASSEMBLED

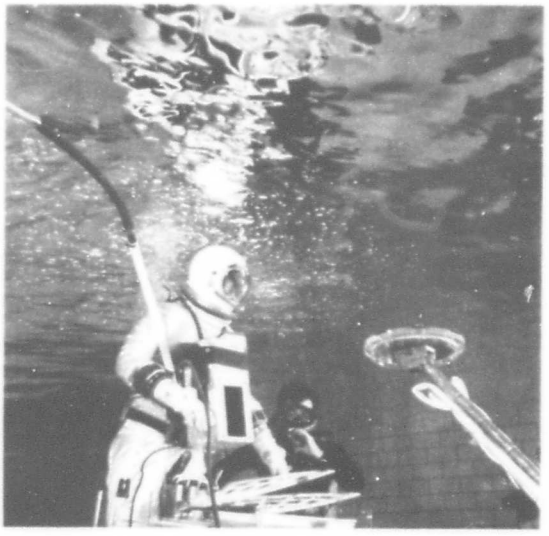

Figure 9

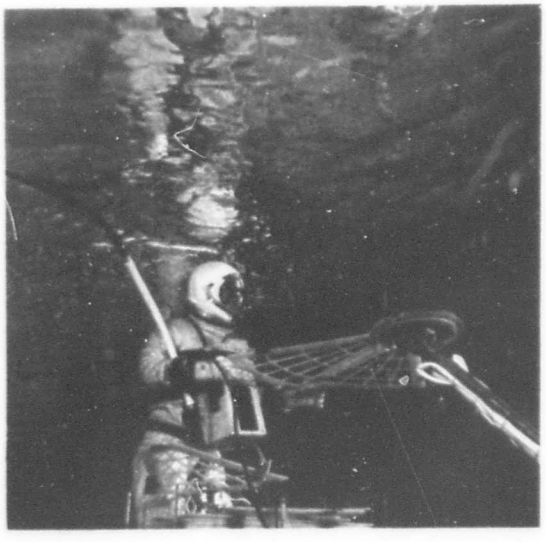

Figure 10

UNDERWATER ASSEMBLY BY PRESSURE SUITED SUBJECT

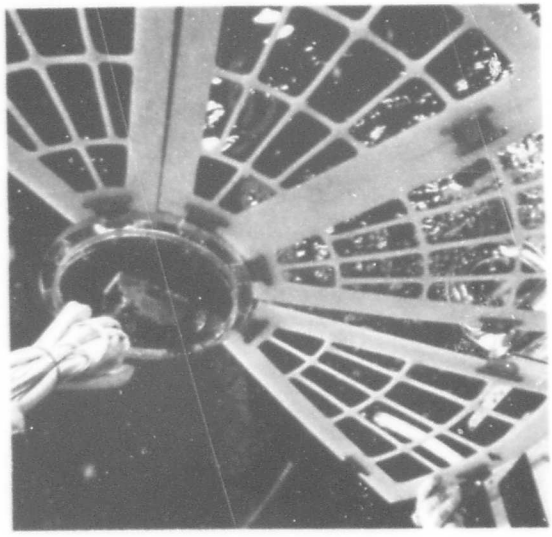

Figure 11

ANTENNA HUB

Figure 12

SUBJECT IN RESTRAINT SYSTEM

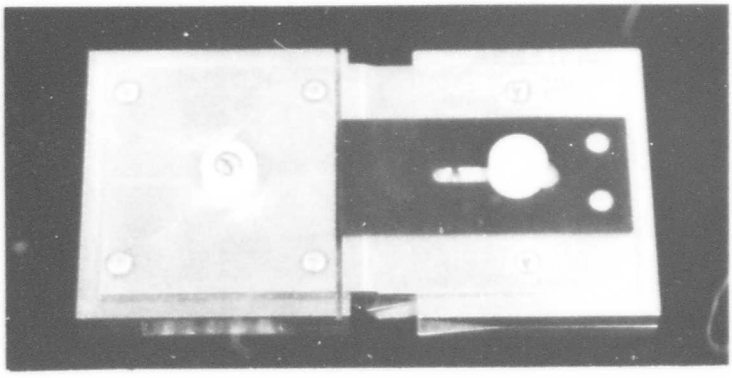

Figure 13

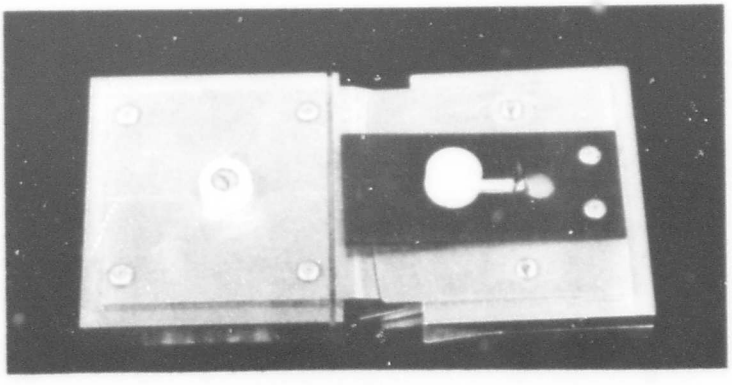

Figure 14

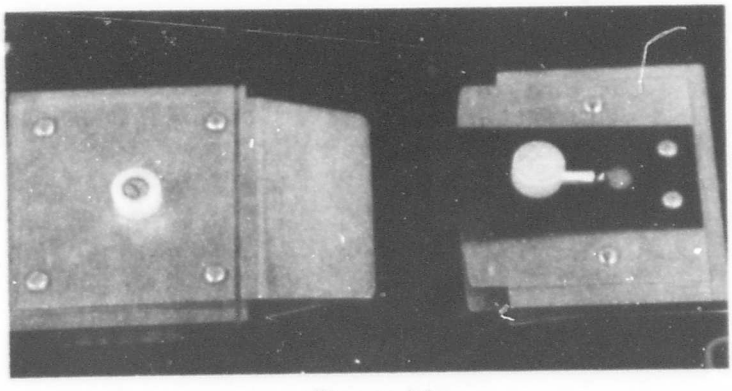

Figure 15

DISASSEMBLY PROCESS OF LATCH

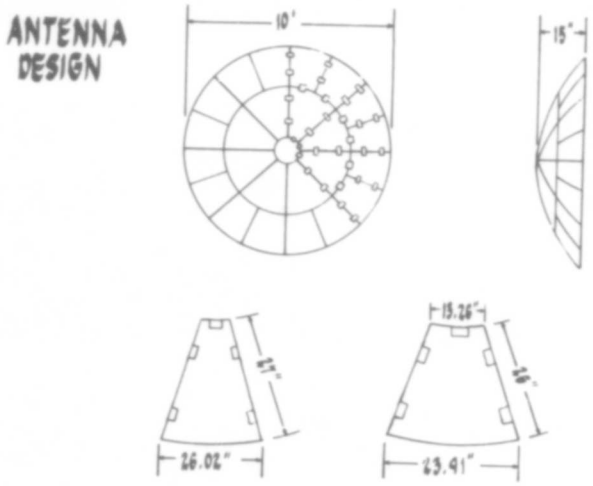

Figure 16

ANTENNA CONFIGURATION

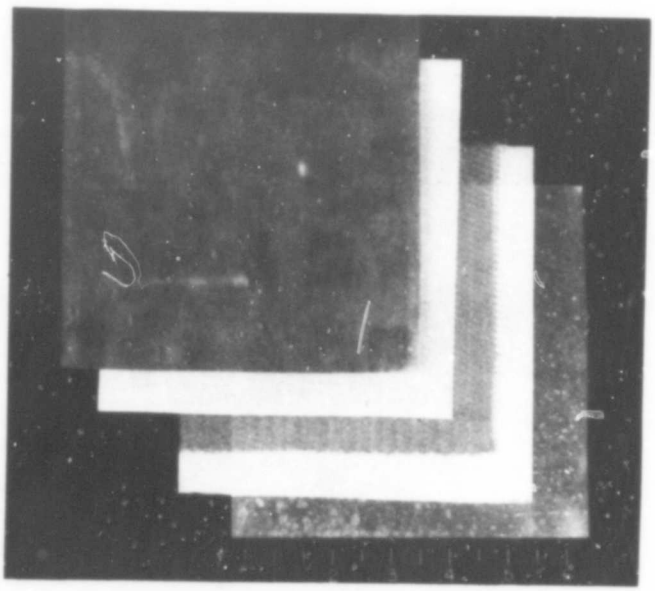

Figure 17

MATERIAL COMPOSITE

CONCEPTS AND DEVELOPMENT OF EXPANDABLE MANNED SPACE STRUCTURES

L. Jurich*

T. L. Hoffman**

SECTION I - INTRODUCTION

The development of expandable structures for manned space applications has been carried on at Goodyear Aerospace Corporation (GAC) for the past six years and for at least the same length of time by both the Air Force and NASA. At Goodyear Aerospace, there has been a transition from terrestrial applications of expandable structures, such as airships and ground shelters, to the more sophisticated structures required for space exploration, represented by space shelters, crew transfer tunnels, and airlocks.

Generally, the development of manned space structures has been highly successful. Starting with early materials-oriented programs, development has progressively advanced to a point where the first expandable manned structure soon will be flown in orbit. This structure is the Air Force D-21 expandable airlock and represents the first effort to evaluate a manned expandable structure under actual space environmental conditions. Certainly, the successful implementation of the D-21 airlock should provide an impetus to continued development of expandable structures and to specific mission applications in the manned space program.

---

*Manager of Manned Space Structures, Astronautics Division, Goodyear Aerospace Corporation.

**Project engineer, Astronautics Division, Goodyear Aerospace Corporation.

SECTION II - DEVELOPMENT APPROACH

1. DEVELOPMENT CYCLE

The general approach of Goodyear Aerospace in the development of manned space structures consists of a progressive series of steps, starting with materials development and culminating in orbital test and evaluation. The development cycle logically embodied in this approach is:

1. Materials development
2. Fabrication method development
3. Preprototype structure development and test
4. Prototype structure development and test
5. Flight hardware development and orbital test

The Air Force D-21 expandable airlock experiment is the only manned expandable structure program that has been planned to undergo a complete development cycle. Previous structure programs conducted by the Air Force and NASA generally have been limited in scope and confined to ground test of preprototype structures.

2. MATERIALS DEVELOPMENT

Goodyear Aerospace is conducting a continuing in-house program of materials research and development (R&D) specifically for manned space structure applications. One outcome of this R&D program is a four-layer composite embodying the "elastic recovery materials technique." This approach has been applied successfully to a number of preprototype structure development programs and is being used on the D-21 airlock program. The Goodyear Aerospace concept of materials for space structures was evolved as an overall composite materials approach that would meet all the requirements of a space environment. The general concept was established by differentiating the various functions performed by the structure into what is essentially a four-layer composite of materials:

1. Pressure bladder and flame barrier
2. Structural layer
3. Micrometeoroid barrier
4. Outer cover and thermal coating

The development objectives pursued in the materials approach were:

1. Nondetectable toxicity
2. Compatibility with O_2 environment
3. Flame resistance

4. Environmental thermal compatibility - maximum temperature of outer surface, +300 F, and minimum temperature for deployment, - 100 F
5. Resistance to space radiation, 10^7 rad tolerance
6. Resistance to micrometeoroid penetration
7. Minimum off-gassing, 0.5 percent weight loss
8. Minimum gas leakage
9. Variation in structural approach

All materials development for manned space structures has been conducted in pursuit of the above objectives and within the general concept of a four-layer materials composite. Since this development is a continuing effort, improvements in materials and techniques are constantly being incorporated. The D-21 airlock represents the latest development of the elastic recovery materials approach applied to a structure design.

3. FABRICATION METHODS DEVELOPMENT

In conjunction with materials developments, Goodyear Aerospace is carrying out an in-house R&D effort on fabrication methods for manned space structures. The objective of this effort is to provide the necessary technology that will permit a practical application of materials development to some specific structure design. The consideration of fabrication methods is usually a governing factor in the final design and selection of materials. In each of three separate space structures development programs conducted at Goodyear Aerospace, the practical consideration of fabrication techniques determined the specific design approach used in the structural layer.

Figure 1 shows a mandrel form fabrication technique used on a lunar shelter development structure that incorporated a steel filament-wound structural layer. Figure 2 also shows a mandrel form fabrication technique used for the development of a crew transfer tunnel. For this application, the practical aspects of geometry consideration dictated a structure layer approach based on multi-ply layup of dacron structural fabric. A tape structural layer approach (see Figure 3) was used in the development of a large structure, 12-1/2 ft in diameter and 37 ft long. The sheer size of the structure alone determined the fabrication method needed and consequently the best design approach for the structural layer.

The development of fabrication methods is a vital link in the overall development of expandable structures for manned space application. Material R&D combined with consideration for fabrication methods provides the technology needed to translate design into hardware.

4. PREPROTOTYPE STRUCTURE DEVELOPMENT AND TEST

Materials development and the companion development of fabrication methods are meaningful only when applied and proved with preprototype

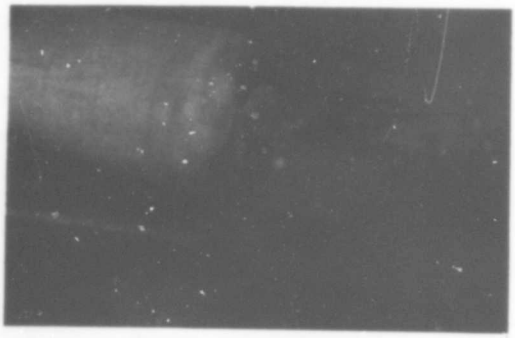

Figure 1 - Filament-Winding Technique

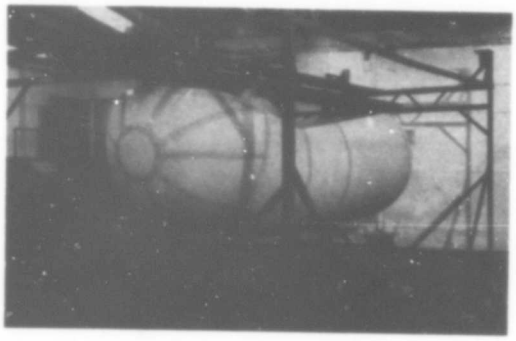

Figure 2 - Fabric Layup

structure development. This fact has been recognized by planners responsible for the development of expandable structures and explains why most R&D structure programs that are not flight-oriented have been carried out at least to this level of development.

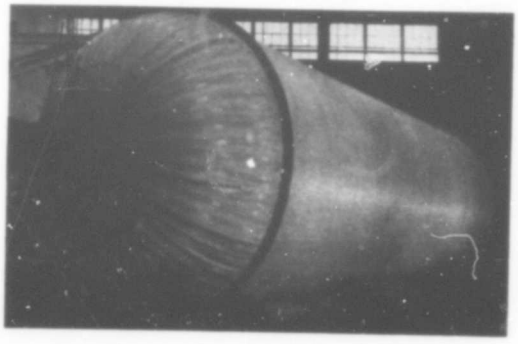

Figure 3 - Large Structure

The objectives of preprototype structures development are somewhat limited, but do provide the first attempt at establishing the feasibility of a specific expandable structures approach. The objectives generally pursued may be summarized as follows:

1. Apply a specific materials and fabrication methods approach to a full-scale structure design
2. Fabricate a representative preprototype structure (preferably full scale) to demonstrate and validate the materials approach and fabrication techniques
3. Conduct the limited ground tests mentioned below to establish feasibility
   a. Gas leakage tests to determine gas loss under design pressure conditions. Development goals are generally in the range of 0.25 to 0.50 lb/day and/or two to three percent of the volume per day for large volume structures
   b. Structural tests under proof-pressure loading
   c. Packaging test to demonstrate packaging concept and establish packaging loads

d. Deployment tests to demonstrate deployment dynamics under vacuum conditions

While the goals or objectives of preprototype structures development do not meet the developmental level required for flight hardware, the successful attainment of even these limited goals represents a significant advance in technology.

5. PROTOTYPE STRUCTURE DEVELOPMENT AND TEST

The next logical step in the development cycle is the fabrication of a prototype structure followed by extensive ground testing that simulates prelaunch, launch, and orbit. While this level of development approaches flight hardware requirements, the final feasibility of an expandable manned space structure design cannot be established without this development. The objectives to be pursued at this level of development might be as follows:

1. Implement a full-scale structure design to fulfill the requirements of the test program
2. Fabricate a full-scale prototype structure under rigid standards of processing and quality control
3. Conduct extensive testing to simulate the extremes of critical conditions listed below that would occur during prelaunch, launch, and orbit
   a. Prelaunch (packaged configuration)
      Humidity
      Salt fog
      High temperature
      Low temperature
      Shock
      Fungus
   b. Launch (packaged configuration)
      Acceleration
      Random vibration
      Sea level-to-orbit pressure simulation
   c. Orbit (packaged configuration)
      Deployment low temperature
      Deployment high temperature
   d. Orbit (deployed configuration)
      High-temperature endurance at proof pressure

Low-temperature endurance at proof pressure

Pressure cycling at high temperature

Pressure cycling at low temperature

The degree of testing required for a prototype item is not as extensive as that for a flight article. The indicated tests, however, do include all those critical environmental effects having a major impact on the feasibility of a specific expandable structures design.

6. FLIGHT HARDWARE DEVELOPMENT AND ORBITAL TEST

The final proof in the development cycle of expandable manned space structures is, of course, the development of flight hardware with subsequent testing under actual orbital conditions. The level of effort and the degree of development testing required prior to launch has been defined in considerable detail in the D-21 expandable airlock experiment. Generally, the effort required will encompass "prototype structure development and test" and additional testing will reflect the compatibility between the installed test item and the spacecraft.

SECTION III - ELASTIC RECOVERY MATERIALS CONCEPT

1. DESCRIPTION

The concept developed to meet the overall requirements of manned space structures was a material composite. Figure 4 depicts the composite, which is comprised of four distinct layers bonded together into a homogeneous structure. The inner layer is an unstressed pressure bladder, whose only function is to maintain pressure tightness and to transmit pressure loads to an adjacent structural layer. The structural layer carries structural loads resulting from internal pressure.

The flexible foam layer acts first as a micrometeoroid barrier, protecting the pressure bladder from penetration, and second in the deployment and shaping of the structure by assuming the shape that it possessed before packaging. The outer cover also has a dual purpose. It is used as a smooth base for the application of a thermal coating and encapsulates the total composite for evacuation and compression prior to packaging for launch. Off-gassing for the total composite is stabilized in about 24 hr with an approximate 0.25 percent weight loss.

2. PRESSURE BLADDER AND FLAME BARRIER

The pressure bladder is a laminate of three individual sealant layers (see Figure 5). The inner layer is a laminate of Capran film and lightweight nylon cloth. This layer is bonded with polyester adhesive to a second layer of closed-cell EPT (ethylene propylene terpolymer) foam, 1/16 in. thick. The outer sealant is again a laminate of Capran film and nylon cloth. To minimize combustion hazards, an 0.3 mil layer of aluminum foil is bonded to the inner surface to provide a flame barrier. The total weight of the bladder composite is about 0.164 psf and is independent of design pressure.

Tests were conducted on the pressure bladder to determine the permeability rate, possible toxicity, and environmental effects due principally to vacuum. Permeability was determined with oxygen as a test gas at 7.5 psia using a Dow cell. The measured rate was less than 10^{-4} psf per day. In relating this rate to a practical structure design, the permeability loss is negligible and accounts for only about one percent of the loss normally incurred through seal and joint leakage. A survey of toxic materials known to be used in the construction of the pressure bladder indicated the possible presence of toluene, xylene, methyl ethyl ketone, methylene chloride solvents, and toluene diisocyanate. Although carbon monoxide was not known to be present, tests for it also were included. The bladder material was exposed to 5 psia of oxygen for 24 hr prior to a chemical analysis and check for toxic gases. Test results indicated that all the above contaminants were below the threshold limits established by the National Bureau of Standards for occupational exposure.

The principal environmental effect for which the bladder was checked was a hard vacuum. This check was made first to ensure that delamination

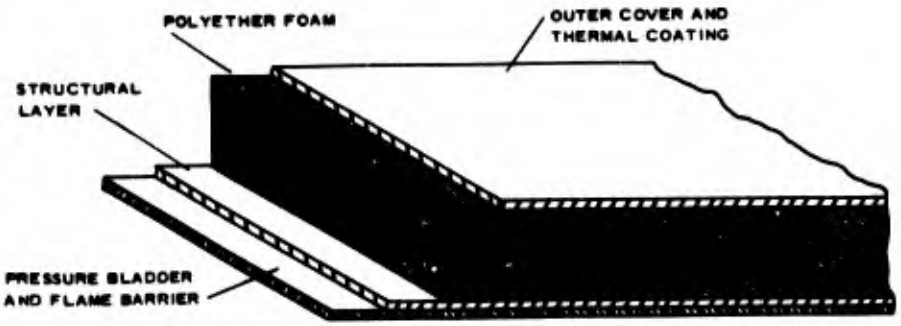

ITEM	WEIGHT (PSF)
PRESSURE BLADDER AND FLAME BARRIER	0.173
STRUCTURAL LAYER	VARIES
FOAM LAYER	VARIES
OUTER COVER	0.068
INTERLAYER POLYESTER ADHESIVE	0.063

Figure 4 - Elastic Recovery Materials Concept

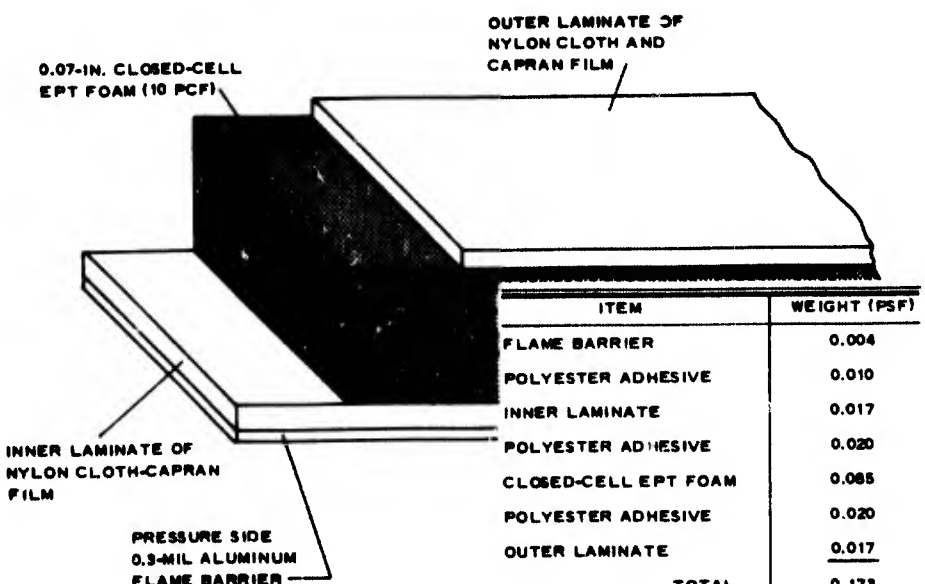

ITEM	WEIGHT (PSF)
FLAME BARRIER	0.004
POLYESTER ADHESIVE	0.010
INNER LAMINATE	0.017
POLYESTER ADHESIVE	0.020
CLOSED-CELL EPT FOAM	0.085
POLYESTER ADHESIVE	0.020
OUTER LAMINATE	0.017
TOTAL	0.173

Figure 5 - Pressure Bladder and Flame Barrier

of the composite bladder would not occur and second to determine the degree of off-gassing to be expected. The bladder construction technique proved successful, both in preventing delamination and in minimizing off-gassing. Off-gassing stabilized in about 24 hr with less than one-percent weight loss.

The EPT foam used in bladder construction governs the lower limits of materials flexibility for the overall materials composite. The material retains sufficient flexibility for dynamic deployment at temperatures as low as -100 F. Embrittlement occurs at about -110 F.

3. STRUCTURAL LAYER

The overall materials concept permits variations in the structural approach as determined either by general geometry requirements or by optimum methods of fabrication. Table 1 presents five basic structural techniques developed for expandable structures applications. A relative weight comparison indicates advantages for dacron filament or tape type structures. However, the higher modulus of flexible steel structures can offer better overall weight saving in some structure designs in addition to better geometry control.

Successful joint designs have been developed for all of the techniques indicated. The variation in safety factor (based on the parent virgin material) is somewhat arbitrary, but is intended to reflect the decrease of material strength due to joints in dacron structures. A 100-percent efficiency has been obtained with flexible steel structure designs. Thus the ultimate structural design factors for all of the techniques indicated are approximately equal.

4. FOAM LAYER

Protection from micrometeoroid penetration is provided by a layer of flexible polyether foam. Based on hypervelocity particle impact tests conducted by Goodyear Aerospace and on tests conducted at the micrometeorite testing facility at Wright-Patterson AFB, flexible foam with a 1.0-pcf density has been selected as a suitable barrier material. The tests at Wright-Patterson were conducted with a particle that had an average mass of 0.005 g, traveling at 27,000 fps. Both series of tests indicate that a foam barrier has the same effectiveness as a single sheet of aluminum with 15 times the mass per unit area.

Figure 6 shows the Air Force near-earth micrometeoroid environment spectrum in terms of particle mass and accumulative particle flux. When the test results are correlated with single-sheet aluminum penetration theory, the critical penetrating flux level is about 5.23×10^{-7} particles/sq ft-day. By relating the critical flux, the exposed surface area of a structural design, the mission time, and single-sheet penetration theory to each other, the probability of zero penetration for various foam thicknesses can be determined.

While the foam layer is primarily a micrometeoroid barrier, it can serve also as a structure deployment aid. During packaging, the foam layer is compressed to about 10 percent of its original thickness and is restrained by a

TABLE 1 - COMPARISON OF STRUCTURAL TECHNIQUES

Technique	Design factor	Ultimate stress (psi)	Design stress (psi)	E modulus (psi × 10^6)	Relative weight
Woven dacron fabric	5	100,000	20,000	*	1.0
Dacron filament wind	5	112,000	22,000	1.4	0.62
Dacron structural tape	5	112,000	22,000	1.4	0.62
Steel filament wind	3	300,000	100,000	30.0	0.75
Steel structural tape	3	300,000	100,000	30.0	0.75

*270,000 fill direction; 115,000 warp direction

packaging canister. Upon deployment in orbit, the canister is jettisoned, and the elastic recovery characteristics of the foam tend to shape the structure to its fully expanded volume. Figure 7 shows the recovery characteristics of the foam under vacuum conditions and for varying temperatures. From Figure 7, note that the packaged structure must be insulated against extreme cold if full recovery is to be achieved.

Environmental effects have been evaluated to establish compatibility with the environment. The effects of vacuum, temperature, and high-energy radiation are of main concern. Off-gassing induced by vacuum is negligible; it amounted to a 0.4-percent weight loss and stabilized in 1.5 hr. Expected temperature extremes are dependent on thermal coatings and are not expected to exceed a 300-F tolerance for the material. High-energy radiation is not expected to present any problem because the foam can withstand a significantly higher amount than the anticipated dose.

5. OUTER COVER

The construction of the outer layer is shown in Figure 8. Since the outer cover encapsulates the composite wall, it serves as an aid in packaging the structure prior to launch. By a vacuum technique, the wall thickness can be compressed from the fully expanded thickness to about 3/8 in., suitable for folding and subsequent packaging in the canister.

Various thermal coatings, either vacuum deposited or spray painted, may be

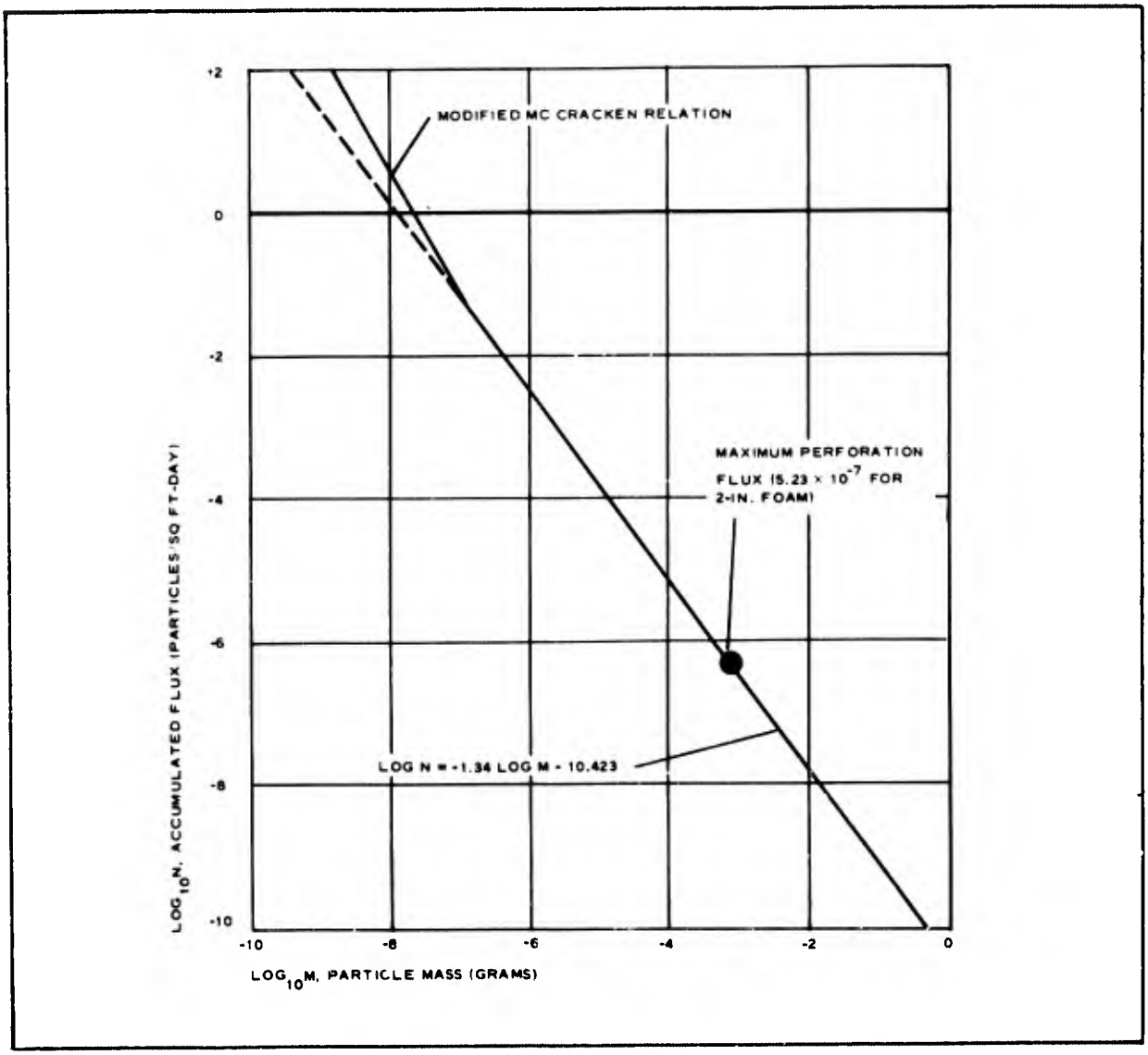

Figure 6 - Near-Earth Micrometeoroid Environment

applied to the film surface of the outer cover. The purpose of the thermal coating is to maintain material temperatures within acceptable limits during full solar flux. Maximum temperatures are limited to about 300 F; minimum temperatures will be limited by the emissivity of the coating, the thermal conductance of the composite wall, and the heat capacity of the structure. A computer program is currently underway to evaluate various coatings along with these factors relative to orbital inclination, orbital altitude, and orientation of a structure with respect to the earth. The objective of the computer program is to establish temperature gradients of the composite wall. These gradients will be used to establish minimum and maximum temperatures and will permit the correlation of material thermal characteristics with the expected temperature extremes.

The compatibility of environmental effects requires the consideration of combined vacuum and ultraviolet radiation, the thermal environment, and

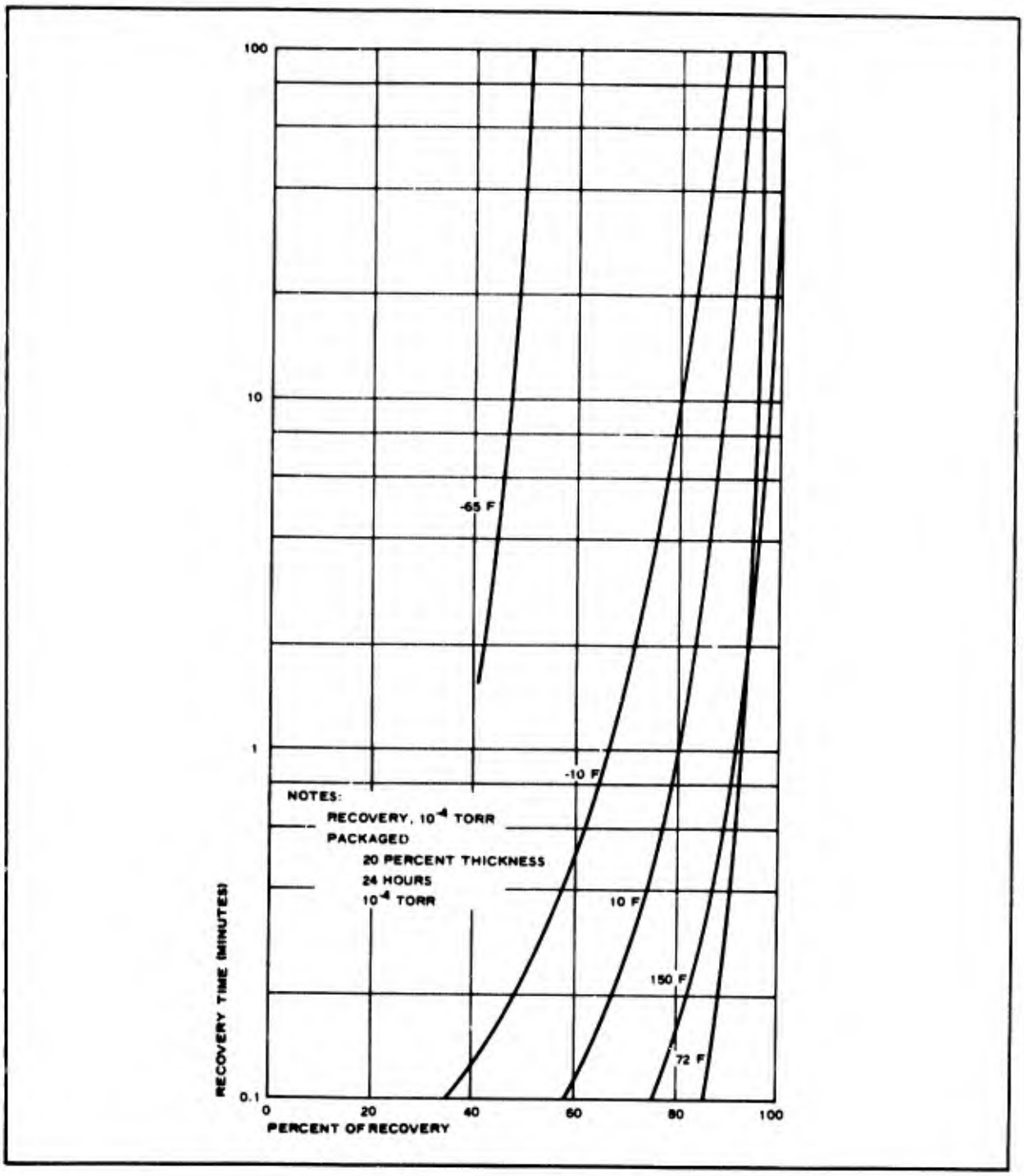

Figure 7 - Foam Thickness Recovery versus Time

high-energy radiation from Van Allen electrons. The portion of the outer cover most sensitive to the orbital environment will be the thermal coating. The combined effect of vacuum and ultraviolet radiation will cause some degradation of the coating, leading to an increase in materials temperature. Off-gassing due to vacuum is a minute effect: less than 0.5-percent weight loss

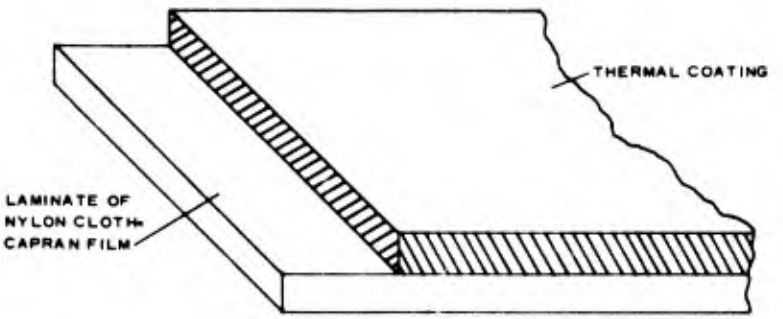

ITEM	WEIGHT (PSF)
FILM CLOTH LAMINATE	0.015
THERMAL COATING	0.053
TOTAL	0.068

Figure 8 - Outer Cover of Composite Wall

and stabilizing in 1.5 hr. Thermal effects relative to extremes in temperature must be evaluated for each specific structure design and coating selection. The tolerance of the outer cover to high-energy radiation is on the order of 10^7 to 10^8 rads.

SECTION IV - DEVELOPMENT OF MANNED SPACE STRUCTURES

1. BACKGROUND

The developments conducted in materials and in fabrication techniques have been successfully applied to the development, fabrication, and test of several preprototype structures. Three specific structure developments already have been completed with the fourth, the D-21 airlock, currently underway.

2. STAY-TIME EXTENSION MODULE

The Stay-Time Extension Module (STEM) is a lunar shelter developed under a contract directed by the Langley Research Center of NASA. The shelter, an integrated structure shown in Figure 9, was fabricated as two structural entities comprised of an airlock and the main shelter bolted together at a common interface. For this design, the elastic recovery material approach was used that incorporated a filament-wound steel structural layer in both the shelter and the airlock. The general characteristics of this design were as follows:

STEM Airlock	Dimensions
Design pressure	5 psi
Factor	3
Diameter	80 in.
Length	4 ft
Volume	100 cu ft
Weight	116 lb

STEM Shelter	Dimensions
Design pressure	5 psi
Factor	3
Diameter	80 in.
Length	13 ft
Volume	400 cu ft
Weight	200 lb

Multiple packaging, deployment, pressurization, and leak rate tests were conducted on the integrated structure both at Goodyear Aerospace and at the Langley Research Center. The results of these tests indicated that repeated folding, packaging, and deployment had no noticeable degrading effect on the structural characteristics of the design.

Some leakage problems were encountered at the pressure bladder

attachment to the rigid frame of the airlock entry hatch. The subsequent development, however, of improved fabrication techniques has overcome this problem for any future design. After repair, the measured leak rate was less than 0.5 lb/day, comparable to the initial gas loss measured immediately subsequent to fabrication.

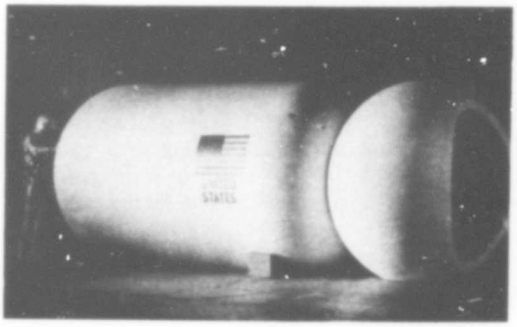

Figure 9 - Lunar Shelter

3. CREW TRANSFER TUNNEL

An equally successful development effort was conducted on the crew transfer tunnel program. This program was conducted under contract with the Air Force Aero Propulsion Lab at the Research Technology Division (RTD). The tunnel configuration as a preprototype structure is shown in Figure 10. The tunnel structure represents a major integration of rigid and expandable structure design techniques shown in the structural joint detail presented in Figure 11. The expandable structures approach also is based on the elastic recovery materials concept, incorporating multi-ply dacron cloth instead for the structural layer. The structural approach is determined by the nonsymmetrical geometry of the structure design. The general characteristics of this structure development are tabulated below:

Tunnel	Dimensions
Design pressure	7-1/2 psi
Factor	5
Width	3-1/2 ft
Length	12 ft
Volume	103 cu ft
Weight	227 lb

Repetitive packaging, deployment, pressurization, and leak tests were conducted. The results of repeated testing produced no degrading effects on either structural characteristics or leakage loss. Throughout the test program, gas loss did not exceed a rate of 0.4 lb/day, compared to an allowable rate of 0.5 lb/day.

4. LARGE STRUCTURES FEASIBILITY DEVELOPMENT

A development program recently completed at Goodyear Aerospace was directed toward establishing the feasibility of fabrication methods, packaging techniques, and deployment characteristics for large structures. This program is being conducted under the direction of the Langley Research Center.

The preprototype structure in the final phase of fabrication is shown in Figure 12. This design again incorporates the elastic recovery materials

approach. The structural approach for this design was dictated by the sheer size of the unit. Dacron structural tape appeared to be the optimum solution, both structurally and from the standpoint of fabrication methods. The tapes are good for about 4000 lb in ultimate tensile test with approximately three miles of tape needed to fabricate the structure. The characteristics of the preprototype structure are as follows:

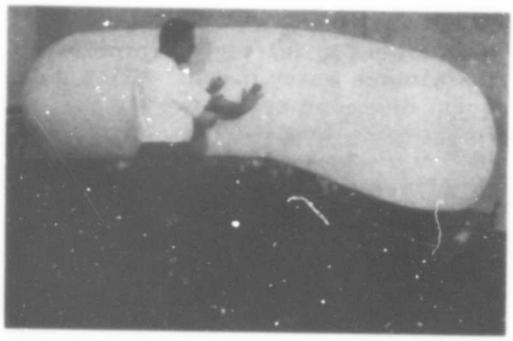

Figure 10 - Crew Transfer Tunnel

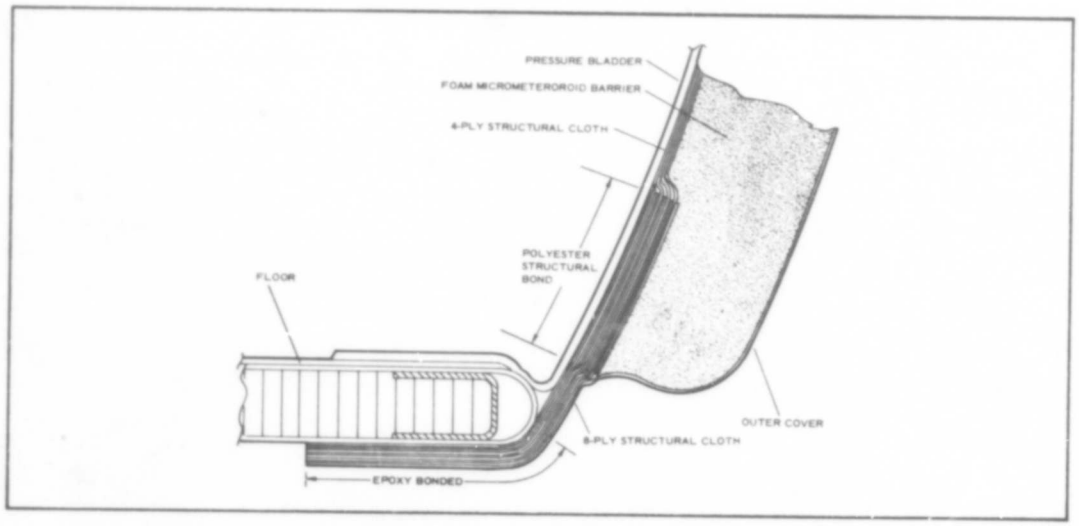

Figure 11 - Structural Joint between Expandable Wall and Rigid Floor

Large Structure	Dimension
Design pressure	5 psi
Factor	5
Diameter	12-1/2 ft
Length	37 ft
Volume	4400 cu ft
Weight	1500 lb

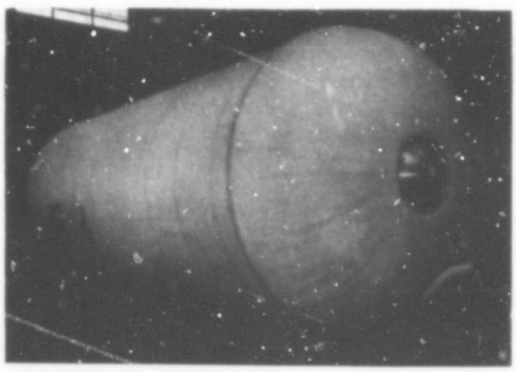

Figure 12 - Preprototype of Large Structure

Since this program is current, no testing has been conducted yet relative to packaging, deployment, and pressurization. Preliminary leak tests have been conducted, indicating a predicted gas loss of about 2.0 lb/day during orbital conditions which is well under the design goal of two percent loss.

5. D-21 AIRLOCK FLIGHT EXPERIMENT

Another current development program is the D-21 airlock flight experiment being conducted by the Air Force Aero Propulsion Laboratory. This program represents the first time that an expandable structure will be subjected to the complete cycle of development testing and then flown in orbit for subsequent orbital testing. Figure 13 shows an artist's concept of the D-21 airlock in a flight experiment during a NASA S-IVB workshop flight.

The elastic recovery materials approach is being used on the D-21 design also. Structurally, the approach is to use a steel-filament-winding technique, selected as optimum for this design. The expandable structures portion of the airlock covers an area of 77 sq ft with the total composite weighing about 35 lb. Out of this total composite weight, the steel filament wound structure weighs about 5 lb. There are no structural joints anywhere in the expandable portion of the airlock design, which should provide ultimate structural integrity and reliability.

Figure 13 - Concept of Airlock

SECTION V - CONCLUSIONS

The use of expandable materials for manned space structures can best be developed by applying materials R&D to a specific end item structure. Feasibility of a specific approach, in the final analysis, can be judged only by the meaningful test results obtained from the final structure and not from material specimens.

Goodyear Aerospace has found fabrication methods to be extremely important in the overall development cycle. This development step forms a bridge between a particular materials approach and a final structure. In addition, fabrication generally indicates where modifications might be required in a materials concept if that concept is to be successfully translated into a piece of hardware.

Finally, the depth of development testing conducted on an end item structure is important from the standpoint of establishing a degree of feasibility. The greater the depth of testing, the more credible the ultimate feasibility of a particular design. In this respect, the D-21 airlock experiment is extremely important because it is the only program in expandable manned space structures that will travel along the complete development path.

ADVANCED ORBITING GRID SPHERE PASCOMSAT

Frederick J. Stimler*

INTRODUCTION

Earth satellites have proved to be excellent means for global radio links. While orbiting, electronic repeaters (active satellites) sooner or later cease their operations and can be jammed in time of conflict. Orbiting reflectors (passive satellites) can provide long-lasting relay points. To be effective, passive satellites must combine large size with small weight; in essence, they must be expandable structures. When large, lightweight bodies are exposed to solar pressure or particle drag, their lifetime in orbit is very low. At increased altitudes the solar pressure becomes predominant and can perturb the orbit to preclude satisfactory use of the passive satellite as a radar or optical reflector. Orbit perturbations were noted with the Echo satellites. The open wire mesh surface of the sphere meets the size/weight requirements and minimizes the effects of solar pressure and drag.

Ylo E. Stahler of SEG/RTD has conducted theoretical and experimental analyses on wire-grid sphere surfaces, using small models. He found that a gain of 7 db can be achieved over that of an equivalent metal sphere at certain radio frequencies to enhance the value of this "grid sphere effect" for passive communications satellites. Details of this effect are given in References 1 and 2 and will not be discussed here.

Several 14-foot diameter wire-grid spheres were constructed for ground and tethered tests to verify the grid sphere reflection signature (References 3 and 4). It was not possible to obtain the necessary frequencies in outdoor tests of the 14-foot spheres to determine the actual effects of high, partial, or low grid transparency during these early contracts. An actual space experiment was considered advisable to make use of the wide frequency range available with the ground radar network.

Goodyear Aerospace Corporation (GAC) prepared a 30-foot diameter wire-grid experimental satellite (PasComSat) for a space launch to verify deployment, film photolyzation, rf effectiveness, and payload design parameters. This satellite is shown in Figure 1. Two complete payloads (canister, sphere, and deployment control assembly, as shown in Figure 2) were

---

*Astronautics Programs, Goodyear Aerospace Corporation, Akron, Ohio.

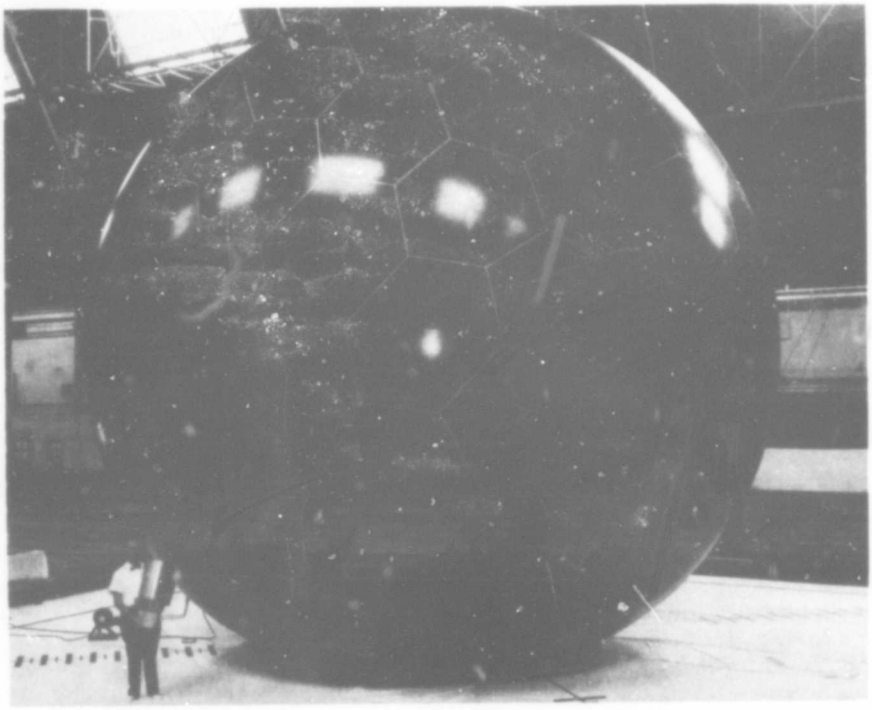

Figure 1. 30-Foot Diameter Grid-Sphere Satellite and Payload Hardware

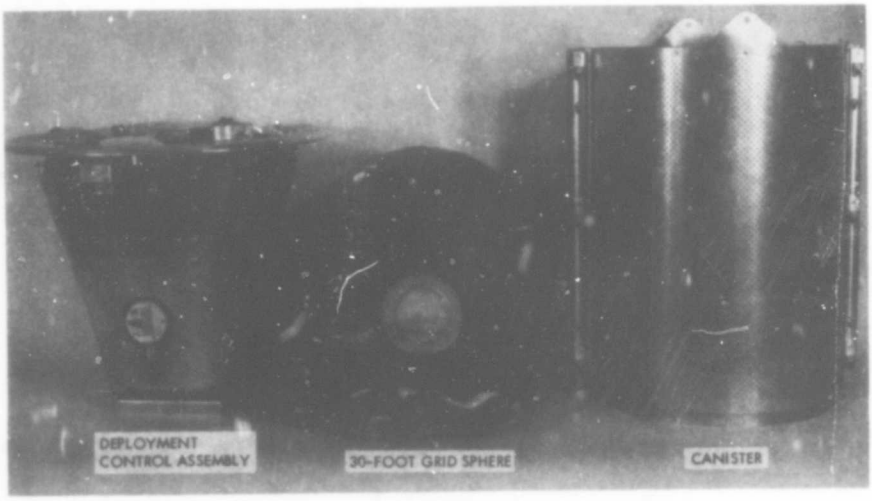

Figure 2. Major Parts of Grid-Sphere Payload

designed, fabricated, ground tested and readied for a later vertical launch (Reference 5). The Air Force desired to place the sphere into a retrograde circular orbit of approximately 540 nautical miles with the OV1 vehicle. This entailed additional design and testing effort, as reported in Reference 6, to meet the launch vehicle requirements as established by the Office of Aerospace Research (LOOAR) and General Dynamics/Convair. The total satellite weight was 54.6 pounds, made up of the sphere at 23.2 pounds, the canister at 10.3 pounds, and the deployment control assembly at 21.1 pounds.

The sphere was placed into a retrograde circular orbit of approximately 540 nautical miles from the Air Force Western Test Range (Vandenberg AFB) at $02^h\ 10^m\ 02^s$ Universal Time (UT) on 14 July 1966. The sphere remaining in orbit weighs about seven pounds after photolyzation of the film. It has been given the international designation of 1966 63A and SPADATS Number 2324.

MATERIALS DEVELOPMENT

Extensive sphere material development tests were conducted to develop a suitable photolyzable film and composite material, to determine a structural seam for operating temperatures of 225°F, and to improve fabrication techniques. Development and fabrication of the photolyzable film was done at the Research Division of The Goodyear Tire & Rubber Company. Processing and testing of the prototype laminate material was conducted at GAC.

Polybutyl methacrylate (PBMA) was chosen as the best photolyzable film candidate, because its volatility under the space environment could be controlled in an acceptable manner and early quantity fabrication seemed possible. Reference 7 gives a good discussion of other plastic materials considered during the course of this program and summarizes the reasons for the final choice of PBMA.

Several dyes were tested with the PBMA film to ensure a temperature of approximately 225°F in space for adequate photolysis action. The prototype material had sufficient dye material added to provide a ratio of solar absorptance to infrared emittance (α/ϵ) in the range of 1.8. The choice of dyes is limited, for the dye must not be a stabilizer, must not be so volatile as to escape before its job is done, and must be generally compatible with handling, fabrication, and testing of the PBMA material.

Figure 3 shows the rate of weight loss of the grid sphere photolyzable film material for various temperature conditions as measured in laboratory tests. Addition of the wire grid, dye, and adhesive to make up the prototype sphere material alters the weight loss rate somewhat, as shown in Figure 4. As indicated by the curves, the grid surface is fairly well open after 200 minutes of exposure with the film, adhesive, and dye residue attaching itself to the wire. It is expected that approximately 70 to 90 percent of the film will eventually be lost; however, additional test data must be taken over a longer time period to predict and understand the end product. It is emphasized that the film will only photolyze when reacted upon by the ultraviolet rays of the sun in the vacuum of space, or under simulated conditions, and

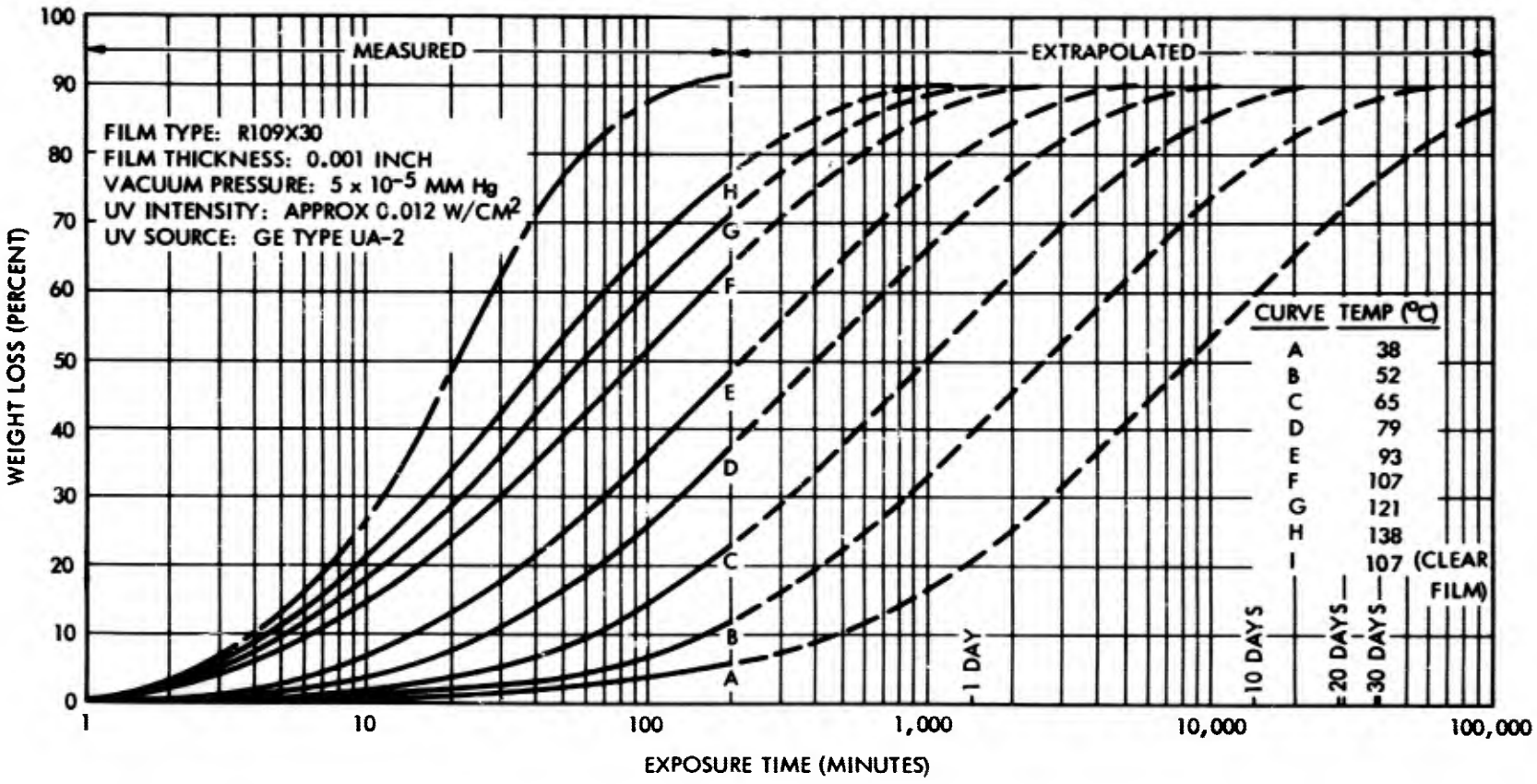

Figure 3. Predicted Weight Loss Behavior of Grid-Sphere Photolyzable Film at Various Temperatures

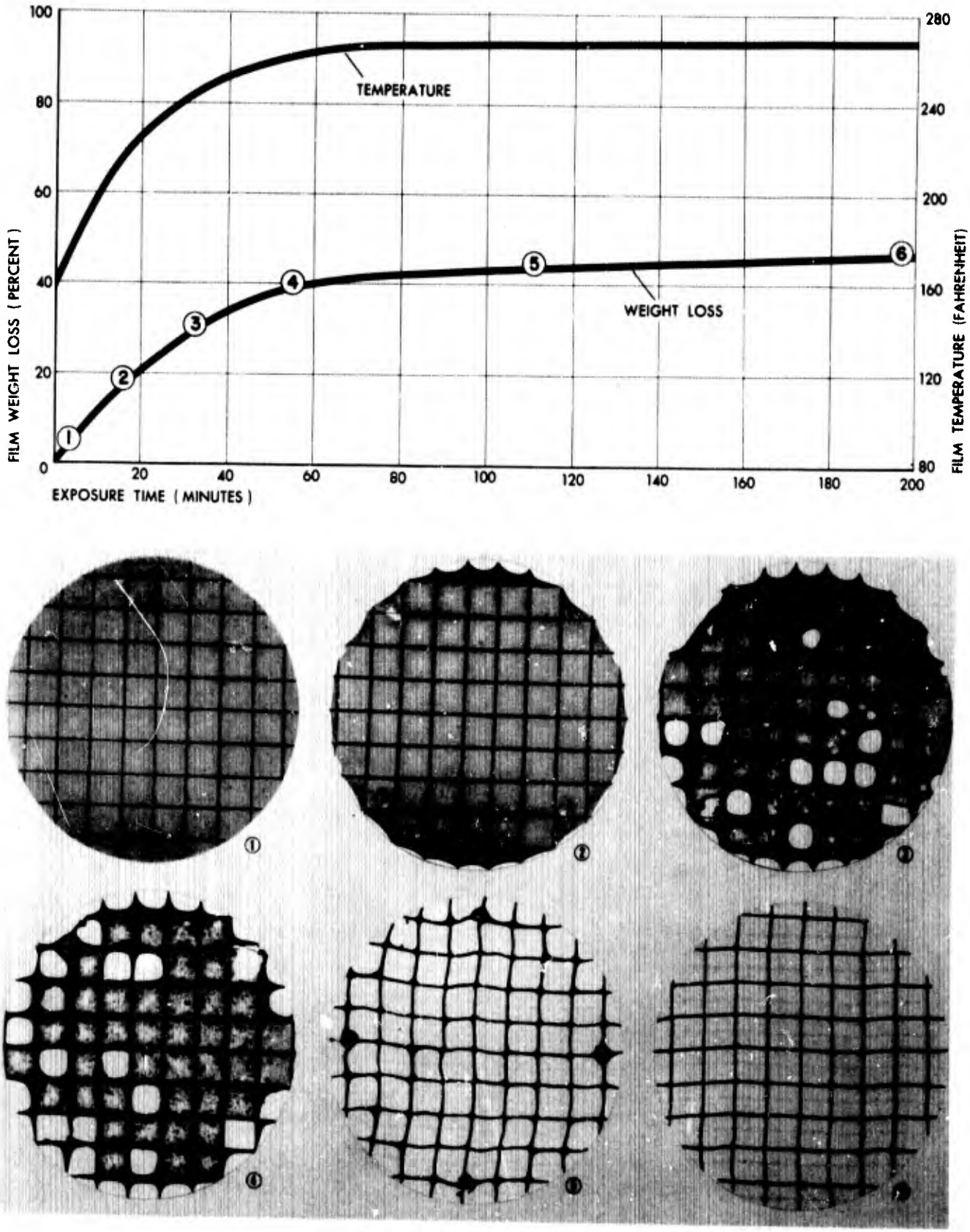

Figure 4. Photolysis of Grid-Sphere Prototype Material

will not disappear as a result of temperature alone. Additional information on design and test details of the wire grid photolyzable film material appears in Reference 5.

Extensive testing was conducted on the Instron test apparatus of the soft 3-mil diameter aluminum wire to ensure that the yield load was within 0.05 and 0.07 pound and that the elongation was over 15 percent. Many spools were rejected and the wire either replaced or reprocessed. It was necessary to establish these stringent requirements to enhance the balloon sphericity following the material elongation that occurred during the rigidization process.

The sphere prototype material was made as depicted in Figure 5. Starched cheesecloth was mounted on the 24-inch diameter by 7-foot long winding drum to facilitate removal of the sphere material. Two pieces of photolyzable film (approximately 3 x 6 feet) were placed side by side on the drum with a slight overlap. After the first winding of 3-mil wire at 6 per inch was completed, the material was removed, rotated 90 degrees, and replaced on the drum. An orthogonal winding at 6 per inch was then applied over the other wire layer. The wire was drawn through an adhesive bath and then through a hyperdermic needle, leaving an adhesive coating of about one-half mil. Two pieces of photolyzable film were placed over the wire side to complete the laminate, and then curing was effected for 10 minutes under a vacuum of 4 inches Hg and a temperature of 190°F. The second set of films was placed at right angles to the first set. This procedure, plus the use of the sandwich concept itself, reduced gas loss due to pinholes in the film and the overlap seam. The vacuum was released after cooling at laboratory conditions to a temperature of 120°F. These 6 x 6 foot panels served as the basic stock from which the sphere geodesic panels were cut.

The composite material and representative seams were tested at 0 to 225°F for tensile strength, creep, yield, optical characteristics, and simulated radiation characteristics. The detail test results are presented in Reference 5. The design strength of the prototype material was 0.6 pound per inch. A yield of 0.1 percent in the wire structure was anticipated during sphere rigidization at the design pressure of 0.0033 psi. The approximate weight breakdown of the prototype material is as follows:

3 mil Al wires at 6 per inch	0.0012 psf (15%)
Photolyzable film (2-1/2 mil layers)	0.0065 psf (81%)
Vitel adhesive	0.0003 psf (4%)
	0.008 psf

SPHERE FABRICATION AND ASSEMBLY

The 30-foot diameter wire-grid sphere is constructed of 162 pentagonal and hexagonal panels to form its geodesic pattern. This pattern was chosen rather than lune or orange peel construction for the following reasons:

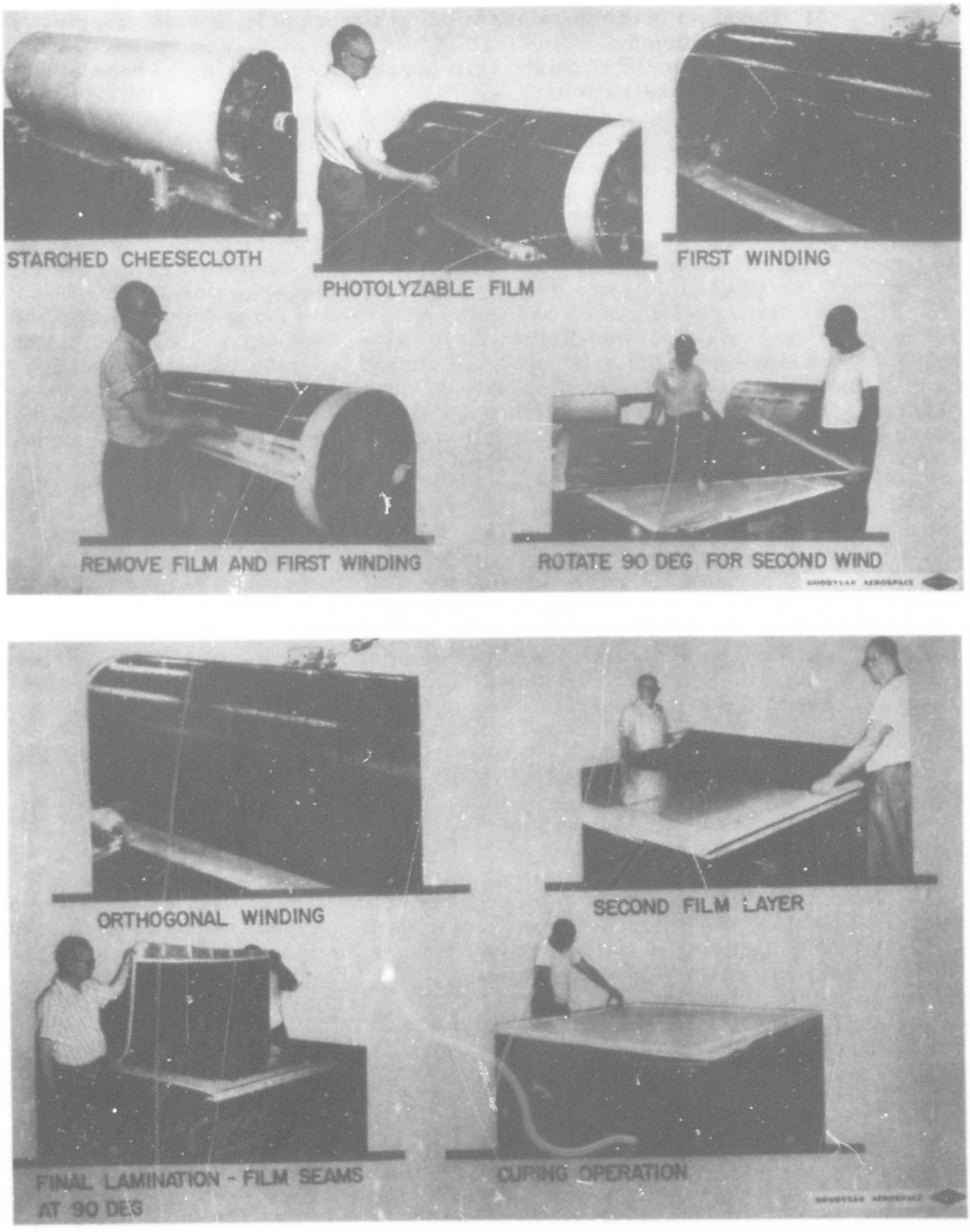

Figure 5. Grid-Sphere Prototype Material Fabrication

(1) The geodesic pattern has less seam length.
(2) Better sphericity and surface accuracy is possible.
(3) Since no continuous seam occurs from pole to pole, ripping is precluded.
(4) Small panels of this fragile material are easier to handle during fabrication.

Figure 6 generally shows the panel fabrication and assembly technique used on the program. One pentagon and two hexagon templates were used. The basic material was first draped over a tool with a 15-foot radius. The panel pattern was placed over the material, and the material was then trimmed. Provision was made for the one-half inch overlap seam by cutting the panels larger and marking seam overlap points to minimize assembly tolerances. As the panels were overlapped during the assembly procedure and positioned with a heat gun, three coats of a mixture of Vitel adhesive and aluminum powder were painted in the seam areas, one after the other. Using the proper mixture and room temperature curing techniques ensured sufficient strike-through of the Vitel adhesive to provide a seam with sufficient structural integrity at 225°F. Panel fabrication, subassembly, assembly, and sphere closure were accomplished in a clean room under controlled conditions. A special opening was provided to inflate the sphere on the ground for check-out and leakage rate studies. A diffusion sock was attached inside the space inflation valve to disperse the inflation gas and preclude surface material punctures from the high pressure during inflation.

The wire-grid photolyzable film was a lot flimsier and harder to handle than the Echo I and Echo II materials. Therefore, special techniques and precautions were developed during this study program. For this reason the prototype or a similar material could be considered for application to larger bodies with probably some modification of such procedures as fabrication, assembly, handling, and packaging.

HARDWARE CONSIDERATIONS

The grid sphere payload hardware was a rather simple and reliable design. Space-qualified hardware and fabrication techniques were used as much as possible within the program requirements. The payloads were designed for a vertical boost to check deployment and rigidization of the balloon. Wherever feasible the payloads were later modified to meet the requirements of an OV1 launch into circular orbit and those of the Western Test Range. The payload was completely self-contained, requiring only a signal to start the programmer following separation from the boost vehicle. Battery power, pyrotechnic initiators and cutters, helium gas at 3000 psi, circuit boards, explosive valves, pressure reducers, electrical controls, etc, were the main items of the deployment control assembly. Further definition of the parts is given in References 5 and 6.

The balloon pressure was controlled by allowing the helium gas to flow through fixed valves in a programmed manner and effecting sphere cut-off from the deployment control assembly at the proper time. No instrumentation or telemetry was incorporated on the payload. Close coordination was maintained with GD/C to expedite the interface structure definition and maintain experiment simplicity.

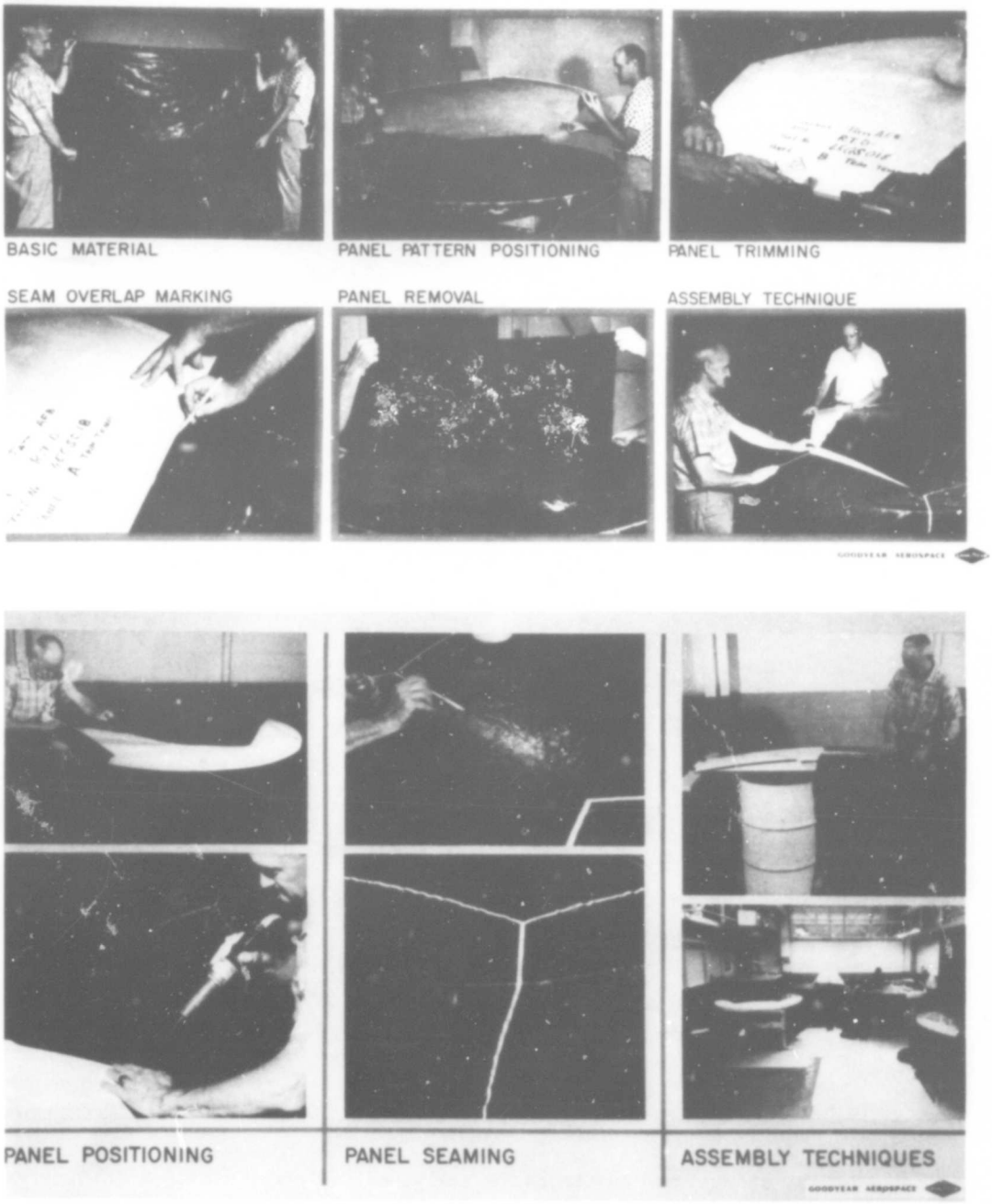

Figure 6. Grid-Sphere Panel Fabrication and Assembly

COMPONENT TESTS

Component and subassembly performance tests were conducted under anticipated environmental conditions, first for the vertical shot requirements (Reference 5) and then for the orbital launch requirements (Reference 6). The principal tests conducted on the assembled payload were canister separation, timer performance, inflation system check-out, resistance and continuity checks, and vibration and acceleration. Suitable design verification tests (DVT's) were performed on the back-up payload, and flight acceptance tests (FAT's) were performed on the flight unit.

Four-foot diameter spheres were fabricated and tested to verify fabrication techniques, packaging, and deployment characteristics of the prototype sphere. Figure 7 shows the four-foot sphere packaging sequence. Figure 8 shows the deployment test conducted in a 6-foot diameter, 10-foot high vacuum chamber at an initial chamber pressure of approximately 1/4 mm Hg. Pleats and accordion folds were utilized in the sphere to ensure rapid deployment. This packaging technique and final volume was representative of that used with the 30-foot sphere. A package volume equal to four times the sphere material volume was considered satisfactory. A non-pressurized canister is used on the payload for simplicity and economy. Rapid deployment of the sphere is expected, as seen in Figure 8. Soapstone and tissue paper were used on the flight sphere to ensure deployment, since the sphere was packaged several weeks prior to the actual space test. Extensive precautions were taken to keep the temperature of the packaged sphere between 60 and 70°F during handling and shipment and when assembled into the payload. A special insulated box was designed, fabricated, and tested to solve this thermal problem (Reference 6).

Simple sphericity measurements of the inflated sphere at about 2/3 design pressure were taken photographically on the ground. These measurements showed that the sphere diameter was within 1/4 percent (<1 inch) of the design value of 30 feet. The sphere surface, including the seam areas, was smooth and free of wrinkles.

FLIGHT TEST

The grid-sphere payload was orbited using a nose-mounted dual OV1 vehicle on an Atlas-D Missile. The OV1 vehicle, which was developed by General Dynamics/Convair (GD/C), consists of three integrated, self-contained units: the payload or satellite, the propulsion module, and the booster-retained structure. The two payloads of this launch were the OV1-7, a GD/C experimental payload, and the OV1-8(P), the GAC grid-sphere payload. The propulsion module is a complete final stage with its own programmer, guidance, attitude control, radar beacon, telemetry, and electrical power systems. The booster-retained structure supports and protects the satellite and its propulsion module during boost vehicle ascent. All OV1 operations usually are controlled by the programmer on board the propulsion module. Figure 9 summarizes the payload and launch vehicle concept used for the grid-sphere program. Figure 10 is a close-up of the nose-mounted dual OV1 vehicle on the Atlas-D missile. The vehicle was mounted while the booster was in the horizontal position.

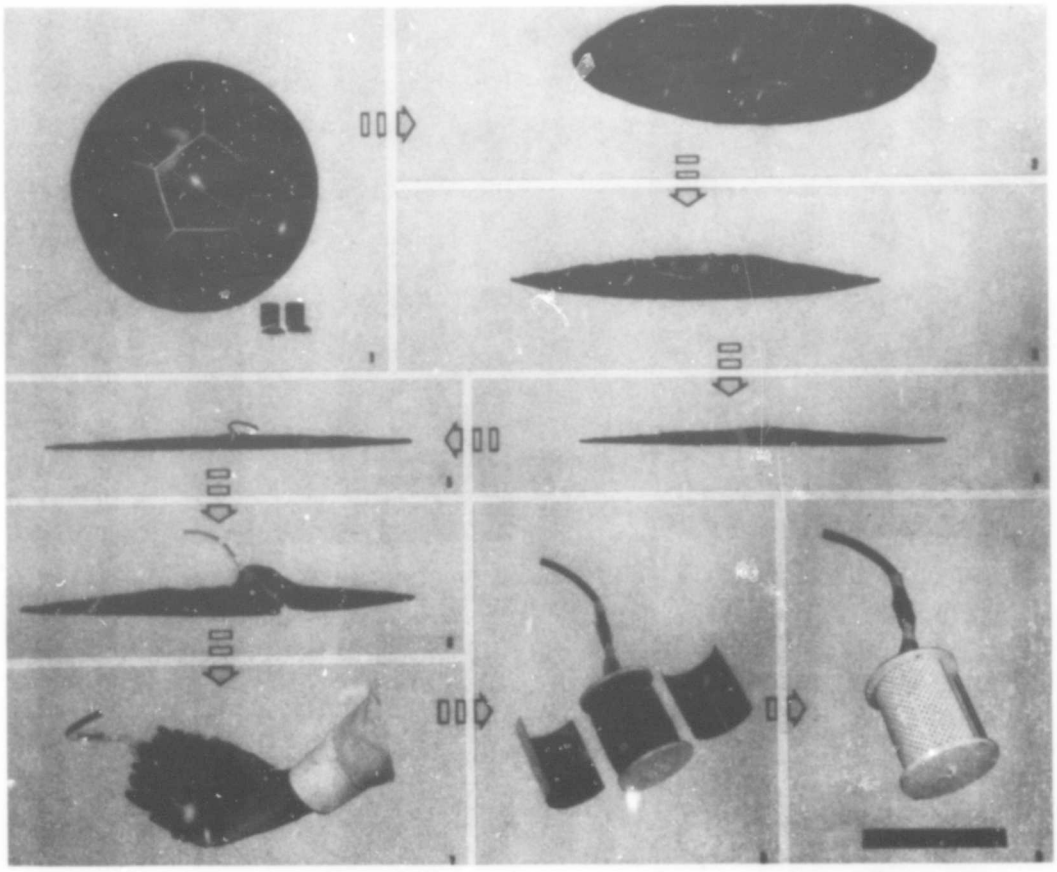

Figure 7. Four-Foot Sphere Packaging Sequence

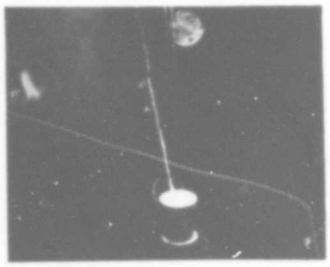

TIME = 0

TIME ≈ 0.5 SEC

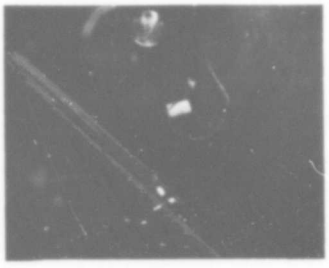

TIME ≈ 0.56 SEC

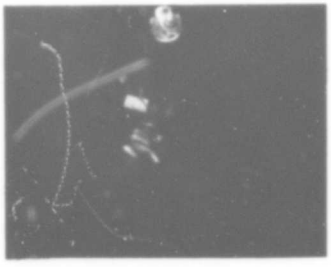

TIME ≈ 0.59 SEC

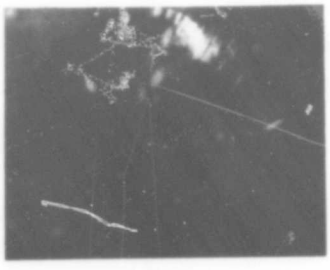

TIME ≈ 0.66 SEC

TIME ≈ 0.69 SEC

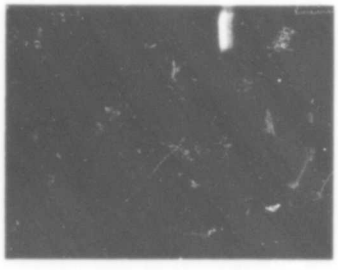

TIME ≈ 0.72 SEC

Figure 8. Four-Foot Sphere Deployment Sequence

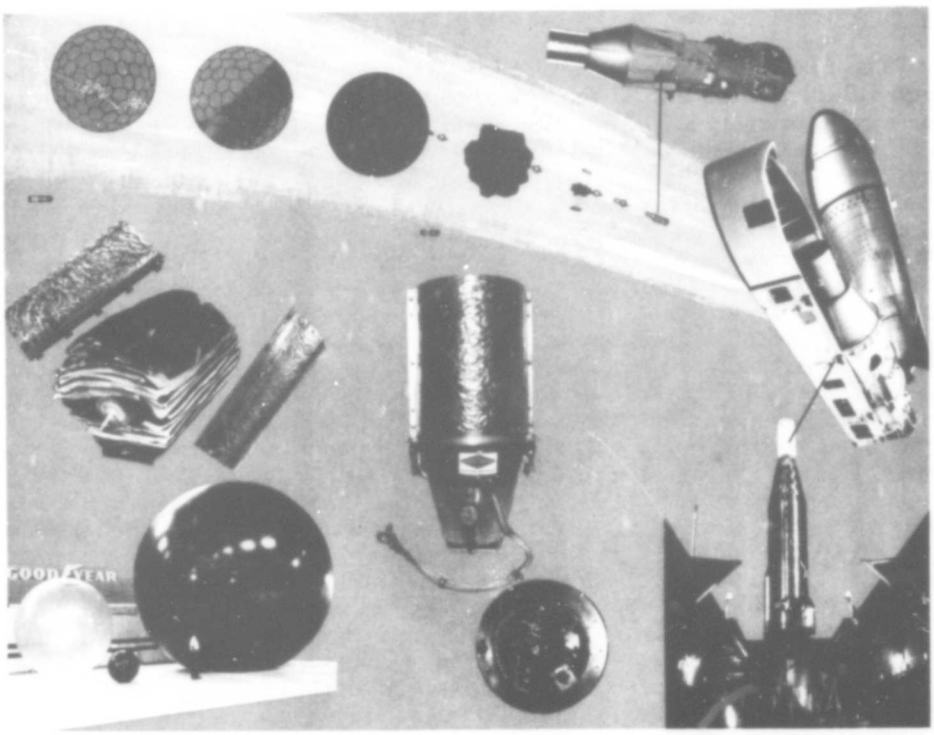

Figure 9. Summary of Wire-Grid Sphere Experiment

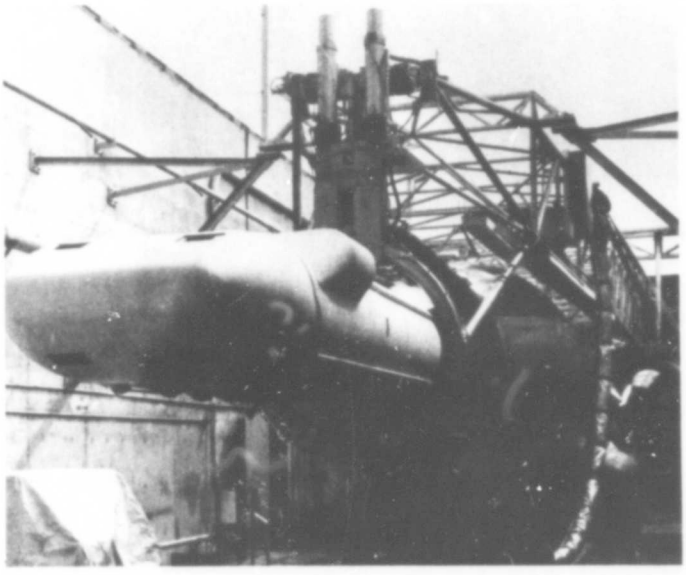

Figure 10. Nose-Mounted Dual OV1 Vehicle on the Atlas-D Missile

The two payloads and their propulsion modules separated from the launch vehicle at the end of the powered phase of the Atlas vehicle ascent. After approximately an 11-minute coast period to ballistic apogee, the propulsion-module solid-fuel motor was ignited and burned for approximately 24 seconds to effect circular orbit injection. During the coast period, the propulsion-module attitude control system maintained proper vehicle attitude until and during rocket ignition. The OV1-8(P) payload separated from the propulsion module at a velocity of approximately 9 (±3) feet per second approximately 100 seconds after motor burnout. At this point, the payload included the interface structure that attached the GAC grid-sphere payload to the GD/C propulsion module. After an additional 60 seconds delay, the canister halves separated at 20 feet per second relative velocity, perpendicular to the orbital velocity vector. Sphere inflation started 5 seconds later. Complete inflation and rigidization was attained at the end of 60 seconds, after which the sphere was separated from the hardware structure through a guillotine action. Separation of the sphere and the hardware was effected through release of sphere pressure at cut-off and the residual pressure in the inflation bottle. Elapsed time from lift-off to the sphere-in-orbit phase was approximately 20 minutes. After payload separation, the propulsion module telemetry rf carrier and C-band radar beacon functions were maintained in operation until battery exhaustion for the purpose of downrange tracking and obtaining initial orbit parameters. The Atlas booster continued its ballistic flight path after engine shut-off and impacted into the Pacific Ocean. The remaining five items - the sphere, the two canister halves, the deployment control assembly and interface or adapter structure, and the propulsion module - remained in retrograde orbit.

This was a unique use of the OV1 vehicle, where scientific black-box experiments are the usual payload. Additional data on the OV1 can be obtained from Reference 8.

DATA ANALYSIS

The Air Force had the primary responsibility for obtaining orbital flight test data and correlation of rf and optical information. However, GAC did provide coordination for acquisition and orbit determination before and after film photolyzation and made some cursory analyses to determine the photolyzation effect on the W/C_DA of the sphere.

A summary of the OV1-8(P) orbital characteristics obtained from Reference 9 is shown in Table 1. The three debris items are the two canister halves and the deployment control assembly including the adapter section. Official launch data is given in Reference 10, which also includes an analysis of problem areas and a comparison of predicted and actual launch and orbital performance.

Figure 11 gives a view of the 24-inch mobile telescope system which GAC has developed for NASA-Langley Research Center for the study of satellite surface characteristics from the ground. Complete design and performance data of this unit can be obtained in Reference 11. At the time of sphere launch this telescope was located at Palomar Mountain and several data runs were made through NASA's cooperation. At the same period the Aeronautical

Table 1. OV1-8(P) Payload Objects in Orbit

1966 Launch Object	Code Name	Catalogue Number	Source	Launch	Period (minutes)	Inclination (degrees)	Apogee (km)	Perigee (km)
1966 63A	30-ft dia grid sphere	2324	US	14 Jul	105.2	144.23	1041	957
1966 63B	Debris	2327	US	14 Jul	105.3	144.25	1012	998
1966 63C	Propulsion module	2328	US	14 Jul	105.3	144.26	1016	994
1966 63D	Debris	2329	US	14 Jul	105.5	144.27	1018	1010
1966 63E	Debris	2337	US	14 Jul	105.3	144.25	1011	1004

Research Laboratories at WPAFB obtained optical data with their fixed 24-inch telescope. Photometric data was also taken by GAC with a 5-inch telescope from the Smithsonian Astrophysical Observatory tracking station in North Canton, Ohio.

Analysis of flight data verifies that the sphere structure and related equipment operated as designed and that the rigidized wire-grid PasComSat will remain in a stable orbit indefinitely. A regression analysis of preliminary photometric data determined from ground stations indicates that the wire sphere surface is 30 percent specular (70 percent diffuse) in its photolyzed state. The orbiting sphere initially had a stellar magnitude of approximately 5 and represents one of the few, if not the only, satellite in hard retrograde orbit (going east to west) that is clearly visible with minimum optical aids.

Recent data has shown that exposure to the space environment has slightly reduced the stellar magnitude of the sphere. This data is presently being analyzed by the Air Force and GAC. Reference 6 gives a comprehensive analysis of the grid sphere performance in orbit from analyses of both optical and rf data observed during the first six weeks following launch. Figure 12 shows a typical relationship of stellar magnitude versus phase angle as noted a few days after launch. As you can see, the data points seem to fit the diffuse curve showing dependence on phase angle.

CONCLUSIONS

Analysis of the flight data verifies that the sphere structure and related equipment operated as designed and that the wire-grid PasComSat will remain in a stable orbit indefinitely. Correlation with previous rf data on grid spheres and agreement between the Air Force and GAC independent optical evaluations have led to a better understanding of the cross check capable with these two types of observations. Indeed, more flight analyses must be made to be sure of the overall performance of the grid sphere. The Air Force is continuing in-house studies in this area and will report these findings in the future.

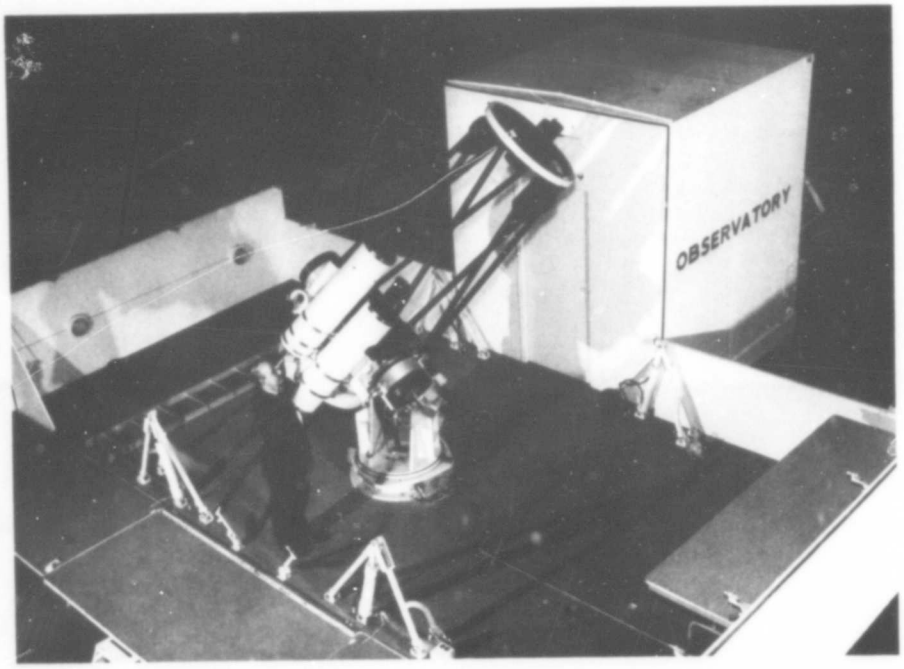

Figure 11. 24-Inch Mobile Telescope for Tracking and Measuring Satellites (Developed for NASA-LRC)

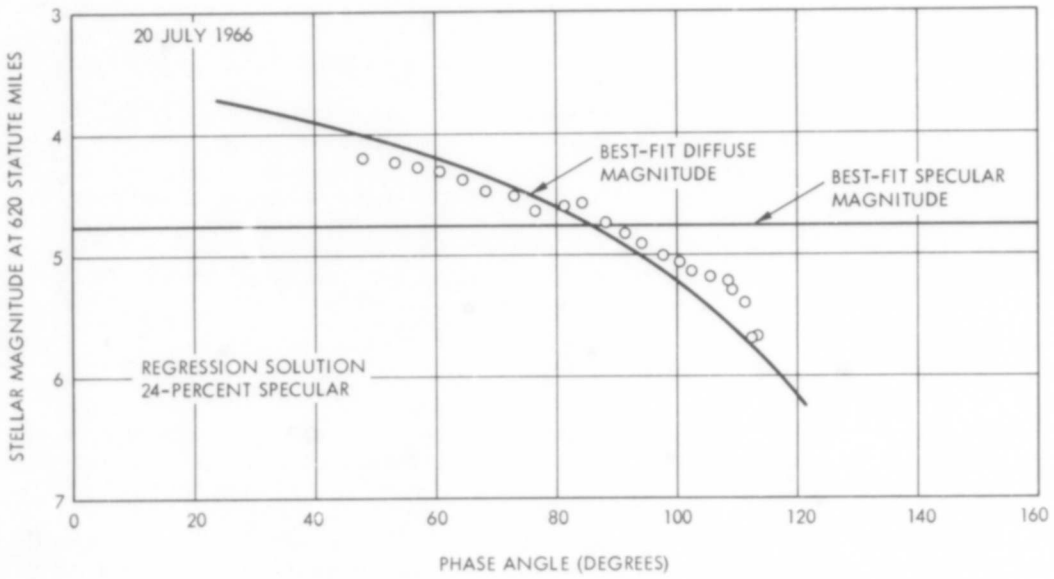

Figure 12. Normalized Stellar Magnitude Versus Phase Angle (20 July 1966)

The main purpose of this pioneering endeavor was accomplished completely. This purpose, you will recall, was to verify deployment, inflation, rigidization, and surface film photolyzation of the wire-grid sphere. Preliminary data analysis has verified the reduced solar pressure and drag effects on the open grid sphere, which should indicate other desirable space applications for the unique material tested. Environmental test results of the sphere material, payload components, and subsystems have shown the design concept to be simple and reliable. Similar expandable structure applications, such as other types of passive communications satellites, wire film tube structures, exo-atmospheric decoys, radar calibration targets, etc, can be solved with an adaptation of this same design technique. It is, however, suggested that a positive means of pressure control and measurement be provided for complicated expandables to enhance deployment, inflation, and rigidization.

Prior to development of an operational PasComSat system, it is recommended that additional rf and optical measurements be made immediately of the 30-foot grid sphere satellite from ground installations to fully evaluate and correlate these data over the frequency range of interest. Photographing of the satellite with Baker-Nunn cameras is also recommended. Additional rf tests of scale models of representative sphere construction should be made to eliminate scintillations experienced to date and to verify the rf enhancement phenomena predicted for the wire-grid mesh concept.

A thorough analysis and understanding of the optical and rf signatures of simple spheres may provide significant design information for other applications. In addition, a dynamic analysis of the orbital parameters through use of computers will provide a better understanding of the drag and solar pressure phenomena in a potential tactical altitude region.

As depicted in Figure 13, we have progressed from the Echo satellites to the grid sphere concept, and now look toward the development of the advanced lenticular passive communications satellite (PasComSat) system which has gravity gradient stabilization and station-keeping characteristics. The data learned during the grid sphere program will be very helpful in advanced studies of large, lightweight, expandable structures of the future.

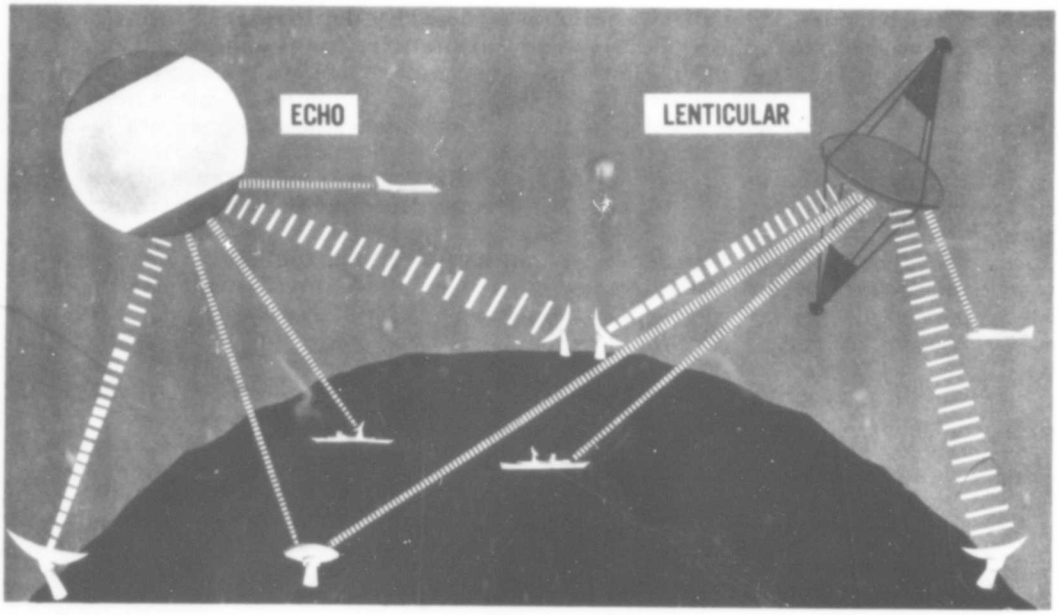

Figure 13. Passive Communication Satellite Concepts

REFERENCES

1. Stahler, Y. E.: Enhanced Radio Reflection of Grid Structures (The Grid-Sphere Effect). Technical Report SEG-TR-65-44, January 1966.

2. Research and Technology Briefs. United States Air Force, Air Force Systems Command. Volume IV, No. 12, December 1966, pp 1-8.

3. Study, Fabrication, and Testing of Passive Satellite Models, Grid-Sphere Type. Technical Report SEG-TDR-64-52, Contract AF33(657)-11537, GER 11568, Goodyear Aerospace Corporation, Akron, Ohio, August 1964.

4. Grid-Sphere Passive-Communication Satellite Performance Tests of Preliminary Model. Technical Report SEG-TR-65-43. Contract AF33(615)-1962, WPAFB, Ohio, August 1965.

5. Grid-Sphere Passive-Communications Satellite. Technical Report SEG-TR-65-66, Wright-Patterson AFB, Ohio, November, 1965.

6. Orbital Experiment of a Grid-Sphere Passive-Communications Satellite. Technical Report SEG-TR-66-62, Wright-Patterson AFB, Ohio, November, 1966.

7. Cross, W. B., Snyder, C. E., and Wier, D. S.: Controlled Instability of Polymer Films for Use in Grid Type Satellites. GER 12670, Goodyear Aerospace Corporation, Akron, Ohio, April 1965.

8. Applications Guidebook for OV1, Report No. GDC AAX65-015, General Dynamics Corporation, Convair Division, 20 December 1965.

9. GSFC Operations Control Center, Satellite Situation Report, X-512-66-51, Vol. 6, No. 15, Goddard Space Flight Center, Greenbelt, Md., 15 August 1966.

10. Flight Evaluation Report, OV1-7 and OV1-8 Propulsion Modules, Report No. GDC/BKF66-058, General Dynamics Corporation, Convair Division, 12 September 1966.

11. Hostetler, R. L., et al: Ground-Based Photometric Surveillance of the Passive Geodetic Satellite. GER 12762, Goodyear Aerospace Corporation, Akron, Ohio, 1966.

SESSION II

FLEXIBLE REINFORCED COMPOSITE WINDOW MATERIAL

By Jerry G. Williams*

INTRODUCTION

To date, all spacecraft for manned space flight have contained windows. These windows have proven extremely useful in conducting photographic-type experiments and in providing the capability for visual horizon and relative spacecraft referencing. Advanced applications of expandable space structures such as those shown in figure 1 also find it extremely desirable to provide windows for visual observations. A flexible window in the expandable lunar shelter[1] would allow observation of shelter support equipment and lunar experiments and would take advantage of external illumination for lighting. A window in a large expandable experiment module would be useful in viewing external phenomena. A window in the expandable airlock[2] would permit observation of space experiments located externally without requiring extravehicular activity (EVA) and would provide the means for initial orientation and referencing for EVA. Also the psychological aspects of a window in a manned space structure should not be overlooked. The purpose of this investigation was to determine if a flexible window compatible with the space environment could be developed for such applications.

Existing flexible transparent polymeric materials do not possess sufficient strength to resist the pressure loads developed in a manned spacecraft structure. The approach taken to meet this high-strength structural requirement for the flexible window is illustrated in figure 2. Basically a rectangular grid network of girth and axial filaments was embedded in a flexible transparent matrix, thus forming a flexible biaxially high-strength composite material. Rectangular space areas between filament groups were required to permit light transmission and viewing, as in a common window screen. The girth-to-axial-strength ratio was taken to be 2:1; the stress ratio developed in a pressure-loaded cylinder. Guidelines for the window were that it be capable of carrying a load of 840 lb/in. (147,000 N/m) in the girth direction and that the window display good optical properties under a 7-psi (48,300 N/m^2) pressure differential. In addition, the matrix was required to be capable of carrying the pressure loading within each grid without "blowout" up to a pressure differential of 35 psi (241,000 N/m^2).

The investigation approach taken was, first, to screen (including simulated space environment testing) available transparent polymers and reinforcement materials for suitable materials; second, to parametrically evaluate the reinforcement pattern; third, to develop an end attachment concept; and, last, to test the resulting composite materials and attachments. The results of this investigation will now be described.

---

*Aerospace Engineer, NASA Langley Research Center.

MATERIALS INVESTIGATION

Matrix

Following a survey of available transparent materials,[3] the optical and mechanical properties of four generically different types of flexible transparent polymers were evaluated. These included: (1) ethylenepropylene, (2) polyurethane, (3) silicone, and (4) polyisoprene. These materials were either cast or molded in sheets against ferro-type plates (1/2 rms finish) in thicknesses of approximately 0.030 inch (0.0762 cm), 0.060 inch (0.152 cm), and 0.120 inch (0.305 cm). Transparency and strength data for samples of each of the four polymers are given in table 1. The ethylene-propylene copolymer and polyisoprene materials were both considered to be unsatisfactory for the application due to their initiation of crazing, embrittlement, and reduced transparency after heat exposure of 100° C for 7 days. Heat exposure also darkened the polyester urethane and very slight crazing was noticed after 10 days of ultraviolet radiation exposure in a fadometer (ASTM procedure D-750-55T) with output strength of 3.15 watts/m^2 of wavelength below 4000 Å. The silicone polymer exhibited excellent resistance to both heat and ultraviolet exposure. The strength at 100-percent elongation and at break both before and after heat, vacuum, or ultraviolet exposure is also shown in table 1. Since these tests were of an exploratory nature, insufficient numbers of tests were conducted to give statistical significance to the differences noted. Apparently, however, the strength of the polyester urethane and silicone polymers was not appreciably changed by the environmental test conditions considered.

Figure 3 presents data for the percent of incident light transmitted by samples of dimethyl RTV silicone and polyester urethane corresponding to wavelengths ranging from 2400 Å to 150,000 Å. Thicknessess for the silicone and urethane were 0.111 inch (0.282 cm) and 0.075 inch (0.190 cm), respectively. Of particular interest is the visible spectrum ranging from 4000 Å to 7000 Å. It is noted that the silicone transmitted approximately 93 percent of the incident light throughout this range while the urethane was essentially opaque at 4000 Å and increased to approximately 88 percent at 7000 Å. Window anomalies are noted in the ultraviolet and infrared regions.

Additional information generated in the study showed the effect of thickness on the percent light transmission through the visible spectrum for the silicone to be negligible for the range of thicknesses tested (0.037 inch (0.094 cm) to 0.171 inch (0.435 cm)). This was not true, however, for the urethane which, for example, at a wavelength of 5750 Å showed a decrease from 84-percent to 71-percent transmission corresponding to an increase in thickness from 0.048 inch (0.122 cm) to 0.133 inch (0.338 cm).

The effect of heat exposure (100° C for 7 days) on the percent incident light transmitted by the silicone through the visible spectrum was found to be insignificant. Heat exposure, however, exhibited a notable effect on this property for the polyurethane, with a more pronounced effect occurring at the blue end of the spectrum than at the red. For example, a 0.133-inch- (0.338 cm)

thick sample of urethane transmitted 35 percent of the incident light of 4240 Å before heat exposure and only 1 percent after exposure. At 7000 Å, 85 percent was transmitted before and 79 percent after heat exposure. The effect of the ultraviolet radiation exposure (previously described) on the percent incident light transmitted in the visible spectrum was determined to be insignificant for both the silicone and the urethane.

It should be pointed out that the optical clarity one obtains in looking through a window is not only dependent on the amount of light which is transmitted, but is also influenced by the degree of resolution provided by the window. The preceding discussion has dealt only with the amount of light transmitted by the matrix material. The second consideration, resolution, will be taken up in a later discussion involving human factors evaluations of reinforced pressure-loaded windows.

The ability of the matrix material to resist bending and repeated folding during packaging is of extreme importance for a flexible window concept. To determine the ability of the matrix materials to meet this requirement, a flexometer instrument, the essential elements of which are described in table 2, was used. Both the polyester urethane and the dimethyl RTV silicone successfully completed 349,000 flex cycles without failure. It should be pointed out, however, that one disadvantage of using silicone for the window application is its notch sensitivity and corresponding low tear resistance. Urethane, on the other hand, is quite tough and resistant to tear propagation. Study is currently under way to investigate the possibility of laminating the two materials in order to combine the desirable properties of both materials.

Reinforcement Material

Three different candidate window reinforcement materials were evaluated including glass, steel, and polyester filaments. Each reinforcement material was embedded in silicone test samples 1 inch (2.54 cm) wide as uniformly spaced uniaxial strands. The test samples were 5 inches (12.7 cm) long and were prepared so that the center 3 inches (7.63 cm) of the sample filaments were embedded in dimethyl RTV silicone while 1 inch (2.54 cm) at each end was "plotted" into an epoxy impregnated glass cloth. The tensile strength of the candidate reinforcement materials was then measured before and after heat exposure (100° C for 7 days) using the above-described test specimen in a constant strain rate test machine with a crosshead separation rate of 2 inches (5.08 cm) per minute. Results of these tests are shown in table 3.

Of the fiberglass materials evaluated, the S-901 glass (S-glass with HTS finish) gave the highest ultimate tensile strength (5.3 lb (23.6 N) per end). The 0.010-inch- (0.0254 cm) diameter polyester filament gave a tensile strength of 6.9 lb (31.7 N) per filament and the 0.004-inch- (0.0102 cm) diameter steel wire gave a tensile strength of 6.3 lb (28.0 N) per wire. The effect of heat exposure (100° C for 7 days) is noted in the right-hand column of table 3. As expected, significant differences in tensile strength from unexposed samples were not obtained for the glass reinforcement. However, polyester reinforced test samples distorted and wrinkled badly after heat exposure due to shrinkage of the reinforcement. It was also found necessary, using the polyester, to fill almost the entire window viewing field with filaments in

order to get the required design strength (840 lb/in. (147,000 N/m) in the girth direction). For these reasons, polyester reinforcement was considered unsatisfactory for the application.

Both the steel wire and S-901 fiberglass filaments appeared to be satisfactory for the window reinforcement material and were both used in the remainder of the study. One problem area, however, which was uncovered during the study and is particularly acute for the steel wire, was the poor adhesion developed between the matrix and reinforcement materials. Improvement in the compatibility of the finish used on the filament or wire with the matrix material should improve this property.

For design purposes, the reinforcement material was considered to carry all the girth and axial loads. However, as noted earlier, the matrix was required to resist blowout within the reinforcement grid. For calculation purposes, the design strength of the S-901 fiberglass and steel wire was considered to be 6.0 lb (26.7 N) per end (wire). This then required 140 filaments (wires) per inch (2.54 cm) to meet the 840-lb/in. (147,000 N/m) strength requirement in the girth direction and 70 filaments (wires) per inch (2.54 cm) to meet the 420-lb/in. (73,500 N/m) strength requirement in the axial direction.

REINFORCEMENT PATTERN

Various spacings of filaments were evaluated in this study to determine the effect of spacing on optical resolution both for a nonstressed and pressure-loaded condition. Reinforcement pattern properties for 15 different panels are shown in table 4. These panels included specimens whose reinforcement filaments were uniformly spaced as in panel number 1 where, for example, a bundle of 40 ends was spaced every 0.25-inch (0.635 cm) in the girth direction; and panels such as number 3 whose bulk of filaments was bundled in one uniformly spaced group with additional filaments uniformly spaced in between.

Thicknesses and weights for some of these panels are also given in table 4. It is believed that these thicknesses and weights can be reduced, although it appears that a thickness of approximately 0.120 inch (0.304 cm) is necessary in order to insure complete coverage of the reinforcement filaments by the transparent matrix material. If filaments are cast too close to the surface, local stress-induced surface straining seriously affects resolution characteristics.

To measure the optical clarity obtainable with nonloaded reinforced panels, photographs were taken of a test chart with the test panel located between the camera and the test chart. The test panel was located 1 foot (0.305 m) from the camera lens and 5 feet (1.27 m) from the 28-inch (0.711 m) x 36-inch (0.91 m) test panel. Some of the photographs resulting from this experiment are shown in figure 4. Lighting and development conditions were identical for all photographs. Test panels are shown below the corresponding photograph. For reference, the photograph in the upper left-hand corner was taken without any intervening test sample. The middle two photographs of the top row were

taken with unreinforced dimethyl RTV silicone and polyester urethane, respectively, as the test panels. All the reinforced specimens shown are composed of fiberglass reinforcement embedded in a silicone matrix with the exception of the panel in the upper right-hand corner which uses steel reinforcement rather than glass.

The data from light transmission tests conducted on the reinforced panels revealed that the presence of the filaments reduced the percent of incident light transmitted by approximately the percent of projected area taken up by the filaments (from 10 to 30 percent depending on the pattern and wavelength). It should be pointed out that the optical resolution obtained by human viewing is normally superior to that obtainable in photographs. This, of course, is because of the superiority of the human eye and because of unconscious body movements which allow one to shift viewing angles slightly to compensate for view blockage caused by the filament pattern.

To measure the resolution obtainable under loaded conditions, the test panels were pressure loaded to 7 psi (48,300 N/m^2) and a human factors evaluation made. The individual making the evaluation viewed the test chart, located 6 feet (1.52 m) beyond the window, through the pressure-loaded test panel and made a comparative judgment based on the criteria set forth in table 5. Results for the first five panels shown in table 4 are given in table 6. For comparison, a rating of 1.0 was obtained for the three main points (blurriness, ability to focus, and readability) for a test conducted without intervening panel. The smallest legible print size which is readable looking through the panels is also given. Of these five panels, number 4 gave the best results.

ATTACHMENT DESIGN

The window geometry chosen for the attachment study was an ellipse whose major and minor axes were 11.4 inches (0.289 m) and 8.0 inches (0.203 m), respectively. Two systems were developed for attaching the flexible window element to a flexible expandable structure. The essence of these two concepts (adhesive bonding and mechanical clamping) is shown in a cross-sectional drawing in figure 5.

Since the reinforcement filaments carry the principal stresses, the attachment approach involved anchoring the filaments around the periphery of the window to meet the "pull-out" strength requirement, thereby transferring the window stresses into the flexible structure. Tests conducted on fiberglass rovings embedded in a silicone matrix showed the silicone to possess insufficient strength for this purpose. It was thus found necessary to terminate the reinforcement filaments in a stronger, higher modulus material. A nitrile polymer anchor flange approximately 2 inches (5.08 cm) wide was found satisfactory for this purpose. Two fiberglass doilies, wound to the elliptical shape of the nitrile flange, were adhered to both faces of the nitrile anchor flange for reinforcement.

The silicone-nitrile flange butt joint was found to form an inadequate joint for gas sealing purposes. Therefore, a seal consisting of a 0.015-inch (0.038 cm) nitrile sheet was bonded to both sides of the attachment in the

joint interface region. It was found necessary, however, to provide an unbonded region on the nitrile seal at the silicone-nitrile flange interface in order to prevent stress concentration induced failures in the silicone. This condition was insured by the incorporation of an unbonded Mylar ring in this region.

Silicone polymer bonds poorly to most adhesives other than those with silicone base. Experimental investigations showed a combination of silicone adhesive A-4000 and an epoxy-based adhesive 943 to be satisfactory for bonding the silicone matrix to the nitrile rubber.

For the adhesively attached window, the attachment to the flexible structure was achieved by a nitrile cement bond between the anchor flange and the flexible structure. For the mechanical attachment, it was developed by a pair of rigid metal rings contoured to the cylindrical curvature of the window and fastened together by a uniformly spaced array of bolts.

The processes involved in fabricating a window and its attachment are shown in figure 6. First, the fiberglass filaments are laid up in a predetermined pattern on a frame-mold tooling fixture and a nitrile flange is placed beneath the fiberglass reinforcement. The glass rovings are then coated with nitrile cement in the flange region. The top half of the nitrile flange is then placed over the fiberglass and the entire system including fixture is placed in a press and cured at 154° C for 1 hour at a pressure of 100 psi (689,000 N/m^2). After the system is removed from the press, the silicone matrix is slowly cast in the elliptical section of the window and allowed to cure at room temperature for 12 hours. The nitrile flange is then trimmed and the glass rovings cut from the frame. The fiberglass ends are then tied in knots and brush coated in place with a nitrile cement. The Mylar ring is placed in the areas where nonadhesion is desired (not shown) and the nitrile seal is bonded into place.

TEST RESULTS

Permeability

Since the flexible window will be used as a pressure retainer, the permeability of the composite materials is of interest. Permeability data for five silicone fiberglass reinforced panels and for unreinforced silicone and polyurethane are shown in table 7. The permeability of the nonreinforced silicone and fiberglass reinforced silicone panels is of the same magnitude, indicating that the reinforcement had negligible effect on permeability. Heat exposure (100° C for 7 days) it will be noted did not apparently affect the permeability of the two polymers. For comparative purposes, Mylar, one of the better low-permeability materials, has a permeability to pure helium of 0.0722 cc(STP)/cm^2-mm-day-atmosphere.[4] This is two orders of magnitude lower than the silicone. Even so, however, the silicone permeability would probably be tolerable for space window application. However, if the composite material were used for large sections of a spacecraft with a long-duration mission, a composite with lower permeability would be desirable. A reinforced window with a laminated matrix using constituent materials such as silicone and Mylar would probably reduce the permeability.

Attachment Study

The flexible window attached to a 3-feet- (1.02 m) square flexible fiberglass fabric using both adhesive and mechanical-type attachments was evaluated in the 4-foot- (1.02 m) diameter pressure chamber shown in figure 7. The flexible window withstood pressures up to 29 psi (200,000 N/m^2) using the adhesive attachment and up to 59 psi (406,000 N/m^2) using the mechanical clamp. All failures encountered were due to filaments "pulling out" of the nitrile flange, which resulted in breaking of the pressure seal and leakage. No reinforcement filament breakage was encountered and the strength of the silicone matrix to resist "blow out" between the reinforcement grid was concluded to be satisfactory for the test conditions considered.

Optical human factors tests were conducted on reinforcement pattern panels numbers 6, 9, and 13; previously described. The results of these tests are shown in table 6 for the panels pressure loaded at 7 psi (48,300 N/m^2).

Filament Wound Chamber

As a final test, conducted to evaluate the flexible window while focusing attention on more closely simulating the real structural application edge conditions, a flexible window was adhesively attached as an integral part of an 18-inch- (45.8 cm) diameter flexible fiberglass filament wound chamber. The chamber with an elliptical shaped, reinforced cut-out is shown in figure 8 along with an enlarged photograph of the window and flange.

The first flexible chamber and window constructed were pressurized to failure. Leakage developed at the window-flange interface at a pressure of 65 psi (448,000 N/m^2) which in an 18-inch- (45.8-cm) diamter cylinder is equivalent to a stress of 585 lb/in. (1025 N/cm) in the girth direction.

A folding test in which the window was bent to a radius of 1.5 inch (3.81 cm) is shown in figure 9. After 25 cycles of folding, the chamber was pressurized to 21 psi (145,000 N/m^2) without failure.

Figure 10 shows the flexible window and chamber while pressurized at 7 psi (48,300 N/m^2). The letters of the chart which reads "FLEXIBLE WINDOW STUDY" were 1 inch (2.54 cm) high and the chart was located inside the chamber approximately 18 inches (45.7 cm) from the window. The camera lens was located 5 feet (1.27 m) from the window. An internal light source was used to illuminate the test chart.

CONCLUDING REMARKS

The results of this investigation indicate that a flexible window is feasible for expandable structures application. A flexible window composed of a composite material of steel or fiberglass reinforcement embedded in a transparent silicone rubber matrix shows particular promise. Simulated space environment experiments conducted on flexible window elements have shown no serious degradation effects on the mechanical and optical properties of the composite,

and good optical resolution was observed under a 7-psi- (48,300 N/m^2) pressure differential. Existing systems for attaching the flexible window into an expandable structure are insufficient to develop the full structural capability of the composite window material and improved attachment concepts should be developed.

REFERENCES

1. Tynan, C. I.: Lunar Stay Time Extension Module. Selected Papers on Environmental and Attitude Control of Manned Spacecraft. NASA TM X-1325, Dec. 1966.

2. Williams, J. G.: Development of an Expandable Airlock Utilizing the Elastic Recovery Principle. Second Aerospace Expandable Structures Conference, Minneapolis, Minn., May 25-27, 1965.

3. Kohrn, R. C.; Kelsheimer, G. E.; Uhlig, E. C.; and LaBelle, B. S.: Feasibility Study for Development of a Flexible Reinforced Window. Uniroyal, NASA CR 66299, March 1967.

4. Rogers, C. E.: Permeability and Chemical Resistance. From book entitled "Engineering Design for Plastics," edited by Eric Baer. Reinhold Publishing Corp., 1964.

TABLE 1.- FLEXIBLE TRANSPARENT POLYMER PROPERTIES

	Strength, psi (N/m^2)						
	Transparency		100 percent elongation			Break	
	Heat exposure 7 days - 100° C	Ultraviolet exposure 10 days	Original	Heat exposure 7 days - 100° C	Ultraviolet exposure 10 days	Original	Vacuum exposure 254 days ~ 3×10^{-8} torr
Ethylene propylene copolymer	unsatisfactory	unsatisfactory	270 (1.86×10^6)		320 (2.21×10^6)	1390 (9.59×10^6)	
Polyisoprene	unsatisfactory	unsatisfactory	140 (9.65×10^5)				
Polyester urethane	darkened	slight crazing	570 (3.93×10^6)	605 (4.17×10^6)	700 (4.83×10^6)	5780 (3.99×10^7)	
Dimethyl RTV silicone	satisfactory	satisfactory	615 (4.24×10^6)	625 (4.31×10^6)	560 (3.86×10^6)	744 (5.12×10^6)	877 (6.05×10^6)

TABLE 2.- FLEXIBILITY DATA

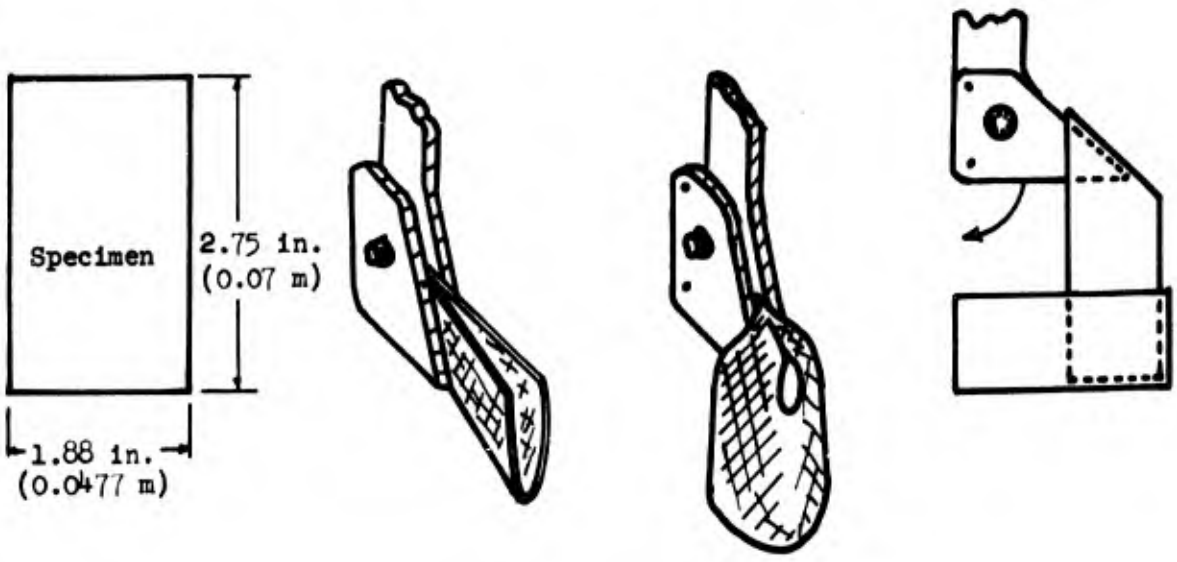

Unreinforced polymer	Thickness in. (cm)	Number of flex cycles
Polyester urethane	0.073 (0.185)	349,000 - test terminated
Dimethyl RTV silicone	0.066 (0.168)	349,000 - test terminated

TABLE 3.- REINFORCEMENT MATERIAL STRENGTH

Reinforcement material, (finish and type glass)	Ultimate tensile strength, lb/end (N/end)	
	Original	Heat exposure, 7 days ~ 100° C
Glass[1] (901-S)	5.3 (23.6)	5.5 (24.5)
Glass (1014-S)	4.9 (21.8)	5.3 (23.6)
Glass (1026-E)	3.1 (13.8)	2.9 (12.9)
Glass (801-E)	3.0 (13.3)	3.4 (15.1)
Glass (902-E)	2.9 (12.9)	3.9 (17.4)
Glass (810-E)	2.3 (10.3)	2.5 (11.1)
Glass (711-E)	2.2 (9.8)	2.5 (11.1)
Glass (1033-E)	1.3 (5.8)	0.7 (3.1)
Polyester[2]	6.9 (30.7)	--
Steel[3]	6.3 (28.0)	--

(1) All glass filaments were G size (0.00038-inch (0.00097 cm) diameter).
(2) 0.010-inch (0.0254 cm) diameter filament.
(3) 0.004-inch (0.0102 cm) diameter wire.

TABLE 4.- REINFORCEMENT PATTERN PROPERTIES

Panel No.	Matrix	Reinforcement	No. of groups of filaments per in. (No. per 2.54 cm)		No. of ends per group		No. of ends per in. (No. per 2.54 cm)		Thickness, in. (m)	Weight, lb/ft^2 (N/m^2)
			Girth	Axial	Girth	Axial	Girth	Axial		
1	Silicone	S-glass*	4	4	40	20	160	80	0.151	0.92
2	Silicone	S-glass	2	2	80	40	160	80	0.181	1.14
3	Silicone	S-glass	2 14	2 6	60 1	40 2	134	92	0.194	1.24
4	Silicone	S-glass	4 4	4 4	20 8	10 4	112	56	0.160	0.92
5	Silicone	S-glass	2 2	2 2	60 8	40 4	136	88	0.171	1.02
6	Silicone	S-glass	4 4	4 4	27 8	14 4	140	72		
7	Silicone	S-glass	16	16	9	5	144	80		
8	Silicone	S-glass	4 4	4 4	15 6	8 3	84	44		
9	Silicone	S-glass	16	16	6	3	96	48		
10	Polyurethane	S-glass	2 14	2 6	65 1	32 1	144	70		
11	Silicone	S-glass	2 14	2 6	65 1	32 1	144	70		
12	Silicone	S-glass	2 6	2 4	40 1	20 1	86	44		
13	Silicone	Steel**	2 2	2 2	60 8	40 4	136	88		
14	Silicone	S-glass	2	2	80	40	160	80		
15	Polyurethane	S-glass	4	4	35	18	140	72		

*S-901 glass filaments.
**0.004-in. (.01 cm) diameter steel wire.

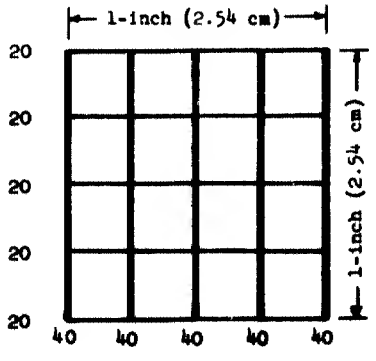

Pattern Number 1

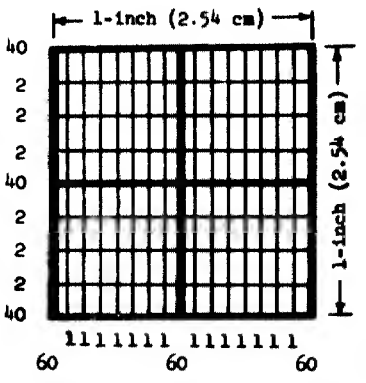

Pattern Number 3

TABLE 5.- HUMAN FACTORS OPTICAL TEST RATING

A. Blurriness (distortion)

1. No distortion

3. Blurred but still comfortable

5. Highly distorted, uncomfortable

B. Ability to Focus

1. Eyes focus immediately

3. Strands change focus but still comfortable

5. Strands interfere with focusing

C. Readability

1. Reading clear - minimum of magnification disturbance

3. Letters change magnification but still comfortable

5. Reading moves with eye movement (high degree of magnification change)

TABLE 6.- HUMAN FACTORS WINDOW EVALUATION

	Human factors optical test (pressurized 7 psi (46,300 N/m^2))			
Panel No.	Blurriness	Ability to focus	Readability	Smallest legible print size, in. (points)
1	3.0	3.5	3.5	0.30 (14)
2	3.7	4.0	3.8	0.156 (11)
3	3.2	3.0	3.6	0.156 (11)
4	2.0	2.0	2.0	0.0937 (6)
5	3.1	3.2	3.4	0.30 (14)
6	3.0	3.0	3.0	0.156 (11)
9	2.5	2.5	2.5	0.156 (11)
13	2.5	2.5	2.5	0.0937 (6)

TABLE 7 .- PERMEABILITY DATA

Sample[1]	Permeability[2] cc(STP)/cm^2-mm-day-atmosphere	
	Original	Heat exposure, 7 days ~ 100° C
Dimethyl RTV silicone, unreinforced	10.7	10.4
Polyester urethane, unreinforced	0.23	0.29
Panel 1	6.4	
Panel 2	6.7	
Panel 3	14.2	
Panel 4	10.7	
Panel 5	4.5	

(1) For description of reinforced panels see table 4.
(2) Gas composed of 95 percent helium, 5 percent oxygen.

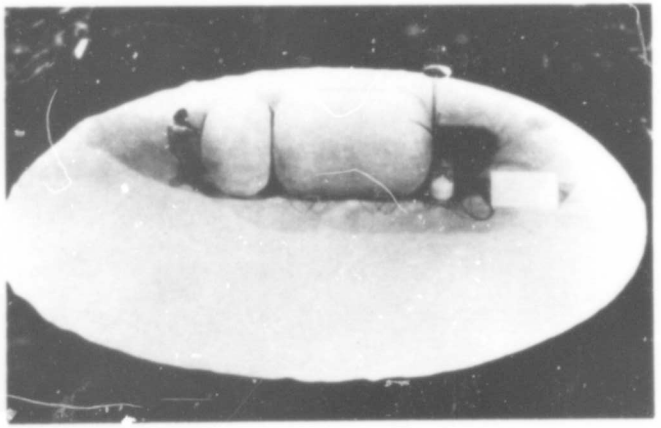

Lunar Shelter

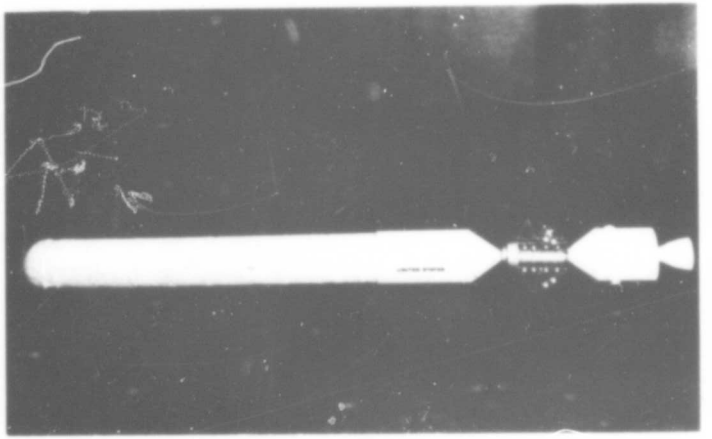

Expandable Experiment Mocule

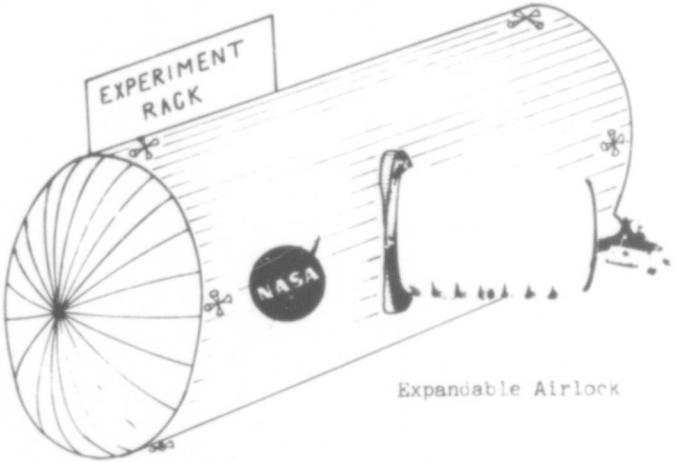

Expandable Airlock

Figure 1.- Expandable structures application for flexible window.

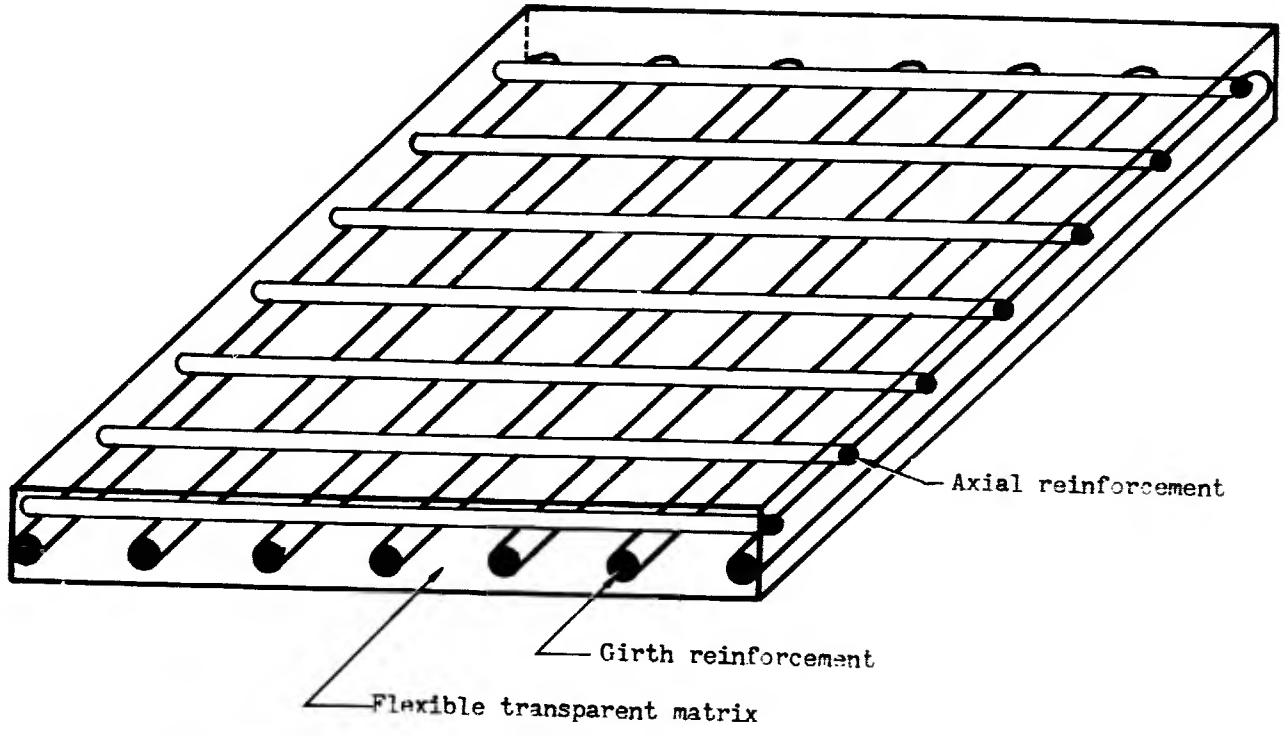

Figure 2.- Flexible window model.

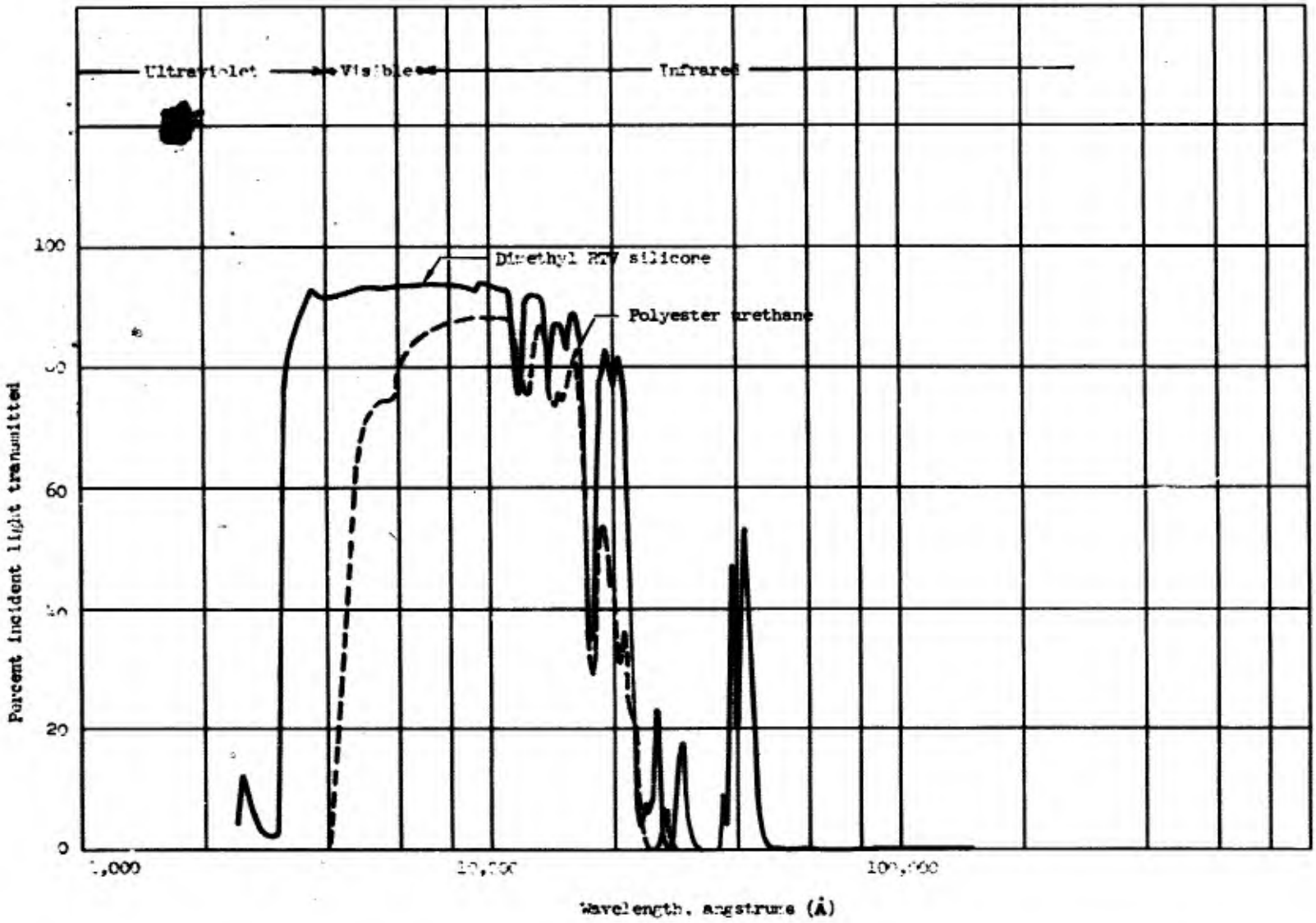

Figure 3.- Percent incident light transmission versus wavelength for polymeric specimen.

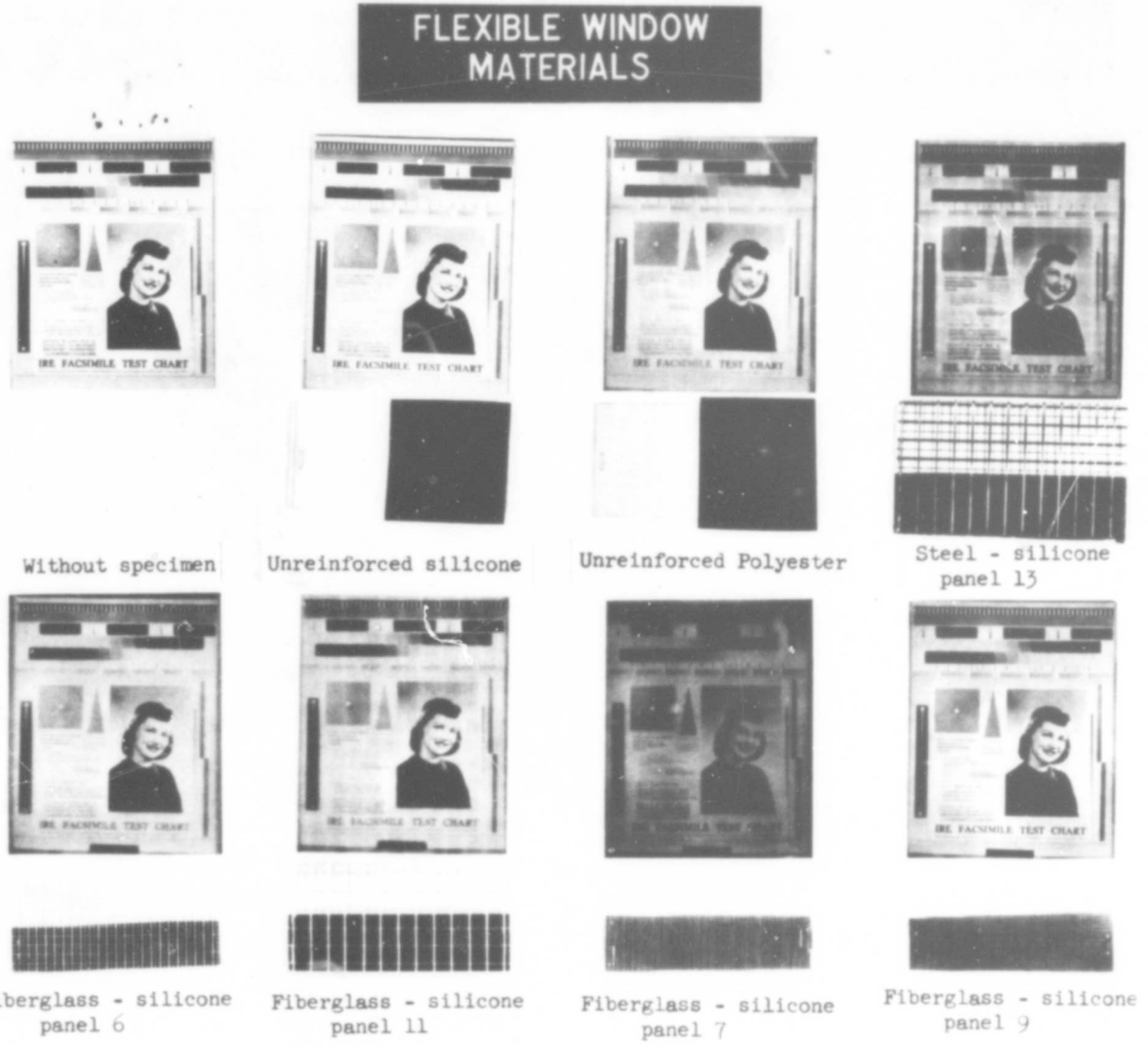

Figure 4.- Photographic test of materials and reinforcement patterns.

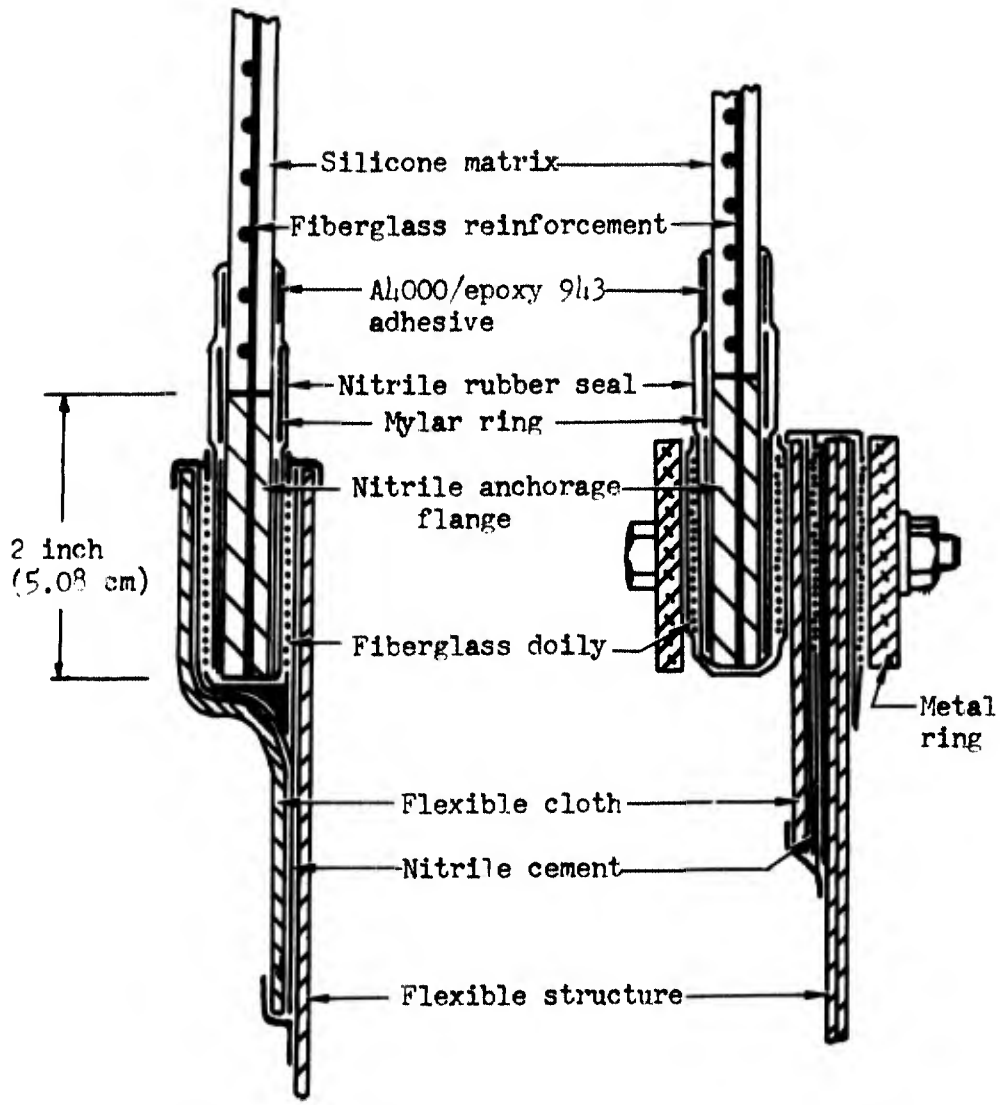

Figure 5.- Window attachment designs.

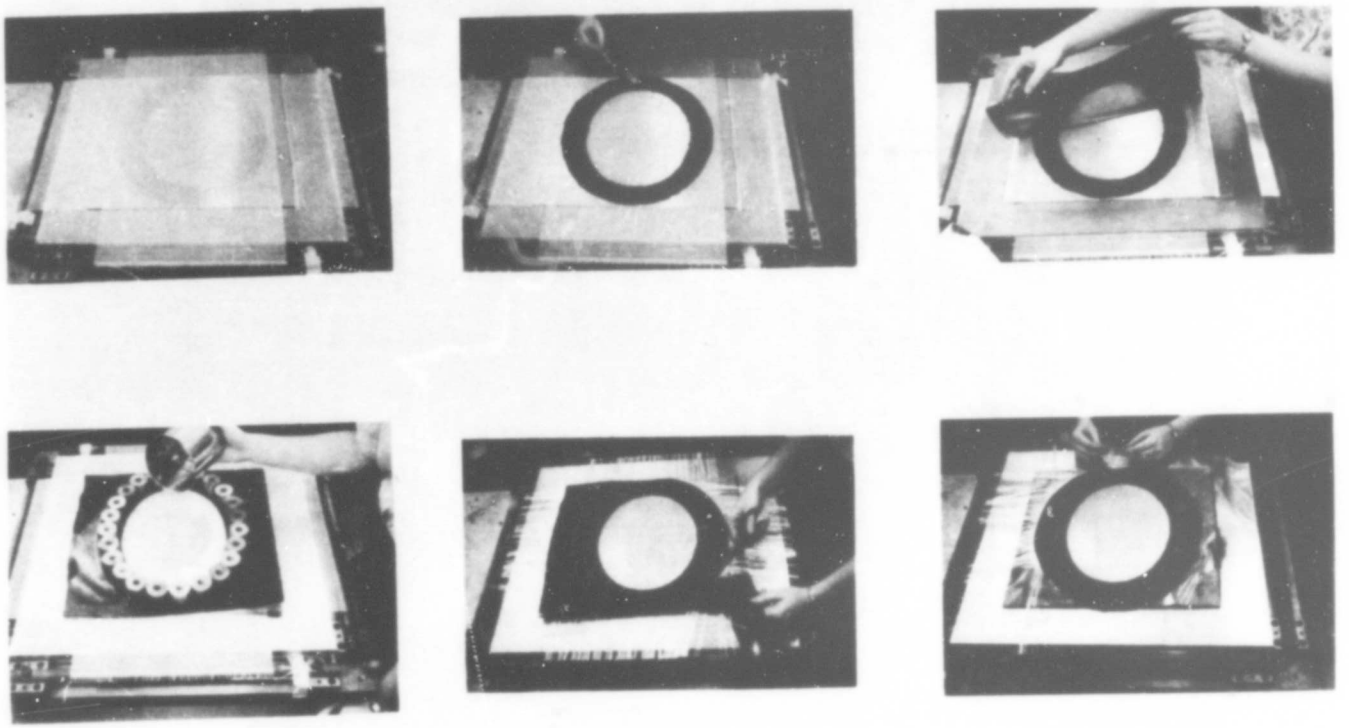

Figure 6.- Photographs showing fabrication techniques for making window.

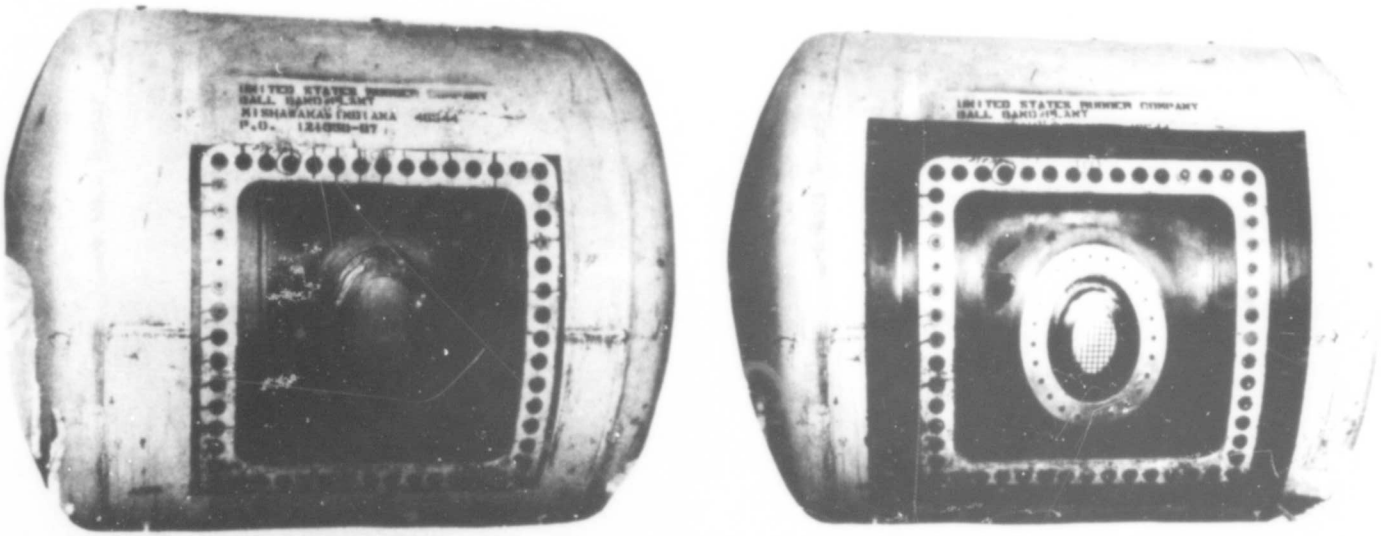

Adhesive attachment

Mechanical attachment

Figure 7.- Four-foot- (1.22 m) diameter test fixture with adhesive and mechanical window attachments.

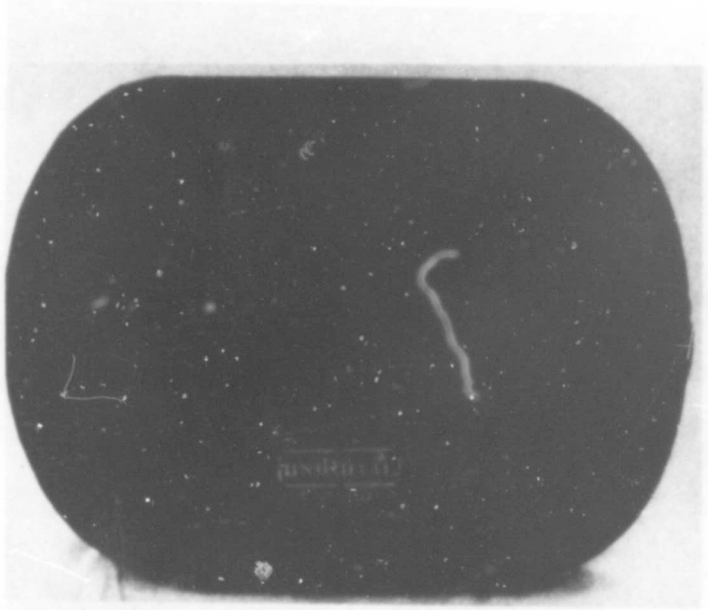

Flexible pressure vessel with reinforced opening

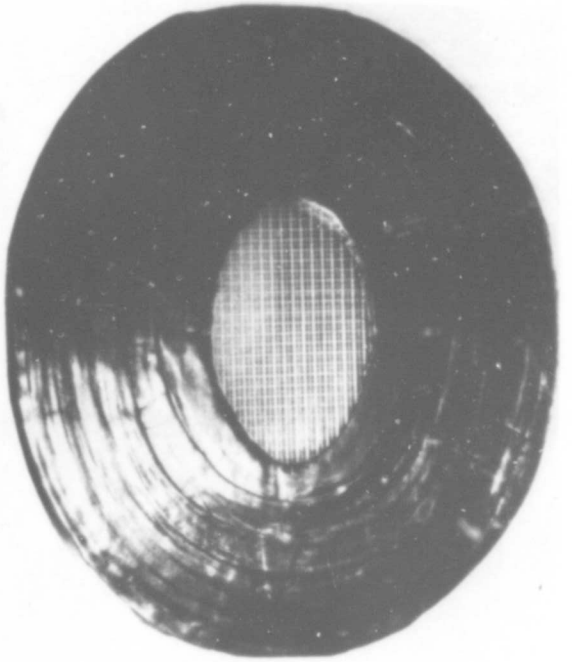

Flexible window

Figure 8.- Flexible filament wound pressure vessel and window.

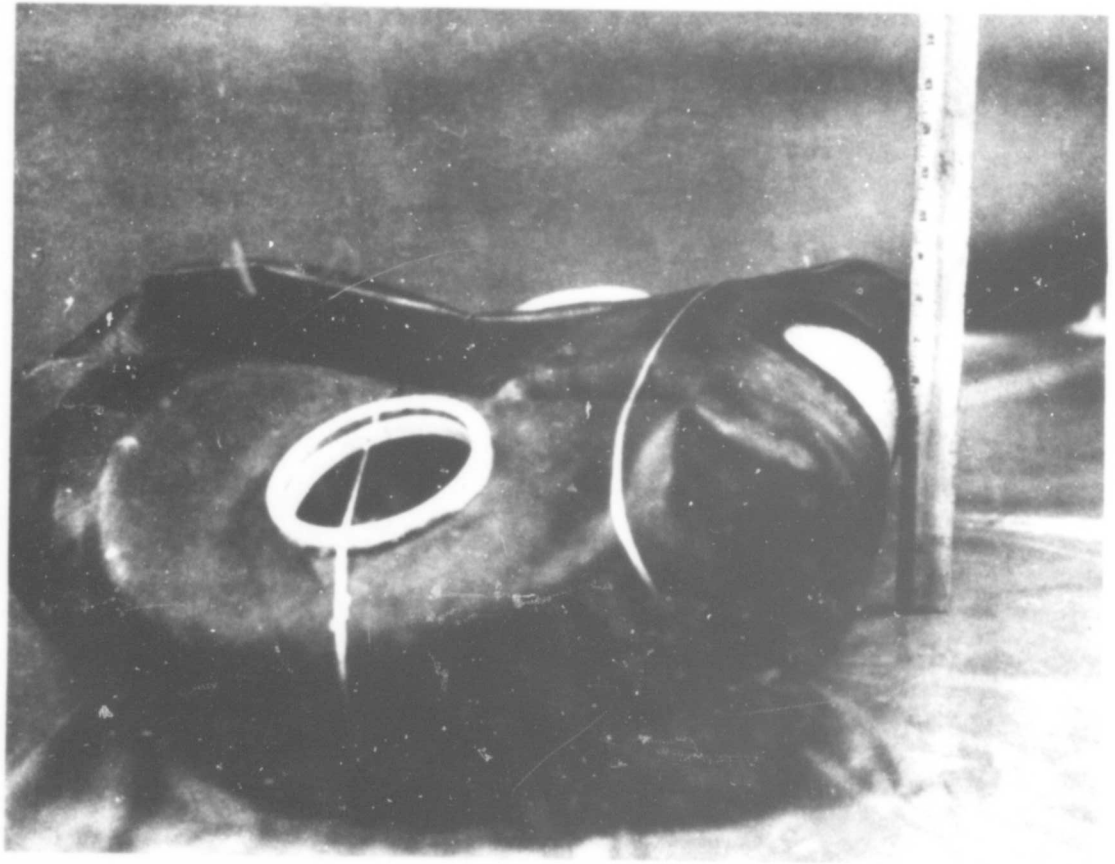

Figure 9.- Window folding demonstration.

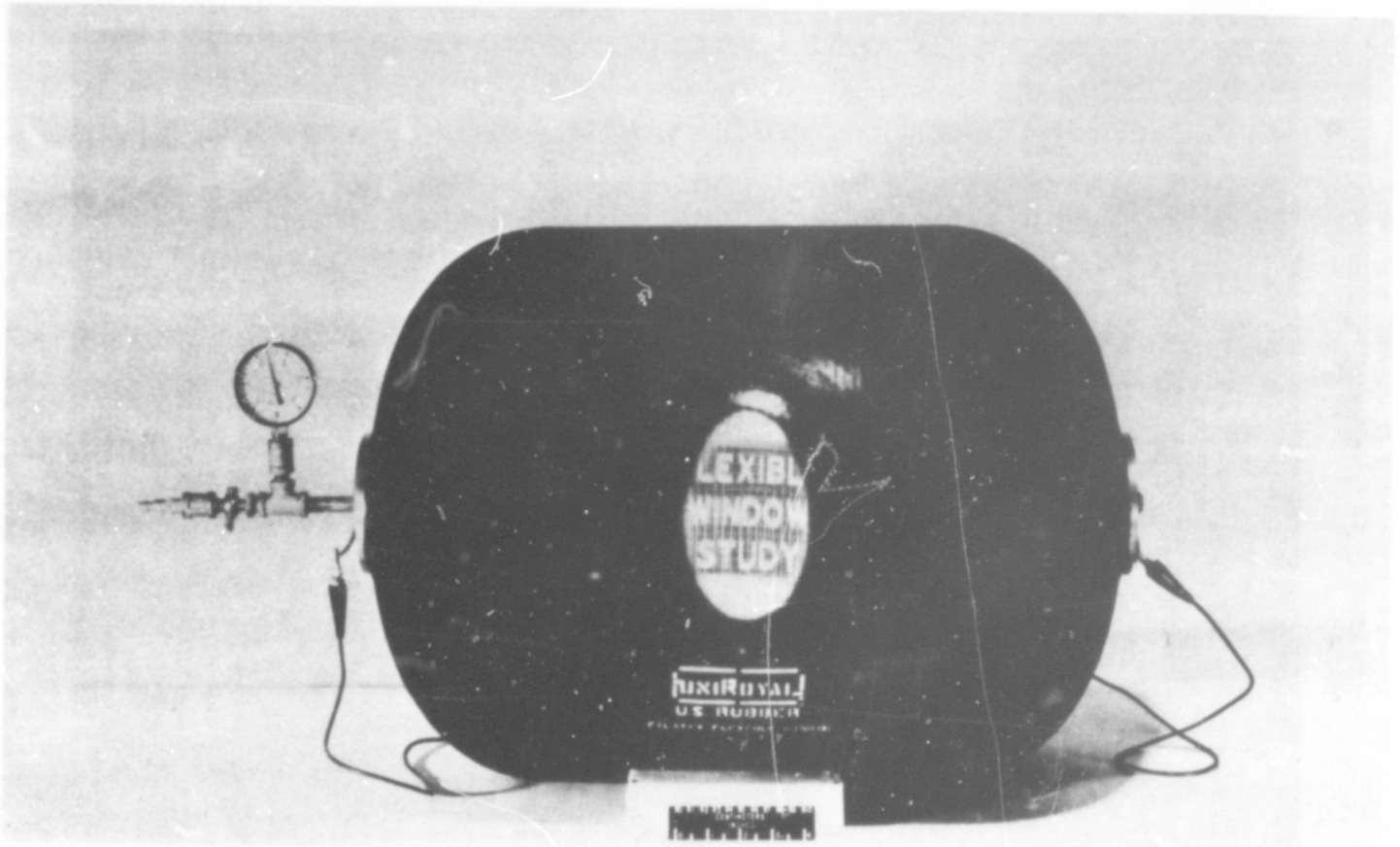

Figure 10.- Flexible window in flexible pressure vessel pressurized at 7 psi (48,300 N/m^2).

GAS-CURED URETHANE RESIN SYSTEMS FOR SPACE STRUCTURES

W. McKillip,* J. Lee,* and R. French**

INTRODUCTION

In recent years, several Air Force-sponsored programs have been conducted to develop a material system that can be used to rigidize packageable, expandable structures after deployment in space. One of the most prominent of these materials is an Archer Daniels Midland Company (ADM) developme · It is a urethane resin that is rigidized by its exposure to a small amount of water vapor.

As a subcontractor on ADM development Contract AF33(615)-2435, Goodyear Aerospace Corporation recently completed a program in which techniques were investigated for applying this material to space-type structures; namely, 10-ft diameter parabolic solar collectors and four-foot diameter by eight-foot long cylinders. This paper summarizes Goodyear Aerospace work on this program and emphasizes the work on the solar collectors, since this task was the most difficult.

PREPROTOTYPE MATERIAL APPLICATION DEVELOPMENT

The chart below shows the significant properties of the Vaporset rigidizing resin refined as part of this program by ADM and used for the models described.

Raw Material Properties

1. Supplied at 60 percent (weight) solids in ethyl acetate
2. Viscosity is 50 centipoise
3. Solution contains 10 percent reactive sites (NCO)
4. For curing, 0.0214 lb of water per pound of solution

*Archer Daniels Midland Company, Minneapolis, Minn.

**Astronautics Design Department, Goodyear Aerospace Corporation, Akron, Ohio

5. Shelf life of solution is more than one year

Application Properties

1. Formulated for vacuum impregnation
2. Nitrogen drying to 95 percent of solids prepared for rapid cure
3. Impregnated fabric samples give shelf life of more than one month
4. Cure rate: three-ply 181 glass laminate 0.040-in. thick, 50 percent ultimate strength in two hours with 20-mm Hg water vapor pressure
5. Cure rate is proportional to water vapor pressure

Cured Properties

1. Ultimate flexural strength equals 50,000 to 60,000 psi
2. Flexural modulus equals 1.8 to 2 × 10^6 for three-ply 181 glass laminate
3. Stability in near earth, ultraviolet, infrared, and gamma radiation environment is more than 700 hr

Figure 1 shows the concept on which the early development effort was

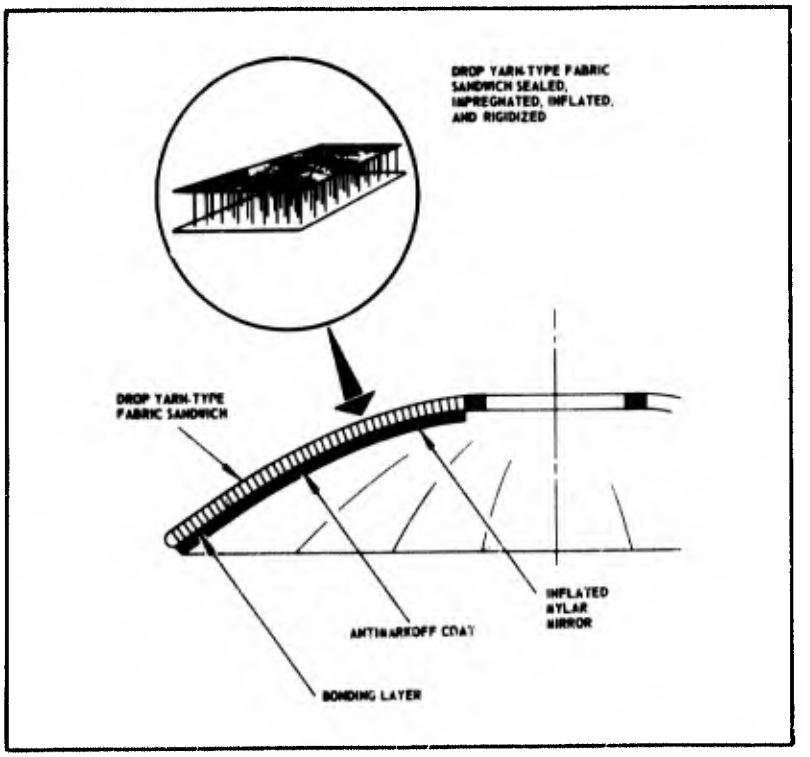

Figure 1 - Drop Yarn-Type Fabric Sandwich

based. The main elements of this composite structure are (1) the mirror (made of thin metallized film), (2) an antimarkoff coat on the back side of the film to prevent show-through of adjacent material texture, (3) a sealed fabric sandwich structure (Dacron AIRMAT*), and (4) a bonding layer for joining the two subassemblies. Figure 1 also shows the construction of the fabric sandwich material, which is essentially two layers of cloth integrally joined by drop yarns extending from one surface to the other.

Prior to folding and packaging, this fabric is vacuum impregnated with the rigidizing resin. After deployment by inflation in space, this resin is reacted by a small amount of water vapor. A rigid structure is achieved.

PROBLEM AREAS

To make such a concept feasible, several interrelated problems had to be solved:

1. Contour accuracy
2. Sealing of AIRMAT structure
3. Mirror surface quality
4. Bonding layer
5. Packaging

CONTOUR ACCURACY

The sandwich structure, when inflated, must hold the mirror surface to an accurate parabolic contour. This depends on the accuracy of the sandwich structure itself and its ability to hold the mirror film. When in its proper shape, the film is stressed to approximately four pounds per inch. The sandwich material initially is flat. Contour is achieved by trimming the AIRMAT into pie-shaped gores. The developed shape of each side is different; each approximates a paraboloid, with one side larger than the other. Care must be exercised to obtain a configuration that when inflated has the drop yarns oriented as nearly as possible normal to the contoured surface. Figure 2 shows a sandwich structure constructed in this manner. Using the techniques developed, a 10-ft diameter parabolic structure can be fabricated to $\pm 1/2$ in. In the future, this task will be optimized through the combined techniques of heat forming and procuring AIRMAT woven with a specified curvature. This work is being done by Goodyear Aerospace under Contract AF33(615)-3874 and is summarized in another paper at this symposium, "Development of Compound Curvature AIRMAT" by J. T. Harris.

SEALING OF AIRMAT STRUCTURE

The sandwich structure must be sealed to permit inflation to contour. This seal also is needed in vacuum impregnation. The problem of sealing the fabric material can be solved by (1) application of a film seal by laminating or

*TM, Goodyear Aerospace Corporation, Akron, Ohio.

(2) application of a coating. The film technique was chosen because it is inherently lighter and the fabric is not saturated with the sealant and therefore is capable of later absorbing more rigidizing resin. A 1/2-mil Mylar film barrier was used in early specimens. Later, 0.4-mil nylon was used. In addition, VITEL* PE-207, Goodyear polyester, was used as the adhesive. Lamination was achieved by using vacuum bagging techniques and oven cure. The resulting composite is not affected by prolonged exposure to the resin solution, which contains ethyl acetate solvent. Lamination is done before trimming the sandwich fabric into pie-shaped gores for joining into the three-dimensional curved shape. Film fabric tape is used to join the gores and seal the edges. The tape is applied using the same thermosetting adhesive and is cured with a hot iron.

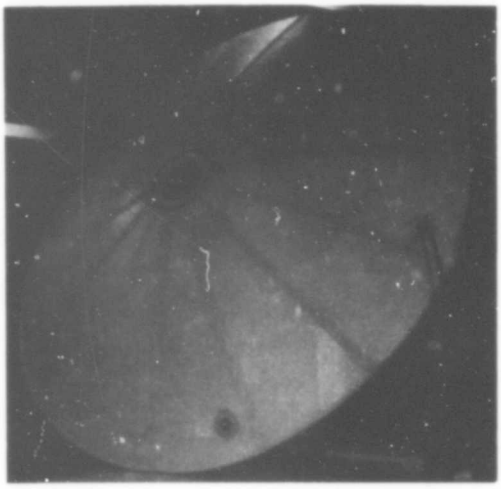

Figure 2 - Inflated Parabolic AIRMAT Structure

MIRROR SURFACE QUALITY

A coating was sought for the back side of the metallized film that would (1) minimize permanent degradation resulting from folding and packaging, (2) prevent any show-through on the mirror surface of adjacent textured materials, and (3) help capture the parabolic shape of the mirror, obtained by inflating the Mylar film.

The best back-side coating was 8 to 10 mils of urethane elastomer applied by spraying. This improved (but did not eliminate) folding degradation and eliminated show-through of adjacent material texture. The coating's ability to hold the Mylar film in its parabolic contour was insignificant; thus, the structure had to hold the film in its contour, and all loads were transmitted through the bonding layer.

BONDING LAYER

The bonding layer has to satisfy several rather difficult requirements: (1) it has to be soft enough to permit packaging, (2) it has to transmit uniformly sufficient load from the deployed sandwich structure to the coated film to stretch the film to the desired contour, and (3) the tolerance of fabrication of the sandwich structure has to be compensated for by varying the thickness of the bonding layer.

A flexible foam system would be most appropriate. This system was investigated and was used on several five-foot diameter models. A flexible

*TM, The Goodyear Tire & Rubber Company, Akron, Ohio.

urethane foam was used. This material was applied by pouring, and the reaction time was slow enough to permit installation of the inflated sandwich assembly after applying the foam. A layer of very open cell foam (1/4-in. thick) was bonded to the concave side of the sandwich assembly before placing in position over freshly poured foam. This layer served as a bleeder to prevent air entrapment and helped take up difference in gap between structure and inflated assembly due to tolerance by allowing the fresh foam to flow into the open cell layer.

Figures 3 and 4 dipict the level of development at this stage; Figure 3 also shows mirror surface quality. Figure 4 shows the variation of flexible foam thickness and penetration of the flexible poured foam into the open cell layer.

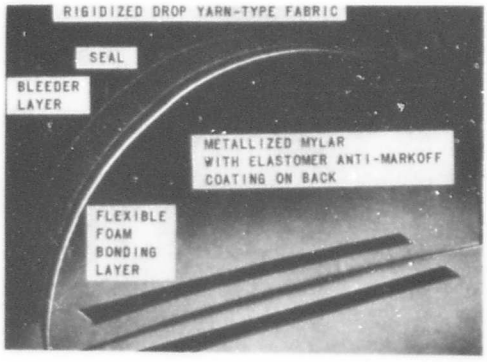

Figure 3 - Composite Mirror Specimen

Figure 4 - Composite Mirror Specimen (Cross-Section View)

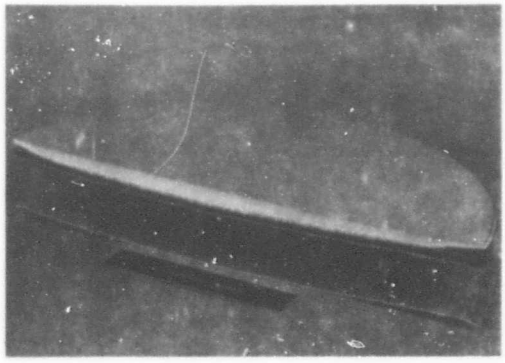

Despite the significant advances derived from the above-described effort, it was questionable whether the structure contour could be controlled well enough to permit using a foam bonding layer of reasonable thickness without costly tooling effort. In addition, packaging of the structure still promised significant degradation of the mirror surface.

PACKAGING STUDIES

While the preceding work was being carried out, some concentrated effort was expended toward solving the packaging problem. In carrying out this study, a somewhat different design philosophy was developed. If a mirror is to be folded, the fold pattern first must be determined. As soon as the fold locations are defined, stiffer materials can be used between the folds. The propagation of folding wrinkles from the fold lines is thereby virtually eliminated.

This philosophy led to the development of a fold pattern that was used on all remaining mirrors made on this contract. This pattern, in effect, permits the folding of the outer portion of the mirror inward toward the hub by first taking tucks in the outer portion. Secondary tucks then are taken in the already folded assembly so the entire unit can be brought up into a cylindrical shape, which is slightly larger than the hub in diameter and has a length approximately equal to one-half the mirror radius.

Figure 5 shows a five-foot diameter model constructed to evaluate this concept. This mirror was built by first making a conventional five-foot diameter inflated Mylar layup and applying approximately 0.020 in. of epoxy to the back. This was followed by a heavy layer of fabric, which simulated the folding characteristics of the AIRMAT planned for structural material. The mirror then was cut at the fold lines, the cuts extending through the Mylar and epoxy shell; thus, the fabric could act as a hinge for packaging.

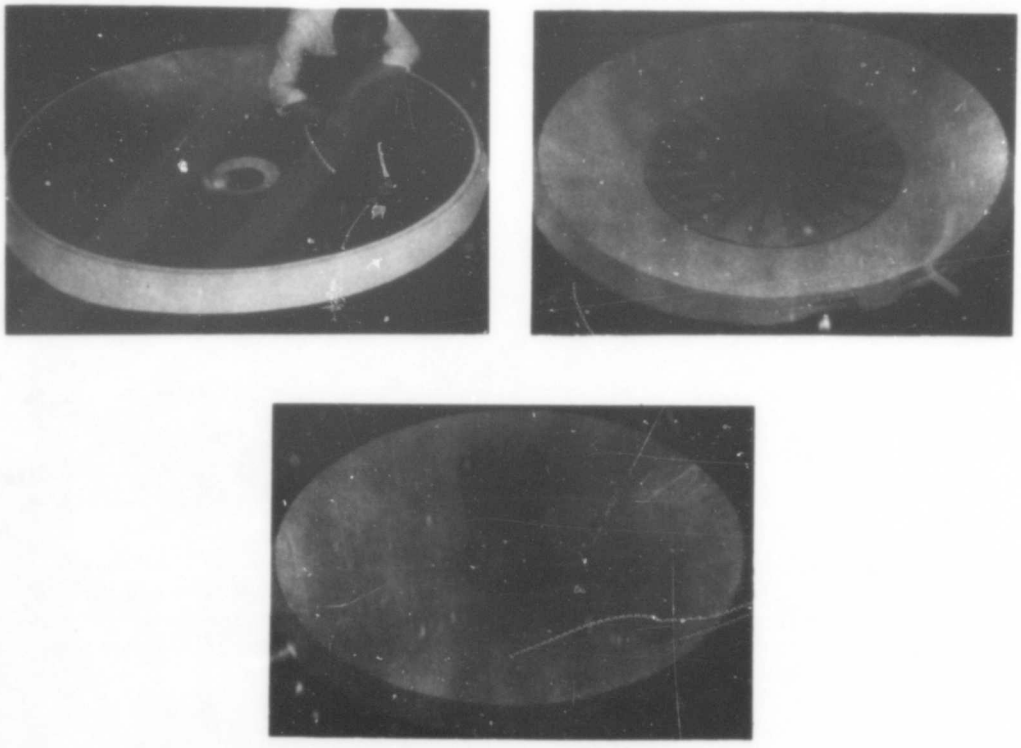

Figure 5 - Folding Study of Five-Foot Diameter Mirror Specimen

NEW DESIGN CONCEPT

The new design philosophy that emerged was based on the following factors:

1. Make an inflated film mirror (see Figure 6) in the

conventional manner. While inflated, apply a shell coating to the back side stiff enough that when the coating is cut into segments the individual pieces will retain the shape of the inflated shell. Add a fabric layer to act ultimately as a hinge after the shell is cut at the fold lines.

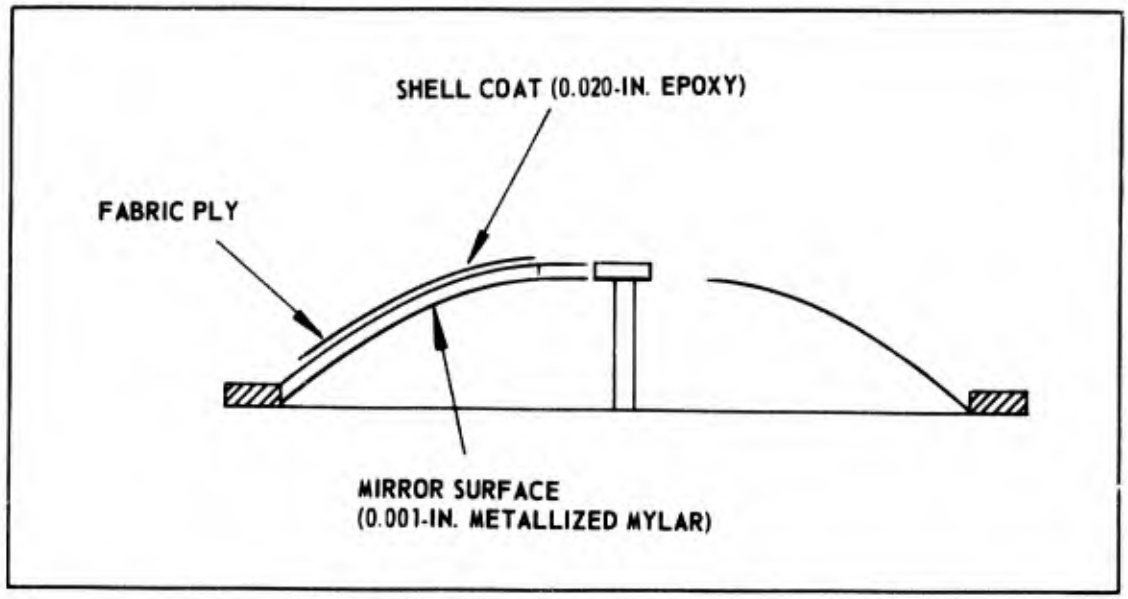

Figure 6 - Inflated Film Mirror

2. Make an AIRMAT sandwich structure as previously used; however cut the gores on the bias (see Figure 7) and seal with 0.4-mil nylon film. The combination of thin, low-modulus film and bias cutting will make the assembled structure somewhat soft. It then can be easily made to conform to the shape of the inflated assembly.

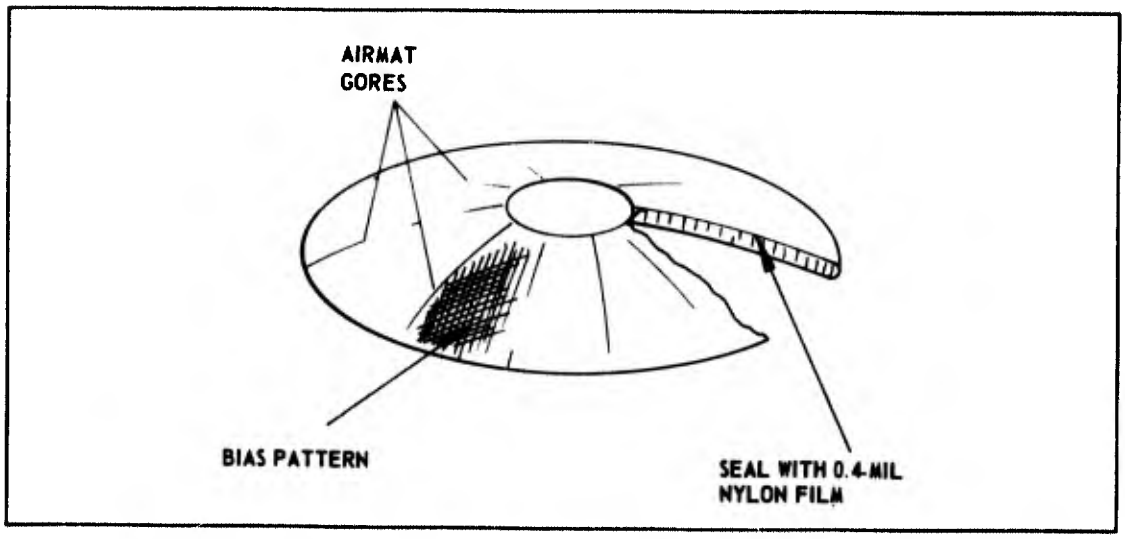

Figure 7 - AIRMAT Sandwich Structure with Bias-Cut Gores and 0.4 Mil Nylon Film

3. Inflate the AIRMAT assembly and bond to the inflated mirror assembly (see Figure 8).

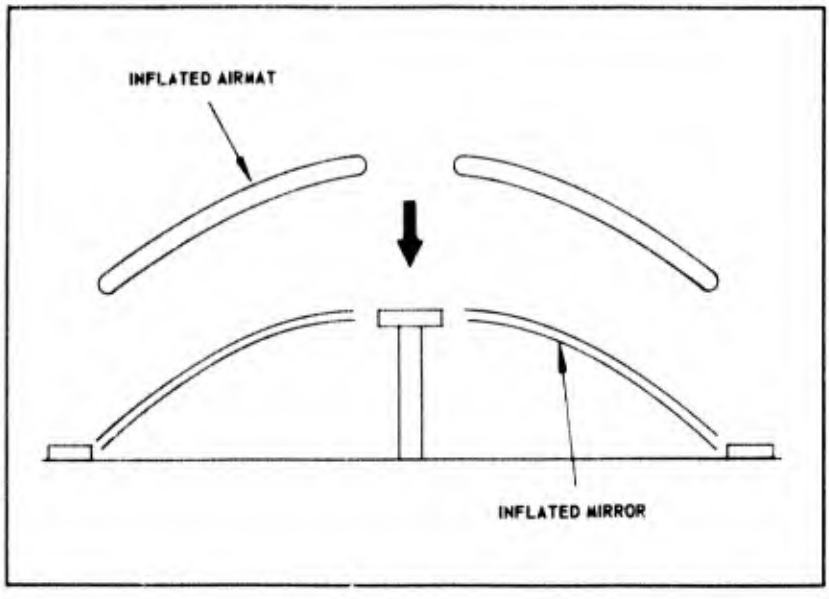

Figure 8 - Bonding AIRMAT Assembly to Inflated Mirror

4. While the structure is still inflated, apply a back ply of fabric (see Figure 9). Orient this fabric so the yarns are radial and circumferential.

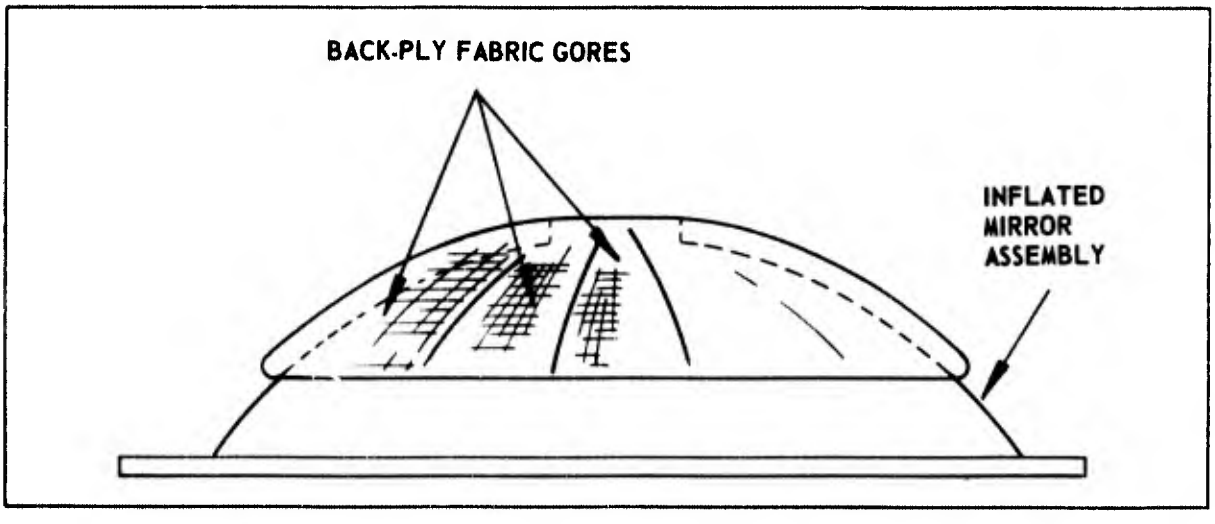

Figure 9 - Inflated Mirror with Back Ply of Fabric

The resulting structure is a sandwich of which the contour is primarily controlled by the shell coat on the back of the film and the back ply of fabric. Both structural layers are applied while the proper contour is held.

5. Invert and cut through the Mylar and shell coat to permit folding. Model is now ready for folding.

FABRICATION AND TESTING OF 10-FT DIAMETER MIRROR

The next program phase involved 10-ft diameter mirrors. The system used closely followed the concept derived from the early screening effort.

Inflated Film Subassembly - Figure 10 shows the layup, which was comprised of 60 one-mil Mylar gores. Inflation to proper contour was achieved with an internal pressure of two inches of water. This was followed by spraying on a urethane primer coat. Next, two coats of epoxy were applied by pouring. A good reflective surface was achieved, although not so uniform as that which could be obtained by spraying. The material used was a mixture of three parts DER 332 to two parts Versamid 140. Two coats were applied, which resulted in a total thickness of approximately 0.025 in. The epoxy coats were followed by a urethane coat (applied by spraying). This material was elastomeric urethane with an amine curing agent.

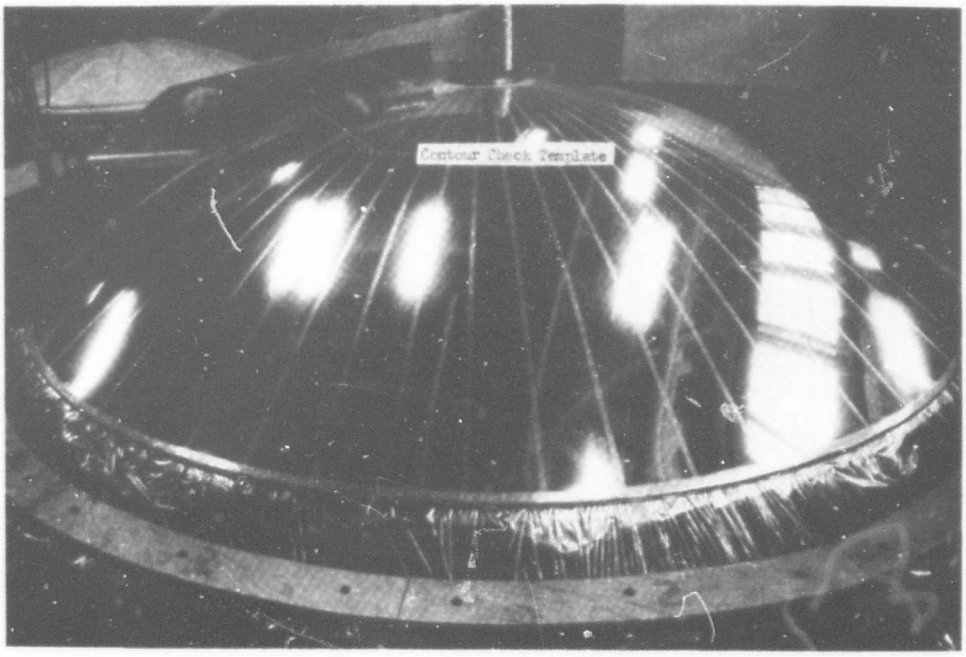

Figure 10 - Inflated 10-Ft Diameter Mirror Layup

The shell coat was followed by application of a Dacron cloth layer (8.9 oz/sq yd). This cloth was applied in eight gores and was bonded using the urethane described above. The urethane again was applied by spraying. Figure 11 shows the inflated Mylar with the shell coat applied and in the process of having this cloth applied.

AIRMAT Subassembly - The AIRMAT used was Dacron and was made to the specifications given in Table 1.

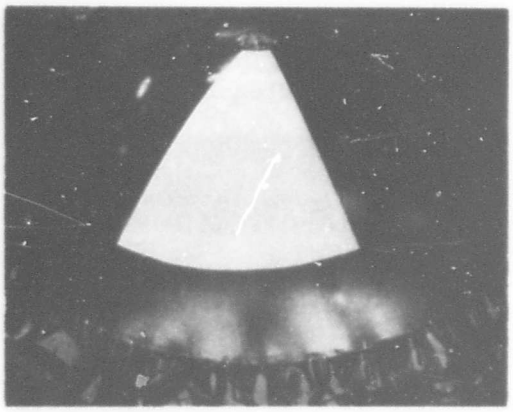

Figure 11 - Inflated Mirror Shell with Dacron Buffer Fabric Being Applied

TABLE 1 - AIRMAT SPECIFICATIONS

Item	Specification
Thickness	1.8 in.
Width	60 in.
Warp material	220 denier, Type 52 Dacron, 84 ends per inch, 7 turns, heat stabilized for minimum shrinkage at 275 F
Fill material	440 denier, Type 52 Dacron, 40 ends per inch, 3-1/2 turns, heat stabilized for minimum shrinkage at 275 F
Drop threads	1100 denier, Type 52 Dacron, 1/2 to 3/4 turn, drop-thread count 4 wide × 5 long (35 sq in.) in plain weave arrangement, heat stabilized for minimum shrinkage at 325 F

The above fabric was sealed with 0.4-mil nylon film by vacuum bag laminating and oven cure. The gores were pretrimmed to the proper developed pattern (see Figure 12). The outer edge seal then was made on the individual gores. The next step was to assemble 15 of these gores into a complete three-dimensional parabolic shape (see Figure 13). The assembly then was attached to the hub ring and the entire structure unit placed on the inflated Mylar envelope to check conformity of shape to the Mylar assembly.

A primer coat of urethane then was applied to both sides of the AIRMAT assembly and to the inflated mirror assembly. Using the same material, the two subassemblies were joined (see Figure 14). The back ply of Dacron fabric (8.9 oz/sq yd) was bonded to the back side in gores, with the warp and fill yarns oriented radially and tangentially. At this time, the basic shape was established and was the same when the Mylar film was first inflated.

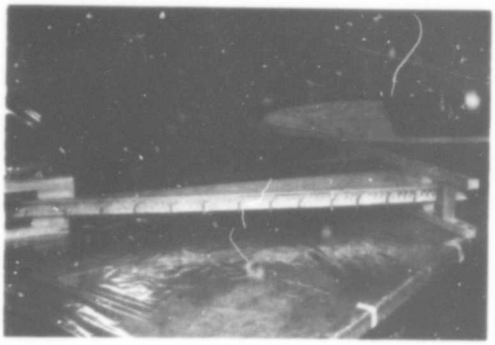

Figure 12 - Pretrim of AIRMAT Gores

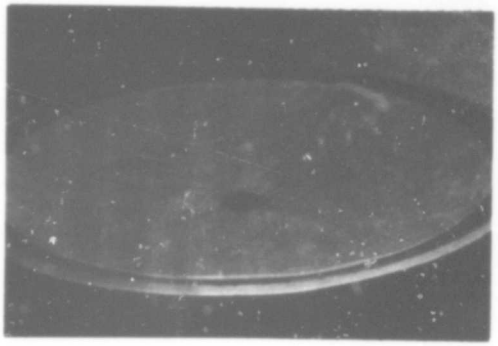

Figure 13 - Preassembly of AIRMAT Structure

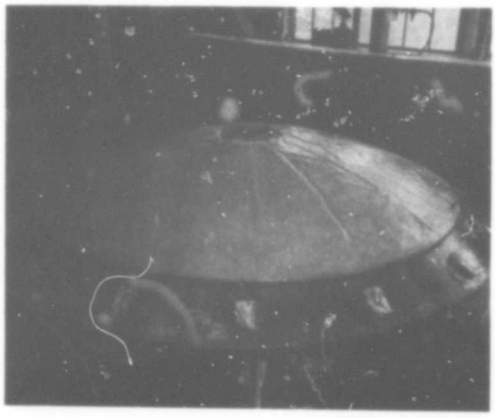

Figure 14 - Inflated Mirror After AIRMAT Attachment

Next, the mirror was suspended (see Figure 15) and a strippable protective coating applied to the mirror surface. The mirror surface then was cut at each fold line. The cuts extended to the buffer ply of fabric. These cuts were wide enough to permit folding without severe strain on the sandwich structure and to minimize peeling effect between the shell coat and the buffer ply. Figure 16 shows the mirror after cutting. The mirror was supported at the hub only; the shape was maintained by the pressure in the sandwich structure.

The next step was to fold the mirror in its packaged condition. Figures 17 and 18 show the unit as the folding operation progressed. Figure 19 is a different view of the mirror after the folding was completed.

After folding, the mirror was returned to its open position, after which the inflation/rigidizing system was installed. The rigidizing gas inlet was manifolded inside the hub. The six gas outlet ports were spaced equally on the back of the AIRMAT near the periphery. The flexible lines were attached

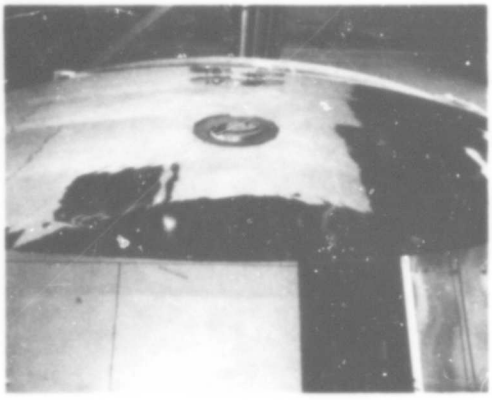

Figure 15 - Inflated Mirror Suspended at Hub Before Folding Cuts

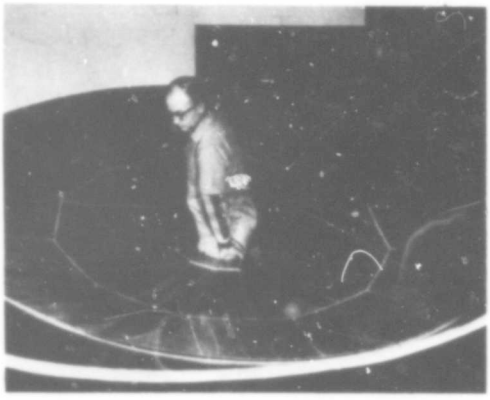

Figure 16 - Inflated Mirror Supported at Hub After Folding Cuts

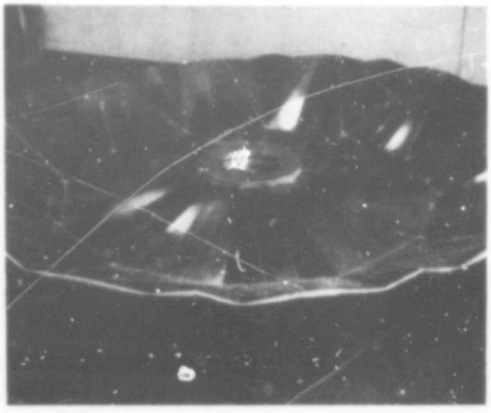

Figure 17 - Deflated Mirror (Folding Started)

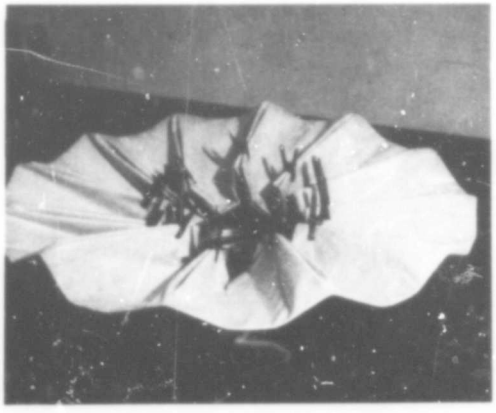

Figure 18 - Deflated Mirror (Partially Folded)

radially to the back side of the AIRMAT and also brought together inside the hub (see Figure 20). The mirror was refolded and shipped to Wright-Patterson AFB, Dayton, Ohio.

Testing - Deployment was first demonstrated in ambient conditions before impregnating. The mirror was placed over a male tool and impregnated (see Figure 21).

The resin (8000 gm) was introduced at the six ports near the periphery. The ports were closed and, using a vacuum pump attached to the one-inch inlet port at the hub, the specimen was evacuated. This moved the resin from

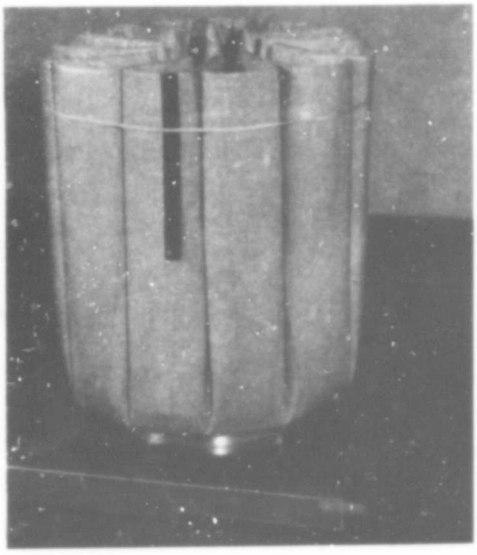

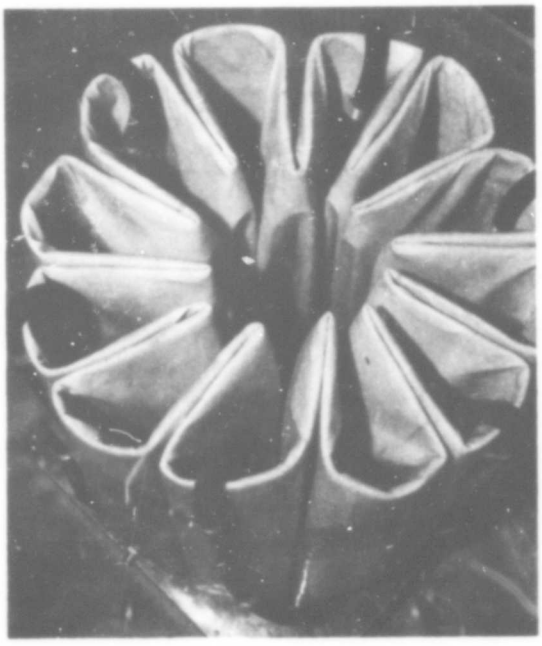

Figure 19 (Above) - Folded Mirror (Side View); Figure 20 (Right) - Ten-Foot Diameter Mirror Ready for Vacuum Chamber Deployment

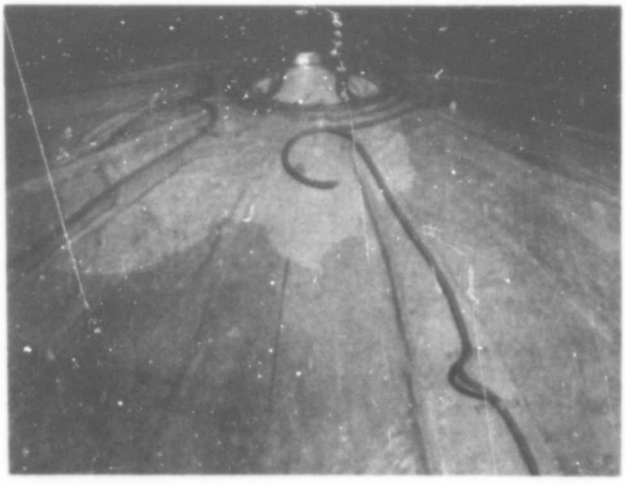

Figure 21 - Ten-Foot Diameter Mirror During Impregnation

the periphery to the hub. This flow was helped by using Teflon paddles to force the movement in the proper direction.

Immediately following impregnation, the mirror was folded, the hot wire cut off, and the Mylar sleeve put in position. The mirror was placed in the vacuum chamber, and all connections were made to permit deployment, solvent boiloff, and rigidization in the vacuum chamber.

The initial phase of pumpdown was achieved in one hour. During this period, the chamber pressure was dropped from atmospheric to 100-mm Hg absolute pressure. By use of auxiliary pumps attached to the specimen through the outlet ports, the absolute pressure within the specimen was kept 25 mm lower than the chamber pressure.

When 100-mm chamber pressure was obtained, the specimen internal pressure was raised to a positive differential of 5.7 mm Hg. Using the hot wire cutoff of the Mylar sleeve, the mirror was deployed. Deployment was smooth, with the mirror first unfolding to the circumferential fold lines and then the outer petals unfolding. After deployment, a positive differential of 25 mm Hg was maintained in the structure.

The deployment was executed at 100-mm Hg absolute chamber pressure because the excess solvent had not been removed from the specimen after impregnation. The vapor pressure of the solvent is approximately 75 mm and might have caused too rapid deployment. (At the time of this test, it was anticipated that another mirror would be similarly tested later. It was intended that the second unit would have the solvent removed prior to insertion into the chamber. That test would have been conducted by evacuating the chamber without simultaneously pumping the specimen; deployment would have been at low vacuum chamber pressure.)

The solvent was boiled off by purging the specimen for two hours with dry nitrogen. Chamber pumpdown continued. A positive differential was maintained in the specimen of 25 mm Hg.

By the time the chamber was in the 10^{-6} range (approximately five hours after the 100 mm Hg hold was complete), it was apparent that a restriction existed in the test outside ports. A gradual local buildup and foaming of the resin had occurred in the ports.

At this point, the inlet and outlet lines were reversed in an attempt to get better flow but with little or no effect. Water was introduced into the inflation gas; however, the amount of water that could be inserted into the specimen was very small due to the very limited flow. The flow was mostly a result of the leakage of the test article. This flow was continued for approximately nine hours.

The chamber then was gradually brought to ambient pressure. During this period, ambient air was throttled into the specimen to prevent collapse. When the chamber was opened, the test article was immediately inspected; it was apparent that rigidization was virtually complete.

After removal from the chamber, the mirror was judged to be of good quality, although not quite so good as the first 10-ft diameter mirror that was rigidized under ambient conditions.

Inspection of a preshaped section cut from the rigidized mirror revealed that the resin had not foamed in the mirror itself but had uniformly coated and rigidized the sandwich faces and drop threads. Figure 22 shows this reflector before and after deployment and the rigidization in the vacuum chamber.

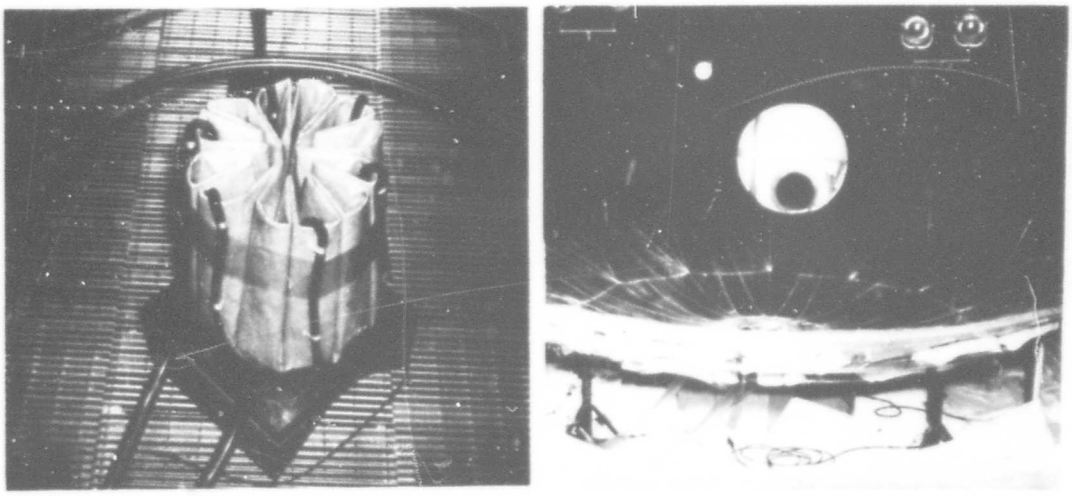

Figure 22 - Before and After Deployment in Vacuum Chamber

Four-Foot Diameter by 8-Foot Long Cylinder - One four-foot diameter by eight-foot long cylinder was built. Dacron fabric was used as the structural textile material in the cylindrical section. This material was sewn into a fluted configuration. The flute geometry was designed so all internal pressure of the cylinder was carried on the inner fabric, which was three plies thick. The fluted assembly was sealed with nylon film, and an internal pressure bladder was used for the primary internal pressure seal. The cylinder ends were hemispherical and constructed from fiberglass laminate and aluminum components. Manifolds were incorporated at the interface of the fabric cylinder and rigid ends as a means of acquiring uniform impregnation and gas flow for drying and rigidization. This unit was impregnated at Goodyear Aerospace; most of the solvent in which the resin was dissolved was boiled off. The specimen was sealed and transported to Arnold Engineering and Development Center in Tennessee. The unit was placed in the vacuum chamber and the chamber evacuated. Deployment then was attempted; however, premature rigidization had taken place, and deployment was impossible. This apparently was due to a small amount of moisture having reached the resin, which is quite reactive at this solvent level. The article had been impregnated 12 days prior to the deployment attempt.

The present state of the art of the rigidizing resin system indicates that proper drying procedures of the structure prior to impregnating and accurate control of solvent removal level would result in a reliable system.

CONCLUSIONS

The Vaporset resin rigidizing system utilized in this program has good potential for future use. The solar collector concept developed and demonstrated is feasible and with refinement ultimately could be used in a space system. The resin system also can be considered seriously for application to other structure types.

BLANK PAGE

DEVELOPMENT OF COMPOUND CURVATURE AIRMAT

By James T. Harris*

INTRODUCTION

Space Age requirements have stimulated many unique technologies to new and surprisingly useful life by altering some restricting limitations or adding a requirement which places a premium on a specific property.

One of the affected technologies is that of Expandable Structures. One unique property of fabric structures, packageability, has sparked an interest in these materials and structures for many space mission requirements. It has also stimulated renewed interest in this construction medium for terrestial and aeronautical applications.

DISCUSSION

Expandable Structures is a term generally attributed to the broad field of structures constructed of coated fabric materials, tailored to the final configuration, deployed to and maintained in the useful shape by an inflation gas. The shapes used are generally bodies of revolution such as spheres or cylinders.

Figure 1 shows the evolution of shape control from these basic body shapes through parallel cylinders of lobe type construction with common interconnecting webs to Airmat**; a continuous material consisting of two woven faces with interconnecting threads.

Although Airmat in flat panels is the most common configuration, many other Airmat shapes have been generated. These vary from airfoil sections used in the Inflatoplanes and helicopter rotor blades, to wedge sections used to seal the fuselage cavity behind a variable sweep winged aircraft.

For many applications, flat panel Airmat can be tailored to a desired configuration by patterning prior to assembly. Examples of this construction technique are shown in Figure 2, wherein an Airmat supported ablative liner provided a foldable extension to a rigid rocket engine nozzle, which, when deployed after stage separation, provides a minimum weight means for engine efficiency increase.

* Engineering Specialist - Goodyear Aerospace Corporation

** TM - Goodyear Tire and Rubber Company

Even though flat and symmetrically shaped Airmat panels are finding new utilization daily, it was recognized that this utilization could be greatly increased with compound curved Airmat.

An example of this occurred during the course of the development of a space rigidized solar concentrator.

The concentration, Figure 3, consisted of a highly reflective metalized Mylar film as a reflecting medium which was very accurately located on a parabolic dish shaped mold. To the back side of this reflecting surface, was attached a conical dish made of pie shaped sections of Flat Dacron Airmat. The fit between the molded reflective surface and the mating Airmat was not uniform but was close enough that the bonding material filled the void areas at the panel to panel junctures of the Airmat.

On very large concentration of the type needed for high electrical power space systems, the overall dimensional accuracy could be improved and the bonding material weight reduced if the Airmat backing could be made of compound curvature Airmat.

The Manufacturing Methods Branch of the Air Force Systems Division, recognized this requirement and awarded Contract AF33(615)-3874 to Goodyear Aerospace Corporation for the development of a method for construction of compound curvature Airmat cloth.

APPROACH

The approach used was to consider each direction, warp and fill, separately developing a technique for creating curvature in each individually and then combining the techniques to accomplish compound curvature.

WARP DIRECTION CURVATURE

On an Airmat loom, Figure 4, the warp yarns for the upper and lower facecloths are stored on separate spools or beams. As these facecloths are woven, they are extracted from the loom in a horizontal direction by a take-off mechanism. The takeoff mechanism was modified on the GAC Research Loom so that the takeoff of the upper facecloth could be accomplished faster than takeoff of the lower facecloth.

These takeoff rates were programmed for a constant difference and the resulting manufactured Airmat had a constant radius of curvature. The curvature existed in the warp direction only and the takeoff mechanism adjustment could be controlled to produce any amount of curvature from radial to parabolic.

Since the contract was slanted toward a solar concentrator application, a radius of curvature of 112 inches was selected to represent the curvature required for a ten foot diameter dish formed from two inch thick Airmat.

Proof of the differential rate takeoff technique was established by weaving a four foot square Airmat panel with the 112 inch radius in the warp direction only as shown in Figure 5.

FILL DIRECTION CURVATURE

A study of the Airmat weaving machinery operation failed to reveal any simple methods for establishing a curvature in the fill direction similar to that achieved in the warp direction. Therefore two alternate methods offering promising solutions to the problem were investigated.

VARIABLE STIFFNESS METHOD

The first method involved weaving Airmat using different weight or stiffness fill yarn in each facecloth. When the Airmat was inflated, different strain or elongation would occur in the fill direction of each face because of the different rate of extension under load of the material used. The result would be a curvature of the inflated Airmat in the fill direction. To evaluate this method, load vs strain information on several combinations of facecloth materials were investigated. One investigation involved a comparison of nylon and Dacron* facecloth of equivalent weight and another involved examining load vs strain data on stretch nylon cloth.

The target differential strain between the two facecloths was 1.80 percent which corresponds to the 112 inch radius on 2 inch thick Airmat.

Three Samples of Airmat facecloth were woven on the loom using Dacron warp threads but with Dacron, nylon, and stretch nylon fill threads so that not only various material properties could be compared but also the effect of weaving variables such as crimp would be included in the investigation. The load-strain curves for the three cloth constructions are shown in Figure 6 and demonstrate that the strain differential between nylon and Dacron range from 5 to 7 percent except for very low loadings. The stretch nylon has a considerably larger elongation. Since the elongations obtained were significantly in excess of the 1.8 percent requirement, this method was considered unsuitable as a means of obtaining fill direction curvature.

HEAT SETTING METHOD

The second method investigated for creating fill direction curvature, involved weaving Airmat with fill yarns of heat set material in one face and non heat set fill yarns in the opposite face. The woven Airmat cloth would then be oven heated to a predetermined temperature thus shrinking the non heat set yarns to the length desired to obtain the required 1.8 percent length differential.

The Airmat was woven on the GAC loom using standard warp and drop yarns, heat stabilized at 275°F, however, the fill yarns on one face were the standard Dacron, while the fill yarns on the opposite face were non heat stabilized Dacron yarn.

*TM - E.I. DuPont

Heat shrinkage tests were conducted to establish shrink rates for cloth at various temperatures. This data plotted on Figure 7 shows that the required 1.8 percent differential length could be achieved by heat setting the Airmat at 186°F. Therefore the heat setting method was selected as the most practical method for obtaining curvature in the fill direction but it is limited to radial curvature. Some consideration was given to using the heat set method for warp curvature but with the limitation to radial curvature only and the added complication of two different warp materials, it was rejected as impractical.

DEMONSTRATION

Proof that the systems for creating warp curvature and fill curvature could be incorporated into Airmat cloth simultaneously was established, Figure 8, by weaving a four foot demonstration panel incorporating both techniques into the single panel. After weaving a panel with warp curvature established by differential takeoff rate, the panel was heat set to establish the fill curvature. Finally the cloth was coated with elastomer, the edges were sealed and the panel inflated to five pounds per square inch. Dimensional checks made on the finished panel indicated equal curvature in both warp and fill directions and close agreement with the target radius.

SUMMARY

It is evident that the differential rate weaving method is the preferred method for obtaining single curvature Airmat. The curvature is obtained purely by mechanical weaving procedures and is independent of yarn materials used. This method can be programmed to weave parabolic curvature, however, it is limited to single direction curvature and must be combined with another method when double curvature is desired.

The differential shrinkage or heat setting method is the most practical method for obtaining curvature in the fill direction but is limited to radial curvature.

The methods of differential rate weaving for warp curvature and heat setting for fill direction curvature when combined, produces compound curvature Airmat with predictable results. The accuracy control is sufficient for application of the material to solar concentrator mirror support structure and therefore opens a new area for Airmat structural applications.

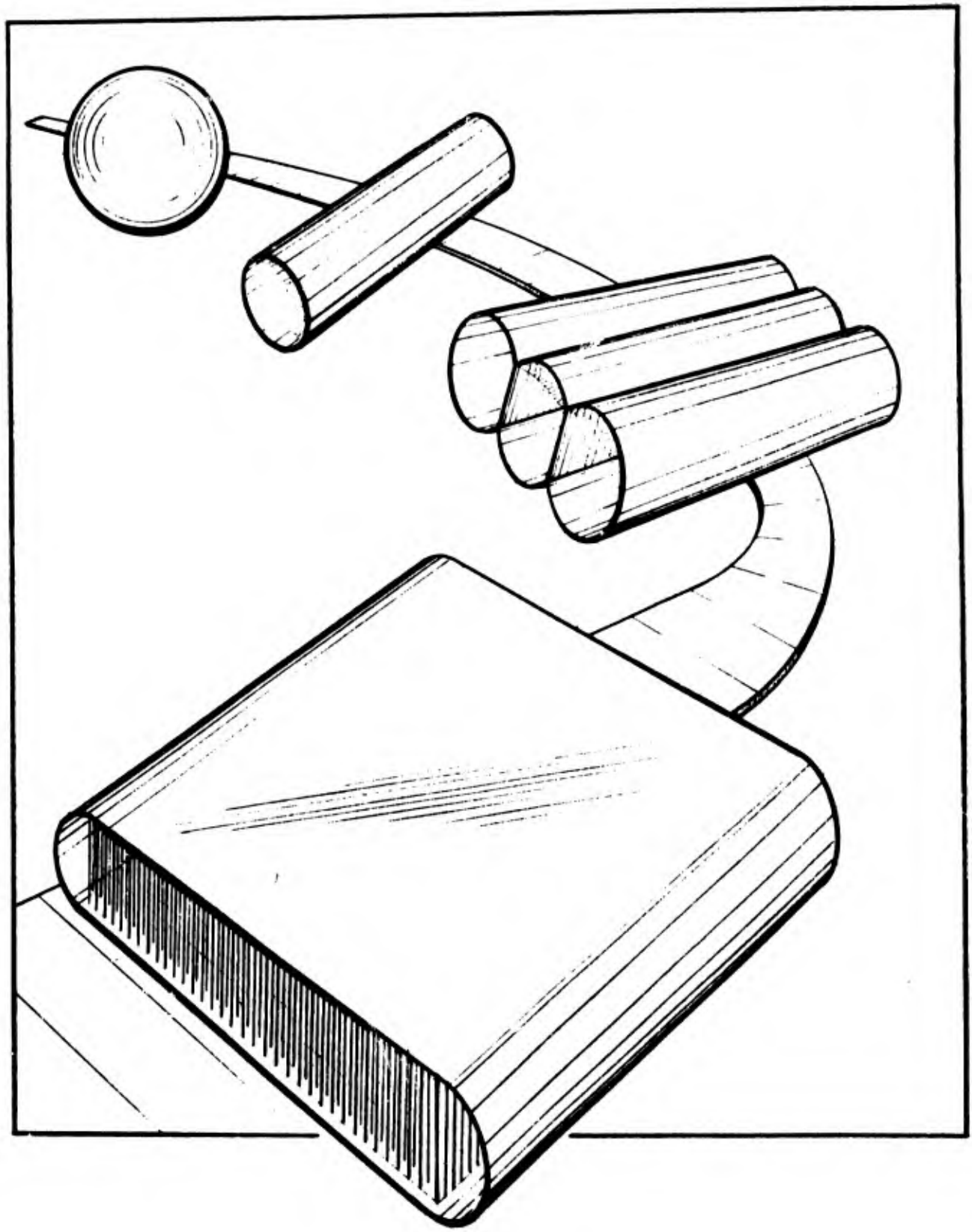

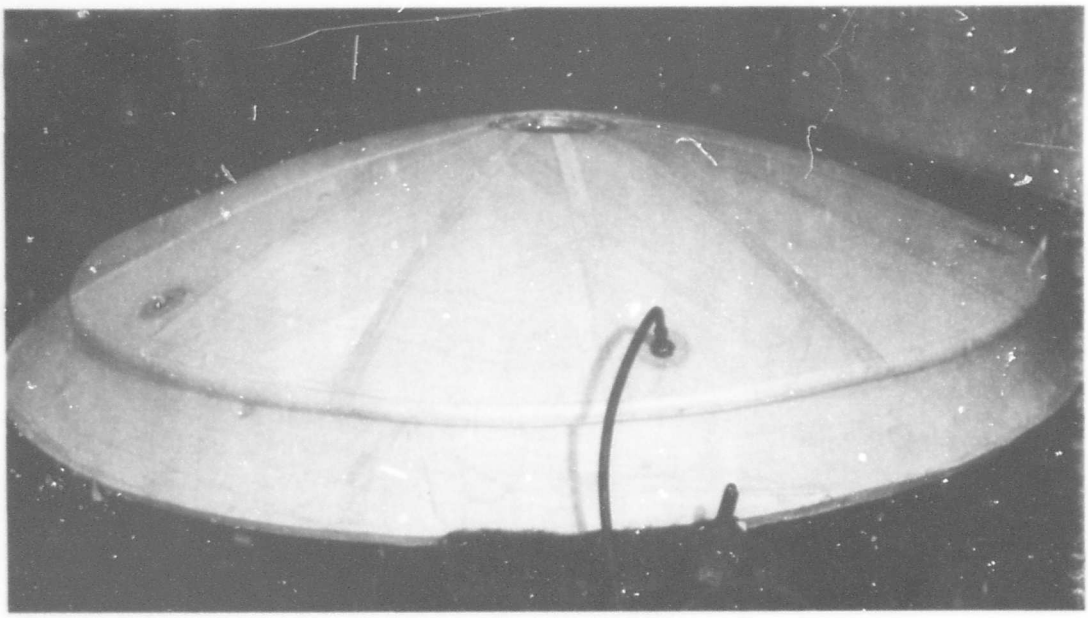

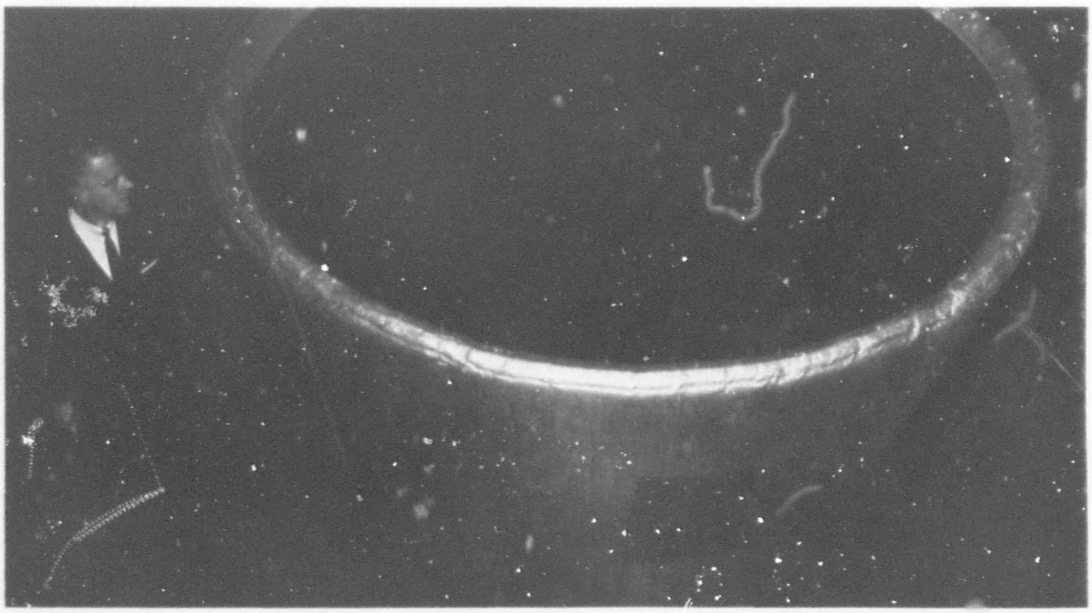

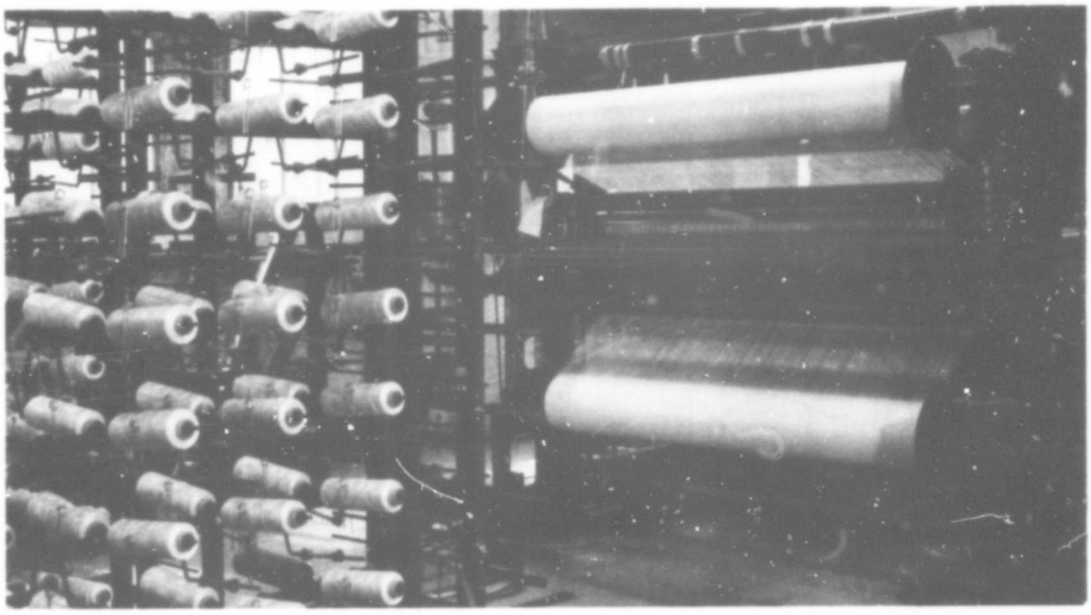

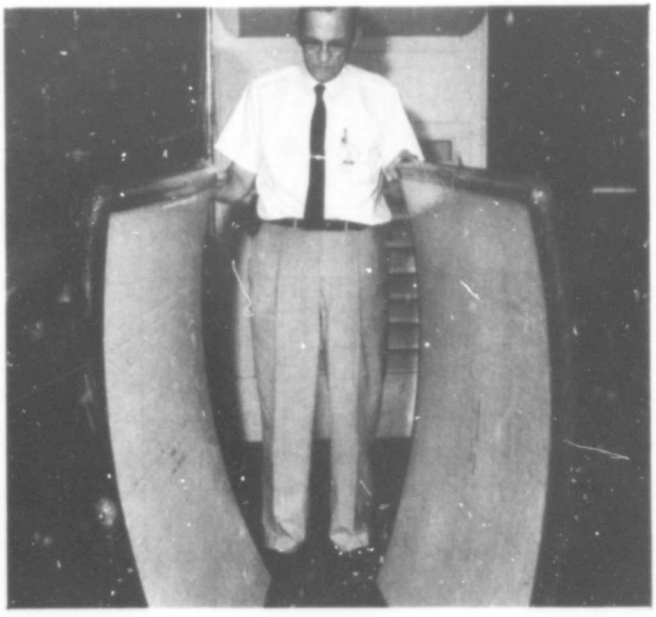

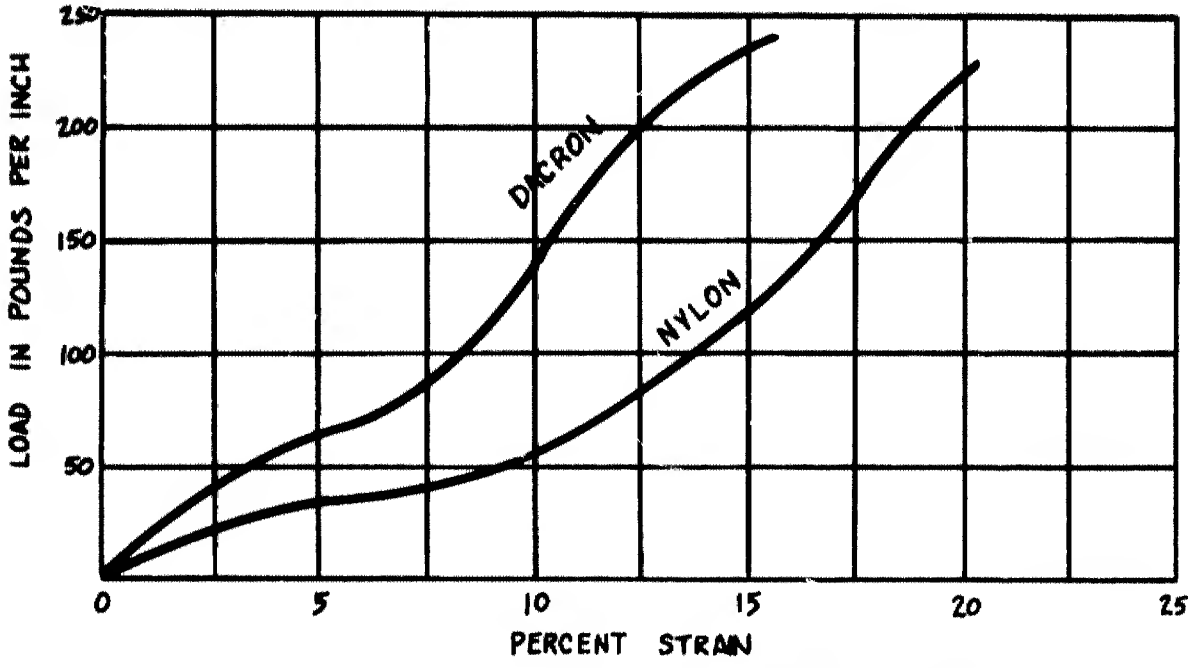

FIGURE 6 LOAD VS STRAIN FOR NYLON AND DACRON CLOTH

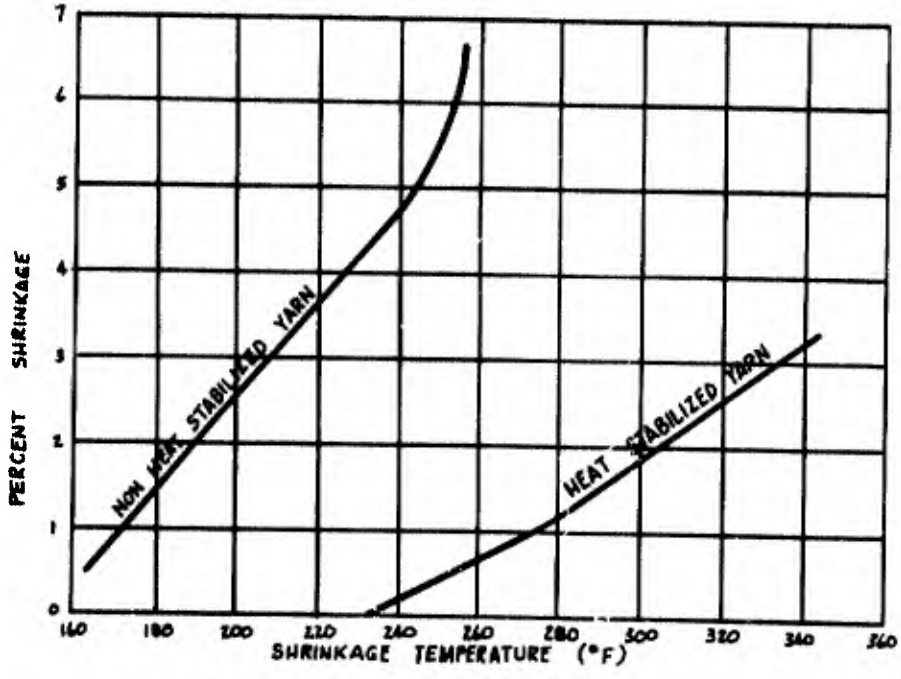

FIGURE 7 SHRINKAGE VS TEMPERATURE FOR DACRON CLOTH

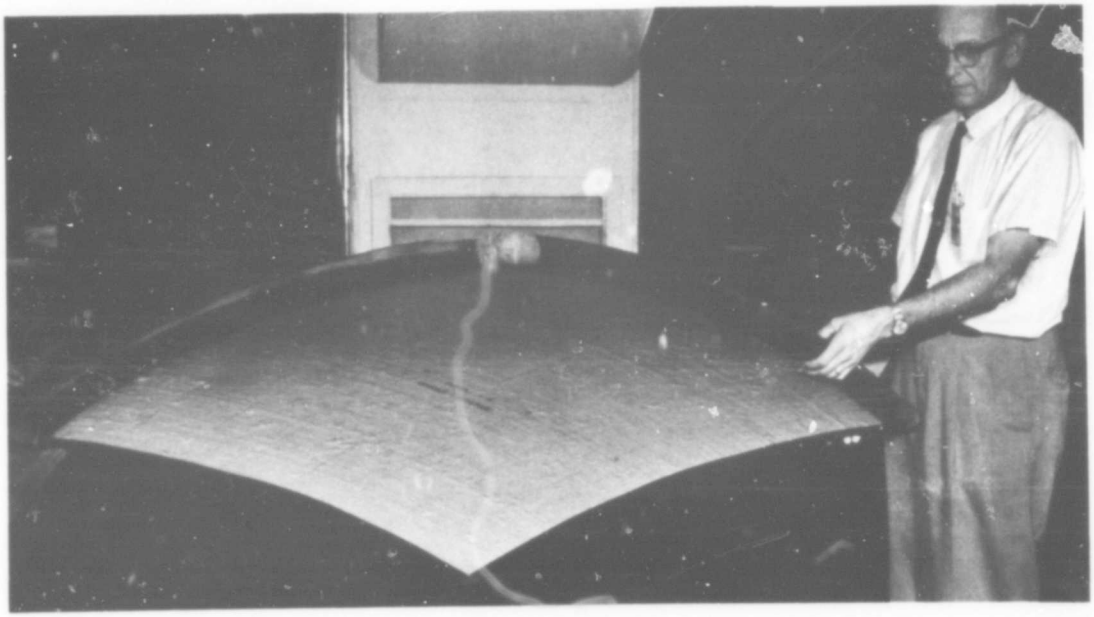

BLANK PAGE

EXPANDABLE AIRLOCK EXPERIMENT FOR THE SIVB WORKSHOP

F. Forbes,* L. Jurich,** and A. Cormier*

assisted by

G. Reid,† L. Manning,** and J. Williams‡

INTRODUCTION

The purpose of this technical paper is to describe the D-21 expandable experiment scheduled for orbital flight testing on the NASA SIV Workshop Flight AAP-2. This paper summarizes the background conditions that led to the D-21 experiment definition, the objectives of the experiment, and a technical discussion of the experiment.

With the rapid advancement in space technology, the United States will be orbiting a series of manned space laboratories from which astronauts can perform various experiments and tasks. Some of these experiments and tasks will necessitate astronaut extra-vehicular activity (EVA). An airlock system will be necessary to alleviate the repeated decompression and compression cycles imposed on the laboratory work area during egress and ingress maneuvers associated with EVA. An expandable airlock would minimize weight and volume requirements imposed on the vehicle and would permit maximum utilization of the internal volumes already available in these laboratories and spacecraft.

Since 1960, considerable Air Force in-house work has been performed on various expansion and rigidization systems, including gelatin rigidized structures and expandable self-rigidizing honeycomb. Additionally, a number of contractual efforts were initiated to investigate expandable elastic recovery material concepts. The level of contract efforts included basic materials research, design and fabrication studies, and construction and ground tests of full-size prototype structures.

Several contract efforts monitored by NASA also have resulted in the successful construction and test of large expandable space structures. These

*Space Technology Branch of Air Force Aero Propulsion Laboratory, Wright-Patterson AFB, Dayton, Ohio.

**Astronautics Programs Department, Goodyear Aerospace Corporation, Akron, Ohio.

†6570th Aerospace Medical Research Laboratory, Wright-Patterson AFB, Dayton, Ohio.

‡NASA Langley Research Center, Hampton, Va.

structures, based on the elastic recovery materials approach, were successfully demonstrated, tested, and then evaluated in vacuum chamber deployment tests. As an outgrowth of this development, two structure concepts have emerged: (1) the chemically rigidized structure concept (see Figure 1) and (2) the elastic recovery materials technique (see Figure 2).

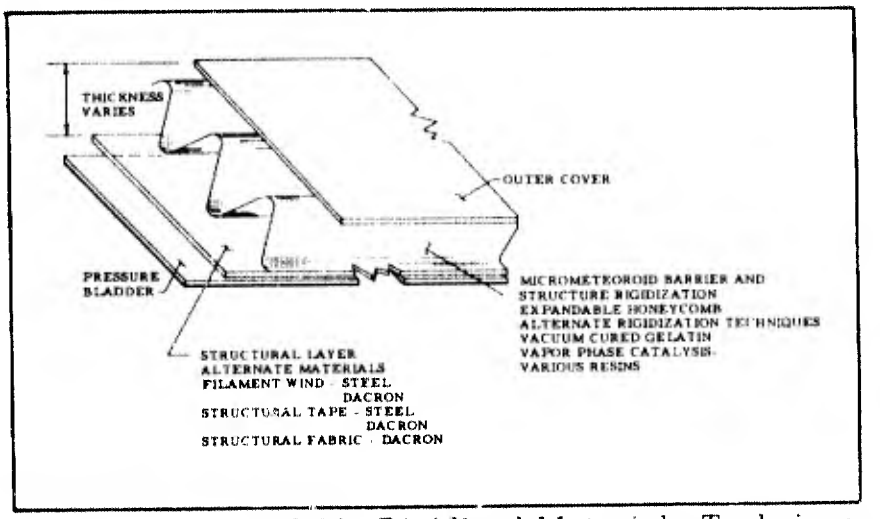

Figure 1 - Expandable Rigidized Materials Technique

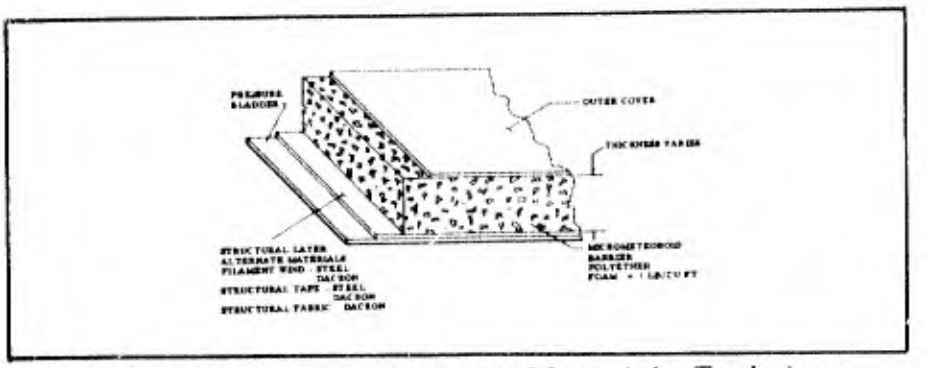

Figure 2 - Elastic Recovery Materials Technique

Both structure techniques are designed to do essentially the same job. The chemically rigidized approach, however, provides an added capability of structure rigidization subsequent to deployment in orbit. The chemical system is more complex and, therefore, has not been so extensively developed as the elastic recovery approach has.

The elastic recovery materials technique rests on a solid background of development. Technology is at a point where the next logical and needed step is a manned orbital flight demonstration. Extensive development of this materials technique conducted by both NASA and the Air Force in the form of full-scale prototype structure fabrication and testing is summarized below. Because of these programs, the Air Force has selected, as a basis for the D-21 flight experiment, the elastic recovery concept.

A crew transfer tunnel was developed by the Goodyear Aerospace Corporation under contract to the Space Technology Branch of the Air Force

Aero Propulsion Laboratory (AFAPL). The tunnel structure is 4-ft wide and 12-ft long, integrated with a rigid metal honeycomb slab structure 3-ft wide and 12-ft long, along one side. Successful structural, gas leakage, packaging, and deployment tests were conducted on the full-scale structure along with extensive materials environmental compatibility testing.

A Stay Time Extension Module (STEM), an integrated lunar shelter airlock, was developed by Goodyear Aerospace under contract to the NASA Langley Research Center. The shelter is 7-ft in diameter and 13-ft long, with an integral airlock 7-ft in diameter and an additional 4-ft long. The test program included structural evaluation, gas leakage, packaging, and deployment.

A retractable airlock was developed by the Whittaker Corporation for the Langley Research Center. This airlock design is 4-ft in diameter and 7-ft long and incorporates a mechanism for retracting the structure when it is not in use.

These advances in elastic recovery materials technology clearly indicated that the next logical step was a manned orbital flight demonstration. Therefore, an expandable airlock system was defined and submitted for approval to both the Department of Defense (DOD) and NASA for flight experiment. In September 1966, the expandable airlock flight experiment was formally approved and designated D-21. This approval was followed in December by a competitive contract award to Goodyear Aerospace for developing the D-21 experiment hardware.

SCOPE OF D-21 EXPERIMENT

The D-21 experiment probably is the most extensive program to have been implemented in the manned application of expandable structures technology. The scope of the D-21 airlock program extends from initial human factors evaluations to establishing size and geometry of the airlock structure to final retrieval of data and definition of experiment results subsequent to orbital testing.

Human Factors

One of the first tasks to be implemented was intensive human factors testing to establish the baseline definition of the experiment design. Testing was conducted by AFAPL and the Air Force Aero Medical Laboratory to establish optimum geometry requirements for the D-21 airlock design and to establish the minimum hatch size consistent with the Apollo space suit and use of a PLSS (Portable Life Support System). Neutral buoyancy tests were conducted in the underwater facility at Wright-Patterson AFB (WPAFB) to establish optimum maneuvers of ingress/egress and to define locomotion aids necessary for these maneuvers and, therefore, for the orbital experiment.

Step-by-step procedures have been established for the overall experiment. These procedures have been defined in a "time line" established for the experiment; about three hours of EVA are required of each of two astronauts to perform the overall experiment. It is expected that the time line

and experiment procedures will be continually refined as crew training is implemented. The proposed training plan includes using both underwater facilities and the KC-135 zero "g" airplane to implement practice maneuvers of the experiment procedures prior to flight.

Hardware Requirements

The experiment plan was established by AFAPL in conformance with experiment guidelines stipulated by the NASA Manned Spacecraft Center (MSC). This plan calls for the developing and extensive qualification testing of experiment hardware used specifically for this purpose. Additional experiment hardware also is required to support astronaut crew training in conformance with experiment procedures stipulated in the experiment plan. This hardware will consist of airlock mockups (of both rigid and expandable materials) to be used both underwater and in the KC-135 to simulate zero "g" maneuvers in experiment procedures. Duplicate sets of flight hardware will be required as the primary and backup flight units. All hardware, except that used for training, must comply with the NASA requirements of NPC-200-2 and NPC-200-3 for quality control and inspection.

Documentation and Design Reviews

Documentation will be required substantially beyond the requirements normally associated with a research and development project. In addition to the usual status reports normally required, documentation in various forms consistent with the experiment requirements and schedules will be submitted for review and approval throughout the program. These documentation forms will include (1) definitive experiment plan, (2) failure mode and effects analysis, (3) qualification test specifications and procedures, (4) qualification test status and final report, and (5) quality control plan and inspection system.

In addition to the documentation stipulated above, periodic design reviews will be held to ensure final integration of the D-21 experiment with the flight vehicle and subsequent implementation of the experiment during flight. These reviews will include (1) initial design review, (2) design certification review, (3) qualification test design review, (4) postqualification test design review, (5) acceptance review, and (6) flight readiness review.

Test Requirements

Extensive ground testing will be required prior to flight acceptance of the D-21 experiment. This testing will be performed on one set of flight design hardware fabricated specifically for this purpose. The test program is directed toward attaining two objectives: (1) to ensure compliance with manned mission requirements and (2) to ensure a high probability that the experiment will succeed.

The test program will be conducted on an integrated assembly of the D-21 hardware. Testing will be environmental in nature and will simulate

the three categories of environment expected: earth environment, spacecraft environment, and space environment. Testing under the first two categories will be performed with the D-21 hardware in a packaged configuration (see Figure 3). Space environment testing will be performed with the D-21 in both a packaged configuration and in a deployed configuration (see Figure 4). Space environment testing also will include the functional aspects of the D-21 experiment defined by the experiment procedures.

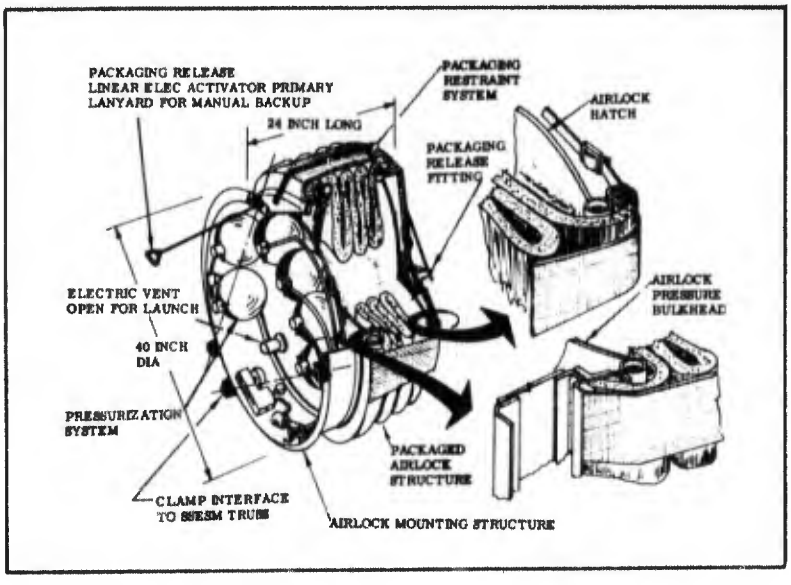

Figure 3 - D-21 Packaged Configuration

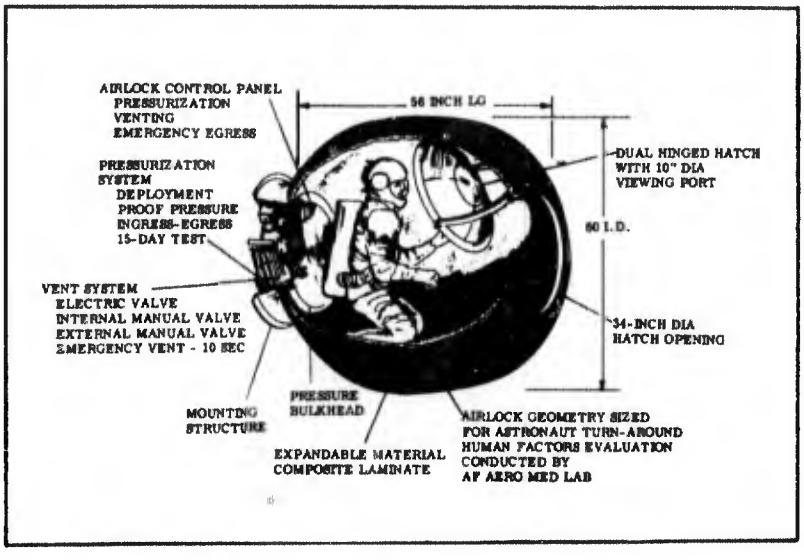

Figure 4 - D-21 Expanded Configuration

Experiment Data

Data from the D-21 orbital experiment will be obtained via telemetry,

motion picture coverage, and voice recordings. The D-21 airlock will be instrumented for temperature and pressure data via telemetry to establish the leak rate of the D-21 airlock in orbit.

Biomedical data will be obtained during astronaut ingress/egress demonstration of the D-21 airlock to evaluate the airlock design relative to the dynamics of ingress/egress and human factors suitability.

Motion picture coverage will permit visual monitoring of the key functional phases of the experiment, such as deployment of the structure and the ingress/egress demonstration.

Voice recordings will be obtained during the entire period of the functional phases of the experiment. These recordings, along with other methods of data return, will permit a thorough assessment of the results of the D-21 experiment. Evaluation and analysis of the experiment results will be published in a final report.

SIVB MISSION OBJECTIVES

Fundamentally, the objective of the SIVB mission is to evaluate the feasibility of using the empty shell of the spent SIVB stage to support crew operations for a 30-day orbital mission.

The SIVB orbital workshop mission will consist of two flights. AAP-1 is manned and AAP-2 is unmanned and is launched five days later. Rendezvous and docking will occur at an approximate orbital altitude of 260 naut mi followed by the 30-day operational mission. The basic orbital hardware of AAP-2 consists of the SIVB spent stage, an airlock support module for subsystem support of the spent SIVB (such as stage pacification, environmental control system, power, and communications), and a multiple docking adapter (MDA) for subsequent linkup of the Apollo Command Service Module (CSM) and resupply modules.

Corollary experiments (such as D-21)will be carried on AAP-2, either in the MDA or on the airlock support module. All experiments will be performed during the 30-day mission period and will be integrated into an overall time line for overall experiment procedures.

Figure 5 shows an artist's concept of the expanded configuration of the D-21 airlock deployed from its mounting location atop one of the four truss structures used to support the airlock support module. The experiment is located external to the thermal curtain used to shield the support module subsystems and is near the EVA panel, thus providing astronauts access to the experiment.

D-21 FLIGHT EXPERIMENT OBJECTIVES

The objective is to obtain the maximum amount of data for use in future airlock designs. These data must necessarily be obtained under a constraint

Figure 5 - D-21 Airlock Deployed from Mounting Location

of minimum astronaut participation considering the large number of individual experiments to be performed on NASA Flight AAP-2. Specifically, the objectives of the experiment are as follows:

1. To ascertain the ability of expandable structures to withstand the boost and launch phase of a typical mission profile with subsequent successful deployment in orbit

2. To validate the successful performance of expandable materials in operational use when subjected to the total orbital space environment

3. To evaluate structure packaging techniques and deployment dynamics

4. To evaluate space environment effects on expandable materials after prolonged exposure (six months)

5. To demonstrate the compatibility of expandable elastic recovery materials in airlock designs with the dynamics of astronaut ingress/egress

6. To establish design parameters and requirements for elastic recovery airlocks for future manned orbital laboratories

7. To provide a baseline from which to extrapolate the application of expandable structures technology to other uses such as crew transfer tunnels, space shelters, and controlled maintenance stations and storage depots

TECHNICAL DISCUSSION OF D-21 EXPERIMENT

The experiment total flight package consists of four distinct units of hardware: (1) the integrated D-21 airlock package, (2) a control panel mounted inside the NASA airlock module (AM) for remote control of the experiment, (3) a wiring harness interconnecting the D-21 package with the remote control panel, and (4) a container for earth return of material specimens.

The D-21 airlock package, shown in Figure 4 and in an exploded view in Figure 6, is comprised of the following subassemblies: (1) packaging system, (2) airlock structure assembly, (3) hatch assembly, (4) pressure bulkhead assembly, (5) pressurization system, (6) telemetry data system, (7) electrical system, (8) mounting structure assembly, and (9) experiment control system.

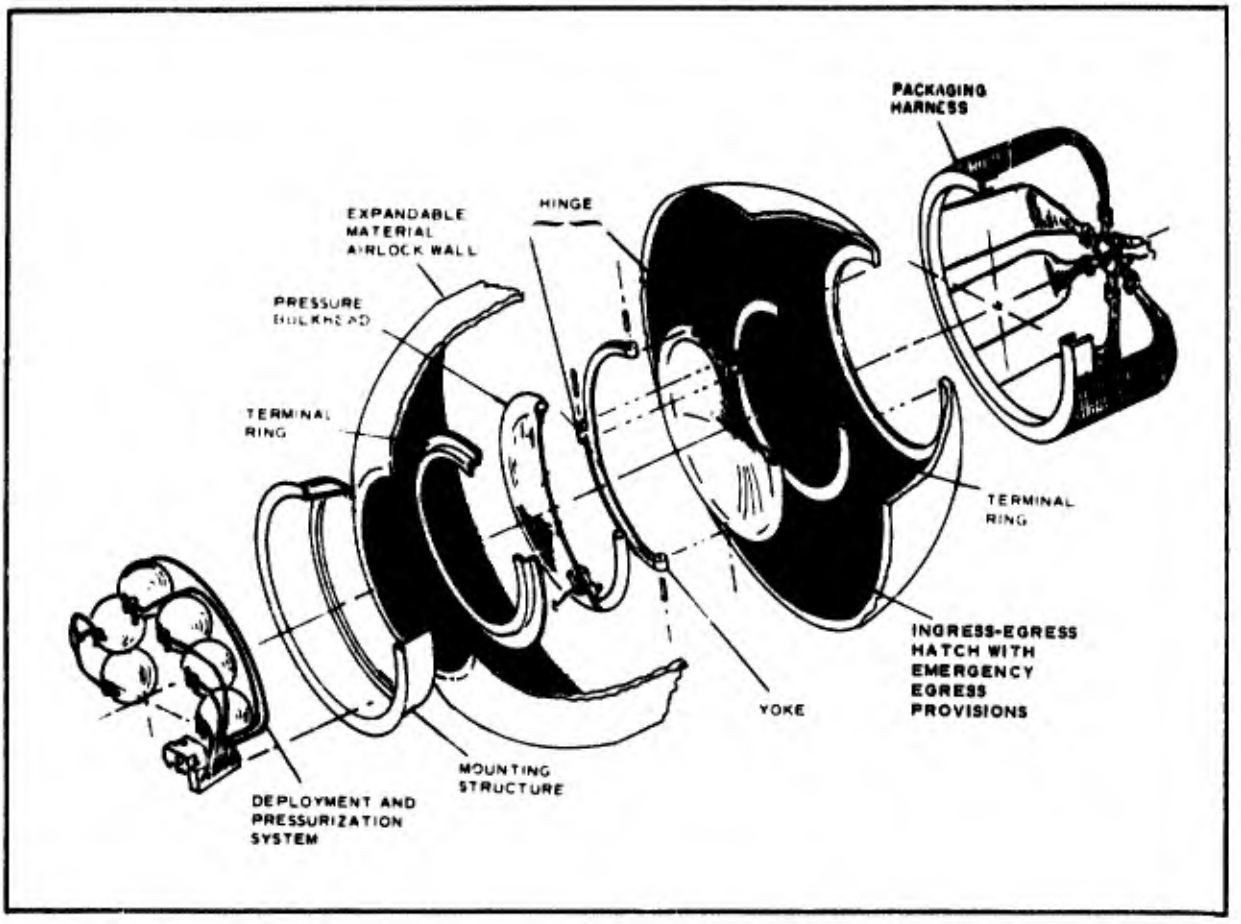

Figure 6 - D-21 Airlock (Exploded View)

Packaging System

The packaging system consists of a series of flexible nylon straps located around the periphery of the mounting base to restrain the expandable portion of the airlock structure in a packaged configuration (see Figure 3). The restraining straps terminate at a release fitting located at the apex point of the package. To deploy the airlock structure to its expanded configuration, provisions are incorporated to release the restraint system either by remote control (electric actuator located in mounting base structure) or by a manually actuated lanyard located on the D-21 airlock package. Provisions are incorporated into the packaging design to position and retain the restraining straps after the airlock is deployed. These straps are secured to the wall structure to lie along the contoured airlock wall material after expansion until full and final geometry has been attained.

Airlock Structure Assembly

The structural assembly consists essentially of the expandable structure material comprising the airlock wall, which is intimately bonded and joined with rigid structure design terminal rings.

The terminal rings, at each end of the airlock configuration, are fabricated of light gage aluminum sheet material. The function of these rings is to provide a rigid termination to the flexible material of the airlock and also to provide a smooth flat surface for hatch and pressure bulkhead seals. The rings are nonstructural in the sense that no tension load transfer occurs between the wall structure and the rings themselves. The rings do, however, function as a load path (via the seals) to transfer hatch and pressure bulkhead pressure loads into the reacting expandable structure.

The expandable portion of the airlock structure uses the elastic recovery materials technique to permit folding and packaging of the structure into a small compact configuration for launch. Once in orbit, the airlock is deployed to its full expanded configuration by the recovery action of the wall material and augmented by low level pressure (less than 0.5 psi) for final shaping. After final shaping, the inherent stiffness of the wall structure will ensure final shape rigidity even under zero pressure conditions.

Basically, the structure wall is a four-layer composite of flexible materials in accordance with Figure 7 and as described below.

Pressure Bladder - The pressure bladder is a laminate of three individual sealant layers with an inner layer of 0.3-mil aluminum foil. The inner sealant layer is a laminate of nylon film-cloth. This layer is bonded with polyester adhesive to a second layer of closed-cell EPT foam 1/16-in. thick. The outer sealant is a nylon film-cloth laminate coated with a polyester resin. The total weight of the bladder composite is 0.159 psf and is independent of design pressure.

Structural Layer - The filament winding manufacturing process is used for the structural layer and provides near the optimum in lightweight load-carrying flexible structure. The structure layer will be wound with three 0.0036-in. stainless steel wires interlaced with a rayon yarn in a winding pattern of 32 hoop filaments and 29 longitudinal filaments per inch.

Micrometeoroid Barrier - Micrometeoroid protection is achieved by a one-inch layer of flexible polyester foam. Flexible foam of 1.2 psf density has been selected as suitable barrier material, based on hypervelocity particle impact tests. While the primary function of the foam would be to act as a micrometeoroid barrier, it also serves as a deployment aid. During packaging, the foam layer would be compressed to about 10 percent of its original thickness and restrained by the packaging canister. Upon deployment in orbit, the canister would be released and the elastic recovery characteristics of the foam would help shape the airlock to its fully expanded volume.

Outer Cover Layer - The outermost layer of the composite wall structure encapsulates the wall to provide a smooth base for the application of a thermal coating. Inasmuch as the outer cover would encapsulate the composite wall, it would serve as an aid in packaging the structure prior to launch. By a vacuum technique, the wall thickness can be compressed from the fully expanded thickness to about 1/4 in., suitable for folding and subsequent packaging in the canister. A passive thermal control coating would be applied to maintain material temperatures within acceptable limits.

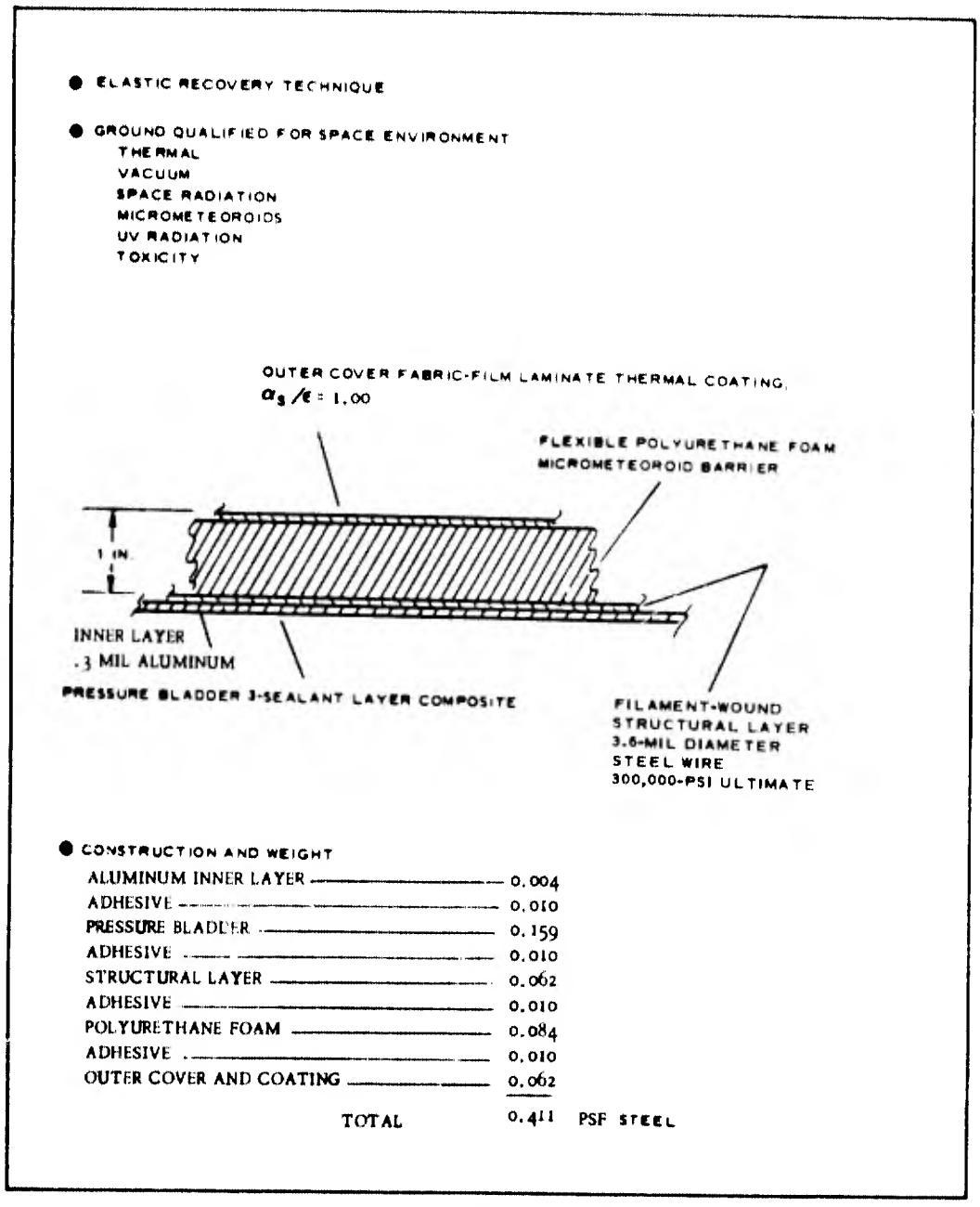

Figure 7 - Expandable Materials Approach

The structural approach being used in the D-21 design is based on a filament winding technique as indicated above. The structural characteristics of this technique are summarized in Table 1.

The compatibility of the expandable materials approach with respect to operations in a space environment has been tentatively established with extensive ground testing. Table 2 presents the environmental compatibility characteristics of the selected materials approach. The materials capability indicated appears to be well within the range of expected environmental conditions without constraining the basic Saturn-Apollo SIVB flight in any way.

TABLE I - STRUCTURAL CHARACTERISTICS

Item	Characteristic
Design pressure	3-1/2 psi
Safety factor	3
Structural approach	Filament wind
Structural material	8-mil diam stainless steel cable
Unit weight	0.109 lb/1000 ft
Ultimate	300,000 psi
"E" modulus	30×10^6 psi
Winding angle	30 deg
Winding area	77 sq ft
Total weight	4.8 lb
Folding effects	
Single cable with sharp 180-deg crease fold	15 percent decrease in ultimate
Pressure bladder backing with sharp 180-deg packaging fold	1000 cycles, no degradation

Hatch Assembly

The hatch assembly shown in Figure 4 consists of a basic dome and compression ring structure; a dual yoke-type hinge and latch hardware; hatch separation provisions for emergency egress; and a 10-in. diameter viewing port. The hatch latches and seals against the terminal ring and can be operated either from the interior or exterior of the airlock.

The basic pressure dome and compression ring structure is fabricated of aluminum and is separable from the overall hatch assembly as a provision for emergency egress. Although the emergency egress feature of the hatch is not required for the experiment procedures as now stipulated, this feature will be incorporated into the hardware design to be available if needed. Controls to separate and jettison a portion of the hatch under emergency conditions are provided at three locations:

1. At the interior of the D-21 airlock on the airlock control panel

TABLE 2 - ENVIRONMENTAL COMPATIBILITY

(EXPANDABLE MATERIALS)

Item	Characteristic
Toxicity	Nondetectable
Oxygen compatibility	5 psi at 200 F
Flame resistance	0.3-mil aluminum foil flame barrier
Thermal characteristics	
Maximum temperature (F)	Outer surface materials, +300; inner surface materials, +250
Minimum temperature (F)	Deployment flexibility, -100; expanded static, -150
Vacuum effects	One-half of one percent weight loss at 10^{-6} Torr
Space radiation	Material tolerance, 10^7 rad; expected dose (one year), 10^5 rad
Micrometeoroids	P_0 = 0.9999 for 30 days

2. At the interior of the D-21 airlock on the mounting base structure
3. Inside the NASA AM on the remote control panel

Actuation of any of these three controls activates pyrotechnics that first vent the airlock down in 10 sec and then jettison the hatch dome structure. Figure 8 presents the schematic functioning of the emergency egress system. Figure 9 shows the diagram of the vent valve used to effect 10-sec venting. This valve is located on the pressure bulkhead and is not part of the hatch assembly. Figure 10 shows how jettisoning of the dome structure is incorporated into the hatch design.

The dual hinge arrangement shown in Figure 4 permits the hatch, in opening or closing, to slide along the interior wall of the airlock rather than sweeping out in a fixed arc as with a single-hinge design. The advantage of the design is the lesser volume swept out in hatch operation, which allows greater usable volume in the airlock. Two latches are provided on the hatch and are located 180 deg apart and 90 deg from the yoke-hinge attachments. The hatch can be jettisoned with the latches in either the open or closed positions.

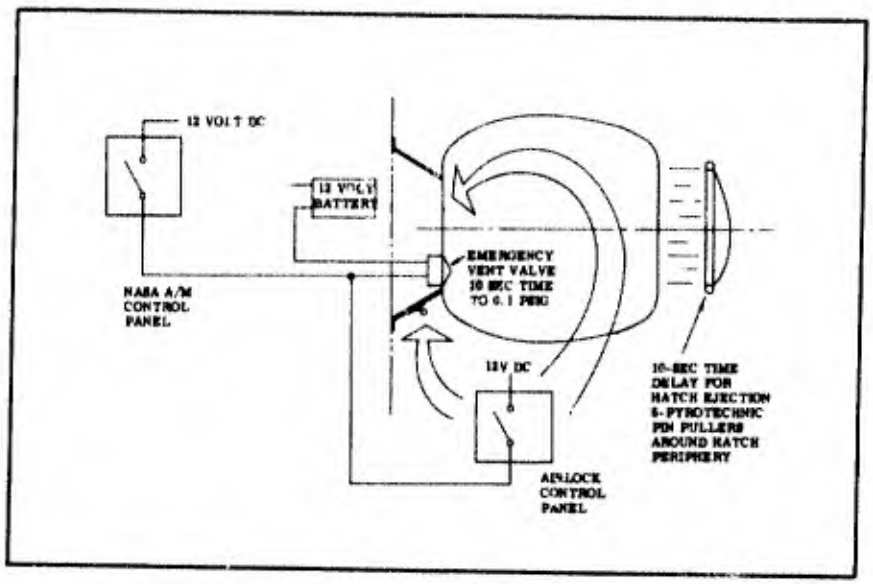

Figure 8 - Emergency Egress System

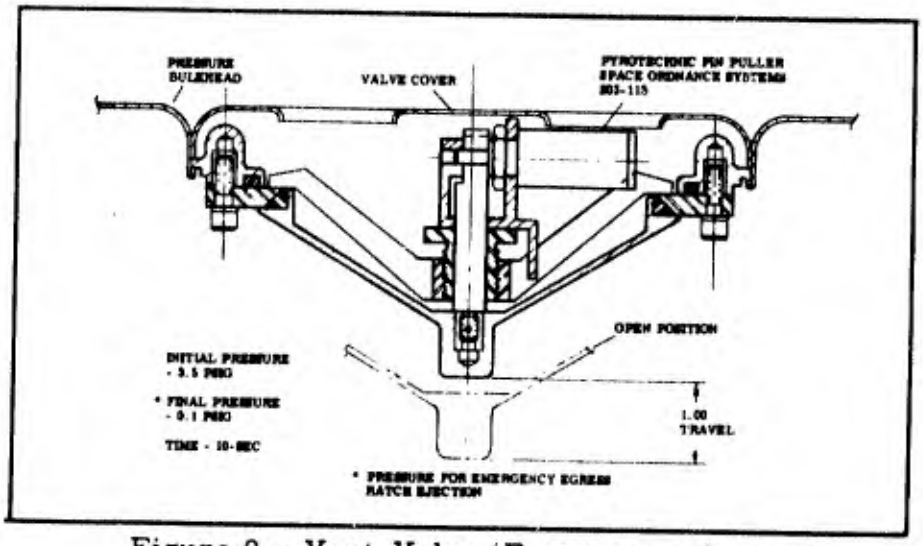

Figure 9 - Vent Valve (Emergency Egress)

The hatch also incorporates a 10-in. diameter viewing port. This port is located off center of the pressure dome to clear the hatch handles. Handles are provided at the center of the pressure dome on both sides. The handle is used to actually open and close the hatch, with latches used only for initial opening or final closing of the hatch.

Pressure Bulkhead Assembly

The pressure bulkhead assembly shown in Figure 4 consists of a basic dome and compression ring structure of aluminum, similar in concept to the dome structure of the hatch. The bulkhead assembly seal and connection is made at the 34-in. diameter terminal ring of the airlock structure and also

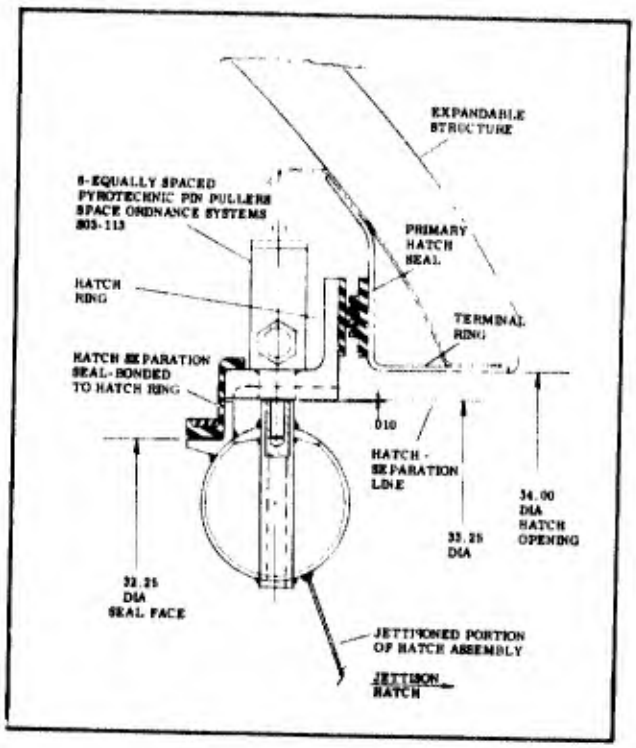

Figure 10 - Emergency Egress Hatch

attached to this ring with six equally spaced bolts. Provisions are incorporated into this assembly for a control panel; a future connection for an astronaut umbilical; and subsystem connection requirements for pressurization, venting, electrical wiring, and instrumentation.

Subsystem Interface Connection - The bulkhead design provides an eight-inch diameter connection pan and plate adjacent to the control panel for interfacing exterior subsystem requirements with the interior of the D-21 airlock. The opening of this pan is provided with a cover plate that is flush with the pressure dome contours.

The pan depth is approximately five inches, with equipment-mounting bosses located on the lower surface and around the periphery. The following equipment provisions are incorporated into this pan connection design:

1. A one-inch diameter manual vent valve located under the pan cover plate. The operating handle for this valve is above the cover plate accessible to the astronaut and adjacent to the control panel.

2. A one-inch hose connection at the bottom of the pan. This connection is used for a vent line to an exterior manual vent valve located on the exterior surface of the mounting structure for the D-21 airlock.

3. A 3-1/2-in. emergency vent valve submerged within and located on the lower surface of the pan (see Figure 9).

4. A one-inch diameter pressure relief valve set at 3-1/2 psig and mounted on the exterior surface of the pan face.

This valve is normally "locked" inoperable when not in use. The purpose of this valve is to limit airlock pressure to 3-1/2 psig and to eliminate excessive pressure buildup from astronaut suit dumping of excess oxygen and water (umbilical rate of 7.9 lb per hour).

5. A one-inch diameter pressure relief valve set at 5.25 psig and also mounted on the exterior surface of the pan face. This valve limits airlock pressure to a proof pressure level.

6. A one-inch diameter electric motor-driven vent valve. This valve is mounted on the exterior surface of the pan face and controlled either from within the D-21 airlock or from the remote control panel.

7. A 1/4-in. connection is provided on the lower pan surface for a pressure line tie to the airlock pressurization system.

8. A 1/4-in. connection is provided on the exterior periphery of the pan for the manifold connection of two pressure transducers to monitor airlock pressure.

9. Three electrical connectors are provided on the periphery of the pan to interface the exterior and interior electrical and instrumentation systems integrated into the D-21 airlock.

Pressurization System

The pressurization system for the D-21 experiment consists of six 150 cu in. high-pressure gas storage bottles charged with nitrogen. The gas is released from each storage bottle through a pyrotechnic valve to flood the airlock to a specific level of pressure established by a predetermined charge in the bottle. Gas flow from any pyrotechnic valve is directed through a common manifold fitting and then through a 1/4-in. supply line to the inlet fitting on the pressure bulkhead of the airlock. All elements of the pressurization system, including pressure storage bottles, pyrotechnic valves, and manifold fitting, are supported off the mounting base structure assembly.

Controls for gas release are located either inside on the D-21 airlock control panel or on the remote control panel located within the NASA AM. These controls are established for conducting the D-21 experiment and include pressurization provisions for deployment, proof pressure, astronaut ingress/egress, and a final 15-day test.

Deployment - Release of the airlock canister restraint is actuated by a switch located on the remote control panel in the airlock module. A mechanical backup system manually operated at the base of the D-21 airlock also is provided. An initial deployment of the structure is partially effected upon

release of the restraint system. Final deployment is achieved through pressurization by release of nitrogen from the 485 psig nitrogen storage bottle. Figure 11 shows the deployment system and method of control.

Proof Pressure - As soon as the airlock has been fully deployed, it is pressurized to a 5-psig proof level from two of the pressure bottles manifolded together for this purpose. The proof pressure level is to be held for about 30 min and then vented. Figure 12 shows the proof pressurization system and the method of control.

Ingress/Egress - Individual pressurization is provided for two cycles of astronaut ingress/egress. This portion of the pressurization system is shown in Figure 13. Pressurization controls are provided both within the D-21 airlock package and within the NASA AM.

15-Day Test - The pressurization system also provides for a 15-day pressure test during which time pressure and temperature data will be obtained via telemetry for determining long-time leak rates of the airlock experiment. Provisions for this pressurization also are shown in Figure 13.

Venting Provisions - Four distinct venting provisions are incorporated in the D-21 experiment design:

1. Manual Vent - A one-inch diameter manual vent valve is located within the D-21 airlock adjacent to the D-21 control panel.

2. Electric Vent - A one-inch diameter electric motor-driven vent valve is located on the exterior of the pressure bulkhead assembly. This valve is switch controlled from either the D-21 control panel or from the remote control panel located in the NASA AM.

3. Manual Vent - Another one-inch diameter manual vent valve is located exterior to the D-21 on the outside surface of the airlock base structure. This valve is provided as a backup to the electric vent in case of malfunctioning.

4. Emergency Vent - A 3-1/2-in. diameter vent valve (see Figure 9) is provided for rapid venting as an emergency feature. This valve is used only in conjunction with the emergency egress feature of the hatch design.

Telemetry Sensors

Pressure and temperature data will be monitored during the course of the D-21 experiment using the NASA support module telemetry system. Eight sensors will be provided, two for airlock pressure and six for surface temperature of the expandable material wall structure.

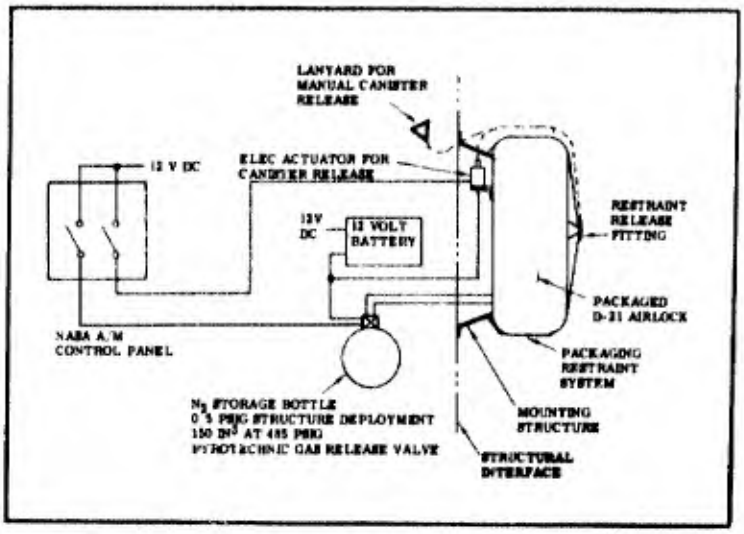

Figure 11 - Pressurization Cycle (0.5 psig)

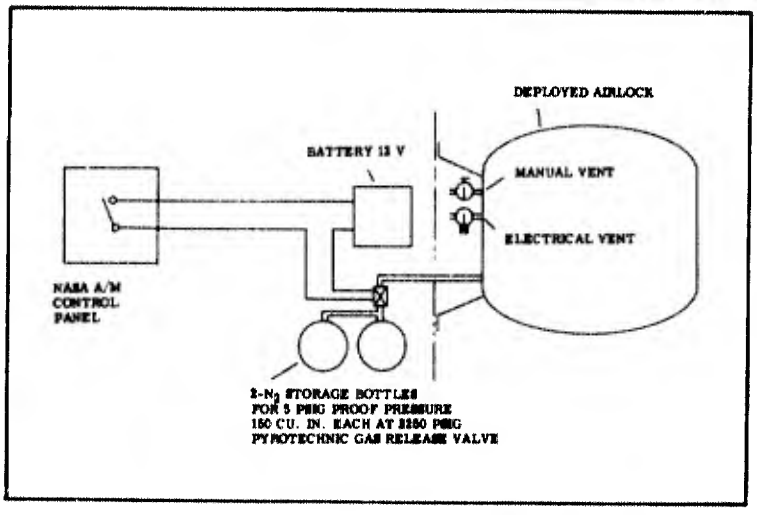

Figure 12 - Pressurization Cycle (5.0 psig)

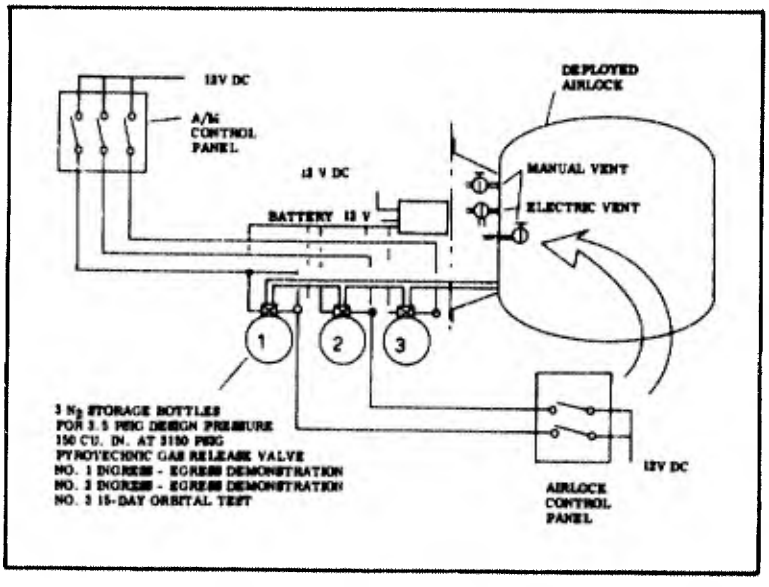

Figure 13 - Pressurization Cycles (3.5 psig)

The pressure transducers will be mounted on the airlock pressure bulkhead and will have a range of zero to 6 psig. Accuracy of these sensors is expected to be about ±4 %.

Two temperature sensors (thermistors) will be mounted on the interior surface of the expandable wall structure located at the midpoint of the structure and 180 deg apart. The range of these sensors is -50 to +150 F, with an expected operational range of 50 to 100 F.

Four additional temperature sensors (also thermistors) will be attached to the exterior surface of the expandable wall material. These will be located 90 deg apart around the periphery of the airlock. The range of these sensors is -150 to +250 F. The operational range expected is -125 to +250 F.

Electrical System

Power for the D-21 experiment will be supplied from a self-contained battery pack and from the 28-v power source of the NASA support module. The self-contained power source will be a dual pack of nickel-cadmium batteries. These batteries will supply power only for the pyrotechnics included in the D-21 design and will be used for no other purpose.

The NASA support module will provide all remaining power requirements for the D-21 experiment including telemetry power, lighting, vent valves, canister release, and control panel lighting. Table 3 presents the power profile for the D-21 experiment for various operating modes.

Mounting Structure

The mounting base structure shown in both Figures 3 and 4 is contructed of light gage aluminum sheet. The basic geometry is a cylindrical shell 34 in. in diameter and 10 in. high. Stiffener rings are provided at each end of the shell, with axial stiffeners located circumferentially around the shell.

The mounting structure provides the physical integrating function for all hardware components of the experiment. The airlock structure assembly is attached to one ring face of this structure with 24 equally spaced bolts. All subsystems exterior to the airlock itself are located within and supported on the mounting shell structure.

The physical interface between the D-21 experiment and the NASA support module is at the face of the mounting structure opposite the airlock. The mounting interface will include provision for 24 equally spaced bolts to provide optimum mounting load distribution. Physically, this interface will be made at the McDonnell Company in St. Louis, where the D-21 experiment will be installed and integrated with the NASA support module.

Experiment Control System

Controls for conducting the D-21 airlock experiment are provided in three locations:

1. A remote control panel located inside the NASA AM

TABLE 3 - POWER PROFILE (SUPPORT MODULE POWER SOURCE)

Operating mode	Duration (min)	Average load (amps)		Total load (amps)			
		Remote control panel	D-21 airlock	Average	Peak	Peaks/ mode	Peak duration
Experiment, on	5	0.36	0.50	0.86	. . .	. . .	. . .
Telemetry calibration	5	0.36	0.58	0.94	. . .	. . .	. . .
Canister release	5	0.40	0.50	0.90	1.10	1	1 min
Pressure system armed	10	0.44	1.56	2.00	. . .	. . .	. . .
Deploy	5	0.36	1.64	2.00	3.00	2	1 sec.
Proof pressure	30	0.40	1.69	2.09	3.09	2	1 sec
Ingress No. 1	40	0.44	3.86	4.30	5.30	2	1 sec
Ingress No. 2	40	0.48	3.99	4.47	5.47	2	1 sec
Start 15-day test	5	0.52	2.04	2.56	3.56	1	1 sec
15-day pressure test	15 days	0.16	0.42	0.58	. . .	. . .	. . .
Final vent	1 sec	0.16	0.42	0.58	1.58	1	1 sec

2. The D-21 control panel located inside the D-21 airlock and mounted on the pressure bulkhead

3. Emergency and/or backup controls mounted on the exterior surface of the D-21 airlock mounting base structure

The remote control panel provides the principal control method for conducting the D-21 experiment. Located in the pressurized environment of the airlock module, this control panel location will still permit implementation of the D-21 experiment in the event that possible limitations may be imposed on EVA.

The control panel located inside the D-21 airlock will not be used during the D-21 experiment. This piece of hardware is redundant to the experiment as now planned but is included in the experiment design and hardware to permit future pressurized ingress/egress demonstrations.

Backup controls are provided exterior to the D-21 and located on the base support structure. The purpose of these controls is to ensure implementation of experiment sequence performance in the event of possible malfunction of the primary control system operated from the remote control panel.

Remote Control Panel - The remote control panel will be located within the airlock section of the NASA AM. This panel, along with appropriate interconnect wiring to the D-21 experiment, will be supplied and installed by McDonnell in conformance with overall experiment design requirements. This panel, diagrammed in Figure 14, incorporates the following controls and indicators:

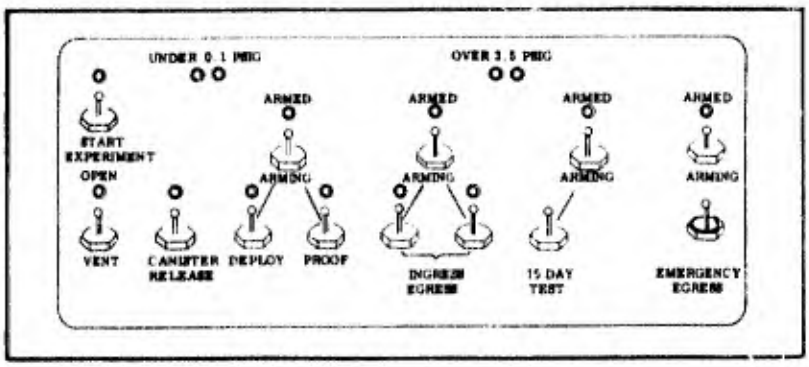

Figure 14 - Remote Control Panel

1. START EXPERIMENT switch to energize panel lighting and indicators on all control panels, the electrical vent control, and the pressure and temperature telemetry sensors in the D-21 airlock

2. VENT switch to control the electrical airlock vent. An indicator light is on when the airlock vent valve is open

3. CANISTER RELEASE switch to release the airlock restraints system, which permits the airlock to deploy

4. ARMING switch to arm the pyrotechnic gas release valves of the pressurization system. An indicator light will come on when the system has been armed

5. DEPLOY switch to actuate pyrotechnic valve for release of gas to deploy the airlock

6. PROOF switch to actuate pyrotechnic valves for release of gas from two bottles into the airlock for proof pressure test

7. D-21 LIGHTS switch to illuminate the interior of the D-21 airlock. Two 21-candle power lamps are provided for this purpose

8. INGRESS/EGRESS switches, one for each ingress/egress pressurization, to actuate pyrotechnic release valves to release gas into the D-21 airlock for two ingress/egress tests

9. 15-DAY TEST switch to actuate pyrotechnic release valve to release gas into the D-21 airlock for the 15-day pressure/exposure test

10. High-pressure dual indicator light that goes on when pressure in the D-21 airlock exceeds 3.5 psig, the normal operating pressure

11. Low-pressure dual indicator light that goes on when pressure in the D-21 airlock is less than 0.1 psig, at which time the airlock hatch can be opened

12. An emergency egress system is provided for rapid venting and subsequent jettisoning of the D-21 airlock hatch. An ARMING switch is provided for arming the squibs of the emergency vent valve and the emergency jettison of the airlock hatch. An EMERGENCY EGRESS switch activates the emergency airlock vent and jettisons the airlock hatch.

D-21 Airlock Internal Control Panel - This panel, shown in Figure 15, is located inside the D-21 airlock and is mounted on the pressure bulkhead assembly and has the following controls:

1. VENT switch to control operation of the electrical airlock vent

2. ARMING switch to arm the pyrotechnic valve squibs of the two ingress/ingress pressurizing gas bottles

3. INGRESS/EGRESS switches to release gas into the D-21 airlock for the two ingress/egress tests

4. High-pressure dual indicator lights that go on when pressure in the D-21 airlock exceeds 3.5 psig, the normal operating pressure

5. Low-pressure dual indicator lights that go on when pressure in the D-21 airlock is less than 0.1 psig, at which time the airlock hatch can be opened

6. MANUAL VENT to vent mechanically the airlock in case of malfunction of the electrically operated vent

7. EMERGENCY EGRESS has the same function as those controls provided on the remote control panel

Backup Controls - In addition to the experiment controls, there also are some local backup controls provided on the exterior surface of the D-21 supporting base structure. A diagram of these controls is shown in Figure 16, with the following functions:

1. MANUAL RESTRAINT RELEASE to release the airlock canister restraint in case of malfunction of the electrical restraint release.

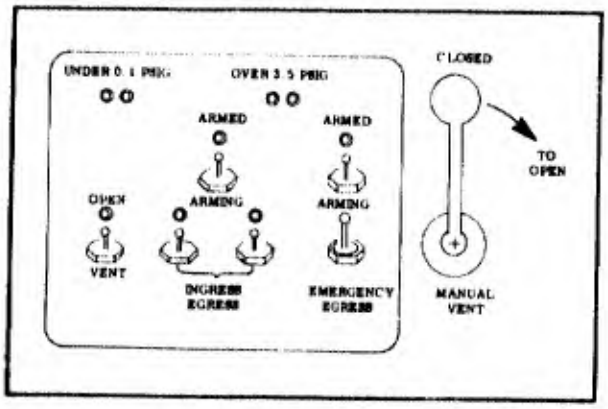

Figure 15 - D-21 Airlock Internal Control Panel

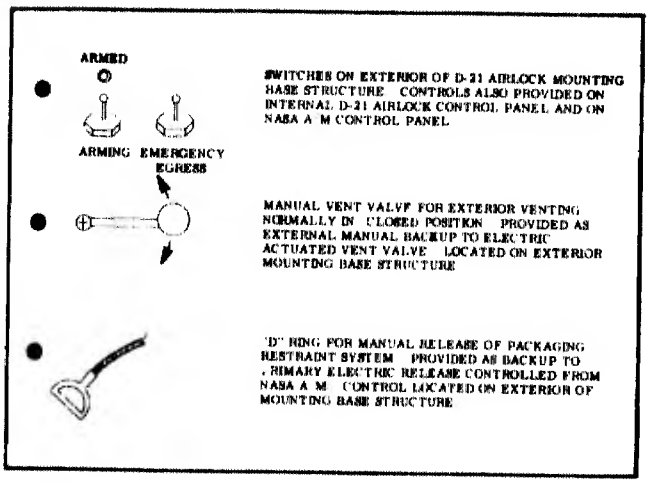

Figure 16 - Miscellaneous External Controls of D-21 Airlock

2. MANUAL VENT VALVE, located on the exterior of the airlock base, to vent the airlock from outside in the event of malfunction of the electrically operated vent.

3. EMERGENCY EGRESS has the same function as those controls provided on the remote control panel.

EXPERIMENT PROCEDURES

Procedures for conducting the D-21 experiment have been established consistent with attaining the objectives stipulated for the orbital test demonstration.

Deployment will be demonstrated to evaluate the effects of launch and boost on structure packaging and to evaluate deployment dynamics on the airlock structure. Proof pressure will next be tested to ensure and to establish structural integrity prior to initiating manned operations.

Astronaut ingress/egress will be demonstrated to evaluate the compatibility of expandable elastic recovery materials in airlock designs with the dynamics involved in operational use. The objective is to determine if material stiffness is adequate for airlock designs and to evaluate the effects of stiffness on ingress/egress performance by the astronaut.

A 15-day long-term exposure test will be conducted with the airlock under pressure. Multiple objectives of the D-21 program will be achieved by this test sequence in the experiment procedures. First, the test results will be used to evaluate the performance of expandable materials in operational use when subjected to the total combined effects of the orbital environment. Second, the test results will be used to establish parameters and requirements for future specific airlock designs. Third, this 15-day test will be used to establish a baseline from which other applications of expandable structures technology can be extrapolated.

The final sequence in the experiment procedures is a revisitation mission six months subsequent to the initial launch. The purpose of this final phase is to evaluate space environment effects on expandable materials after prolonged exposure. This evaluation will consist essentially of earth return of a material specimen with subsequent laboratory analysis.

The procedures to be followed in conducting the D-21 airlock experiment are presented as a functional sequence diagram in Figure 17 and in the experiment procedures summary below. The total elapsed time required to conduct the overall experiment is estimated at 191.4 min. The total EVA requirements for each of two astronauts required to perform the experiment are estimated at 166.1 min.

The experiment procedures are to be conducted in three distinct time periods or phases:

1. Phase I - Deployment and structural test demonstration
   a. Total elapsed time - 52.8 min
   b. Total EVA (each of two crewmen) - 30.9 min
2. Phase II - Astronaut ingress/egress demonstration
   a. Total elapsed time - 93.1 min
   b. Total EVA (each of two crewmen) - 91.8 min
3. Phase III - Postenvironment exposure examination
   a. Total elapsed time - 45.5 min
   b. Total EVA (each of two crewmen) - 43.4 min

A revisitation mission to the SIVB orbital workshop will be conducted approximately six months subsequent to the initial experiment. During this visit, another postenvironment exposure examination will be conducted in accordance with the procedures and time estimates stipulated for Phase III.

The experiment procedures summary follows:

1. Phase I - Deployment (EVA 30.9 min, elapsed time 57.8 min
   a. Depressurize AM
   b. Crewman Number 1 (CM1) moves to anchoring station outside thermal curtain and photographs

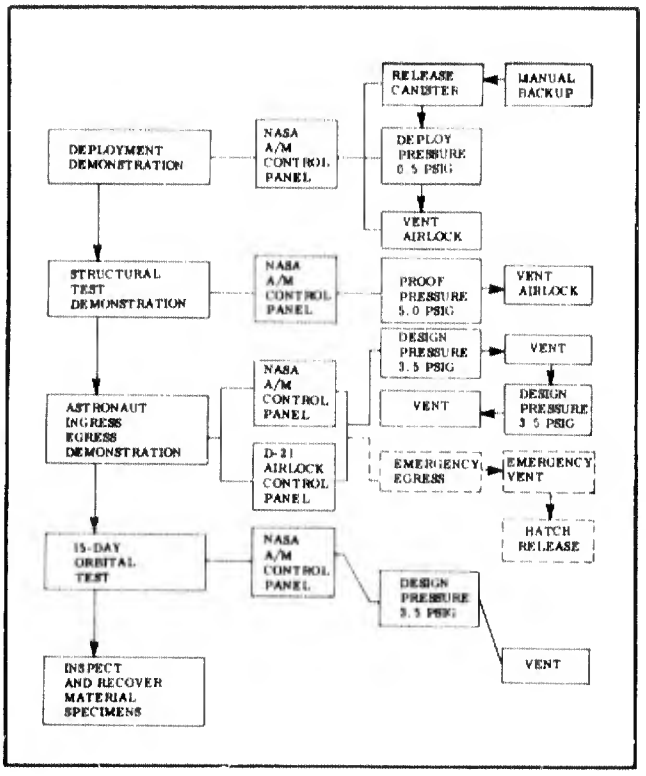

Figure 17 - Experiment Procedures Diagram

deployment while CM2 controls deployment from inside the AM

c. CM1 visually inspects D-21

d. CM1 photographs D-21 as CM2 initiates proof-pressure test

e. CM1 returns to AM

f. AM is sealed and repressurized

g. Proof pressure test will continue for at least 30 min before Phase II begins

2. Phase II - Ingress/egress demonstration (EVA 91.8 min, elapsed time 93.1 min

a. Depressurize AM

b. CM1 moves to anchoring station outside thermal curtain

c. CM1 photographs D-21 as CM2 activates depressurization valve from inside AM

d. CM1 moves to D-21 and works hatch between pressurization cycles initiated by CM2 and examines seal during D-21 pressurization

e. CM1 and CM2 both move to anchoring station where camera is transferred to CM2

f. CM2 photographs CM1 during two ingress/egress cycles conducted without D-21 pressurization

g. Both CM1 and CM2 return to AM

h. AM is sealed and repressurized

3. Phase III - Postenvironment exposure examination

a. Depressurize AM (EVA 43.4 min, elapsed time 45.5 min)

b. CM1 moves to anchoring station and photographs D-21 as CM2 activates D-21 depressurization switch

c. CM1 moves to D-21 and visually examines interior and exterior surface and actuation at hatch, photographing where appropriate

d. CM1 receives sample patches and returns to AM

e. AM is sealed and repressurized

4. Revisitation

a. Same as a. above

b. CM1 moves to anchoring station and photographs D-21

c. Same as c. above

d. Same as d. above

e. Same as e. above

DATA AND INSTRUMENTATION

Data from the D-21 experiment will be obtained from all sources available on the SIVB flight. These data will include photographic coverage, astronaut voice recordings, biomedical data pertaining to ingress/egress maneuvers, and airlock temperature and pressure data via telemetry.

Photography (16 mm Color)

Movie coverage of the D-21 experiment is requested. Table 4 gives this film coverage. Movie coverage by portable hand-held cameras is desirable. Photographic coverage will be effected from either the MDA or the Apollo CSM if viewing areas are appropriate. Fixed camera mounting also can be used. However, this method is least desirable.

TABLE 4 - MOVIE COVERAGE OF D-21 EXPERIMENT

Experiment period	Time (min)	Frames per second
Airlock canister release	1	16
Pressure deployment	5	6
Ingress/egress demonstration	30	1
Postenvironment inspection, end of 15-day test	3	1

Voice Recording

A voice recording of astronaut comments concerning the D-21 experiment is being requested. The recording will cover all phases of EVA appropriate to the experiment procedures. The total period involved is 191.4 min; recording has been requested to cover the entire period.

Biomedical Data

Biomedical data have been requested during the astronaut ingress/egress portion of the D-21 experiment. No special data are required. Only those data normally recorded during the SIVB orbital workshop flight will be obtained.

Telemetry data follows:

Telemetry

1. Data channels (eight analog data items can be commutated)
   a. Two pressure
   b. Six temperature
2. Temperature (inner surface of D-21 airlock)
   a. Two sensors 180 deg apart
   b. Range - -50 to +150 F
   c. Operating range - 0 to 100 F
   d. Accuracy - ±1 percent
   e. Vendor - Yellow Springs Instrument Company, Part No. 427
3. Temperature (outer surface of D-21 airlock)
   a. Four sensors 90 deg apart
   b. Range - 150 to 250 F
   c. Operating range - 125 to 250 F

d. Accuracy - ±1 percent

e. Vendor - Rosemont Engineering, similar to Part No. 118L(Goodyear Aerospace Specification Control 66QS1293)

4. Pressure of D-21 airlock

a. Two sensors on pressure bulkhead

b. Range - 0 to 6.0 psig

c. Accuracy - ±4 percent

d. Vendor - Fairchild Controls, similar to Part No. TP-200-948A491 (Goodyear Aerospace Specification Control 66QS1294)

5. Sensor output signal range (all channels)

Zero to 5 v, dc

6. Data channel frequency response

Two cycles per second (minimum)

7. Data sampling rate

a. Continuous (from start of experiment to start of 15-day test)

b. 5 sec/4 hr (first two days of 15-day test)

c. 5 sec/12 hr (remaining 13 days of 15-day test)

SUMMARY OF DEVELOPMENT SCHEDULES AND TESTS

The hardware development schedule is shown in Figure 18. Four sets of experiment hardware will be fabricated in addition to two mockup units that will represent the packaged and deployed hardware configurations. The first hardware unit will be used for qualification testing. This test unit will be shipped to WPAFB after qualification tests have been completed for continued structural testing to destruction. The second hardware unit will be used during astronaut training for experiment procedures.

Two flight units will be fabricated. These are scheduled for delivery 1 March and 1 April of 1968. Flight hardware along with aerospace ground equipment will be shipped to McDonnell for final integration of the D-21 experiment.

Table 5 shows the sequence of testing to be performed and the facility where testing will be done. All space environment testing will be conducted at AEDC (Arnold Engineering Development Center). Table 6 summarizes the specific types of space environment tests to be performed. These tests all will be performed under vacuum conditions with varying thermal environment and airlock pressures to simulate the extremes of the conditions anticipated for the D-21 experiment.

Qualification test requirements for the D-21 experiment represent a

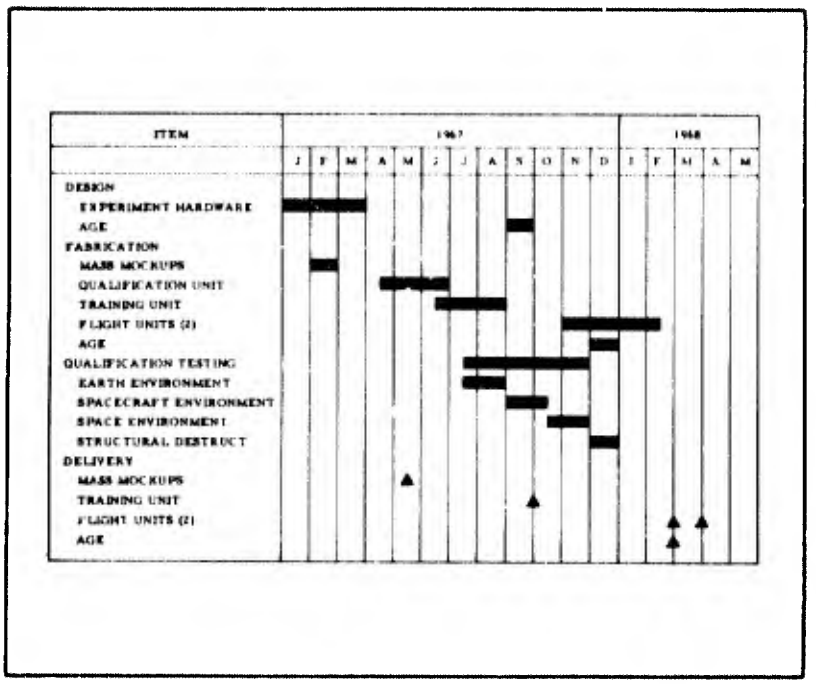

Figure 18 - Hardware Development Schedule

TABLE 5 - TEST SEQUENCE AND FACILITY

Test	Test facility
Functional-operational	Goodyear Aerospace
Humidity	Goodyear Aerospace
High temperature	Goodyear Aerospace
Low temperature	Goodyear Aerospace
EMI compatibility	Goodyear Aerospace
Electrical compatibility	Goodyear Aerospace
Magnetic fields	Goodyear Aerospace
Salt fog	Wylie Labs
Acoustic noise	Wylie Labs
Shock	Goodyear Aerospace
Acceleration	AEDC
Vibration	AEDC
Space environment	AEDC
Fungus	Wylie Labs

TABLE 6 - SPACE ENVIRONMENT TESTS

Test	Airlock pressure	Environmental conditions	Conditions
Launch	Packaged	Vacuum	Packaged airlock installed in test chamber. Maximum available vacuum applied to chamber in two-minute time span.
Operational	0	Vacuum: 1×10^{-6} mm Hg Temperature: -65 F	Airlock, in a packaged configuration, to be placed in the space chamber and required conditions obtained. Canister to be ejected and unit deployed and inflated.
Endurance	0	Vacuum: 1×10^{-6} mm Hg Temperature: -150 F	With zero pressure in airlock, subject unit to environment for 12 hr.
Cycling	0 to 5.25 psi	Vacuum: 1×10^{-6} mm Hg Temperature: -150 F	Cycle pressure in the airlock 30 times. Minimum internal temperature is -50 F.
Endurance	5.25 psi	Vacuum: 1×10^{-6} mm Hg Temperature: -150 F	With 5.25 psi in airlock, proof pressure unit for 12 hr and conduct leak test. Minimum interval temperature is -50 F.
Endurance	0	Vacuum: 1×10^{-6} mm Hg Solar radiation	With zero pressure in airlock, subject unit to solar radiation impinging on top surface of airlock.
Cycling	0 to 5.25 psi	Vacuum: 1×10^{-6} mm Hg Solar radiation	Cycle pressure in the airlock 30 times. Solar radiation impinging on side surface of airlock. Maximum internal temperature is +150 F.
Endurance	5.25 psi	Vacuum: 1×10^{-6} mm Hg Solar radiation	With 5.25 psi in airlock, proof pressure unit for 12 hr and conduct leak test. Solar radiation impinging on side surface of airlock. Maximum internal temperature is +150 F.
Emergency egress	. . .	Vacuum: 1×10^{-6} mm Hg Temperature: -150 F	Operate emergency egress system.

comprehensive and extensive testing program. Successful completion of this program will be a significant achievement in itself and certainly will indicate successful performance of the D-21 airlock in orbit.

CONCLUSIONS

Conclusions of the D-21 experiment follow:

1. Flight demonstration of the elastic recovery structure is the next logical and needed step in the timely development of the expandable structures for manned space flight applications.

2. The D-21 experiment hardware can meet the space experiment schedule and requirements.

3. The experiment procedures as defined will achieve all the experiment objectives.

SESSION III

BUCKLING RESISTANCE OF INFLATED CYLINDERS IN BENDING

A. D. Topping*

INTRODUCTION

The first expandable aerospace structure was the free balloon, an inflatable type. The first balloons were approximately spherical and practically pressureless. When the need to give the balloon dirigibility led to streamlining, there was some difficulty in maintaining the shape of the balloon under the aerostatic and aerodynamic forces it encountered (see Figures 1 through 4).[1**] Two solutions to this problem developed. One solution (by Count Zeppelin) was to house the balloons inside a rigid framework, whereupon the airship ceased to be an expandable structure. The other solution was to use a higher pressure in the envelope of the airship (as dirigible balloons are called; all airships flying today are pressure airships). Increasing the pressure also increases the tensile stresses; perhaps the first problem in optimizing an expandable structure, then, was to determine the minimum pressure necessary for its proper functioning and safety. Today, the aerospace industry deals with other applications and other shapes. But determining pressure is still the first order of business in the design of any inflatable structure, and the cylinder remains an important basic inflatable configuration element.

In preliminary design, the maximum bending moment that an inflated membrane cylinder can carry often is assumed to be that bending moment required to reduce the stress in an outer fiber to zero according to the Navier hypothesis, which was shown by Haas[2] in 1912 to be applicable with reasonable accuracy to an inflated fabric cylinder. The cylinder will, however, carry appreciably more bending moment than this, although Burgess[3] (in 1930) spoke of the "impossibility of a bending moment producing by itself longitudinal forces greater than pR/2." Burgess's statement implies that

$$M_c = M_{wr} = \frac{p\pi R^3}{2} . \tag{1}$$

But if one supposes a constant cross section with all but one outermost fiber is wrinkled and ineffective, then this fiber carries the load $p\pi R^2$. The maximum resisting moment is

$$M_c = p\pi R^3 = 2M_{wr} . \tag{2}$$

More recently, Leonard, Brooks, et al.,[4, 5, 6] have argued that this equation should give both an upper and lower bound to the collapse moment for a

---

*Senior engineer specialist (stress), Goodyear Aerospace Corporation, Akron, Ohio.

**Superior numbers in the text refer to items in the List of References.

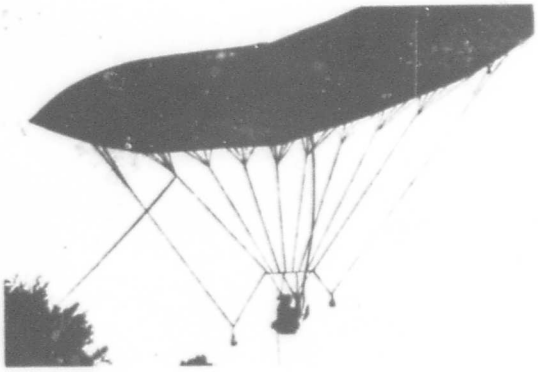

Figure 1 - Collapse of Santos-Dumont's Airship No. 2, 11 May 1899 (First Phase)

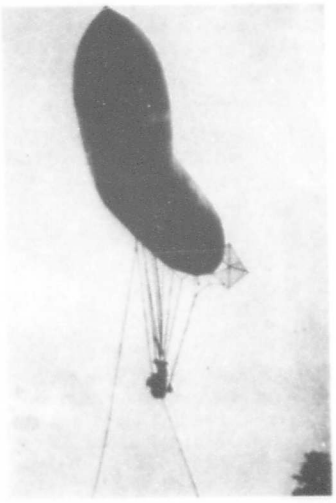

Figure 2 - Collapse of Airship No. 2 (Second Phase)

Figure 3 - Collapse of Airship No. 2 (Third Phase)

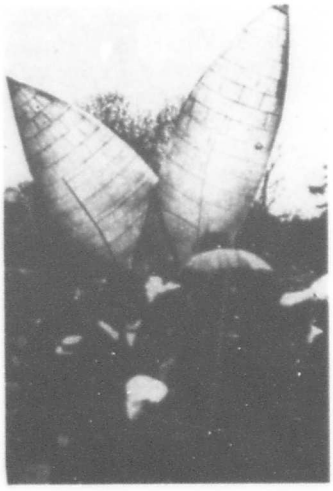

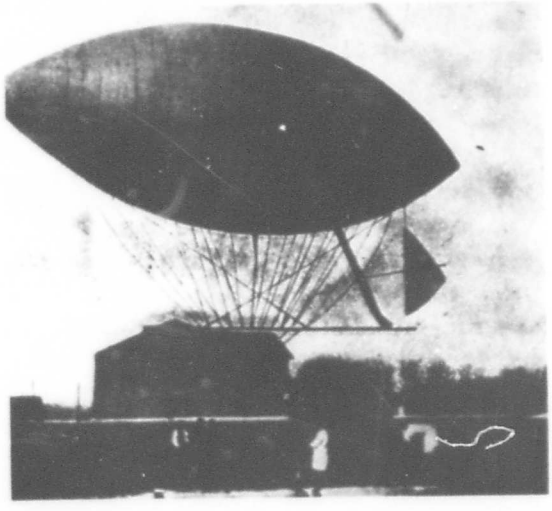

Figure 4 - Santos-Dumont's Airship No. 3

pressurized circular cylinder if the skin has no bending stiffness. Stein and Hedgepeth[7] arrived at the same result by an independent method. An obvious objection is that, as the area of the unwrinkled periphery approaches zero, the unit stress in the outermost fiber approaches infinity. Failure would be expected, therefore, to occur by rupture of the material; yet cylinders can be and have been collapsed in pure bending without rupture.

The paradox can be explained by considering that the cross section does not remain constant but is reduced in area locally by the wrinkle or wrinkles. Goodyear Aerospace studied the collapse problem from this point of view in 1954 and 1955 with encouraging results; this study is reported in Reference 8. The theory will be racapitulated before additional work is discussed.

POSTWRINKLING BEHAVIOR - AREA CONSTANT

First, some relationships will be established assuming the area of the cross section remains circular and does not change. If no longitudinal stress can be carried across the wrinkled part of the cross section, the centroidal axis of the unwrinkled periphery shifts by some amount, e. If the envelope is thin and of constant thickness, the properties of a line can be dealt with and the following obtained from Figure 5:

$$\left.\begin{aligned} e &= \frac{R \sin \beta}{\beta} \\ I &= R^3 \left(\beta + \frac{\sin 2\beta}{2}\right) - 2R\beta e^2 \\ c_1 &= e - R \cos \beta \\ s &= 2R\beta \end{aligned}\right\} \qquad (3)$$

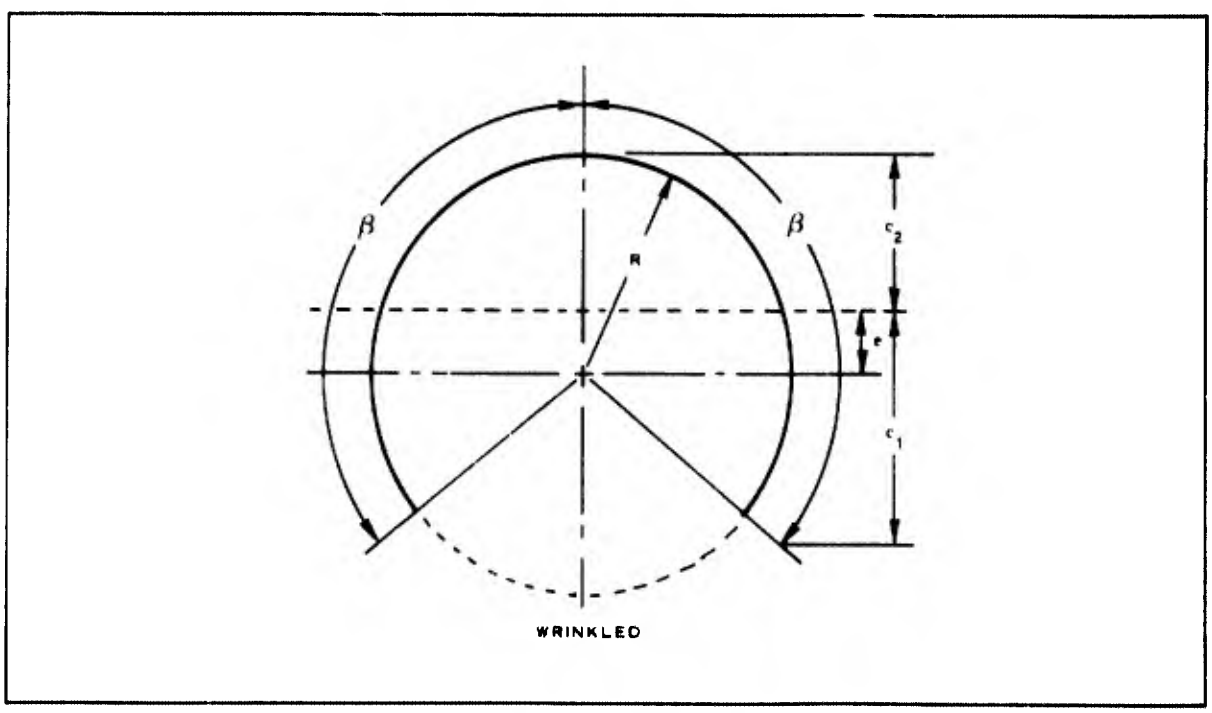

Figure 5 - Wrinkled Cylinder Cross Section

As the centroidal axis shifts, a relieving moment is created by the internal pressure equal to

$$M_{eo} = pA_o e. \tag{4}$$

The bending moment that can be resisted by the unwrinkled portion of the envelope is

$$M_{uo} = \frac{pA_o I}{sc_1} , \tag{5}$$

and the total resisting moment is

$$M_o = M_{eo} + M_{uo} . \tag{6}$$

By using Equations 3 through 6, one obtains

$$\frac{M_o}{p\pi R^3} = \frac{\sin \beta}{\beta} + \frac{2\beta^2 + \beta \sin 2\beta - 4 \sin^2 \beta}{4\beta (\sin \beta - \beta \cos \beta)} . \tag{7}$$

Since

$$f_{eo}t = \frac{pA_o}{s} = \frac{M_{eo}}{es} , \tag{8}$$

the maximum stress is

$$f_o t = \frac{M_{eo}}{es} + \frac{M_{uo} c_2}{I} . \tag{9}$$

With the help of Equations 3, 4, and 5, a nondimensional stress, $f_o t/p\pi R$, can be obtained as a function of β and hence of M_o.

Strains due to circumferential stress have no effect on wrinkling if the ends of the cylinder are assumed free to move longitudinally. If plane sections remain plane, the displacements of the outermost wrinkled fiber should correspond to

$$Et\epsilon_{wr} = \frac{pA_o}{s} - \frac{M_{uo}(R + e)}{I} . \tag{10}$$

When this strain is negative, wrinkling has occurred, and its magnitude determines the size of the wrinkle. Expressed in terms of β with the help of Equation 8, Equation 10 becomes

$$\frac{Et\epsilon_{wr}}{p\pi R} = \frac{M_{uo}(1 + e/R)}{p\pi R^3 \left| \beta + \frac{\sin 2\beta}{2} - 2\beta (e/R)^2 \right|} - \frac{M_{eo}}{2p\pi R^3 \sin \beta} . \tag{11}$$

POSTWRINKLING BEHAVIOR - AREA REDUCED BY WRINKLE

If the form of the wrinkle is assumed to be that of a sine wave,

$$y = a \sin x . \tag{12}$$

Then, since y is maximum when sin x = 1, $a = y_{max}$ and the total wave height is 2a. The length of the sine wave is (for $0 \cdot x \cdot 2\pi$)

$$\ell = 4(1 + a^2)^{1/2} E(k), \tag{13}$$

where E(k) is a complete elliptic integral of the second kind with

$$k^2 = \frac{a^2}{1 + a^2} . \tag{14}$$

By proportion, one can write

$$\frac{\ell}{2\pi} = \frac{1 + \epsilon_{wr}}{1} \text{ or } \frac{1}{1 - \epsilon_{wr}} . \tag{15}$$

For small strains, there is no significant difference between these alternate expressions. For large strains, the second expression may seem preferable, but the first expression is used in the discussion that follows on the grounds that the strains be referred to the base of the wave and not to its curved length. Further, from the properties of the assumed sine curve

$$\frac{a}{\pi} = \frac{h}{b} . \tag{16}$$

From Equations 13 and 15,

$$\pi(\epsilon_{wr} + 1) = 2(1 + a^2)^{1/2} E(k); \tag{17}$$

thus, the wrinkle height can be found if b is known. $R(1 + \cos \beta)$ - see Figure 5 - cannot be assumed to be h, since β does not depend on the material stiffness, E, as ϵ_{wr} does. An assumption must be made here as to the wrinkle pattern. Assume that the buckle is as wide as it is long (thin sheet metal cylinders buckle this way: see Reference 6); then

$$b = 2R\delta . \tag{18}$$

If the bottom of the wrinkle is straight and R does not change significantly,

$$h = R(1 - \cos \delta) . \tag{19}$$

From Equations 16, 18, and 19 is obtained

$$\frac{1 - \cos\delta}{2\delta} = \frac{a}{\pi} . \tag{20}$$

This equation can be solved for δ by trial, the value, a, being known from Equation 17. Given δ, the new cross-sectional area can be found from

$$A = R^2(\pi - \delta + \sin\delta\cos\delta). \tag{21}$$

The centroid of this area is no longer at the center of the original circle but at a distance from it, e_A, where

$$\frac{e_A}{R} = \frac{2\sin^3\delta}{3(\pi - \delta + \sin\delta\cos\delta)} . \tag{22}$$

Then the resisting moment is

$$M = pA\left(e - e_A + \frac{I}{sc}\right). \tag{23}$$

It follows that

$$\frac{M}{p\pi R^3} = \frac{A}{A_o}\left(\frac{M_o}{p\pi R^3} - \frac{e_A}{R}\right) . \tag{24}$$

From the equations given, the resisting moment can be found as a function of β for various values of the parameter pR/Et. If Equation 11 is used to find ϵ_{wr}, the result will be slightly conservative since the stresses (and hence ϵ_{wr} and δ) will appear larger than an exact theory would indicate.

Note that ϵ_{wr} cannot exceed 1.0, since that would mean that the fabric is sliding over itself instead of forming a sine wave. But there is another limitation. If Equation 20 is differentiated and the result is set equal to zero,

$$\frac{1 - \cos\delta}{\delta} - \sin\delta = 0. \tag{25}$$

The value of δ satisfying Equation 25 is approximately 2 1/3 radians and must be a maximum. This limits h/b and in turn ϵ_{wr} and shows that the determination of ϵ_{wr} from the constant-area equation is far from accurate when δ approaches this angle. The solution provides, nevertheless, a lower bound, and the constant-area solution provides an upper bound. If desired, better approximations of ϵ_{wr} can be made when M has been found as $f(\beta)$, and the calculation repeated until satisfactory agreement is obtained.

Equation 24 is plotted in Figure 6 for several values of pR/Et. The constant-area solution represents the case pR/Et = 0. Figure 7 shows the effect of pR/Et on the maximum longitudinal tension that can be applied to a fabric cylinder in pure bending.

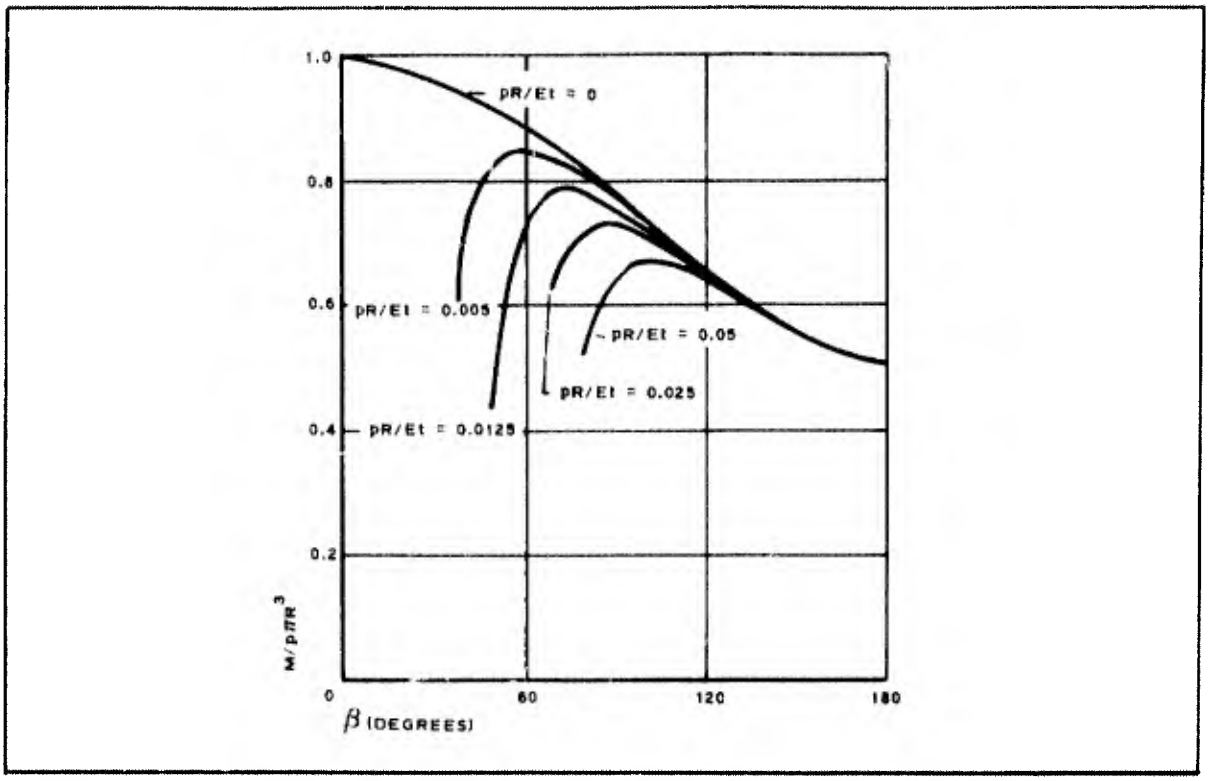

Figure 6 - Collapsing Moments for Inflated Cylinders as a Function of Unwrinkled Periphery

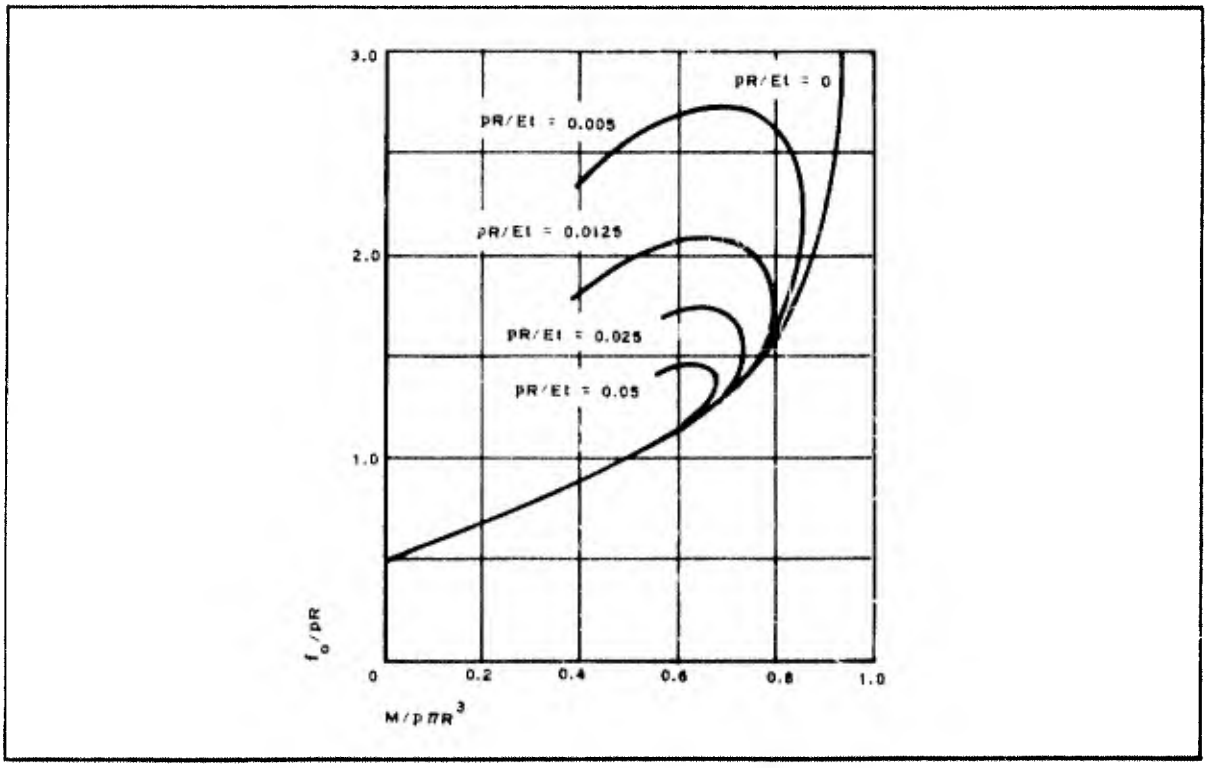

Figure 7 - Maximum Tensile Stress as a Function of Bending Moment and pR/Et

EXPERIMENTAL INVESTIGATION

The original experimental work reported in Reference 8 and supporting the theory was performed on a single cotton-neoprene fabric cylinder. Additional tests were made with two purposes in mind: (1) to get additional confirmation of the theory and (2) to investigate the effect of packaging on subsequent collapse resistance.

The specimens were all made to the same nominal size, 5 in. in diameter and with 26 in. of free length between end blocks. The cylinders were secured to wooden end blocks by two clamps at each end. Figure 8 shows the Dacron-neoprene specimen under load. Pure bending moments were applied by hanging equal loads, P (in this case bags of shot), 10 in. from the attach points for the support cables, which were about 20-ft long. The cable length ensured that no significant longitudinal tension would be introduced into the specimen. Angular deflections, θ, were measured by means of protractors at both ends to evaluate (1) the flexural stiffness, EI, and (2) the moment arm of the applied couple (10 cos θ in.). The pressure was held constant during each test.

The materials used were as follows (two cylinders of each, one packaged):

1. Dacron-neoprene - Code N363A10, single ply; 7 oz/sq yd; specification strength 170 × 150 lb/in.; base cloth Code 477 (4 oz/sq yd, plain weave, 220 × 220 denier, 60 × 55 count); fill longitudinal
2. Metal fabric - Type 304 stainless steel cloth, single ply; monofilament, 200 × 200 count, 0.0016-in. diameter wire; silicone coating; warp longitudinal
3. Mylar - 1/2-mil thick (0.0005 in.); roll direction longitudinal

For simulated packaging, each cylinder was pressed flat and creasing at the seams was avoided. Each cylinder then was folded once with a lengthwise crease and finally folded accordion style into a square package. The folded packages were subjected to 11.53 psi by a vacuum-bag method for five days before being fitted with the wooden end pieces for testing. The packaged volume was obtained by making a mold around the packaged specimen and later measuring the amount of mercury the mold would hold. The packaging ratios (package volume over theoretical volume) were Mylar, 1.218; Dacron-neoprene, 1.186; and stainless steel-silicone 1.122.

For the bending test, the pressures were selected to give a nominal safety factor of 4.0 on the hoop tension. Table 1 gives the basic input data for the tests. Loads were applied in increments of 0.5, 1.0, or 7.5 lb depending on the test pressure (which was lowest for the Mylar and highest for the Dacron-neoprene cylinder). Figure 9 shows typical resulting angular deflection diagrams, normalized by using M/M_{wr} as the ordinate. Tests were repeated five times; results are summarized in Table 2.

Packaging reduced the effective flexural modulus, averaged from five repetitions of load, by five or ten percent. On the first test, where the

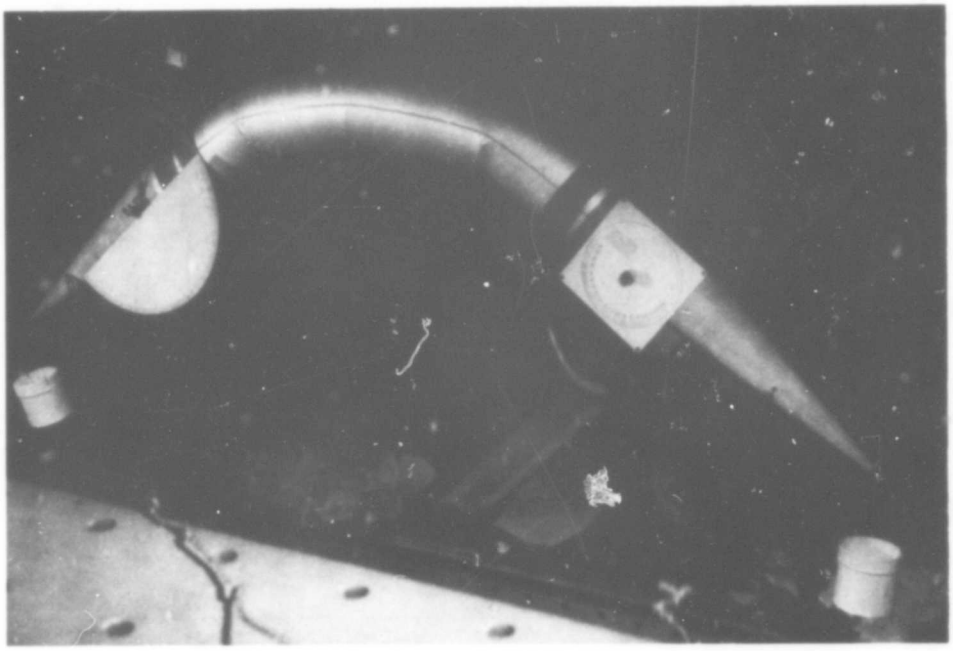

Figure 8 - Unpackaged Dacron Bending Specimen at Near Collapse Load

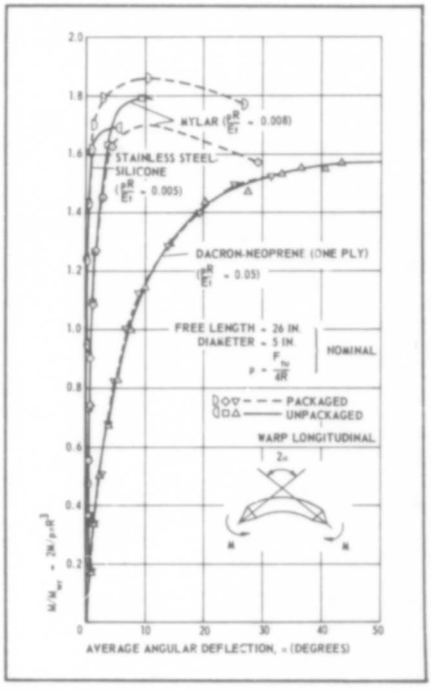

Figure 9 - Moment-Deflection Relations for Inflated Cylinders in Pure Bending

TABLE 1 - INPUT PARAMETERS FOR BENDING TESTS

Dacron	Metal	Mylar
p = 17.0 psig	p = 4.20 psig	p = 1.10 psig
t = 0.0082 in.	t = 0.0081 in.	t = 0.0005 in.
Unpackaged L = 26.00 in.	Unpackaged L = 26.00 in.	Unpackaged L = 26.125 in.
Unpackaged 2R = 5.123 in.	Unpackaged 2R = 5.043 in.	Unpackaged 2R = 5.031 in.
Packaged L = 26.125 in.	Packaged L = 26.00 in.	Packaged L = 26.00 in.
Packaged 2R = 5.14 in.	Packaged 2R = 5.04 in.	Packaged 2R = 5.045 in.
Unpackaged M_{wr} = 448.8 in./lb	Unpackaged M_{wr} = 105.8 in./lb	Unpackaged M_{wr} = 27.5 in./lb
Packaged M_{wr} = 453.3 in./lb	Packaged M_{wr} = 105.6 in.	Packaged M_{wr} = 27.7 in./lb

TABLE 2 - COLLAPSING MOMENT OF INFLATED CYLINDERS VERSUS pR/Et

		Unpackaged						Packaged					
Material	Test no.	$p\pi R^3$	pR	M_c	$\frac{M_c}{p\pi R^3}$	$\frac{pR}{Et}$	$\frac{pR}{Et}$	$p\pi R^3$	pR	M_c	$\frac{M_c}{p\pi R^3}$	Et	$\frac{pR}{Et}$
Dacron	1	897.6	43.55	705	.785	831	.0524	906.6	43.69	715	.789	925	.0472
	2	897.6	43.55	705	.785	1201	.0363	906.6	43.69	730	.805	861	.0507
	3	897.6	43.55	705	.785	978	.0445	906.6	43.69	730	.805	957	.0457
	4	897.6	43.55	705	.785	906	.0481	906.6	43.69	730	.805	949	.0460
	5	897.6	43.55	705	.785	961	.0453	906.6	43.69	730	.805	941	.0464
Metal	1	211.6	10.59	179	.846	4200	.0025	211.2	10.58	196	.928	5151	.0021
	2	211.6	10.59	170	.803	2650	.0040	211.2	10.58	170	.805	1784	.0059
	3	211.6	10.59	170	.803	1796	.0059	211.2	10.58	170	.805	1923	.0055
	4	211.6	10.59	170	.803	2967	.0036	211.2	10.58	170	.805	1784	.0059
	5	211.6	10.59	170	.803	2730	.0039	211.2	10.58	170	.805	2184	.0048
Mylar	1	55.0	2.767	49.3	.895	376	.0074	55.4	2.775	47	.850	326	.0085
	2	55.0	2.767	49.3	.895	374	.0074	55.4	2.775	47	.850	319	.0087
	3	55.0	2.767	49.2	.893	361	.0077	55.4	2.775	47	.850	358	.0078
	4	55.0	2.767	49.2	.893	372	.0074	55.4	2.775	47	.850	356	.0078
	5	55.0	2.767	49.3	.895	361	.0077	55.4	2.775	47	.850	333	.0083

difference would be expected to be most marked, only the Mylar showed a loss while the packaged Dacron and metal fabrics actually were stiffer than their unpackaged counterparts.

The effects of the packaging on the buckling resistance of the cylinders does not appear to be great. There is a decrease of perhaps five percent in M_c/M_{wr} for Mylar; for the metal fabric, the packaged specimen surprisingly reached a higher ratio than the unpackaged specimen by 10 percent in the first test of each, although this advantage disappeared when the tests were repeated on the same specimens. The Dacron-neoprene material evidenced no appreciable effect of packaging at all, and the differences for the other materials (in view of the metal fabric behavior) suggest that the observed variation is within the limits of experimental error. The increments of load used were such that, for the packaged Mylar, the maximum resisting moment was reached between increments; its value, therefore, had to be estimated. For the packaged Dacron, the loading was stopped apparently just short of true collapse, and a short extrapolation based on the curves for the unpackaged specimen was necessary.

Repetitions of the loadings yielded surprisingly consistent results (see Figure 10), although some permanent set was evident each time the load was removed. The metal fabric exhibited a marked decrease in Et in the first test after being buckled once, but no further decrease was observed after subsequent loadings. The other materials showed no decrease at all.

Figure 11 shows moment-deflection curves similar to the curves in Figure 9, obtained from a two-ply cotton-neoprene cylinder in tests made several years earlier using the same technique. Reference 8 describes these tests. Only one specimen was used, and the parameter pR/Et was varied by changing the pressure.

None of the moment-deflection curves in Figures 9 and 11 is linear even for $M < M_{wr}$; therefore, the modulus of elasticity, E, is not constant. A useful value of the parameter pR/Et can be obtained, however, by assuming E to be the secant modulus at the theoretical first wrinkling moment,

$$M_{wr} = \frac{p\pi R^3}{2} \quad . \tag{26}$$

Since the moment is uniform,

$$\theta = \frac{M_{wr} L}{2EI} \tag{27}$$

or

$$E = \frac{M_{wr} L}{2\theta I} \quad . \tag{28}$$

Since $I = \pi R^3 t$ and using Equation 26,

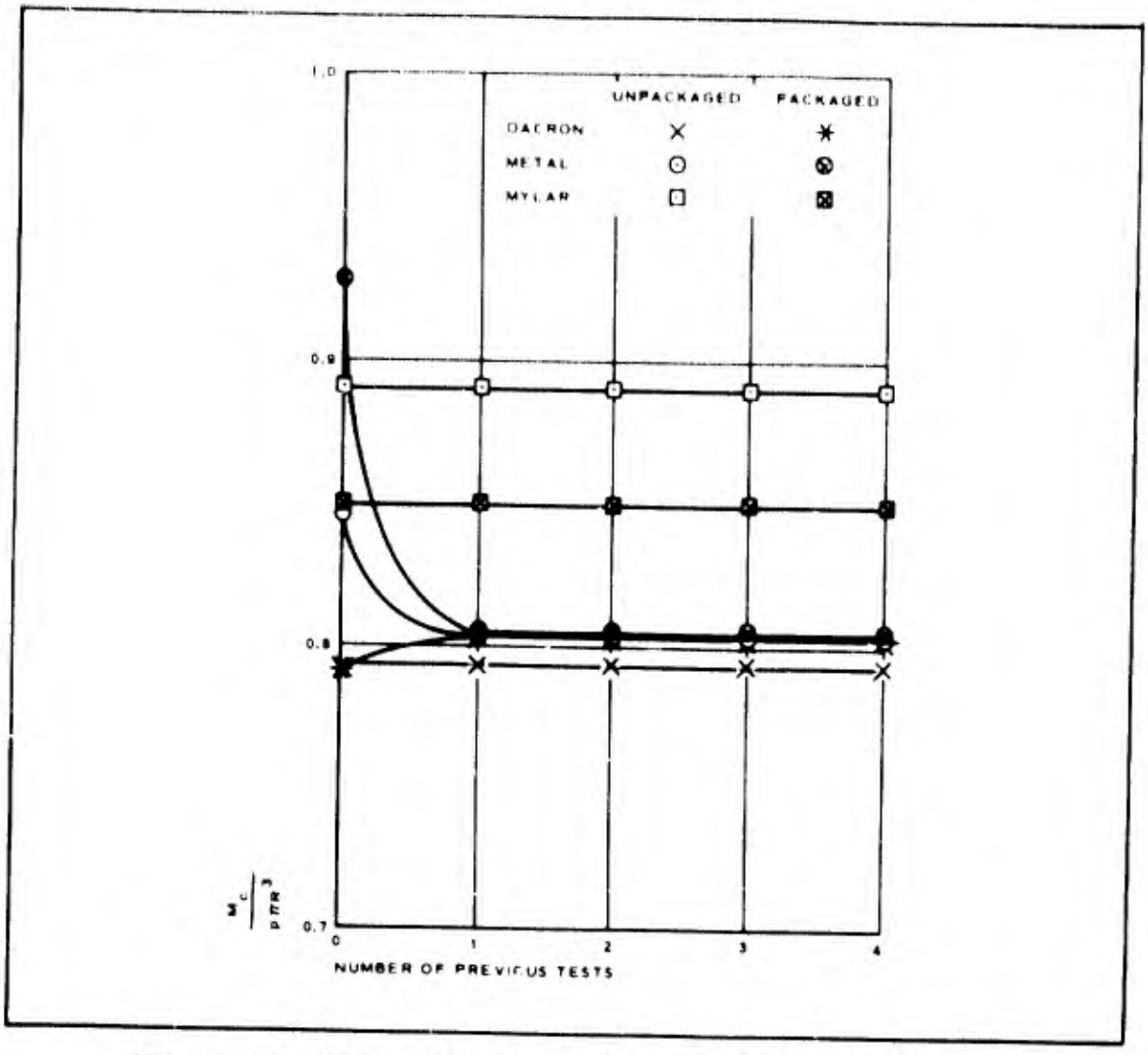

Figure 10 - Effect of Repeated Tests on Collapse Strength

$$Et = \frac{pL}{4\theta} \quad . \tag{29}$$

When there is a permanent set, θ_o, θ in Equation 29 must be replaced by $(\theta - \theta_o)$. This is the value of Et used in the parameter pR/Et to compare experiment with theory in Figure 12.

COMPARISON OF THEORY WITH TEST

Figure 12 shows a theoretical curve, obtained by plotting the maximum values of the curves of Figure 6. The test results also are shown. As found in Reference 8, the theory forms a good lower bound to all the data, except for the metal fabric specimens, which agree, nevertheless, fairly well with the theory. The Dacron-neoprene test values, on the other hand, exceed the theoretical estimate by some 15 to 20 percent. This is possibly due to the

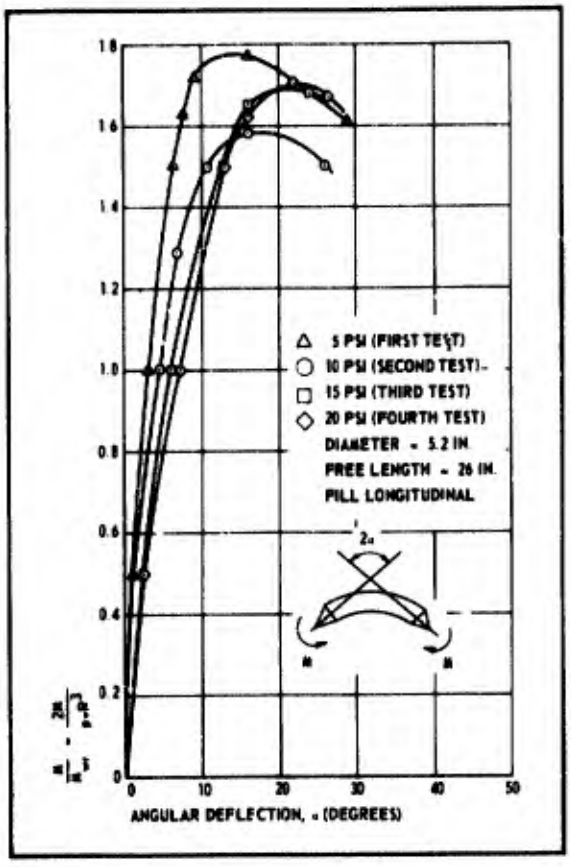

Figure 11 - Moment-Deflection Curves for a Two-Ply, Bias-Straight, Cotton-Neoprene Cylinder

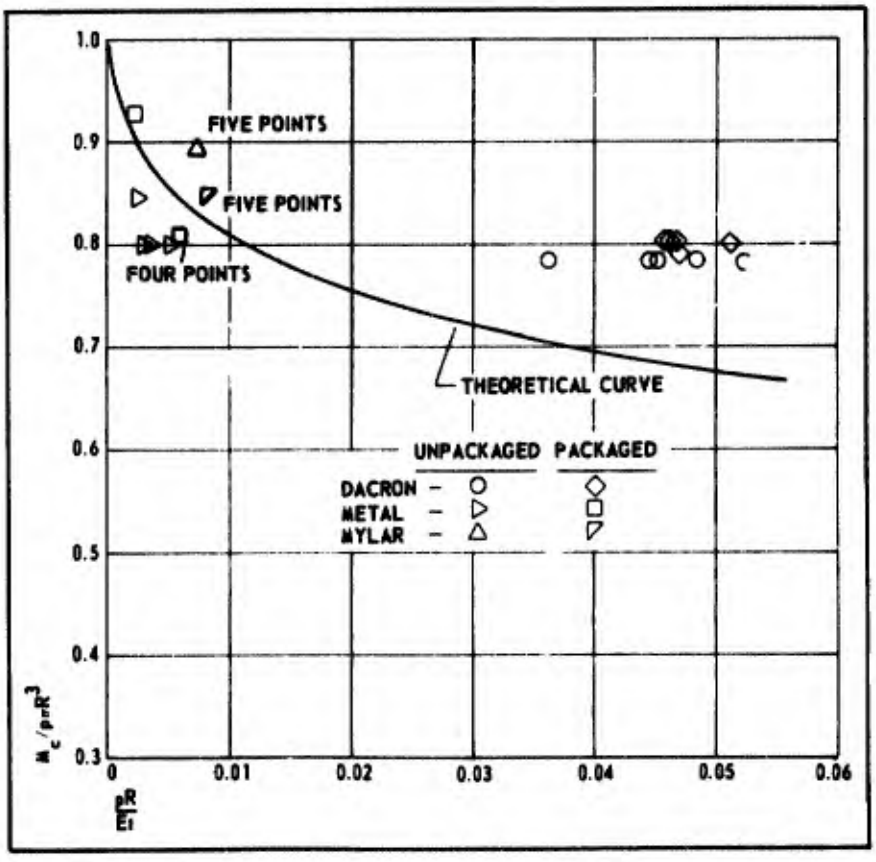

Figure 12 - Collapsing Moment of Inflated Cylinders

manner of wrinkling. The Dacron cylinders wrinkled in two or more places simultaneously (see Figure 8), whereas the theory envisions only a single wrinkle. Since length does not appear in the analysis, the cylinder is assumed to be very long. If more than one wrinkle forms, the cylinder is in effect shortened, the material available to form a wrinkle is not so great, the cross section change is less severe, and a higher collapse moment can be expected (a too-short test specimen may produce the same result). The metal fabric specimens buckled primarily at a single place (see Figure 13).

The relatively low test values of M_c/M_{wr} for the metal fabric specimens may be due to another factor. The modulus of elasticity of this material in compression (measured in a column test) was found to be less than half the flexural modulus in the first bending test. Further, after being buckled once, the apparent flexural modulus of elasticity was sharply reduced (see Table 2). The value of E in the vicinity of the wrinkle, therefore, is considerably lower than the measured E, for the modulus on the tension side of the beam would not be much affected by previous loading. The neutral axis would be moved toward the tension side, and a lower collapse moment would be expected.

COMPARISON WITH OTHER WORK

Figure 14 shows data from other sources (see References 6, 8, 10, and 11), compared with the present theory, as well as some other theories (see References 12 and 13). The only data to fall below the deep-wrinkle membrane theoretical curve, except for a single point among 32 from tests of a cotton-neoprene cylinder (see Reference 8), are all from tests of metal fabrics.

Most work on the collapse of pressurized thin-walled cylinders has approached the problem from the shell theory viewpoint, and tests have been confined to sheet materials. Zender,[12] for example, has examined test data for Mylar and 7075-T6 aluminum-alloy cylinders from References 14 and 15, and has compared them with the theory that assumes the compressive stress in the wrinkled region to be

$$Et/R\left|3(1-\nu^2)\right|^{1/2}$$

and that gives

$$M_c = p\pi R^3\left\{1+\frac{2Et^2}{pR^2\left|3(1-\nu^2)\right|^{1/2}}\right\}. \tag{30}$$

The test data fell below the theory but always fell above $M_c = p\pi R^3$ and along a geometrically similar curve. Zender found that a semiempirical modification of Equation 30,

$$M_c = p\pi R^3\left\{1+\frac{Et^2}{2pR^2\left|3(1-\nu^2)\right|^{1/2}}\right\}, \tag{31}$$

which is still asymptotic to $M_c = p\pi R^3 = 2M_{wr}$ (the constant cross section membrane solution), formed a very good lower bound to the data. Equation 31

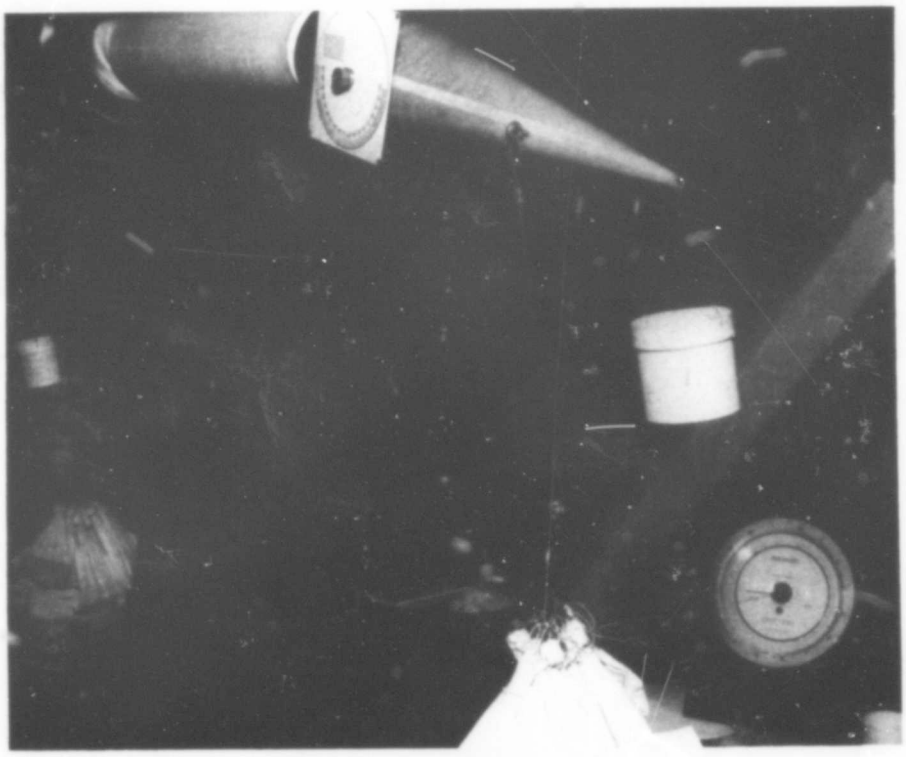

Figure 13 - Metal Fabric Bending Specimen at Near Collapse Load, Packaged Metal (p = 4.2 psig; P = 21 lb)

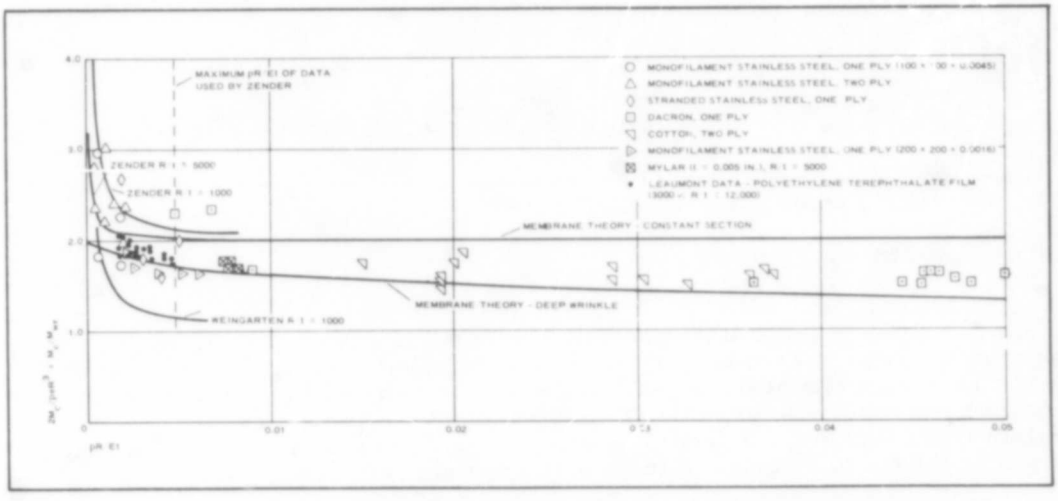

Figure 14 - Collapse Moments for Pressurized Fabric Cylinders

is compared with the present theory and test data in Figure 14 for R/t = 1000 and R/t = 5000 (the latter corresponding to the tests reported here on Mylar). The data of Suer, Harris, et al.,[9] from tests of stainless steel sheet cylinders are consistent with data used by Zender. The maximum value of pR/Et for the data Zender used, however, was 0.00475. Equation 31 with R/t = 5000 does not agree well with the Mylar data nor with the data of Leaumont[11] on polyethylene terephthalate cylinders with 3000 < R/t < 12,000.

In Reference 8, the difference between Zender's observations on tests of sheet materials and the deep-wrinkle membrane theory as checked by fabric materials was suggested to be due to (1) relatively low value of pR/Et used in the sheet cylinder tests and (2) a difference in wrinkling behavior between fabric and sheet materials. Figure 14, with additional (more recent) data, indicates that these factors are insufficient to explain all the differences. Since the deep-wrinkle membrane theory implicitly assumes a very long cylinder, Table 3 suggests that another factor, the test cylinder L/R ratio, is more important than (2).

TABLE 3 - COMPARISON OF TEST SPECIMEN PARAMETERS

Reference no.	L/R	pR/Et
6	6	$0 < \frac{pR}{Et} < 0.0007$
8 (also present paper)	$5 < L/R < 6$	$0.0025 < \frac{pR}{Et} < 0.052$
9	2.85	$0.00017 < \frac{pR}{Et} < 0.0025$
10	$14 < L/R < 16$	$0.0004 < \frac{pR}{Et} < 0.009$
11	3	$0.0017 < \frac{pR}{Et} < 0.0046$
14	$0.875 < L/R < 2^{*}$	$0.00003 < \frac{pR}{Et} < 0.00475$
15	$0.246 < L/R < 0.987^{**}$	$0.00003 < \frac{pR}{Et} < 0.0014$

*Except for some tests with R/t = 100

**Between stiffening rings

The high values of the collapse moment obtained in References 9, 14, and 15 apparently are at least partially due to end effects. These effects would depend on the material stiffness and, although the values of L/R for References 9 and 11 are not much different, the difference in E for the respective materials (steel and polyethylene) is about two orders of magnitude. The ranges of pR/Et for the two series of tests also are very different.

Weingarten,[13] using a small deflection shell theory with a modified Donnell equation, arrived at a criterion for "the moment at which significant deformations appear in the cylinder, rather than the maximum moment able to be carried," but which he thought might prove a good approximation. His solution is not closed, and he presents numerical results for $100 \leq R/t \leq 1000$. The latter yield the curve attributed to him in Figure 14. The curve is asymptotic to $M_c/M_{wr} = 1$, as in the deep-wrinkle membrane theory, but is obviously not a good fit to the data.

CONCLUSIONS

The deep-wrinkle membrane theory presented here and in Reference 8 is the only theory in reasonable agreement with experiment. This theory provides a satisfactory estimate of the maximum bending moment an inflated cylinder with $pR/Et >$ about 0.002 can carry and is superior to other theories and empirical formulas that have been proposed. It is basically conservative and provides a good lower bound. With adequate knowledge of the mechanical properties of the material, this theory is suitable for design. Packaging and previous buckling appear to have only a minor effect on the buckling resistance of the materials tested. The constant cross section theory gives a good upper bound for membranes with negligible flexural stiffness.

LIST OF REFERENCES

1. Santos-Dumont, A.: My Airships: The Story of My Life. London, Grant Richards, 1904.

2. Haas, R., and Dietzius, A.: "Stretching of the Fabric and Deformation of the Envelope in Non-Rigid Balloons" National Advisory Committee for Aeronautics (Report No. 16), Third Annual Report, 1917, pp 144-271. Translated by K. K. Darrow; originally published by Springer Verlag, Berlin, 1913.

3. Burgess, C.: Bursting Tests of Cylinders of Balloon Fabric. U.S. Navy Department of Aeronautics, Technical Note No. 10, series of 1930.

4. Leonard, R.; McComb, H.; Zender, G.; and Stroud, W.: "Analysis of Inflated Re-entry and Space Structures," Proceedings of the Recovery of Space Vehicles. Symposium, Los Angeles, August 31 and September 1, 1960; Institute of Aerospace Sciences, New York, 1960 (pp 62-78).

5. Leonard, R.; Brooks, G.; and McComb, H.: Structural Considerations of Inflatable Re-entry Vehicles. NASA Technical Note D-457, September 1960.

6. McComb, H.; Zender, G.; and Mikulas, M.: "The Membrane Approach to Bending Instability of Pressurized Cylindrical Shells" in Collected Papers on Instability of Shell Structures. NASA Technical Note D-1510, 1962, pp 229-237.

7. Stein, M., and Hedgepeth, J.: Analysis of Partly Wrinkled Membranes. NASA Technical Note D-813, July 1961.

8. Topping, A.: Buckling Characteristics of Inflated Fabric Cylinders in Pure Bending. Preprint 65-AV-5, ASME Aviation and Space Conference, Los Angeles, March 14 through 18, 1965.

9. Suer, H.; Harris, L.; Skene, W.; and Benjamin, R.: "The Bending Stability of Thin-Walled Unstiffened Circular Cylinders Including the Effects of Internal Pressure" in Journal of the Aeronautical Sciences. May 1958; Vol 25, No. 5; pp 281-287.

10. Foerster, A., et al.: Analytical and Experimental Investigation of Coated Metal Fabric Expandable Structures for Aerospace Applications. Air Force Aernautical Systems Division, TDR-63-542, August 1963.

11. Leaumont, W.: Collapse Tests of Pressurized Membrane-Like Circular Cylinders for Combined Compression and Bending. NASA Technical Note D-2814, May 1965.

12. Zender, G.: "The Bending Strength of Pressurized Cylinders" in Journal of the Aerospace Sciences. March 1962; Vol 29, No. 3; pp 362-363.

13. Weingarten, V.: "Effects of Internal Pressure on the Buckling of Circular Cylindrical Shells Under Bending" in Journal of the Aerospace Sciences. July 1962; Vol 29, No. 7; pp 804-807.

14. Seide, P.; Weingarten, V.; and Morgan, E.: Final Report on the Development of Design Criteria for Elastic Stability of Thin Shell Structures. Space Technology Laboratories, STL/TR 60-0000-19425, December 1960.

15. Dow, M., and Peterson, J.: Bending and Compression Tests of Pressurized Ring-Stiffened Cylinders. NASA Technical Note D-361, April 1960.

LIST OF SYMBOLS

f_b = bending stress
M = bending moment
y = distance from neutral axis of a beam
I = moment of inertia of a circular arc
f_t = tensile stress
p = inflation pressure
A = area enclosed by periphery of cross section
A_o = original area enclosed by periphery of cross section
s = unwrinkled peripheral length
M_{wr} = moment at beginning of wrinkling = $p\pi R^3/2$
c, c_1, c_2 = distances from neutral axis to outermost fiber
R = radius of circular cross section
M_c = maximum moment section can sustain
β = half angle describing unwrinkled periphery
e = distance from center to neutral axis (centroid of unwrinkled periphery)
e_A = distance from center to center of pressure
M_{eo} = resisting moment due to eccentricity
M_{uo} = resisting moment of unwrinkled periphery
f_{eo} = pA_o/s
f_o = total stress based on original cross-sectional area
ϵ_{wr} = strain available to form wrinkles
ℓ = length of a sine wave
$2a$ = height of a sine wave
h = wrinkle height
b = wrinkle base
E = secant modulus of elasticity
δ = angle defining width of a wrinkle
θ = angular deflection at end of beam
L = length of beam
t = skin thickness
ν = Poisson's ratio

BLANK PAGE

PERFORMANCE OF AN EXPANDABLE WHIRLING MEMBRANE SOLAR ENERGY CONCENTRATOR

By John M. Jerke*

INTRODUCTION

Solar energy concentrators used in conjunction with electrical conversion devices are being considered for space power systems. Most of these concentrators are reflecting paraboloidal mirrors that concentrate solar energy on a heat receiver in the focal region. The method of conversion of heat to electrical power, required power output, weight, and payload packaging influence the basic materials and type of construction used in fabricating the concentrator. As a result, concentrators ranging from lightweight inflatable plastic mirrors to relatively heavy one-piece nickel mirrors have been built and quantitative data on their ground test performance are available.[1]

Expandable concentrators are of interest for large power systems that require concentrators much larger than launch vehicle diameters since they can be compactly packaged for launch and then deployed for use in space. Although expandable concentrators have not been fabricated with highly accurate surface geometry, most have optical accuracies capable of attaining temperatures suitable for dynamic conversion systems. One of the expandable types that has been proposed is the whirling membrane concentrator.[2] The whirling membrane concentrator is a thin aluminized plastic membrane that has been preformed to an approximate paraboloid and is rotated about the optical axis to maintain the desired paraboloidal shape. The centrifugal loading, plus axial loading applied at the rim, stretch the approximate paraboloid into the desired paraboloid. The results of an experimental investigation to determine the feasibility of this concept and to measure the concentrating ability are presented in this paper.

The units used for the physical quantities defined in this paper are given in the International System of Units (SI). Factors relating this system to U.S. Customary Units are presented in reference 3.

DESCRIPTION OF TEST MODEL

A sketch of the whirling membrane solar concentrator model is shown in figure 1. The model consists of a shaft, metal hub, aluminized plastic paraboloid, cables, and cable hub. The paraboloid design diameter is 3.05 meters, the design rim angle is 60°, and the design focal length is 132.1 centimeters.

*Aerospace Engineer, Structures Research Division, Langley Research Center, Langley Station, Hampton, Va.

The membrane is constructed of 13-μm-thick aluminized polyethylene terephthalate plastic and is formed of 45 gores assembled on a convex mold. The reflective gores are attached to the edge of the metal hub and, by means of plastic tabs, to the cables at the concentrator rim. There are seventy-two 0.8-mm-diameter steel cables which extend from the cable hub mounted on the shaft to the plastic tabs in which they are embedded. Three 3.05-m-diameter models with ratios of metal hub to concentrator diameters of 0.20, 0.35, and 0.50 were tested. The metal hubs are flat disks and are mounted on the shaft below the cable hub.

The models were tested at a rotational speed of 71 rad/sec in an 18-m-diameter vacuum sphere at approximately 130 N/m^2* pressure. The angular velocity was chosen in order to have membrane maximum stress well below the material yield stress of about 100 MN/m^2. The vacuum condition was necessary in order to eliminate undesirable aerodynamic forces which would cause membrane flutter.

DESIGN CONCEPT

The membrane for the whirling concentrator was preformed as an approximate paraboloid so that the desired paraboloidal shape would be obtained under the stresses imposed by centrifugal and axial loading. In order to construct the proper preformed membrane, it was necessary to know the stress distribution of the spinning paraboloid. This stress calculation was based on equations derived in reference 2. Having determined the stresses in the spinning membrane, it was possible to calculate the spatial displacement which the membrane would experience as a result of the stress distribution. The membrane was then constructed according to ordinates which differed from a perfect paraboloid by this displacement. In this way, the loading experienced during rotation would stretch the approximate paraboloid into the desired paraboloid.

According to reference 2, the meridional stress decreases with radial distance from the optical axis while the circumferential stress increases. For a hub of small diameter relative to the overall membrane diameter, reference 2 indicates that the meridional stress, at least over the outer portion of the membrane, becomes insignificant compared with the circumferential stress. If a thin sheet of material is tested in tension in one direction, large-scale wrinkles tend to form parallel to the applied force. These wrinkles may be eliminated by applying slight tension in the plane of the sheet at right angles to the wrinkles. Therefore, in order to prevent the formation of circumferential wrinkles in the spinning membrane due to the relatively large circumferential and small meridional stress values, a certain minimum ratio of meridional to circumferential stress appears to be necessary. One method of varying the meridional to circumferential stress ratio that was suggested in reference 2 is to vary the diameter of the fixed hub to which the membrane is attached. For this purpose, three models of the same overall diameter, but with different hub diameters were tested.

---

*1 $N/m^2 = 1.45 \times 10^{-4}$ psi.

A further requirement for the formation of a paraboloid by spinning a preformed approximate paraboloidal membrane is the presence of an axial load at the membrane rim. This axial load was achieved by means of the cables extending from above the rim plane at the optical axis to the membrane rim. It was necessary to estimate the cable length and distance above the theoretical rim plane where they intersect the optical axis which would result in a cable configuration capable of properly supporting the spinning paraboloid. It was assumed that at the tab-membrane juncture, the tabs would make an angle with the rim plane equivalent to that of the cone-paraboloid configuration of reference 2. This assumption was used with a numerical process to determine the cable parameters.

TEST SETUP

The apparatus for testing the whirling membrane concentrator models is shown schematically in figure 2, and a photograph of one of the models under test conditions is shown in figure 3. A steel framework provided a support for the concentrator and associated optical ray trace measuring equipment. A variable-speed motor coupled to the shaft was used to rotate the models. A fixed polyethylene sheet was stretched horizontally just below the metal hub to support the membrane when at rest and during spin-up. As the rotational speed was gradually increased, the membrane lifted off the supporting sheet and assumed the shape of a concentrator by the time the desired speed was obtained.

The optical ray trace equipment used to determine the concentrating ability of the models consisted of a light source to provide a well collimated beam of light and 10 silicon solar cells to measure the reflected light distribution in the focal region. The zirconium arc lamp with its collimating lens gave a 7.6-cm-diameter light beam with a 0.025° collimation angle and was driven along an overhead track by means of a remotely controlled motor. A silicon solar cell located just below the lens of the light collimator continuously monitored the irradiance from the light source. The 10 other solar cells were spaced 2.5 centimeters apart in a line on the solar cell bar. The solar cell bar had three degrees of freedom as follows: (1) rotation about the concentrator optical axis, (2) translation perpendicular to the optical axis, and (3) translation along the optical axis. All three modes were remotely controlled, and the positions of the solar cell bar were determined by remote indicators. The solar cell in the light beam and the cells on the bar had heaters and thermocouples for maintaining a constant temperature and thus constant cell sensitivity.

Procedure for acquiring typical data consisted of placing the solar cell bar at a vertical location in or near the design focal plane, positioning the light source, and then surveying the plane by rotating and moving the solar cell bar. The light source was then moved to another radial location, and the survey was repeated. In all, the light source was positioned at five radial locations for each survey plane in order to obtain data representative of different areas of the membrane.

RESULTS AND DISCUSSION

Data from the investigation yield such factors as the shape and size of the distribution of the reflected energy in and near the design focal plane. Using this information, it is possible to estimate the shape, focal length, and geometric efficiency of the concentrator.

An illustration of the type of data obtained during the investigation is presented in figure 4. In this figure, irradiance ratio is shown as a function of radial distance from the optical axis in a survey plane 3.8 centimeters below the design focal plane and with the light source located at a radial distance of 1.20 meters from the optical axis. Irradiance ratio is the ratio of the reflected light irradiance occurring in the survey plane to the light irradiance approaching the concentrator. This ratio represents the factor by which the irradiance of the incident light beam has been modified by concentrator geometry and specular reflectance of the aluminized plastic. The magnitude of the irradiance ratio will also vary directly with the diameter of the collimated light beam used. However, this ratio provides a convenient means of analyzing the data as the magnitude does not affect determination of the membrane properties such as shape, geometric efficiency, and focal length. In figure 4 the two irradiance ratio distributions represent cross sections of the reflected energy distribution in the survey plane, taken 90° apart. The 0°-180° distribution is in the plane containing the light source and the optical axis. The incident light beam, with its circular cross section, would produce an elliptic image in the focal plane if reflected from a perfect paraboloid. The major axis of the elliptic image for the whirling membrane test setup should lie along the 0°-180° axis of figure 4(a) while the minor axis should lie along the 90°-270° axis of figure 4(b). With the test light source at the radial location indicated for figure 4, a perfect whirling membrane concentrator would produce an elliptic image having a major axis length of 0.16 centimeter and a minor axis length of 0.11 centimeter. Figure 4(a) shows an image spread of about 15 centimeters along the 0°-180° axis. This dispersion of energy was probably caused by circumferential wrinkles in the membrane, which were visually observed, indicating that apparently the meridional stress was not sufficient to remove the wrinkles resulting from the relatively large circumferential stress. Figure 4(b) shows an image spread of about 7 centimeters along the 90°-270° axis. The energy spread in this direction was probably caused by deviations in the circular shape of the membrane similar to cusping or scalloping. Although there is considerable dispersion of energy along the two axes shown in figure 4, the distribution peak occurs on the optical axis. The location of the peak value relative to the optical axis is used to determine concentrator focal length which is discussed with figure 5.

Data such as those in figure 4 were obtained for each concentrator model with the light source at five different radial locations. Data from the five light source locations were used to prepare figure 5 which shows the displacement of the irradiance ratio distribution peak from the optical axis and the peak magnitude as a function of distance along the concentrator radius. Whenever the survey plane is below or above the focal plane, the peak of the irradiance ratio distribution along the 0°-180° axis will lie to one side of the optical axis. Therefore, the concentrator focal length is determined by

locating the survey plane position in which the distribution peaks fall closest to the optical axis. Figure 5(a) shows that only one of the irradiance ratio distribution peaks occurs slightly off the optical axis which indicated that this survey plane is the focal plane for most of the membrane. Therefore, most of the membrane has assumed a parabolic radial cross section, but with the focal plane 3.8 centimeters below the design focal plane or about 3 percent less than the design value. The variation of peak magnitude with radial distance in figure 5(b) shows that the center region of the membrane is producing the least dispersion of the incident light.

The data from the five light source locations were averaged to obtain the irradiance ratio distribution in the focal plane that would result from illuminating a complete radial band of the concentrator with a well collimated beam of light of cross-sectional area equal to that of the test light source. The average irradiance ratio distributions were obtained for the focal plane of each test model, and figure 6 shows these distributions along the 0°-180° axis. The focal lengths are 130.7 centimeters, 129.1 centimeters, and 128.2 centimeters for the 0.20, 0.35, and 0.50 hub diameter ratio models, respectively, as compared to the design value of 132.1 centimeters for all models. These focal plane distributions also represent the best concentration of energy, or the most energy in the smallest area, occurring in the various planes surveyed for each model. To obtain these optimum energy distributions, it was necessary to locate the cable hub above the design position on the shaft as much as 14 centimeters. As compared with the other models, the distribution for the 0.20 hub model shows an image of greater width and smaller peak magnitude. Since data for the three models indicate that each membrane was a body of revolution with essentially a parabolic radial cross section, it appears that the greater dispersion of reflected light for the 0.20 hub model was due to the presence of additional circumferential wrinkles. The difference in energy concentration between the 0.35 and 0.50 hub models is not very significant, indicating that the amount of circumferential wrinkling was relatively comparable for the two models. This circumferential wrinkling was visually observed for all three models.

The best concentration of energy in a focal plane appears to have been produced by the 0.50 hub model. Therefore, data were used from this model to calculate the geometric efficiency of a whirling membrane concentrator. The variation of the geometric efficiency with aperture diameter ratio of a completely illuminated 0.50 hub whirling membrane is presented in figure 7. The geometric efficiency is defined as the ratio of energy passing through an aperture in the focal plane to the total energy reflected from the concentrator. The aperture diameter ratio is the ratio of aperture diameter to concentrator diameter. Curves for two other expandable solar concentrators,[1,4] which also use aluminum-coated plastic are presented in the same figure for comparison purposes. It should be noted that the data for the inflatable-rigidized and split-rib umbrella concentrators are for solar illumination with an 0.533° angle of collimation, while the whirling membrane data are for the test light source illumination with an 0.025° angle of collimation. Calculations indicate that for solar concentrators of the quality of the whirling membrane, the angle of collimation over the range, 0.025° to 0.533°, has little effect on the geometric efficiency curve. On this basis, the efficiency of the whirling membrane under solar radiation would still be comparable to that of the two other expandable-type concentrators.

It might be expected that the whirling membrane could be packaged into a very small volume because the thin plastic film requires no backup structure. However, the relatively large fixed hub which is necessary to suppress circumferential wrinkles limits the packaging capabilities of the whirling membrane. Estimation of the packaged volume for the 0.50 hub whirling membrane model gave a value of 0.14 m^3. This value includes a one-piece paraboloidal mirror to replace the flat hub. Such a paraboloid would serve the same structural purpose as the flat hub but by having an identical focal length to the membrane, it could provide the concentration of additional energy. A packaged volume of 0.15 m^3 for a 3.05-m-diameter umbrella concentrator is reported in reference 5, and an estimated packaged volume of 0.12 m^3 for a 3.05-m-diameter inflatable-rigidized concentrator with predistributed foam is given in reference 6. Therefore, the whirling membrane concentrator appears to be comparable with the two other types of expandable concentrators shown in figure 7 as regards geometric efficiency and packaged volume. However, since the focal plane data for the 0.50 and 0.35 hub models are relatively similar (e.g., see fig. 6), the efficiency of the 0.35 hub model should nearly equal the efficiency of the 0.50 hub model, and the packaged volume could be reduced approximately 50 percent.

CONCLUDING REMARKS

In summary, the results of a program to investigate the whirling membrane solar concentrator concept have been presented. An optical ray trace method was employed in order to estimate such concentrator properties as shape, focal length, and geometric efficiency. Three 3.05-m-diameter models with ratios of hub diameter to concentrator diameter of 0.20, 0.35, and 0.50 were examined and results are given for each model.

All models generally achieved a parabolic radial cross section, but with focal lengths of 130.7 centimeters, 129.1 centimeters, and 128.2 centimeters for the 0.20, 35, and 0.50 hub models, respectively, as compared to the design value of 132.1 centimeters. Undesirable dispersion of the reflected image probably resulted from circumferential wrinkles and deviations in the circular shape of the membrane similar to cusping or scalloping. Comparison of the data for the three models shows that there was considerably less circumferential wrinkling in the 0.35 and 0.50 hub models, which were similar in behavior, than in the 0.20 hub model.

Estimation of the geometric efficiency at various aperture ratios for the 0.50 hub model indicates that the whirling membrane has a concentrating ability comparable to two other expandable-type solar concentrators, an inflatable-rigidized and split-rib umbrella, which also use an aluminized plastic membrane. The whirling membrane appears to be capable of efficient operation (greater than 0.90) in the aperture ratio range near 0.04 which would make it applicable for relatively low-temperature space power conversion systems.

REFERENCES

1. Heath, Atwood R., Jr.; and Hoffman, Edward L.: Review of Solar Concentrator Technology. Paper presented at Intersociety Energy Conversion Engineering Conference (Los Angeles, California), September 1966.

2. Simmonds, James G.: The General Equations of Equilibrium of Rotationally Symmetric Membranes and Some Static Solutions for Uniform Centrifugal Loading. NASA TN D-816, 1961.

3. Mechtly, E. A.: The International System of Units - Physical Constants and Conversion Factors. NASA SP-7012, 1964.

4. Camp, John D.; and Nowlin, William D.: Investigation of the Calorimetric Efficiency of a Split-Rib Umbrella-Type Paraboloidal Solar Energy Concentrator. NASA TN D-2015, 1964.

5. Heath, Atwood R., Jr.: Status of Solar Energy Collector Technology. Vol. 11 of Prog. in Astronaut. and Aeron., Morris A. Zipkin and Russell N. Edwards, eds., Academic Press (New York), 1963, pp. 655-668.

6. Heath, Atwood R., Jr.: Review of Inflatable-Rigidized Solar Energy Concentrator Technology. Paper presented at Annual Solar Energy Society Meeting (Boston, Mass.), March 1966.

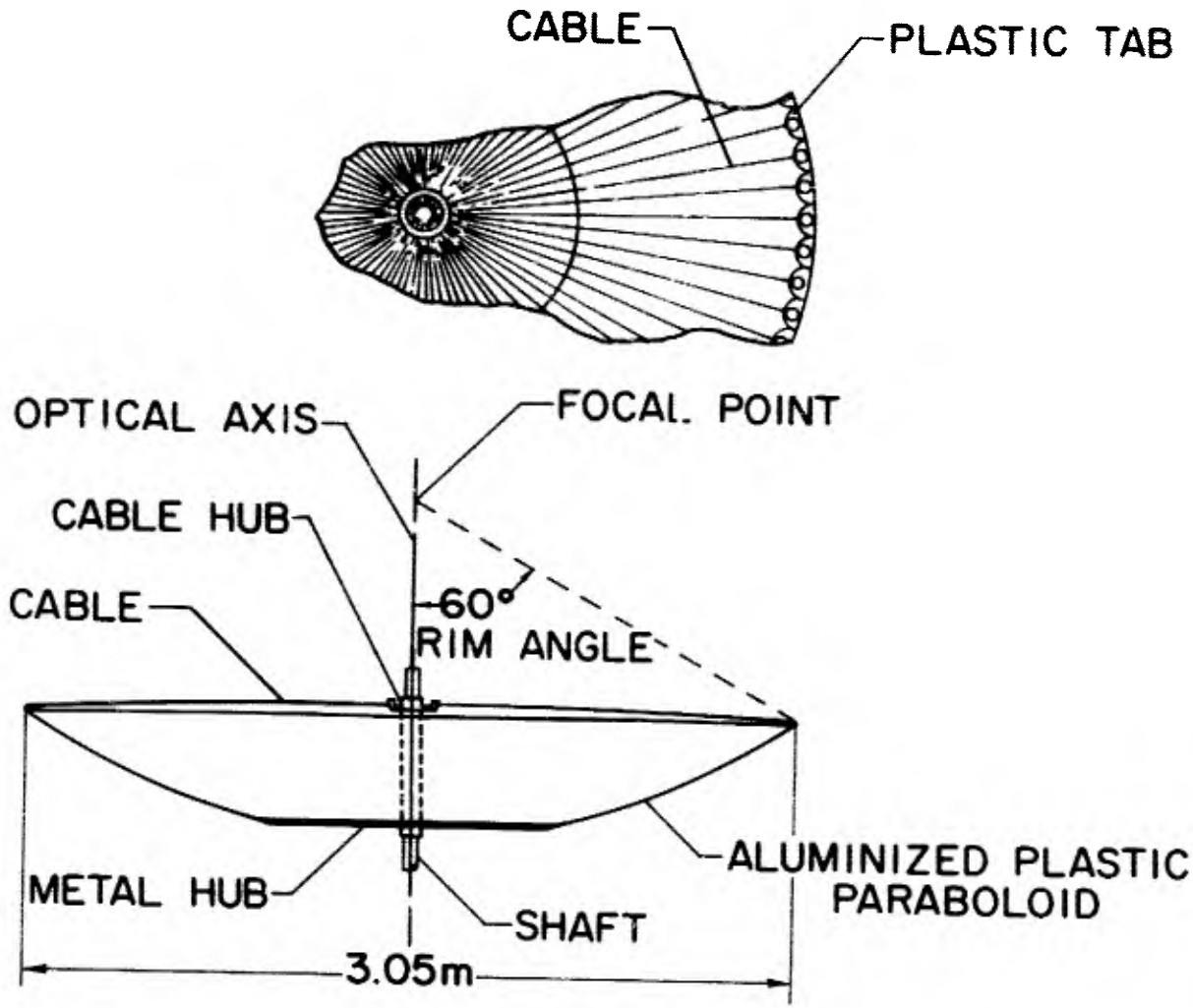

Figure 1.- Sketch of whirling membrane solar concentrator.

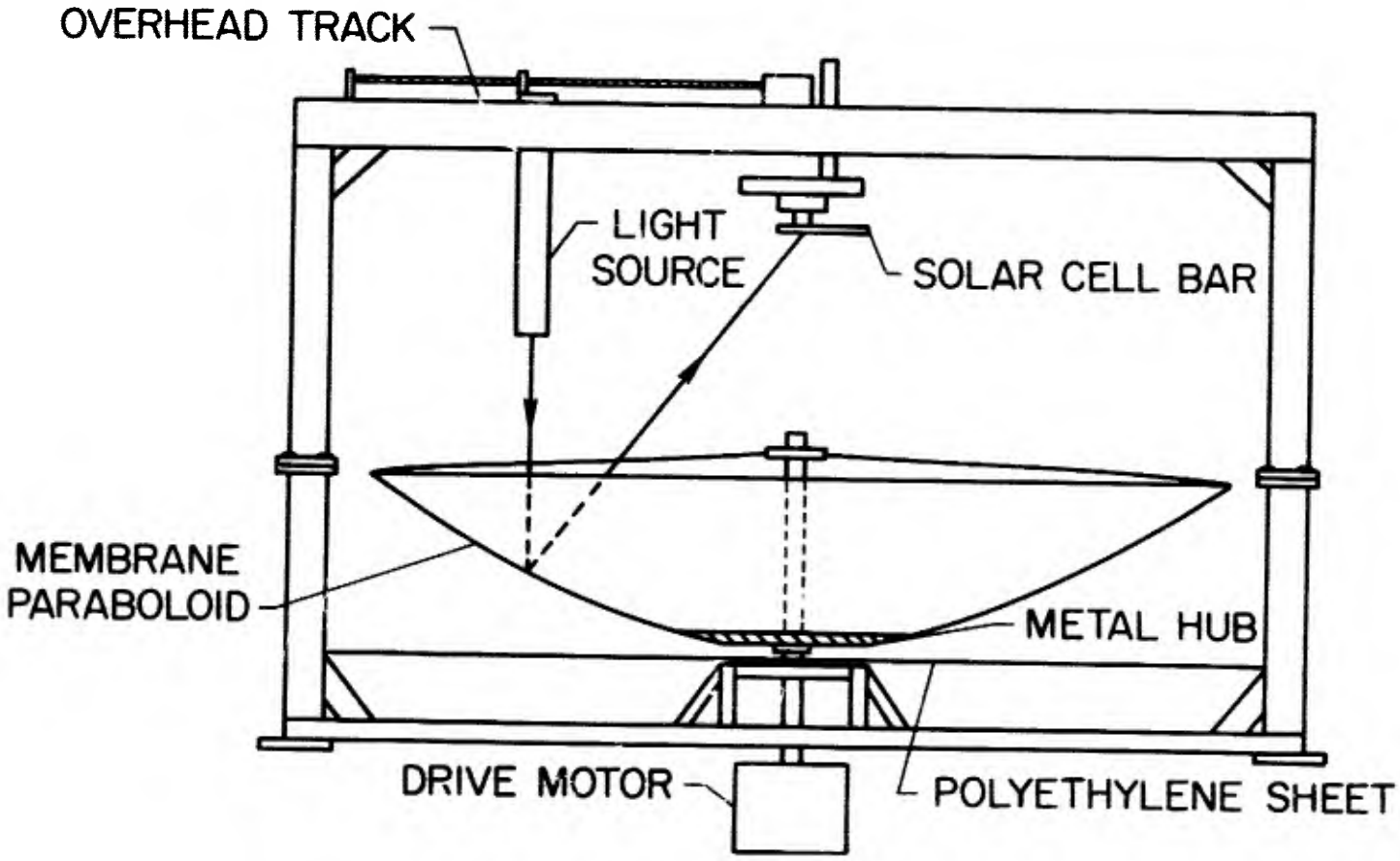

Figure 2.- Schematic of test apparatus.

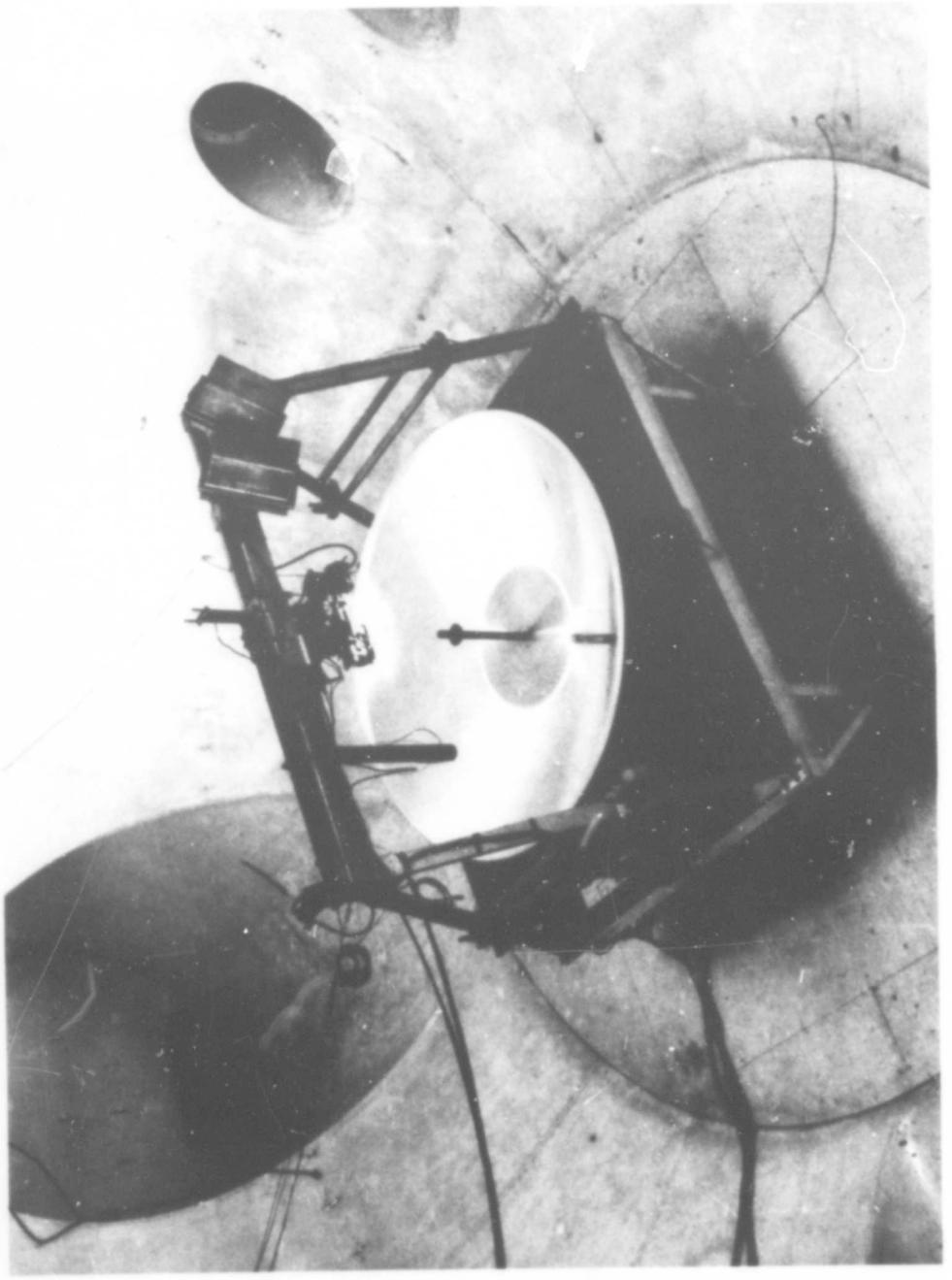

Figure 3.- A whirling membrane model during tests.

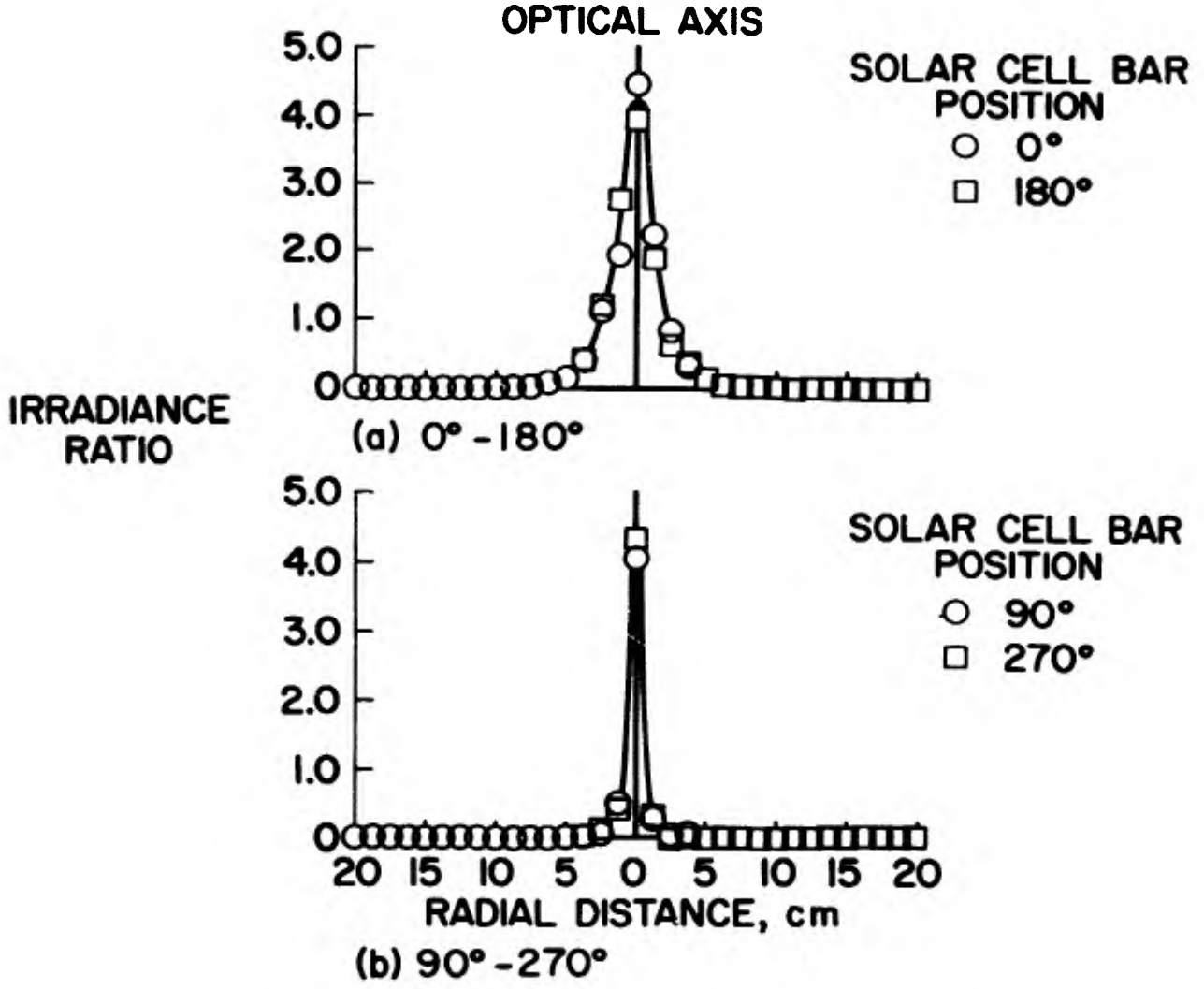

Figure 5.- Irradiance ratio distributions along two orthogonal axes in the focal plane of a whirling membrane model. (0.50 hub diameter ratio.)

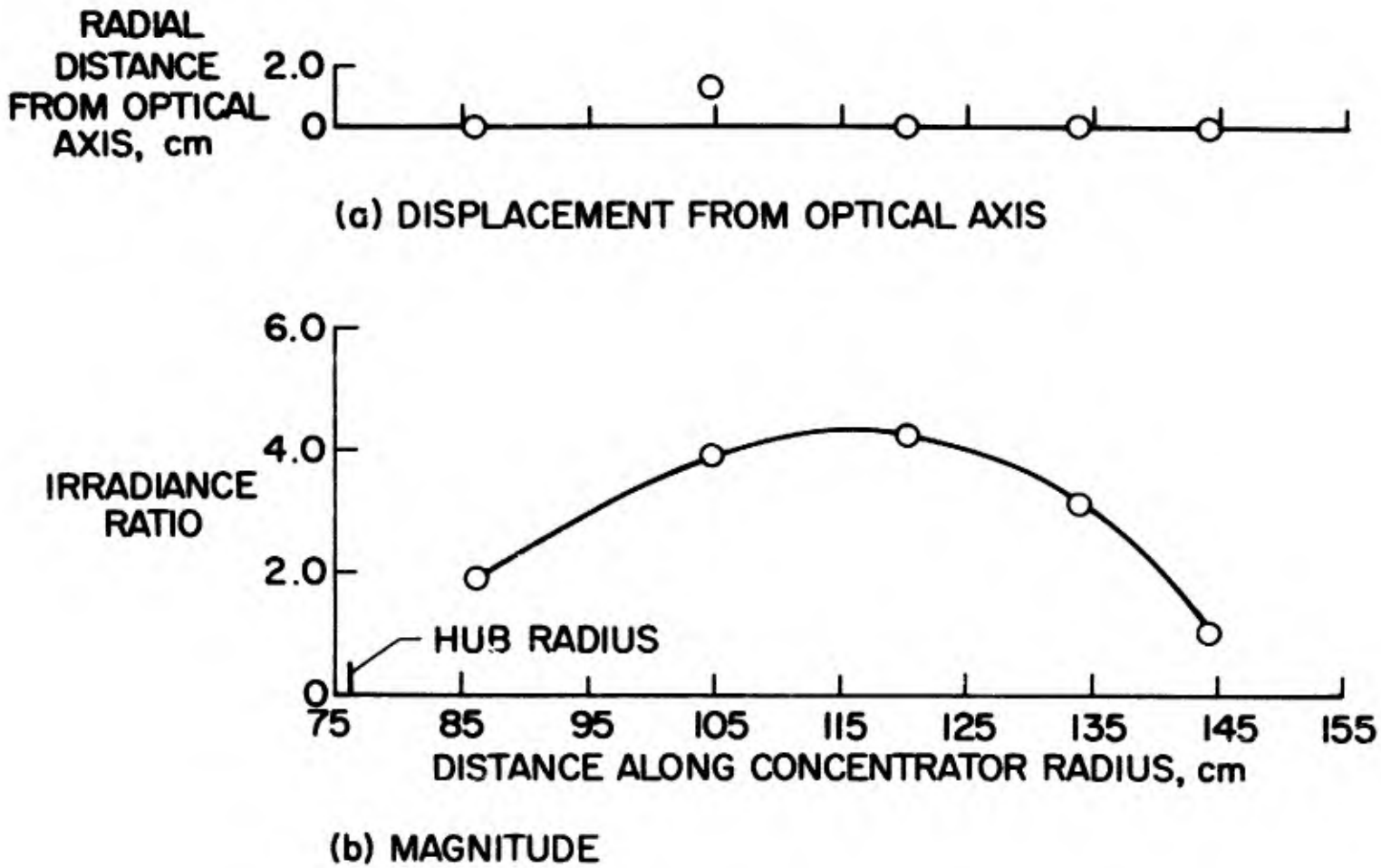

Figure 5.- Variation of displacement of the irradiance ratio distribution peak from the optical axis and the peak magnitude with distance along the concentrator radius. (0.50 hub diameter ratio.)

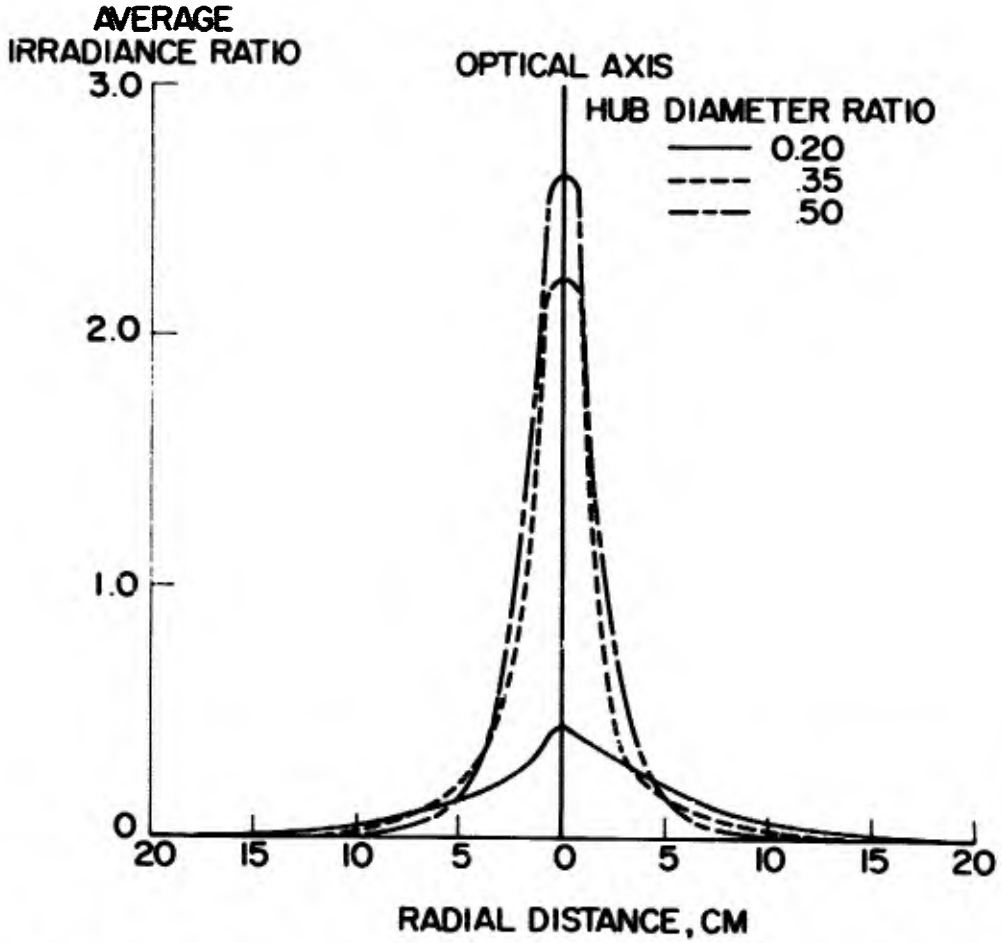

Figure 6.- Focal plane average irradiance ratio distribution along the 0^{o}-180^{o} axis of the three whirling membrane concentrator models.

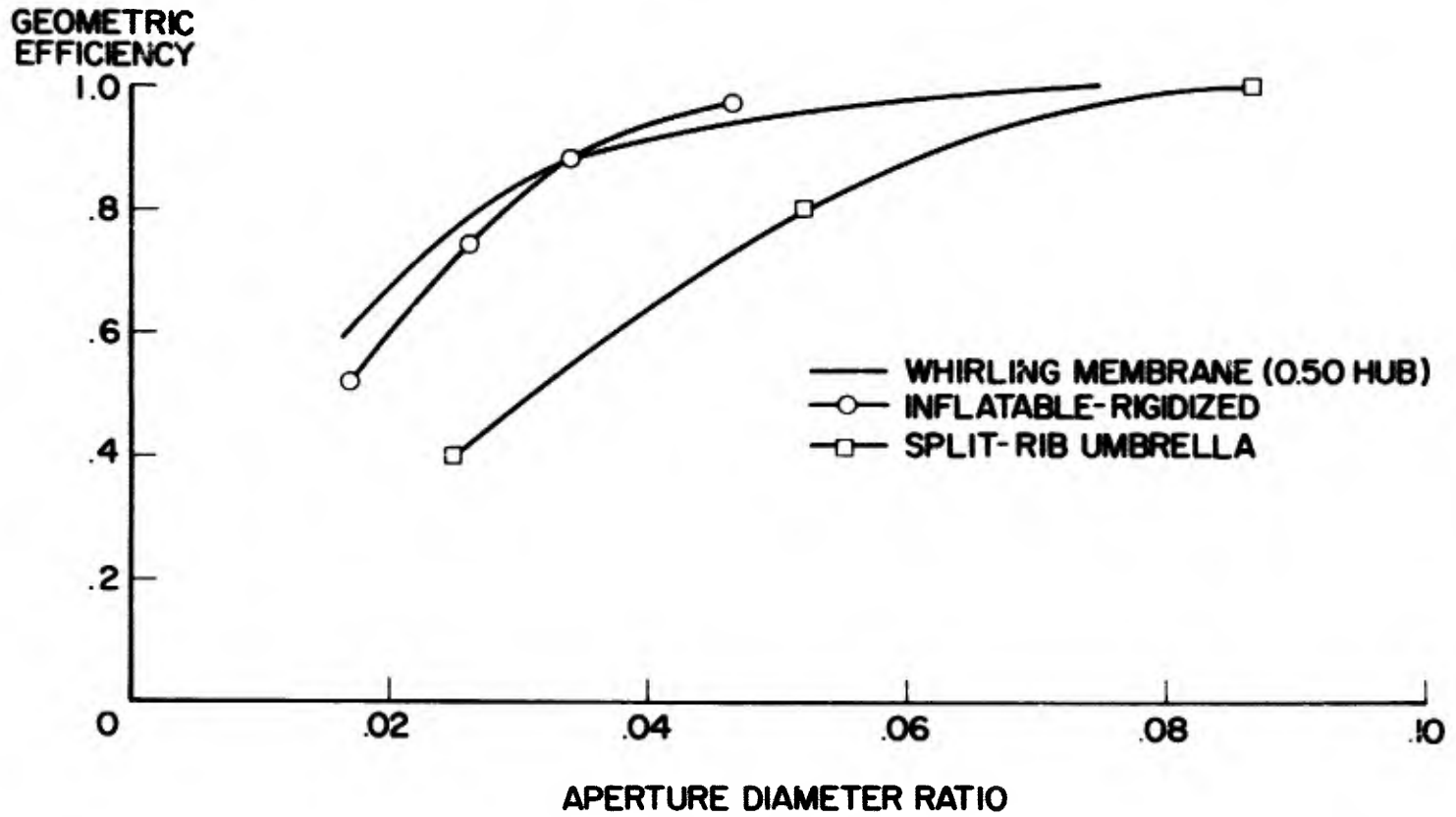

Figure 7.- Geometric efficiency of the whirling membrane and two other expandable concentrators.

ABSTRACT

PAGEOS FABRICATION ACCURACY AND RELIABILITY

S. J. Stenlund

The PAGEOS program was the first time that a Space Satellite Reliability Program has been used in the design and fabrication of a very large inflatable satellite. This paper covers the design and performance of the 100-foot diameter PAGEOS Satellite and the Reliability Program used in predicting its reliability. The mathematical technique for reliability prediction was developed.

The technique utilizes known theory of probability in evaluating representative random samples of component characteristics. The end result is component, operational phase, and ultimately system reliability prediction including estimation of failure rates.

This model was successfully applied to the recently launched PAGEOS inflatable satellite. Other typical applications are to structures such as passive communications satellites, high altitude balloons, expandable space shelters, expulsion bladders, erectable penetration aids and space microwave structures.

MISSION

As a continuation of the NASA effort in support of the National Geodetic Satellite Program, an Echo I type Satellite was launched from Vandenburg Air Force Base on June 23, 1966 into a near-polar orbit at about 2,200 miles in altitude. The 100-foot diameter, aluminum-coated, spherical satellite can be observed from the ground as a point source of light while it reflects the incident sunlight. Simultaneous photographs of this light source taken against the star background by two or more widely separated ground-based cameras will enable geodesists to determine the spatial coordinates of each camera position. An interconnected series of camera positions has been established to cover the entire surface of the earth, thereby permitting geometric determination of each camera position within a single reference system. The use of this satellite for geodetic purposes will continue for a five-year minimum period during which the necessary photogrammetric observations will be made to provide, for the first time, a purely geometric determination of the shape and size of the earth.

DESCRIPTION OF SATELLITE

The PAGEOS satellite is a spherical shell of 1/2-mil Mylar coated with vapor-deposited aluminum approximately 2,000 Å thick, giving a surface resistance of less than 1 ohm per square. The aluminum film serves to reflect most of the incident sunlight and protect the plastic film from the degrading ultraviolet radiation.

The aluminized material was initially processed in long flat sheets (10,000 feet long by 54 inches wide). This material was then treated and inspected before being cut into 84 gores required for the sphere. The gores, 45 inches wide at the center and 157 feet long, were then butted together and sealed with a 1-inch wide tape made from the same material. The tape was coated with a thin layer of thermosetting adhesive specially formulated to withstand the temperature extremes and vacuum of space.

Polar caps were sealed over the gore tips to provide structural integrity at the terminating gore points. Since the gores were insulated from each other by the plastic film and adhesive dielectric along the seams, the gores were electrically connected to each other by a ring of conductive paint at the polar cap.

To ready the sphere for flight, an inflation system* was added, and after the final seal was made, the sphere folded into a small canister. Upon completion the package was sent to Vandenburg Air Force Base, mounted on a Thor Agena vehicle, and rocketed into space. When the canister was in orbit it separated, leaving the sphere free to inflate to its full (100-foot diameter) size.

*A mixture of subliming powders, namely benzoic acid and antraquinone.

FABRICATION ACCURACY

The PAGEOS satellite is the most accurately fabricated, large inflatable ever built. During the full-scale inflation test, measurements showed that the polar and equatorial diameters were less than ± 1/2 per cent from the design. Measuring the 100-foot diameter sphere accurately was an engineering challenge. The polar diameter was measured directly by fastening a measuring tape at the top, or north pole, of the sphere, and allowing it to hang through a duct at the bottom of the sphere. The equatorial diameter was measured at eight different points with a system of theodolites. As measurements were taken, the information was put into a desk computer at the test site, and diameter measurements became available within a few minutes after the theodolite readings. The accuracy of this system was believed to be within 2 inches for a 100-foot length measurement. Figure 1, a picture of Echo I, should be compared with Figure 2, which shows PAGEOS at approximately the same skin stress (4,000 psi). Comparisons of the reflected images, the smoothness of the seals, and the flatness of the gores, show the results of the much improved fabrication techniques used on PAGEOS. A closer view, Figure 3, shows the meaning of fabrication accuracy with an apparent optical illusion. This picture is actually a reflection taken by the photographer standing in the lower center portion of the picture. Careful examination of the upper right-hand corner of the picture shows a seal which is just visible under proper lighting conditions taken at this range. This picture clearly shows the excellent optical reflective qualities of the spherical surface.

This high degree of accuracy was attained by using an accurate gore pattern, by maintaining seal tolerances, and by lowering the sealing temperature. Continual and vigorous inspection during all stages of fabrication insured the proper use and control of tools and procedures.

For the 157-foot long gore pattern, the length tolerance established was ± 1/4-inch, while the width tolerance was ± 0.030 of an inch at the mid-point, reduced to ± 0.015 of an inch near the tip. The center reference line was held straight within ± 0.060 of an inch. These tolerances were measured and verified with conventional engineering tools such as a theodolite, a calibrated steel measuring tape, and vernier calipers.

In butt joining the gores, the maximum allowable gap was 0.030 of an inch and the maximum allowable overlap was 0.040 of an inch. Frequent measurements during fabrication showed that these tolerances were rarely exceeded, indicating the capability of sealing techniques to maintain such tolerances.

Mylar has a tendency to shrink and distort when heat is applied. To minimize this effect, it was necessary to reduce the normal sealing temperature from 390 F to 340 F. The result was the distortion-free seals shown in Figure 2.

The gore cutting template was accurately laid out and then periodically remeasured to insure continued accuracy. Random measurements were made daily and checked against the last periodic measurement to insure no changes beyond tolerance limits were taking place. During sealing, each of the seals was inspected with go-no-go gages and optical comparitors.

To verify the design before orbiting a sphere, a static inflation test was planned of a full-scale sphere to determine polar and equatorial diameters, structural integrity of the sphere, degree of seam creep over a period of time, and to evaluate workmanship and the effectiveness of inspection.

The static inflation sphere required two modifications, attachment points (tie-down patches), and ducts, or openings, in the sphere wall. The tie-down patches were to hold the sphere in place and the ducts to add or discharge air. Both were necessary because the sphere was to be flown ten feet off the hangar deck as a tethered, hot-air balloon to facilitate accurate measurements of the diameter.

To insure that the modifications would not degrade the performance of the sphere during the static test, each was thoroughly tested. Figure 4 shows the tie-down patch being tested with a dead weight of 60 pounds. Further loading caused it to fail under a load of 430 pounds. Since the maximum operating load expected was 50 pounds, the results of the test showed the design more than adequate.

The duct installations were tested by constructing spherical segments and pressurizing them. Figure 5 shows a spherical segment with an unmodified polar cap of the design to be used in the final sphere. This was the control segment for the modified spherical segments. Figure 6 shows a polar cap modified in its center with an inflation duct for adding air to the bottom of the sphere and for discharging air from the top. The opening was reinforced so that loads were transmitted across it.

Figure 7 shows a side duct segment used for discharging air. This opening differed from the polar ducts since less reinforcing and reinforcing tapes were available away from the poles. Test data were satisfactory, as failure levels were verified to be well above the maximum to be encountered during the static inflation test. The results of these tests gave us confidence in the reliability of design for the static inflation test sphere.

The final design test was the actual inflation of the full-scale sphere in an air ship hangar at Lakehurst Naval Air Station, Lakehurst, New Jersey. The results of this test showed that the key objectives had been met, but that blocking, the adhesion of the material to itself, was present. As a result, special emphasis was placed on solving the problem. It was found that chemically treating the Mylar side of the material with a solution of Freon TF and Valclene No. 1 virtually eliminated blocking. Testing, manufacturing, and inspection procedures were modified to reduce the potential for blocking to take place. A final redundant change, to further prevent blocking, consisted of dusting the inflatant powder over the entire inner surface of the sphere since it served as a lubricant and release agent. Although these changes were overlapping, they were felt necessary since blocking would surely cause catastrophic failure of the sphere when inflated in space.

A successful simulated deployment test of the full-scale sphere in a large vacuum chamber showed the results of these changes. A few minor changes were required in other parts of the system, but the last high hurdle had been passed, and fabrication of the flight spheres was ready to begin. After hold-

ing a design review and considering every design aspect as required by the NPC documents, fabrication began.

During the manufacture of the flight spheres routine material tests were conducted to assure quality and reliability of the sphere. For each sphere built there were 750 tensile strength tests, 350 tensile impact tests, 170 thermal shock tests, 170 thermal flex tests, 170 seam creep tests, and 175 reflectance tests. These nearly 1800 tests measured the variable characteristics of the material. In addition, 530 adhesion tests, 530 hot-wheel-blocking tests, 170 seam-peel tests, and 550 aluminum-adhesion tests were conducted, making a total of nearly 3,500 individual tests on each sphere. The results of this test effort were used in estimating failure rates. Reliability prediction for components and the system were based on these estimated failure rates.

Meanwhile, special emphasis was placed on minimizing handling and workmanship defects by manufacturing. Only 9 material defects (due to handling) in over 31,000 square feet of material and not one single seal defect in over two miles of seal were detected in the flight sphere. The final reliability prediction for the flight sphere was .9602. The reliability goal had been established at .96 earlier in the program.

How were these results accomplished? During the early stages of the program, we were required to plan the quality program and submit it for approval. The plan included the approach that was to be used throughout the program to implement, staff, and maintain the program; and the requirements to be met during all phases of engineering design, development, fabrication, processing, assembly inspection, testing, check-out, packaging, shipping and storage. The contract required conformance to the NASA Documents NPC 200-2 and 250-1.

What was management's role in reliability? The program management motivated those working on the job so that they had an intense desire to avoid failure. The people were well trained in their jobs and their morale was kept high by keeping them informed on how well the work they had done was performing downstream. Test results were made known, pictures and movies were shown, and program management showed high interest in the work as it progressed.

RELIABILITY APPLIED TO AEROSPACE SYSTEMS

How can the PAGEOS experience benefit aerospace programs? The tools for doing the job were found. A technique for reliability evaluation and prediction has been developed. The mathematical approach developed is applicable to aerospace programs where full-scale item testing (reliability demonstration testing) is not practical or feasible. The approach can be used as a guide to aid programs with similar quality requirements.

The approach in building a product is straightforward and logical. However, the proof and confidence of its reliability is usually not as easy. It is desirable to have a full-scale test of the end item in actual or simulated operating conditions and data on ultimate performance which requires destructive tests. When the end item is very large and costly, actual testing is not economical or even feasible. Because it is usually difficult to fully simulate atmospheric and space conditions and to anticipate the operating environ-

ment, extensive planning and ingenuity are required. Tests of materials, parts and components can be substituted for the full-scale test. Sometimes testing well beyond the expected conitions is done to achieve confidence and assure reliability. Random sampling of basic materials and subassemblies is a useful technique. Destructive tests of representative samples is another way of evaluating the quality of an untestable device. No matter what innovation is used, the important point to keep in mind is the validity of test techniques and effectiveness of results.

Every aspect of performance and mode of failure should be considered. But, it is not sufficient to consider only the expected results; the unexpected must also be looked for when conducting tests and analysing data. Overlooking, misinterpreting and underestimating information from preliminary tests can easily occur. The result can be a costly failure in a later test or in the mission. Watch words in testing are, "Keep alert and look for the unexpected -- it usually comes."

Reliability should be designed into every aerospace system. A quality and reliability program should be set up for each program, even if a very simple one. It will evaluate on its own merits all of the aspects associated with the flight and will predict the failure modes of the mission.

I will summarize with the following conclusions:

1. The PAGEOS program substantially reduced fabrication and inspection arts to a science.

2. Large spheres can be accurately built and measured to an accuracy of $\pm$ 1/2 per cent using state-of-the-art equipment and methods.

3. A reliability prediction can be made without large-scale testing of the whole unit either in a huge environmental system or in space.

4. Reliability techniques developed during the program have application in other aerospace systems.

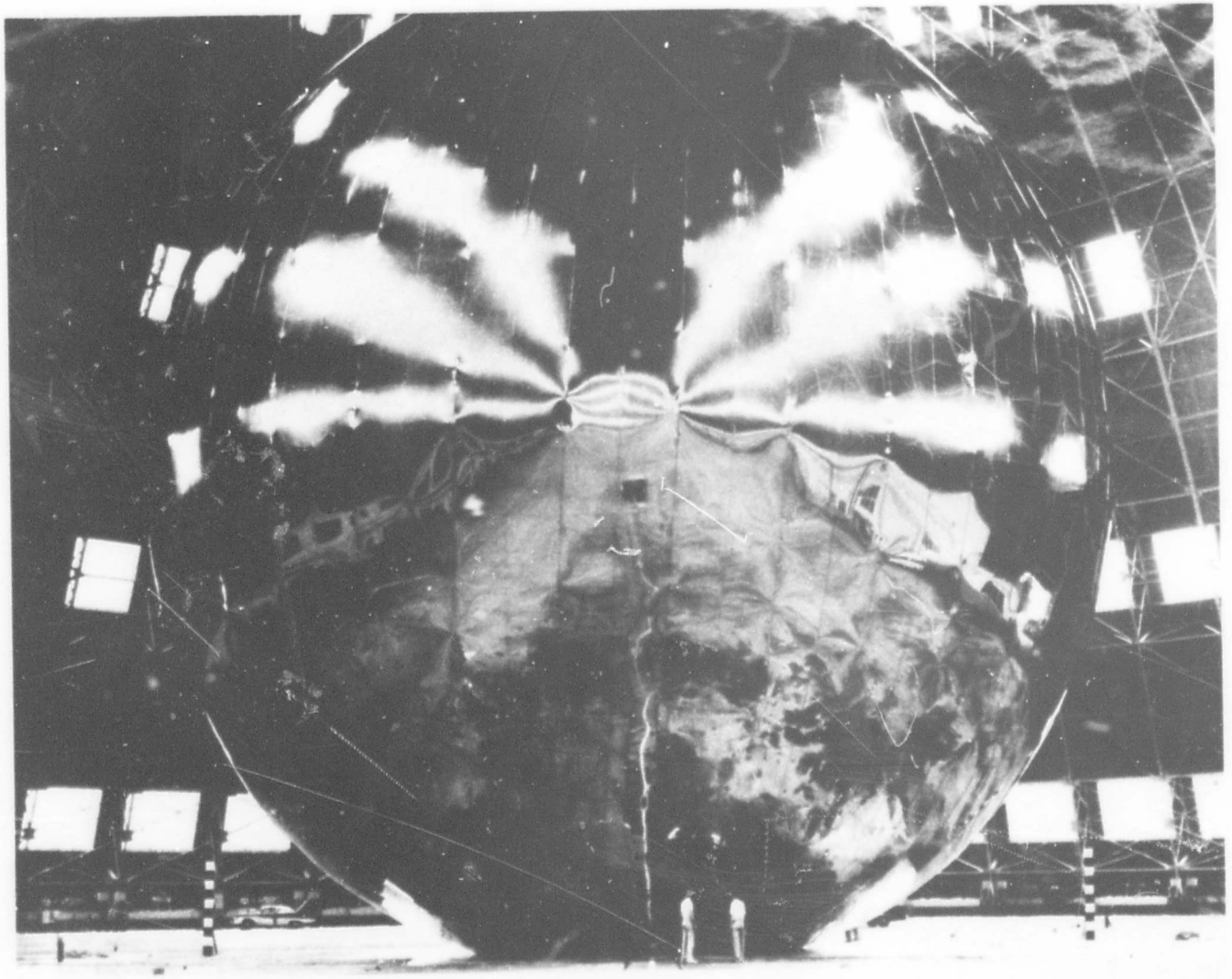

Figure 1

ECHO I STATIC INFLATION

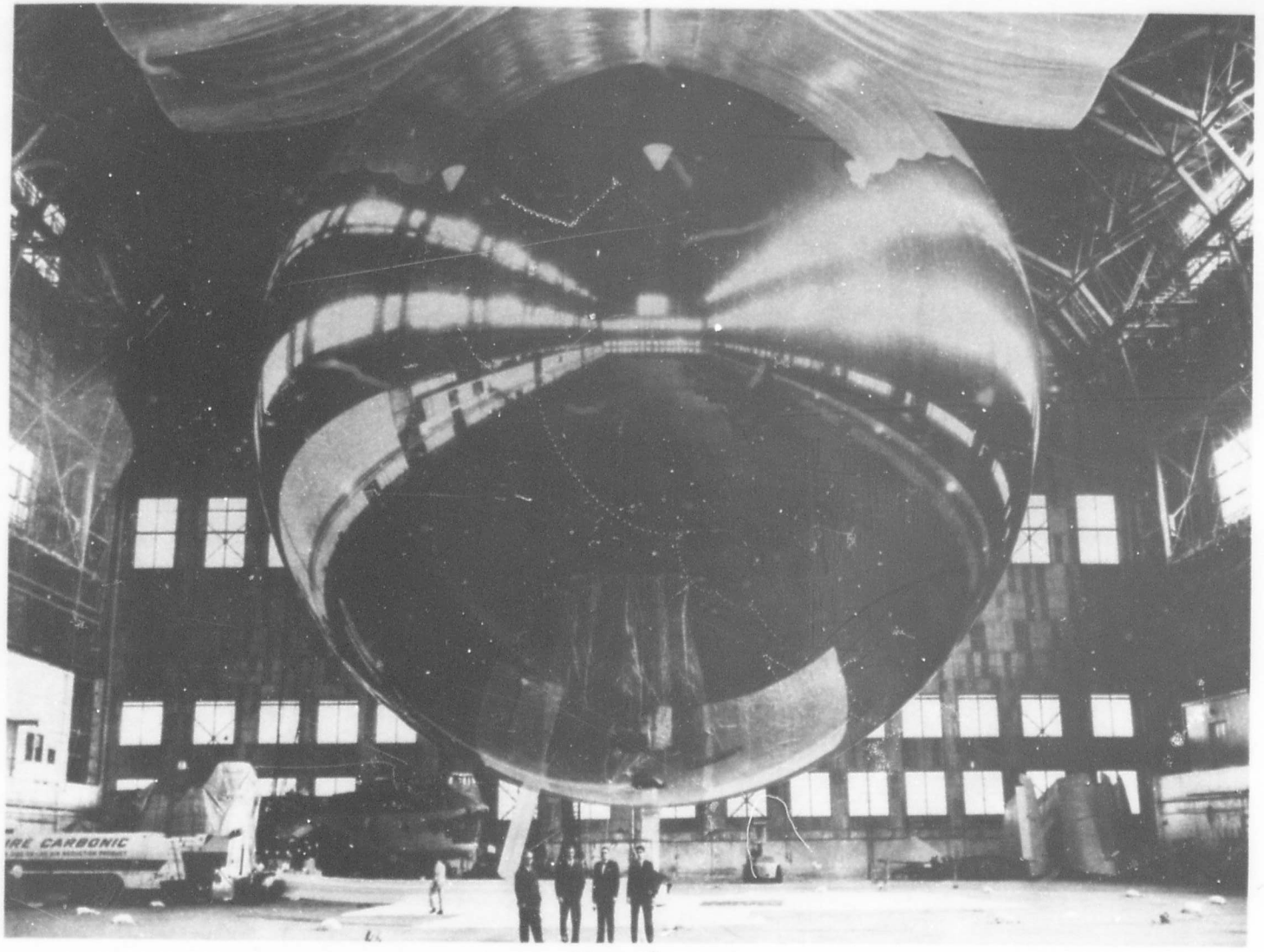

Figure 2

PAGEOS STATIC INFLATION

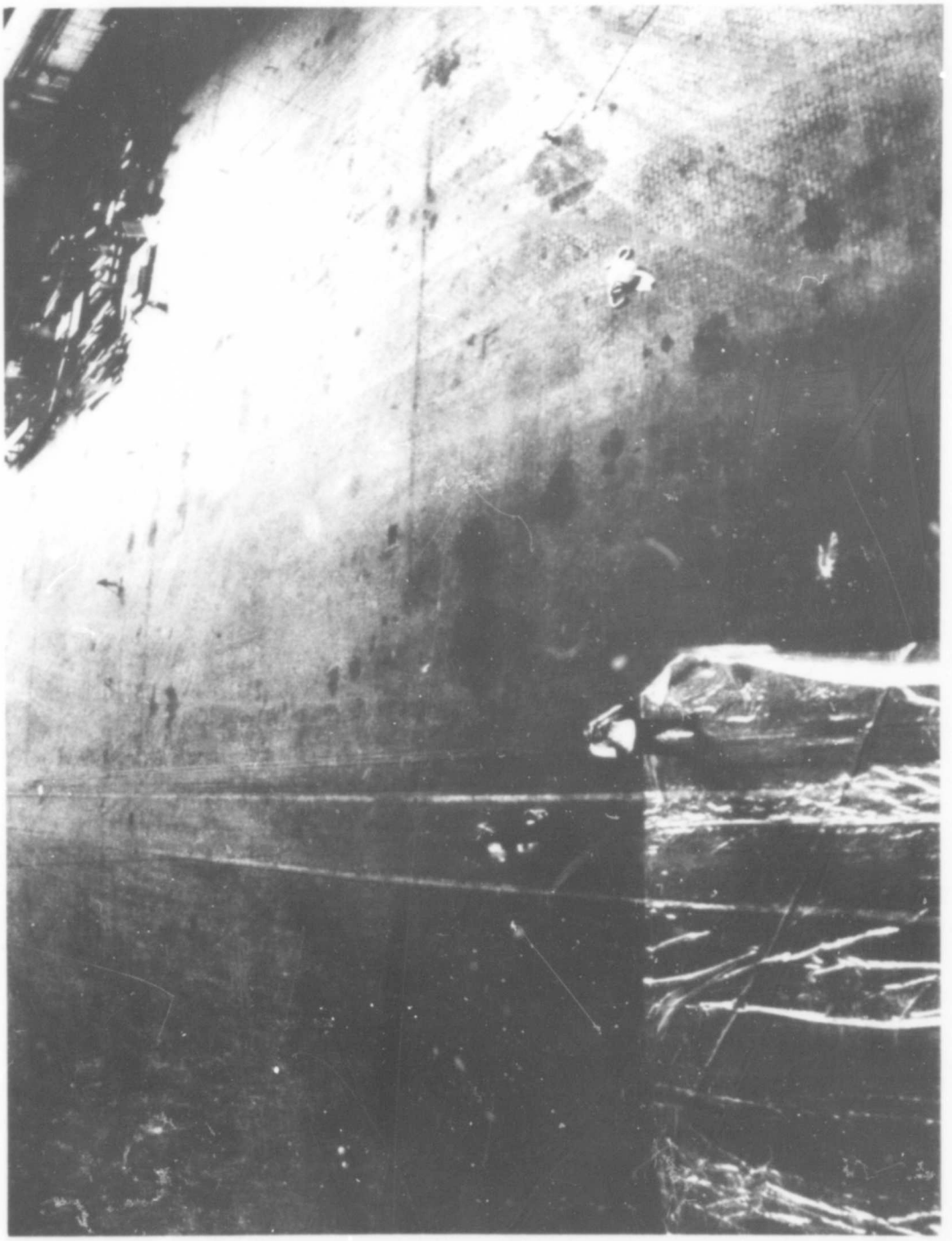

Figure 3
REFLECTED IMAGES

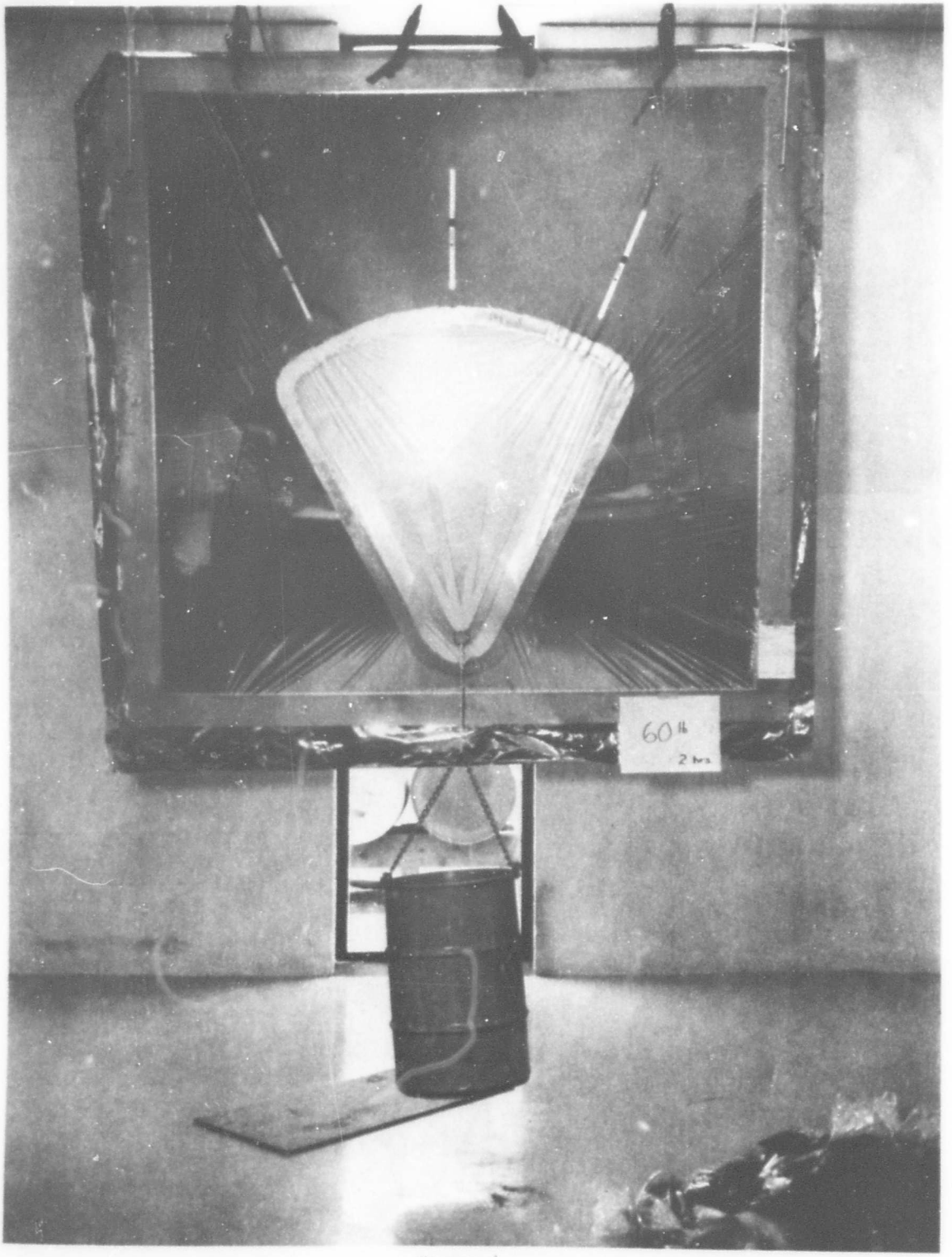

Figure 4

TESTING THE TIEDOWN ATTACHMENT

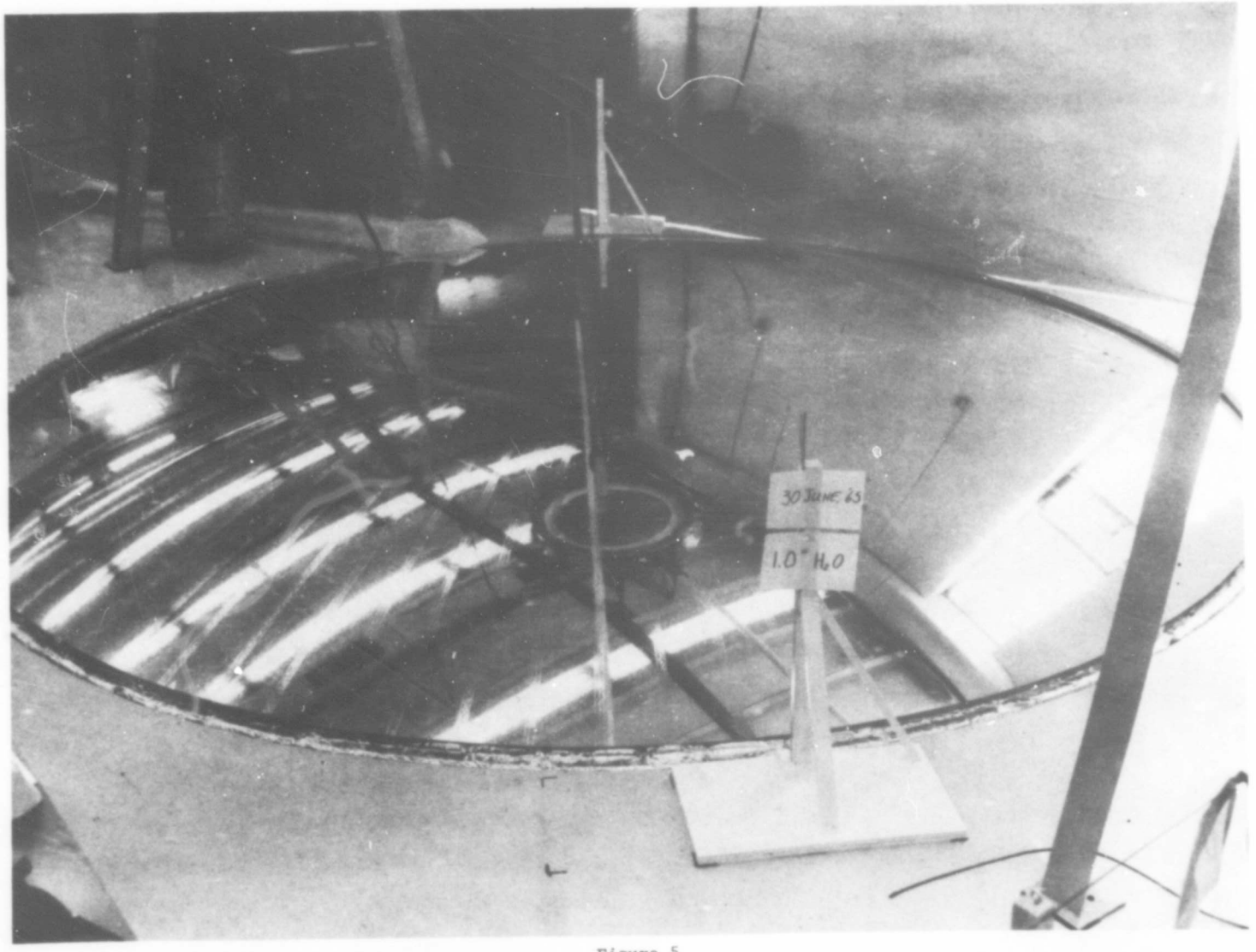

Figure 5
POLAR CAP

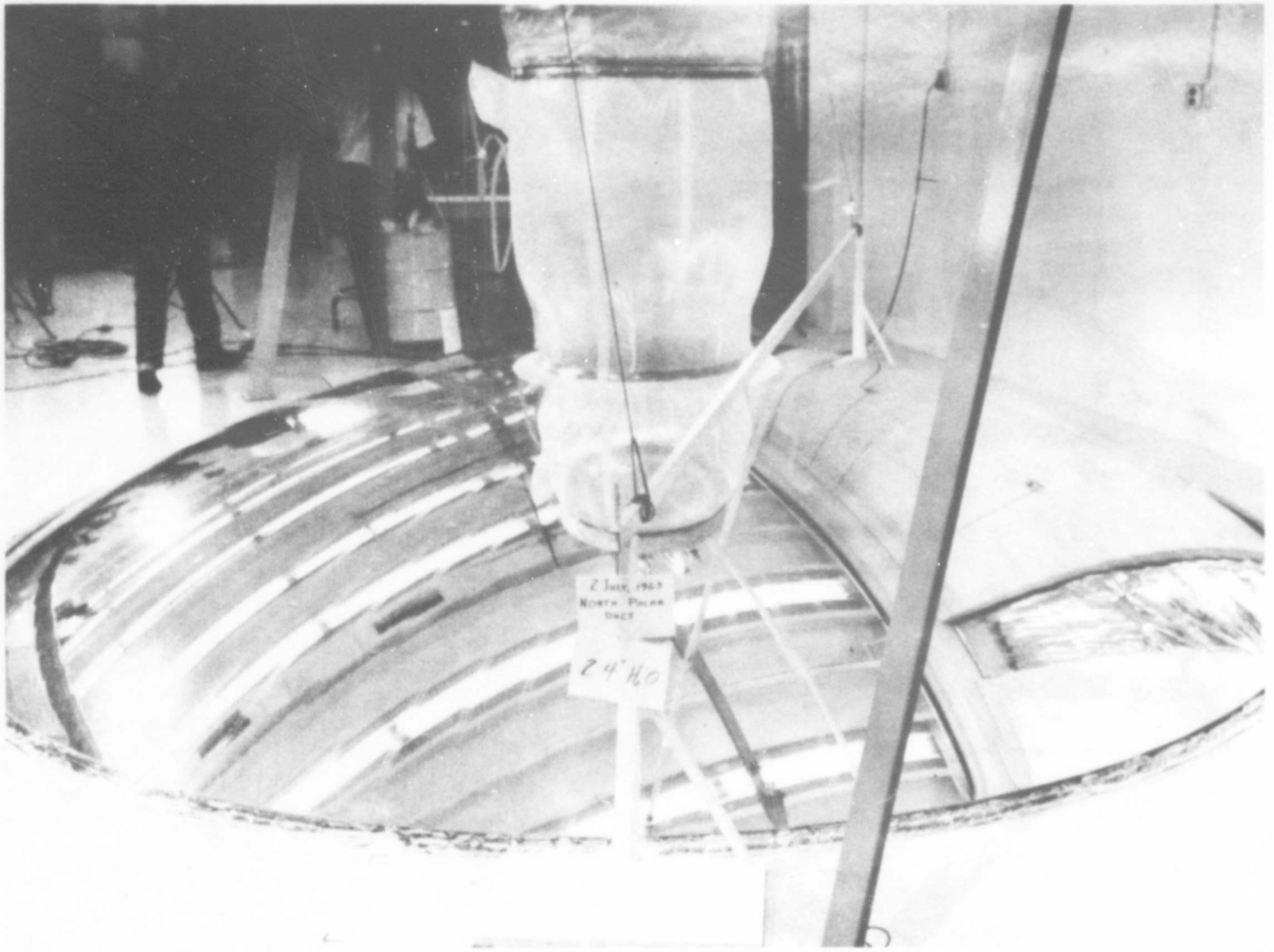

Figure 1

NORTH POLAR CAP WITH DUCT

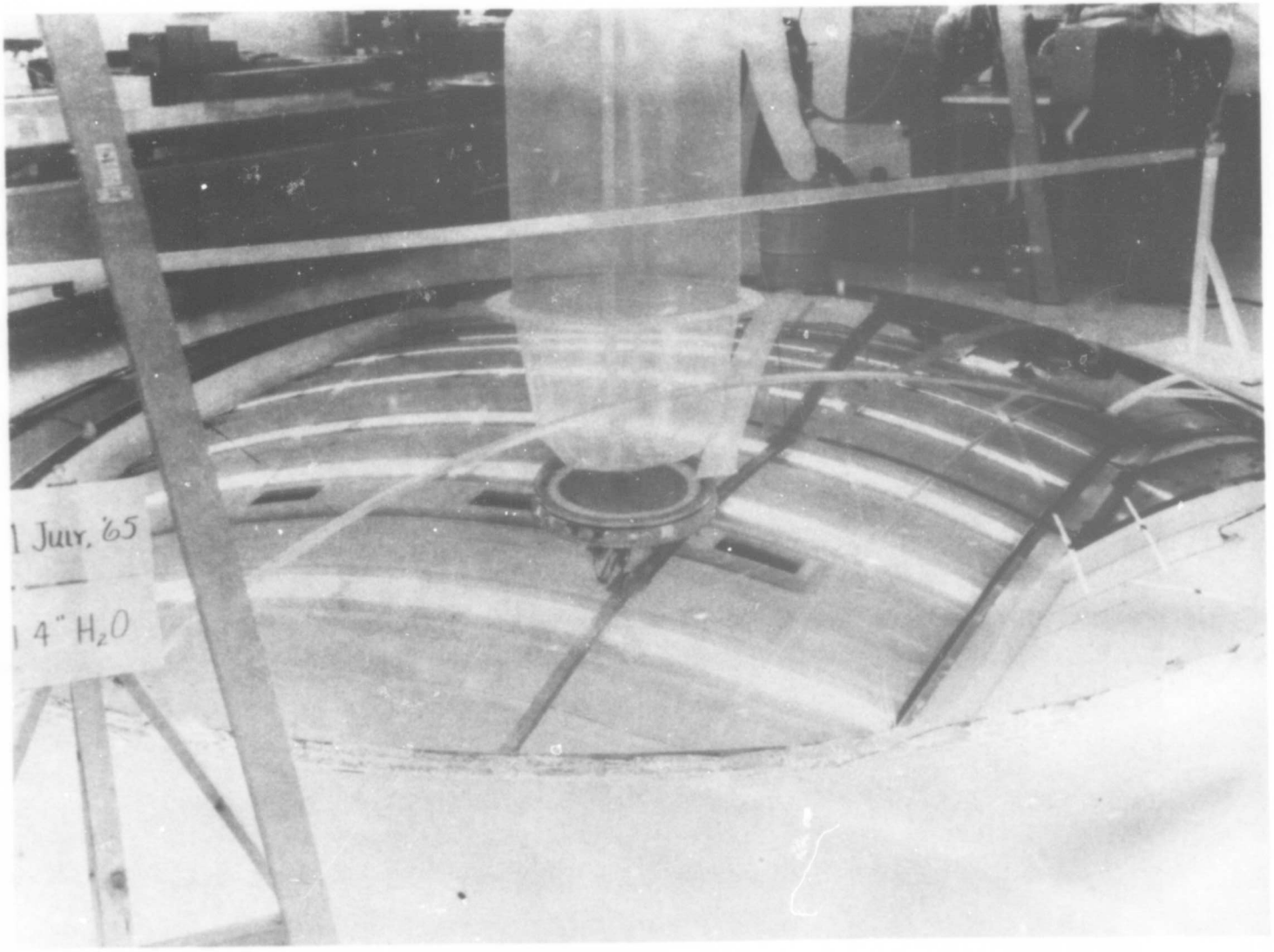

Figure 7

EXHAUST DUCT

BLANK PAGE

VACUUM TESTING OF EXPANDABLE STRUCTURES AND MATERIALS*

N. C. Latture, F. W. Nelms and R. E. Southerlan**

INTRODUCTION

Vacuum tests are needed to insure that expandable structures can be deployed in a simulated space environment and that once deployed they can withstand the space environment. The Aerospace Environmental Facility (AEF) (Figure 1) at the Arnold Engineering Development Center (AEDC) Arnold Air Force Station, Tennessee has the capabilities to conduct these tests. This paper will present the capabilities of three AEF chambers (Aerospace Environmental Chamber Mark I, Aerospace Research Chambers (12V) and (7V) [ARC (12V) and ARC (7V)]) and the results of four tests which were conducted for Goodyear Aerospace Corporation, GCA Viron Division and the Research and Technology Division (RTD) Aero-Propulsion Laboratory, Wright-Patterson Air Force Base, Ohio.

The first articles tested were inflatable, self-rigidizing structures which are characterized by a fabric substrate. The fabric is woven or assembled into a sandwich construction, impregnated with resin, and packaged for deployment. Four 1/6 scale models of a space shelter were tested in the ARC (12V) for GCA Viron Division, a division of GCA Corporation. The test objective was to determine if the models would deploy and rigidize in a simulated space environment.

A 10 foot diameter by 25 foot long expandable, cylinder-type aerospace shelter was tested in the Mark I chamber. The structure's 18 foot cylindrical portion was constructed of woven fiberglass flutes sandwiched between layers of urethane coated nylon. The cylindrical portion was terminated by two 10 foot diameter aspheric fiberglass and epoxy bulkheads which served as the structure's canister before deployment. The test objective was to determine if the vehicle would deploy and rigidize in a simulated space environment and to record the deployment and rigidization with motion-picture photography.

*The research reported in this paper was sponsored by the Arnold Engineering Development Center, Air Force Systems Command, under Contract No. AF 40(600)-1200 with ARO, Inc. Further reproduction is authorized to satisfy needs of the U. S. Government.

**Project Engineers, ARO, Inc., Aerospace Environmental Facility, Arnold Engineering Development Center, Arnold Air Force Station, Tennessee

The other Mark I test was of an inflatable crew transfer tunnel designed and fabricated by Goodyear Aerospace Corporation. The tunnel is made from eleven separate layers of materials. It is packaged in a canister which will be remotely ejected once the space vehicle and space laboratory are in orbit. The tunnel will be deployed and pressurized to 0.5 atmosphere. The test objectives were to: (1) determine the stress loads in the canister separation screws by the packaged tunnel applying some additional pressure against the canister during vacuum chamber pumpdown to 10^{-4} torr, (2) demonstrate the functional separation of the canister and deployment of the unpressurized expandable tunnel at 10^{-4} torr or lower, and (3) determine the appearance of the tunnel and the leakage rate from the tunnel during a 24 hour period while pressurized to 0.5 atmosphere at 10^{-4} torr or lower.

Many of these expandable structures will be subjected to low pressure and to the combined environments of low pressure and solar radiation. To determine the effects of these factors, rigidized fiberglass samples from Hughes Aircraft Company, Archer Daniels Midland Company (ADM) and National Cash Register (NCR) were tested in the Aerospace Research Chamber (7V) under simulated orbital conditions.

Test conditions included a 60 day vacuum exposure at mid-10^{-8} torr with solar coverage 56.9 minutes per 90 minutes simulating a 200 nautical mile orbit. One set of materials was exposed to the vacuum only and the other set to combined vacuum and solar environments. Tensile and flexural properties were determined for the two cases and compared with the results obtained after a five day vacuum drying period. Effects on density, thermal expansion, dimensional stability, surface reflectivity and light transmission were also determined.

TEST CHAMBERS

Aerospace Research Chamber (12V)

The Aerospace Research Chamber (12V) (Figure 2) is specifically designed and constructed for the conduction of thermal balance tests requiring a high pumping speed, solar simulation, albedo simulation and complete cold wall.

The chamber shell and cryoliner are constructed of stainless steel to give low outgassing and good corrosive resistance. The usable test volume is 10 feet in diameter by 12 feet high. A solar simulator ("top sun") has been designed and fabricated and is now operational. This is an off-axis, integrator type system with an array of 20-kw Xenon lamps irradiating (via an optical integrator and a collimating mirror) a test area 8 feet in diameter (Figure 3). Albedo simulation is supplied by tungsten filament lamps.

The chamber has a conventional pumping system. A liquid-nitrogen-cooled (77°K) surface completely enclose the 10-foot-diameter by 12 foot high test volume. The LN_2 surface shields 120 ft^2 of gaseous helium-cooled (20°K) surfaces which cryopump nitrogen, oxygen and argon. A 500-cfm mechanical pump is used to rough the chamber down and a 140-cfm mechanical pump backs a valved, 32-inch oil diffusion pump. The performance of this pumping system (Figure 4) may be improved for special applications by optional cryosorption or titanium gettering.

Aerospace Environmental Chamber Mark I

General Description

The Mark I chamber (Figures 5 and 6) is a cylindrical vessel 42 feet in diameter and 82 feet in height with 0.875-inch thick walls and 1.5-inch thick elliptical heads. The chamber shell is constructed of 304L stainless steel to give low outgassing and good corrosion resistance.

The inside working dimensions of the chamber are 35 feet in diameter and 65 feet in height. Vehicle entrance to the chamber is through a 20 foot diameter hatch located in the top of the chamber. Personnel access to the chamber is through a hatch 8 feet in diameter near the bottom of the chamber.

Pumping Systems

Three pumping systems are available for evacuating the Mark I chamber: (1) a three-stage increment of the Propulsion Wind Tunnel Facility (PWT) plenum evacuation system, (2) a conventional vacuum pumping system consisting of roughing pumps, fore pumps, booster pumps, and diffusion pumps, and (3) a cryopumping system cooled by 90-kw liquid nitrogen and a 10-kw gaseous helium system.

The plenum evacuation system is capable of evacuating the chamber from atmospheric pressure (760 torr) to 50 torr in approximately 80 seconds as shown in Figure 7.

The conventional pumping system consists of two 850-cfm roughing pumps and one to eighteen mechanical fore pumps which are used to evacuate the chamber from atmospheric pressure to 15 torr in approximately two hours; where two 4000-cfm Roots® blowers are started. They lower the pressure to 10^{-1} torr in two hours; next, one to eighteen booster pumps are placed in operation; and at approximately 10^{-2} torr the roughing pumps and Roots blowers are valved out and then from one to forty-eight 32-inch diffusion pumps can be placed in operation. This will complete the evacuation of the chamber to the 10^{-6}

® The named commercial product(s) in this paper is not to be considered in any sense as an indorsement of the product(s) by the United States Air Force or Government.

torr region in a total of approximately 4.5 hours (see Figure 8). The total pumping speed of this system for hydrogen is 2.5×10^6 liters/sec and 1.0×10^6 liters/sec for air.

The cryopumping surfaces are aluminum alloy finned copper tubes shielded by liquid nitrogen cooled stainless steel shields (Figure 9). The cryopump surfaces are maintained below 20°K by a gaseous helium refrigeration system which can absorb 10-kw at that temperature. This system has two 5-kw refrigerators in parallel (Figure 5). In combination with the stainless steel wall panels cooled to an average of 72°K by subcooled liquid nitrogen, the cryopumps provide a pumping capacity for nitrogen of 30×10^6 liters/sec; the panels will pump water vapor or carbon dioxide at a speed of 140×10^6 liters/sec. The cryosurfaces require about twelve hours to reach operating temperature, and cooldown can be started at 10^{-1} torr. Figure 10 is a typical pumpdown curve with cryopumping and Figure 11 shows typical throughput curves for the gases of principal interest.

Thermal Environmental Systems

To conduct thermal balance tests, the Mark I will have a solar simulator. Presently available is a tungsten lamp heat flux simulator for planet albedo, planet radiation simulation and solar heat flux simulation. Cold surfaces for simulating the cold, black sky of space are being installed, and a handling system is available to support and maneuver the test vehicle with respect to the solar simulator. These systems will allow thermal balances to be carried out under deep space or earth orbital conditions.

The planet albedo (reflection of solar energy from a planet) and planet radiance are simulated by one system with as many as 1500 T-3 quartz-envelope tungsten filament lamps mounted in individual reflectors which may be spaced around the test vehicle to irradiate it to the desired amount. This system can also be used as a solar heat flux simulator for tests not requiring the spectral match and decollimation angle provided by a solar simulator. Each lamp has an output continuously adjustable from 0 to approximately 24 w/ft^2 at a distance of 30 inches in front of the lamp reflector unit. This output is uniform to within ±5 percent and extends approximately ±40 degrees on each side of the output centerline. The lamp units may be installed in multiples to further increase the level of radiant energy. The lamps may be grouped in banks, each with an individual control circuit, so that the desired distribution of energy can be achieved on the vehicle surface. There are fifty channels of control circuits, each capable of delivering up to 15-kw.

The simulator units will be attached to a bird cage arrangement surrounding the test vehicle (Figure 12). The bird cage is supported by the vehicle handling system and is adjusted and tailored to adapt to different test vehicle shapes, sizes and requirements.

Efforts are currently underway to procure and install a solar simulator with a well collimated uniform beam which will more nearly duplicate the sun.

Vibration System

A vibration system is provided to simulate the vibrations which may be imparted to the vehicle during powered phases of flight. Vibrational testing is conducted with the vehicle supported near the bottom of the chamber. In general, it cannot be accomplished simultaneously with thermal testing, but it can be conducted during pressure trajectories and under steady-state low pressure conditions.

Two vibration systems are provided and each is capable of both sine wave and random excitation.

The heavy load, low frequency vibrations transmitted to the vehicle from the booster engine during the launch phase of flight can be simulated by four hydraulic exciters mounted below the chamber on a 100-ton concrete reaction block (Figure 13). Each exciter can operate from 5 to 500 cps and provide a maximum force output of 50,000 pounds.

The low load, high frequency vibrations imparted to the vehicle from staging and maneuvering rockets can be simulated by a 30,000-pound force capacity electrodynamic exciter operating over a frequency range from 5 to 3000 cps. This shaker is mounted on the chamber centerline (Figure 13) and utilizes the 100-ton concrete reaction block.

Aerospace Research Chamber (7V)

Vacuum and thermal environments for the radiation study were provided in the Aerospace Research Chamber (7V), Figure 14. A liquid nitrogen cooled liner completely encloses the test area providing a radiation heat sink and a pump for 77^{o}K condensables. Two 32" oil diffusion pumps backed with 6" oil diffusion and mechanical pumps provide the basic vacuum pumping.

Low temperature gaseous helium is available from two systems. One of these systems can also produce 60 liters/hour of liquid helium. A new inner liner is under construction that can be cooled with either gaseous or liquid helium. This will be used to provide low radiation backgrounds and a highly efficient molecular sink (Figure 15).

SCALE MODEL SPACE SHELTER TEST IN ARC (12V)

Test Article Description

The test structure in both the package and deployed positions is shown in Figure 16. The model consists of two epoxy domed halves 10 inches deep and 20 inches in diameter joined by a fabric substrate center section. The halves are sealed with an O-ring and held together by a spring loaded clamp with an explosive bolt. The deployed model is 20 inches in diameter, and the center fabric between the domed halves is 38 inches in length.

The fiberglass sandwich section was impregnated with a resin which was activated by a catalyzing vapor (H_2O). Figure 17 shows the catalyst container mounted on top of the domed half of the model. Two solenoid valves are used to control the catalyst flow to the fiberglass fabric sandwich section. A heater was used to maintain the proper catalyst temperature (approximately 80°F).

Test Configuration

The test setup (Figures 17 and 18) shows the model mounted in a cage in the test chamber. The strain-gage-type load cell which was used to measure the vehicle weight was located at the top of the cage (Figure 17). This cage was used to support the heat flux lamps (quartz envelope tungsten filament lamps), which were used to maintain the proper curing temperature on the model surface. The front surfaced mirrors shown in Figure 18 permitted visual monitoring of the back side of the test model.

Instrumentation

Chamber instrumentation was monitored with an alphatron and two ionization gages. Copper-constantan thermocouples were used to monitor the LN_2 liner temperature. The power input to the heat flux lamps was measured by standard a-c voltmeters and ammeters. Variable transformers were used to change the output level of the lamps. A total radiation thermopile detector was used to determine the output level from the heat flux lamps. A strain-gage-type load cell was used to monitor the weight of the test model. A 25-channel data logger system and strip chart recorders were used to record all test data. A camera located outside a chamber port was used to obtain permanent motion-picture coverage of the deployment and rigidization. A closed-circuit television located inside the test chamber was used to monitor the deployment of Model No. 4.

Procedure

Pre-Test Preparation

Reflectance measurements were made on a sample of model surface material over the wavelength range from 0.3 to 7 microns. These measurements were then used in conjunction with the output of the heat flux lamp (0.3 to 7 microns) to determine what output would be required from the lamps to produce the desired temperature on the model surface. The lamps were then spaced around the vehicle surface to give the desired distribution and output. The total radiation detector was used during the test to monitor the lamp outputs, which were used to calculate the model surface temperature.

Preparation of Test Model

The deployed model before being prepared for the test is shown in Figure 16. The outer mylar or polyethylene covering was used to seal the fiberglass section from the water vapor in the atmosphere. That section was purged with dry nitrogen prior to impregnation. A vacuum pump was attached to this section and the section pumped to a low pressure to help impregnate the fiberglass of the model with resin (Figure 19). After the impregnation was completed, the model was packaged (Figure 20), sealed with the spring loaded clamps and explosive bolt, and suspended in the test chamber as shown in Figure 21.

Test Procedure

The ARC (12V) was evacuated to 10^{-5} or 10^{-6} torr, depending on the outgassing load from the test model. After the chamber pressure stabilized, the heat flux lamps were energized, the motion-picture camera was started, and two seconds later the explosive bolt was fired to initiate deployment (time = 0) of the test model. Figure 22 shows the model partially deployed. Approximately 10 minutes were allowed for the chamber pressure to recover from the deployment. Then the model was pressurized with CO_2 (2 to 12 torr) to obtain the desired shape. The CO_2 was used instead of air because it is easily pumped with a 77°K cryopump. The model is shown deployed and properly shaped in Figure 23. After the model was shaped the flow of the catalyst (H_2O) was started for rigidization. The heat flux lamps maintained the model surface temperature above 65°F during rigidization.

Results and Discussion

Model 3 Results

Deployment and rigidization were successful as can be seen in Figures 22 and 23 taken from the motion pictures. A chamber pressure of 4×10^{-6} torr (Figure 24) was attained prior to deployment and pressures in the low 10^{-5} torr region were

maintained during the time the model was being rigidized. The heat lamps were energized 2 minutes prior to deployment. These points can be seen on Figure 24 as well as the pressure surges caused by the catalyst. The test model weight loss (Figure 25) was as expected. The model was maintained at a higher temperature (Figure 26) during this test and this tended to speed up rigidization. At 74 minutes, power to the lamps was reduced, resulting in the temperature decrease shown. Figure 27 shows Models 3 and 4 after rigidization.

Model Deployment

The deployment of Models 2, 3 and 4 was successful. As soon as the explosive bolt was fired to release the spring loaded clamp, the model immediately dropped to its fully expanded length. Model 1 did not deploy properly. When the clamp was released, the model did not drop but had to be forced down with air pressure. Indications were that rigidization had started before the model was deployed. This may have been caused by excess heat on the model prior to deployment. In addition, chamber pumpdown required approximately 3.3 hours or 1 hour longer than the pumpdown time required for the other models.

Model Rigidization

Although no structural strength tests were conducted on the models they were checked for rigidization. Each model was well hardened and very rigid.

Model Weight Loss

Model weight loss should remain constant prior to deployment and drop sharply during deployment. The weight should continue to decrease during rigidization as portions of the catalyst vaporized and the resin outgasses. Models 2, 3 and 4 lost weight as expected (Figure 25). They showed a drop during deployment as the entrapped excess resin and gases were allowed to escape. They continued to lose weight during rigidization as the catalyst was used and the resin cured. Model 1 started to lose weight prior to deployment and did not show a drop during deployment. The resin had started to cure prior to deployment. Weight loss continued during rigidization as the catalyst was used and the resin continued to cure.

Chamber Pressure

Chamber pressures maintained throughout the test were satisfactory considering the large gas loads (mainly H_2O vapor) which had to be removed. Approximately 4.0 pounds of the catalyst (H_2O) were used during the 1-hour rigidization time required to cure the resin. Gas loads (H_2O) in the range from 10^2 to 10^4 atmosphere cc/sec were removed in order to maintain the chamber pressure shown in Figure 24.

Heat Flux System

It was necessary to use the chamber heat flux system to maintain the model surface temperature above 65°F so that the resin would cure and rigidization would occur. The heat flux system is capable of producing a wide range of model surface temperatures. The higher curing temperatures (110 to 120°F) desired to accelerate the curing process were easily attained in these tests (Figure 26).

LARGE SPACE SHELTER TEST IN MARK I

Test Article Description

The expandable structure was similar to the small models tested in the Aerospace Research Chamber (12V) described earlier. Figures 28 and 29, respectively, show the test article in the packaged and deployed condition.

The domed bulkheads which served as the predeployment canister were constructed of fiberglass and epoxy. Each bulkhead weighed approximately 1000 pounds and was 10 feet in diameter by approximately 3.5 feet deep.

The fiberglass fabric was of a sandwich type construction with the fluted core parallel to the axis of the cylinder, Figure 30. Elements of the fiberglass sandwich consist of a 26 oz/yd^2 inner facing fabric, an 8 oz/yd^2 core fabric, and a 10 oz/yd^2 outer facing fabric. The outer covering was identical to the urethane-coated inner bladder fabric except that it was not pigmented. Fiberglass sections of the fabric sandwich were joined continuously at the flute lines by an integral weaving process. The bonds between the pigmented urethane-coated bladder, the 0.25-inch thick foam rubber, the fiberglass, and the urethane-coated nylon outer covering were made with flexible adhesives, Figure 30. An O-ring seal was used between the two halves of the canister which were restrained by a large spring-loaded ring clamp. The clamp was released by the simultaneous firing of two explosive bolts positioned 180 degrees apart on the periphery of the canister's 10 foot diameter.

The fiberglass sandwich section was impregnated with a resin which was activated by water vapor. The catalyst container and the two solenoid valves used to control the catalyst flow rate to the fiberglass fabric section are shown in Figure 31. Two 2500 watt heaters were installed in the container to maintain the proper catalyst temperature.

Test Configuration

Two test configurations were used. The first, for a shakedown run, had no resin in the fiberglass. The second was used in the rigidization test.

The first configuration was an assembly of the non-resin impregnated aerospace shelter and a full scale model of the Gemini vehicle (Figure 32). The purpose of using this assembly was to perform an operational check of the chamber, the test article and the support equipment. The second configuration did not include the Gemini model since it contributed significantly to the chamber pumping system gas load.

Instrumentation

The chamber pressure was monitored with two alphatron and two ionization gages. Copper constantan thermocouples were used to monitor the LN_2 liner temperatures, the three solenoid valve temperatures and the catalyst temperature. Four strain gage type load cells were used to monitor the weight of the test article (Figure 31). Transducers were used to make the required pressure measurements. All data were recorded using a strip chart recorder and a 25 channel data logger system. Two cameras were used to provide the motion picture coverage of the deployment and rigidization. These cameras were mounted outside the chamber and viewed the test article through portholes. One of the cameras was mounted to view the side of the extended cylinder and provided 400 frame/sec coverage for the first 10 seconds of its operation, then shifted automatically to 24 frame/sec coverage. The second camera was mounted on top of the chamber and operated at 24 frame/sec. A closed-circuit television camera located inside the chamber was used to monitor the deployment of the test article.

Test Procedure

The fabric portion was assembled to the bulkheads and the resin introduced to the fluted section of the cylinder. After resin impregnation was completed, the cylinder was packaged. The two bulkheads which served as the canister were brought together and fastened with a spring loaded clamp and the two explosive bolts. The packaged shelter was then installed in the test chamber.

The Mark I chamber was evacuated to the low 10^{-6} torr range for the shakedown run and to the low 10^{-4} torr range for the actual test. The higher pressure for the actual test was a result of the outgassing load (primarily resin-solvent vapor) from the test article. After the chamber pressure had stabilized and a final scan had been made of all the sensors, the motion picture cameras were started. Approximately 2 seconds later the explosive bolts were fired to initiate the deployment of the test article. After firing of the explosive bolts, the procedure was to have been to deploy the cylinder slowly by filling the bladder with CO_2 to a pressure of 6 inches of water. Figure 33 is a diagram of the CO_2 piping and valving arrangement. After complete deployment the catalyst

solenoid valves were to be operated as required to release the catalyst at approximately 20 lb/hr. The vapor distribution solenoid valves were to be used to release excess catalyst and solvent vapor. Pressure was to be maintained in the bladder at 6 inches of water until the rigidization process was completed.

Results

The shakedown run was accomplished successfully. Deployment of the shelter was performed using the CO_2 to pressurize the bladder section to approximately 16 torr. At this pressure the shelter was fully expanded and supported the Gemini model without assistance from the overhead support cables.

Motion pictures were made of the shelter Gemini model assembly's deployment and expansion. Shelter internal pressures, several test article temperatures, and the load cells' output were monitored during the run.

The rigidization test run was not completely successful. A chamber base pressure of 4×10^{-4} torr was attained for the test of the resin impregnated cylinder. The chamber pressure was limited because of the large gas load presented by the approximately 240 pounds of solvent (butyl-acetate) in the 600 pound of resin-solvent mixture used to impregnate the fiber-glass section of the cylinder.

All systems operated normally until immediately after firing the explosive bolts. Complete deployment of the cylinder occurred almost immediately after the bolts released the restraining ring. The cylinder expanded unevenly, bending and leaning toward the side containing the heavy, eccentrically positioned floor. Figure 36 shows the shelter floor location. The expansion rate and the asymmetrical weight distribution caused the almost fully expanded shelter to fall to the chamber floor. The violent deployment with its resultant damage precluded continuation of the test with the expanded cylinder resting horizontally on the chamber floor. The chamber was returned to atmospheric pressure. The cylinder was positioned with its longitudinal axis vertical and was pressurized to 8 inches of water gage. Rigidization of the resin-impregnated fiberglass section of the shelter was then accomplished at ambient conditions. Figure 35 shows the rigidized cylinder after removal from the chamber.

The shelter was inspected immediately after removal from the chamber. Although no structural tests were conducted, the fabric section was examined closely and was found to be very hard and completely rigidized. Most of the damage suffered during the violent deployment and fall was to the interior portion of the shelter.

The pressure in the resin-saturated fluted fiberglass section of the fabric cylinder was 13 inches of water prior to deployment of the shelter. Although this pressure was higher than desired, the decision was made to deploy since indications were that pressure would not be reduced significantly during an extended period of pumping.

The cause of the expansion of the cylinder to its full length in such a violent manner was traced directly to high pressure in the volume between the bladder and the outer covering, which contained the 600 pound of resin-solvent mixture. Analysis of the data and subsequent work done by the resin suppliers indicate that approximately 63 percent of the solvent (150 pound) should have been removed from the resin-impregnated fabric to prevent the violent deployment. It is quite unlikely that this amount of solvent could have been pumped by the chamber pumping system in a reasonable time since the lower portion of the cylinder contained a substantial amount of resin in the liquid phase that could very well have been trapped within the folds of the packaged fabric, thereby preventing the solvent from vaporizing.

One method of reducing the amount of solvent in the impregnated fabric would be to purge the fluted area with dry nitrogen until the required reduction in the solvent content is attained. To keep the resin solids suspended homogeneously in the impregnated fabric after drying, the resin suppliers recommend minute amounts of certain inert additives in the resin solvent mixture.

CREW TRANSFER TUNNEL TEST IN MARK I

Crew Transfer Tunnel Assembly

An inflatable expandable crew transfer tunnel (Figure 36) was packaged inside a canister and mounted to a carrier bed (Figure 37) which contains two hatches to simulate the space vehicle and space laboratory hatches. The deployed tunnel is shown in Figure 38 prior to being packaged. Solenoid valves were attached to lines leading to both hatches. Using vacuum pumps, the tunnel and the 2-inch foam layer were evacuated to 2 or 3 psi below atmospheric pressure and folded as shown in Figure 39. The canister was then placed over the tunnel and fastened to the carrier bed with twelve separation screws (Figure 39) installed in guillotines, which cut the screws and allowed separation to take place. The carrier bed with tunnel and canister was then hoisted and fastened to the test carrier support frame (Figure 40).

Test Configuration

Figure 41 shows the test article being lowered into the Mark I test chamber. The test article (Figure 40) is shown in

the test carrier support frame with a canvas catcher installed to the support frame to catch the canister after deployment. The test article is shown (Figure 40) in the test chamber, with all instrumentation and pressure lines connected, ready for canister separation and tunnel deployment. Four cameras mounted outside three viewing ports were used to obtain high speed and standard speed motion pictures of the canister separation and tunnel deployment and pressurization. A closed-circuit television located inside the test chamber monitored the canister separation, tunnel deployment and pressurization.

Pumping System Used

The pumping system used to test the crew transfer tunnel consisted of two 850-cfm roughing pumps and four mechanical fore pumps to evacuate the chamber from atmosphere to 15 torr, where two 4000-cfm Roots blowers were started; at 10^{-1} torr four booster pumps were placed in operation; and at 10^{-2} torr the roughing pumps and Roots blowers were valved out, and two 32-inch diffusion pumps were placed in operation. Approximately 100 ft^2 of LN_2 cryopumping surfaces was used. Figure 42 shows the pumpdown curves obtained with this system.

Instrumentation

Chamber pressure was monitored by two alphatrons and three ionization gages. The tunnel internal pressure was monitored by two transducers and an absolute mercury pressure gage. Iron-constantan thermocouples were used to monitor the tunnel wall foam temperature. Strain gages were used to monitor the loads in the canister separation screws during chamber pumpdown. A 25-channel data logger system, strip chart recorders, and multipoint recorders were used to record the test data. Canister separation, tunnel deployment and pressurization were monitored by a closed-circuit television and recorded by four motion-picture cameras.

Test Procedure

The normally closed solenoid valves were energized to allow gas in the packaged tunnel to escape into the chamber during pumpdown. Still photographs were taken of the packaged, assembled tunnel (Figure 40) and initial strain-gage readings were recorded. Chamber evacuation was then started.

During chamber pumpdown, vacuum chamber pressure (Figure 42) tunnel wall foam temperature, solenoid valve temperatures, tunnel internal pressure (Figure 42) and separation screw loads were monitored and recorded.

Tunnel wall foam temperature was to be maintained above 50°F, and the solenoid valve temperature was to be maintained below 200°F during pumpdown. The separation screw loads were not to exceed 200 lb/screw.

When the chamber stabilized below 10^{-4} torr, the solenoid valves were de-energized and the tunnel was ready for deployment. With the tunnel wall foam temperature at 82°F and the chamber pressure at 3.2×10^{-5} torr, (Figure 42) and the tunnel internal pressure of 4 torr, the chamber lights were turned on and the four motion picture cameras were started to record the canister separation, deployment and pressurization at 400 and 24 frames/sec. One second later, the twelve pyrotechnic guillotines were simultaneously fired. The guillotines cut the canister separation screws, the canister fell into the canvas catcher on the test carrier and the tunnel started to deploy (Figure 43).

Deployment of the tunnel was completed by inflating it with carbon dioxide. The tunnel was pressurized to 0.5 atmosphere, and the chamber lights and cameras were turned off. The tunnel temperature and pressure were allowed to stabilize over a 2-hour period, and the tunnel leakage was measured over a 24-hour period. The tunnel internal pressure, foam wall temperature and chamber pressure were recorded initially and at 0.5-hour intervals during the 24-hour leakage test. At the end of the 24-hour period, the chamber and tunnel were both returned to atmospheric pressure.

Results and Discussion

The test data obtained from this test consisted of motion pictures of the canister separation, tunnel deployment, and pressurization. Chamber pressure, tunnel internal pressure and wall foam temperature were recorded during the chamber pumpdown and the 24-hour leakage test. The loads on the canister separation screws were recorded during chamber pumpdown. Results indicate that all test objectives were successfully accomplished.

Canister Separation, Tunnel Deployment, and Pressurization

As described in the section on Test Procedure, separation, deployment and pressurization were successfully accomplished and recorded by four movie cameras, one viewing each end of the tunnel and two broadside. Figure 43 shows the tunnel during three different stages of deployment and pressurization.

Chamber and Tunnel Internal Pressure

The curve on the left of Figure 42 shows how the tunnel pressure followed the chamber pressure during the pumpdown prior to deployment. The flat spots on the initial pumpdown curve at 10^{-3} and 2×10^{-4} torr are the results of leaks in the chamber that developed and were temporarily repaired during the pumpdown. This curve also shows the repressurization of the tunnel prior to the 24-hour leakage test.

The curve on the right of Figure 42 shows the second pumpdown and the 24-hour leakage test. During the 24-hour test, the tunnel internal pressure decreased from 397 to 362 torr. The total leakage during the 24-hour period was 0.54 pounds or 2.25×10^{-2} lb/hr. The chamber pressure gradually decreased from 5.5×10^{-5} torr to 2.4×10^{-5} torr during the 24-hour test. Figure 44 shows the pressurized tunnel after completion of the 24-hour leakage test.

Tunnel Wall Foam and Solenoid Valve Temperature

The tunnel wall foam temperature was 82°F at deployment and increased to 129°F because of the heat load from the chamber lights, which were required for motion-picture coverage. During the 24-hour leakage-test, the tunnel wall foam temperature increased from 90 to 92°F. These temperatures are all satisfactory since the requirement was a minimum allowable temperature of 50°F. The solenoid valves were easily maintained at temperatures below the 200°F maximum allowable.

Loads in Canister Separation Screws

The strain gages indicated a very negligible load change, compared to the 200 pound allowable, on the canister separation screws during chamber pumpdown.

COMBINED ENVIRONMENTAL TESTS IN THE ARC 7V

Apparatus

The solar environment for this study was provided by a Genarco carbon arc unit, Figure 14. The unit produces one solar constant over a 30" diameter area. Radiometers located in the test plane monitored the radiation level throughout the 60 day test period, Figure 45.

Two tensile test assemblies were fabricated; one installed in the solar beam and one shielded from the radiation, Figure 45. This allowed a determination of tensile properties without exposure of the test samples to atmospheric conditions.

Procedure

Flexural and tensile specimens were cut with the warp direction lengthwise, Figure 46. As many samples as possible were cut from the 8" x 10" fiberglass laminates received. Twenty samples of each shape were exposed to mid-10^{-8} torr vacuum for 108 hours to dry. These samples were then tested and the results used as a basis of comparison for later results. One flexural sample from each supplier was mounted for optical observation. Thermocouples were attached to smaller pieces to determine sample temperature before pulling. (LN_2 liner was cooled during the vacuum soak.) (Figure 45)

Eighteen tensile samples were mounted in each test assembly for the 60 day test phase. Nineteen flexural samples were exposed to combined solar and vacuum, eighteen samples to vacuum only. After the various exposure periods, the chamber was repressurized with dry nitrogen and the flexural samples removed for testing. Several small samples were instrumented with thermocouples to measure the temperature change during the 90 minute period and to measure temperature differences across the samples.

Tensile tests using strain rates of .055 in/in min were made under vacuum to the extent possible. Samples mounted in the solar beam slipped in the tester clamps and only six samples were successfully tested. After a nitrogen pressurization and removal of the flexural samples, additional clamping was added, Figure 45. The samples were again vacuum soaked for two days and six more were successfully tested. The remaining samples were removed and tested outside the chamber for mechanical strength only.

The ASTM standard method of test for flexural properties of plastics was used as a guide for the bending tests. The samples were supported on .25" diameter supports 1" apart. This gave a span-to-depth ratio of about 32 to 1. The mid-span deflection rate used was .037 in/min.

Throughout the 60 day phase, ten minute data scans were made of the radiometer and thermocouples. Two minute time lapse photography from two outside locations were also obtained. Optical measurements and continuous temperature monitoring were made at various times during the 60 day test phase. A statistical distribution of solar intensity at the two locations is shown in Figure 46.

Results

A summary of the mechanical properties is shown in Table 1. No proportional limit was indicated by the tensile data. In general, an increase in strength was measured after exposure to solar and vacuum. The combined vacuum and solar effects increased the density from 3 to 10 percent but little change was noted after vacuum exposure only.

Slight changes were noted in the dimensional properties. An elongation of .02 mm/2 inches was measured during the solar period. A slight curl in the NCR sample mounted for optical observation (Figure 45) was noted during the "off" cycle amounting to 2 mm displacement at the bottom. No other movement was detected by the photography on the other two samples.

Temperature differences of $4^{O}F$ between the illuminated and non-illuminated sides were measured throughout the test even though the samples darkened as the test progressed. During

the solar exposure maximum temperature varied from 20°F to 85°F averaging near 60°F. In the "off" cycle, temperatures dropped 90°F to 100°F, Figure 56.

Discussion

General Appearance of Materials

The sample sheets were constructed of interwoven and laminated fiberglass impregnated and rigidized with resin. No information was provided as to how the laminates were made nor the composition of the resin. Samples supplied by National Cash Register had the appearance of being pressed at some point during fabrication. Hughes and Archer Daniels Midland samples did not appear to be pressed. Figures 48 and 49 show comparisons of surface texture and warpage before the test samples were cut.

Tensile Tests

A comparison of tensile failures and cross sections of non-failed areas of these samples under 10X magnification are shown in Figures 50 and 51. In most cases failure occurred at the minimum cross section on the Hughes and NCR samples. The light spot on the NCR sample is a partially failed area. A much larger area of resin failure was noted in the Hughes samples. One of these samples was tested at -200°F and the resin separated from the fibers the entire length of the 2" test section. The ultimate tensile strength of this sample was 43,500 and the modulus of elasticity near 825,000 psi. Most of the ADM samples failed at the face of the holding clamp indicating a high notch sensitivity. Some of these samples were retested and failed in the minimum cross section at ultimate values near those previously obtained.

No set pattern of change in tensile strength or modulus of elasticity was established for the three materials tested. After vacuum exposure only the Hughes samples decreased in strength and after the combined exposure the ADM samples weakened. Further, there was no correlation between the ultimate strength and the modulus of elasticity. In all cases the modulus of elasticity decreased after 60 days of only vacuum exposure and increased under the effects of combined exposure. Typical tensile data are shown in Figure 52.

Bending Tests

The flexural test data gives additional indications of the environmental effects. All averages of the load at failure (Table 1) increased after the 60 day exposure to vacuum only. Further increases were measured on the sample exposed to both vacuum and solar when flexed with the solar exposed side in compression. This was most apparent with the Hughes samples

as a 45 percent decrease in strength and a 41 percent decrease in flexibility was measured with the non-illuminated side in compression. Comparative runs are shown in Figure 53. On more than half of these flexural samples, failure occurred on the side not directly exposed to the solar beam irrespective of the bending direction. This indicated a definite increase in resin strength after solar exposure. Comparisons of failed specimens and corresponding cross sections (unfailed) are shown in Figures 54 and 55.

Density, Dimensional and Thermal Properties

The mechanical properties of this type of fiberglass proved desirable for several reasons. No change in length greater than .01 mm was measured after any of the test conditions. An average coefficient of thermal expansion of 4.0×10^{-6} in/in ^{o}F was measured over a $100^{o}F$ temperature excursion during the simulated orbit. Typical temperature response of a sample is shown in Figure 56.

Some indication of the heat conduction properties was obtained by temperature measurements on each side of samples exposed to the solar beam. Thermocouples were cemented to both sides of several samples and temperature differentials of $4^{o}F$ were measured. There are many factors affecting the accuracy of this measurement and it should only be considered as an indicator rather than a measurement of thermal conductivity.

Spectrophotometer studies gave some further experimental measurements of thermal properties. Reflectivity and transmissivity properties were determined on samples subjected to vacuum exposure only and compared to similar samples exposed to the combined vacuum and solar. The transmissivity was measured in the wavelength band from .35 to 2.5 microns and the reflectivity from .27 to 2.5 microns. Maximum changes in reflectivity near 100 percent were measured from .350 - .600 microns on two Hughes samples, Figure 57. Maximum reflectivity for the ADM and NCR samples was 50 percent.

Transmissibility curves for the Hughes sample discussed above and the NCR samples are shown in Figures 58 and 59. Maximum transmission was less than 30 percent for all samples. One fact concluded from the data is that long term solar exposure does increase the energy absorption in the .300 - .600 micron wavelength band.

CONCLUSIONS

Scale Model Space Shelter

Deployment and rigidization of scale models 2, 3 and 4 in a simulated space environment of 10^{-5} to 10^{-6} torr and $77^{o}K$ surroundings were successful. Deployment of Model 1 was not as desired, but rigidization was successful.

The heat flux system provided an effective and convenient means to maintain the model surface temperature at a level necessary for the successful curing of the resin.

Large Space Shelter

Deployment of the large aerospace shelter in a simulated space environment was not successful; however, the shelter was rigidized at atmospheric conditions. The violent expansion certainly was not desirable, but it appeared that had the structure been constrained to prevent structural damage, a successful deployment and rigidization would have been achieved. The dramatic, though undesirable, results of this test graphically pointed to the need for further study and development of rigidizing agents for expandable space shelters.

Crew Transfer Tunnel

Canister separation, deployment and pressurization of the tunnel in a simulated environment of 10^{-5} torr were very successful. A nominal amount of leakage was recorded from the tunnel during the 24-hour test period while pressurized to approximately 0.5 atmosphere and maintained in a simulated environment of 10^{-5} torr. The leakage rate was considered to be satisfactory.

Radiation Effects

Rigidized fiberglass of the type tested is not adversely affected by the combined environmental effects of vacuum and solar for the simulated 60 day orbital period. Increases in both the tensile and bending strength were measured after this period. The materials are dimensionally stable under these environments but small density changes can be expected. The absorptivity of the materials increases between .300 - .600 microns. A closer investigation of these changes will be necessary before the long term effects of solar exposure can be assessed.

TABLE I

TENSILE PROPERTIES

SUPPLIER	Ultimate (psi) VACUUM EXPOSURE			Modulus of Elasticity VACUUM EXPOSURE (psi)		
	5 Days	60 Days	60 Days and Solar	5 Days	60 Days	60 Days and Solar
Archer Daniels Midland Co.	28,600	32,200	27,400	703,000	627,000	643,000
Hughes Aircraft Co.	25,500	24,300	26,900	619,000	401,000	540,000
National Cash Register Co.	25,600	26,200	27,800	656,000	550,000	673,000

FLEXURAL PROPERTIES

	LOAD AT FAILURE (lbs)			DEFLECTION (inches)		
Archer Daniels Midland Co.	55.6*	62.0	63.2* 62.1	.100	.090	.089* .089
Hughes Aircraft Co.	29.0*	39.2	43.6* 23.9	.090	.109	.124* .073
National Cash Register Co.	31.8	38.3	47.2* 37.6	.101	.103	.109* .022

*Side exposed to solar in compression

DENSITY (Grams/cc)

	0 Days	5 Days	60 Days	60 Days and Solar	Average Thickness
Archer Daniels Midland Co.	1.43	1.56	1.42	1.55	.042"
Hughes Aircraft Co.	1.48	1.50	1.45	1.61**	.050"
National Cash Register Co.	1.64	1.66	1.68	1.81	.044"

**Sample density before 60 day period = 1.56 grams/cc

SUMMARY OF MECHANICAL PROPERTIES

Fig. 1 Aerospace Environmental Facility

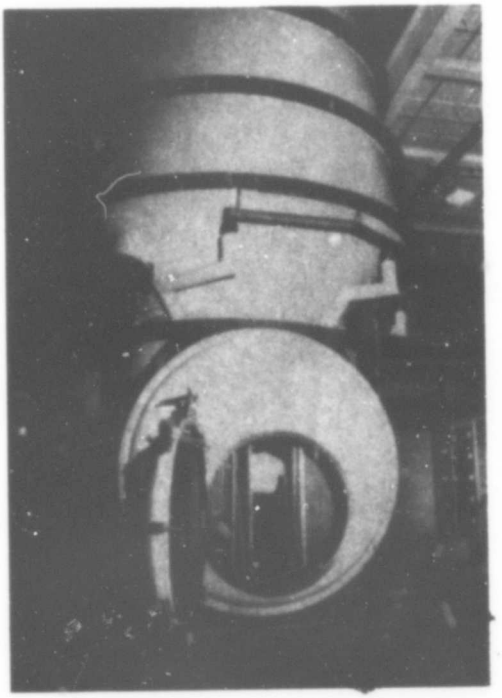

Fig. 2 Aerospace Research Chamber (12V)

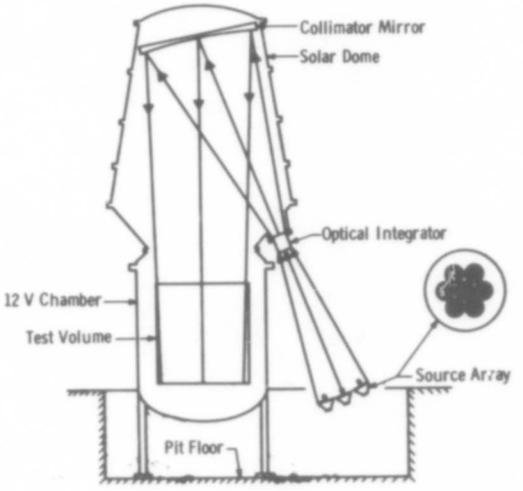

Fig. 3 Optical System for Solar Simulator

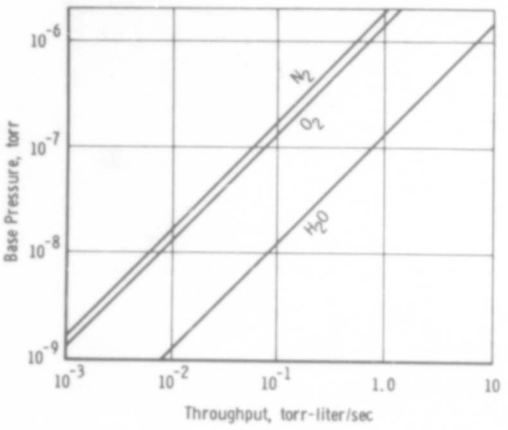

Fig. 4 Performance of Aerospace Research Chamber (12V)

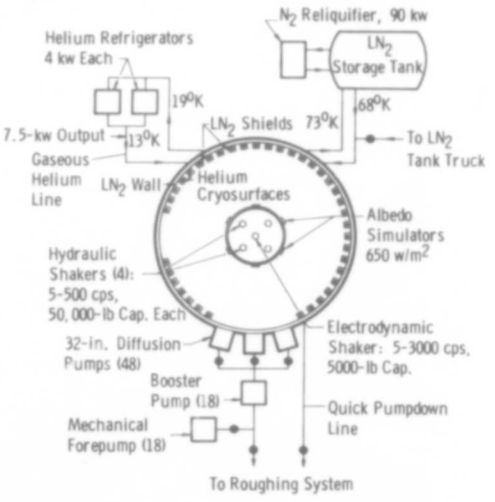

Fig. 5 Mark I Schematic

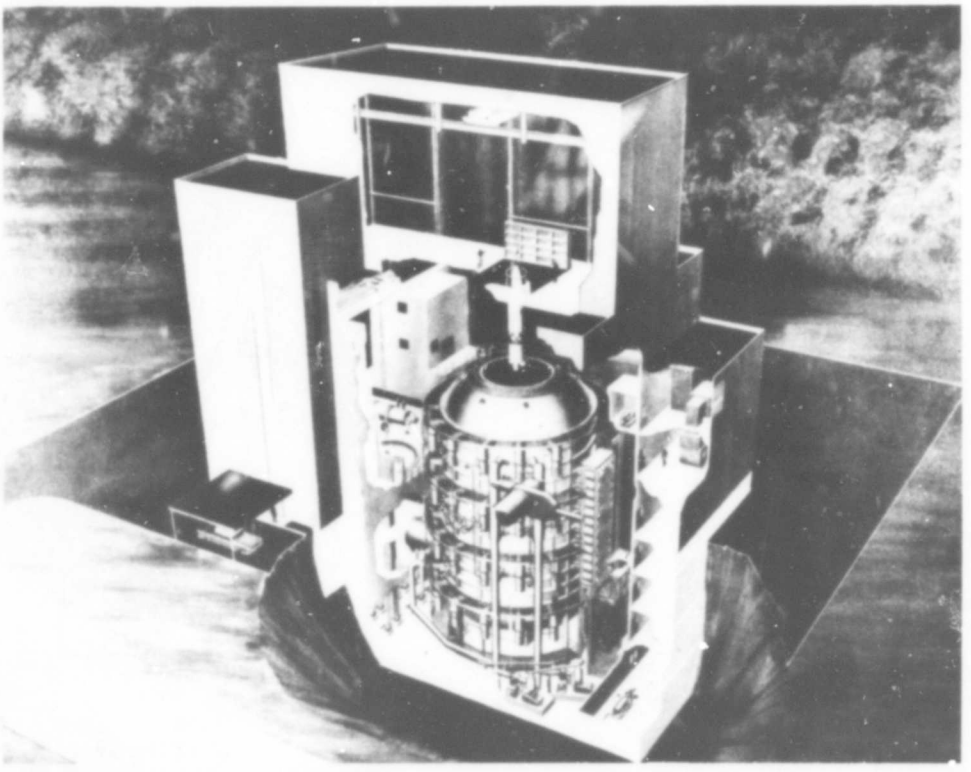

Fig. 6 Mark I Facility Arrangement

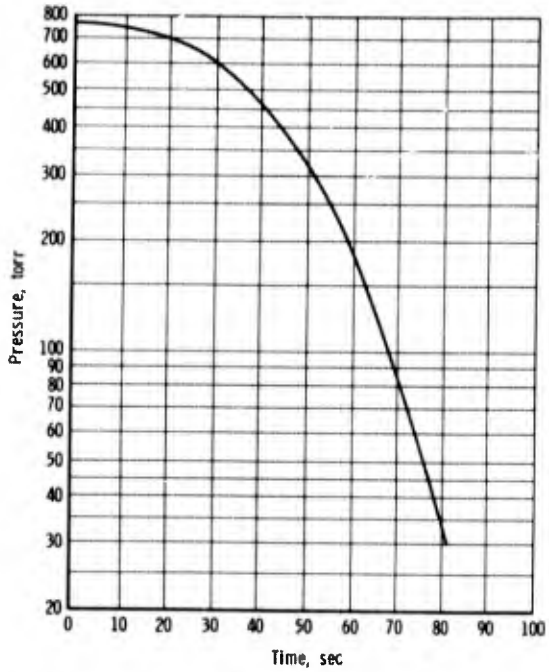

Fig. 7 Pressure/Time Trajectory

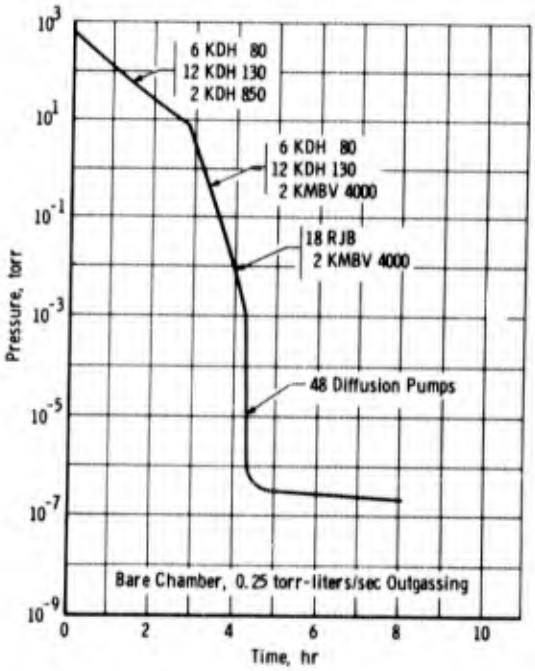

Fig. 8 Mark I Pumpdown Curve with Diffusion Pumping

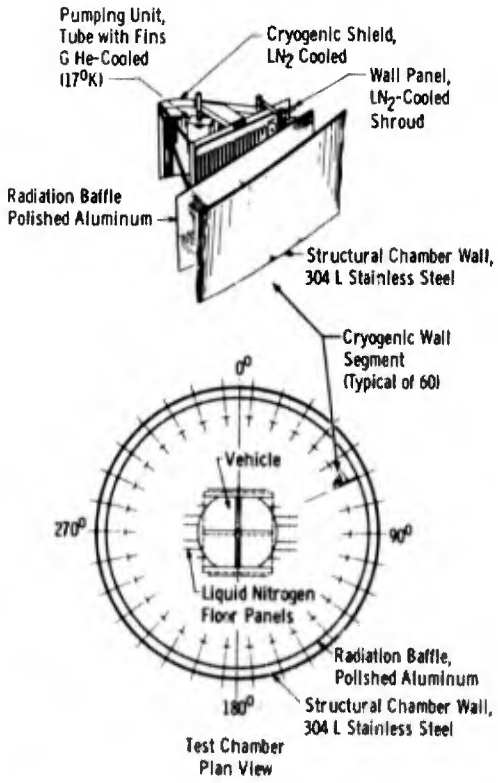

Fig. 9 Cryopump Configuration

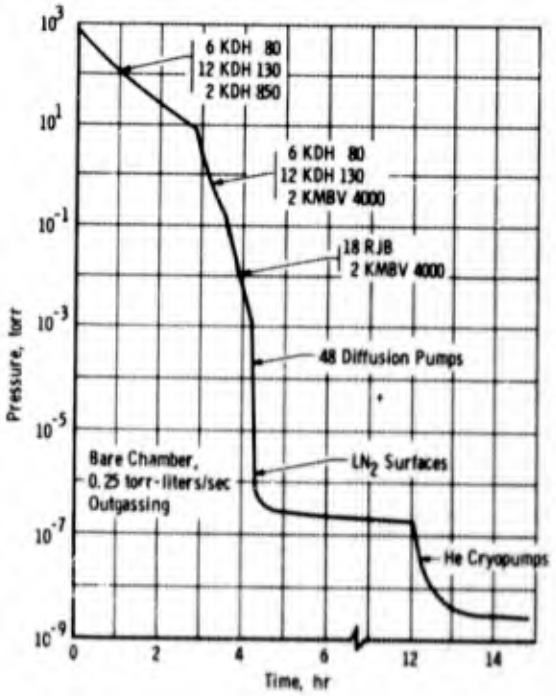

Fig. 10 Mark I Pumpdown Curve with Cryopumping

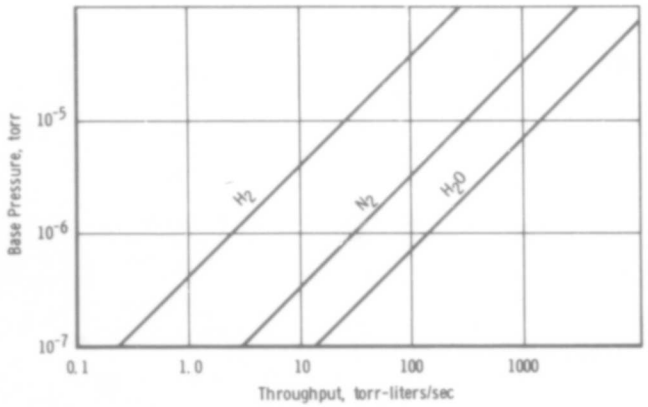

Fig. 11 Mark I Throughput Curves

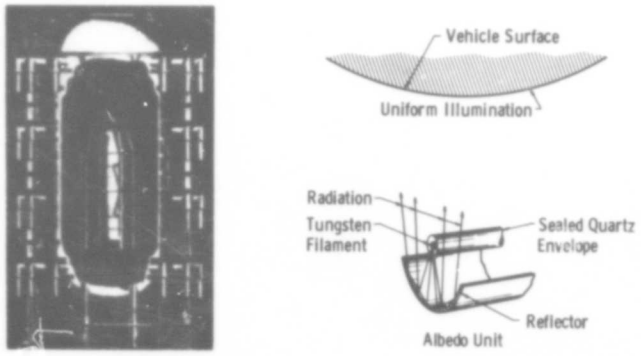

Fig. 12 Planet Albedo and Radiance System

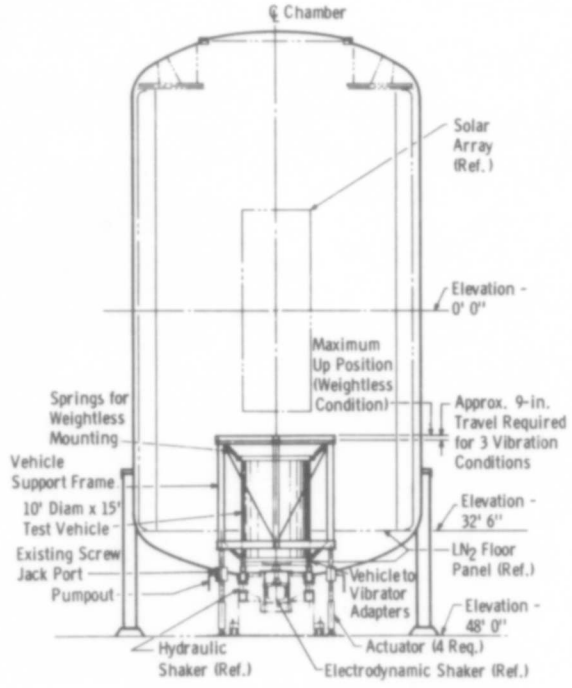

Fig. 13 Vehicle Vibration Support

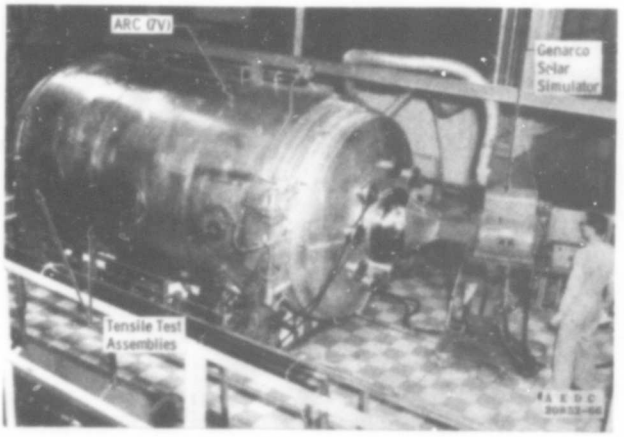

Fig. 14 Aerospace Research Chamber with Solar Simulator

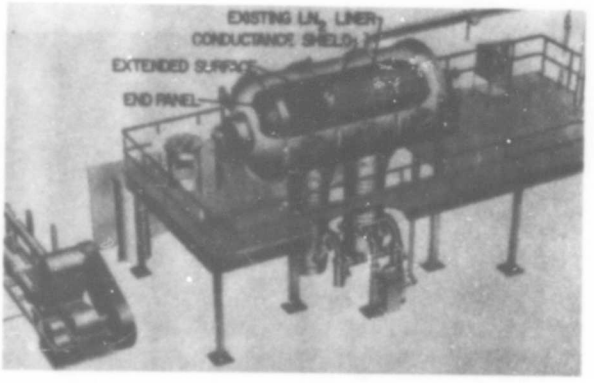

Fig. 15 Aerospace Research Chamber (7V) with He-Cooled Liner

Fig. 16 Packaged and Deployed 1/6-Scale Model, Space Shelter

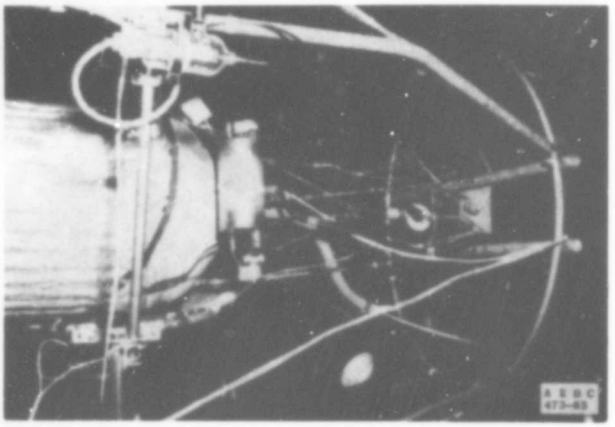

Fig. 17 Model 2 Mounted on Load Cell

Fig. 18 Model 4 Test Configuration

Fig. 19 Model 3 Resin Impregnation

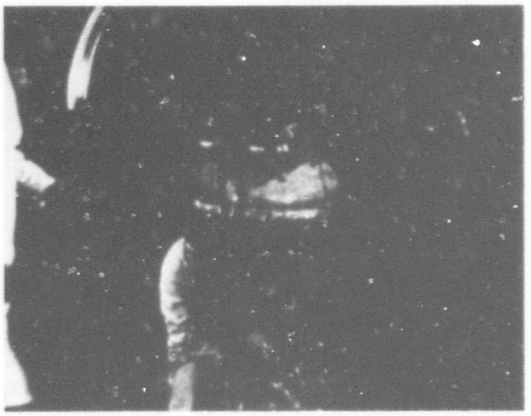

Fig. 20 Packaging Model after Impregnation

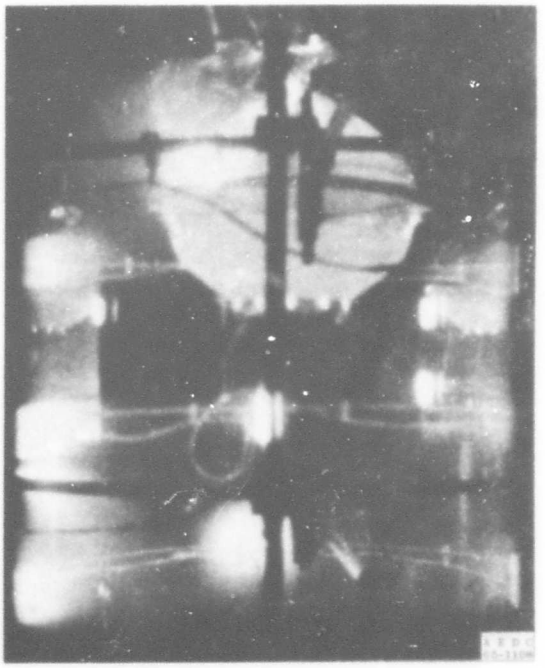

Fig. 21 Packaged Model in Test Chamber

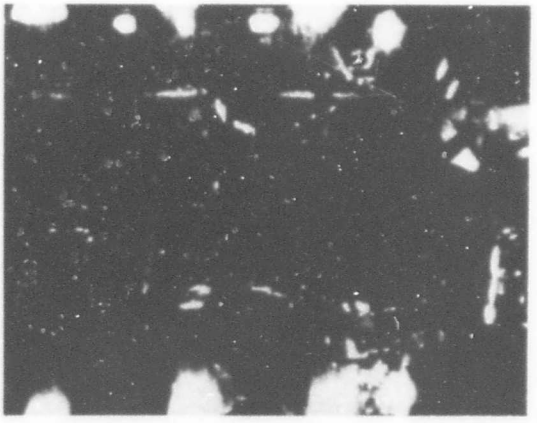

Fig. 22 Model 3 Partially Deployed

Fig. 23 Model 3 Completely Deployed

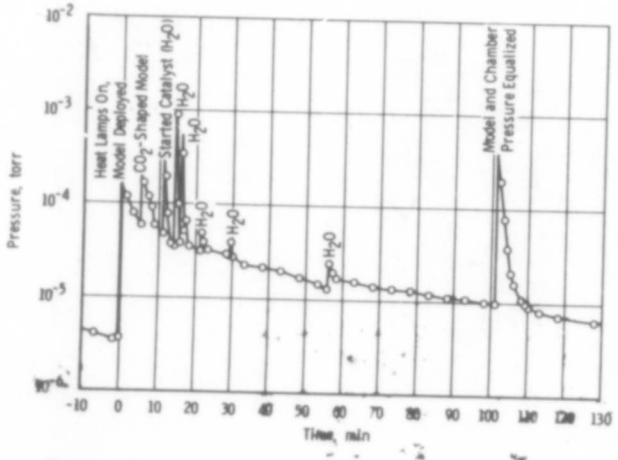

Fig. 24 Model 3 Chamber Pressure

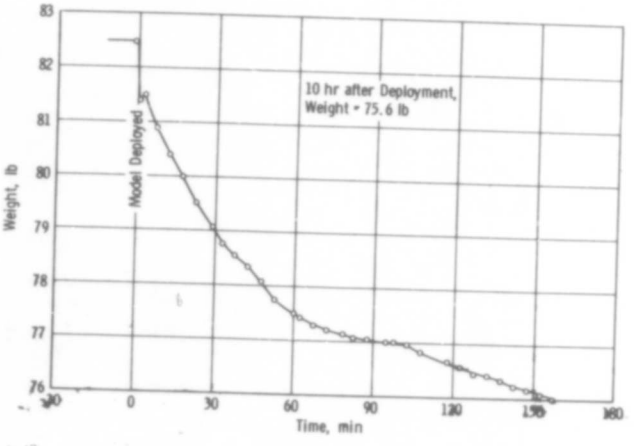

Fig. 25 Model 3 Weight Loss

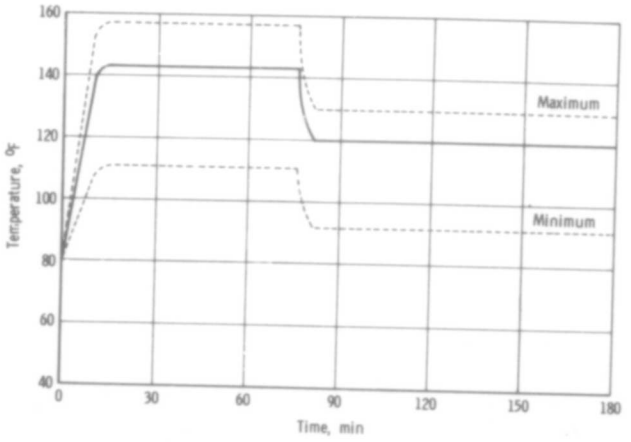

Fig. 26 Model 3 Temperature

Fig. 27 Models 3 and 4 after Rigidization

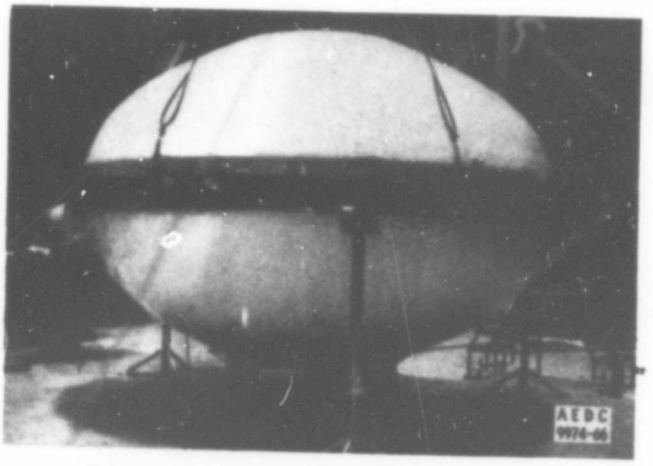

Fig. 28 Packaged Expandable Aerospace Shelter

Fig. 29 Deployed Expandable Aerospace Shelter

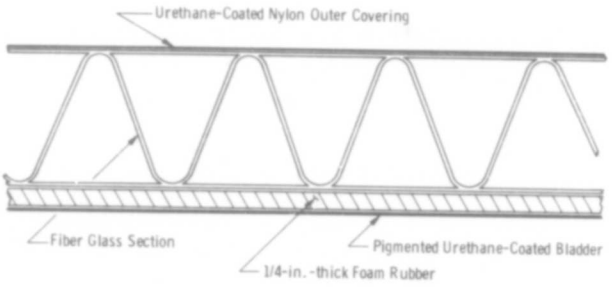

Fig. 30 Cross Section of Fabric Cylinder Wall

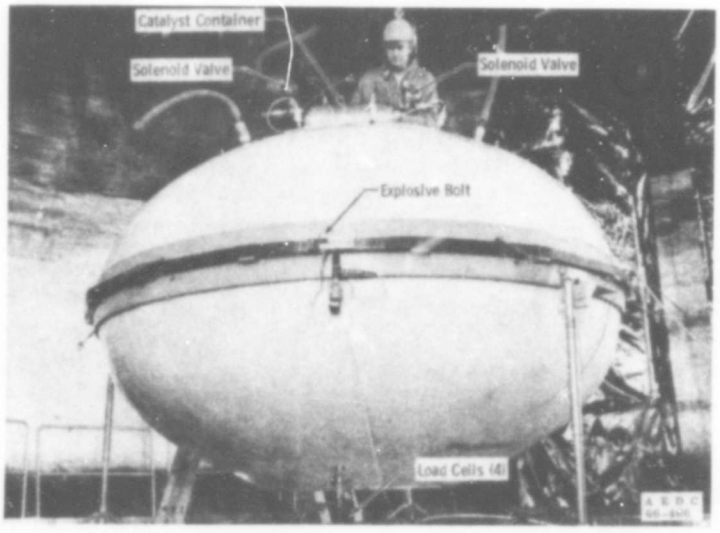

Fig. 31 Catalyst Container and Valves on Packaged Shelter

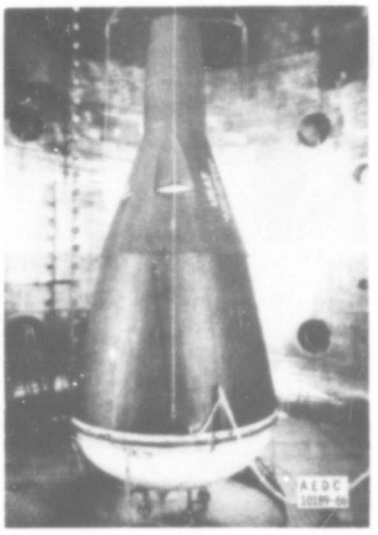

Fig. 32 Packaged Shelter and Gemini Model

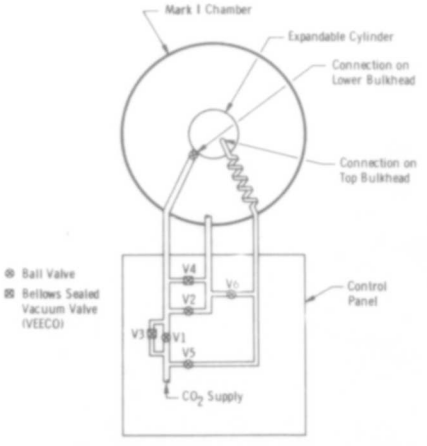

Fig. 33 Expandable Shelter Evacuation and Pressurization Schematic

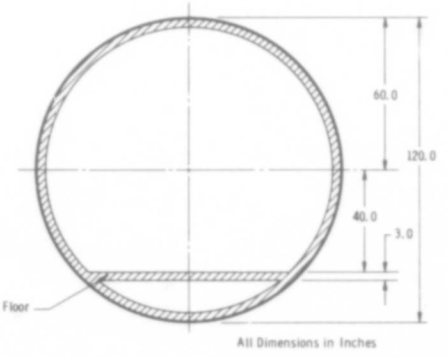

Fig. 34 Cross Section of Cylinder Showing Floor Position

Fig. 35 Expanded and Rigidized Shelter

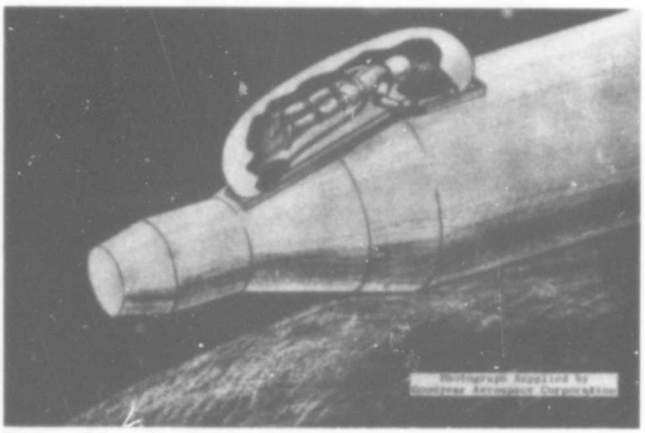

Fig. 36 Inflatable Crew Transfer Tunnel

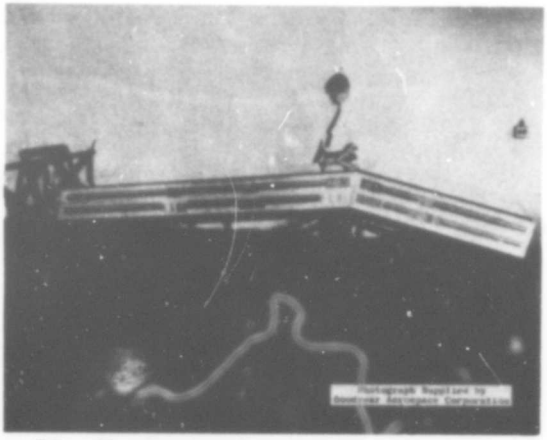

Fig. 37 Packaged Tunnel Inside Canister Mounted on Carrier Bed

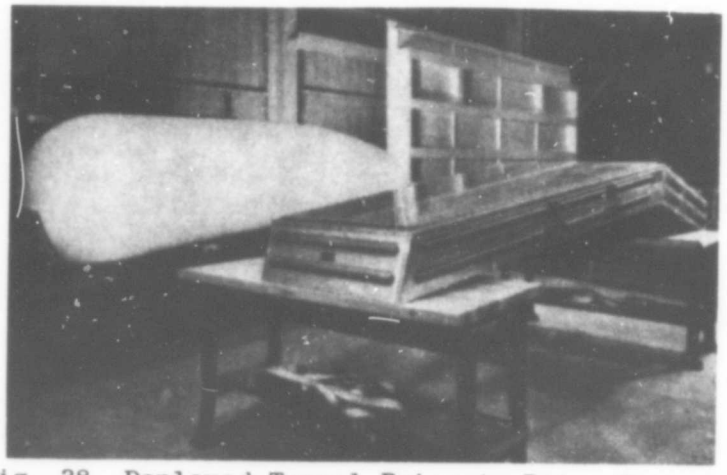

Fig. 38 Deployed Tunnel Prior to Being Packaged

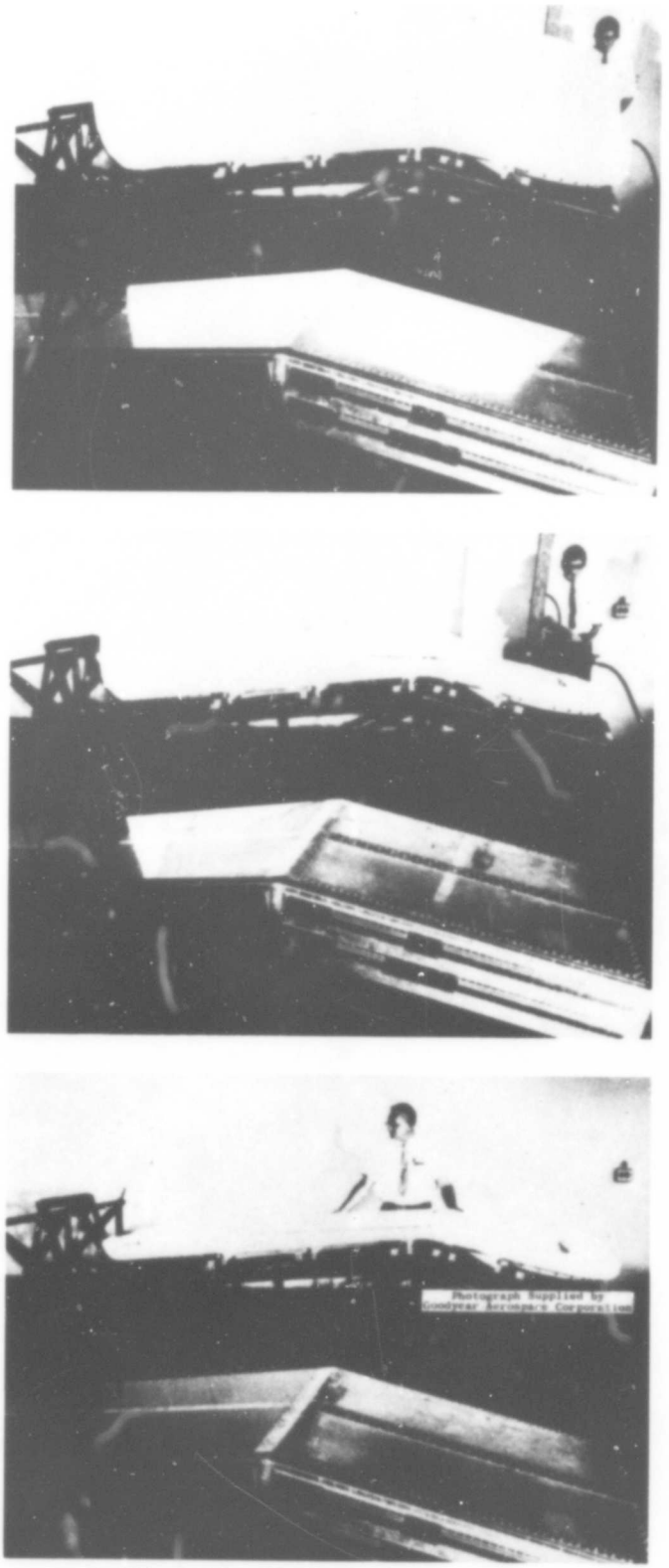

Fig. 39 Tunnel Packaging

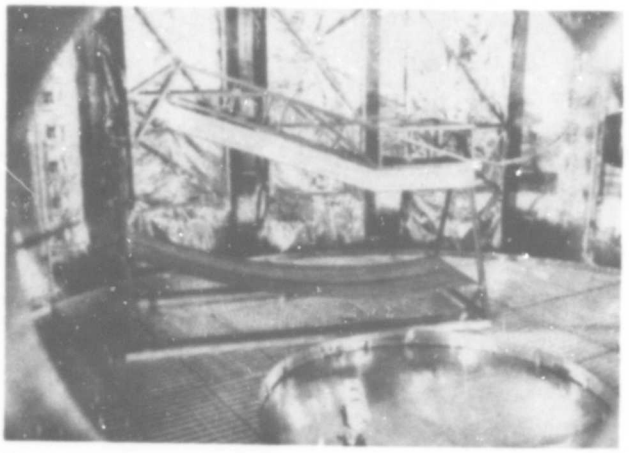

Fig. 40 Tunnel Installed in Test Chamber

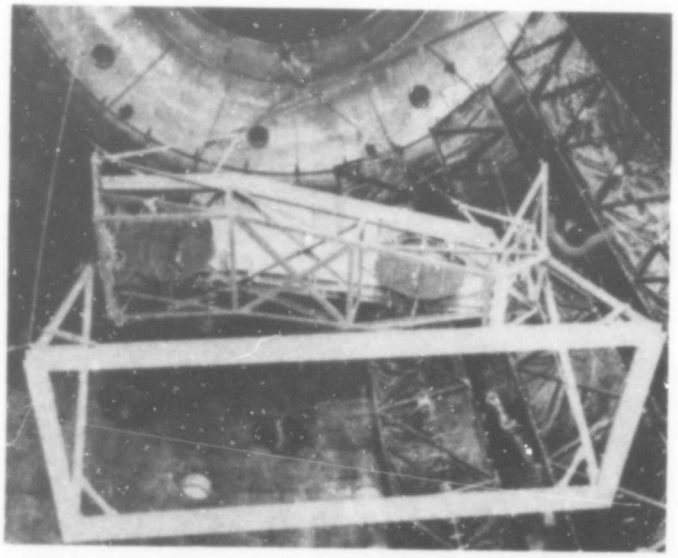

Fig. 41 Assembled Tunnel Being Lowered into Test Chamber

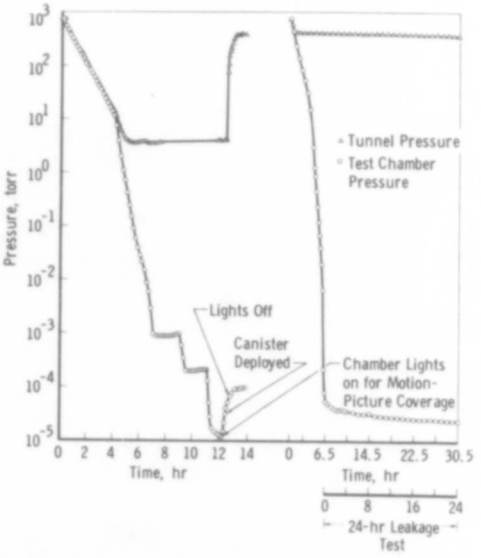

Fig. 42 Chamber and Internal Tunnel Pressure

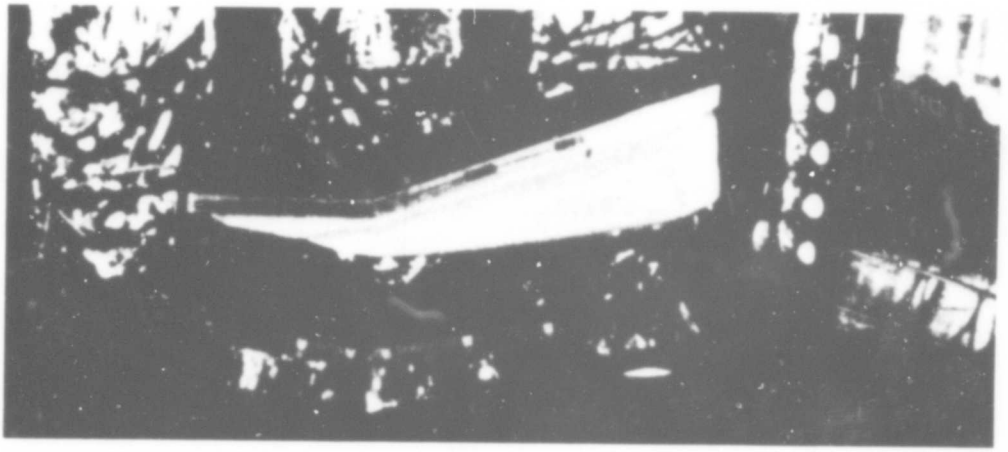

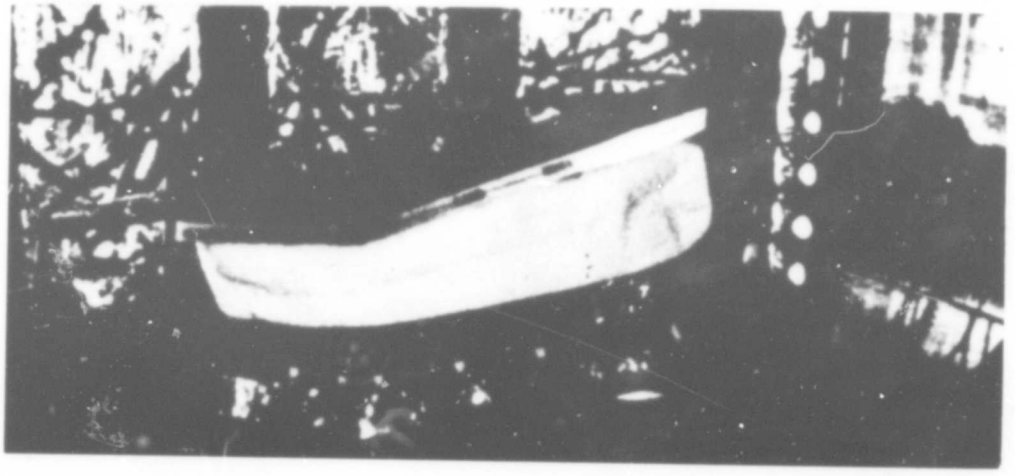

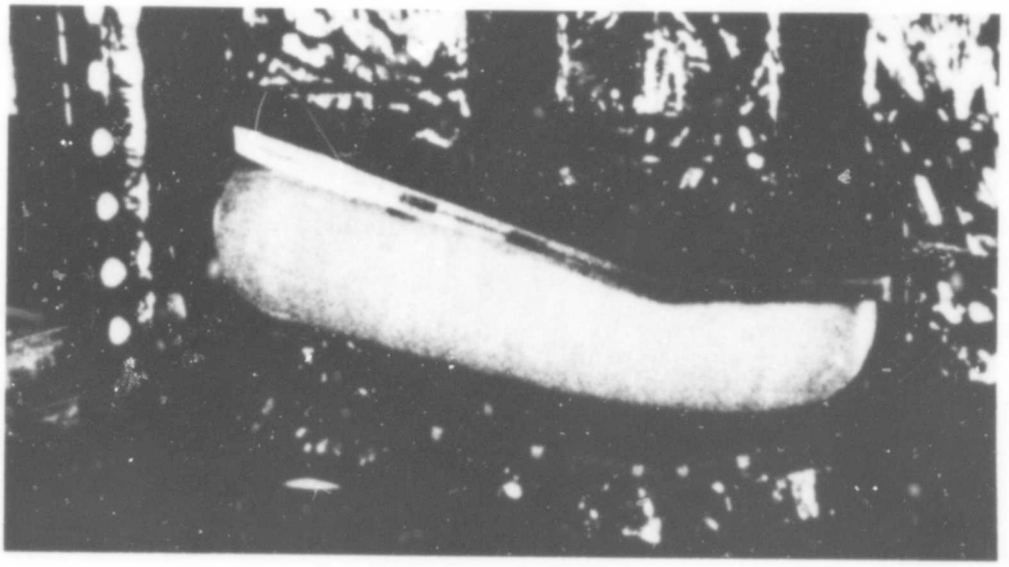

Fig. 43 Tunnel Deployment

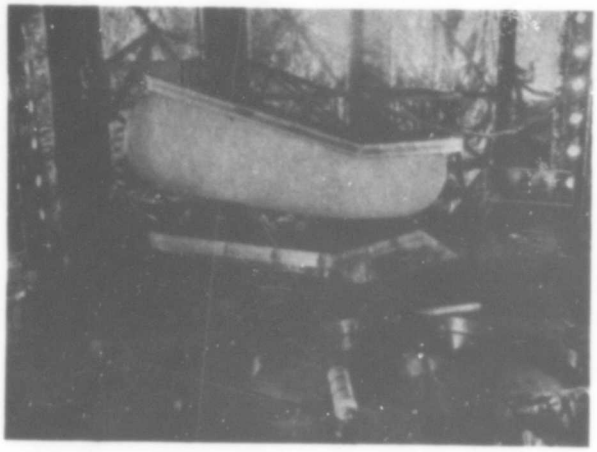

Fig. 44 Pressurized Tunnel after Completion of the 24-hr Leakage Test

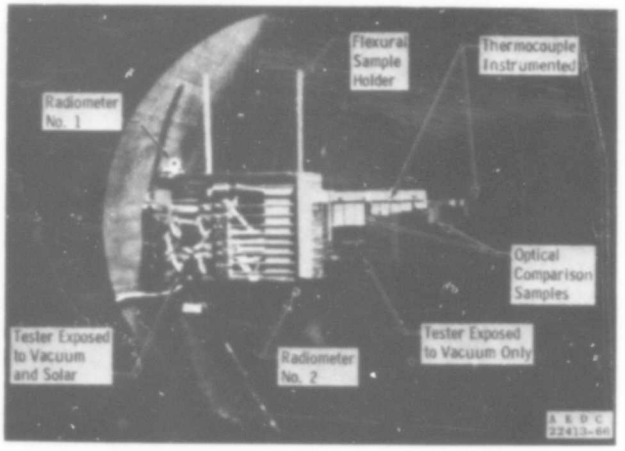

Fig. 45 60-Day Vacuum and Solar Test Installation

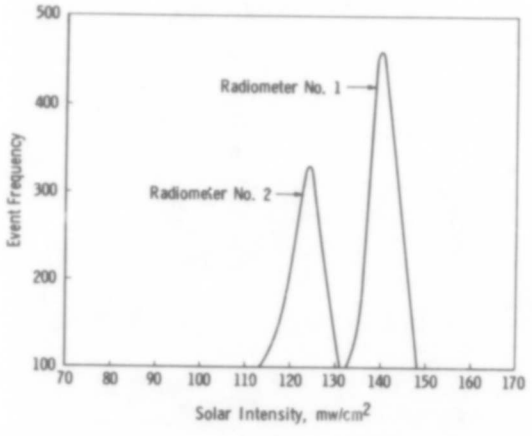

Fig. 46 Statistical Distribution of Solar Intensity during the 60-Day Vacuum and Solar Exposure

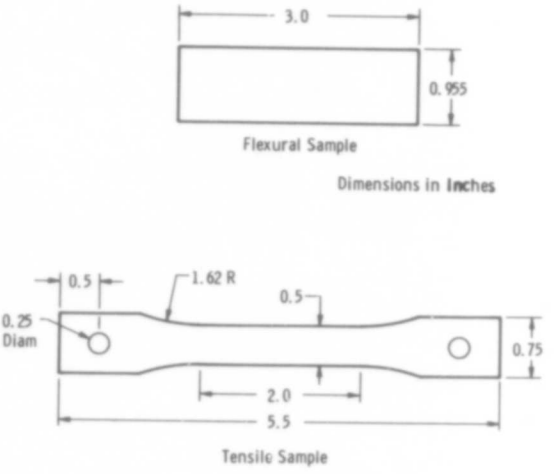

Fig. 47 Flexural and Tensile Shap

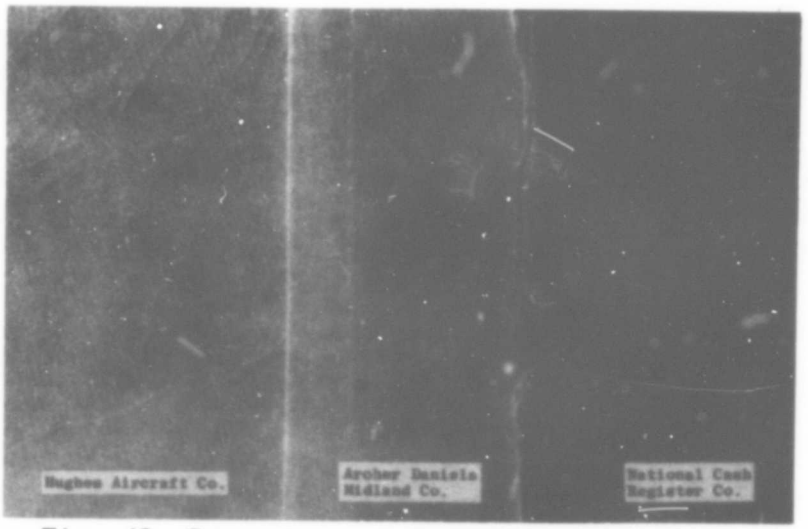

Fig. 48 Comparison of Samples before Testing

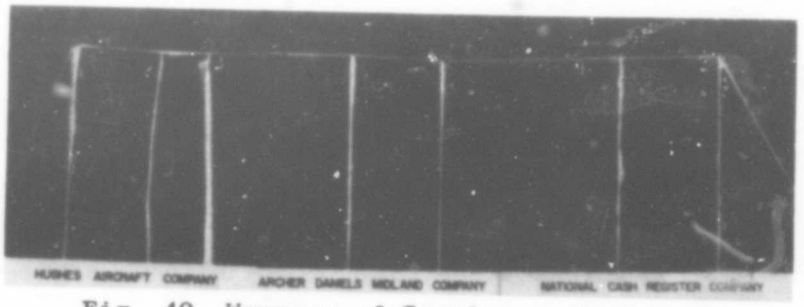

Fig. 49 Warpage of Samples as Received

Fig. 50 Comparison of Samples Failed in Tension

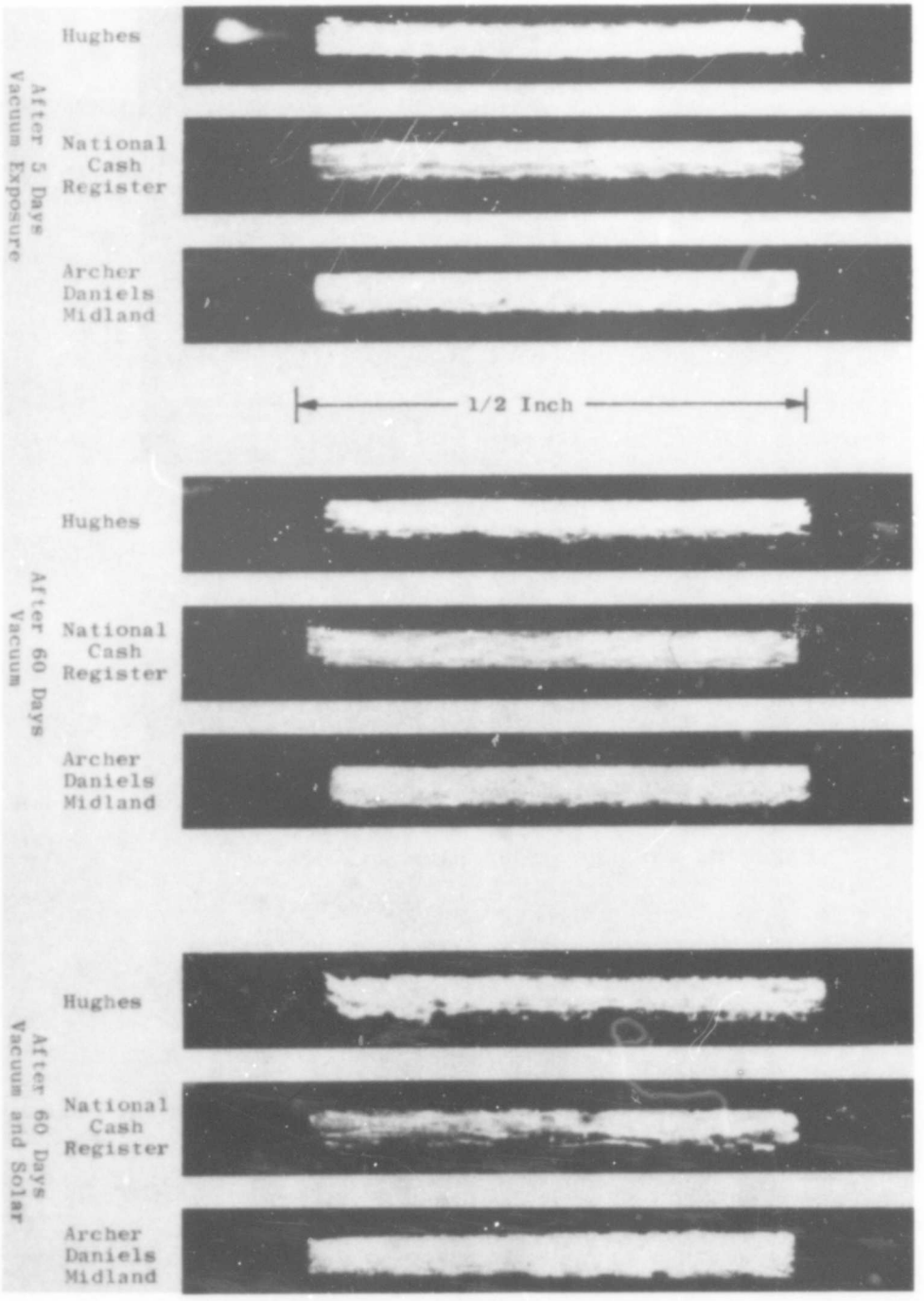

Fig. 51 Cross Sections of Samples Failed in Tension

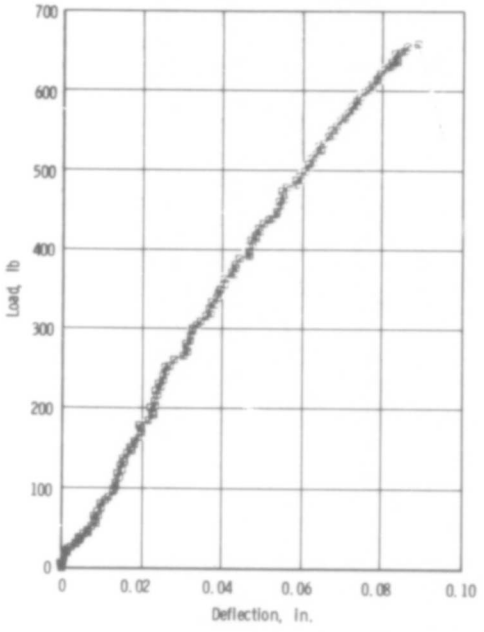

Fig. 52 Typical Tensile Data (Hughes Co. after Vacuum and Solar Exposure)

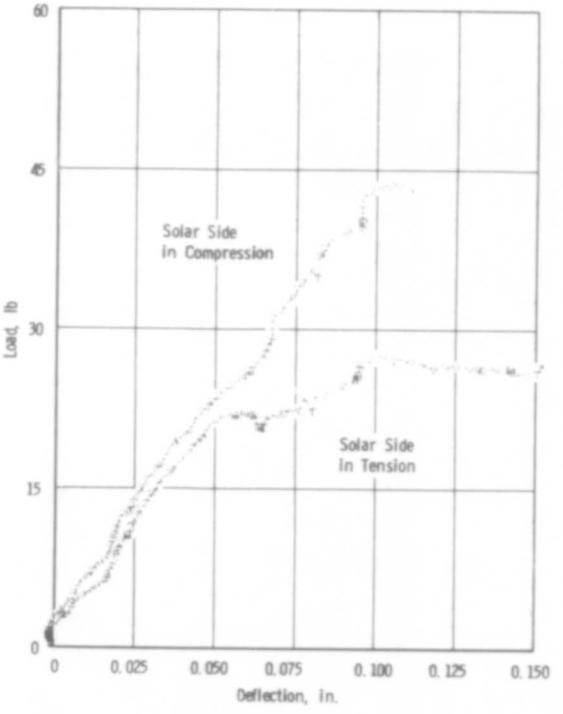

Fig. 53 Bending Data on Hughes Fiberglass Material after 60 Days Solar and Vacuum Exposure

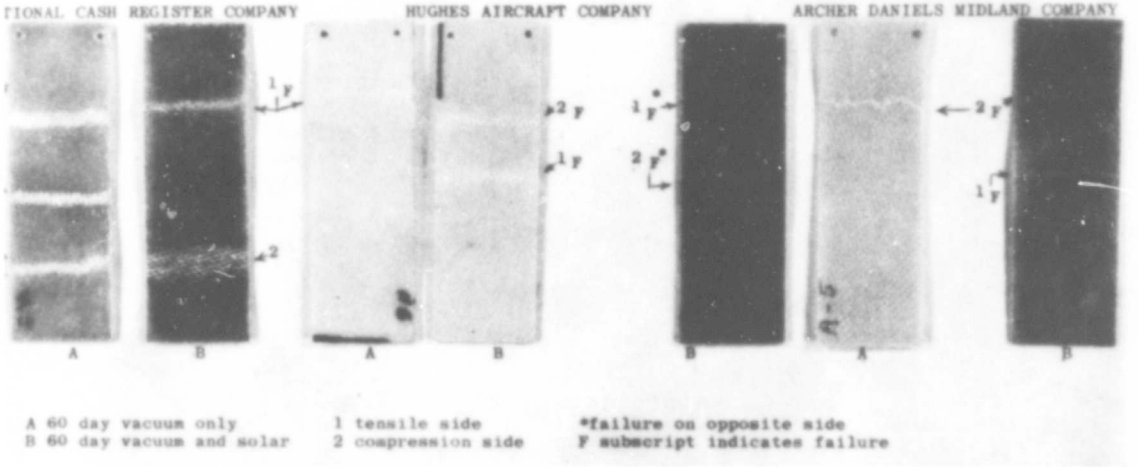

Fig. 54 Comparison of Flexed Samples

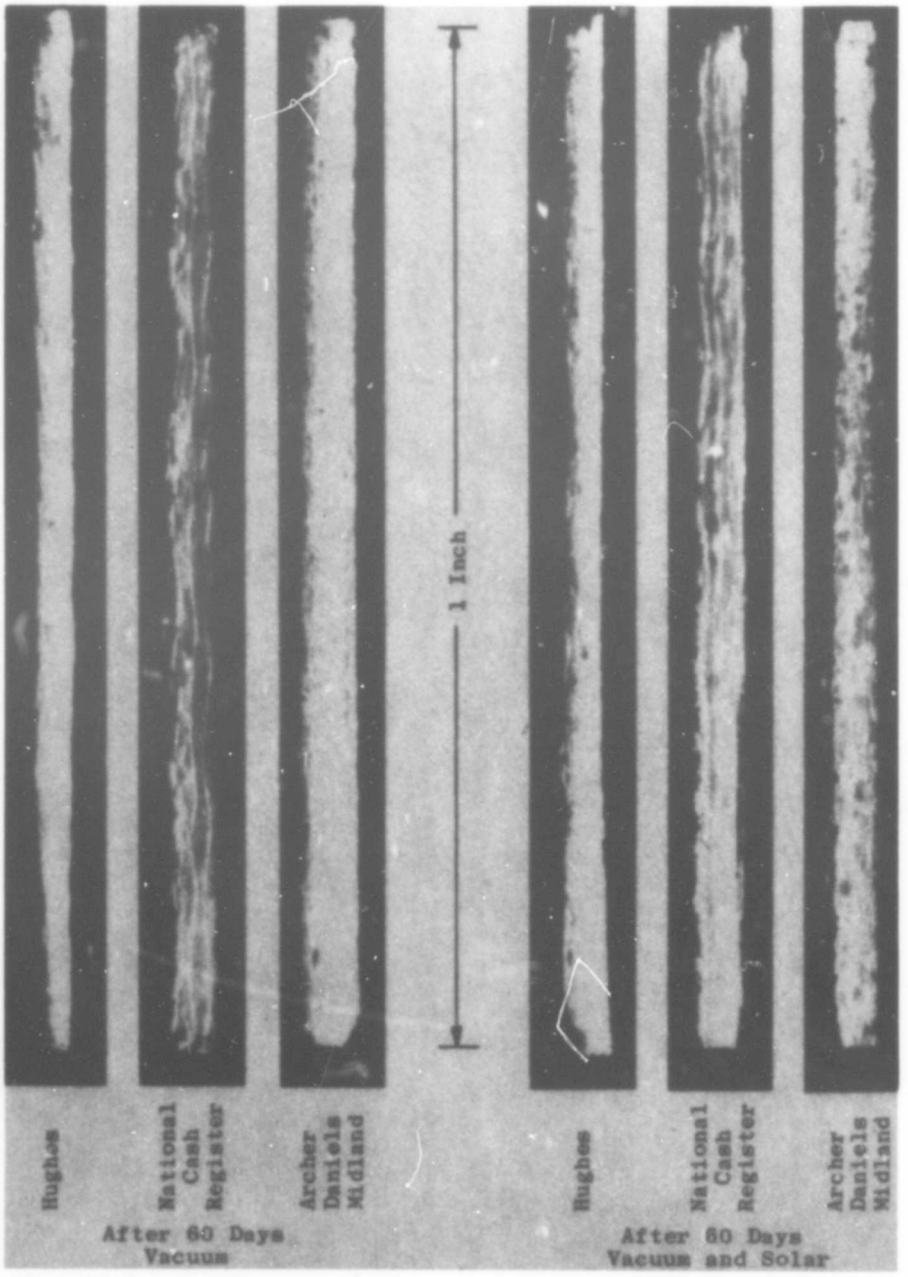

Fig. 55 Cross Section of Flexed Samples

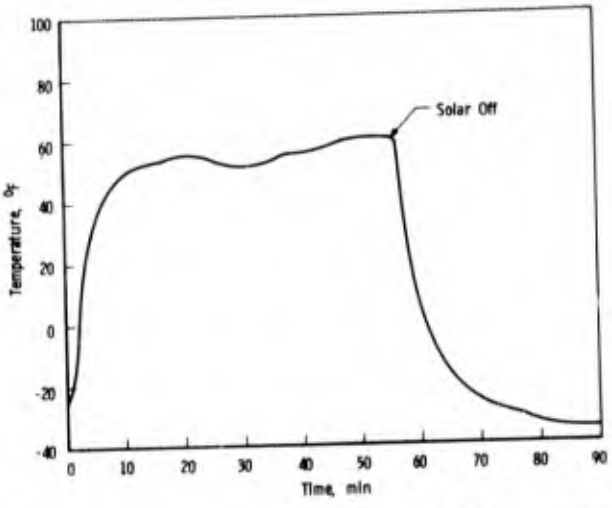

Fig. 56 Typical Temperature Response of Fiberglass to Solar Radiation

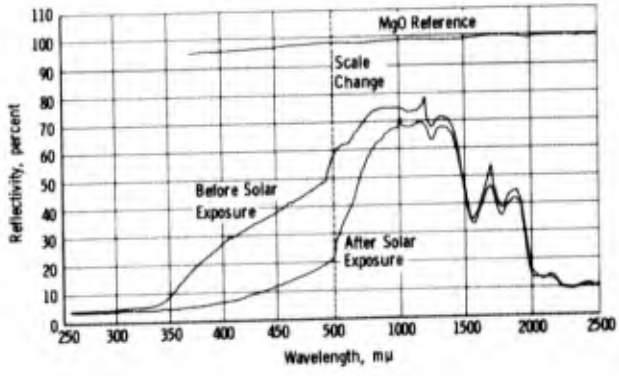

Fig. 57 Solar Effects on Reflectivity of Hughes Fiberglass Samples

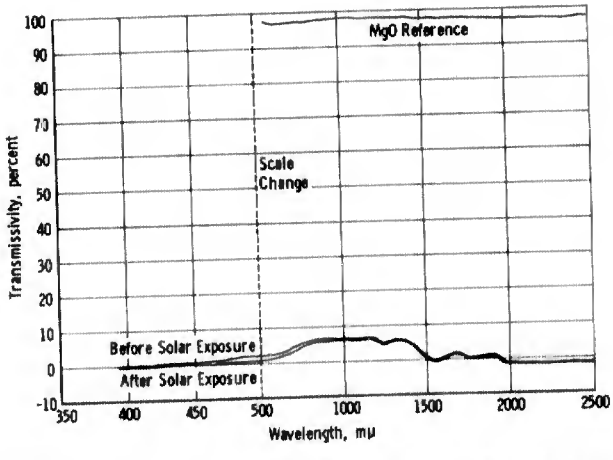

Fig. 58 Solar Effects on Transmissivity of Hughes Aircraft Co. Fiberglass Samples

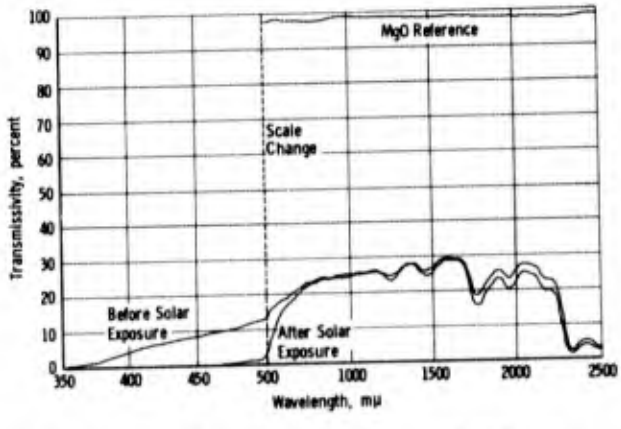

Fig. 59 Solar Effects on Transmissivity of National Cash Register Co. Fiberglass Samples

BLANK PAGE

FEASIBILITY DEVELOPMENT OF A SELF-DEPLOYING ELECTROMAGNETIC ENERGY FOCUSING REFLECTOR FOR SPACE OR TRANSPORTABLE GROUND BASED APPLICATIONS

BY

William Korvin*

Hossein Bahiman*

John Gates*

*Systems Division - NASA/Goddard Space Flight Center

INTRODUCTION

The need for enhanced communications capabilities inherent in a world of expanding technology could be alleviated through the use of a large aperture, lightweight, high gain, easily packaged and deployed parabolic antenna system. Development of a single optimized design technique for such an antenna system for all possible design environments becomes a rather complicated trade-off problem. Therefore, in this effort the design restraints are predicated upon the environmental effects presented by ground test, launch, and orbital operation of the

antenna system in the space application. At the same time, but to a lesser extent, versatility for use as a deployable reflector antenna in other environments (such as that imposed by ground based transportable applications which presents formidable design restraints) was considered. In this case concern with ruggedness and dependability would be the major design considerations.

The basic philosophy governing this developmental effort, in an attempt to optimize the structural principles, was concentration on the possibilities for obtaining the simplest and lightest material application, capable of high surface accuracies which include consideration of fabrication, assembly, packaging, deployment and operation techniques.

Many reflector design techniques have been or are being involved in this general problem area so that mention of the various generic types may be apropos in order to place the technique under discussion in its proper context.

Certain design techniques lend themselves to classifications because of similar deployment mechanisms and gross structural characteristics. For the purpose of this discussion, four main subheadings are defined as: 1) Inflatable (any technique using gas pressurization as the primary method of deployment/erection and whose primary structural material possesses extreme flexibility in the prior-to-deployment state); 2) Mechanical (any technique using a mechanical method of deployment/erection other than inflation and whose primary structural material possesses a minimal amount of flexibility); 3) Memory (any technique using the structural material characteristics as the primary means for obtaining deployment/erection and whose structural material possesses great to extreme flexibility at some period in the prior-to-deployment state); 4) Hybrid (any technique using a combination of the above mentioned techniques as the method of deployment and/or structural material).

The present effort falls under the subheading of High Modulus Materials of the Memory Techniques. This material, in brief, consists of a fiber glass grid core covered with a thin flexible resin system plated by a metallic vacuum deposit which can be preformed in the desired shape, deformed into a packaged condition, and when released, because of its stored elastic strain energy, resumes its original fabricated contour (See Figure 1).

SYSTEM DESIGN APPROACH

To implement this high-modulus memory material approach for a practical design, a review of candidate material properties for the reflector design was carried out. Not only did this include physical properties as such, but fabrication techniques and, therefore, structural application and to a large extent the possible deployment mechanism.

It is believed that functional simplicity is compatible with light weight, and that a flexure joint incorporating its own deployment mechanism is more desirable from a reliability and weight standpoint than that of a mechanical hinge with its accompanying motivating mechanism. Therefore, effort was started on the design and fabrication of a single piece, flexible, preformed mesh reflector. A mesh material configuration was chosen for its ability to form complex curves and to alleviate self-shrouding of the structure with solar radiation as well as reducing wind loads in possible ground use. Since the flexibility of a simple parabolic disch for packaging without degradation is not in keeping with the stiffness necessary (e.g. deployed configuration stability in a one "g" field), radial ribs of the same material were added. The parabolic dish was designed with marginal ability to maintain its preformed configuration without support as were the ribs, however, when assembled the composite structure became self-supporting. Although the ribs themselves in the deployed configuration contribute greatly to the stiffness of the overall structure in radial vertical planes of the upright parabola, these ribs can be flexed sideways for folding. The transverse flexing of the ribs reduces the moment of inertia contributed by the ribs and thus allows folding and packaging of the composite structure.

In order to accommodate a hard interface between the antenna system and attachment points, to facilitate fabrication, and to take advantage of allowable pre-erected protions of the reflector within shroud restraints, a sheet metal hub was designed. The hub also presents a base for attachment of the feed support, either Cassegrain or prime, which although not an erectable structure in the design task, nevertheless was approached in a somewhat unorthodox manner. Generally the approach to feed support structures has been the design use of high strength, metallic or high dielectric materials which presents an RF blockage problem due to the support members themselves. Some effort was expended to reduce this blockage problem and at the same time shield the feed mechanism from alternating solar radiation (i.e. varying sun angles) with the use of a hollow monocoque, conical structure composed to the maximum extent possible of dielectric material.

As was indicated previously, this concept is applicable to both space and transportable tactical ground communications. Since major concern at Goddard Space Flight Center is with space communications rather than ground based tactical applications, the design effort was concentrated on space deployment capabilities.

SYSTEM DESIGN CONSIDERATIONS

The need and general availability of design restraints and environmental factors dictate to a large extent the prime design parameters. Some design requirements and environmental factors which must be necessarily taken into account during design consideration are:

1. Achievement of tolerances in fabrication and assembly.

2. Preserving integrity and tolerances in the packaged state during the launch standby environment.

3. Preserving integrity during launch environment:

    a. lateral vibration and acceleration
    b. axial vibration and acceleration
    c. axial torsion vibration and acceleration

4. Achievement of tolerances in deployment.

5. Maintenance of tolerances in the deployed orbital operation and environment:

    a. axial torsion acceleration
    b. lateral torsion acceleration
    c. hard radiation
    d. ultra-violet
    e. infrared
    f. vacuum

Rather stringent reflector tolerance requirements are necessary for high antenna gain using a large (thirty-foot diameter) reflector at a frequency in the vicinity of seven GHz. Since fabrication of a full scale antenna system was neither practical nor desirable from a cost viewpoint, a one-fifth scale effort was selected as a reasonable compromise between size and the scaled frequency (i.e. thirty-five GHz). This scaling resulted in requiring no peak surface deviations normal to the theoretical surface greater than approximately 0.02 inches. Restriction in the largest opening in the reflector mesh should be of the order of 0.03 inches to assure 90 to 95% RF reflectivity at K band.

The focal length to diameter ratio of the reflector considered for this design was 0.5.

The method of packaging consists of introducing straight radial folds in the mesh reflector as its periphery is moved away from the tangential apex plane of the paraboloid and inwards toward the focal point. This package configuration does not take full advantage of possible packaging compactness, but is in keeping with the reliability goal in deployment with restriction to a minimum of sharp inflection fold lines in the material. The convoluted folded periphery is clamped and held in position with a tension ring. The tension ring is resisted by a plastic foam fixture which was formed to receive the fold pattern in a controlled bend radii grasp. Deplovnent is initiated when the tension clamp is severed and the stored elastic energy of the mesh forces the folded periphery away from its packing fixture and into its deployed state. The edge of the rib sockets do not coincide with the edge of the hard reflector hub surface, but rather extend beyond the metal hub surface. This allows some transition between complete restraint (in folding) of the mesh and the sharp bend at the hard surface of the reflector.

To determine surface tolerances for RF considerations the assembled antenna reflector was replaced over the reflective surface mold before and after packaging in order to estimate any discernible tolerance deviation. Maximum measured deviation from the mold was no greater than 0.050 inches for an estimated 5% of the area and no greater than 0.010 inches for the remaining area.

Accurate determination of major model frequencies, mode shapes, and "q" factors both for the deployed and packaged reflector configurations is believed possible only with full scale testing in view of the complicated analysis required for the mesh and the possible non-uniform use of materials during fabrication. Although the resonant frequencies are expected to be low, improvement may be made by placing the mesh under tension in the folded configuration and by judicious use of additional ribbing (e.g. circumferential ribs) in the deployed condition.

Ultra-violet radiation is not expected to be a problem because of the protection offered to the resin system by the over-layer of vacuum deposited aluminum. Dimensional stability and brittleness due to exposure to hard radiation may be a possible problem area and may necessitate search for an alternate resin system with similar mechanical characteristics but greater radiation resistance. An indication of compatibility of the reflector material and vacuum is given in the vacuum deposition process where the mesh is subjected to a pressure of 10^{-5}mm of Hg for a period of thirty (30) minutes. It is estimated that the use of thin, flexible, thermal control coating will limit the maximum temperature rise of the mesh surface to one hundred degrees centigrade or less when exposed in orbit to solar infrared radiation.

FABRICATION

A six foot diameter mold and ribs were designed and fabricated. (See Figures 2 and 3). The reflector mesh design was based on the stiffness and flexibility available in material samples produced from a previous program for the development of self-erecting materials and with the possibility in mind that with the variation of the resin system and glass core used, mechanical properties of the composite material could be varied to suit the design. Design and fabrication of the molds themselves proceeded under the assumptions that a room temperature or near room temperature cured resin could be utilized in the fabrication of the mesh and also that vacuum bagging might be necessary to insure proper material conformation. The parabolic mold surface and the flange or attachment area of the rib mold were considered of prime importance with regard to tolerances. These surfaces were carefully hand finished to an estimated tolerance of $\pm$0.005 inches from the theoretical configuration. Various material and resin systems were sample fabricated from the molds using a three rib sector of the reflector assembly (fifteen ribs are used in the complete assembly) in order to evaluate the physical properties of these variations in the composite assembly and simultaneously improve the handling and material layup techniques.

Fabrication of the complete assembly model was [illegible]ved in the following manner. The general Technique involving the [illegible]h composite material consisted of laying the glass cloth across flat frames slightly larger in area than the mold surface in the desired number of layers and orientation (See Figure 4). The edges of the cloth were lightly constrained to the frames by the use of tape (See Figure 5). The glass cloth layers were then impregnated and a thinned polysulfide liquid polymer using hand rollers, blotted to remove the excess resin, and blown with air to eliminate bridging of the interstices (See Figure 6). The composite was then immediately draped over the male molds and hand shaped to conformation (See Figures 7 and 8). Curing consisted of raising the temperature to 160°F either in an oven (as was the case with ribs) or with overhead heat lamps (as was the case with the parabolic shell) for approximately seventy-two hours (See Figure 9). During cure, clamping was applied to a small area of the outer tips of the rib mold in order to prevent bridging of the material at a place of compound curvature. This was also done at the extreme edge of the reflector shell for the same reason which facilitated proper lay-down of the material over the whole paraboloid. Assembly of the ribs to the parabolic shell and then to the metal hub was accomplished by bonding with the same resin system (See Figure 10 and 11). Fabrication of the metal hub was done by spinning aluminum sheet to a parabolic surface. The rib sockets were formed by compressing aluminum sheet over molds (See Figure 12). Upon completion of the bonded assembly, the composite mesh structure was processed (metalizing lacquer applied and heat cured) to provide a suitable substrate for vacuum metal deposition (See Figure 13). Aluminum was vacuum deposited to both concave and convex sides of the composite mesh structure to provide the necessary reflective and UV protection characteristics. The RF feed support structure (See Figure 14) was fabricated and bonded to the center metal hub parabolic surface and the circular packaging fixture for the mesh reflector, shaped from a styrofoam slab, was mounted near the upper end of the feed support (See Figure 15).

A surface tolerance of ±1/16 of the operating frequency wavelength is used for assurance of an RF reflector efficiency of 50% to 60%. For 35,000 mc this is approximately ±.02 inch. With the fabrication technique of using a mold (diameters of 6 to 9 feet), tolerance achievement is not an extremely difficult task. However, beyond this diameter, extreme care must be taken as far as the mold material is concerned, i.e. the ambient room temperature and humidity, to avoid variable surface tolerances in the mold.

The antenna system weight breakdown is shown in Table No. 1, based on a total weight of 14.2 pounds. The estimated total minimum weight for the reflector and hard point attachments (considering testing in earth's gravity field) is 6.4 pounds as delineated in Table No. 2.

Possible conversion of this antenna system to an infrared energy collector could be accomplished by bonding a preformed parabolic elastomeric material of minimal thickness to the concave side of the antenna reflector. This material would, of necessity, possess adequate thermal stability. Vacuum deposition of aluminum on the concave side of the parabola should then provide the necessary reflective qualities.

RF CHARACTERISTICS OF THE SYSTEM (PRIMARY AND SECONDARY PATTERN)

To determine the effect of various foam materials used for supporting the RF feed at the focal point, several measurements were made of the primary feed energy distrivution. Ideally, its energy is spread across the reflector aperture such that when it is reflected, a collimation of the radio frequency energy takes place producing a highly directive high gain beam. Figure 16 shows what is considered as an optimized primary pattern which distributes energy across the reflector aperture. Figure 17 shows the resulting secondary beam. Since the highest test frequency available at the time of RF testing was 7.6 GHz, this frequency was used to make measurements on different foam structures which produced the primary patterns shown in Figures 18 and 19. Secondary patterns are shown in Figures 20, 21, and 22.

It should be noted that where severe primary pattern distortion occurred, the second pattern also deteriorated. The secondary pattern of the dielectric parabolic reflector is shown in Figure 23 with the testing rig and setup pictured in Figures 24 and 25. The asymmetry of the secondary pattern is believed due to the large asymmetric feed support as shown in the test setup illustrations. A gain of 38 db was achieved in Figure 23, which, considering the distortion of the dish introduced by the test setup position and feed support degradation, is approximately normal efficiency for a frequency of 7.6 GHz.

SUMMARY

The state of material development has been completed under the systems feasibility study. The next developmental phase requires more rigorous material testing as well as composite assembly environmental testing data for an enhanced material development and optimized design. Areas of possible material and design improvement include:

1) Resin system development for greater resistance to hard radiation such as the use of natural rubber for coating the fiber glass.

2) Alleviation of creep or plastic flow of the resin system during prolonged packaging of the composite assembly. This may be possible with the use of cryogenic temperatures and/or lamination of thin narrow radial steel springs between the material layers in either the dish or ribs.

3) Improved rib designs to meet special environmental specifications such as merging the box rib at the periphery of the assembly into the flat shell adjacent to the inner parabolic shell at its edge to provide additional edge stiffness and shape conformation.

The lightweight, dielectric, memory material described in this paper allows an extremely versatile reflector system to be formed. The dielectric reflector systems thus formed may be used for RF and solar concentrators and in either space applications or for portable ground systems. It can be made lighter in weight than other presently developed concepts when surface tolerance as a function of reflector diameters is considered.

Acknowledgement is given for extremely helpful advice and services furnished by the following groups at the Goddard Space Flight Center:

ATS-4 Project Staff

Communications Research Branch

Fabrication Engineering Branch

Flight Programs Office

Materials Research & Development Branch

Plastics Model Shop

Structural Dynamics Branch

Thermal Systems Branch

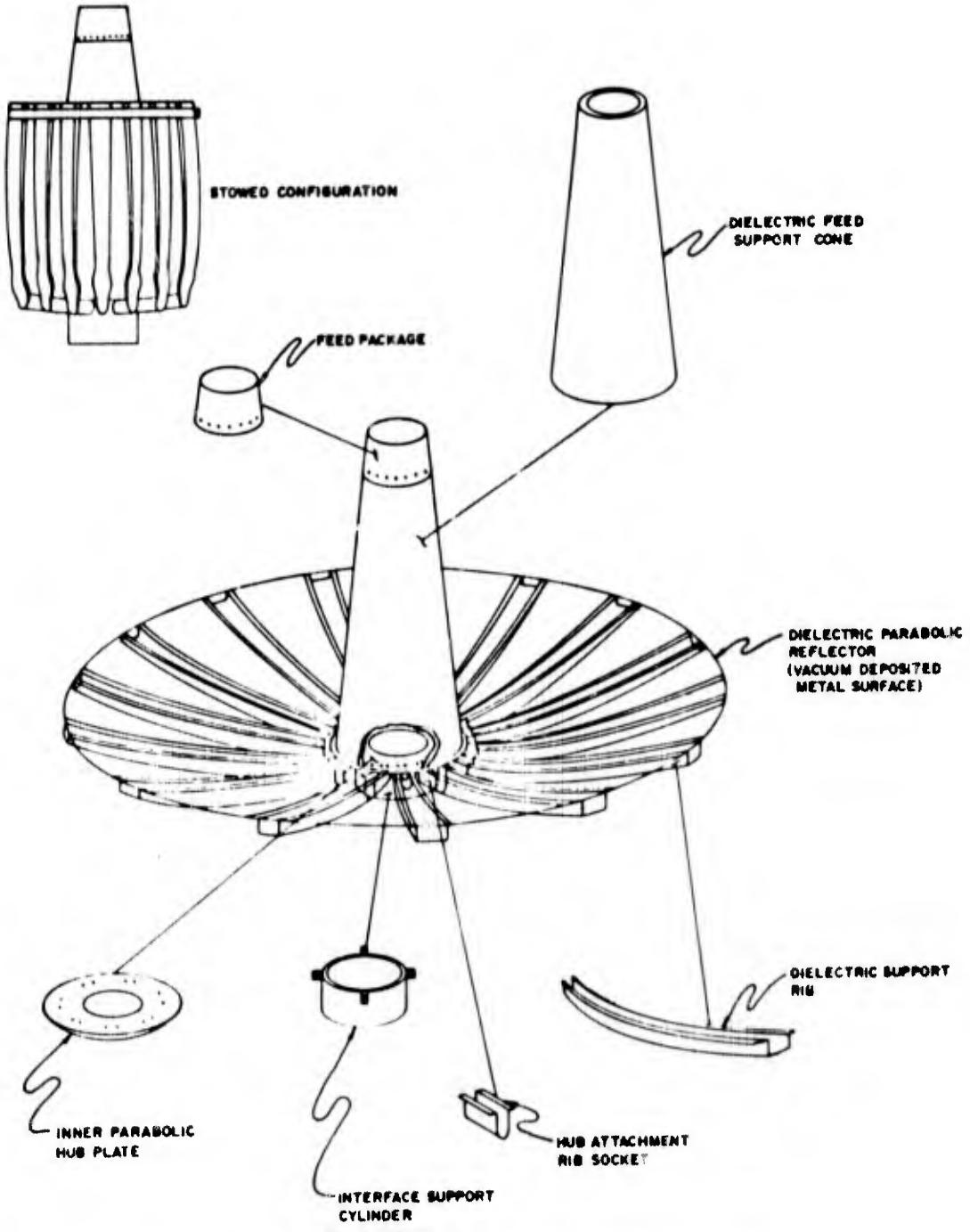

FIGURE I
DEPLOYABLE DIELECTRIC PARABOLIC ANTENNA SYSTEM

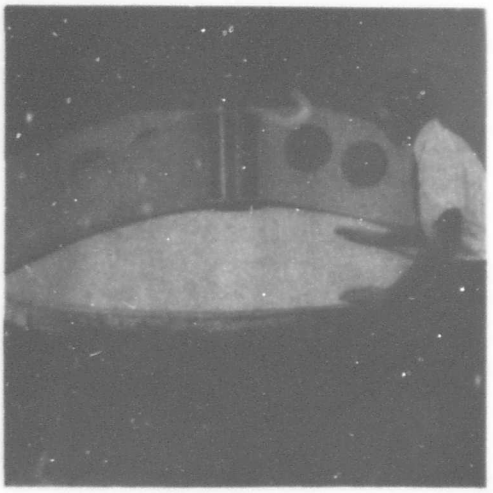

FIGURE 2

PARABOLIC MOLD FABRICATION

FIGURE 3

RIB MOLD

FIGURE 4

FIBERGLASS CLOTH

FIGURE 5

CLOTH AND FRAME LAYOUT

FIGURE 6
CLOTH IMPREGNATION
WITH POLYSULFIDE

FIGURE 7
DRAPE OF IMPREGNATED CLOTH

FIGURE 8
HAND FORMING OF IMPREGNATED
CLOTH TO MOLD

FIGURE 9
OVEN CURING OF IMPREGNATED
CLOTH ON MOLD

FIGURE 10

ATTACHMENT OF RIB

FIGURE 11

ASSEMBLY OF PARABOLIC MESH SHELL WITH RIB SOCKET AND RIB

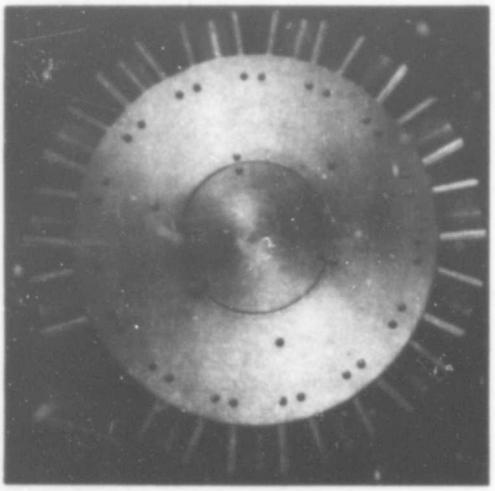

FIGURE 12

FABRICATED ALUMINUM HUB

FIGURE 13

APPLICATION OF VACUUM DEPOSITION SUBSTRATE

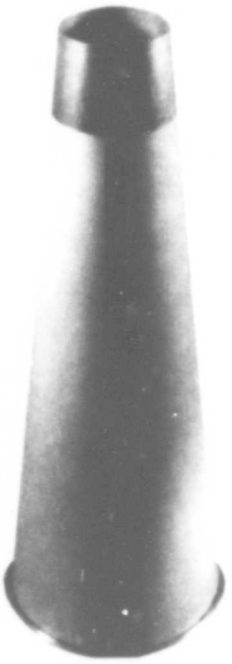

FIGURE 14
FEED SUPPORT STRUCTURE

FIGURE 15
PACKAGED CONFIGURATION USING
STYROFOAM PACKAGING FIXTURE

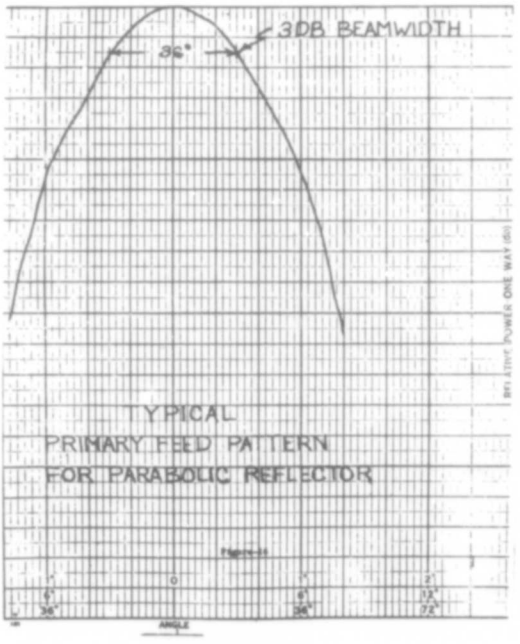

FIGURE 16

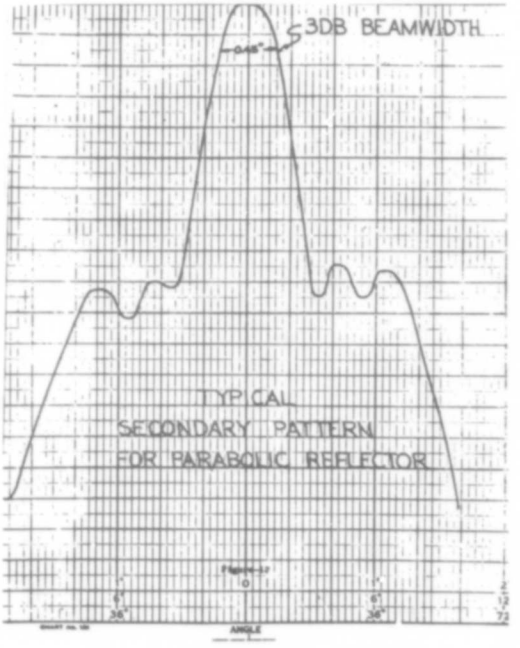

FIGURE 17

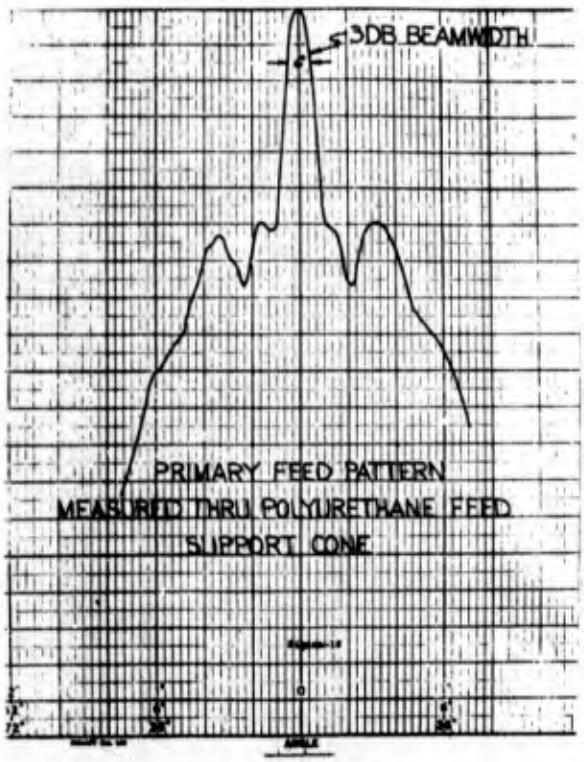

FIGURE 18

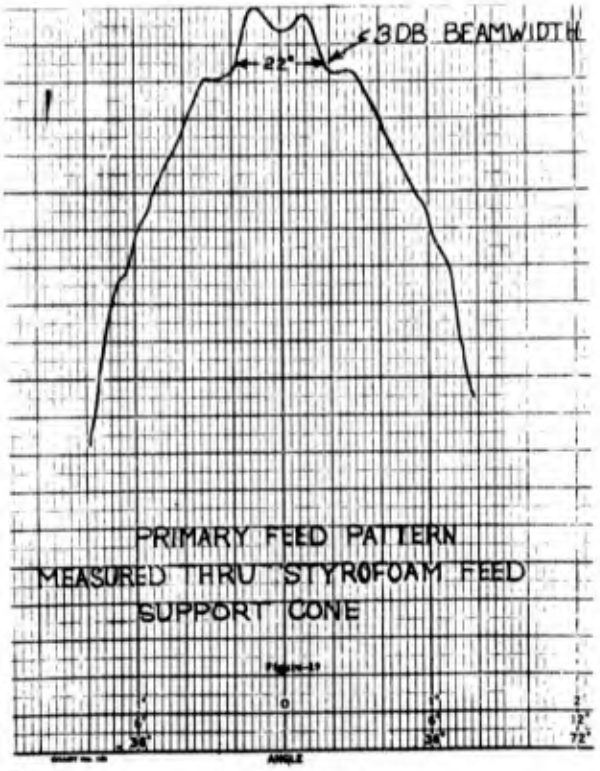

FIGURE 19

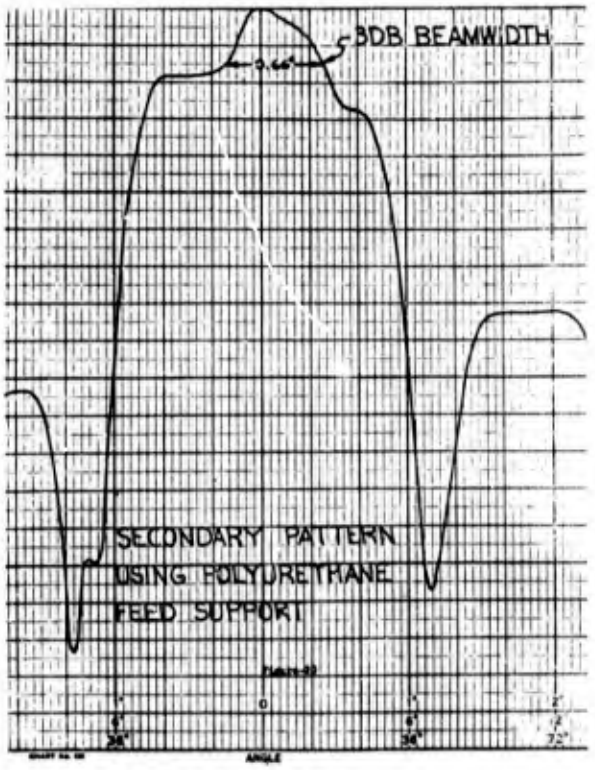

FIGURE 20

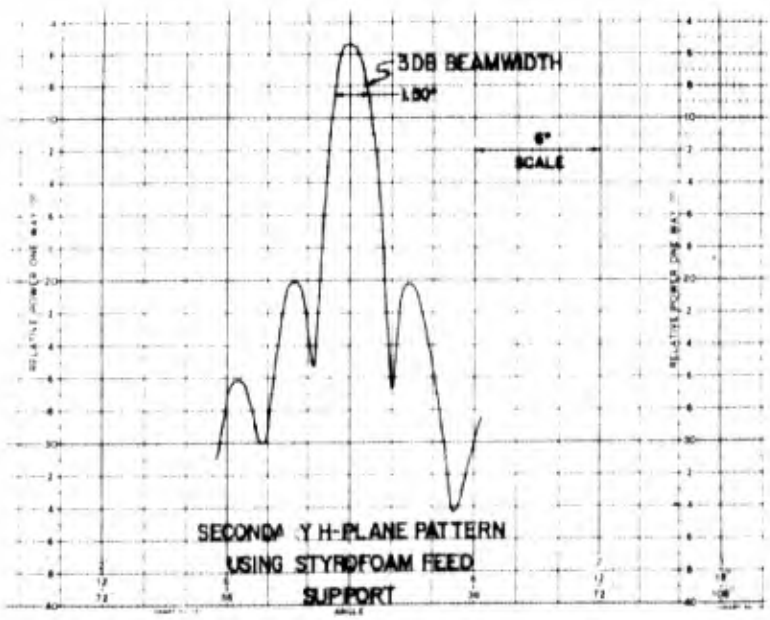

FIGURE 21

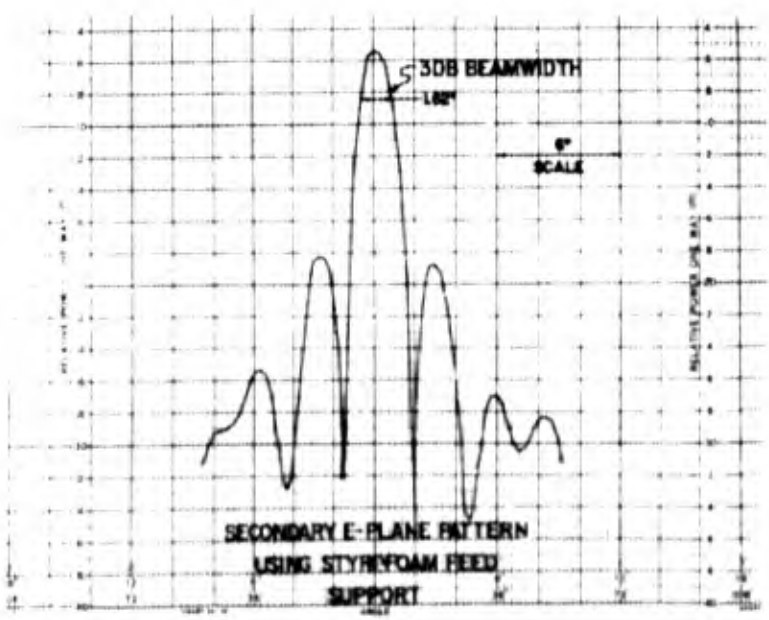

FIGURE 22

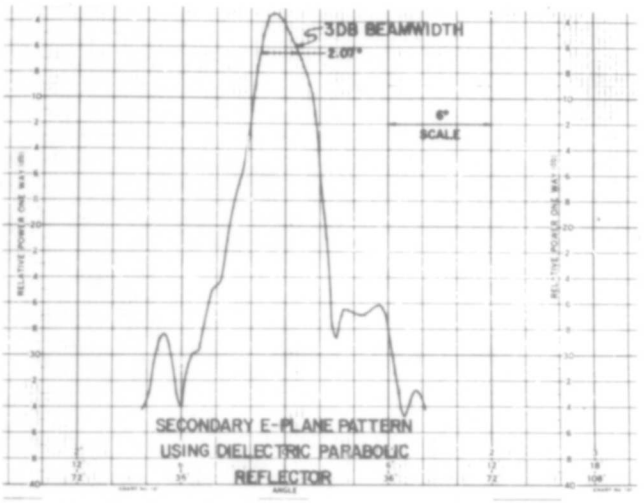

FIGURE 23

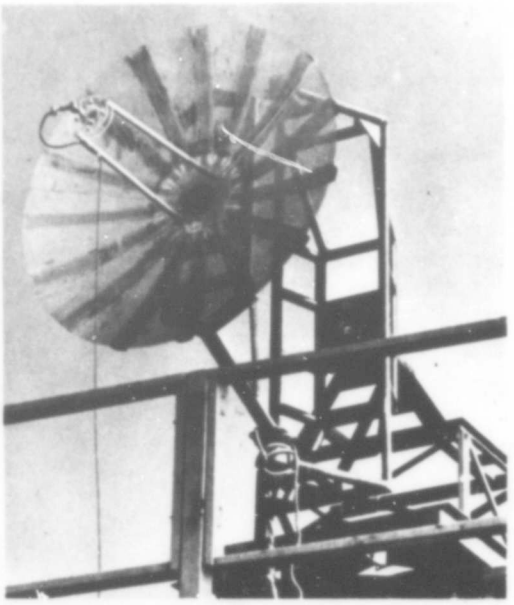

FIGURE 24
TEST MOUNTS FOR DIELECTRIC
PARABOLIC REFLECTOR

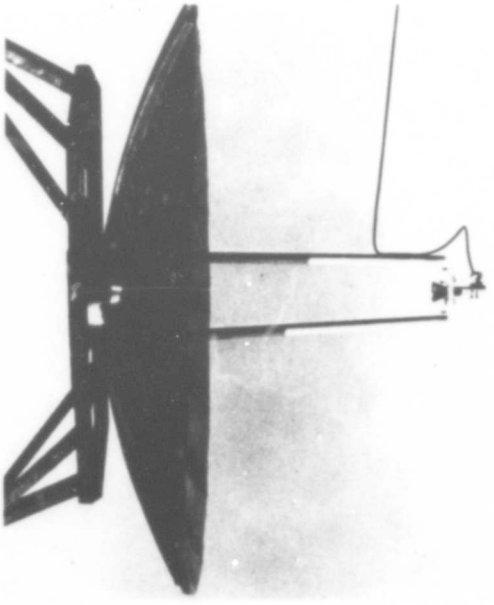

FIGURE 25
DIELECTRIC PARABOLIC REFLECTOR
TEST SETUP SIDE VIEW

TABLE NO. 1

WEIGHT BREAKDOWN OF ANTENNA SYSTEM

ITEM	WEIGHT (lbs)
(1.) MESH REFLECTOR SHELL (1 ea.)	1.45
(2.) MESH SUPPORT RIBS (15 TOTAL)	3.51
(1.) AND (2.) MESH REFLECTOR TOTAL	4.96
(3.) ALUMINUM PARABOLIC HUB PLATE (1 ea.)	1.08
(4.) ALUMINUM RIB SOCKETS (15 TOTAL)	1.65
(5.) ALUMINUM SUPPORT CYLINDER (1 ea.)	0.72
(3.), (4.), AND (5.) HUB BASE SUPPORT TOTAL	3.45
(6.) URETHANE FEED SUPPORT CONE (1 ea.)	2.75
(7.) ALUMINUM CAP, FEED SUPPORT CONE (1 ea.)	0.40
6., AND 7. FEED SUPPORT TOTAL	3.15
(8.) PACKAGING FIXTURE (1 ea.)	2.36
(9.) MISCELLANEOUS CONNECTIONS AND BONDING JOINTS	0.30
(1.) THROUGH (9.) ANTENNA SYSTEMS TOTAL	14.22

TABLE NO. 2

ESTIMATED WEIGHT BREAKDOWN FOR FUTURE DEVELOPMENT OF REFLECTOR STRUCTURE AND HARD POINT ATTACHMENTS FOR MINIMUM WEIGHT.

ITEM	WEIGHT (lbs)
(1.) MESH REFLECTOR SHELL (1 ea.)	2.0
(2.) MESH SUPPORT RIBS (15 TOTAL)	3.0
(1.) AND (2.) MESH REFLECTOR TOTAL	5.0
(3.) PARABOLIC HUB PLATE (1 ea.)	0.5
(4.) RIB SOCKETS (15 TOTAL)	0.8
(3.) AND (4.) HARD POINT ATTACHMENTS	1.3
(5.) MISCELLANEOUS BONDED JOINTS	0.1
(1.) THROUGH (5.) REFLECTOR AND HARD POINT ATTACHMENTS TOTAL	6.4

BLANK PAGE

BURSTING STRENGTH OF FILM AND FABRIC PLASTIC CYLINDERS CONTAINING AN AXIAL SLIT

By Jerry W. Deaton*

INTRODUCTION

The designer of expandable space structures is often faced with a choice between film or fabric materials. The choice is often in favor of the film although fabric materials are generally regarded to be better rip stoppers than film material. Few direct comparisons of film and fabric materials as regards advantages in the presence of rips or slits are available in the literature. The purpose of this investigation is to compare the residual tensile strengths of film and fabric forms of a material in the presence of a slit. Results are presented herein on the effect of varying slit lengths on the bursting strength of cylindrical shells made from polyethylene terephthalate film and fabric. In addition, the bursting strengths of the film and fabric cylinders are compared with the predicted results obtained from two different procedures that are currently used to predict the bursting strength of pressurized metal cylinders containing cracks.

SYMBOLS

$2a_o$ slit length, in.

b width, in.

C_1 coefficient in equation (A1)

C_2 coefficient in equation (A4)

C_m constant appearing in equation (A2), $in^{-1/2}$

K_b finite width correction $= \sqrt{\dfrac{1 - \dfrac{2a_o}{b}}{1 + \dfrac{2a_o}{b}}}$

K_{cn} nominal fracture toughness based on initial slit length for flat sheet (stress intensity factor), $lb/in.\sqrt{in.}$

K_u factor of stress concentration for flat sheet at failure

$K_{u,cyl}$ factor of stress concentration for cylinder at failure

*Aerospace Engineer, Langley Research Center

L	length, in.
N_{gross}	critical uniform load per unit width for sheet based on gross width, lb/in.
N_{hc}	critical membrane hoop loading, lb/in.
N_{net}	critical uniform load per unit width for sheet based on net width, lb/in.
N_u	tensile ultimate load per unit width, lb/in.
N_y	tensile yield load per unit width, lb/in.
N_{YB}	tensile yield load per unit width in 2:1 biaxial stress field = $(1.15)N_y$, lb/in.
P	pressure, psi
r	radius, in.
w	weight per unit surface area, lb/in^2

MATERIAL AND TEST SPECIMENS

The material under consideration, polyethylene terephthalate, is available in rolls of film or fabric as shown in figure 1. In figure 1(b) the fabric is shown to have one set of yarns (warp) with considerable crimp and another set of yarns (fill) which is more nearly straight. Also shown in figure 1 are the unit weights and tensile properties of the two material forms as well as the yarn count of the fabric.

A typical cylinder specimen is shown in figure 2. Each cylinder had a radius of 3.6 inches and was 20 inches long. The film cylinders were made by wrapping the film around a two-piece collapsible cylindrical mandrel. These cylinders had a single longitudinal overlap seam which was held together by double-back tape (see fig. 2). The single longitudinal seam in the fabric cylinders was formed by folding and sewing as illustrated in figure 2. The test program included 20 film and 16 fabric cylinders. The slit lengths chosen for the cylinder specimens were 0.25, 0.50, 1.0, and 2.0 inches. Each slit was located centrally along the cylinder length, diametrically opposite the seam and was made with a sharp instrument while the cylinder was on the collapsible mandrel.

TEST PROCEDURE

The setup for testing the cylinder specimens is shown schematically in figure 3. A 1/32-inch-thick neoprene bladder slightly larger in diameter than

the cylinder specimens was attached to thick circular end plates which were separated by a manifold. One of the end plates was rigidly attached to the manifold while the other was free to move. This configuration was placed inside a cylinder specimen (see fig. 3(b)). After the specimen was clamped to the end plates it was placed in a water tank and slowly filled with water. Care was taken to avoid trapping air inside the cylinder. The internal pressure was measured by a transducer connected to the cylinder and was autographically recorded. The water tank was pressurized and the pressure recorder and a movie camera operating at 24 fps located directly above the slit of the cylinder were started. The pressure inside the cylinder was gradually increased until the test cylinder burst. A typical pressure-time record is shown in figure 4. The time required to burst most cylinders was between 20 and 60 seconds; the shortest time was 3 seconds and the longest time was 1.5 minutes. The tests were limited to these relatively short times in order to avoid significant creep behavior of the material. Observation during the tests and studies of the movie frames indicated that in all cases the cylinders failed suddenly without detectable prior crack growth. A typical failure consisted of a rapid extension of the crack for approximately the entire length of the cylinder, as shown by the unwrapped cylinder specimens in figure 5.

RESULTS AND DISCUSSION

The values of the critical hoop loading N_{hc} are given in table 1 and plotted against slit length in figure 6. The values of N_{hc} for zero slit length were obtained by using the uniaxial ultimate strength values given in figure 1 for each material. Comparison of the experimental data corresponding to the different orientations of the film material indicates that, within the scatter of the data, material orientation has no effect on the critical hoop loading for the film cylinders (see fig. 6(a)). It is evident from figure 6(b) that the fabric cylinders having the warp yarns in the hoop direction have slightly higher values of the critical hoop loading than those with the fill yarns in the hoop direction. Since the warp yarn count is less than the fill yarn count the individual warp yarns support greater loads than the fill yarns. The reason for this behavior may be related to the difference in the amount of crimp existing in the warp and fill yarns. When the warp yarns are in the direction of principal loading they tend to straighten out and thus transfer the crimp to the fill yarns. Due to this crimp, interchange friction between warp and fill yarns is increased thus establishing a means for transferring load from one warp yarn to an adjacent warp yarn. When the fill yarns are in the direction of principal loading there is less crimp interchange, therefore less friction between yarns and thus less load transfer between adjacent fill yarns.

It is evident from figure 6 that for a given slit length the fabric cylinders have a much higher bursting strength than the film cylinders. For the slit lengths investigated the average value of the bursting strength for the fabric cylinders is about twice the bursting strength of the film cylinders. The results shown for zero crack length represent the uniaxial strengths given in figure 1 and show that the fabric strength is inherently about

1.6 times the film strength. A direct comparison of the film and fabric cylinders is given in figure 7. The ordinate N_{hc}/w is equivalent to the familiar stress-density ratio used to express the tensile efficiency of materials. The curves shown for the film and fabric represent the average values of the critical hoop loading obtained for both orientations of the material. For the cylinders with slits, figure 7 shows that the strength-weight ratio of the fabric cylinders is approximately twice that of the film cylinders. The results shown at zero slit length are for uniaxial loads and indicate that the fabric strength-weight ratio is inherently about 1.8 times that of the film. It should be noted that woven materials generally require coatings or liners in order to retain pressure, and any such coating or liner would reduce this advantage.

Figure 7 also indicates that for the shorter slit lengths the fabric is less sensitive to rupture than the film cylinders. This can be seen by comparing the values of N_{hc}/w for cylinders with and without slits. For the shortest slit length, the value of N_{hc}/w for the fabric is greater than 90 percent of the zero slit length value whereas for the shortest slit length for the film the value of N_{hc}/w is only about 75 percent of the zero slit length value.

The decrease in bursting strength with increasing slit length noted for the film and fabric cylinders is consistent with predicted results obtained by other investigators working with pressurized metal cylinders (see refs. 1 and 2). Although the methods of analysis that have been developed to predict the failure of pressurized metal cylinders containing cracks may not be valid for plastics, a comparison with the experimental data is of interest. The details required to make such comparisons are presented in appendixes A and B. The results are shown in figure 8. The curves shown in figure 8 represent the extremes of the predicted bursting strength obtained for each method of analysis presented in appendix A. The dashed curves give the extremes of the notch-strength analysis and the solid curves give the extremes of the fracture mechanics analysis while the symbols indicate the experimentally obtained values of the bursting strength. The comparisons indicate that large errors can result from the application of the notch-strength analysis to film or fabric cylinders whereas the fracture mechanics analysis yields a scatter band which is consistent with the data scatter and follows the trend of the data. Although the fracture mechanics analysis describes the overall behavior of the film or fabric cylinders, it is clear from figure 8 that substantial errors can result by using this method.

CONCLUDING REMARKS

The bursting strengths of film and fabric plastic cylinders containing an axial slit as obtained from water pressurization tests have been presented. The results demonstrate that the fabric material is superior to the film material as regards residual strength in the presence of a slit. It has been shown that the strength-weight ratio of the fabric cylinders is approximately twice

that of the film cylinders largely due to the inherent strength advantage of fiber over film. The results were compared with the predicted bursting strength obtained from two different semiempirical analyses, one based on notch-strength analysis and the other employing fracture mechanics concepts. The comparison demonstrates that large errors can result from the application of the notch-strength analysis to film or fabric cylinders whereas the fracture mechanics analysis yields a scatter band which is consistent with the data scatter and follows the trend of the data. Although the fracture mechanics analysis describes the overall behavior, the width of the scatter band is sufficiently large that substantial errors can result by using this method.

APPENDIX A

COMPARISON OF CALCULATED AND EXPERIMENTAL RESULTS

In reference 1 (notch-strength analysis) an empirical relation is presented to predict the bursting strength of pressurized cylinders containing slits. This relationship gives the stress concentration factor for the cylinder as a function of the stress concentration factor of a flat sheet as follows:

$$K_{u,cyl} = K_u\left[1 + C_1\left(\frac{a_o}{r}\right)\right] \tag{A1}$$

where

$$K_u = \frac{N_u}{N_{net}} = 1 + K_b C_m \sqrt{a_o} \qquad \text{(see ref. 3)} \tag{A2}$$

and

$$K_b = \sqrt{\frac{1 - \frac{2a_o}{b}}{1 + \frac{2a_o}{b}}} \qquad \text{(see ref. 4)} \tag{A3}$$

and C_m is a constant having the dimension $\left(in^{-1/2}\right)$.

The constant C_m may be determined experimentally from flat sheet tests as shown in appendix B. The values of C_m obtained from appendix B are given in the following table:

Film			Fabric		
Roll direction	C_m, $in^{-1/2}$		Warp direction	C_m, $in^{-1/2}$	
	Average	Range of values		Average	Range of values
Longitudinal	0.700	0.387 to 1.068	Longitudinal	1.109	0.526 to 2.385
Transverse	1.065	0.474 to 1.146	Transverse	0.852	0.332 to 1.329

These values of C_m along with equation (A3) were used to obtain K_u from equation (A2). With these values of K_u and the experimental values of $K_{u,cyl}$ determined from the burst strengths given in table 1, the value of C_1 which satisfies equation (A1) has been determined for each cylinder tested.

The resulting values of C_1 are shown in figure 9. It is evident from figure 9 that the value of C_1 is not constant for either the film or fabric. Hence, assigning a single value to C_1 could lead to large errors in prediction of burst strength.

The method of analysis used in reference 2 (fracture mechanics analysis) for determining the bursting strength of cylinders containing slits is based on fracture mechanics concepts. This approach considers the stress intensity near the end of a slit in a cylinder to be influenced by membrane stressing in the cylinder wall and bending stresses caused by pressure bulging of the material on either side of the slit. The equation for predicting the bursting strength of cylinders as given by reference 2 is as follows:

$$N_{hc} = \frac{K_{cn}}{\sqrt{\pi a_o + \frac{1}{2}\frac{K_{cn}^2}{N_{YB}^2}\left(1 + C_2 \frac{a_o}{r}\right)}} \tag{A4}$$

where K_{cn} is determined empirically from

$$K_{cn} = N_{gross}\sqrt{b \tan\left[\frac{\pi}{b}\left(a_o + \frac{1}{2}\frac{K_{cn}^2}{N_y^2}\right)\right]} \tag{A5}$$

The values of K_{cn} may be obtained experimentally from tests on flat sheets as shown in appendix B. The values of K_{cn} obtained from appendix B are given in the following table:

Film			Fabric		
Roll direction	K_{cn}, lb/in. $\sqrt{\text{in.}}$		Warp direction	K_{cn}, lb/in. $\sqrt{\text{in.}}$	
	Average	Range of values		Average	Range of values
Longitudinal	135.03	134.85 to 135.22	Longitudinal	186.80	178.78 to 194.81
Transverse	125.01	122.16 to 127.86	Transverse	225.95	224.11 to 227.78

Values of K_{cn} were obtained only for sheet specimens having a slit length in the range of 30 percent to 40 percent of the sheet width which is consistent with suggested testing methods given in reference 5. With these values of K_{cn} and the experimental values of burst strength N_{hc} given in table 1, the value of the coefficient C_2 which satisfies equation (A4) has been determined for each cylinder tested. The resulting values of C_2 are shown in figure 10.

In the analysis of reference 2, C_2 is assumed to be constant for a given material. However, it is evident from figure 10 that the values of C_2 vary considerably. This is particularly true of the film cylinders. Therefore, the selection of a single value for C_2 is not justified by the experimental evidence.

By selecting the highest and lowest values for C_1 and also for C_2 a scatter band for each method of analysis can be calculated for comparison with the experimental data. The results of such calculations are shown in figure 8.

APPENDIX B

STRENGTH OF FILM AND FABRIC PLASTIC SHEETS CONTAINING A CENTRAL SLIT

Experimental data are needed on the strength of film and fabric plastic sheets containing a central slit in order to apply the analyses given in references 1 and 2 to predict the bursting strength of film or fabric cylinders. The results of such tests are presented in this appendix.

The details of the two sheet sizes tested for the film and fabric material are given in figures 11 and 12, respectively. In the fabric sheets some of the longitudinal yarns were removed so that unraveling of the specimen would be minimized. One series of sheets was made 3 inches wide and had a test length between the gripped portion of 6 inches. These specimens had central slits which were made by cutting with a sharp-edged instrument. The slit lengths ($2a_o$) were 0.125, 0.25, 0.50, and 1.0 inch. Two specimens of each slit length and of each orientation of the film and fabric were tested. Another series of sheets was tested with the width and slit length scaled up by a factor of four. The length of these specimens between the gripped portion was made 12 inches or scaled up only half as much as the width and slit length because of the limitation of size which could be accommodated in the testing machine.

The sheet specimens were tested in tension using a screw-driven testing machine with a capacity of 10 kips. Three inches of each end of the specimen were placed in smooth-faced grips and, after careful alinement, were subjected to tensile loading at a strain rate of about 0.33 per minute until failure occurred. Load and motion of the lower platen of the testing machine were recorded autographically so that the load at failure and the elapsed time of the test were readily obtainable. It should be stated that guide plates were not used in the sheet tension test and in some cases considerable out-of-plane deflection was noted in the area of the slit. However, it is likely that any restraint introduced by the use of guide plates would not appreciably increase the strength of the film or fabric sheets. The results of the film and fabric plastic sheet tests are given in table 2. Comparison of the data in table 2 for the 3-inch and 12-inch width sheets indicates that for a given value of $2a_o/b$ the wider sheets support greater failing loads per unit width than the narrower sheets. This trend is opposite to that experienced in metals and, therefore, indicates the need for further research in order to determine reliable parameters for analysis involving plastic materials.

REFERENCES

1. Peters, Roger W.; and Kuhn, Paul: Bursting Strength of Unstiffened Pressure Cylinders With Slits. NACA TN 3993, 1957.

2. Anderson, Robert B.; and Sullivan, Timothy L.: Fracture Mechanics of Through-Cracked Cylindrical Pressure Vessels. NASA TN D-3252, 1966.

3. Kuhn, Paul: The Prediction of Notch and Crack Strength Under Static or Fatigue Loading. Preprint 843C, S.A.E.-ASME, April 1964.

4. Dixon, J. R.: Stress Distribution Around a Central Crack in a Plate Loaded in Tension; Effect of Finite Width of Plate. Jour. R.A.S., Vol. 64, No. 591, Mar. 1960, pp. 141-145.

5. ASTM Special Committee on Fracture Toughness Testing of High-Strength Metallic Materials. Fracture Testing of High-Strength Sheet Materials. Bull. No. 243, ASTM, Jan. 1960, pp. 29-40.

TABLE 1.- BURST STRENGTHS FOR FILM AND FABRIC CYLINDERS

CONTAINING AN AXIAL SLIT

[L = 20 in.; r = 3.6 in.]

Film			Fabric		
Roll direction	$2a_o$, in.	N_{hc}, lb/in.	Warp direction	$2a_o$, in.	N_{hc}, lb/in.
Axial ↓	0.25	68.10	Axial ↓	0.25	140.56
	.25	69.94		.25	127.07
	.50	50.02		.50	111.12
	.50	53.28		.50	111.58
	1.0	29.92		1.0	70.45
	1.0	32.94		1.0	73.68
	1.0	35.55		2.0	33.44
	2.0	23.63		2.0	33.77
	2.0	19.16			
			Hoop ↓	.25	138.60
Hoop ↓	.25	75.38		.25	150.48
	.25	66.26		.50	123.98
	.25	73.60		.50	130.33
	.50	46.64		1.0	78.80
	.50	49.04		1.0	77.57
	1.0	38.23		2.0	45.57
	1.0	27.44		2.0	44.10
	1.0	33.08			
	1.0	39.12			
	2.0	23.98			
	2.0	20.26			

TABLE 2.- TENSILE STRENGTHS FOR FILM AND FABRIC SHEET

Film					Fabric				
Roll direction	b, in.	$2a_o$, in.	N_{net}, lb/in.	N_{gross}, lb/in.	Warp direction	b, in.	$2a_o$, in.	N_{net}, lb/in.	N_{gross}, lb/in.
Transverse	3.0	0	87.33	87.33	Transverse	3.0	0	150.17	150.17
		0	99.33	99.33			0	144.57	144.57
		0	90.66	90.66			.125	123.48	118.33
		.125	75.13	72.00			.125	118.26	113.33
		.125	75.13	72.00			.25	102.91	94.33
		.25	70.18	64.33			.25	110.91	101.67
		.25	70.18	64.33			.50	94.40	78.67
		.50	64.40	53.67			.50	98.00	81.67
		.50	64.00	53.33			1.0	96.00	64.00
		1.0	59.50	39.67			1.0	92.50	61.67
		1.0	60.00	40.00					
	12.0	.50	67.91	65.08		12.0	.50	100.87	96.67
		.50	69.30	66.42			.50	100.00	95.83
		1.0	67.00	61.42			1.0	111.82	102.50
		1.0	68.18	62.50			1.0	112.27	102.92
		2.0	66.10	55.08			2.0	114.00	95.00
		2.0	53.90	44.92			2.0	110.00	91.67
		4.0	61.38	40.92			4.0	110.63	73.75
		4.0	63.50	42.33			4.0	109.38	72.92
Longitudinal	3.0	0	95.33	95.33	Longitudinal	3.0	0	154.40	154.40
		0	98.33	98.33			0	152.63	152.63
		0	90.33	90.33			.125	126.26	121.00
		.125	78.61	75.33			.125	131.83	126.33
		.125	78.26	75.00			.25	109.82	100.67
		.25	75.27	69.00			.25	111.64	102.33
		.25	75.64	69.33			.50	88.80	74.00
		.50	66.80	55.67			.50	76.40	63.67
		.50	65.60	54.67			1.0	74.50	49.67
		1.0	61.00	40.66			1.0	77.00	51.33
		1.0	61.50	41.00		12.0	.50	117.83	112.92
	12.0	.50	72.61	69.58			.50	113.91	109.17
		.50	71.39	68.42			1.0	102.73	94.17
		1.0	71.00	65.08			1.0	110.00	100.83
		1.0	71.64	65.67			2.0	98.00	81.67
		2.0	70.50	58.75			2.0	93.50	77.92
		2.0	69.50	57.92			4.0	100.63	67.08
		4.0	66.00	44.00			4.0	93.75	62.50
		4.0	66.13	44.08					

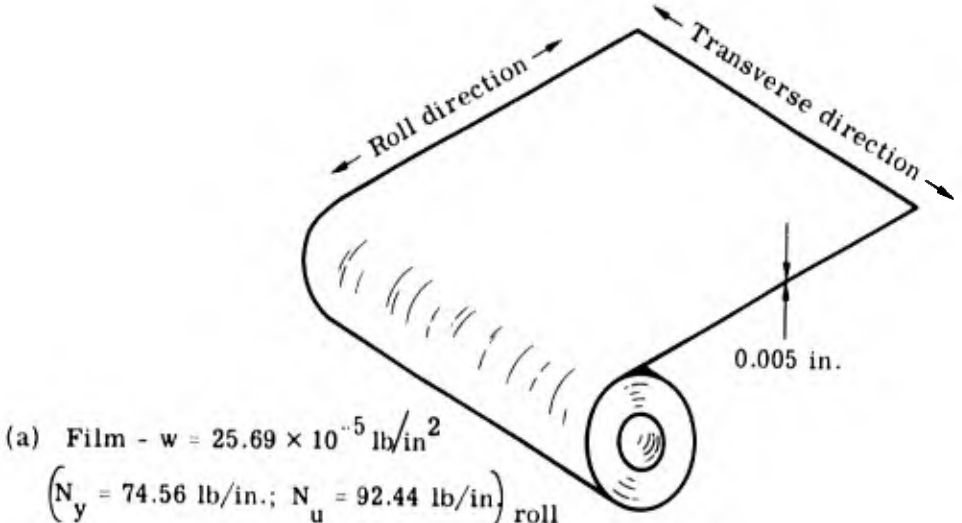

(a) Film - $w = 25.69 \times 10^{-5}$ lb/in^2

$(N_y = 74.56$ lb/in.; $N_u = 92.44$ lb/in.$)_{\text{roll}}$

$(N_y = 72.22$ lb/in.; $N_u = 94.66$ lb/in.$)_{\text{transverse}}$

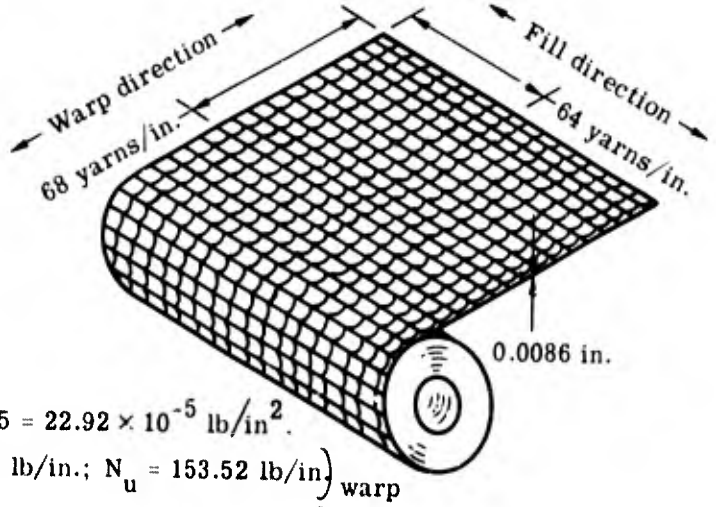

(b) Fabric - $25 = 22.92 \times 10^{-5}$ lb/in^2.

$(N_y = 133.33$ lb/in.; $N_u = 153.52$ lb/in.$)_{\text{warp}}$

$(N_y = 120.83$ lb/in.; $N_u = 147.37$ lb/in.$)_{\text{fill}}$

Figure 1.- Nomenclature and material properties.

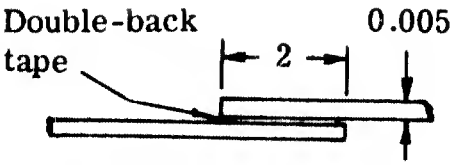

(a) Film cylinder seam

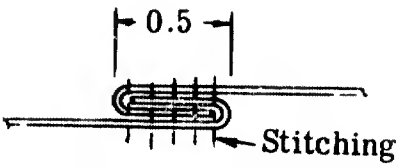

(b) Fabric cylinder seam

Detail A

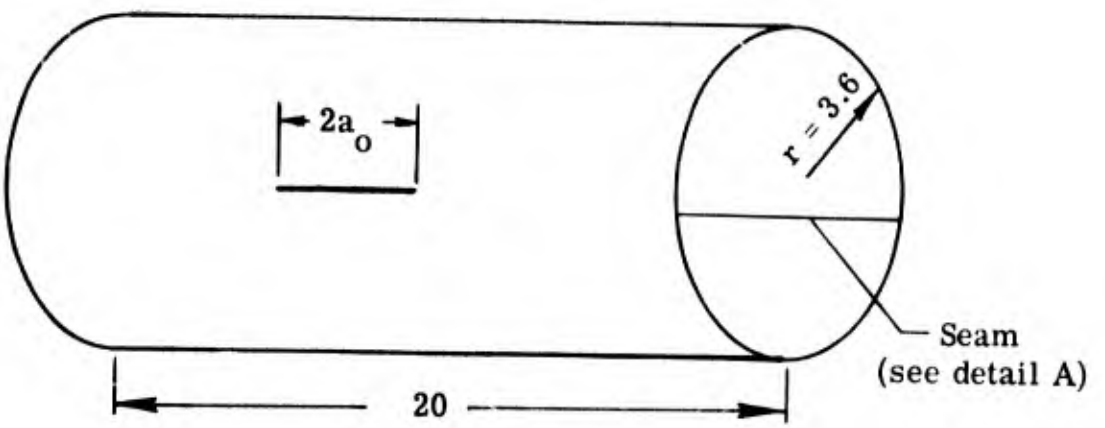

$2a_o$ = 0.25, 0.50, 1.00, and 2.00

Figure 2.- Typical cylinder specimen. All dimensions are in inches.

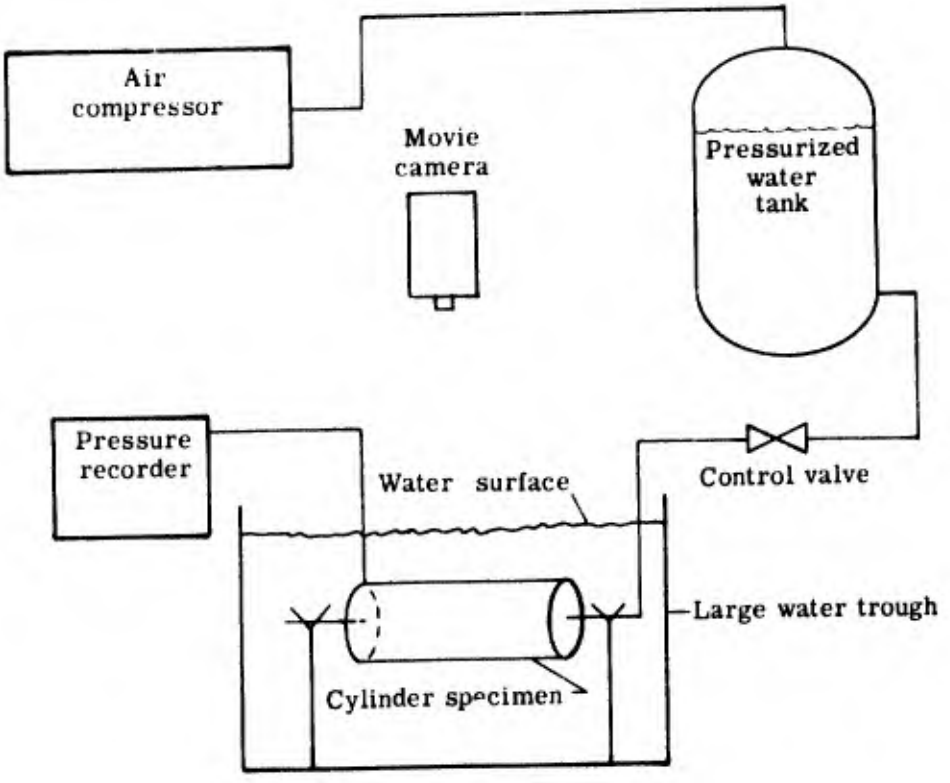

(a) Test setup

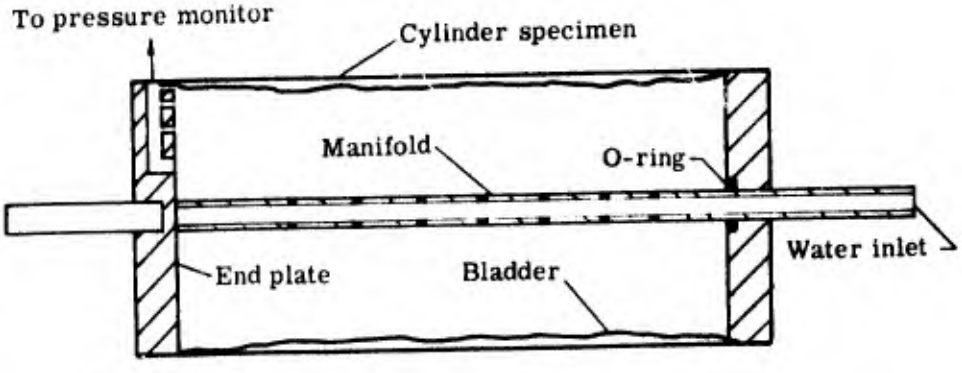

(b) Cross-section of cylinder

Figure 3.- Schematic of cylinder burst test apparatus.

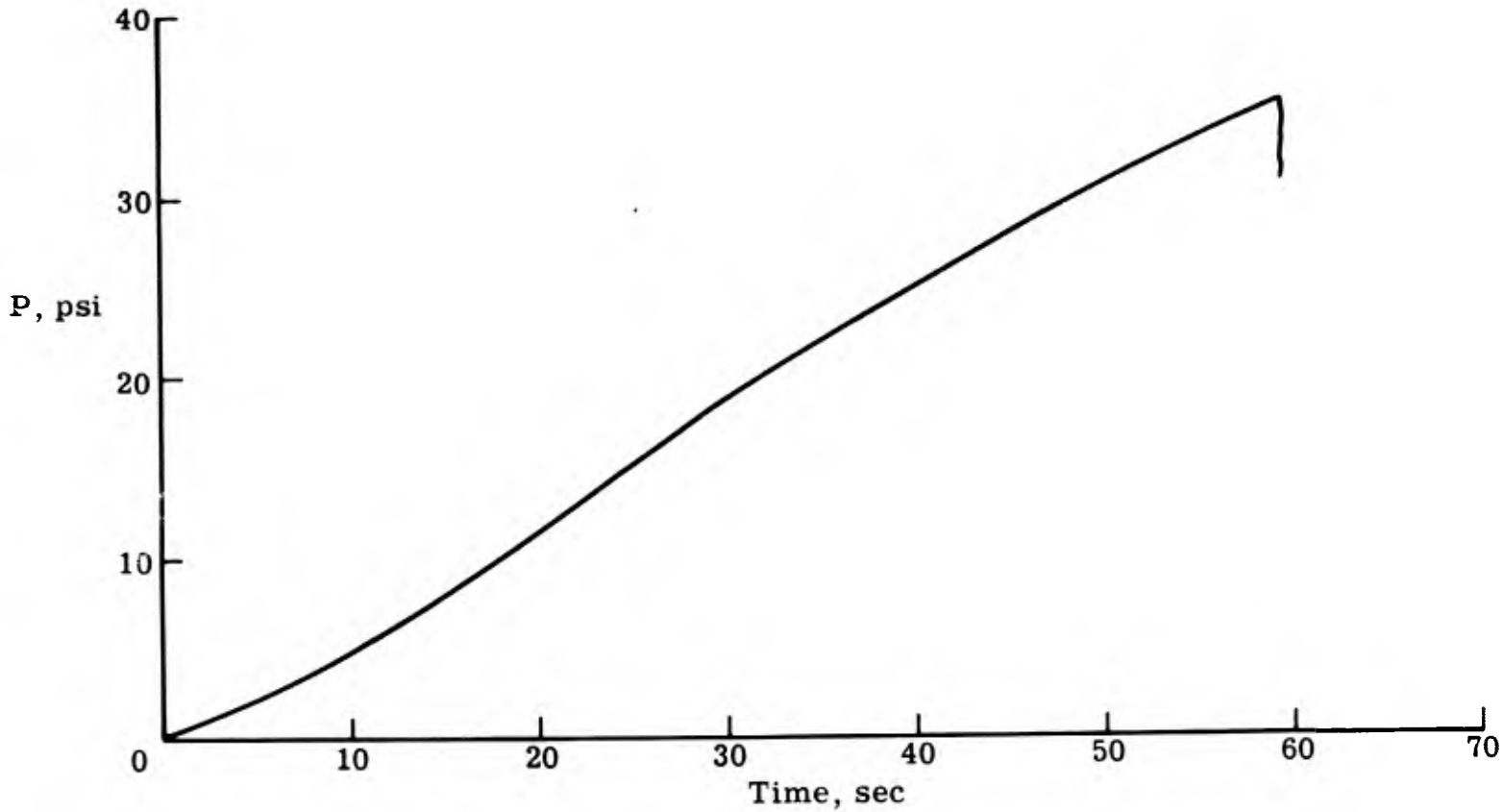

Figure 4.- Typical pressure-time record for cylinder burst test.

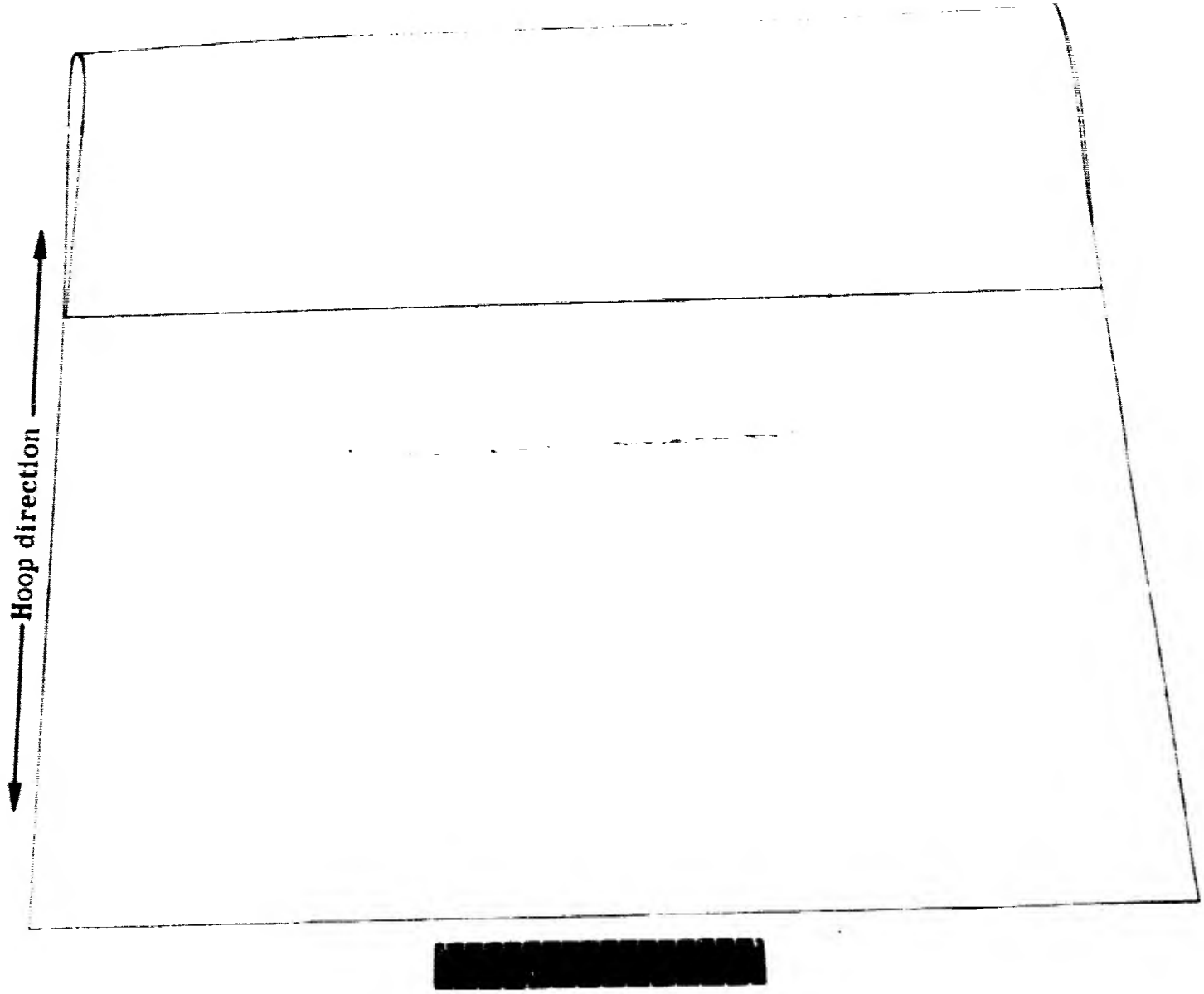

(a) Film.

Figure 5.- Typical failure of unwrapped cylinder specimen.

(b) Fabric.

Figure 5.- Concluded.

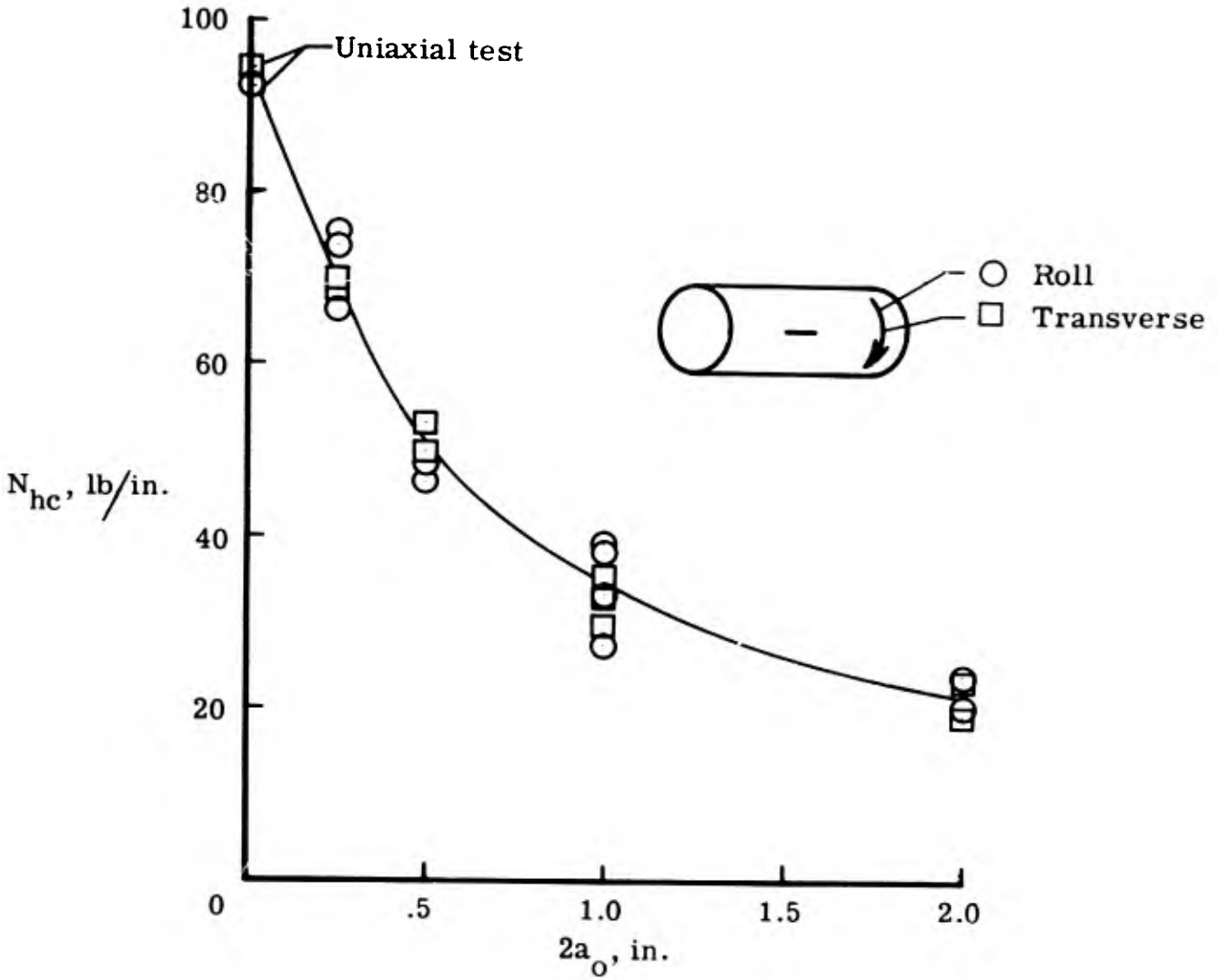

(a) Film.

Figure 6.- Critical hoop loading for film and fabric cylinders.

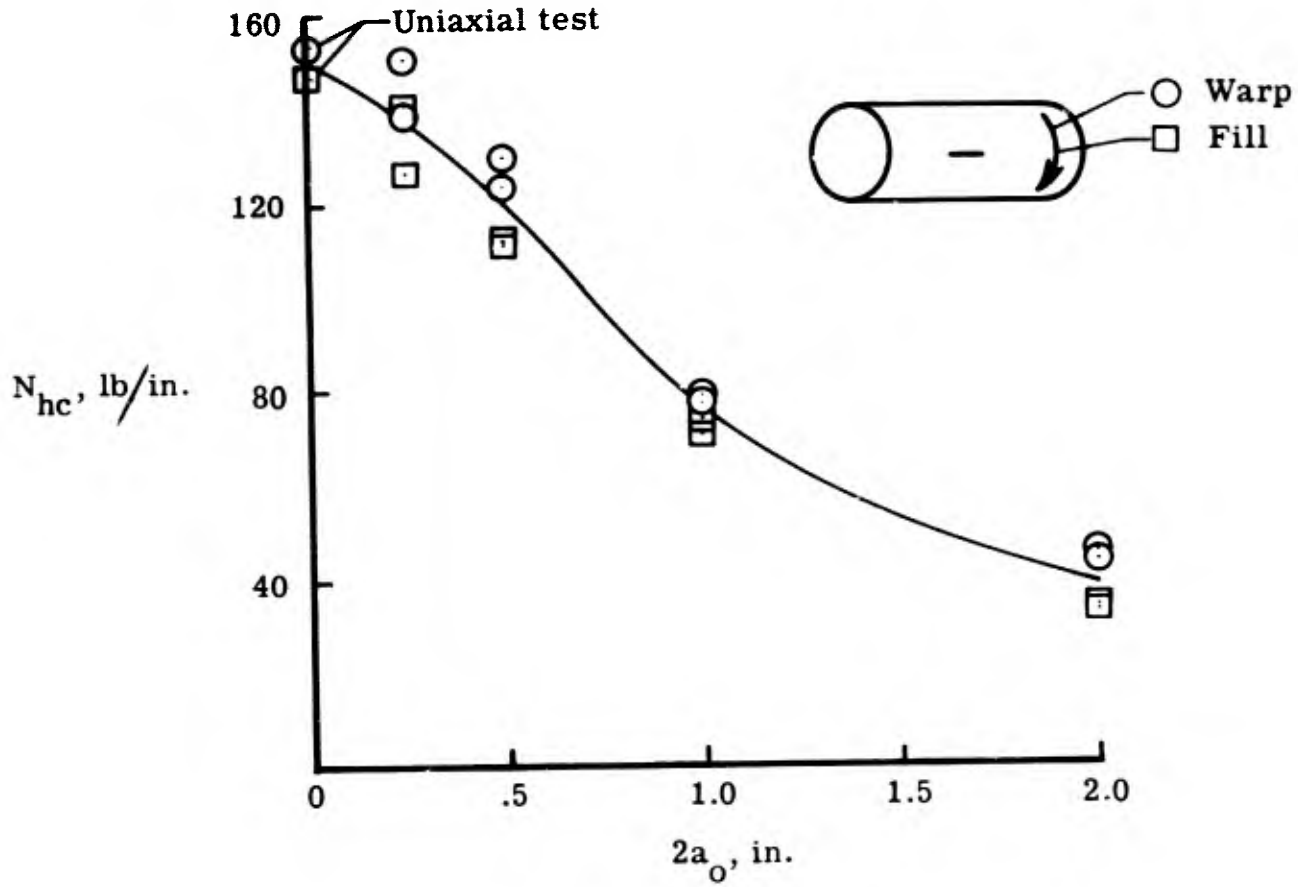

(b) Fabric.

Figure 6.- Concluded.

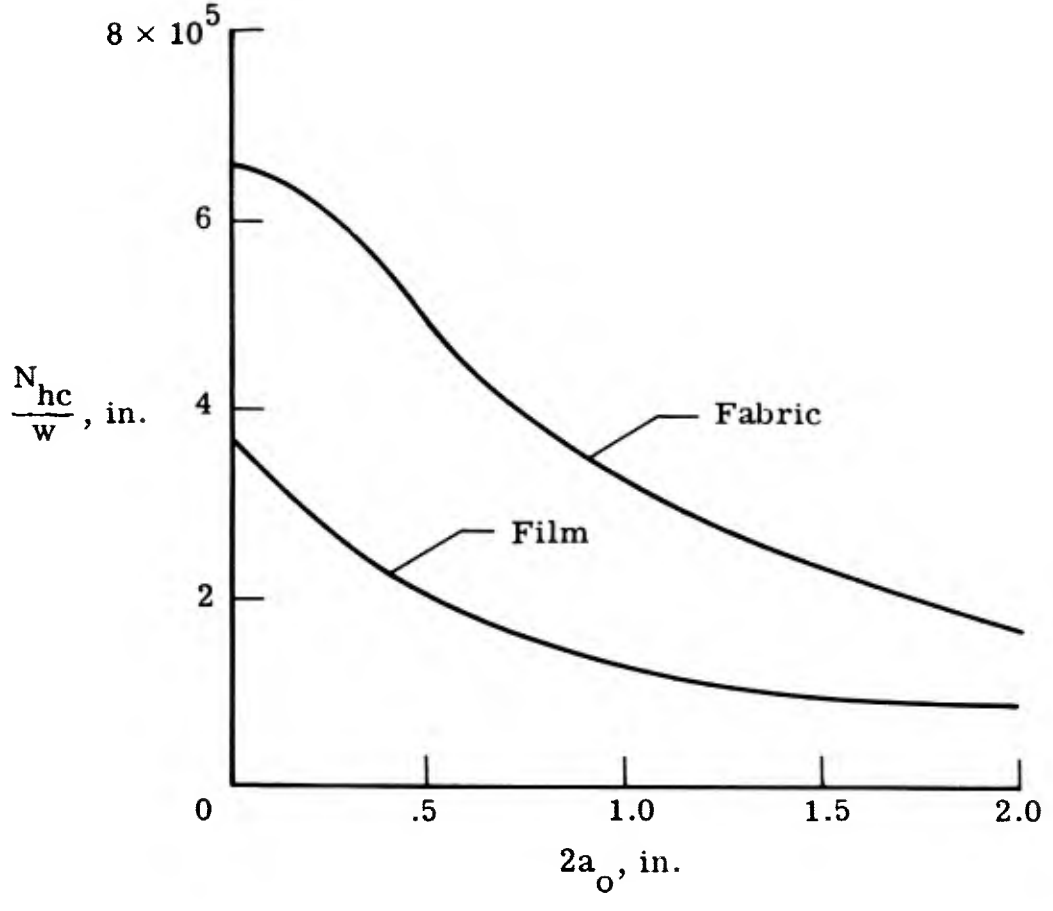

Figure 7.- Comparison of stress-density ratios for film and fabric.

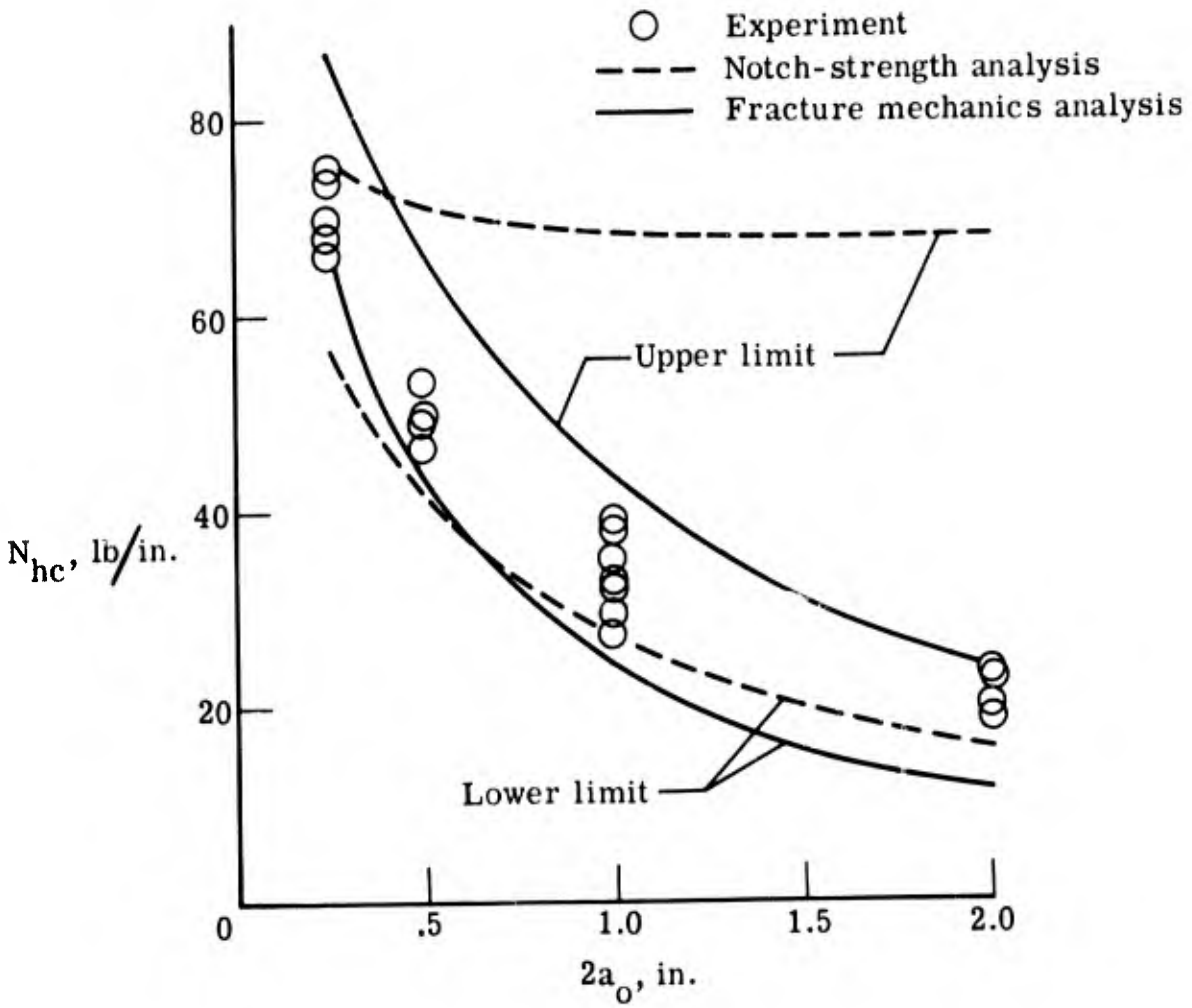

(a) Film.

Figure 8.- Comparison of experiments with extremes of calculations.

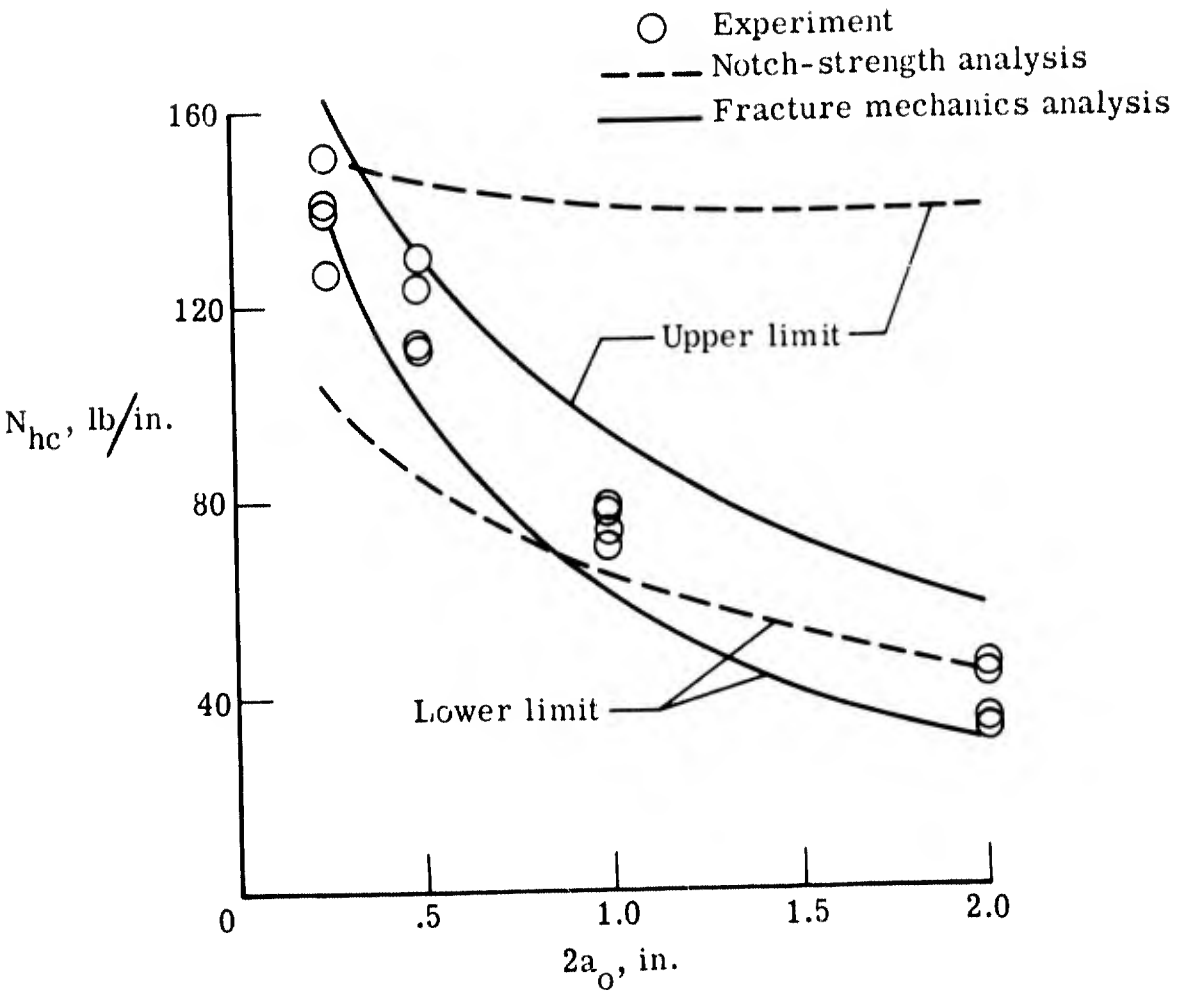

(b) Fabric.

Figure 8.- Concluded.

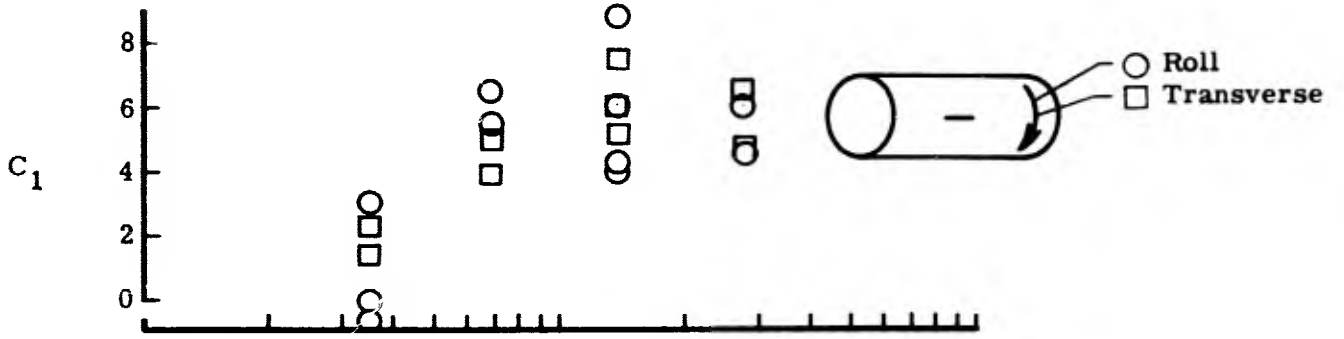

(a) Film.

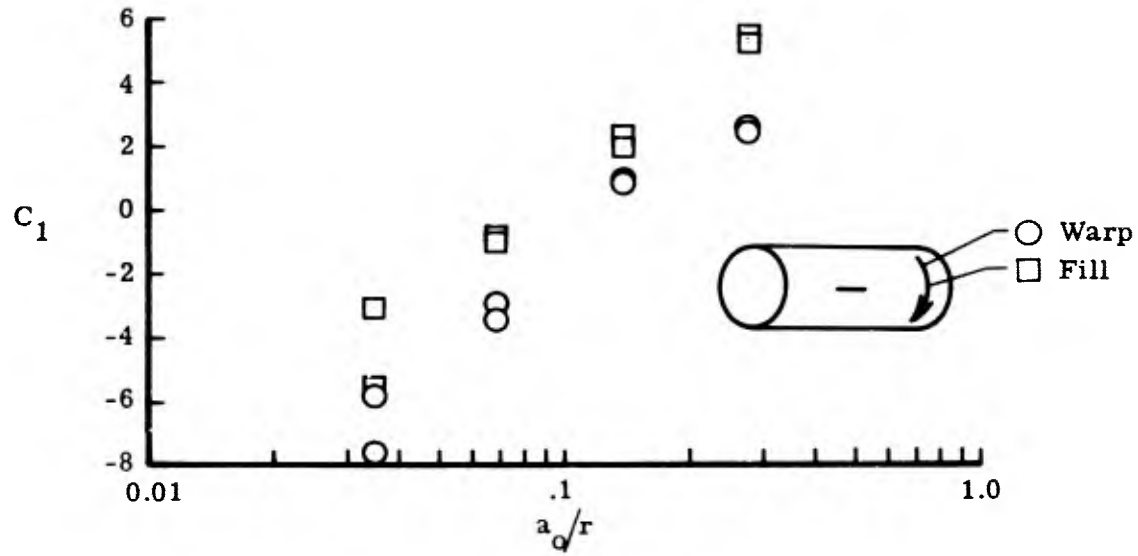

(b) Fabric.

Figure 9.- Values of C_1 for film and fabric.

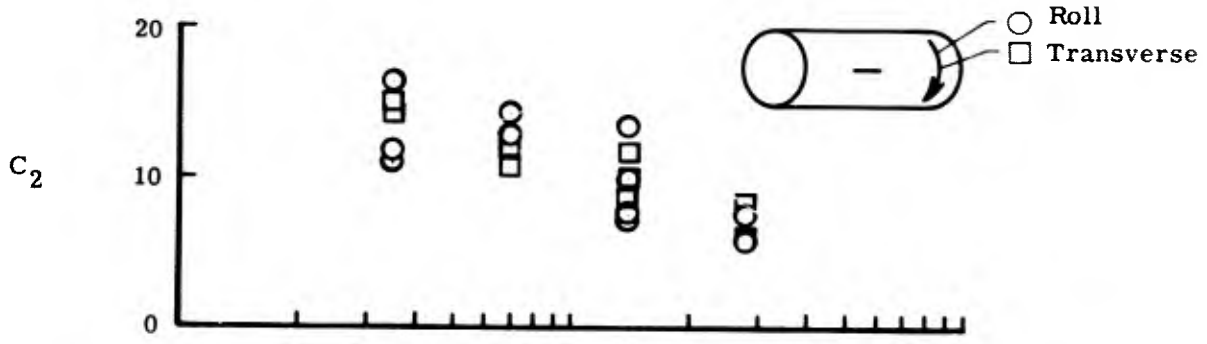

(a) Film.

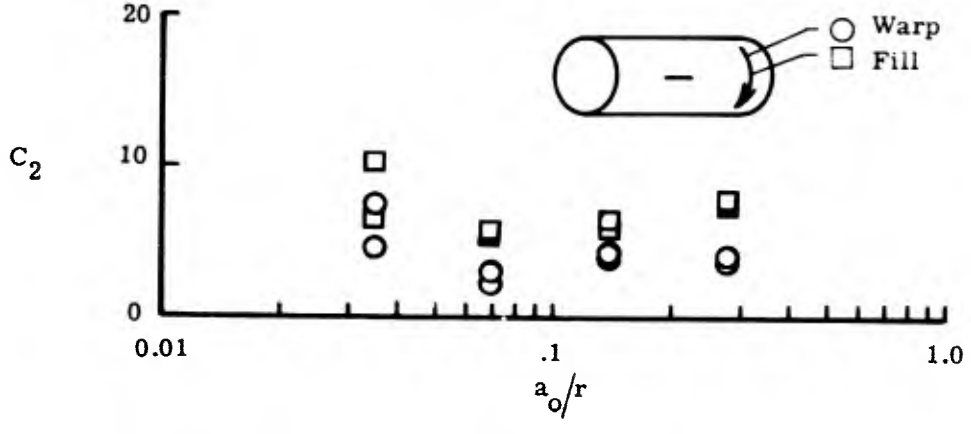

(b) Fabric.

Figure 10.- Values of C_2 for film and fabric.

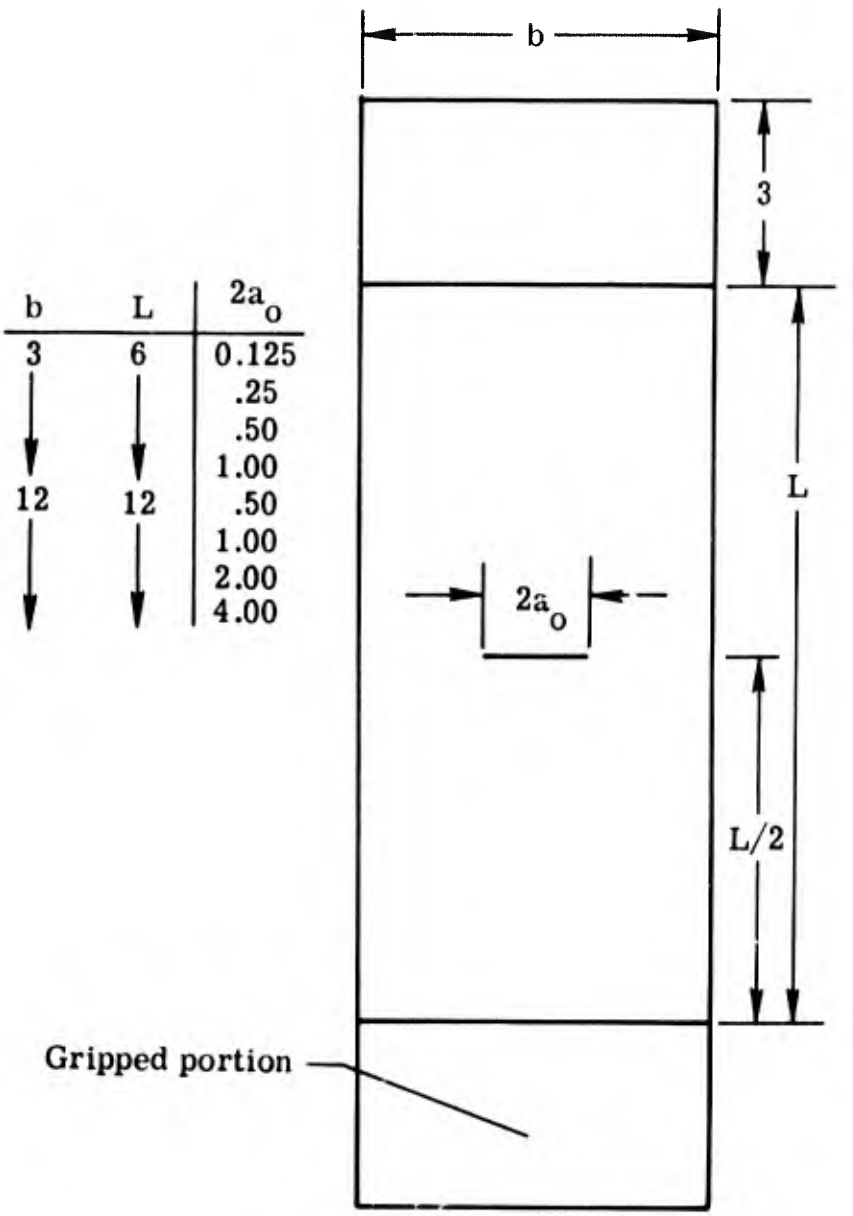

Figure 11.- Details of film sheet specimens with central slit.

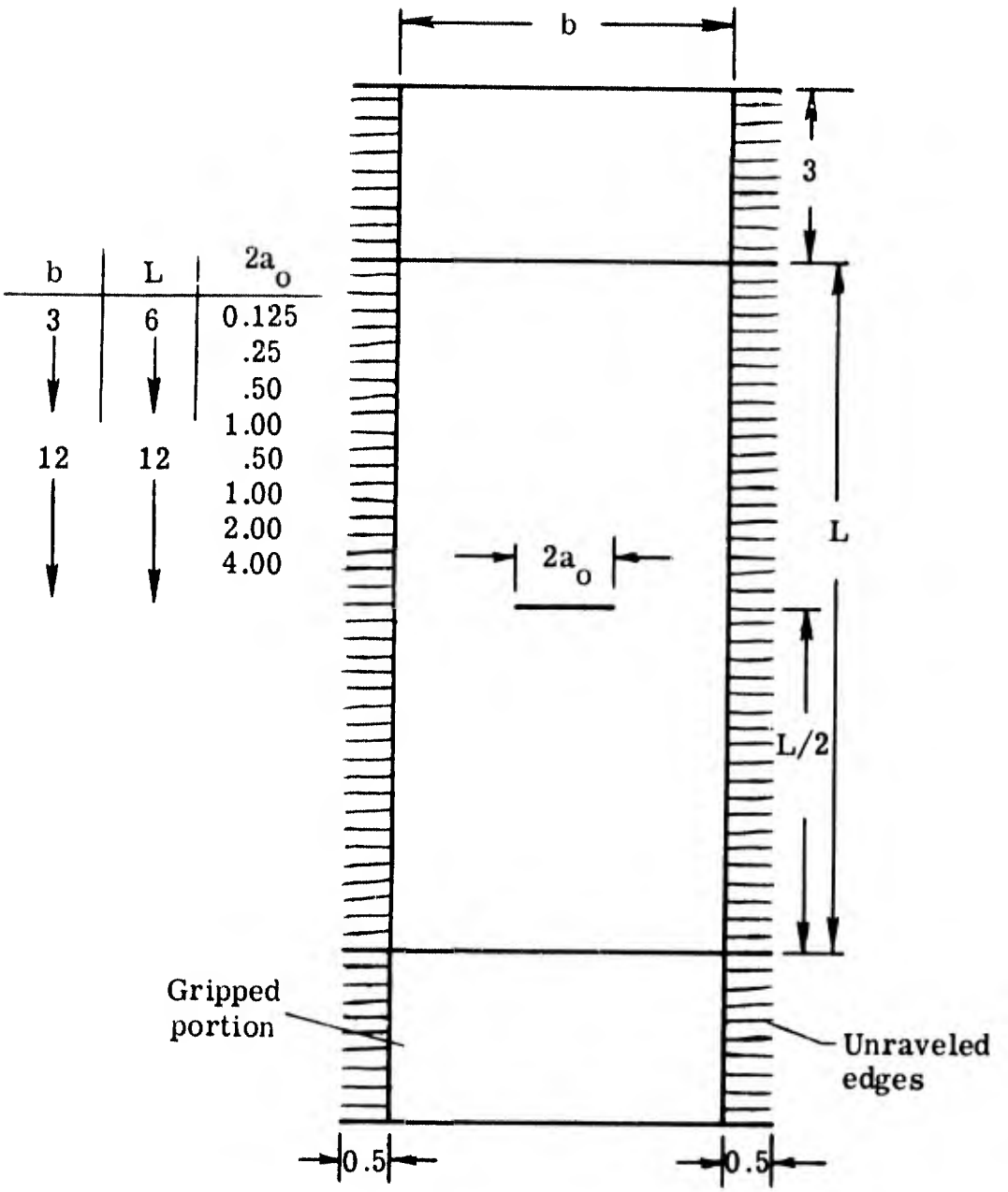

Figure 12.- Details of fabric sheet specimens containing central slit.

SESSION IV

ZERO-G SIMULATION AND ITS RELATIONSHIP TO SPACE EXPERIMENTS

GARY B. REID*

DANIEL R. SEGER **

That the accomplishment of manned space experiments depends to a large degree on the proper definition and design of the man/equipment interfaces, has been made evident by the difficulties recently encountered during the performance of Extra-Vehicular Activity (EVA) tasks on Gemini 9 through 11. If this interface between man, particularly EVA man, and his equipment is so important, how can we insure that it will be properly defined, designed and tested: Part of the answer, of course, is derived through simulation of the actual space experiment. How much of the experiment should be simulated? When does the cost of simulation outweigh the benefits received? The tradeoff point varies with the type of simulation and the complexity and enormity of the experiment, but one thing is abundantly clear.- In order to derive the maximum efficiency from man in his in-space operator's role, he must be well trained to use his properly designed equipment.

Since space experiments are very clearly defined, and the subjects are well trained and highly motivated, simulation for space experiments actually appears to be the running of pilot studies in which the simulation is carefully planned and executed and various data are collected and evaluated. It is then anticipated that the procedures and data will later be verified by the orbital execution of the experiment.

Prior to the running of pilot studies, however, numerous human engineering decisions are required to solve those basic operational problems that will be encountered during the engineering and development phases of experiment definition. Figure 1 describes a simplified methodology wherein a space experiment is conceived, designed, developed and flown in space. Simulation and testing can play an important role in the conceptual design, feasibility determination, detail design and training phases. Based on this philosophy, if an experimenter concludes that zero-g simulation for training and testing is, in fact, necessary, what is his recourse? Presently there exists no technique for the extended generation of a true state of weightlessness short of achieving earth orbital flight. However, there do exist several techniques for achieving short periods (20-30 seconds) of weightlessness or longer durations of mechanically equivalent null gravity.

*Captain, USAF 6570th Aerospace Medical Research Laboratory,
Wright-Patterson AFB, Ohio

**Captain, USAF Air Force Aero Propulsion Laboratory,
Wright Patterson AFB, Ohio

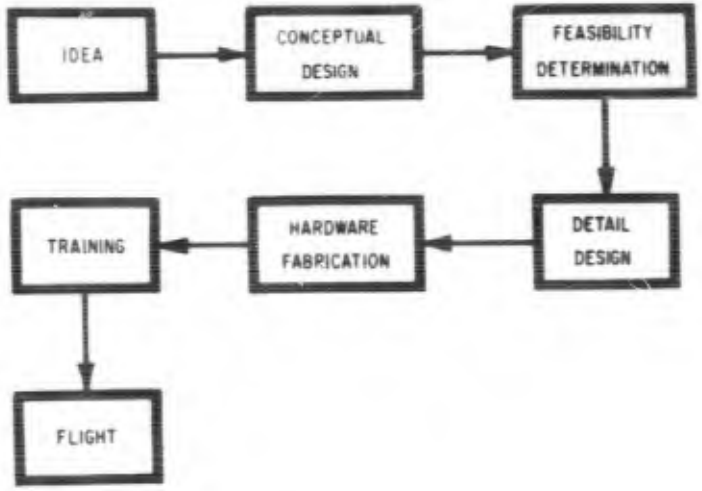

Figure 1

Figure 2

Zero-G Simulation

The three primary methods of achieving or simulating zero-g are: Aircraft flying keplerian trajectories, water immersion to attain neutral buoyancy (Fig 2) and mechanical simulators consisting of frictionless platforms with gimballed support structure.

Considerable effort has been expended to prove (or disprove) the validity of these types of simulation as compared to orbital space flight (Refs 1,2,3). Comparison of simulation schemes or proof of validity is beyond the scope of this paper. However, comments as to the applicability of each type of simulation used for the effort reported herein will be included later. Of the three principal types of zero-g simulation, only two (zero-g aircraft and neutral buoyancy) are being used extensively throughout this effort.

For those unfamiliar with the operation of the zero-g aircraft, weightlessness is achieved by flying an aircraft through a portion of a keplerian trajectory as depicted in Fig 3. Tests conducted during these flights have the advantage of being subjected to true dynamic and physiological weightlessness. However, test time is limited by aircraft operational restrictions to 20 to 30 seconds making the test one of the part-task variety. The number of parabolas flown per mission varies with mission objectives, but averages approximately 30 parabolas per 3 hours of flight. Because of the high fidelity of weightlessness achieved, the zero-g aircraft is frequently used to verify results of other simulations.

Although true weightlessness is not achieved by water immersion techniques, neutral buoyancy, a simulation of zero-g, is accomplished by the addition of weight to the test subject's torso and extremities in order that the resulting volume will have a density at or near that of water. There are currently two schools of thought on pressurizing suits for water immersion use, water pressurization and air pressurization. There are distinct advantages attributable to both modes of pressurization, but a compilation of these and a comparison of methods is yet to be accomplished. The principal value of this simulation is that extended test time is available which permits the subject to experience a realistic fatigue build-up. In addition mock-up size is not limited by aircraft volume. The facility used for neutral buoyancy zero-g simulation at Wright-Patterson AFB, Ohio, is operated by the 6570th Aerospace Medical Research Laboratory. The dimensions of the pool are 40 ft by 30 ft by 8 ft deep and the water temperature is maintained at 77°F. The test setup is graphically depicted in Fig 4. The pressure suited subject is submersed after adding approximately 80 lbs of lead weight and pressurizing the suit to 2 psi. The pressure of the suit is raised to 3.7 psi when the subject reaches the work area and the ballast is rearranged as necessary by the safety monitors to obtain more nearly perfect balance. Ancillary equipment used includes photographic equipment, underwater floodlighting equipment, communications equipment and scuba gear.

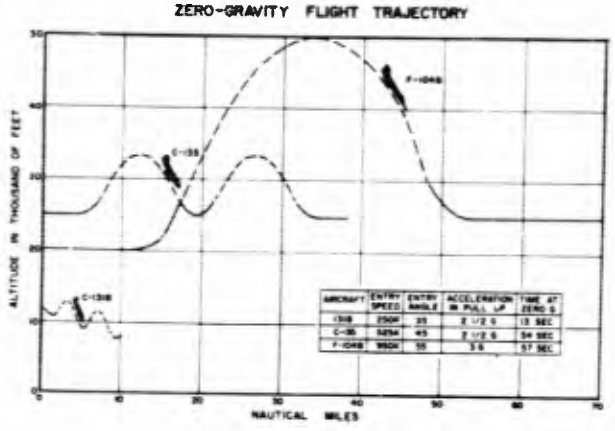

Figure 3

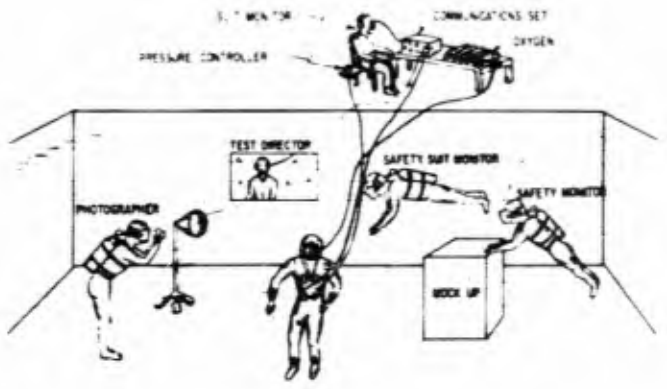

Figure 4

Application of Zero-g Simulation

These techniques for simulating the weightless state were applied directly to the design and procedures determination for the D-021 and D-023 space structures experiments. Because of the constraints imposed by the hardware delivery schedule, the data gained through the simulation effort thus far are largely of the qualitative type, with numerous equipment and procedural changes taking place during the course of a single test. However, it was determined that this type of data did serve as a valuable tool since the simulation effort was primarily applied to minimize operational difficulties involved with the D-021 and D-023 experiments.

The Expandable Airlock Experiment D-021 consists of an expandable airlock module complete with an instrumentation system capable of monitoring all aspects of the experiment. The experiment module is mounted externally between support trusses of the SIVB Spent Stage (Fig 5). The experiment plan consists of several cycles of ingress/egress and pressurization/depressurization. The simulation effort was directed primarily toward solving the problems associated with the ingress/egress operation. Thirteen trials were run in the neutrally buoyant mode utilizing three different sized subjects and three types of pressure suits, (G-2C, G-4C, Navy Mark IV). Three different sized volumetric encumbrances were added to the subject for various trials, a back mounted Astronaut Maneuvering Unit, a chest pack life support system, and a back pack life support system (Figs 6,7,8). In addition, various types of and locations for handholds and restraints were evaluated. Figures 9 and 10 depict the underwater mockup used for ingress/egress tests and indicates the location of handholds and restraint devices. In addition to ingress/egress procedures and time line analysis, an emergency retrieval procedure was developed. This operation involved two pressure suited subjects, one inside the airlock feigning unconsciousness, and the second outside attempting to rescue the "disabled" crew member. (Figs 11 & 12). Several trials were run alternating the "disabled" subjects and varying the original position of the "disabled" crewman, i.e. feet against hatch, head against hatch, etc. Various restraining methods were used to secure the rescuer to the airlock, ranging from knee tether (Fig 13) to no restraint whatever. Given the worst case, the larger subject "disabled" with feet behind the hatch, it was shown that maximum retrieval time (time to clear the D-021 airlock) ran approximately 138 seconds, well within the duration of the emergency oxygen supply.

The zero-g aircraft will also be utilized in the testing of the D-021 experiment, primarily to validate the ingress/egress procedures, the handhold locations and hatch actuation. Two of the subjects involved in the two weightless tests will repeat this performance in the 0-g aircraft. The largest new potential problem to be investigated in the airplane is the effect of the airlock flexibility on ingress/egress operations. The flexible mockup was not used in the underwater tests because the damping characteristics of the water method might reduce the motion induced in the structure due to ingress, and because the sponge-like absorption characteristics of the mockup itself could greatly hamper the refurbishment and maintenance of the mockup.

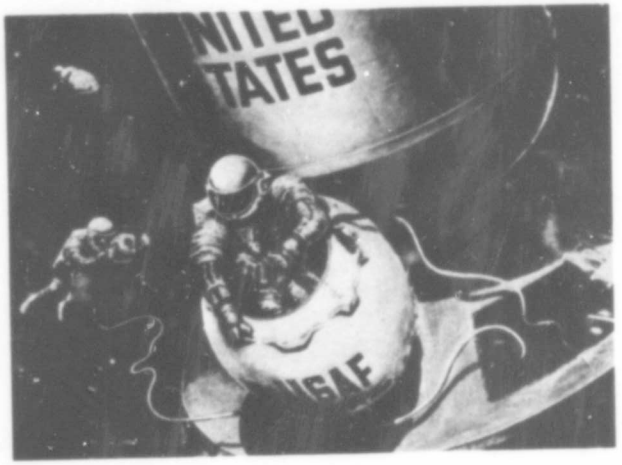

Figure 5

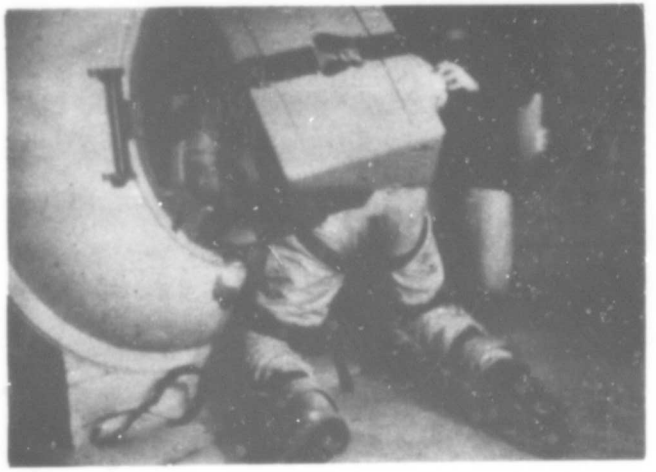

Figure 6

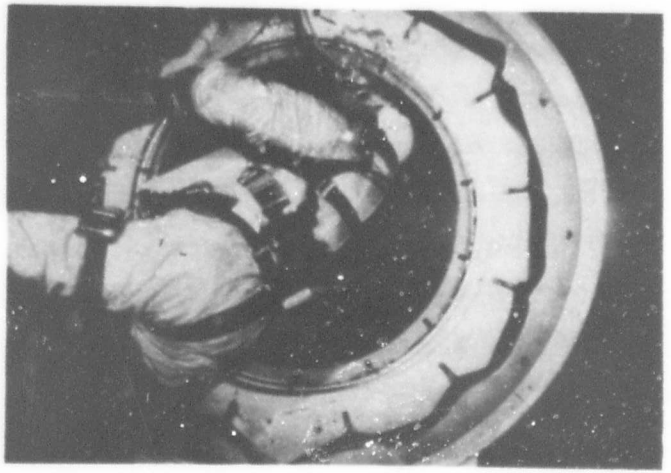

Figure 7

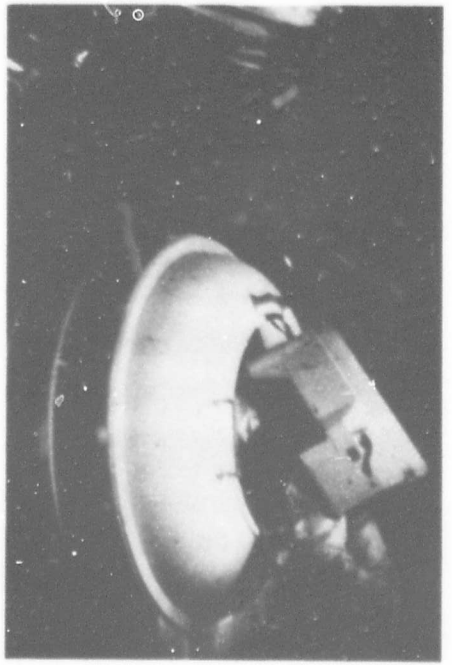

Figure 8

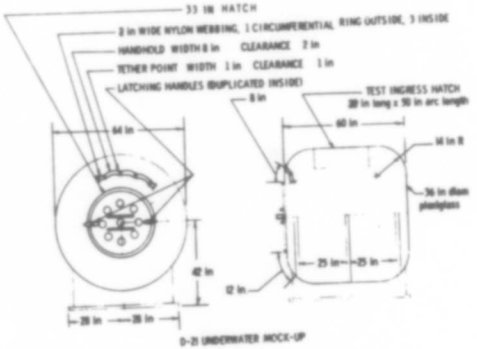

Figure 9

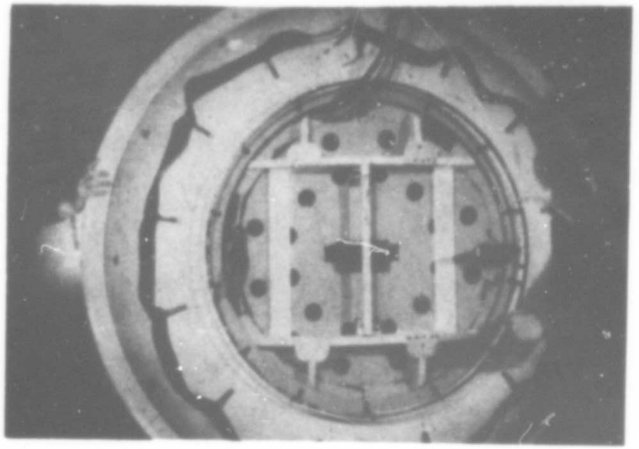

Figure 10

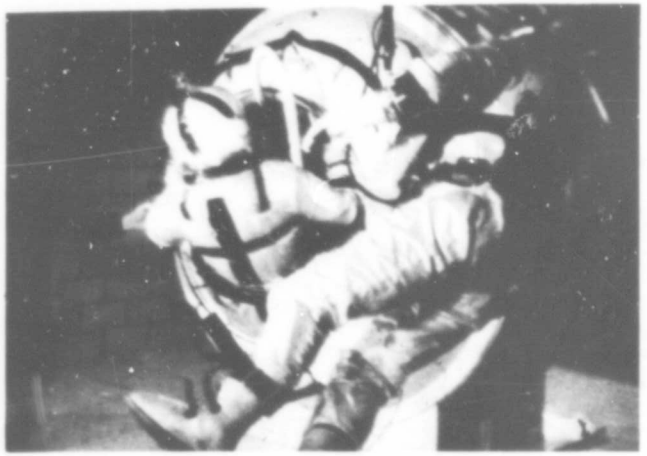

Figure 11

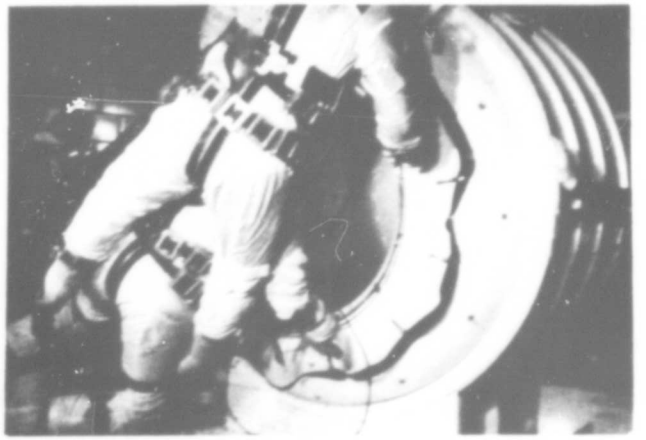

Figure 12

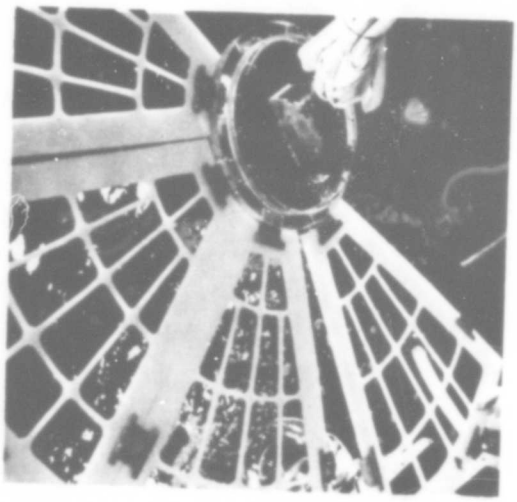

Figure 14

Figure 13

The second experiment simulated consists of a modularly assembled 10 foot diameter parabolic antenna. The experiment is designated D-023 and is planned to be assembled inside the SIVB tank by a crewman in a pressurized suit. The experiment procedure calls for the crewman to retrieve the package from its stowage location, unpackage and set up the major components and proceed with the attachment of panels to the hub until an inner and outer annulus are complete. This procedure is then reversed, until the equipment is once again packaged and stowed. Part task simulation (assembly and disassembly only) has been accomplished by several subjects while neutrally buoyant and wearing pressurized G-2C and G-4C suits (Figs 14, 15, 16). Qualitative and quantitative data accumulated during this simulation resulted in many equipment and procedural changes. The improvements resulting from simulation include: Simpler, more reliable latches, improved foot restraint, less complex hub and boom indexing systems, and a more meaningful assembly procedure. A total task simulation, including package retrieval thro.gh package stowage is planned for underwater simulation in the near future to validate the time line analysis currently representing the experiment. No zero-g aircraft simulation was performed on the D-023 experiment per se, due to the inability of the assembled structure to sustain the 2-g loading encountered in the flight profile.

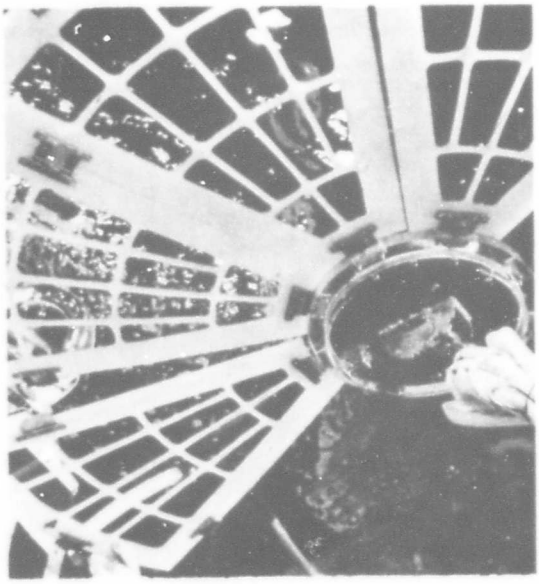

Figure 16

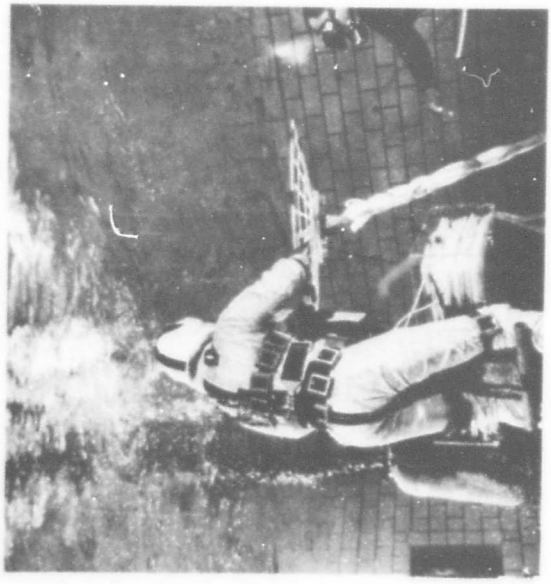

Figure 15

SUMMARY

The simulation effort herein described was planned and executed merely as an engineering development tool. It has provided valuable insight into many potential operational problems. A follow-on series of tests will be conducted to firmly establish procedures and time lines. It is anticipated that equipment and procedures will undergo only minor modifications throughout the remainder of the experiments' lifetime because of the early emphasis on proper design for astronaut compatibility.

If man's capabilities are to be effectively exploited in space operations, proper planning and training are required. This can be done through simulation and testing of the system under consideration with man-in-the-loop. For this reason, subsequent simulation efforts involving D-021 and D-023 will emphasize the optimizing of man's performance, astronaut training and the collecting of pre-flight data.

REFERENCES

1. C.B. May, J.N. Schofield, L.A. Vorst, Air Force-Gemini Space Maintenance Experiment and Simulation. National Conference on Space Maintenance & Extra Vehicular Activities, Orlando, Florida March 1966.

2. Morton, Hunt, et al, Neutral Buoyancy Submersion for the Analysis of Human Performance in Zero-G, AJAA Fourth Manned Space Flight Meeting, St Louis, Mo, October 1965.

3. C.R. Cording, Extra Vehicular Maintenance and Techniques

4. Preliminary Definitive Experiment Plan, Expandable Airlock Experiment D-021, GER 13036, 10 Jan 1967, Goodyear Aerospace Corporation, Akron, Ohio.

5. H.L. Loats, Jr, G.S Mathingly, C.E Brush, A Study of the Performance of an Astronaut During Ingress and Egress Maneuvers Through Airlocks and Passageways, Final Report NAS 1-4059 Phase II, 31 April 1965.

DEVELOPMENT OF SELF-SEALANT TECHNIQUES FOR MICROMETEOROID PROTECTION OF AEROSPACE VEHICLES

S. Schwartz and A. J. Tuckerman*
and
W. F. Anspach**

*
Components and Materials Laboratory, Aerospace Group, Hughes Aircraft Company, Culver City, Calif.
**
Elastomers and Coatings Branch, Air Force Materials Laboratory, Wright Patterson Air Force Base, Ohio

I. INTRODUCTION

The successful utilization of expandable structures in space will require a solution to problems not directly related to design and construction considerations. These are problems created by hazards inherent in the space environment. One is the probability of collision with micrometeoroids. As the flights become longer and actual exploration of the moon becomes a possibility, this hazard increases. The sudden or even slow loss of pressurization could be catastrophic to the spacecraft occupants, to the vehicle itself, or to the occupant of a space suit or structure outside of the vehicle. Expandable structures could not conveniently use the meteoroid bumper concept in their design. Incorporation of a self-sealing mechanism in the vehicle wall will therefore be necessary to reduce the effects of this hazard.

II. IMPACT EFFECTS

A brief discussion of these impact effects would be worth presenting at this time. In almost every self-sealant system studied, some type of high or low viscosity fluid is contained in a small package simulating part of a spacecraft wall. During impact testing, the package is maintained with the vacuum on one surface and either ambient pressure (14.7 psi absolute) or a lower pressure, corresponding to a spacecraft internal pressure of 5 to 7 psi, on the other surface.

On perforation by the simulated micrometeoroid, a number of things happen to the package, depending on its construction and the type of contained sealant. A hole is produced on the impacted face (vacuum side) ranging in size from that equal to the projectile to more than twice its size. The exit face, if fabricated of metal, in many cases, "flowers" out so that a 3/32-inch diameter projectile may produce an exit hole of from 1/2 to 3/4 inch in diameter, or greater. The internal structure of the package may also suffer damage from the shockwave transmitted by the liquid sealant and the materials of construction, particularly if high modulus materials are used. The sealant, depending on its type, also acts in several ways after impact. With a low viscosity fluid, a good deal of material immediately spews out of the entry hole into the vacuum due to the pressure differential, the shockwave pressure and its own vapor pressure. At the same time, however, a portion of the fluid is also forced into the pressurized "cabin" area, partly by the projectile, partly by particles from the impacted front surface, and partly by the accompanying shockwave. With a very high viscosity fluid, these effects are attenuated; however, if an immediate seal results, then continued "cabin" pressure eventually pushes the fluid through the entry hole, unless the sealant at the same time hardens.

The design of the packaging then has to be one which will result in minimum damage from the shockwave, and also allow minimum loss of fluid after impact. At the same time, the package must permit flow of the fluids to the entry hole, while restricting flow to the exit hole. The package also has to be compatible with conventional methods of spacecraft fabrication, such as bonded honeycomb and skin construction and/or skin and stringer construction.

III. PACKAGE DESIGN

The type of package shown in Fig. 1 was initially developed to meet most of the above requirements when used with honeycomb construction and two-component chemical sealants. In this package, the honeycomb section acts as a baffle or sump to minimize loss of liquids into the vacuum while the reaction is proceeding. The chemical reactants are contained in the spacers and the rubber sheet on the exit face acts as a hole size controller to minimize loss of the liquid reactants into the "cabin" section. A number of variations of this basic construction were made during the program. Figure 2 shows one variation using an epoxy-fiberglass entry face.

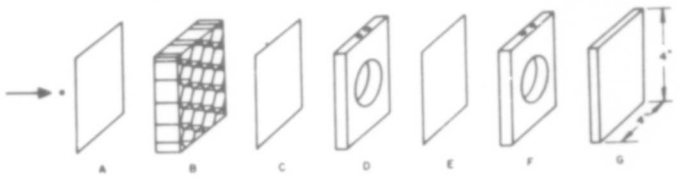

A. 0.020-inch thick 302 CRES face sheet

B. 0.500-inch thick nylon-phenolic, 0.188-inch cell size

C. Same as A

D. 0.188-inch thick aluminum reactant spacer, 3-inch diameter centrally located hole

E. 0.0015-inch thick aluminum foil

F. Same as D

G. 0.188-inch thick neoprene rubber sponge

The entire package is bonded together with 3 M Co. AF-110 adhesive.

Figure 1. Standard three compartment chemical self-sealant package.

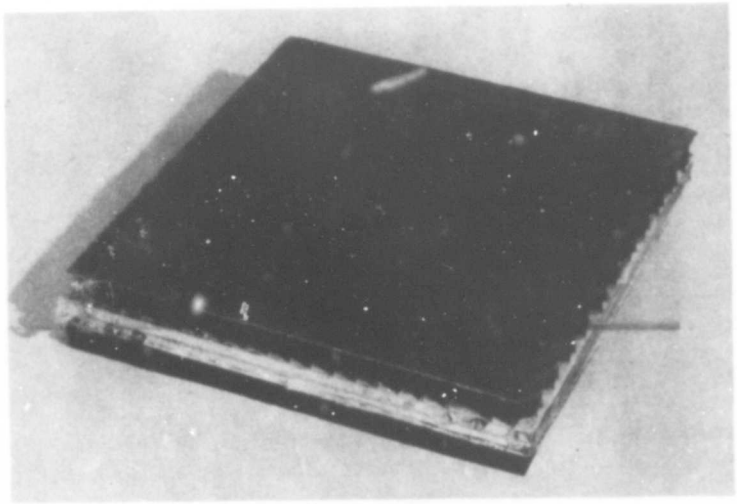

Figure 2. Appearance of three compartment chemical package.

Figure 3 illustrates seal formation in this type of construction and also shows the "flowering" on the exit side of the package when the rubber hole size controller is omitted. Later in the program, a single compartment package was developed which was more applicable to skin and stringer construction. This package was simply an elastomeric container filled with a one-component sealant, held between the wall surfaces. In most cases, both types of packages were made from four to six inches square for ease of handling and for use with the impact test apparatus.

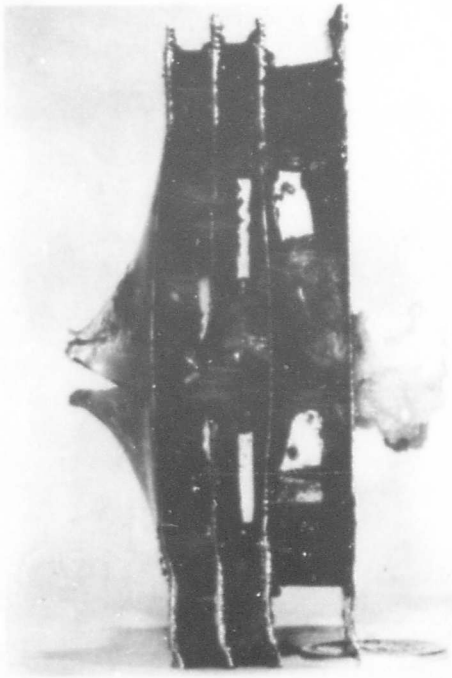

Figure 3. Cross section of an impacted three compartment package showing sealant distribution.

IV. TEST METHODS

An important consideration at the beginning of the program was to establish a satisfactory test method. Initially, a simple, manually operated vacuum perforator was used to test the packages under differential pressure conditions. Evaluation of sealant systems with this device was not adequate since impact shocks and pressure wave characteristics were not present.

The second test method, developed and eventually used for the majority of the tests, used a dynamic particle accelerator shown in Fig. 4. In this apparatus, a 1/8-inch diameter spherical brass or steel projectile is fired through a distance of 8-1/2 feet in a vacuum of approximately 100 microns. The projectile is propelled by an 18 grain charge of #4227 DuPont rifle powder contained in a Remington #222 cartridge case and impacts the target at velocities of from 5500 to 7000 ft./sec. The test apparatus also contains electronic velocity measuring equipment to indicate or record the speed of every shot.

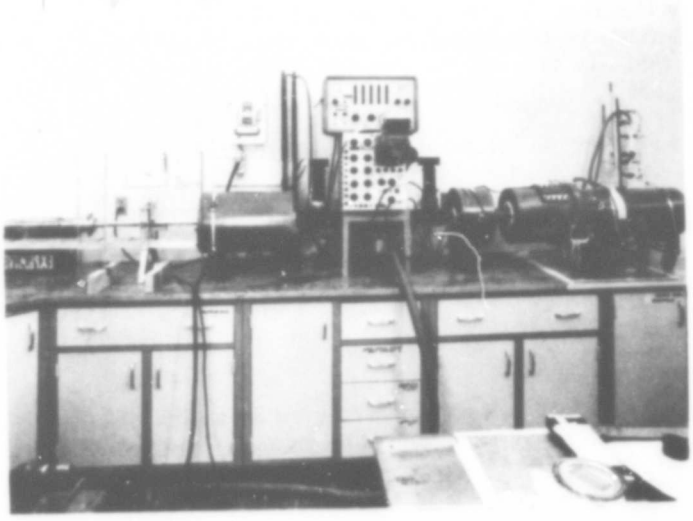

Figure 4. Dynamic particle accelerator used for high velocity impact evaluations

The sample package is mounted at the far end of the vacuum chamber and acts as a seal for a two-inch diameter hole in the chamber. Surrounding the package, and also sealed to the wall of the vacuum chamber, is a second chamber which acts as a particle backstop and also makes it possible to determine the leakage rate through the impacted specimen quantitatively, by means of the flow meter and manometer shown in Figure 5. Constructed in the front and back chambers are viewports and lights to allow visual observation of impacts and seal formation.

Figure 5. Leakage rate equipment for dynamic particle acceleration

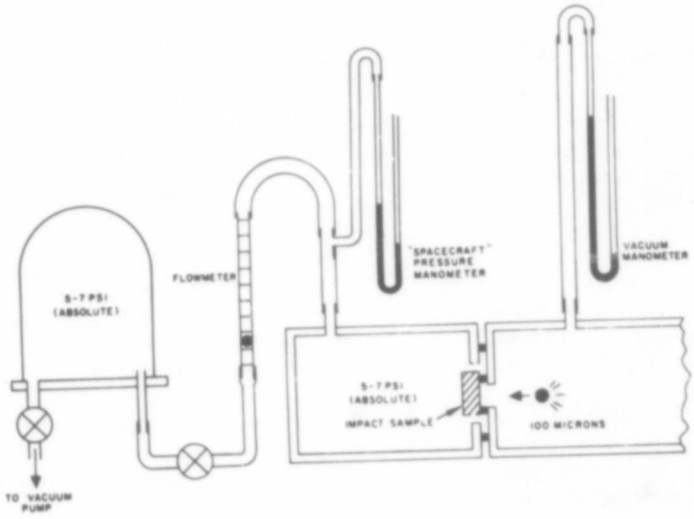

To test a package, the front chamber is evacuated and the rear chamber is kept at room pressure, adjusted to 5 or 7 psi absolute, or as desired. After perforation of the sample, the dynamic leakage characteristics of the seal are determined by the rate of air flow shown by the flow meter and by the drop in pressure shown by the "spacecraft" manometer. The chamber is continuously pumped to assure maintenance of the initial differential pressure.

The initial package and sealant developments were all made using the above equipment. The shockwave effects and initial damage are probably not as severe at these speeds (5000 - 7000 fps) as at light gas gun velocities of 19, 000 to 25, 000 fps, or micrometeoroid velocities of 32, 000 to 200, 000 fps. Nevertheless, the sudden perforations and the differential pressures were present so that a good comparison could be made between various self-sealant systems. After initial tests had established the superiority of particular systems, tests were also made using a light gas gun to obtain impact velocities of 19, 000 to 25, 000 fps.

The light gas gun facilities used were at NASA/Ames Research Laboratories, Moffett Field, California, and at the Utah Research Corporation, Salt Lake City. At Ames, tests were made using 1/8-inch pellets at approximately 20, 000 fps and with differential pressures of 14.7 psi. At Utah Research Corporation, the tests utilized 1/32, 1/16, 3/32, and 1/8 inch projectiles at velocities from 19, 000 to 22, 000 fps with differential pressures of normal ambient pressure and 5 psi.

V. SEALANT PACKAGE DEVELOPMENT

These broad classes of sealant systems were investigated. These included: (1) materials which formed a seal by mechanical or other physical means; (2) those which formed seals through chemical reaction initiated by penetration of two reactant packages; and (3) those which used a combination of physical-chemical and mechanical techniques, such as hardening by solvent loss and the use of mechanical plugging devices.

Mechanical Self-Sealant Systems:

Since mechanical systems appeared to be very simple and inherently reliable, a number of such systems were tested. One of these utilized a one-inch thick, one-inch cell size honeycomb bonded to aluminum skins. Each cell contained three sealed, partially inflated rubber balloons approximately 1/2-inch in diameter. On impact, it was expected that the sudden external pressure drop would cause the balloons to expand, thus plugging the newly formed hole. Even if the balloons were perforated, the rush of air would cause the light rubber to effect a partial seal. Some success was achieved with this method; however, since it did not result in completely satisfactory seals and the reliability was not high, further investigation was discontinued.

The expanding balloon system was also combined with a chemical reactant package. Fair seals were also obtained with this technique, but since the resultant package was quite cumbersome and the results were no better, investigation of this technique was also dropped.

Another type of mechanical seal utilized Dow Corning's Sylgard 51, a one-component, self-sealing gel normally used for dielectric purposes. A one-half inch thick compartment with .010 stainless steel faces was filled with gel and cured. The package sealed instantaneously when a projectile was fired through it, but with continued exposure to the differential pressure, the gel flowed through the hole and the seal was lost. Reinforcement of the gel with such materials as asbestos fibers, polyethylene and Teflon cubes caused loss of the sealing qualities.

The last type of mechanical seal studied was one in which compressively prestressed polyisoprene rubber was used as the sealant material. Several seals were obtained with rubber plugs of .15 to .25-inch thickness; however, these seals were obtained only at velocities of approximately 5000 fps. At velocities of 6500 fps and higher, the projectile apparently did not simply slice through the rubber so that no seal could result.

Chemically Reactive Sealants:

A highly promising concept consisted of chemically self-sealing the perforated wall. In this technique, two packages of rapid-reacting chemical components contained within a multi-compartmented wall are perforated by the projectile. On contact the reactants cure to form an impermeable, resinous mass with sufficient strength, creep resistance and wall adhesion to withstand the one atmosphere pressure differential across its surfaces.* In order to form a good seal, the reaction speed must be such that the sealant mass is formed before total expulsion of the reactants and/or drastic reduction of cabin pressure occurs. Furthermore, when utilizing a multiple walled construction, correct stoichiometric proportions and good mixing would be extremely unlikely on impact. Therefore, the reaction must be one which forms a good sealant mass over wide ranges of proportions and with minimum mixing. In addition to the requirements of fast reaction and high degrees of polymerization, it is also necessary that the reactants be capable of long term storage and subsequent polymerization at temperatures of from $0^{\circ}F$ to at least $120^{\circ}F$. With these criteria in mind, a number of reactive systems were screened to determine their suitability for further evaluation. Simple open cup reactions were made using approximately 1:1 proportions (since stoichiometric mixing would not occur during impact perforations).

One of the first of the two-component systems tested was a series of polyurethane reactants. Several isocyanate prepolymers, both commercial and special Hughes Aircraft Company preparations, were reacted with various amines and commercial polyols. Similar reactions were made utilizing sebacyl chloride and several amine curing agents. A third series of tests was made with a number of epoxy resins and various curing agents. A number of miscellaneous reactions were also tested, but in no case were the results encouraging enough to warrant more extensive evaluations. A summary of the systems tested and the results are shown in Table 1.

*In the early work, a differential pressure of one atmosphere was used exclusively.

Table 1. Two-Component Reactive Systems

Reactants	Sources	Results
Polyurethane Reactions:		
P1010 Isocyanate Prepolymer and Triethylenetetramine	Wyandotte Chemical Corp.	Fast reaction and good elastomeric mass
Pe450 Isocyanate Prepolymer and Triethylenetetramine	Wyandotte Chemical Corp.	Fast reaction, polymer unstable in air
Adiprene L-315 Isocyanate Prepolymer and Triethylenetetramine	DuPont Company	Fast reaction and good elastomeric mass
Nacconate 80 (toluene diisocyanate) and Quadrol [N, N, N', N'-Tetrakis(2-hydroxypropyl) ethylenediamine]		
Mondur MR-Isocyanate Prepolymer and Triethylenetetramine	Mobay Chemical Company	Relatively slow reaction
CPR X8-49-A-Comp R - Isocyanate; CPR X8-49A-Comp T - Polyol	CPR International Corp.	Fast reaction, weak foam formed
CPR X8-49B-Comp R CPR X8-49B-Comp T	CPR International Corp.	Fast reaction, weak foam formed
CPR X8-49C-Comp R CPR X8-49C-Comp T	CPR International Corp.	Fast reaction, weak foam formed
P1010 Isocyanate; Prepolymer CPR X8-49B Polyol	Wyandotte Chemical Corp. CPR International Corp.	Fast reaction forming good elastomeric mass
Adiprene L-167 Isocyanate Prepolymer; CN-X121 Ethylenediamine molecular sieves	DuPont Co. Linde Co., Division of Union Carbide	Slow reaction, frothing under vacuum
Diethylene Glycol-Isocyanate Prepolymer and Triethylenetetramine	-	Prepolymer too viscous for fast reaction
Triethylene Glycol-Isocyanate Prepolymer and Triethylenetetramine	-	Prepolymer too viscous for fast reaction

Polyurethane Reactions (Cont'd.)		
Tetraethylene Glycol-Isocyanate Prepolymer and 20% Dioxane and Diethylenetriamine	-	Fast reaction forming good elastomeric mass
Polyamide Reactions:		
Sebacyl Chloride Triethylenetetramine	-	Fast reaction, good product, some fuming
Sebacyl Chloride Ethylenediamine	-	Very fast reaction and high exotherm, destroys product
Sebacyl Chloride-90% Triethylenetetramine-10% Ethylenediamine	-	Fast reaction, good product, fumes
Epoxy Reactions:		
Epoxides 201 and 206 (peracid diepoxides); Boron Trifluorides (ether, phenol and dihydrate complexes)	Union Carbide Company	Fast reaction, extremely volatile catalysts
Epoxylite 204, Comp A Epoxylite 204, Comp B	Epoxylite Corp. (Proprietary Systems)	Relatively slow reaction
Epoxide 201 Epoxylite 204, Comp B	Union Carbide Co. Epoxylite Corp.	Fast reaction after short induction period, good product
Epoxide 206 Epoxylite 204, Comp B	Union Carbide Co. Epoxylite Corp.	Fast reaction highly exothermic, weak product
Various combinations of Epoxides 201, 206, and Epoxol 9-5 with Oxiron 2000 Boroester 8, Epoxylite 204, Comp B and Methyl Metaborate	Swift and Company, FMC, U. S. Borax Research Corp.	All combinations had a 15 to 30 second induction period followed by highly exothermic reaction. Products ranged from friable to tough and hard.
Miscellaneous Reactions:		
Arylamide-N, N-methylene-bisacrylamide; ammonium persulfate	American Cyanamide	Slow reaction

Miscellaneous Reactions (Cont'd.)

Butyl Cyanosorbate Tetramethyl Guanidine Triethylenetetramine, Tetramethylammonium-hydroxide	-	Fast reaction, high exotherm, but resin too thermoplastic
Silicone Resin Q-9-0063 Catalyst XY-141	Dow Corning Company	Slow reaction
Sulfur Monochloride Castor Oil	-	Fast reaction after short induction period, noxious fumes, spongy product
Terephthalyl Chloride Triethylenetetramine, Ethylenediamine, Triethylamine	-	Poor polymerization

As a result of the preliminary open cup evaluations, it was decided to study in more detail the urethane system utilizing Adiprene L-315 and triethylenetetramine and the polyamide system utilizing sebacyl chloride and a mixture of amines. In both cases, the "standard" package, shown in Fig. 1, was used as the carrier for the sealants. A number of variations of the "standard" package were also made, mainly in order to obtain better shockwave resistance.

A large number of tests at high velocities of 6000 - 7000 fps and a few at hypervelocities of 20, 000 - 22, 000 fps were made with varying proportions of both types of sealants in variations of the "standard" honeycomb package. The results of these tests are summarized as follows:

1. Very reliable, instantaneous seals are obtainable with two-component packages utilizing either the urethane or the polyamide system.

2. The urethane system is preferred since the polyamide reaction liberates toxic hydrogen chloride fumes.

3. Long term storage tests of the reactants kept in hermetically sealed aluminum containers indicate that satisfactory seals can be obtained after at least two years storage at room temperature.

4. To assure reliable formation of seals, it is necessary that the package have a baffle or sump compartment ahead of the reactants to prevent spewing into the vacuum, and a foam rubber hole size control sheet on the rear part of the package. The minimum weight of such an assembly is approximately 8 gm/in^2 or 2.5 lb/ft^2. Furthermore, for minimun shockwave damage, the package should be made using as many low modulus materials as possible.

This is particularly important for the honeycomb material, which stood up much better when made of phenolic-glass than when made of aluminum foil. Reactant containers for long term storage, however, have to be of aluminum foil rather than flexible organic packaging materials such as polyethylene or Aclar because of the small amount of moisture vapor transmission by the organics.

Physical-Chemical-Mechanical Sealants:

The success of the two-component self-sealant materials indicated that the chemical concept of sealing was definitely feasible. However, the high weight and relative complexity of the package and the somewhat noxious fumes, derived even from the polyurethane reactants, pointed out the need for improvements.

In order to eliminate the fume effect of the urethane reactants, tests were made with an entirely new system; one which would minimize the fumes, and hopefully, result in a simpler package. Since after perforation of the package the sealant was exposed to the vacuum and the differential pressure, it was decided to use these phenomena, if possible, to help effect a seal rather than regard them as detriments. (In the two-component chemical systems discussed previously, only the differential pressure was used to facilitate mixing.) Therefore, tests were run initially with high solid content solutions of fast drying materials such as nitrocellulose in acetone. When packages containing a fairly high viscosity solution of nitrocellulose were perforated, the material would spew from the entry hole as before; however, in the vacuum, the materials simply dried to form a seal, or partial seal, about the hole, rather than utilizing a chemical reaction to form the sealant.

With this initial success of a one-part sealant, tests were then made of similar materials using water as the liquid phase. The use of water as the liquid medium virtually eliminates all possibility of noxious fumes. Studies were made of a number of water-resin emulsion systems which rapidly coagulate or dry to a firm sealant. For some materials, tests were conducted with and without a coagulating agent. The materials initially screened, and the results, are given in Table 2.

Table 2. Single-Component Water-Resin Emulsions

Material	Source	Results
Polyvinyl Alcohol (Elvanol)	DuPont Company	30% solution dried too slowly
Polyvinyl Acetate Emulsion	Reichhold Chemicals, Inc.	Dried well when exposed to a vacuum
Polyvinyl Acetate Emulsion	Swift and Company	Dried very fast in vacuum, held up well
Vultex, Natural Rubber Latex (alone and with $Ca(NO_3)_2$ Coagulant)	General Latex and Chemical Company	Dried well, mass had poor adhesion however

Piccopale A-1 Hydrocarbon Emulsion (with acid coagulant)	Pennsylvania Industrial Chemical Company	Requires strong acid coagulant, mass was crumbly
Neoprene Latex #650 and coagulant	U. S. Rubber Company	Coagulates well, but initial viscosity was too high
SBR Latex #LX3118 and coagulant	U. S. Rubber Company	Fair coagulation, product too soft
Hycar #2671 and #1552 and coagulant	B. F. Goodrich Company	Fair reaction, product soft and weak
SBR #305 and #460 and coagulant	Dow Chemical Company	Viscosity initially too low; solids content too low
Polyvinyl chloride, Pliovic #400	Goodyear Rubber Company	Poor coagulation and slow drying
Isoprene #700 and coagulant	Shell Chemical Company	Fair reaction, product somewhat soft

From the various liquid materials, it was determined that the polyvinyl acetate emulsion and the natural rubber latex gave what appeared to be the best products after impact and exposure to the vacuum. Both of these materials could be used alone, or, in the case of the natural rubber latex, with 20% by weight of a 30% calcium nitrate solution to act as a rapid coagulant. When used alone, either material would require only a single compartment in the package, thus resulting in package simplification. When this system was impacted, however, both materials still tended to spew into the vacuum copiously and to a somewhat smaller extent backwards into the cabin section. This meant that the package would require either an empty sump compartment on the vacuum side, or that some method would have to be devised to inhibit the forward surge of material on impact.

In an effort to minimize the loss of liquid materials into the vacuum, various light-weight fillers were added to the sealant. The fillers included 6 - 20 mesh ground cork particles, expanded styrene beads, phenolic microballoons, ground urethane foams and a thixotropic agent, pyrolyzed silica (Cab-o-Sil). It was hoped that these fillers would act as tiny mechanical "plugs", dragged or pushed toward the hole by the initial rush of fluid and escaping air. In this respect, the filler materials worked exactly as planned and considerably increased the reliability of the resulting seals. The use of the light-weight fillers also decreased the density of the composite sealant to a large extent. This was regarded as desirable, since the relatively heavy liquid sealant could be cut down in the total quantity used per square inch. The expanded styrene beads, ranging in size from approximately 1/32 inch to 1/8 inch in diameter, and with a density of approximately 2 lb/ft^3, appeared to be the best from the standpoint of light weight and general applicability. Figure 6 illustrates schematically the package behavior before addition of the "plugs" and after addition of the "plugs".

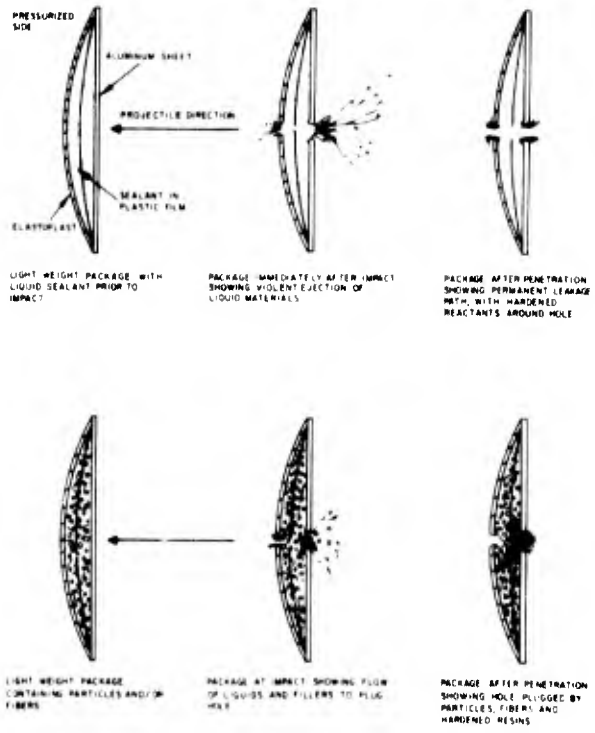

Figure 6. Effect of Filler addition on package behavior of light-weight system.

Although the addition of the light-weight fillers helped considerably in assuring a seal around the entry hole, a hole size controlling agent was still required to prevent excessive loss at the exit hole. A number of tests were made using packages with various low modulus materials. These included multiwall polyethylene bags, back-up pads of rubber, foam, Elastoplast (an elastic bandage material) and thin (.006 inch) natural rubber sheet. The thin natural rubber showed the least damage from the perforation and had the additional advantage of adding the least weight.

After discovering the efficacy of the thin rubber sheet, it seemed advantageous to make the entire sealant container out of an elastomer. This elastomeric container, filled with sealant, could then be inserted between the metal spacecraft walls. Natural rubber toy balloons were found to work very well for this purpose. With the use of the balloon as a complete container, another advantage was found in that in many cases the balloon acted to seal or partially seal the entry hole, as well as the exit hole.

The final self-sealant package then consists of two or more concentric balloons filled with the polyvinyl acetate-emulsion and the styrene beads in the correct proportions. (The natural rubber latex will seal as well, but has poorer storage qualities.) It was also found that causing the package to be under slight compression when in the elastomeric container helped to increase reliability. Tests were made with varying thicknesses of packages to determine the minimum size which gave good reliability. Figure 7 shows packages of 3/4, 1/2, 3/8 and 1/4-inch thickness, and also shows the use of metal film cans to contain the packages and simulate a spacecraft wall. Figure 8 shows a cross section of a metal film can-elastomeric package after impact.

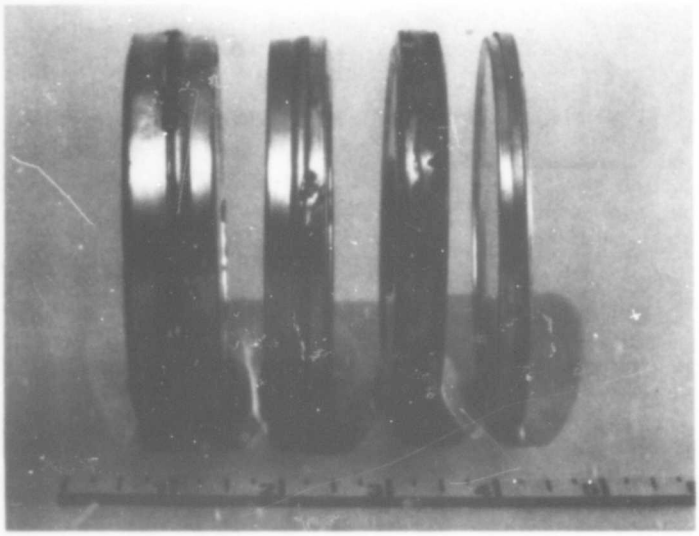

Figure 7. Varying thickness packages

Figure 8. Cross section of a metal film can-elastomeric package

VI. IMPACT TEST RESULTS

During the course of the investigation, a great many shots were fired at many types of sealants contained in several package configurations. Therefore, a simple comparison of the number of shots versus the number of perfect seals is meaningless since many of the tests were with new, untried sealant systems. However, with standardization of the double component and the single component systems, it was then possible to establish some kind of a reliability figure for each system. Table 3 summarizes the performance for each type of sealant when impacted with 1/8-inch projectiles at a velocity of 5500 to 7000 fps.

Table 3. Sealant Reliability

Sealant Type	Perfect Seals	Seals with Leakages	
		0 to 1000cc/min	>1000cc/min
Two-Component System	65%	10%	25%
Single Component	80%	10%	10%

Tests were also run at hypervelocities of 20, 000 - 22, 000 fps using light gas gun facilities. Because of the considerably greater cost of these shots, only a few were made. The tests indicated that the probability of forming perfect seals or seals with low leakage is somewhat less than at the lower velocities, but still about 60%. This probably would be higher with increased testing.

In a final test of the single-component system, a demonstration was held at Wright-Patterson Air Force Base. In this test, a special 2 ft. sq. structure with four separate 1 ft. sq. compartments was placed in a space chamber. Each test compartment was internally pressurized to 5 psia, while the external chamber pressures ranged from 5 to 2 x 10^{-6} Torr during the various shots. Figure 9 shows the appearance of the demonstration structure. Figure 10 shows a typical distribution of the balloon packages inside the test specimen.

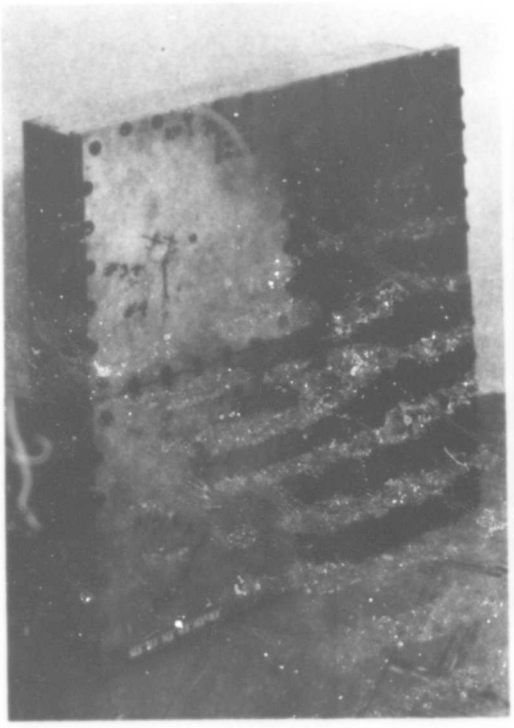

Figure 9. Structures used for demonstration at WPAFB

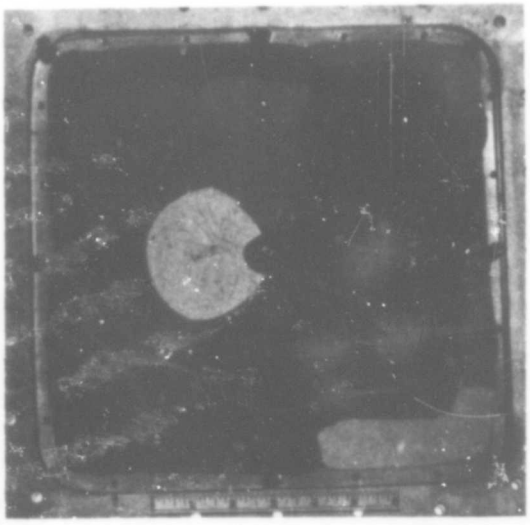

Figure 10. Typical distribution of balloon packages in large impact specimen.

Several shots were fired into each compartment, using 1/8-inch diameter projectiles accelerated to 6000 to 7000 fps. Three chambers received two shots each, one received three, and one received one shot. (Five test panels were used for the tests.) The results of the impact tests are shown in Table 4.

Table 4. Impact Test Results of Demonstration Structure

Panel No.	Shot No.	External Pressure, Torr	Leakage lb/hr	Remarks
1	1	5	0	Instantaneous seal
1	2	5	0	Instantaneous seal
1	3	2	.165	Impact was near edge
2	4	5	0	Instantaneous seal
2	5	1	0	Instantaneous seal
3	6	1	0	Two holes found from projectile and wax shell plug
3	7	1	.025	
4	8	4.7×10^{-2}	.025	
4	9	4.7×10^{-2}	0	Instantaneous seal
5	10	2×10^{-6}	0	Instantaneous seal

These tests then clearly demonstrated the applicability of the system for use with a typical spacecraft structure.

VII. SUMMARY AND CONCLUSIONS

The single component self-sealant system appears to be the simplest and most practical system to minimize the loss of pressure in a spacecraft due to micrometeoroid penetration. Although the sealant system was developed primarily for space vehicles, it appears also to have promise for spacesuits, expandable structures such as lunar shelters, escape capsules, etc., based on preliminary tests conducted with fabric materials. The use of this system, with some additional applications development work, could prove to be a potent life-saving device. The characteristics of the system are summarized below:

1. Weight of sealant package itself - ranging from 1 to 1.6 lb/ft^2.
2. Thickness - 3/8 inch currently appears to be the minimum thickness which can be used with good reliability.
3. Simplicity - the packages can be easily made and are readily adapted to conventional double wall skin and stringer construction.
4. High reliability
5. Attenuation of shockwave effects - due to use of a large discontinuous phase which absorbs the impact energy.

6. Good storage life - if packaged in a low moisture vapor transmission rate material.

7. Good sealability at 14.7 psi absolute.

8. Sealability under multiple impacts within a small area.

ACKNOWLEDGMENTS

The authors wish to express their appreciation to the Air Force Materials Laboratory at Wright-Patterson Air Force Base, Ohio, and to Hughes Aircraft Company for permission to publish this paper. They also wish to acknowledge with thinks the technical assistance and advice of Mr. P. C. Crepeau and Dr. S. Wiener.

REFERENCES

1. Cosby, W. A. and Lyle, R. G., "The Meteoroid Environment and Its Effects on Materials and Equipment", NASA publication, NASA SP-78, 1965.

2. Gros, C. G., "Meteoroids as a Possible Hazard to Space Vehicle Operations", Lockheed Missiles and Space Company, Report No. SB-63-1, May 1963.

ILLUSTRATIONS AND TABLES

Figures

Tables

BLANK PAGE

UNFURLABLE ANTENNAS

A. J. Wendt and L. D. Surber

1.0 INFLATABLE CIGAR ANTENNA

1.1 THEORY OF OPERATION

The cigar antenna is basically a surface wave structure which uses circular disk elements to control the phase velocity of the radiated wave. In this respect, it closely resembles the Yagi-Uda antenna. Figure 1 shows a deployed model of the inflatable cigar antenna mounted in a test fixture. In Figure 2, this same antenna is shown in its stowed configuration.

One driven element at one end of the cigar antenna acts as the source for all the remaining elements. A TE_{11} mode is generated on the structure. Some of the energy from the driven element is radiated, but for the most part, it propagates down the axis of the antenna, inducing currents in each element as it impinges upon it. The induced currents cause these elements to become secondary sources of radiation. These in turn cause more energy to be radiated, and at the same time, act as an additional source for all remaining elements down the axis of the antenna. Thus, each element is fed by energy from the driven element plus each preceeding element. As the energy propagates down the length of the antenna, the current induced on each parasitic element is progressively less. This provides a tapering effect, which reduces the amplitude of the minor lobes at the expense of increasing the width of the principle beam.

Simon and Weill[1] describe the cigar antenna as a transmission line having local discontinuities found upon it in the form of metal disks. These discontinuities cause the line to radiate and also act as an artificial dielectric. Thus the relative phase velocity along the transmission line can be varied by changing the dielectric constant along the line.

1.2 ELECTRICAL CHARACTERISTICS

1.2.1 Feed Structure

The feed system consists of two orthogonal, triangular, dipole elements etched onto a dielectric substrate, located a 1/4-wave length in front of a reflector disk. The dipoles are fed by a hybrid mounted behind the reflector.

The triangular dipoles have a broad impedance bandwidth, thus, this is not considered the criterion for the antenna operating bandwidth. Rather, it is the frequency range over which the hybrid will function properly, along with the minor lobe level that determines the bandwidth of the antenna. As will be shown later, the operating bandwidth of this particular antenna is 1.68:1, based on the minor lobe level.

G. T. Schjeldahl Company

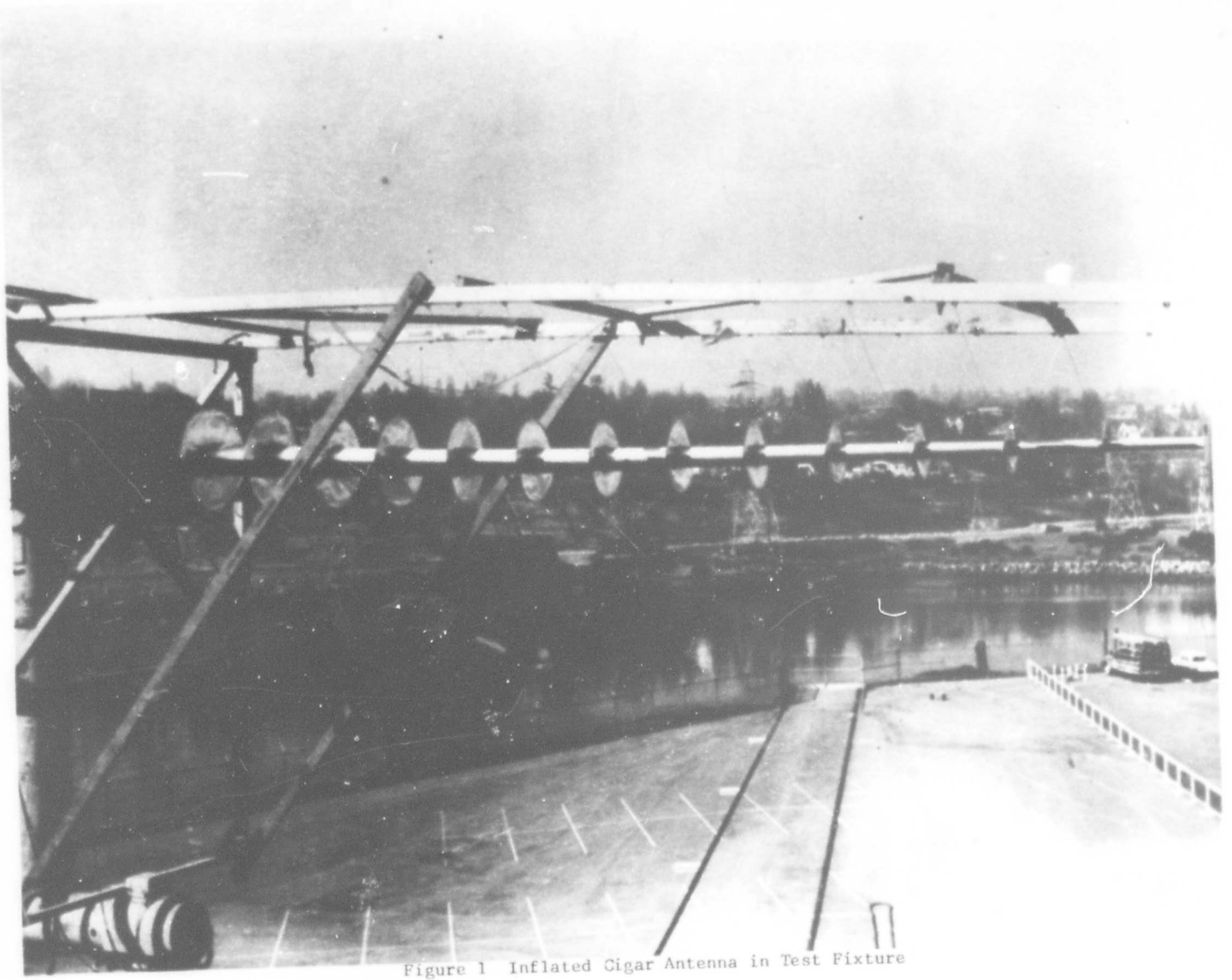

Figure 1 Inflated Cigar Antenna in Test Fixture

Cigar Antenna Model in Stowed Configuration

Figure 2

For narrow band applications, two sets of orthogonal dipoles can be used to excite the disk elements.[2]

1.2.2 Control of Relative Phase Velocity

Proper phase distribution along the axis of the cigar antenna is achieved by varying two parameters: first, the diameter of the disk directors, and second, the spacing of these directors.

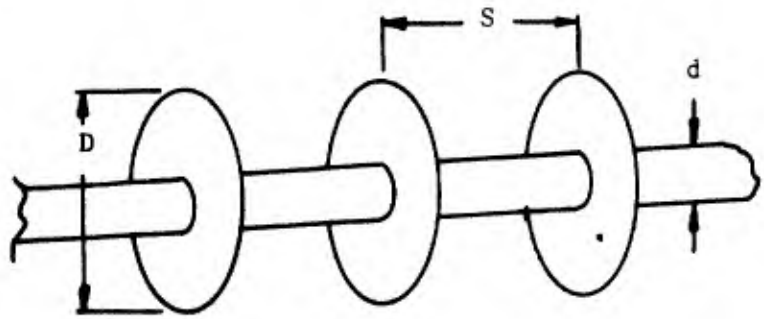

The effect of the mast is accounted for by subtracting its diameter from the disk diameter. Thus, $D-d/\lambda$ and S/λ are the two variables used to control the pattern of the cigar antenna.

If $D-d/\lambda$ is small, less than 0.2, the phase velocity is little effected by a change in S/λ. However, for $D-d/\lambda < 0.2$, quite a variation in the phase velocity can be achieved. At S/λ = 1/4-wavelength, the change in phase velocity is at a minimum. For convenience, the disks are usually spaced so that $\lambda/4 < S/\lambda < \lambda/3$. This provides a maximum amount of phase adjustment with a minimum number of elements.

1.2.3 Radiation Pattern Measurements

Since the antenna was incapable of supporting itself in a horizontal attitude in a 1-g environment, it was necessary to build a wooden test fixture to support it when electrical measurements were performed. The antenna was properly deployed by maintaining a constant internal pressure of 0.7 psi in the antenna boom. The antenna mounted in the test fixture on the antenna range is shown in Figure 1.

The cigar antenna was elevated 42 feet above the ground and was illuminated by a circularly polarized helix antenna located at the same level. Radiation patterns were measured by rotating the cigar antenna 360 degrees in azimuth, and automatically plotting the energy received from the helix.

Radiation pattern measurements were made from 134 MHz to 225 MHz. At frequencies below this band, the beamwidth became very broad and the gain was reduced considerably. Typical patterns are shown in Figures 3 through 6. At the upper frequency limit, something resembling a coma lobe appears. Since the antenna design is circularly symmetric, it appears that the only cause of the coma lobe in the model was a slight bend in the mast located approximately six feet from the tip. Since this bend can readily be rectified by fabricating the tube over a mandrel, it is expected that the coma lobe can be eliminated in any future models.

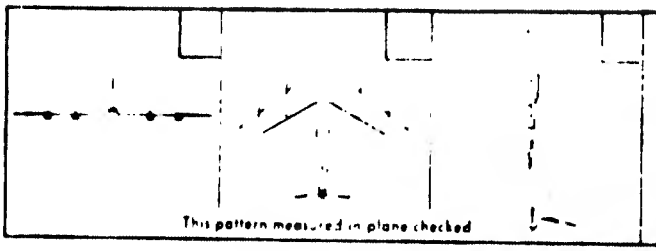

FILE NO. SHEET OF

PLANE TYPE MODEL SCALE

ANTENNA TYPE

ANTENNA LOCATION

FREQUENCY FULL SCALE MODEL 134mc

MODEL SURFACE

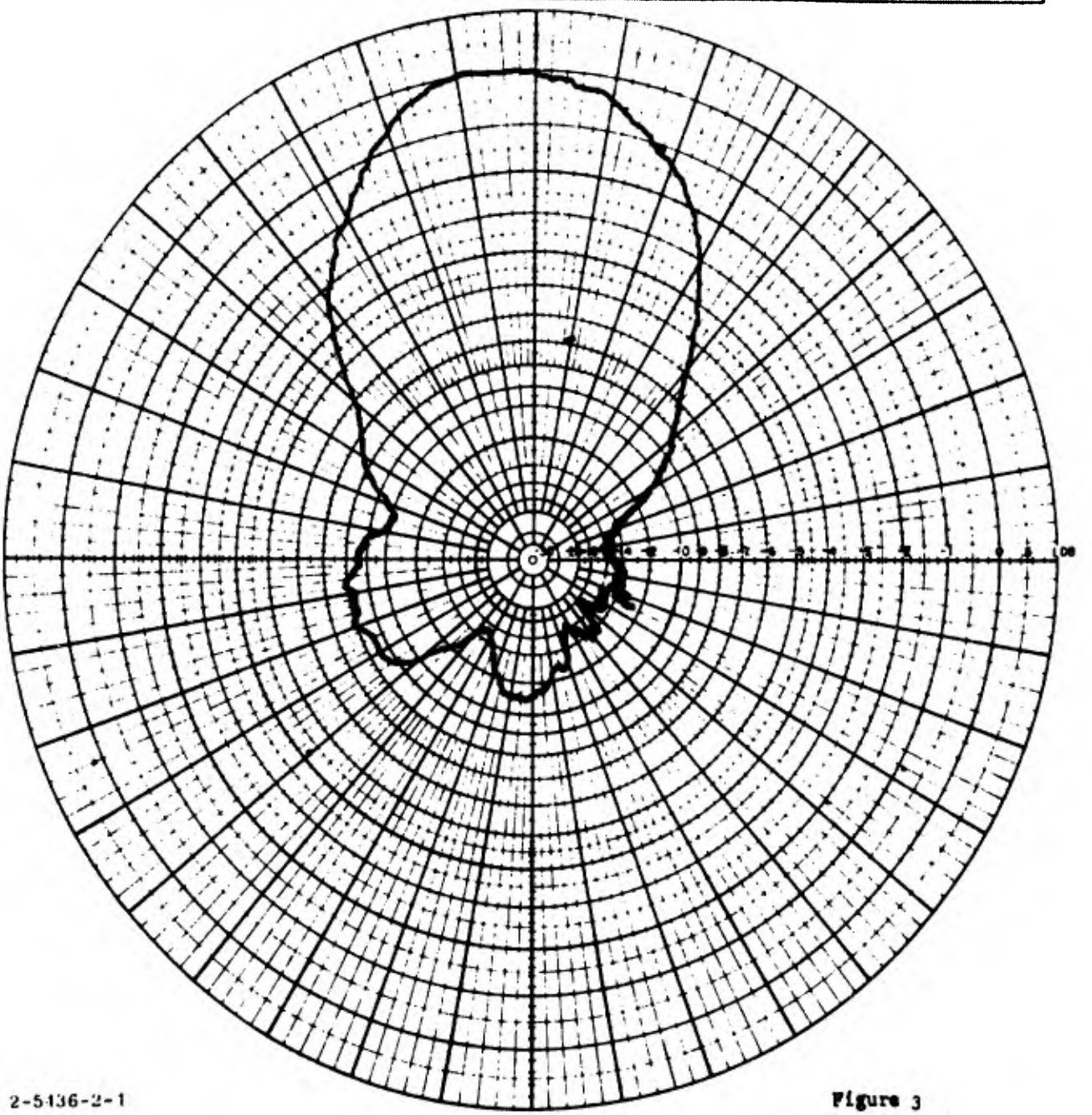

2-5136-2-1

Figure 3

REMARKS R=300

OPERATOR DATE

APPROVED DATE 11 db

VARIABLE ANGLE Φ ( ), θ ( )

CONSTANT ANGLE Φ = —— θ = ——

POLARIZATION E_Φ ( ), E_θ ( ). ——

Φ = Horizontal angle θ = Vertical angle

CURVE PLOTTED IN VOLTAGE (—), POWER ( ), DECIBELS ( )

POLAR RECORDING CHART

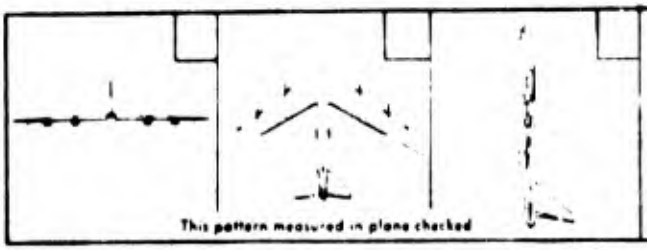

FILE NO _____ SHEET ___ OF ___

PLANE TYPE _____ MODEL SCALE ___

ANTENNA TYPE _____

ANTENNA LOCATION _____

FREQUENCY FULL SCALE _____ MODEL 190 Mc

MODEL SURFACE _____

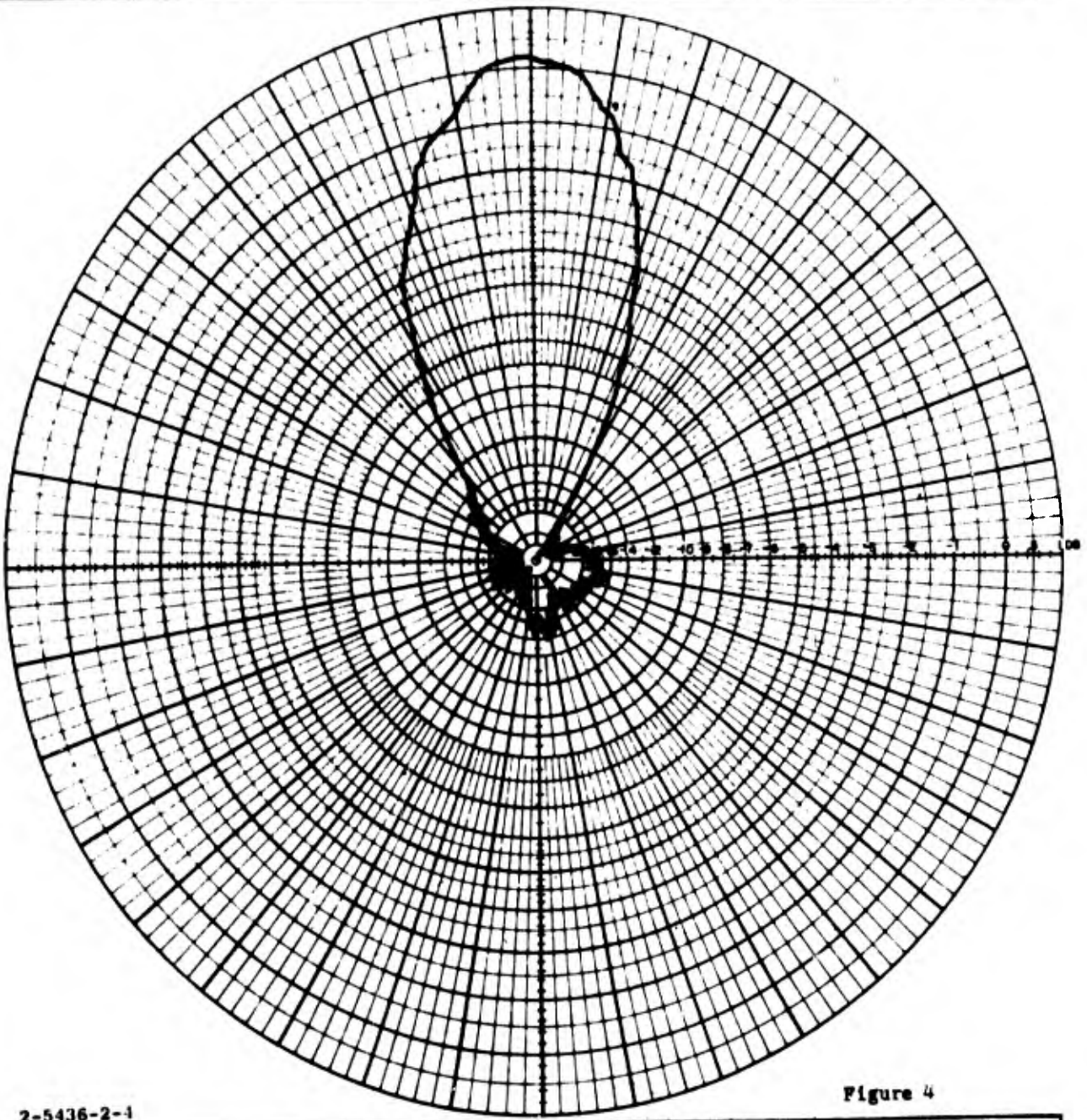

Figure 4

2-5436-2-1

REMARKS R=300

Bolo

OPERATOR _____ DATE _____

APPROVED _____ DATE 11

VARIABLE ANGLE Φ ( ), θ ( )

CONSTANT ANGLE Φ = ____ θ = ____

POLARIZATION E_Φ ( ), E_θ ( ), ____

Φ = Horizontal angle θ = Vertical angle

CURVE PLOTTED IN VOLTAGE ( ), POWER ( ), DECIBELS ( )

POLAR RECORDING CHART

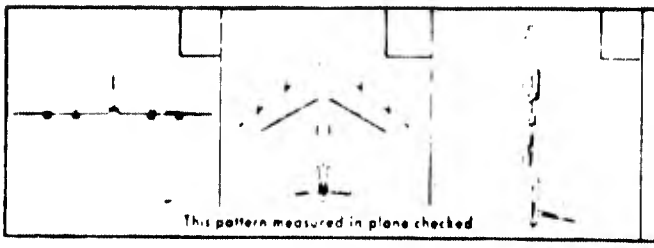

FILE NO _____ SHEET ___ OF ___

PLANE TYPE _____ MODEL SCALE _____

ANTENNA TYPE _____

ANTENNA LOCATION _____

FREQUENCY FULL SCALE _____ MODEL 210 Mc

MODEL SURFACE _____

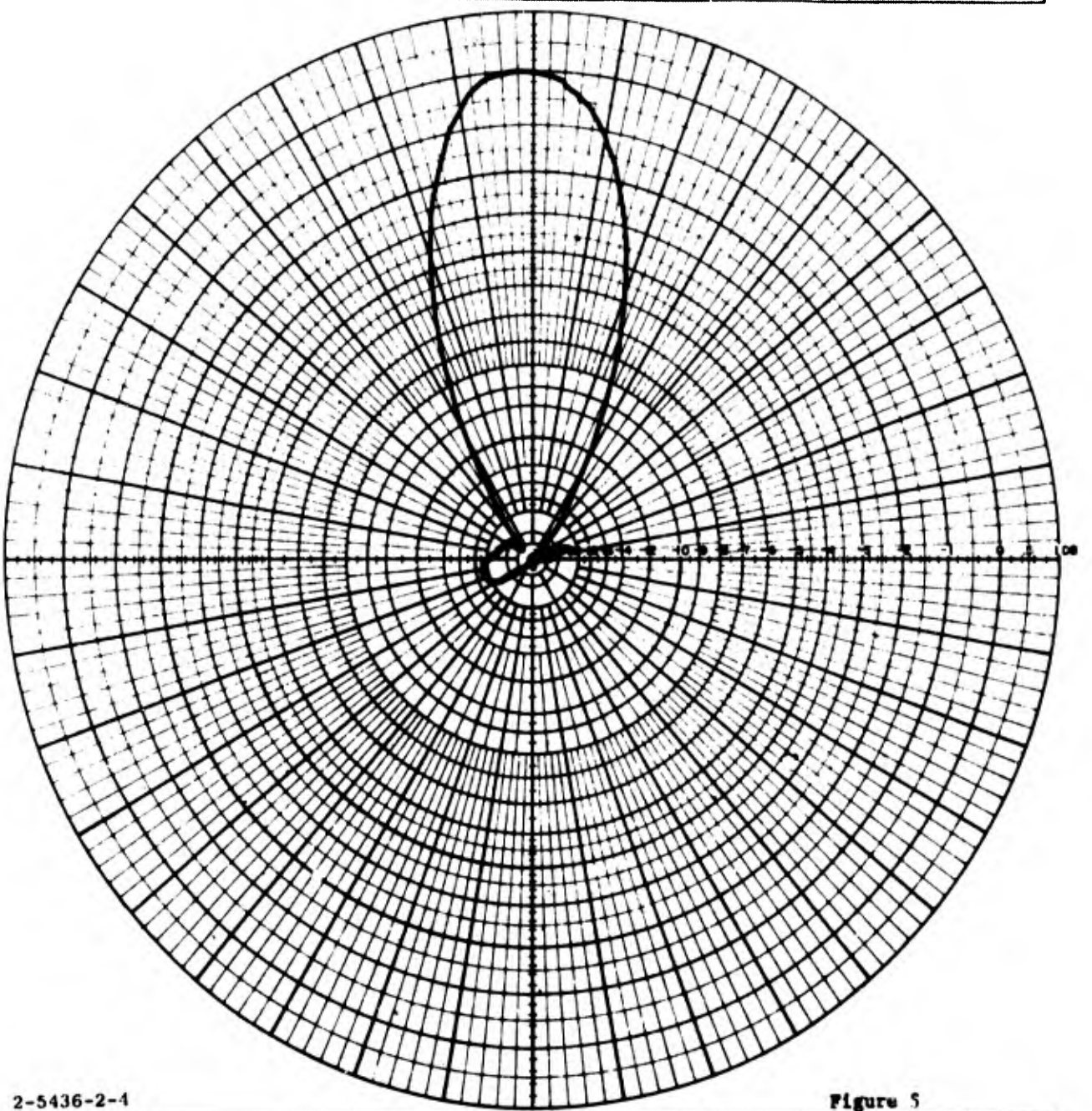

2-5436-2-4

Figure 5

REMARKS R=300

Bolo

OPERATOR _____ DATE _____

APPROVED _____ DATE 23 db

VARIABLE ANGLE Φ ( ), θ ( )

CONSTANT ANGLE Φ = ____ θ = ____

POLARIZATION E_Φ ( ), E_θ ( ), _____

Φ = Horizontal angle θ = Vertical angle

CURVE PLOTTED IN VOLTAGE ( ), POWER ( ), DECIBELS ( )

POLAR RECORDING CHART

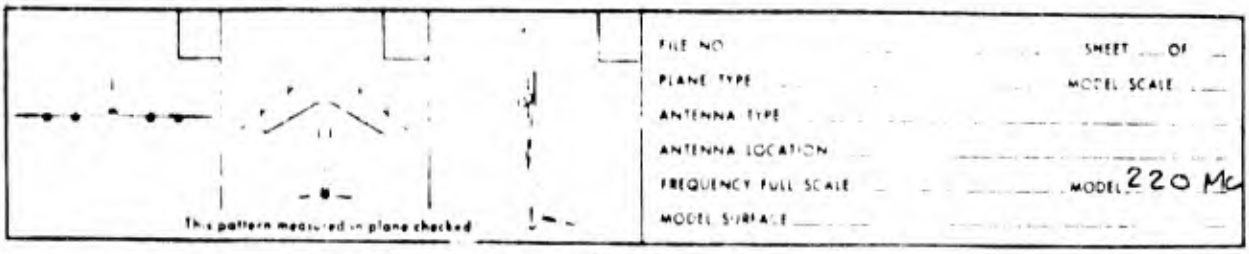

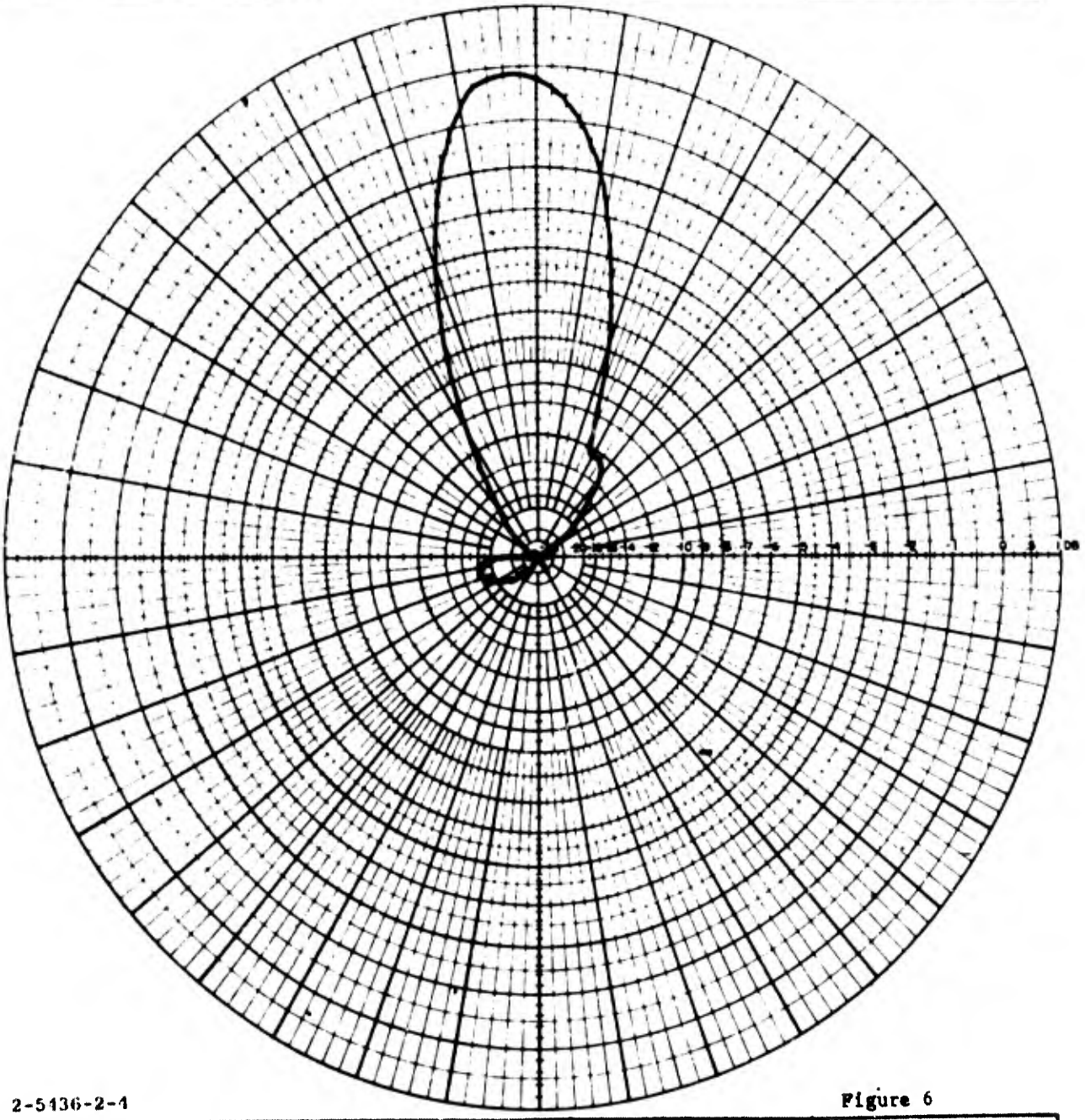

2-5136-2-1

Figure 6

REMARKS R=300

Bolo

OPERATOR DATE

APPROVED DATE 20db

VARIABLE ANGLE Φ [ ], θ [ ]

CONSTANT ANGLE Φ = ____ θ = ____

POLARIZATION E_Φ [ ], E_θ [ ], ____

Φ = Horizontal angle θ = Vertical angle

CURVE PLOTTED IN VOLTAGE [ ] & POWER [ ], DECIBELS [ ]

POLAR RECORDING CHART

1.2.4 Relative Gain

The electrical length of the cigar antenna is 3 wavelengths at 134 MHz and 5 wavelengths at 225 MHz. Thus, the maximum theoretical gain is approximately 15 db at 134 MHz and approximately 17 db at 225 MHz.[3] However, these figures do not allow for minor lobes or insertion losses in the feed system.

The theoretical gain of the cigar antenna can be found from:

$$G_{db} = A_{db} + G'_{db} \qquad (1)$$

A represents the contribution from the feed and G' the contribution of the surface wave. For the antenna designed by the Schjeldahl Company, where the feed is basically a dipole backed by a ground plane 1/4-wavelength away:

$$A = 5 \text{ db}$$

$$G'_{db} = 5 + 10 \log_{10} L/\lambda$$

$$G_{db} = 5 + (5 + 10 \log_{10} L/\lambda)$$

$$\text{at 134 MHz, } G_{db} = 14.75 \text{ db}$$

$$\text{at 225 MHz, } G_{db} = 17.0 \text{ db}$$

As before, these figures represent a maximum level and do not allow for losses. Notice that these levels are almost exactly the same as the values obtained previously which were based on electrical length.

An attempt was made to measure the relative gain of the cigar antenna by referencing it to a standard gain dipole. However, it was discovered that due to the inherent broad beamwidth of the standard gain dipole, the magnitude of the ground reflections at the test frequencies destroyed the accuracy of these gain measurements. Therefore, an approximate method of calculating the gain of the cigar antenna was used, assuming an efficiency of approximately 73 per cent. Using the equation:

$$G \approx \frac{30{,}000}{\theta\varphi}$$

where $\theta = \varphi$ (assuming equal E & H plane beamwidths)

results in the following gain:

Frequency (MHz)	Beamwidth (Degrees)	Relative Gain (db)
134	68	8.11
160	51	10.62
185	39	12.94
190	39	12.94
200	35	13.88
210	34	14.14
215	33	14.39
220	31	14.94
225	30	15.22

The accuracy of these figures should be within ± 1/2 db.

1.2.5 Bandwidth

If the minor lobe level is used as the criteria, the bandwidth of the antenna is 50 per cent, or 1.68:1. Using a minimum gain of 10 db as the criteria, the bandwidth is slightly greater than 39 per cent, or 1.40:1.

1.2.6 Axial Ratio

Since the antenna is fed by a corporate feed structure, the axial ratio is determined by how broadband the phase shifting network is. Difficulty was encountered in measuring the axial ratio at the low frequency end because of ground reflections, however, at the higher operating frequencies, it was within 3 db.

1.2.7 Optimizing Techniques

There are several approaches available for optimizing the gain of the cigar antenna. Some of them are:

1. lengthen the antenna
2. use higher gain feed system
3. reduce bandwidth of antenna
4. increase feed taper section (increase number of full diameter director disks)

If the main consideration is a low minor lobe level, the parameters of the director elements at the center and the tip of the antenna must be varied experimentally.

1.3 MECHANICAL CHARACTERISTICS

The antenna consists of an inflatable mast, having attached to it 14 circular disk directors, the feed element, and a reflector disk. The mast is 23 feet long and is tapered from an 8-inch diameter at the feed end to a 2-inch diameter at the tip. The directors also vary in diameter from 27 inches at the feed end to 8 inches at the tip. See Figure 7.

A strain-rigidization concept was employed in the antenna mast design: therefore, the mast was considered as a pressure vessel (strain rigidization) and as

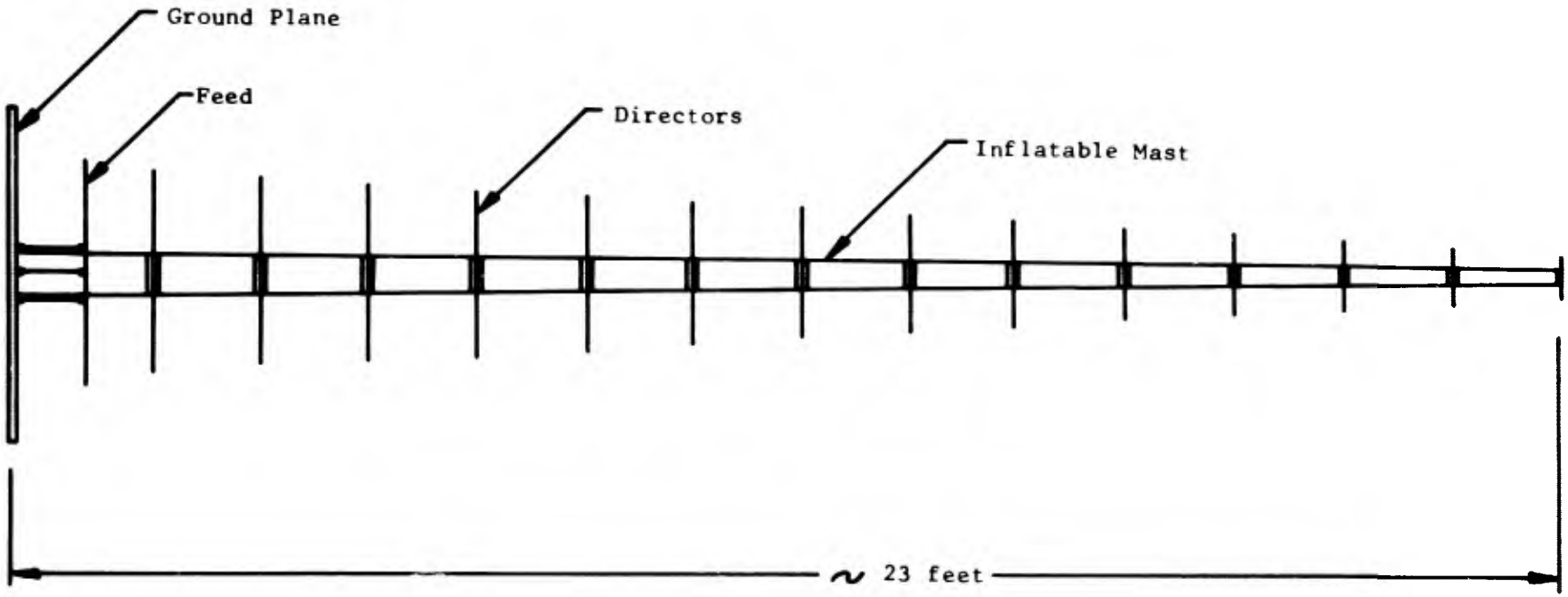

Inflatable Cigar Antenna

Figure 7

a long column (buckling stiffness). The mast was designed to withstand 0.02-g linear acceleration and 0.02-rad/sec^2 angular acceleration about the base with zero internal pressure. Mechanical test data shows that these requirements were met with a safety factor of two.

1.3.1 Structural Design

Since the mast varied in diameter, a multi-layered laminate was used so that adequate stress could be developed at the tip without bursting the tube at the base. The laminate consists of alternate layers of 0.18-mil aluminum foil and 0.35-mil Mylar. The outer shell was a continuous layer of foil-Mylar laminate. A second layer was added to the inside extending 220 inches from the feed end: a third layer of the same laminate was then added inside extending 116 inches from the feed end.

The design was based on having 6,000-psi skin stress at the tip of the mast. This resulted in a mast thickness varying from 1.74 mil at the base to 0.7 mil at the tip.

Stiffness of the laminate was verified by considering the mast as a cantilever beam with a bending moment generated by the angular acceleration and the mass moment of inertia. The bending stress is found in the following manner:

$$\text{Bending Stress} = MC/I_A \qquad (2)$$

where M = bending moment,

C = radius at the base,

and I_A = Area Moment of Inertia.

Let t = material thickness,

x = distance from base at which bending moment is calculated,

A = cross-sectional area,

ρ = density,

g = acceleration of gravity,

dm = element of mass = $(\rho/g)\,A\,dx$,

m = mass of each disk,

ℓ = distance from base at which each disk is located,

α = angular acceleration.

Then the mass moment of inertia is

$$I_m = \int_0^{\ell} x^2\, dm + \sum_{i=1}^{i=n} m_i \ell_1^{\,2} .$$

Since $M = I_m x$, while $I_A = \pi C^3 t$, equation 2 becomes

$$\text{Bending Stress} = \frac{\alpha\left(\frac{7\pi\rho}{6g}\, t\ell^3 + \sum_{i=1}^{i=n} m_1 \ell_1^2\right)}{\pi C^2 t} \qquad (3)$$

The required laminate thickness was determined by equating the bending stress to local buckling stress data obtained by axially loading columns of the laminate. A safety factor of two was used in the design.

The director disks were spun from 6-mil, 1080-0 aluminum foil and attached to the mast with standard sealing techniques using GT-301 Mylar tape. Each director was also attached mechanically to the mast.

The feed elements consisted of two orthogonal triangular dipoles etched on a copper-clad dielectric disk. Ease of construction, rather than weight was the prime consideration here.

1.3.2 Packaging, Deployment, Stowage Volume, and Weight

Several methods of packaging the mast are available. One unit was packaged as shown in Figure 2. Deployment of this package was axial (longitudinal). The time required to fully deploy the antenna can be controlled and can vary from several minutes to a few seconds.

The total height of the package is approximately 8 inches, however, this could have been reduced somewhat. This makes the stowed volume approximately 500 in^3, not including the disk elements. Total weight of the package including the dielectric supported feed and feed cables was approximately 4 pounds maximum.

1.3.3 Structural Loading & Deflection Test Results

The purpose of this test was to determine the ability of the unpressurized, strain-rigidized antenna to carry design loads.

The antenna was initially inflated on the surface of a pool of water to simulate a zero-g field. After the antenna was inflated, each disk was suspended from a spreader bar and the antenna was transported to a test fixture. The antenna was pressurized to 1.5 psig and maintained for one minute. Pressure was allowed to drop to zero prior to applying loads horizontally to each disk at the center line of the mast.

The loading condition represented a 0.02-g side load on the antenna, with each disk being loaded proportionally to its calculated dead weight.

Horizontal deflections at each disk were measured by observing an index card through a transit.

The results of these loading tests are shown in Figure 8. Test run No. 1 consisted of applying loads, one at a time, beginning at the disk nearest the base and proceeding toward the tip. Deflections of all disks were recorded after each disk was loaded. Test run No. 2 was made after unloading, taking a new zero reference, and reloading as before. Deflections were recorded after all the disks had been loaded. Run No. 3 was similar to run No. 2 except that the

loads were applied starting at the tip of the mast. Some of the variation in the results of the three runs can be attributed to the friction of the loading threads.

The antenna mast was then pressurized to 2.5 psig, held for one minute, then reduced to zero. Run No. 4 was then made where loads were applied beginning at the base.

Loads were arbitrarily increased for run No. 5, and were applied beginning at the tip.

As can be seen in the curves of bending moment and bending stress in Figure 8, the antenna mast greatly exceeded these design requirements.

1.4 SUMMARY AND CONCLUSIONS

The design and test results of an inflatable cigar antenna have been described.

The electrical tests indicate that the gain of the antenna is reasonably close to the theoretical value. It should be noted that no attempt was made to optimize the design. Therefore, these test results do not represent the ultimate that can be obtained with this configuration.

Satisfactory radiation patterns were measured from 134 MHz to 225 MHz, a 1.68:1 bandwidth. The gain over this bandwidth varied from approximately 8 db to 15 db.

The mechanical loading and deflection tests show that under zero internal pressure, the antenna structure can withstand a 0.02-g side load with a safety factor greater than two. Arbitrarily increasing the loads until the tips of the antenna deflected 2 inches resulted in only 0.1 inch deflection after removing the loads.

It appears that the inflatable cigar antenna concept provides a very practical design approach to a medium gain VHF communications antenna for space application. Obviously, at higher frequencies this design concept would have many merits. Listed below are four examples of other cigar antenna designs and their electrical characteristics.[1]

Length of antenna L/λ	4	6	20	∞
Gain above isotropic	16db	17.5db	22db	2∞db
1/2-pwr beamwidth	27^{o}	23^{o}	10^{o}	7^{o}
Minor lobe level	12db	12db	15db	17db

These were all hard (solid metal) antennas, however, there is no reason to believe that their performance could not be duplicated with an inflatable design.

A cigar antenna operating at 2 GHz would have a length of approximately 2-1/2 feet if scaled from the antenna built by the G. T. Schjeldahl Company. An array of these could easily be used if increased gain were required. Ideally, an array of four such antennas would provide 20db gain at 2 GHz, based on the test results of the inflatable cigar antenna. A 16 element array (4×4) has been built which provided approximately 25 db gain over a 1.2:1 bandwidth.[4]

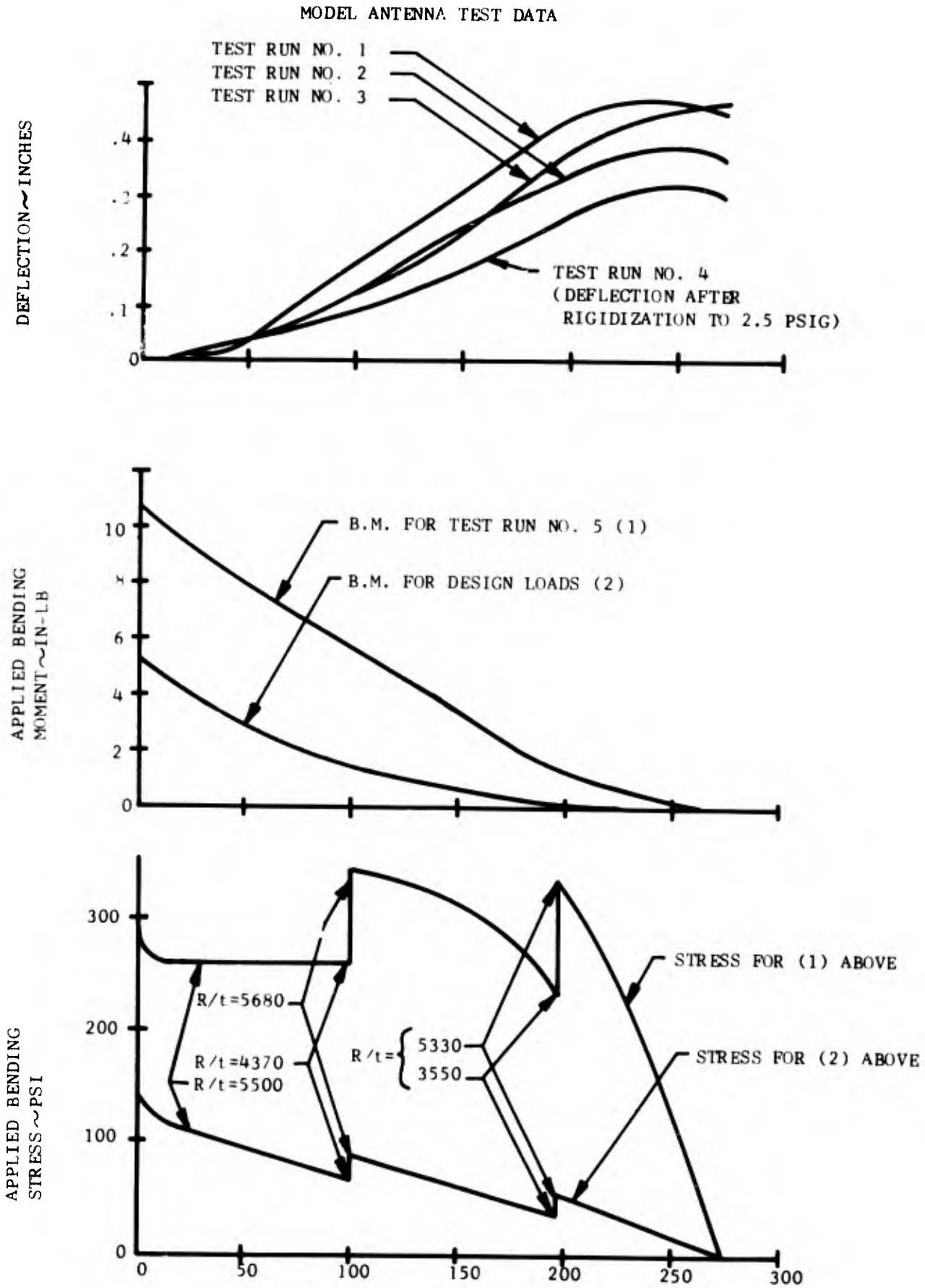
MODEL ANTENNA TEST DATA
TEST RUN NO. 1
TEST RUN NO. 2
TEST RUN NO. 3
TEST RUN NO. 4
(DEFLECTION AFTER
RIGIDIZATION TO 2.5 PSIG)
DEFLECTION ~ INCHES
.4
.3
.2
.1
0
B.M. FOR TEST RUN NO. 5 (1)
B.M. FOR DESIGN LOADS (2)
APPLIED BENDING
MOMENT ~ IN-LB
10
6
4
2
0
STRESS FOR (1) ABOVE
STRESS FOR (2) ABOVE
R/t=5680
R/t=4370
R/t=5500
R/t= 5330
3550
APPLIED BENDING
STRESS ~ PSI
300
200
100
0
0
50
100
150
200
250
300
ANTENNA LENGTH ~ INCHES (FROM ROOT)

Figure 8

2.0 INFLATABLE PARABOLA

2.1 ELECTRICAL CHARACTERISTICS

Two 10-ft diameter inflatable parabolas have been constructed having an f/D ratio of 0.833 and 0.42. The rms surface error on the shorter focal length model was 0.133 inches, making the ratio of diameter to surface error approximately 900. On the longer focal length model, this ratio was approximately 1,000. It should be noted that the reflector surface was not formed over a mandrel or molded with heat. Had this process been used, it is estimated that the rms surface error could be reduced to under 0.05-inches.

Radiation measurements were performed only on the shorter focal length model. The reflector dimensions and feed support structure are shown in Figure 9. Figure 10 shows the basic reflector construction and the materials used in fabrication.

2.1.1 Primary Feed System

The primary feeds used to illuminate the parabola were three cavity-backed dipoles, tuned at 2.0, 3.0, and 4.0 GHz. The entire parabolic antenna system is shown in Figure 11. Primary feed patterns are not included in this report, however, the following table provides all the data of interest.

PRIMARY FEED PATTERN DATA

FREQUENCY	AVE. B.W.	EDGE DIRECTED ILLUM.	EDGE ILLUM.
2.0 GHz	130°	-8.9 db	-11.6 db
3.0 GHz	125°	-10.2 db	-12.9 db
4.0 GHz	135°	-9.0 db	-11.7 db

(For f/D = 0.42, Space Atten. = 2.7 db)

2.1.2 Radiation Pattern Measurements

In measuring the secondary radiation patterns of the inflated parabola, the following items were investigated:

1. Principal plane radiation patterns were recorded with the primary feed located at the reflector focal point.

2. The antenna directivity (maximum directive gain) was measured by comparing it to the maximum directive gain of each primary feed. Each feed was integrated on the antenna pattern range to establish its directivity.

3. Each feed was moved off the focal point to determine the effects of axial defocusing.

Summaries of the data obtained are presented in Figures 12 and 13. Rectangular radiation patterns were recorded and are presented at the end of this

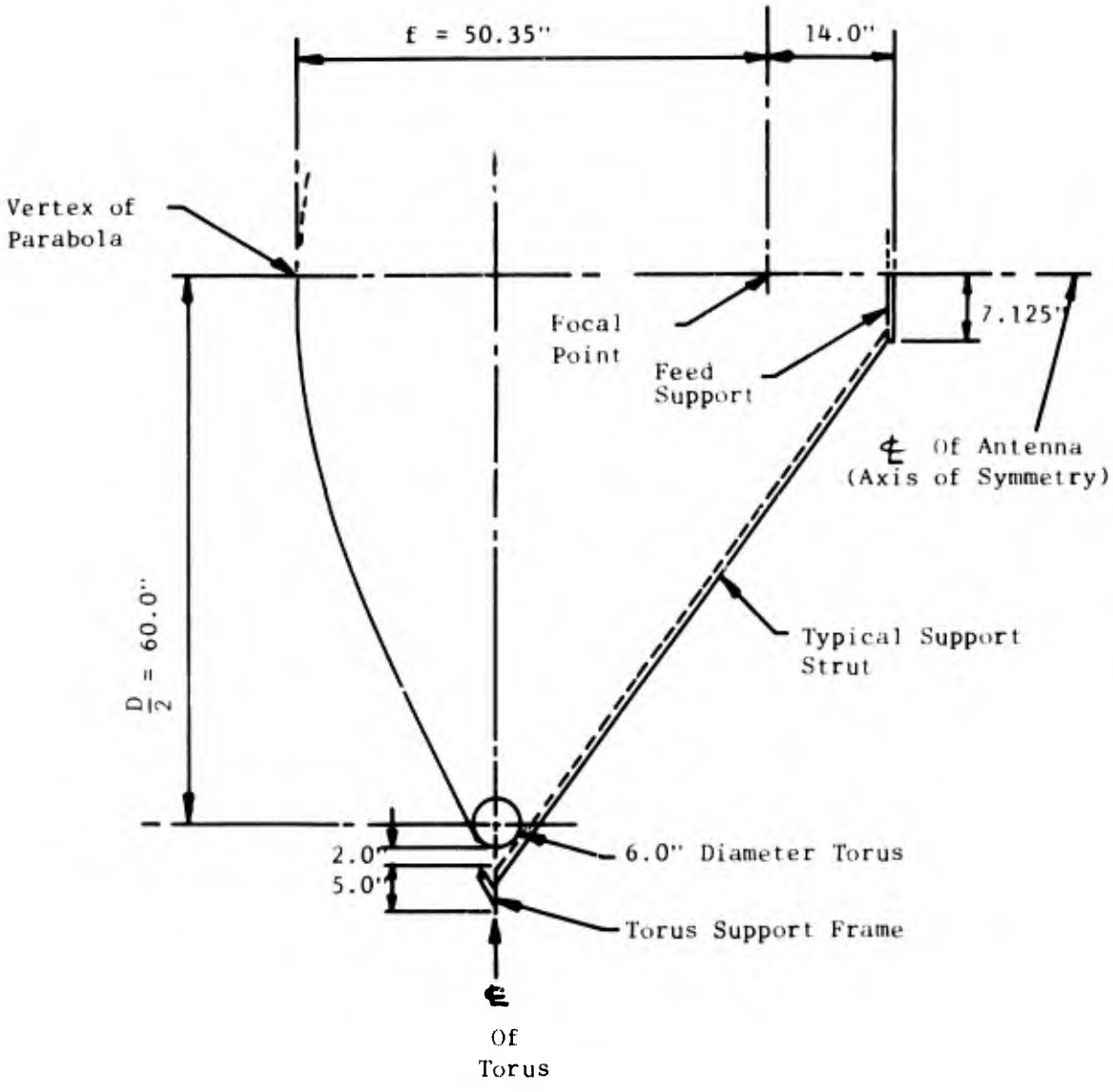

INFLATABLE PARABOLIC ANTENNA
f/D = 0.42

Figure 9

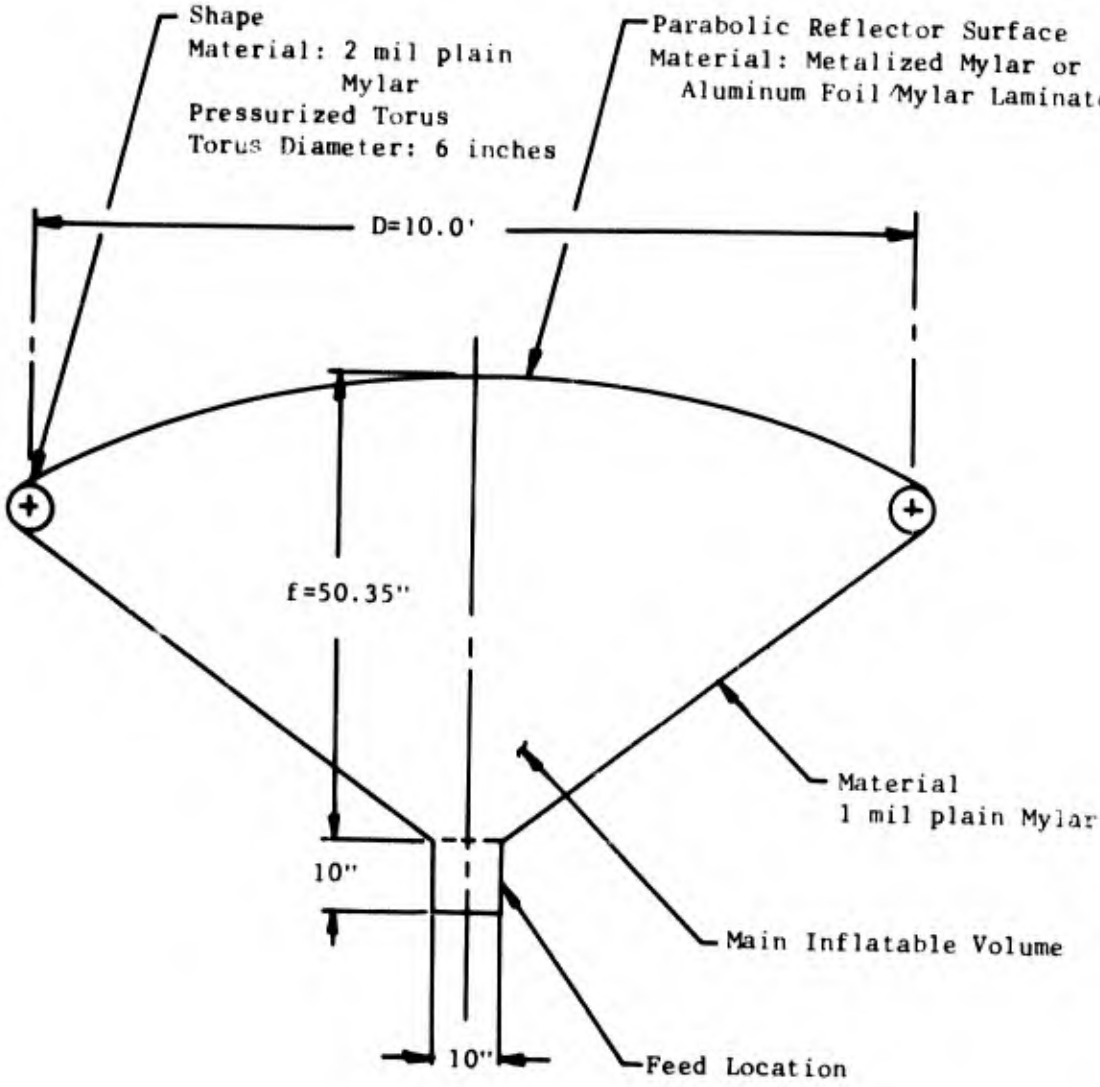

CONFIGURATION OF INFLATED VOLUME

Figure 10

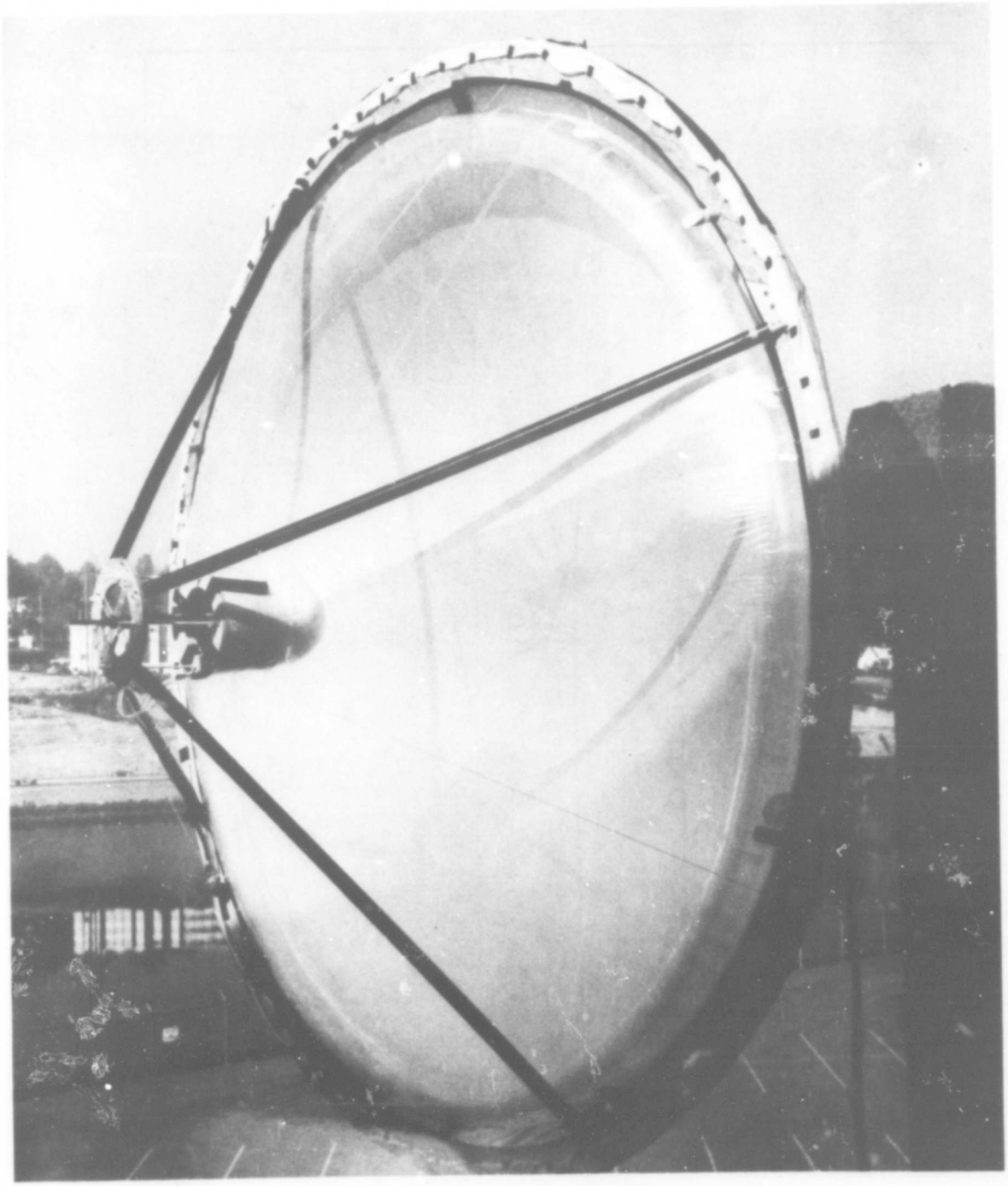

Inflatable Parabolic Antenna
in Test Fixture
Figure 11

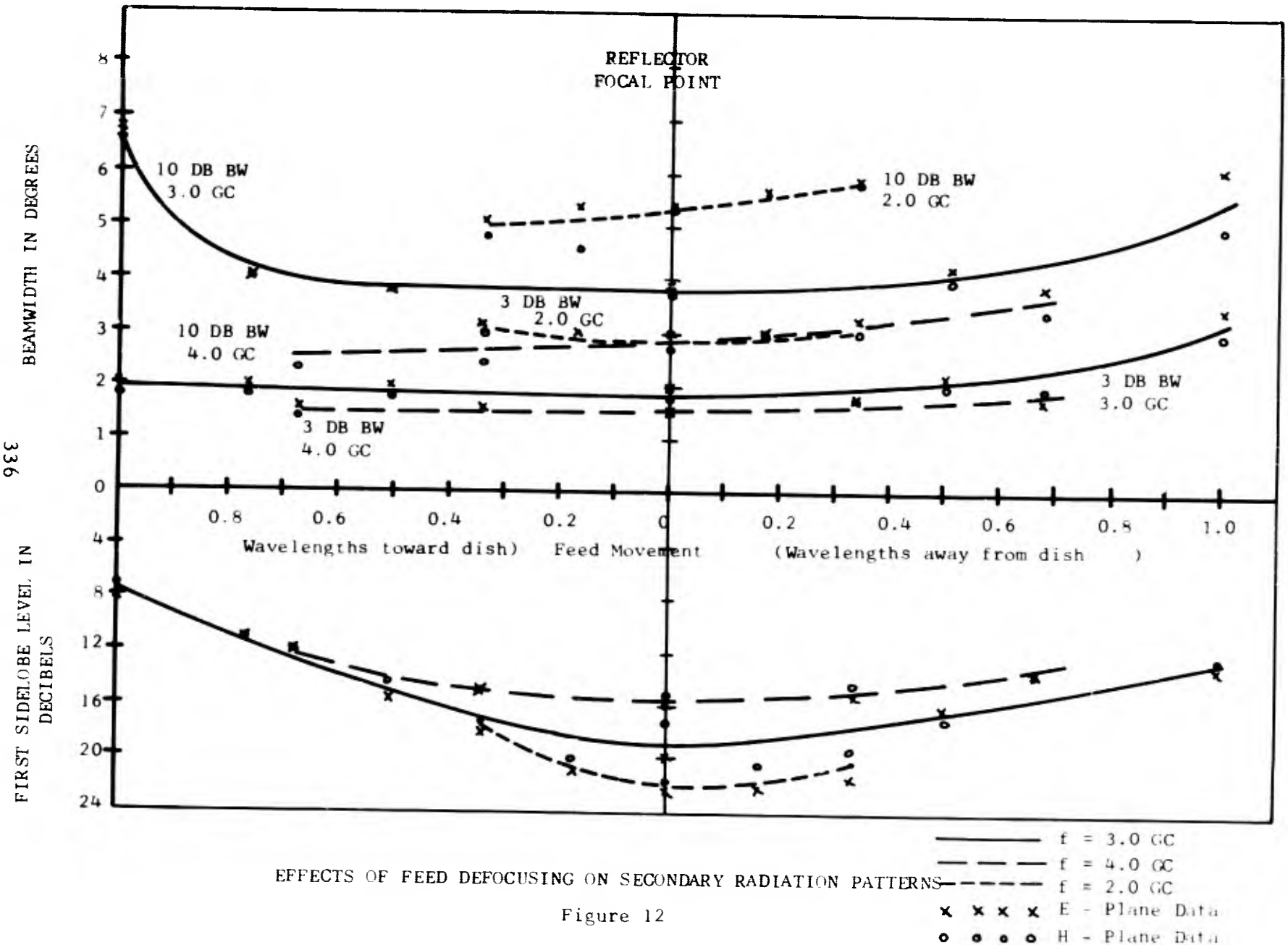

EFFECTS OF FEED DEFOCUSING ON SECONDARY RADIATION PATTERNS

Figure 12

$$G = 10 \log_{10} \frac{4\pi A}{\lambda_o^2} n$$

G = Antenna Gain in Decibels
A = Antenna Aperture Area
n = Aperture Efficiency
λ_o = Free Space Wavelength

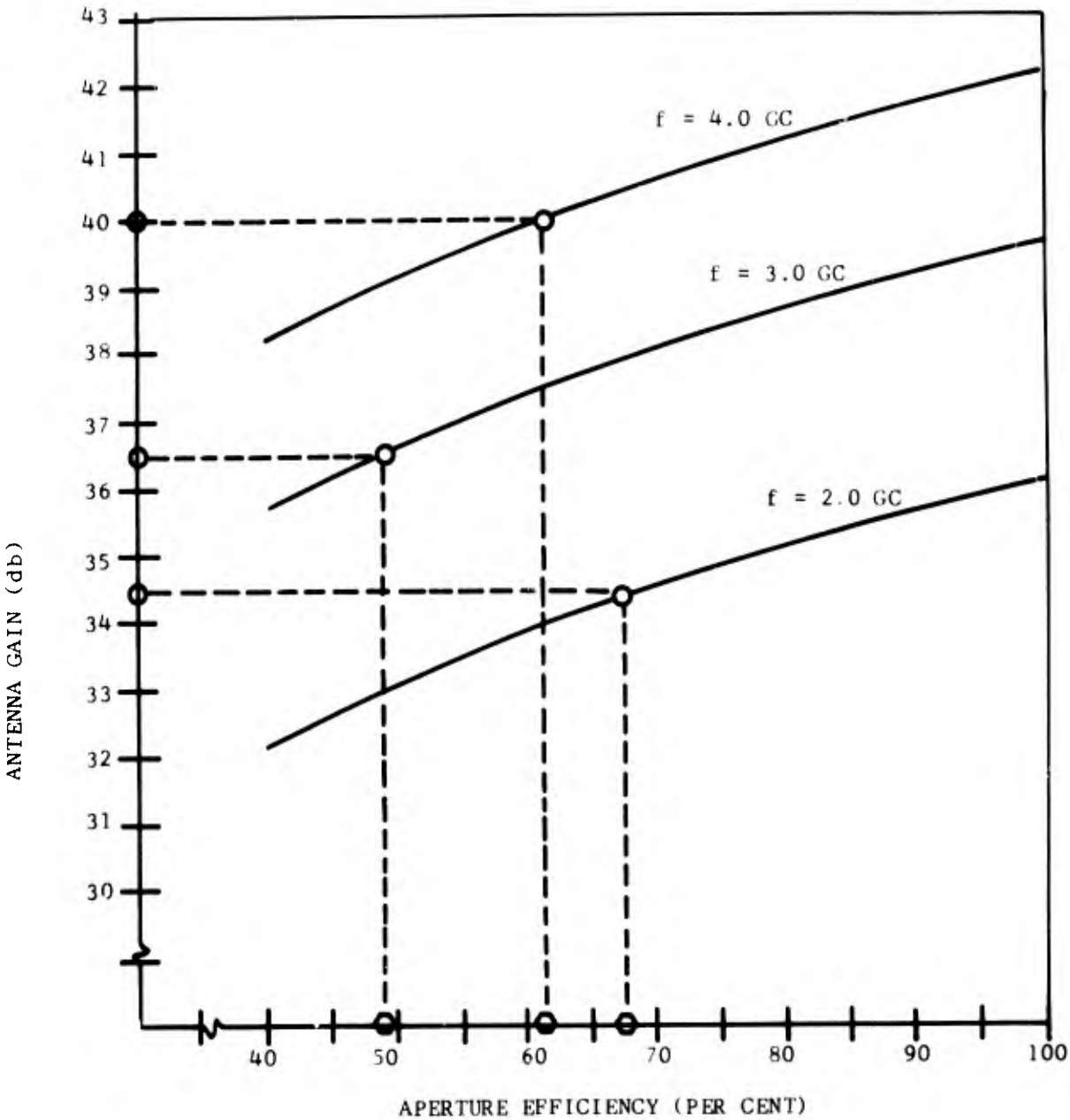

ANTENNA GAIN VS APERTURE EFFICIENCY
10 FOOT DIA. PARABOLIC DISH

Figure 13

report. Tests were performed with 5 psi pressure in the torus and 0.50 inches of water in the reflector volume. The following table is a summary of these measurements.

2.1.3 Secondary Pattern Characteristics

FREQUENCY	REFLECTOR DIRECTIVITY	SIDE LOBE LEVEL	EFFICIENCY
2.0 GHz	34.5 ± 1.0 db	-21.5 db	67.5 %
3.0 GHz	36.5 ± 1.0 db	-17.5 db	49.1 %
4.0 GHz	40.0 ± 1.0 db	-15.0 db	61.5 %

The reflector rms surface error is $\lambda/22$ at 4.0 GHz, or 0.133 inches. This causes a loss in gain of approximately 1.0 db. Assuming that all this energy goes into the first side lobe, only a slight increase in the side lobe level would result. Therefore, the large increase in side lobe level with frequency is attributed to scattering by the feeds and antenna supports.

The parabola is somewhat under-illuminated at 3.0 GHz, as is shown in the primary feed data. This would account for much of the reduced efficiency at 3.0 GHz.

2.2 CONCLUSIONS

Based on the results obtained from the electrical tests, it appears that the inflatable parabolic reflector was a very efficient antenna. Any possible deficiencies in the reflector such as poor surface conductivity, surface tolerances and nonparabolic shape could not be detected within the scope of the measurements made.

In a space application, the parabolic surface could be strain-rigidized by pressurizing the antenna until the metal foil passes its yield point. The same technique could be used to rigidize the feed support system.

As mentioned previously, the rms surface error can be reduced drastically if a machined mandrel is used to form the parabolic surface. The surface skin is then stretched over the mandrel and heat is applied to mold the skin to the contour of the machined mandrel. Using this technique, the surface error of the parabola is then primarily a function of the machined surface accuracy of the mandrel.

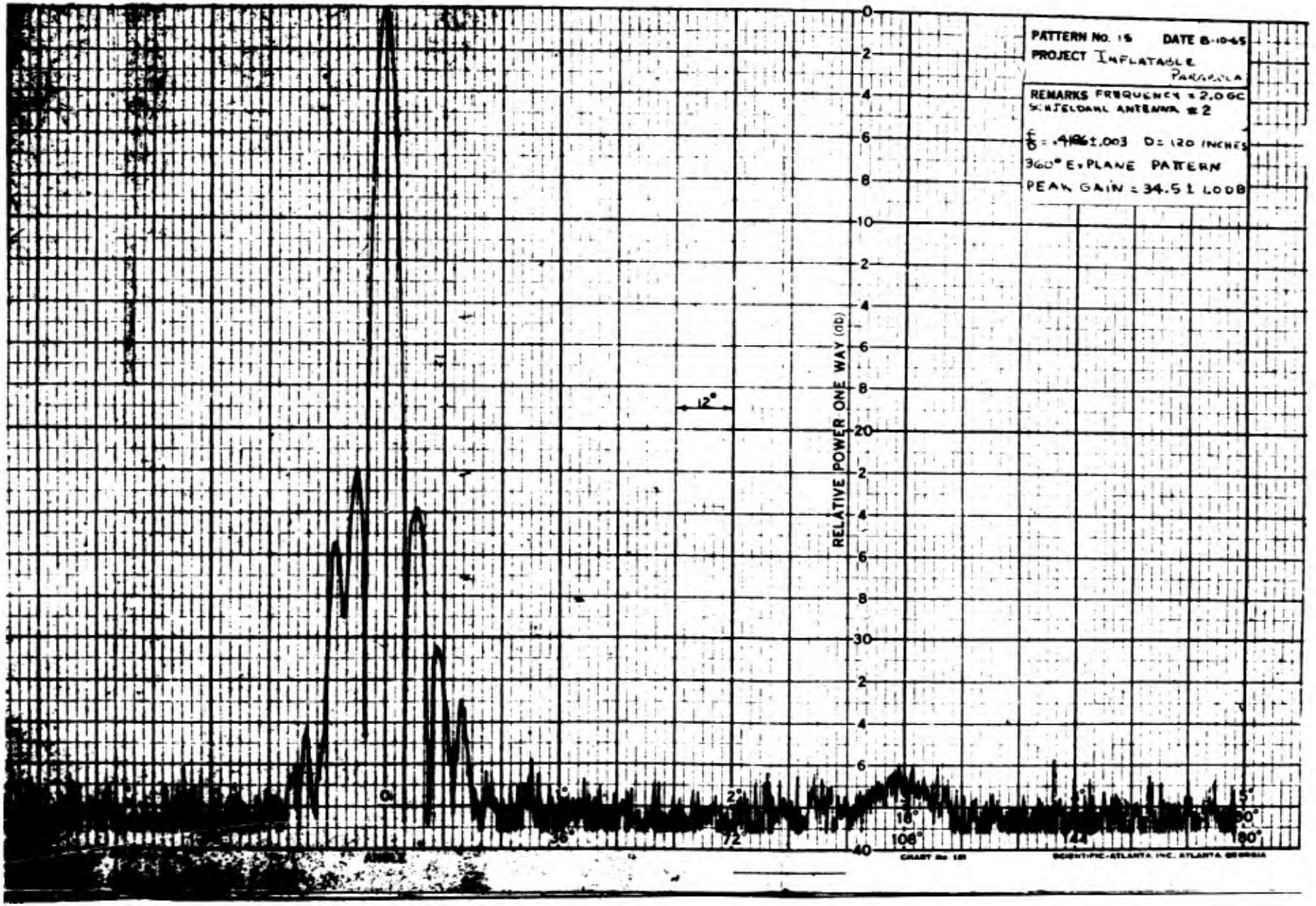
PATTERN NO. 15 DATE 8-10-65
PROJECT INFLATABLE PARABOLA
REMARKS FREQUENCY = 2.0 GC
SCHELDAHL ANTENNA # 2
f/D = .4161.003 D = 120 INCHES
360° E-PLANE PATTERN
PEAK GAIN = 34.5 ± 1 DDB
RELATIVE POWER ONE WAY (DB)
12°
0
2
4
6
8
10
20
30
40
0°
1°
2°
5°
18°
108°
72°
90°
180°
SCIENTIFIC-ATLANTA INC. ATLANTA GEORGIA

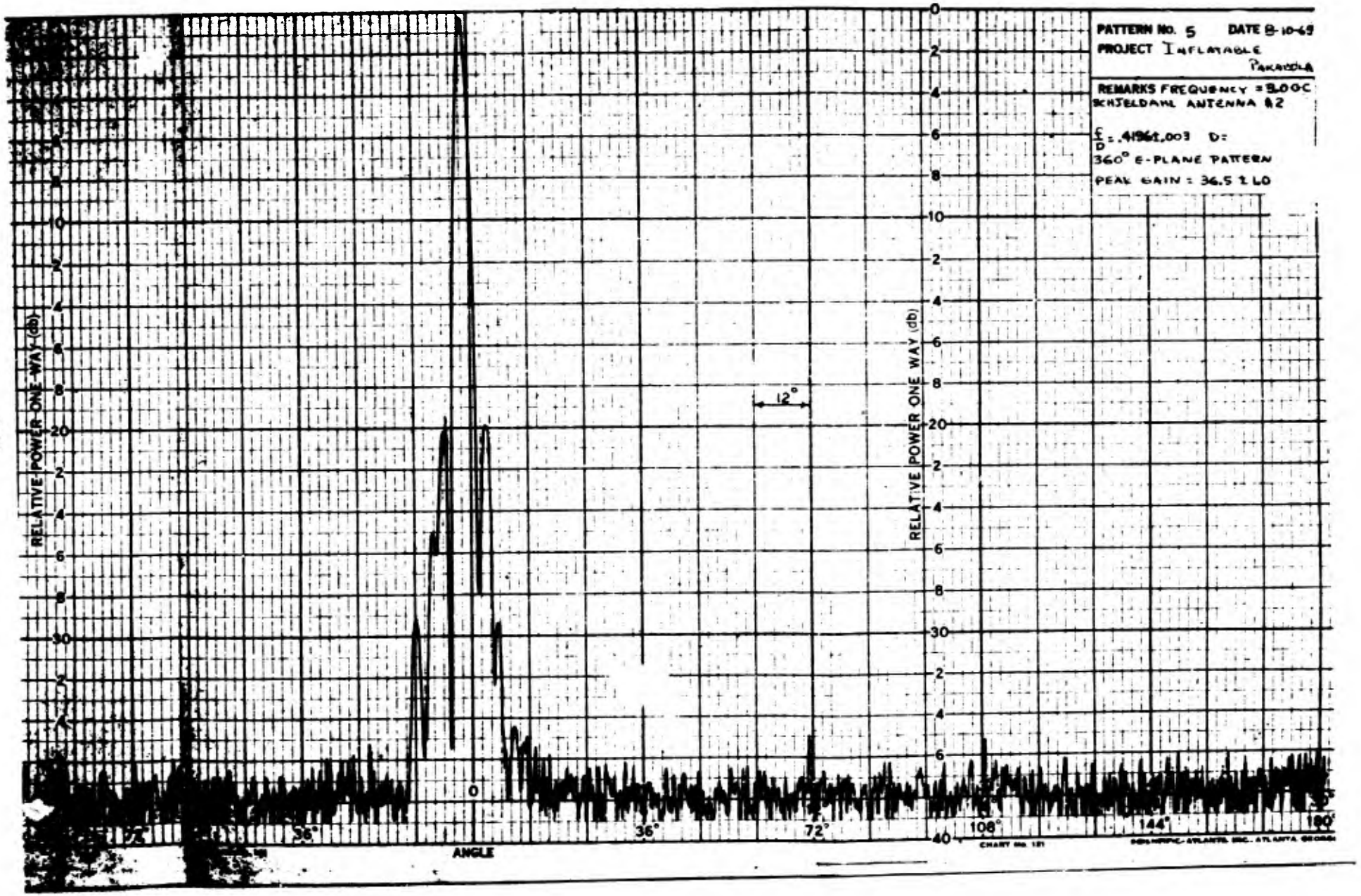

Figure 15 SECONDARY RADIATION PATTERN AT 3.0 GHz

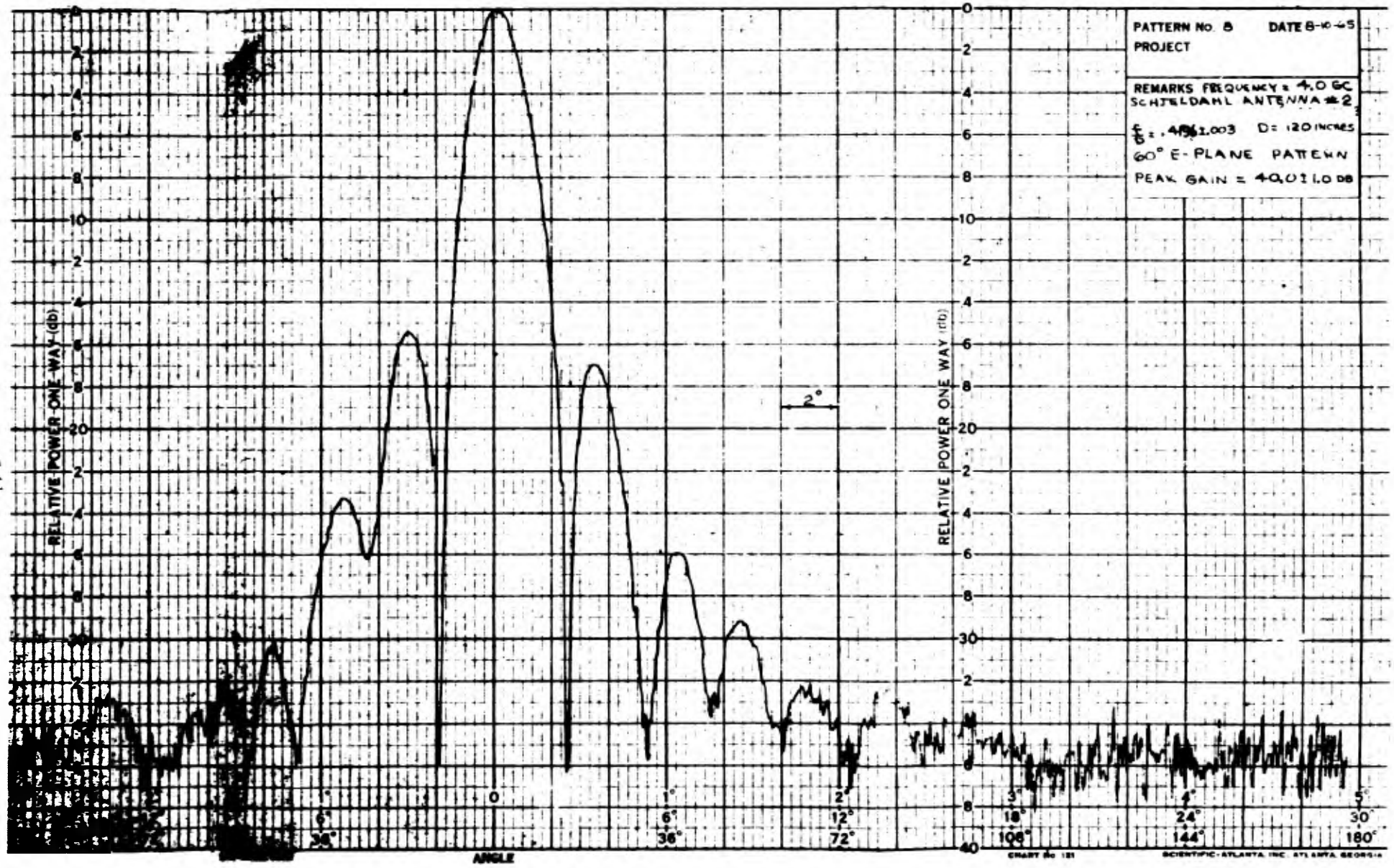

Figure 16 SECONDARY RADIATION PATTERN AT 4.0 GHz

PLANAR EQUIANGULAR SPIRALS

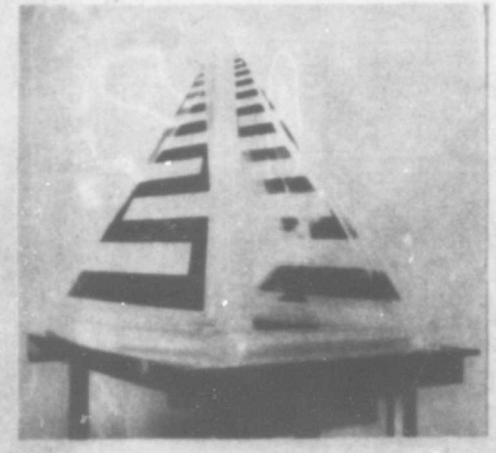

INFLATABLE LOG PERIODIC
TRAPEZOIDAL-TOOTH ANTENNA

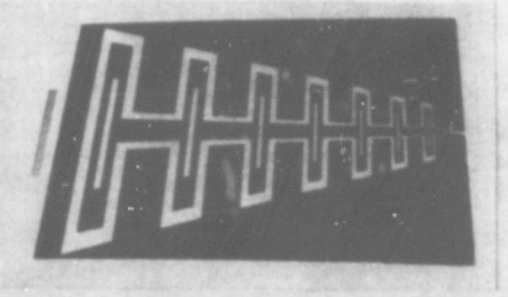

LOG PERIODIC FOLDED
SLOT ARRAY

FIGURE 17
OTHER UNFURLABLE ANTENNAS
DESIGNED BY G.T. SCHJELDAHL CO.

REFERENCES

1. J. C. Simon & G. Weill, 1953, "A New Type of Endfire Antenna", (in French) Ann. Radioelectricite, Vol. 8, pp 183.

2. William Croswell & Melvin Gilreath, 1962, "Erectable Yagi Disk Antennas for Space-Vehicle Applications", NASA Technical Note D-1401.

3. John Kraus, 1950, Antennas, New York, McGraw-Hill Book Co., Inc. pp. 25.

4. Fred Beck, 1965, "A Method for Arraying Yagi-Disk Antennas", NASA Technical Note D-2683.

BLANK PAGE

THE REQUIREMENTS AND ROLE OF EVA ASSOCIATED WITH ORBITAL STRUCTURES

R. G. Clodfelter*

and

R. A. Stewart**

INTRODUCTION

It has become more apparent with the ever-increasing number of manned space flights, even from the first flight of Yuri Gagarin in 1961, that man is conquering these new frontiers in a systematic fashion. He has, through the Vostok, Mercury and Gemini series, established that he can: first, survive the natural and induced environments of his spacecraft, second, can perform meaningful experimentation within the spacecraft, and third, can successfully cope with the environment external to the spacecraft.

Studies conducted over the past several years have identified a large number of in-space erectable structures to be utilized in the conduct of a number of earth orbital missions. These structures have generated by their mission requirements, substantially larger dimensions than the limiting dimension for fixed structures in space, specifically the booster diameter. In the case of the largest booster vehicle in the current national inventory, this dimension is 21.5 feet. It should be further noted that a structure must be erected in a manner which insures its structural fidelity in the accomplishment of the mission objectives. One technique is the utilization of an extravehicular astronaut in the deployment, assembly, and maintenance of these structures.

It is the intent of this paper to relate the role of EVA to the structural requirements, to delineate the relative effectiveness of EVA, and to define the equipment required to provide EVA orbital support to the erection of large structures. It is not the intent of this paper to define all of the structural assembly techniques nor the missions required of these structures, but rather to establish in general that EVA does have a defined and effective role in the support of these structures.

---

* R. G. Clodfelter, Project Engineer, Maneuvering System Spacecraft Technology Branch, Air Force Aero Propulsion Laboratory, AFSC.

**R. A. Stewart, Project Engineer, Space Systems, Textron's Bell Aerosystems Company.

Presented at 3rd Aerospace Expandable and Modular Structure Conference, May 1967.

MISSION IDENTIFICATION

The next logical step in the evolutionary advancement of manned participation in space is the extension of his activity into participation in extravehicular missions such as will be required for the erection, assembly, operation, and maintenance of large structures.

Figure 1 is a partial listing of potential structural assembly, techniques and their related missions. Shown in Figure 1 are five of the more predominant missions that have been analyzed as a result of a number of studies over the past several years. Antenna erection, maintenance, and support operations are shown as one task. Spacecraft vehicle support operations such as construction of RACKS, airlocks, and associated assemblies on vehicles such as the SIVB workshop for in orbit experimentation are shown as another. Total vehicle assembly as in the case of large orbital space stations of the MORL class which will consist of interlocking modules is depicted as another mission. Assembly of structures that might be operative remote from the parent craft, such as large X-Ray telescopes (Reference 1) is still another mission shown.

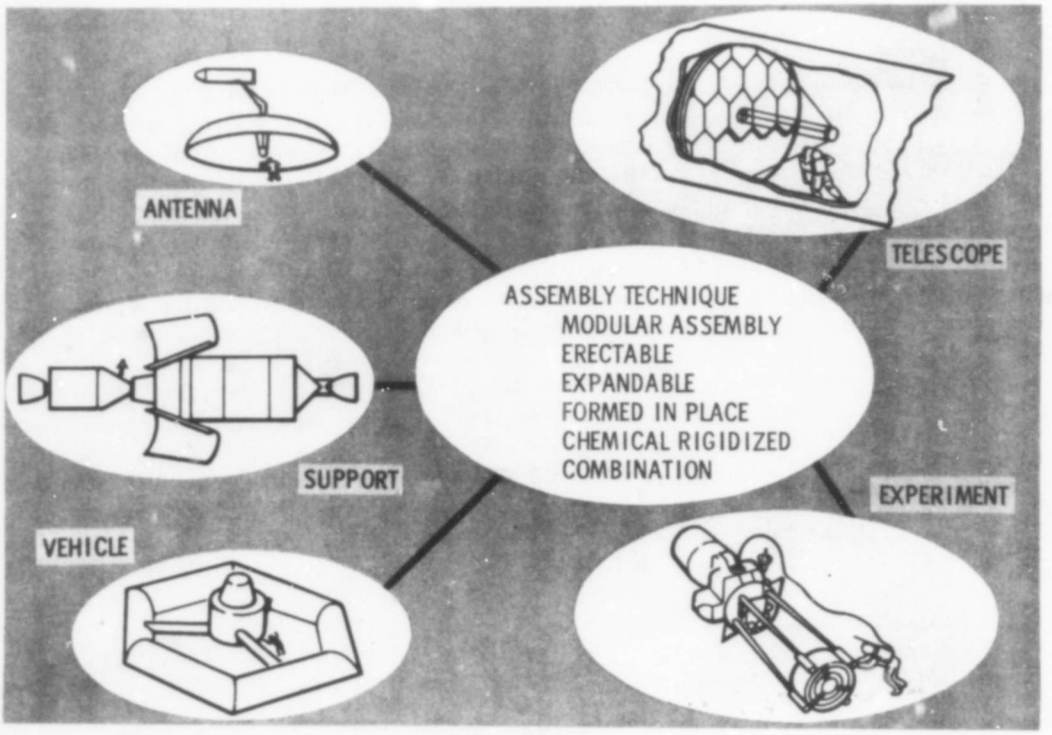

Figure 1. Potential Structural Assembly Technique and Related Mission

From these missions and others studied over the past several years, several elemental erection approaches have been synthesized as shown in Figure 1. These erection approaches consist of: modular assembly (i.e., mechanically erectable structures); erectable (i.e., unfurlable); expandable (i.e., elastic recovery and inflatable structures); formed in place (i.e., chemical evaporative) and chemical rigidized (i.e., catalytic).

EVA POTENTIAL

Only recently has the technical community begun to appreciate more fully the benefits that might accrue from direct manual participation in the development of in-space erectable structures. This has resulted in a delineation of those areas where EVA assistance, of either a manned or remote nature, might provide a valuable contribution to automatic techniques.

Two approaches to EVA in the design of space systems for the 70's have evolved. The first minimizes EVA crew participation to only those activities which cannot be done by automatic means. The second approach would maximize the crew EVA role to encompass as many activities where EVA could provide a performance benefit, e.g., assembly of large structures.

In actual space operations, the crew participation will most probably proceed from the former to the latter in a series of sequentially and logically planned experiments dealing with first, baseline human performance evaluations, developing secondly into planned assistance and finally expanding into full crew participation.

Table 1 identifies the potential EVA role associated with each of the various assembly techniques.

TABLE 1. IDENTIFICATION OF EVA POTENTIAL

ASSEMBLY TECHNIQUE	EVA ROLES
MODULAR	MODULE POSITIONING, ALIGNMENT AND ATTACHMENT
ERECTABLE	ERECTION MONITORING
EXPANDABLE	ADJUSTMENT OF ELEMENTS
FORMED IN PLACE	THERMAL JOINING
CHEMICAL RIGIDIZING	MECHANICAL FASTENING
COMBINATION	OPERATION
	MODIFICATION
	MAINTENANCE

From the table it may be seen that a number of fundamental EVA tasks have been synthesized from a review of the assembly techniques and the joining operations associated with these techniques, i.e., welding, brazing, metal fastening, adhesive, and pyrotechnic, as well as the specific mission requirements.

These fundamental EVA tasks reduce themselves to the following:

Module Positioning, Alignment, and Attachment - This consists of emplacing modules into predetermined locations and mechanically attaching the modules until the complete structure is realized. For example, in the construction of an antenna, segmented panels could be employed around the center in a sequential modular fashion until the complete antenna is constructed in the manner of the D-23 Experiment (Reference 2).

Erection Monitoring - Erection monitoring consists of flying off the spacecraft with either the remote or manned unit to positions which can observe a deployment sequence of a fragile automatic erectable structure.

Adjustment of Elements - In the case of either modularly or self-erecting structures, adjustment made by mechanical or cable type alignment techniques to maintain the accuracy and/or position of the structure.

Thermal Joining - The thermal joining consists of welding, brazing, soldering, or thermal adhesive setting of the elements into the appropriate position of the structure to be assembled.

Mechanical Fastening - This task consists of mechanically joining any segment module, or complete structure, with variety of fasteners while EVA.

Modification - EVA can provide modifications if necessary under certain conditions. For example, to change a frequency spectrum of a given antenna, it would be desirable to change or modify that antenna feed.

Maintenance - Extensive studies (References 3, 4, 5 and others) have established the utility of maintenance tasks for extended duration missions. For example, periods greater than 90 days will require routine operation such as refueling and replacement of solar cells as well as in-orbit repair of malfunctioning equipment.

EVA REQUIREMENTS AND EQUIPMENT

Having briefly addressed the potential role EVA has in conjunction with orbital structures it is appropriate to discuss the operational context of EVA, i.e., the requirements imposed by EVA, and their associated equipments.

Before presenting the equipment requirements, it is desirable to review the EVA crew capability and constraints.

The astronaut's ability to perform manual tasks is significantly influenced by his pressure suit, thermal/meteorite garment and restraint devices. Perhaps one of the most important factors in the design of the successful mission is the understanding of the astronaut's physical limitations when operating in the orbital environment.

Figure 2 presents some pertinent characteristics regarding astronaut capabilities and limitations in a full pressure suit which are primarily guidelines in defining the ability to perform extravehicular tasks. These are based upon results of a recently completed study of the EVA support of the Apollo Experiment Pallet (Reference 6) in which special consideration was given to crew capabilities and limitations within a full pressure suit. Definition of suit constraints, with regard to visibility, accessibility, mobility and manual dexterity received primary emphasis. In addition, the requirements of devices to enable surface locomotion and to minimize danger of suit damage during the performance of extravehicular tasks were investigated. Grasp and reach limits shown are based on the use of the ILC Block II suit. A number of other mobility and dexterity restrictions of interest for EVA operations associated with orbital structures, may be found in Reference 6.

Some of the more pertinent equipment items which have been identified for EVA across the spectrum of orbital structure utilization are summarized in Table 2. These are subdivided across the primary equipment such as personnel life support packs and space suits, EVA secondary support equipment common to all missions such as handrails for surface locomotion, and finally mission support equipment which would

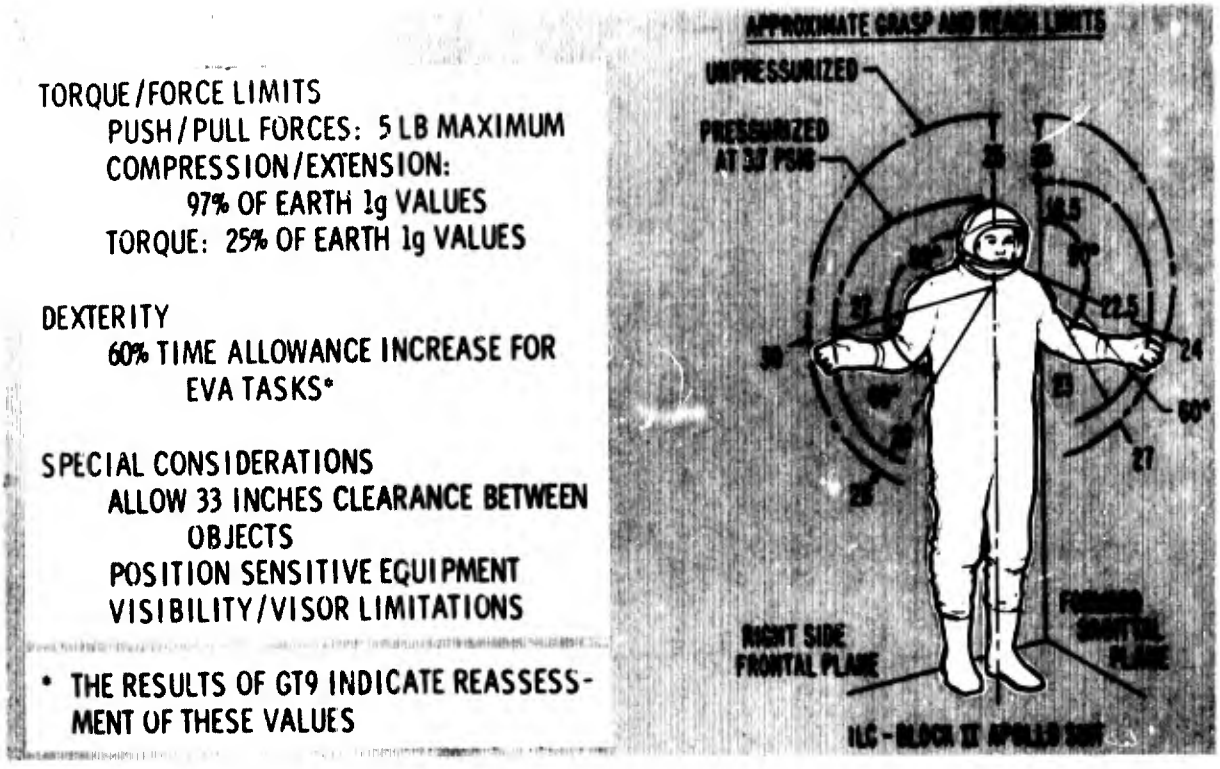

Figure 2. Astronaut Capabilities and Limitations in a Full Pressure Suit

TABLE 2. POTENTIAL EVA EQUIPMENT

	EVA EQUIPMENT	FUNCTION	WEIGHT (LB)	VOLUME (FT^3)
PRIMARY SUPPORT EQUIPMENT	• EXTRAVEHICULAR SUIT			
	SOFT	ASTRONAUT PRESSURIZATION AND PROTECTION	37.9	4.5
	HARD		64.6	8
	THERMAL/METEOROID GARMENT		20.0	1
	• LIFE SUPPORT			
	PORTABLE ECS	LIFE SUPPORT	64.5	2.8
	UMBILICAL		30.0	1.5
SECONDARY SUPPORT EQUIPMENT	• EGRESS/INGRESS			
	AIRLOCK		100	9
	HANDHOLDS		0.5	
	• LOCOMOTION DEVICES			
	HANDRAILS		0.25 LB/FT	
	TETHER	SURFACE LOCOMOTION	8	0.3
	HAND-HELD MANEUVERING UNIT (HHMU)		5	1
	REMOTE MANEUVERING UNIT (RMU)	OFF THE SURFACE LOCOMOTION	132	5
	ASTRONAUT MANEUVERING (AMU)		176	5.8
	DUAL MANEUVERING (DMU)		177.9/241.8	6
	SHUTTLE/MANIPULATOR UNITS (IMMU)		1800	175
MISSION SUPPORT EQUIPMENT	• OTHER SUPPORT EQUIPMENT			
	RESERVICING UNITS	MANEUVERING UNIT, LIFE SUPPORT, AND POWER RE-SUPPLY	475-835	3
	CAMERAS		2	0.25
	LIGHTING PROVISIONS		2-6	
	TOOLS AND JIGS		10-15	1
	CARGO TRANSFER EQUIPMENT	SPECIAL WORK	6	0.25
	MEDICAL KIT	SITE ACTIVITY	2	0.2
	RESCUE DEVICES		20	2-4
	WORK SITE ANCHORING DEVICE		4-15	1
	TV CAMERA		6	0.25

TABLE 2 POTENTIAL EVA EQUIPMENT

be required to support a particular mission. Also delineated in the figure are the pertinent characteristics of each of the equipment items.

Perhaps the most significant item that can be drawn from this table is the EVA compliment of maneuvering units. These units serve multipurpose functions in the support of large structures.

Studies, conducted in Reference 7 identified some 52 potential missions for maneuvering units. Some of these EVA mission include the following:

Antenna support operations

Telescope support operations

Plasma wake investigations

Coronograph alignment

Radiation studies

Physiological/psychomotor studies

Behavioral studies

Assembly of large structures

Astronaut transport

Remote maneuvering investigations

Crew rotation

Cargo transfer

Propellant handling

Maintenance of spacecraft

Space rescue

Equipment retrieval

Deployment aid

The candidate maneuvering units for the accomplishment of these missions (as shown in Figure 3) are:

HHMU (Hand Held Maneuvering Unit)

AMU (Astronaut Maneuvering Unit)

RMU (Remote Maneuvering Unit)

DMU (Dual Maneuvering Unit)

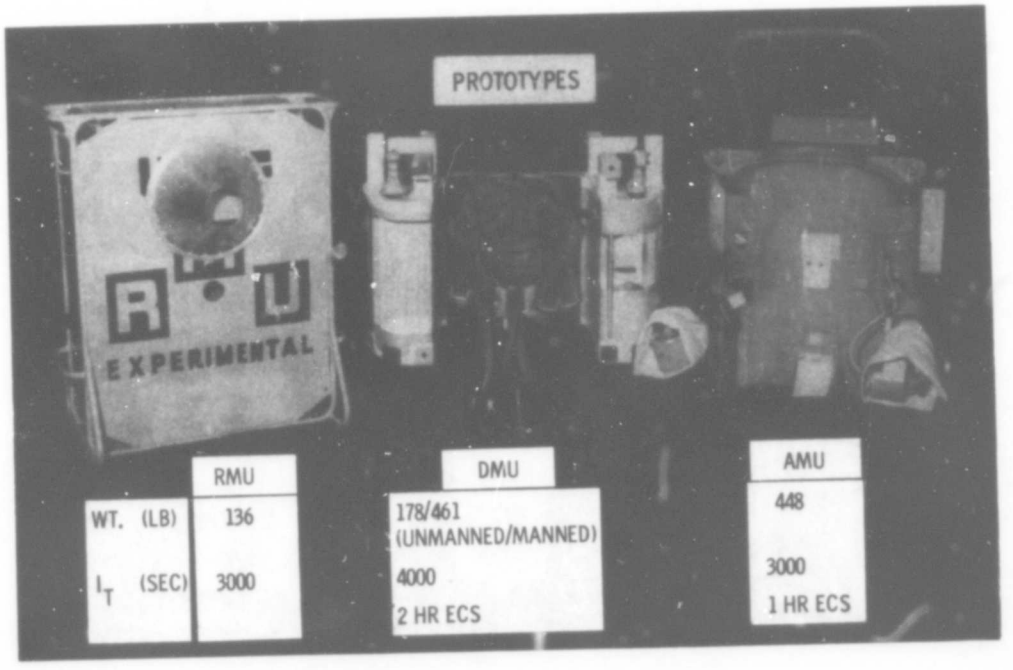

Figure 3. EVA Maneuvering Units

The missions cited were compared on a common performance basis for all the maneuvering units. The principal criteria for selection of an operational maneuvering unit are: mission effectiveness (i.e., the ability of a system to accomplish a given mission and number of missions performed), and cost effectiveness. Certainly, from an operational viewpoint, the mission effectiveness should predominate. In reviewing the candidate units (Figure 4) it may be seen that the HHMU and the AMU can only perform the manned operations. The RMU, only the remote, while the DMU can perform both manned and remote missions ... i.e., the DMU synthesizes the capabilities previously distributed between the Astronaut Maneuvering Unit (AMU) and the Remote Maneuvering Unit (RMU)

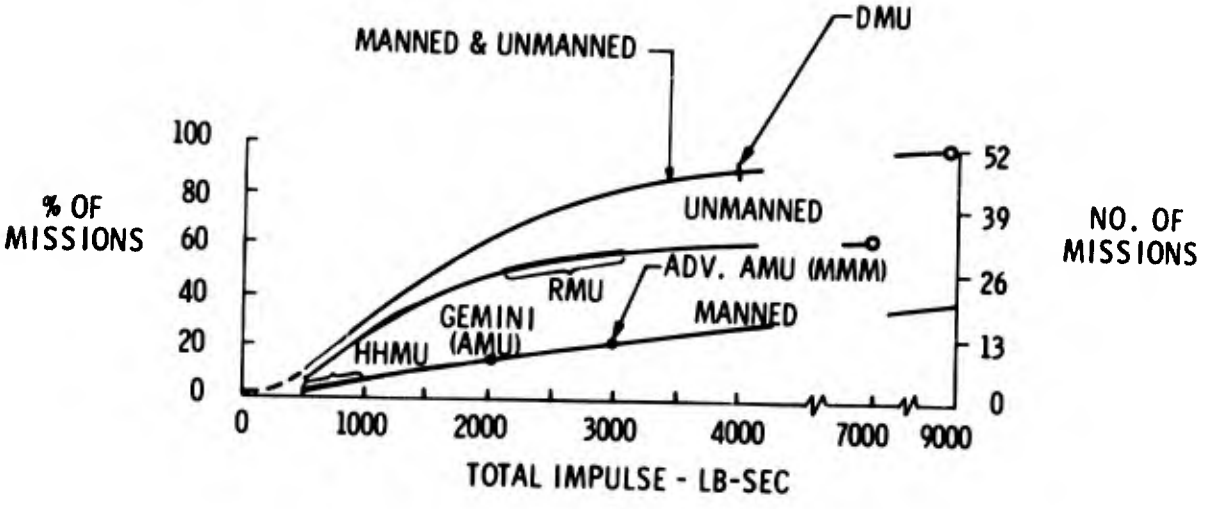

Figure 4. Maneuvering Unit Mission Capability as a Function of Total Impulse

Therefore, in considering the alternatives, either some of the mission requirements must be abrogated or a separate AMU and RMU type vehicle must be compared against a single Dual Maneuvering Unit. It was found in studies of Reference 7, that a Hand Held Maneuvering Unit could not meet the fine control requirements of the missions. Similarly, it was found that with only a small increase in propellant load (~5 lb) the DMU could perform all the AMU and RMU missions with the same degree of precision.

Therefore, as may be seen in Figure 4, the DMU can operationally achieve far greater mission flexibility with no significant degradation in performance. Referring to Figure 4, it may be seen that the DMU can perform 93% of the missions as opposed to 60% for the RMU and 22% for the AMU.

One of the missions of predominate interest is astronaut rescue, which recently was simulated in a KC135 zero-g aircraft flight. If an astronaut working extravehicularly becomes incapacitated, the Dual Maneuvering Unit could be sent out to capture the astronaut and remotely return him to the spacecraft. Some structure and/or container would be required to capture the passive astronaut. If the astronaut becomes

incapacitated while wearing a DMU, it could be remotely commanded back to the parent spacecraft by the pilot in the spacecraft. If the astronaut has simply drifted away from the parent vehicle, the DMU could be sent out unmanned from the vehicle without endangering the remaining astronaut. The stranded astronaut would don the unit and return to the spacecraft. This rescue mode has been simulated in the KC 135 shown in Figure 5. For this test, a remote control package was added to the Gemini D-12 training unit giving it the capability of "flying" as a DMU.

A. Remote Control Station

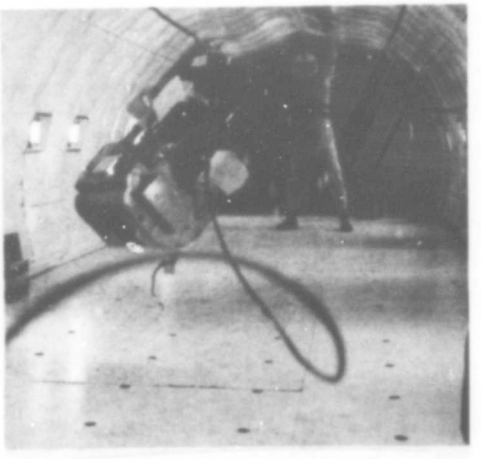

B. Remote Mode Outbound

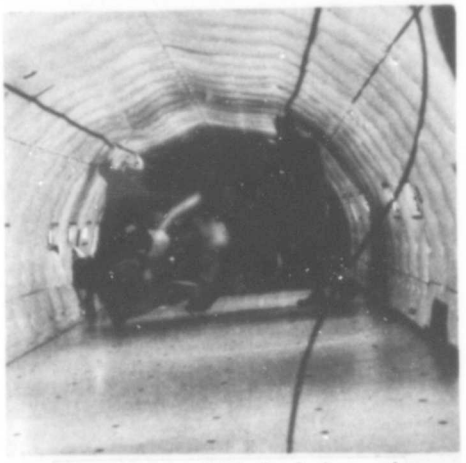

C. Manned Mode Inbound

D. Return Completed

Figure 5. DMU Rescue Simulation

EVA SUPPORT STRUCTURES

In addition to identifying the potential support role of EVA in conjunction with large structures, it is appropriate to consider what structures will be required to support EVA. Figure 6 depicts some of the potential EVA support structures, such as airlocks, restraint devices, and support structures. This section of the paper is a brief discussion of some of the more pertinent EVA support structures.

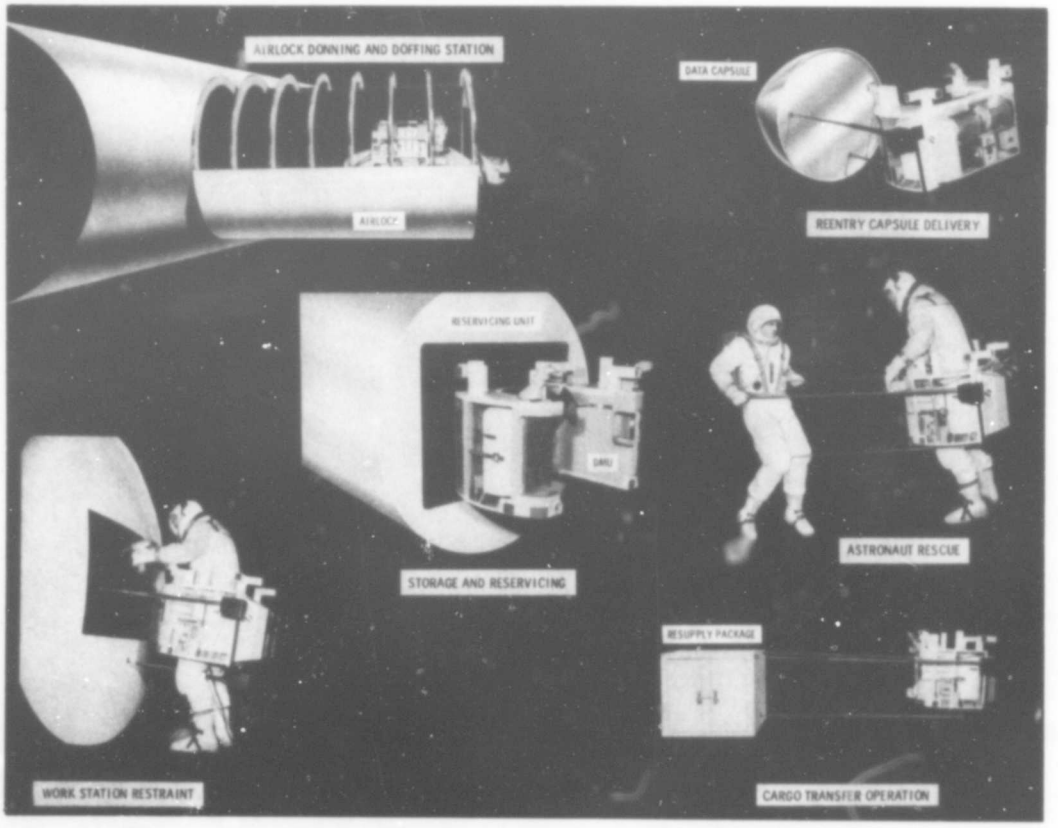

Figure 6. EVA Support Structures

EVA EGRESS/INGRESS

Considering EVA excursions for the performance of any "outside" task, it is necessary to establish the most effective method for astronaut egress/ingress. The penalty associated with the inherent requirement of spacecraft egress/ingress hardware is often overlooked in the evaluation of EVA mission performance.

There are several methods available to satisfy the egress/ingress requirements. They are: (a) vent the entire cabin as in the Gemini program, (b) pump and store the

cabin oxygen for rescue, (c) add an airlock. A preliminary weight tradeoff was conducted based on the assumption that the atmosphere is 100% oxygen at 5 psia and 75°F. The results are present in Figure 7 which gives the total system weight as a function of the number of EVA excursions. A nominal volume for any one compartment of a space laboratory was assumed to be 1000 feet^3, included. To calculate the system weight when the cabin atmosphere is vented overboard and then repressurized from the ECS oxygen supply, the additional oxygen was determined and 20% of this value was added to account for the increase of the ECS oxygen tank weight.

It should be pointed out that the cabin remains unpressurized during the EVA which may be undesirable for long duration excursion times. If it is necessary to repressurize between egress and ingress, the effective number of excursion is increased by a factor of two.

The pumping approach was based on the assumption that 90% of the cabin oxygen was compressed and stored for reuse in a pressure vessel. The electrical power to drive the compressor was assumed to be 0.0075 pounds of fuel cell expendables per cubic foot of cabin volume. A weight of 30 pounds was used for the pump and 20% of the weight of the make-up oxygen was alloted for the larger ECS tank. The weight of a stored oxygen vessel was assumed to weight 40% of the stored oxygen since this oxygen would be stored in a gaseous phase.

The airlock system is based on an SIVB workshop experiment (D-21) sponsored by the Air Force Aero Propulsion Laboratory (Reference 8). The expandable airlock

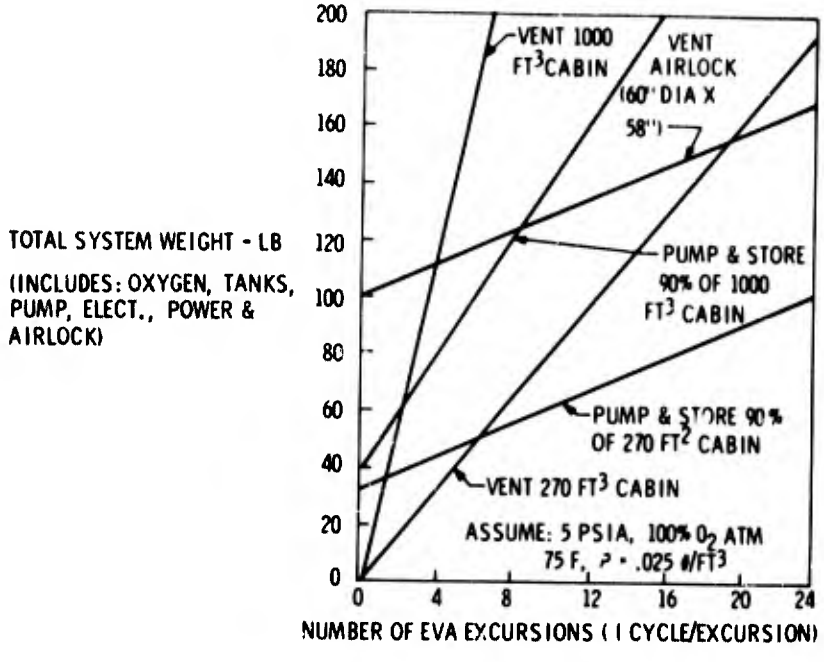

Figure 7. System Total Weight vs. EVA Excursions

(60 inch diameter x 58 inches) has a projected operational weight of 100 pounds including all the hardware necessary to activate the airlock.

Analysis of Figure 7 shows that for up to 20 EVA excursions, utilization of the Apollo vehicle (270 ft^3) as the depressurization chamber has a weight advantage over a vented airlock. The break-even point is reduced to 10 excursions if repressurization is required between egress and ingress. There are disadvantages associated with using a command capsule (Apollo-Gemini) such as a depressurization chamber. They are: (a) lengthy and sometimes difficult operating procedures, (b) size constraints. Also, the continuous operation of a command capsule of an airlock could jeporadize the later use of the vehicle for reentry.

The basic laboratory compartment of 1000 ft^3 could be subdivided to serve as an airlock, with the airlock being a compartment on the order of 300 ft^3. In this case, the weight of the added bulkhead must be added. This would unduly penalize this approach.

If more than six EVA transfers are required, the pump and store approach has a weight advantage over venting the cabin. However, the added system complexity and hazard of pumping oxygen in space may offset the weight advantage. An overall evaluation of the egress/ingress approaches indicate that for more than four EVA transfers a small lightweight airlock would be strongly considered. Analysis of the role of extravehicular operation in the support of space structure assures that several excursions will be required. A detailed discussion of an external lightweight airlock has been given in another paper of this conference (Reference 4) and, therefore will not be pursued here. However, once an external airlock is projected to support EVA egress/ingress, it appears that other extravehicular operations may be included by modification of the basic airlock design. The airlock could serve as a storage and reservicing station for maneuvering units, as a launching and docking boom, as a cargo container and possibly as a rescue/retrieval device and a reentry capsule.

ATTACHMENT/RESTRAINT SYSTEM

The second exemplative EVA support structure is that of a modular attachment system. The success of the Gemini XII in performing EVA tasks has been largely attributed to the development of adequate work area restraints (Reference 9). The relative ease with which Major Aldrin accomplished his EVA tasks was in contrast with previous Gemini extravehicular operations where the lack of adequate restraints appears to have been a major factor in producing excessive work loads on the astronaut.

Proper restraint systems hold the astronaut in position at the work site, thereby relieving him of the exertion of counteracting body forces and torques inherent in the task. They also allow the astronaut to completely relax during the necessary and frequent rest periods. Without restraints the astronaut must continue to exert himself during rest periods simply to prevent drifting out of position because of the ever present physical disturbances. The development of adequate restraint systems are a definite step in the evolution of EVA as a useful and effective operational tool. One restraint device which was considered for utilization with the DMU was the stem attachment

system shown in Figure 6. This is a modular system consisting of three stems, with suitable attachment mounts. The concept was developed to provide a variable length attachment system between the extravehicular astronaut and his work site (Reference 10). The concept is shown in Figure 6 coupled to the DMU. Once the concept is coupled as a module to the DMU, other potential uses may be postulated. Figure 6 also depicts four potential uses of a STEM coupled to the DMU - docking, retrieval, cargo transfer and reentry.

The remote mode docking procedure would involve extending the STEM to about eight feet and positioning the DMU so that the ends of the STEMS can be guided into three conical shaped receptacles. After attachment is insured, the STEMS are retracted which brings the DMU into positive connection with the reservicing system. To launch, the procedure would be reversed. Manned-mode operation could follow much the same procedure.

The STEM system could be used to secure a cargo package for mass transfer missions and in rescue operations where the astronaut would be secured at a safe distance from the maneuvering unit exhaust plume. Recent simulation tests at Bell Aerosystems Company have demonstrated cargo transfers capability with the Dual Maneuvering Unit. These tests evaluated the influence of payload size (400 lb) and location for a short range (400 ft) mass transfer task. Successful transfers were accomplished with the payload c.g. at a distance of five feet from the maneuvering unit c.g. along the longitudinal axis.

The return from orbit of components and data (e.g., biological specimens) analysis without costly premature deorbiting of the parent vehicle is a desirable capability. One approach to this mission utilizes the DMU to align and stabilize the reentry capsule prior to retrothrusting. Using the DMU TV system and radar, the desired reentry angle is achieved by aligning with the stadiometric markings on the parent spacecraft. This can be accomplished too, with $\pm 1^{\circ}$ (Reference 7). The DMU will hold this stabilization to 1.5° of the desired angle. The DMU is then used to rotate the reentry capsule to provide spin stabilization, and in the case of small packages ($<$ 30 lb) the retro thrust.

EVA COMPARISON

Having identified the potential EVA roles (Figure 2) associated with orbital structures, it is appropriate to look at EVA with respect to its effectiveness. However, before making a direct comparison, it is appropriate to point out a number of pertinent facts. The first is that in general, for most of the missions projected for the 1970's and beyond, the crewman will be on board so that the justification for the existence of the crewman and for his EVA activities is not specifically contingent upon any given experiment or operational mission. Therefore, a one to one comparison between EVA and alternate techniques for accomplishing the tasks is not readily achievable, but rather EVA effectiveness should be ascribed proportionally to all of the tasks performed. Further EVA effectiveness is contingent upon the crew capabilities in a full pressure suit as well as the effectiveness of the EVA equipment supplied. To illustrate these facts, an example has been selected which develops the above points.

The example selected in this paper is the assembly support, calibration and maintenance of a large antenna in earth orbit, as will be required for limited area communications, point to point communications, and millimeter wave radio astronomy. Figure 8 is a schematic depicting EVA antenna support operations.

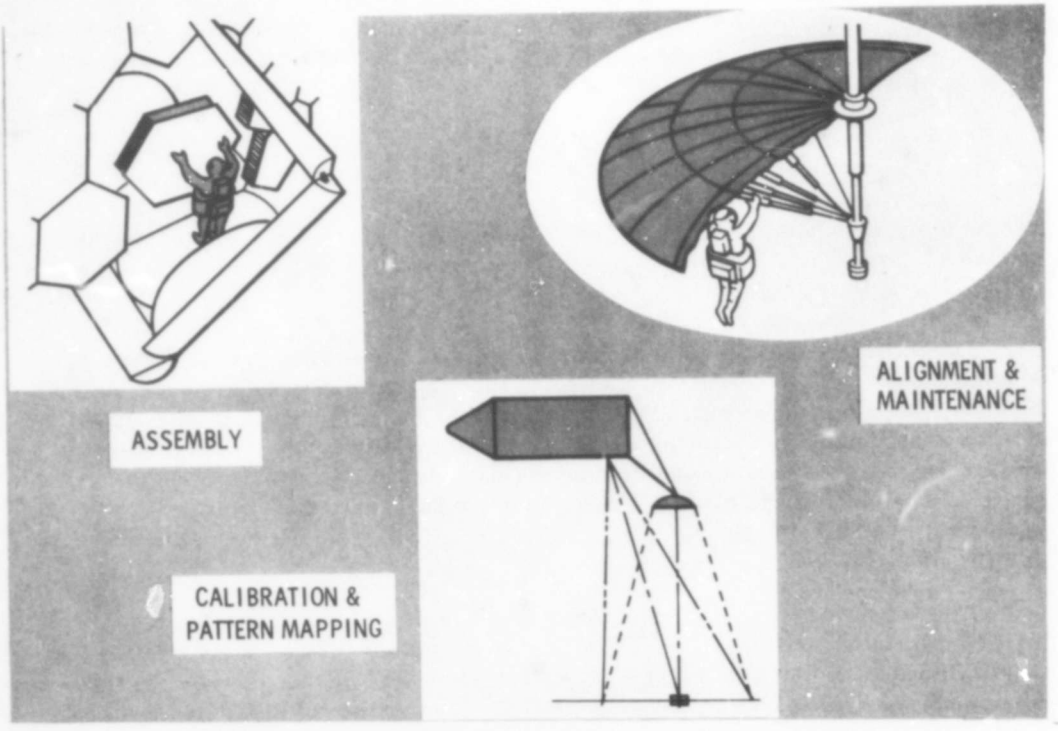

Figure 8. EVA Antenna Support Operations

In-orbit operations are required in order to achieve the large apertures (approximately 100 ft) necessary for these missions, specifically, to determine the boresight axis, beam pattern and field strength of the antenna to verify its operating characteristics, and pointing capability and subsequent in-orbit adjustments of the antenna to maintain the proper surface contour. This is particularly true in the astronomy missions wherein calibration on a known source is necessary.

Figure 9, gives a first approximation of antenna characteristics and required manufacturing and assembly tolerance (K). A K of 1/4000, means that the antenna diameter, surface variation, and relative position of the feedhorn to reflector shall have a mean deviation from nominal values not to exceed one part in 4000. Atpresent, earth manufacturing tolerance is limited to about 1/4000.

High frequency operation will impose severe dimensional tolerance requirements of the order of 0.01 inch rms surface deviation. Referring to the figure, it may

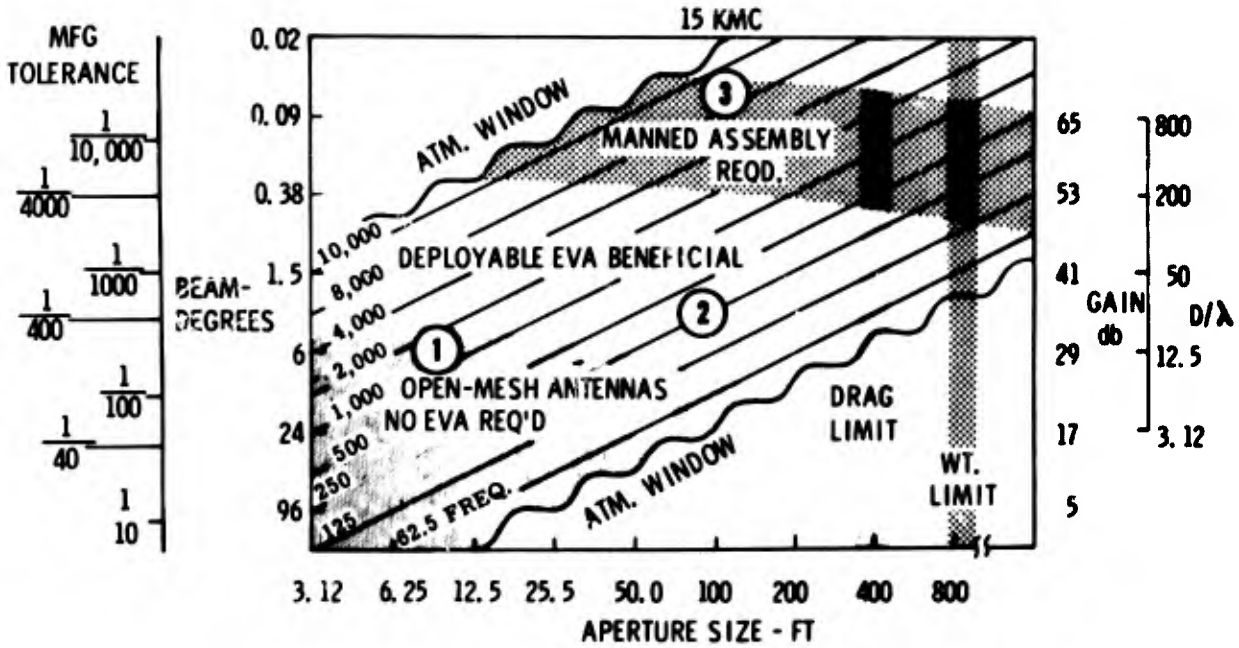

Figure 9. Comparison of EVA for Antenna Assembly

be seen that zone 1 defines the range of values for which expandable open mesh structures may be utilized. Zone 2 defines where deployable structures may be utilized, but EVA is useful for alignment, and maintenance of surface characteristics as well as deployment aids. The open mesh antennas should be limited to openings of $\sim \lambda/8$ or smaller, 7500 MHz or higher. In addition, increases in aperture cause increased difficulty in maintaining surface tolerance over the entire diameter of the structure due to thermal cycling and vibrational problems. The division between zones 1 and 2 is badly defined because of these problems. Zone 3 includes an antenna requirement which necessitates improved earth manufacturing techniques and very careful assembly of modular panels with accurate calibration by extravehicular operations. Analysis shows that as antenna pointing and gain requirement becomes more stringent, greater direct EVA participation is necessary. Zone 3 includes antenna requirements which necessitate careful assembly of modular panels and accurate calibration by extravehicular operations. As may be seen, pointing accuracy may be increased through decreasing beam, and increasing D/λ, hence, a direct benefit may be attributed to EVA.

In order to accomplish the antenna support operations, both manned and remote mission subtasks are required. Assembly and alignment require manned operations, while calibration and pattern mapping require remote operations. The antenna assembly operations will only expend a Δ V of ~50 ft/sec, while the alignment and maintenance operations will expend approximately 250 ft/sec Δ V for maneuvering.

In order to perform this mission, as with all missions, certain unique mission payloads are required. Therefore, it is necessary to examine the effectiveness of the EVA associated equipment as well as the task. In this case, the equipment require-

ments are as follows: for manned assembly, alignment and maintenance an integrated tool kit approximately 16 in. x 10 in. x 8 in. in size and weighing 24.7 lb. In the case of pattern mapping and calibration it is necessary to add a maneuvering unit and a transmitter-receiver package, and pattern mapping antennas, the total package weighing approximately 16 lb, plus the basic maneuvering unit weight.

Certain equippage will also be required on the parent spacecraft such as an automatic tracking scope or a cooperative radar for accurate position determination of the maneuvering unit.

In addition to investigating the mission effectiveness, it is important to assess the cost effectiveness. One such comparison of an EVA system has been conducted on the DMU. Figure 10 presents a cost and weight breakeven comparison for the DMU as opposed to separate AMU and RMU vehicles conducting a representative mission set defined in Reference 7.

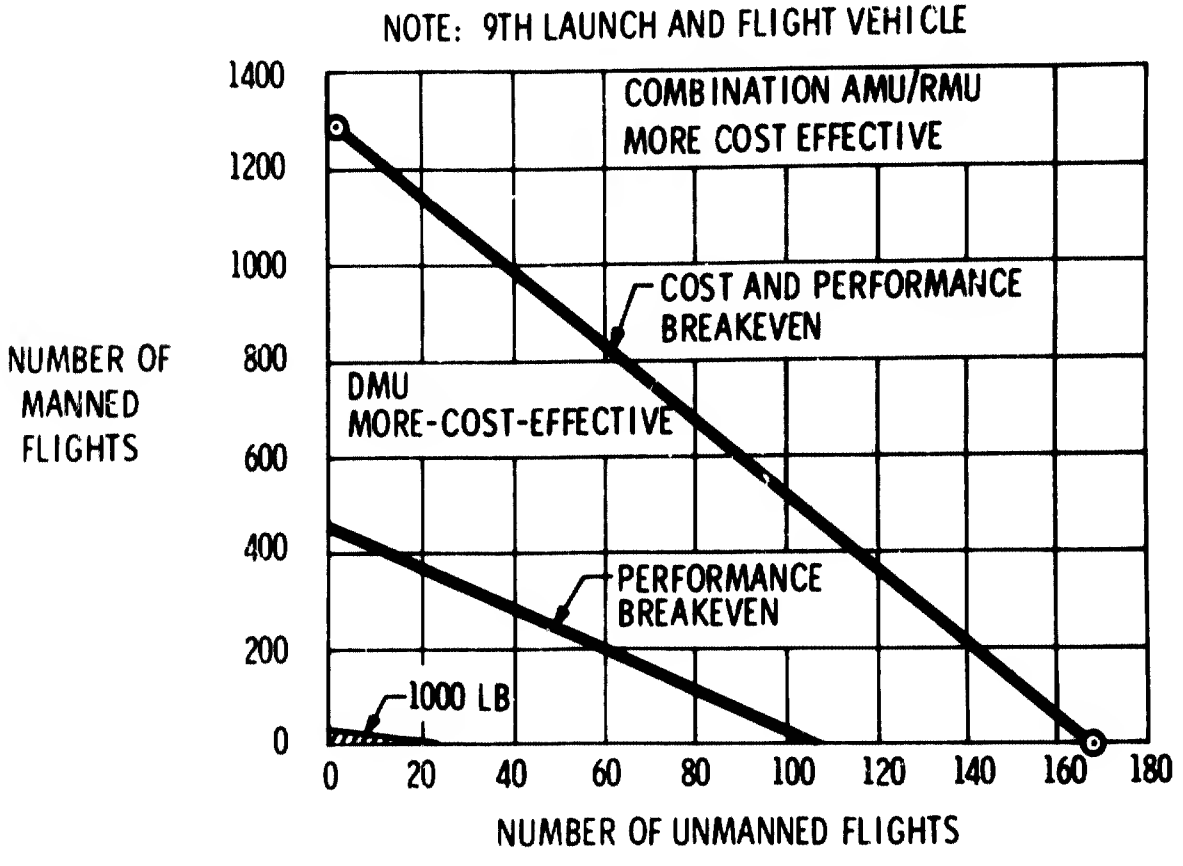

Figure 10. DMU Effectiveness Comparison

As may be seen in the figure, a great number of flights must be conducted on a given parent spacecraft launch, for example, approximately 200 manned and 60 unmanned for a weight breakeven and an even greater number, approximately 600

manned and 90 unmanned for the cost breakeven. Also spotted on the curve is the region of probable maneuvering capability in terms of available payload weight of a typical parent spacecraft. The region depicted upon the curve represents 20% of the nominal payload available or 1000 pounds. The system weight includes both initial weight of all systems (vehicle, reservicing, retrieval devices, etc.) and weight of fuel expended. Weight breakeven represents the number of flights at which the initial advantage of the DMU lower system weight is compensated for by the relatively higher fuel consumption rate of the DMU compared to the AMU and RMU.

The foregoing discussion has attempted to establish the value of EVA for certain antenna operations and the effectiveness of the DMU as an EVA maneuvering unit.

SUMMARY AND CONCLUSIONS

In order to interrelate the items previously discussed in this paper, it is appropriate to show an integrated mission profile. Figure 11 presents an integrated profile for EVA support of an antenna system, as well as the EVA requirements in terms of manned, and remote operations necessary to fulfill that particular mission.

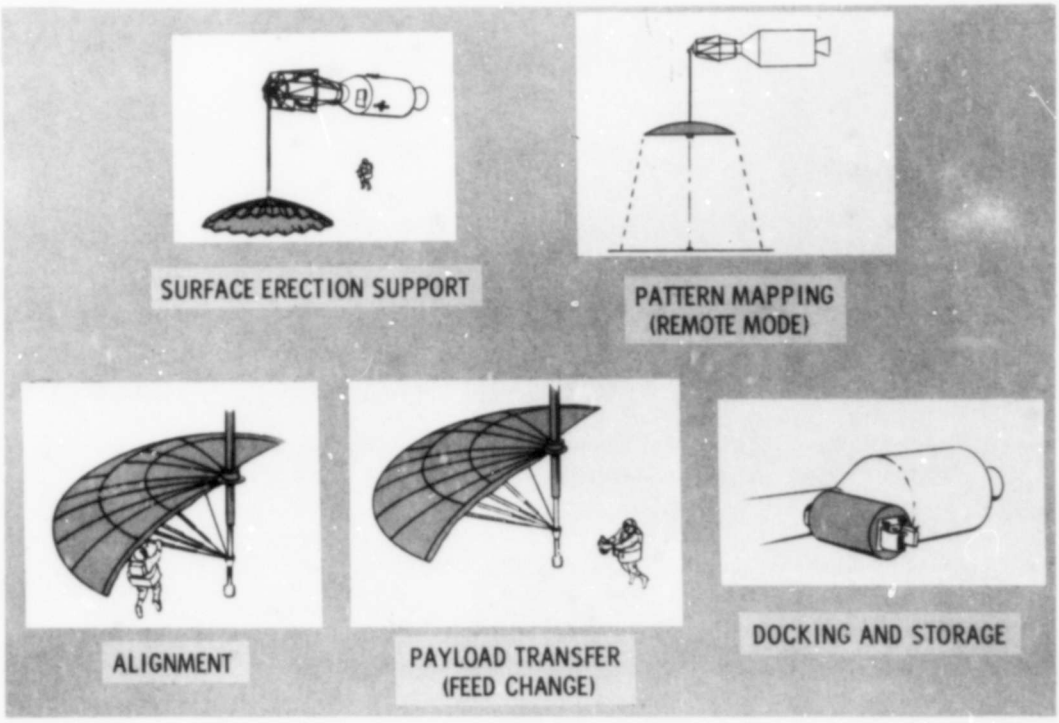

Figure 11. Integrated Mission Profile

In conclusion, this paper has attempted to define in a general fashion the role of EVA in the support of erectable structures and has reached the following specific conclusion:

(1) A number of potential roles have been identified for EVA in support of orbital structures.

(2) EVA provides, in certain mission applications, effective support for orbital structures.

(3) EVA requires a number of support structures, such as Airlocks and maneuvering units.

(4) Maneuvering units offer substantial benefit to EVA orbital operations involving large structures.

(5) Under the certain conditions, the DMU represents both a mission and cost effective maneuvering unit.

While some of the items discussed in this paper are in fact preliminary in nature, and not operational hardware, it is anticipated that in conjunction with increased earth orbital mission capability the role of EVA also will be expanded substantially.

REFERENCES

1. General Dynamics, Large Space Structures Experiments for AAP, Mid-Term Presentation, March 1967.

2. Forbes, F., Huie, R., et. al. "Modular Assembled Antenna Experiment for the SIVB Workshop" 3rd Aerospace Expandable and Modular Structures Conference, May 1967.

3. Seale, L. M., Bailey, W. E. and Powe, W E., "Study of Space Maintenance Techniques", ASD-TDR-63-931, May 1966.

4. Proceedings of the National Conference on Space Maintenance and Extravehicular Activities, AFAPL, March 1966.

5. Griswold, J W., and Schnuder, R. E., "Exploiting the Reliability - Maintenance Relationships for Manned Mission of Extended Duration", October 1964.

6. Stewart, R A., et. al., "Apollo Experiments Pallet Extravehicular Operations Study, Final Report", Bell Aerosystems Company, Report 7276-945001, March 1966.

7. Stewart, R. A., et. al., "A Study of a Dual Purpose Maneuvering Unit, Final Report" AFAPL-TR-67-32, April 1967. (Title Unclassified) Report Secret.

8. "Expandable Airlock Experiment for the SIVB Workshop", Cormier, A., Forbes, F., et. al., 3rd Aerospace Expandable and Modular Structure Conference, May 1967.

9. NASA/MSC, Gemini Summary Conference Slides, February 1967.

10. DeHavilland, "Boom Attachment System", AFAPL-TR-67-14, April 1967.

BLANK PAGE

AUTOMATICALLY ERECTABLE TOWERS AND MASTS (AUTO-MAST)

J. C. Bell[a]

INTRODUCTION

The development of the auto-mast design concept is really the first major achievement in making inflatable masts and towers practical. Previously, handling and erecting long slender inflatable masts more than 100-ft high essentially were impossible, and anything more than 50-ft was extremely impractical. The auto-mast does not have this severe height limitation. A 300-ft LF antenna tower for a long-range navigational aid (LORAN D) is being studied, and a computer program capable of studying much greater heights has been set up. The ultimate height limitation is not known and apparently does not depend on the erection system but only on the structural design.

The extreme height is achieved by a unique building-block feature. During erection, each section of the mast is permanently fixed and secured by guy cables while it is being deployed. In this manner, the lower sections are completely stabilized before proceeding to the next higher sections.

The primary function of the auto-mast is to provide an easily erectable and retractable mast that can elevate and adequately support a payload at any intermediate height up to its fully erectable height or length. The auto-mast's function can be modified somewhat to fit a specific application.

The auto-mast design concept has evolved and progressed as a result of much work in company-supported programs as well as in contracts. Most contract work has been directed toward lightweight, manpack LF, HF, VHF, and UHF communications antenna mast applications. As an example, 60-ft VHF-UHF antenna masts for the Air Force recently have been tested under actual jungle conditions in Vietnam. This 60-ft mast can be erected or packaged in as little as 15 min; the complete unit is designed to be carried by one man in a backpack.

Most of the previous masts have been made of fabric; however, steel panels now are being used in the large tower designs. Steel greatly stiffens and strengthens the mast. A 150-ft tower that uses this new steel-reinforced concept is now being fabricated. This tower will be used in the present study of a 300-ft LORAN D tower.

The automatically erectable mast design also is being applied to (1) sea stilts, (2) automatically extendable causeways or bridges, (3) elevator scaffolding, (4) observation towers, and (5) space structures. The sea stilts program is a

[a] Aero-Mechanical Engineering Division (research and development).

current contract to design and develop automatically extendable vertical floats. Two contracts have been awarded on space structure applications. The remaining programs are company-funded studies.

In most areas, Goodyear Aerospace has resolved the primary problems and is working on secondary problems. Some of the more important inventions and developments significant to auto-mast work are:

1. The auto-mast design concept
2. A variable modulus construction design that greatly improves the mast shear stiffness while at the same time maintaining the flexibility needed for retraction and packaging
3. Highly durable lightweight fabric material
4. Substantial improvements in manual and automatic pressurization systems

This paper discusses the Goodyear Aerospace design concept. Concept features include:

1. Structures normally weigh less than other masts for comparable requirements.
2. Each mast is a self-contained unit, including power supply for pressurization and retraction.
3. Package size is smaller. The ratio of package volume to material volume is less than 2 to 1. A 3-to-1 ratio is required for most vacuum-packed inflatable devices, and a considerably higher ratio is needed for foldable metal structures.
4. Minimum erection and retraction times are provided. A completely automatic system can be provided; however, semiautomatic systems normally are the best compromise. Extension rates are up to 100 ft per minute; times and rates depend on size, configuration, and pressurization.
5. Complete erection is possible in a relatively high wind.
6. Masts are easy to repair and maintain, with few spare parts required. Major components can be replaced easily.
7. When used as an elevator, masts can raise a relatively heavy payload to the fully extended height of the mast and maintain the load at that or any intermediate elevation.

8. Being fabric, the masts present a minimum radar cross section, since they are thin-wall dielectric structures relatively transparent to RF energy. When needed, they can be metallized to increase the radar cross section or to function as the antenna radiator itself.

9. Building block feature to permit great heights.

The complete mast with guys is packaged in a minimum-volume, lightweight, portable container, which serves as the base for the mast structure. In operation, the mast rises automatically from its base container when internal pressure is applied. The retraction system reverses the erection operation as in vacuum packaging and lowers the mast into the base container.

Many masts and towers use their own air-compressor systems to maintain internal pressure automatically. Any pressure source can be used. For ultralightweight masts, Goodyear Aerospace has developed an eight-ounce manual pump.

The mast operation either can be semiautomatic or automatic for a particular application. Semiautomatic operation would be used mostly in ultralightweight, portable masts, while complete automatic operation would be required for post-attack applications.

BASIC DESIGN CONCEPT

Figures 1 through 4 show different examples of Goodyear Aerospace's automatically erectable mast design. Regardless of the specific mast application, the basic configuration consists of the mast assembly, base assembly, reel mechanism deployment and erection system, pressurization system, guy assembly, and elevator platform (when needed). The antenna masts will be used mostly to describe the design concept since most of the development has been performed.

Under an internally funded program, Goodyear Aerospace has initiated a computer program to analyze inflatable mast designs thoroughly. The basic program has been set up, and initial computer runs have been made using the design parameters for the 300-ft mast.

Mast Assembly - The mast utilizes a tapered tubular envelope having a variable-modulus cross section. Guy cables are used at appropriate levels to resist wind loads and to prevent buckling or excessive deflection. Structural integrity is maintained, and buckling is prevented by the compression stiffness of the rigid panels as well as by the internal pressure. The internal pressure induces tension in the material to offset compression loading due to bending moments, vertical components of the guy cable loads, and the weight loads of the mast.

The inflatable portion of the mast will be fabricated of flexible structural materials utilizing Goodyear Aerospace's variable-modulus construction approach. The company considers this approach and the company's unique erection and retraction concept as a breakthrough in inflatable mast design. The variable

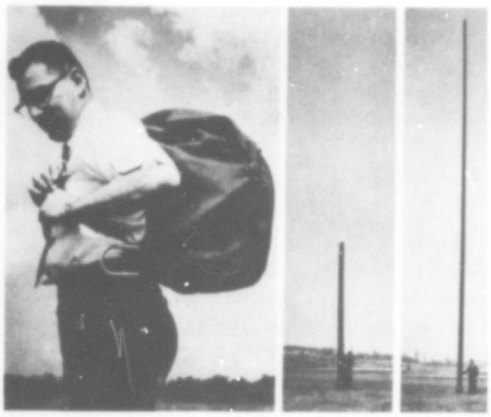

Figure 1 (Above) - Sixty-Foot VHF-UHF Manpack Antenna Mast; Figure 2 (Below) - Top-Loaded LF Antenna Mast

Figure 3 (Above) - Backpack Comparison of 30- and 60-Ft Antenna Masts; Figure 4 (Below) - High-Payload, 50-Ft Inflatable Mast

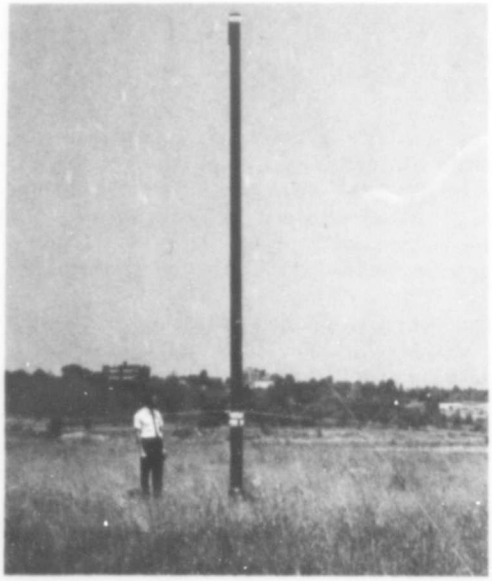

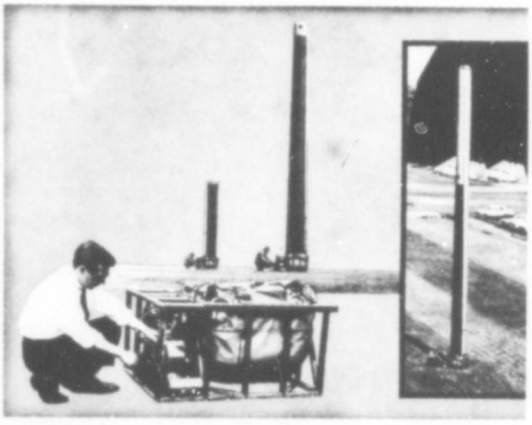

modulus construction approach uses a relatively flexible material to make the tubular section. Mast stiffness is obtained by adding high-modulus panels to make up a large percentage of the mast circumference. These panels can be a series of relatively narrow strips equally spread around the mast with exposed areas of the flexible material in between or can be two wide panels located diametrically opposite to each other.

With this arrangement, the exposed fabric between the stiff material provides flexibility to permit retraction and compact packaging; the stiff material improves the shear modulus of the structure to the point where it is no longer the critical factor, and the bending stiffness (which also is improved) becomes the governing factor. For example, in the 300-ft tower, Goodyear Aerospace will use two longitudinal panels of stainless steel for the high-modulus material. To provide ruggedness and durability, the company proposes to laminate a heavy Mylar film to each side of the steel. A scuff ply of elastomer-coated cloth will be laminated over the Mylar on the outside surface. The width of these panels, which is slightly less than the diameter of the mast, will taper from the top to the bottom. These panels will be located diametrically opposite to each other, with the width parallel to the axis of the reel shaft in the base so the panels roll flat on the reel when the mast is retracted.

These panels will serve a secondary function in that they will be used as the electrically conductive radiating element between the base and the top of the mast. The flexible material of the tubular section will consist of a neoprene-coated multiple-ply Dacron fabric. The bottom of the mast will terminate in an inflatable hemisphere made of the flexible fabric material. Since this material is nonconductive, it will provide the required electrical insulation between the conductive mast and the ground.

Support Base - The base structure of larger masts is usually constructed of a rubberized fabric hemisphere supported by an aluminum tubular framework (see Figure 4). The retraction reel, which stores the inflatable mast and guy lines in the packaged condition, is mounted on bearings supported by the framework. For the lighter masts, the support framework is not provided and uses only the fabric hemisphere (see Figure 5). The reel is contained within the hemispherical base of the inflatable mast; the stub end shafts of this reel extend through the opposite walls of the air chamber, where rubber shaft seals are provided to prevent air loss.

Figure 6 shows that the erection and retraction subsystem is part of the base on the larger masts. The subsystem includes the engine, compressor, gear box, and reel mechanism as well as the control system for operating the mast.

The manpack design simply is a manually operated system and has a double-ratchet arrangement (see Figure 7).

Guy System - The guy system usually consists of three guys spaced radially on 120-deg angles at regular intervals, depending on the height and environmental requirement of the mast. In some antenna systems, the guys can double as top-loading wires or counterpoise wires - for example, the 35-ft manpack antenna (see Figure 8).

The guy system can be made completely automatic with automatic takeup and locking reels. This guy system would be used mainly for relatively permanent site installations, such as a postattack application. In this application, the guys are automatically deployed during erection and reeled in during retraction, thus permitting very rapid operation. The automatic takeup reel operates very similar to constant tension reel, except the reel prevents any length of guy from being pulled back from the reel once it has been retracted.

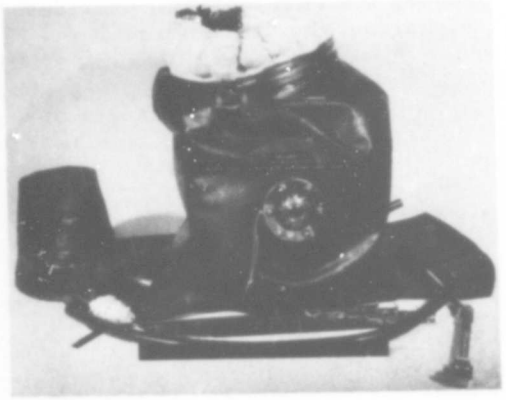

Figure 5 - Sixty-Foot VHF-UHF Inflatable Antenna Mast (Packaged)

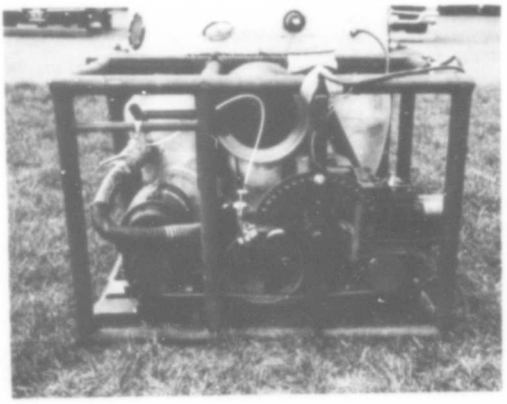

Figure 6 - Erection and Retraction Subsystem

Figure 7 - LF Antenna Mast Model

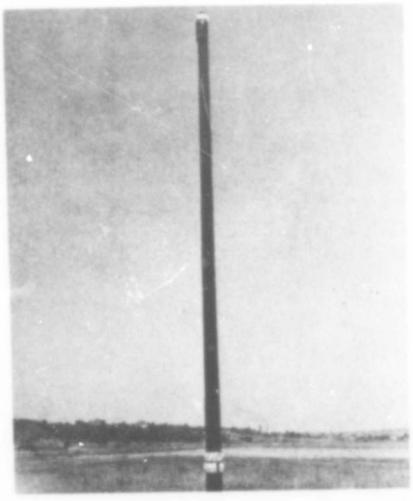

Figure 8 - LF Antenna Mast Model (Fully Erected)

System Operation - Erection and retraction of the mast are controlled by a strap that is attached internally at the top of the mast, extends down through the mast, and is attached to the reel shaft in the base structure. Operation of the reel shaft retracts the control strap, which pulls the mast inside itself until all mast material is rolled on the reel.

The guy cables are permanently attached externally on the mast and are reeled in with the mast. Thus, when the mast is inflated, the guy cables and top-loading

array are automatically deployed with the mast, and it is merely necessary to attach the lower ends to ground anchors and to pretension them.

The erection technique resembles a building block arrangement in that the lower portion of the mast is erected first. This approach allows the lower guys to be deployed first and to be permanently attached to the ground anchors; therefore, the mast is stabilized completely at the lower level before it is erected higher.

Because of this building block arrangement and erection technique, the mast has a maximum attainable height capability limited only by the structural strength that can be built into its walls.

Erection and retraction times vary depending on the application. A manpack mast can be erected or retracted by two men in as little as 5 min, whereas a 300-ft mast is designed for erecting or retracting in about two hours by six men. However, much flexibility is possible, since the limiting factor is the amount of air pressure that can be supplied and the speed with which the guys can be handled. Action of the air pressure automatically extends the mast while it is being inflated; it is retracted by means of a reel in the base.

The erection concept with an exceptional packaging ratio, a 50-ft version of a mast fabricated and tested by Goodyear Aerospace, is shown in Figure 9. This fabric mast averages five inches in diameter and weighs only 2.5 lb (including guy lines but excluding the seven-inch-cube metal base).

When packaged, the guy lines are rolled up on the reel with the mast. When the mast is extended by introducing air pressure, the mast is erected until the lower guys are exposed first. These guys are attached to anchors and adjusted to secure the mast permanently at the lower level before the mast is extended. This procedure is repeated with subsequently higher levels until the mast is fully extended. In this manner, it is possible to erect long, slender, inflatable masts to considerable heights in dense overgrowth or in any situation requiring an efficient and expeditious erection.

The larger masts have basically the same operation except for the added functions of the power pack assembly and the task of driving the high-load ground anchors. These masts also will have an automatic pressure system to maintain a constant pressure.

From an operational standpoint, retraction and packaging are very simple. For a manually operated manpack mast, the operator reels in the mast and stops only periodically when the retraction reaches the guy attachments. At this point, the guys are disconnected from the stakes, and the retraction continues until the mast is completely wrapped into the base. The air pressure in the mast will cause it to be very tightly compressed while the mast is being pulled inside. This compression will result in a very compact package when the mast is completely reeled in.

The buildup of air pressure in the mast will be relieved automatically through the pressure relief valve to maintain constant pressure. If desired, the bleeder valve can be opened to vent air manually. For a completely automatic mast

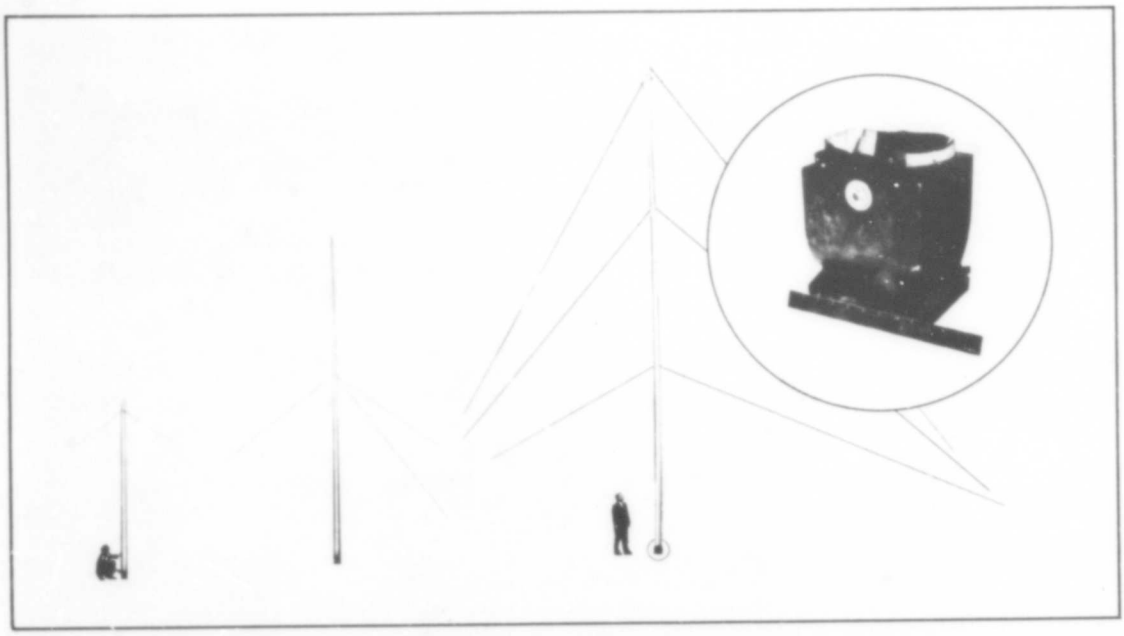

Figure 9 - Extremely Lightweight Antenna Mast (Five-Inch Diameter)

design, erection and retraction are continuous; no intermediate stops at guy stations are necessary.

Experience has shown that packaging ratios as low as 2 to 1 can be expected. That is, the packaged volume is only twice the actual material volume. Normally, a very good packaging ratio would be about 3 to 1 using a standard vacuum-packaging technique.

Inflation Devices - Air compressor systems are used on the larger masts, but much effort has been put into development of manual pumps.

As part of past research and development efforts to find a suitable manual pump for use with inflatable masts, several commercial pumps were evaluated. Figure 10 shows some of the commercial pumps tested. None was satisfactory for the weight, pressure, and volume required; therefore, Goodyear Aerospace initiated a design study to develop a better pump. Goals were set up for minimum weight, minimum package size, pumping capacity, and back pressure for a manual pump. Several pump configurations were fabricated and tested (see Figure 11). The best design was a foot-operated configuration (see Figure 12).

This pump, which weighs eight ounces, can pump at a rate of 3.0 cfm and can operate at a back pressure of up to 10 psig. A version of this pump was supplied to Rome Air Development Center (RADC), N. Y., with the 60-ft VHF-UHF

antenna masts. Later, further improvements resulted in a better and more durable pump (see Figure 12). This pump uses an improved intake and exhaust system.

Material Selection - Material selected for a particular mast design depends completely on the specific application, but some generalized requirements must be considered.

The interrelated parameters of durability and of light weight are primary considerations in designing the lightweight inflatable antenna mast. In selecting a fabric material, the problem is to select one that is light enough and at the same time adequately durable enough for the expected use.

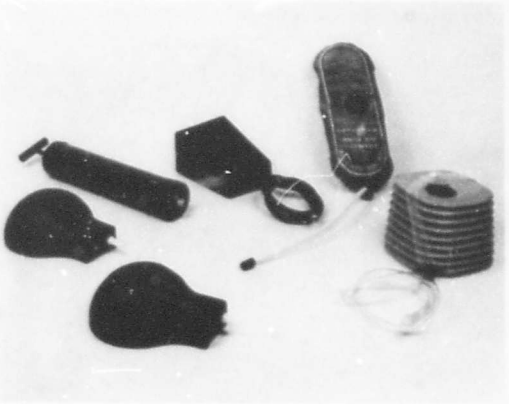

Figure 10 - Commercial Foot Pumps Evaluated

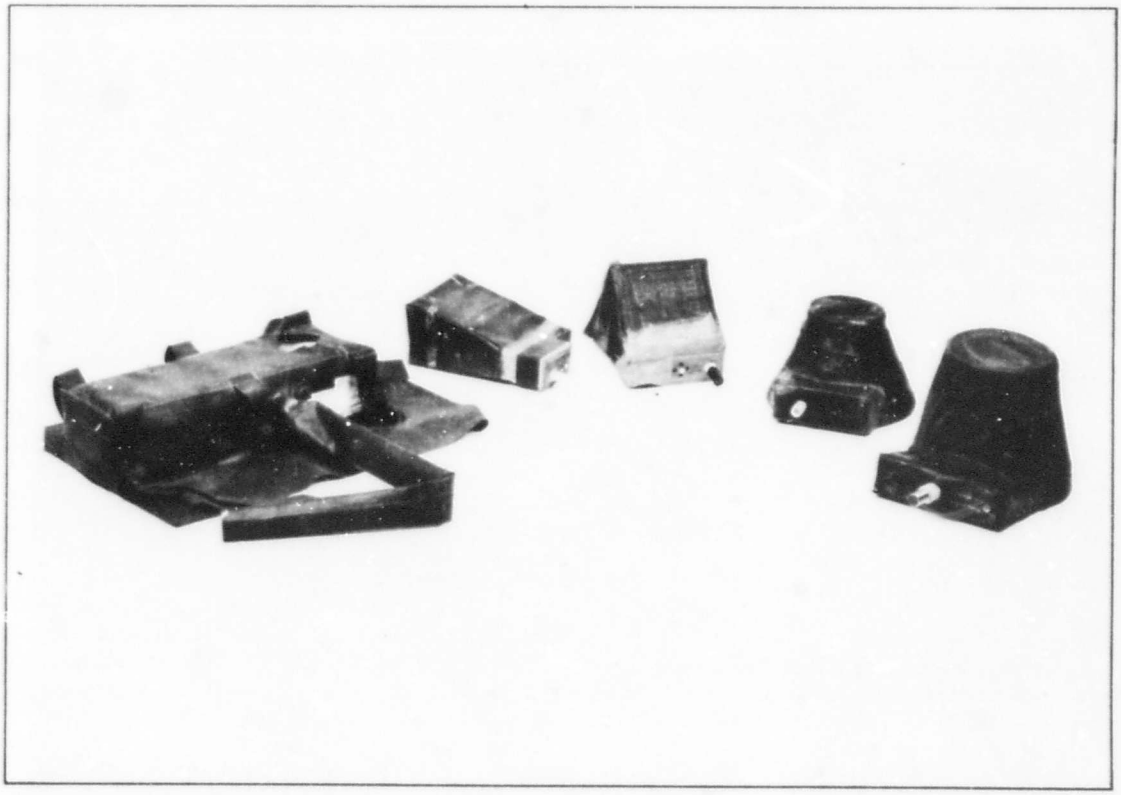

Figure 11 - Mast Inflation Foot Pump (Experimental Models)

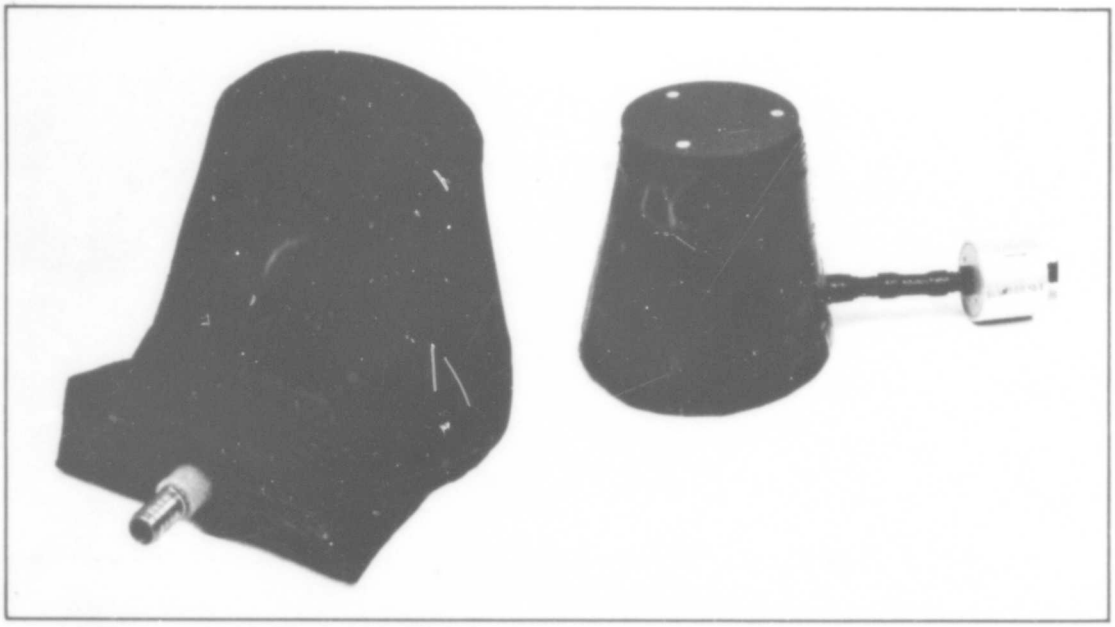

Figure 12 - Mast Inflation Foot Pump, Eight-Ounce Model (Left) and Improved Design of Mast Inflation Pump (Right)

During a past program, full-scale development mast models were tested to study new materials with improved shear stiffness to preclude the bow-string effect. These tests indicated that a mast made of a single material was not adequate. On models using a single material that was flexible enough to provide durability and efficient packaging during erection and retraction, the mast was not stiff enough to prevent bowing and buckling during retraction. Where material stiff enough to prevent bowing was used, it was not flexible enough to provide for durability and easy, efficient retraction. As a consequence, a variable modulus concept was evolved. In this concept, the inflatable mast is made up of alternate vertical panels of stiff and flexible material.

In the design that finally evolved, the stiff material consisted of a lightweight nylon cloth laminated to a heavy Mylar film; the flexible material consisted of lightweight Mylar film laminated to a heavy nylon cloth, with a spread of chloroprene elastomer between plies to act as a flexible pressure barrier.

The panels of stiff material were located diametrically opposite to each other, with the width parallel to the axis of the reel shaft in the base. When the mast was retracted, the panels rolled flat on the reel. The flexible fabric between these panels provided the flexibility to permit retraction, while stiff material provided the necessary shear stiffness to keep the mast rigid and straight. This concept proved to be very satisfactory under test, with no significant deterioration of the mast fabric during erection and retraction cycling. This construction

was used on the 60-ft VHF-UHF antenna masts recently fabricated for RADC [Contract Number AF30(635)-42992].

As a result of testing these masts recently in Vietnam, design modifications appeared necessary to eliminate some "bugs" that can be expected in first units. In considering the recommendations passed on by RADC personnel, Goodyear Aerospace has initiated design improvements in the mast construction. The primary effort is to make the mast more airtight without increasing weight. To determine the effects of wear, pressure leakage versus time tests are being made on the mast and the correlation of leakage to the number of erection cycles is being determined.

Initial pressure tests have been made on a 35-ft mast of similar design. This mast is a prototype design with an improved reel mechanism. The leakage rate in the first 24-hr period dropped the mast pressure from 4.24 to 3.75 psig, which is more than enough to keep it standing over the same period of time. In this test, the mast remained erect four days before collapsing in a wind.

Structural Considerations - Inflatable mast geometry is determined from the inflation pressure required to prevent initial wrinkling of the mast material under the specified wind velocities. The loads on the mast are primarily bending moments due to the distributed dynamic pressure along the mast reacted at the guy cables and ground and the compression loads in the mast due to the vertical components of the guy cable reactions.

The combined bending moment and compression loads are resisted by tension loads in the fabric. When the compression stress (combined bending and compression loads) equals the tension stress in the mast due to the inflation pressure, a point of zero stress occurs and a wrinkle starts. This is the initial wrinkle point. Any additional load causes the wrinkle to become more severe until the mast collapses. In pure bending, the collapsing load is generally 1.5 to 2.0 times the load causing the initial wrinkle, depending on material stiffness.

The loads in the mast, and the cable loads, are generally calculated by assuming that the deflection of the guy cable attach points on the mast remain in a straight line. The cable sizes then are selected to provide the required elongation to achieve this condition. However, this condition may not be attainable, in which case the mast analysis has to be modified to consider the relative movements of the supports. The approach is the same used in analyzing a continuous beam with supports that have settled.

After the bending moments and axial loads acting on the mast have been determined, the required pressure for a given section readily can be determined from the equation

$$p = \frac{2M}{\pi R^3} + \frac{P}{\pi R^2},$$

where

M = bending moments, including beam column effects (lb-in.),
P = axial load (lb),
R = mast radius (in.), and
p = required pressure (psi).

The maximum stress in the fabric (f) then is determined from

$$f = pR.$$

The properties of the mast material must conform to the strength required for the inflation pressure with an appropriate safety factor. Generally, a safety factor of 4.0, based on the fabric's quick-break strength, is used.

In addition to being strong enough to resist the bending moments and axial loads without wrinkling and the internal pressure loads without failure, the mast must have adequate stiffness to prevent collapse as a beam column. In calculating beam column effects, Pcr is defined as the critical column load and is determined from

$$Pcr = \frac{Pe}{1 + \frac{Pe}{A_p + KGt}},$$

where

Pe = Euler column buckling load, $\frac{\pi^3 R^3 Et}{L^2}$ (lb),
p = inflation pressure (psi),
A = enclosed cross-sectional area, πR^2 (sq in.),
R = mast radius (in.),
K = section shape constant, πR for a circular cylinder (in.),
Gt = shearing modulus of elasticity (lb/in.),
Et = modulus of elasticity (lb/in.), and
L = column length between inflexion points (in.).

In preparing the initial feasibility studies for a 300-ft inflatable mast for the LORAN D antenna system, Goodyear Aerospace conducted a preliminary structural analysis to investigate the required material strength, weight, and inflation pressure for the wind load requirements. The mast consisted of a 300-ft inflatable mast that tapered from five feet in diameter at the base to two feet at the top. The mast was supported at 12 equally spaced guy levels by Dacron Nolaro cables. The mast guy attach points were assumed to remain in a straight line when the mast was subjected to a uniform 70-knot wind at a temperature of -65 F. This assumption allowed a Hardy Cross moment distribution to be calculated.

To perform a rigorous, highly redundant analysis by manual calculation is very time consuming, especially when numerous configurations to achieve an optimum design are considered. Therefore, Goodyear Aerospace has started developing a computer program to perform these calculations. The program has been written and prepared on cards. Initial computer runs have been made using

the design parameters for the 300-ft mast. The program still needs to be checked, evaluated, and experimentally verified. These preliminary computer runs indicate that final design results may deviate from those determined in the preliminary analysis.

When the final computer analysis is completed, the results will provide a much more detailed analysis for evaluation. The program then will be available for a parametric analysis of masts in general.

SUMMARY OF BASIC DESIGN FEATURES

The auto-mast design has features that make it adaptable to many applications.

Weight - The structure normally weighs less than other masts when designed for comparable requirements. Except for very small masts, it weighs less than other inflatable masts since they all require a larger cross section to erect the unit. In weight, the auto-mast's main advantage over metal masts is that minimum gage sizes increase the weight of the latter. The gage sizes usually are not determined by the loads involved, but the mast must be beefy to preclude inadvertent handling damage.

For this same reason, inflatable masts can utilize larger diameters that give a more efficient use of the cross-section material, particularly where the external load on the mast is not a function of the mast diameter. To take advantage of high-strength materials, metal fabrics and panels can be used.

In addition, the auto-mast is a pressure-stabilized structure. Internal pressure puts tension in the wall of the structure. In this manner, the compression loads on the mast are resisted by the pretension in the walls as well as the compression load-carrying capability of the stiff panels. This design results in a lighter weight structure.

Package Size - Compared with any type of packageable mast configuration, the packaged size of the auto-mast is smaller. Inherently, the design of the unit provides packaging ratios as low as 2 to 1. This extremely small ratio is possible because the mast retraction technique is essentially the same as a vacuum package rolled tightly around a reel. Figure 13 shows a cutaway view of a mast model and the packaging method used. As the mast turns inside itself, the mast internal pressure tightly compresses the part that has been turned inward. In addition, the mast still under pressure has about one-half the longitudinal pressure load in the strap. This load pulls the mast wrapping tightly around the reel as it is rolled up. As a comparison, vacuum packages of inflatable structures normally have packaging ratios of about 3 to 1. Similar comparisons with folded or packaged rigid structures are not too meaningful since they normally cannot approach this degree of packaging.

Erection and Retraction Times - Minimum erection and retraction times are provided by the auto-mast. Whether the selected design is manually operated, semiautomatic, or completely automatic, there is no comparable erection device that can be put up or down so quickly.

The manual design still is somewhat automatic. It uses a manual pump, a hand-operated reel mechanism, and guys that are manually deployed and tensioned. This mast can be erected or retracted at a rate of about four feet per minute, with guy deployment taking most of the time.

The semiautomatic system has an engine, compressor, and powered reel mechanism but manually deployed guys. The guys still are the major time-consuming factor, but the ease and convenience of the other automatic functions are attractive. Erection rate is about 10 ft per minute.

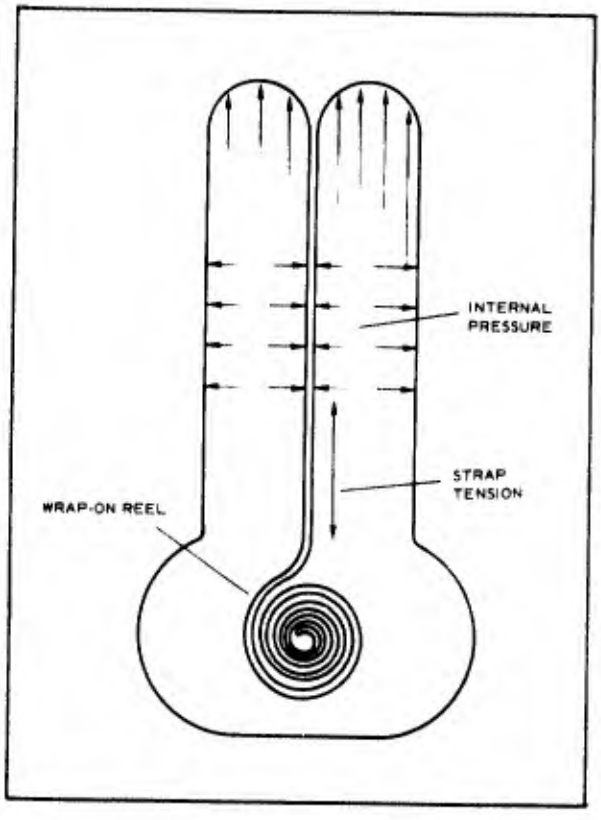

Figure 13 - Cutaway of Mast Model

The completely automatic system normally is used at a semipermanent installation, where the mast will be erected and retracted at the same site a number of times. It could be used where a completely remote operation is required, such as a postattack application. For this system, everything is automatic, including the guy deployment. The guys are automatically deployed, tensioned, and locked in position by a set of tensioned reels; erection and retraction times are limited only by the capacity of the compressor system and retraction reels. For some designs, even 100 ft per minute or more for erection or retraction might be feasible.

Versatility of Operation - Another feature of the auto-mast is its operation in any environmental condition. Even in relatively high winds, the mast either can be erected or retracted without failure or serious problems. This feature is possible since the mast is fully pressurized at all heights and is able to stand nearly the same wind loading during operation as when fully erected.

A self-contained unit is an advantage but not necessarily inherent to the design concept. In every design, however, special consideration is given to the operating subsystem to be used with the mast. Manual pumps having high-capacity outputs have been designed and fabricated for use in lightweight portable masts. For these same units, design of the reel and ratchet roll-up mechanism and of the special guides that effect a smooth wrap onto the reel also is emphasized. For larger masts, tradeoff studies are performed on compressors, gear reduction assemblies, and engine power packs to obtain maximum performance for the minimum weight and size.

Maintenance - The masts are relatively easy to repair and maintain. Any air leaks can be repaired in the field with patch kits. Each subsystem is an

independent assembly and can be designed for easy replacement and maintenance with standard tools normally available in the field. Even a major item such as the upper mast assembly can be designed for easy replacement in the field. Operated like an elevator, the auto-mast can raise a relatively heavy payload to the fully extended height of the mast and maintain it at that elevation. An elevator platform that rides the top of the mast supports the payload.

Payload Capability - Since considerable longitudinal tension is induced by internal mast pressure to resist the bending moments caused by wind load, the addition of a vertical payload usually does not significantly reduce the wind load capability. For example, a mast having a one square foot cross section pressurized to 10 psi would have a vertical tensioning of 144 × 10 = 1440 lb, which would provide 32.8 lb/in. tension in the wall. With a 100-lb vertical load in this relatively small cross section, about 31.4 lb/in. tension for resistance to any bending loads still would remain. Figures 14 and 15 show elevator platform additions to existing mast test models.

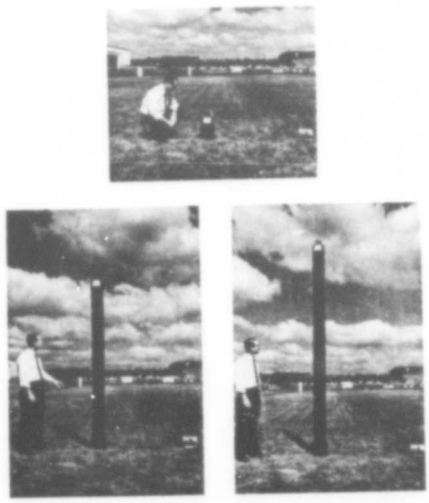

Figure 14 - Twelve-Foot Elevator Mast

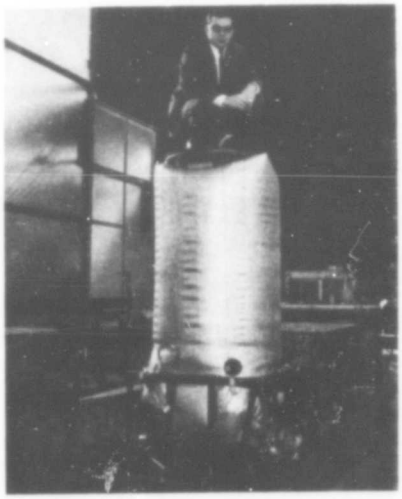

Figure 15 - Fifty-Foot Mast with Elevator Platform

Radar Reflectivity - The masts can be designed to have a minimum radar cross section if thin wall dielectric material is used, or they can be metallized to increase the radar reflection. In some cases (such as the LORAN D antenna design), the 300-ft towers utilize steel panels for added structural strength, which are not only radar reflective but also function as the antenna radiator.

To metallize a mast, a reflective, conductive, and flexible paint has been developed that will not crack or flake when the fabric material is flexed. Figure 16 shows this RF reflective paint on a 60-ft coaxial antenna mast. Test models of this inflatable 6-1/8-in. coaxial antenna mast have carried up to 2.5 kw during high-power testing.

Building Block Design - One of the biggest advantages of the auto-mast is the building-block feature, which allows it to be erected to great heights. Erection is carried out by first deploying the lower section. This section is secured by guys before the next section is erected. Retraction is carried out in the same manner.

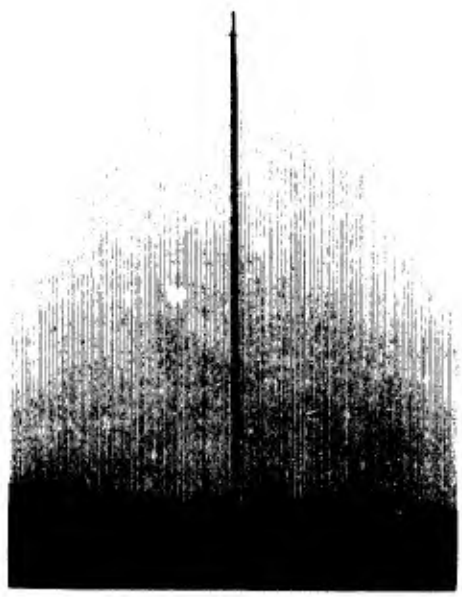

Figure 16 - Sixty-Foot Inflatable Coaxial Antenna Mast

POTENTIAL FUTURE APPLICATIONS

There are many potential applications for the auto-mast design concept. The design actually represents an extremely extendable actuator that has a variety of uses. In some cases, the actuator itself is the main structure; in others, it is a subsystem.

Antenna Mast - The most obvious and most active use is an antenna mast for portable or transportable applications. Overall, the applications could include VLF, LF, HF, VHF, and UHF antennas as well as elevator-type antenna masts for supporting antenna dishes and arrays at much higher frequencies and at different heights. Future designs still will have the lightweight and packaging advantages; however, durability and ruggedness together with speed of erection and retraction will be improved even further with new materials and design modifications.

The LORAN D 300-ft antenna is an extremely durable tower. It is designed for use in almost any environment, including a 70-knot wind with a temperature range of -65 to +125 F. Figures 17 and 18 show a 50-ft test tower during a five-month environmental endurance test.

The 300-ft tower is the largest design studied and illustrates the potential of the basic design. Figure 19 shows the basic configuration. It includes an airlock passage for access inside the tower. As an option, a ladder that can be used for visual inspection and even minor repair is provided on the inside strap.

Retractable Floats - The mast design has an almost exclusive application for retractable vertical floats. The future ASW weapon will require the use of a true open-ocean seaplane or of a high-speed, ocean-going air cushion vehicle to provide a fast sensor-bearing and weapon-carrying capability. The seaplane has not been compatible with rough water conditions encountered in ASW operations due to hull structural limitations and rapid decline in crew performance while the seaplane is pitching and rolling. The auto-mast design used as a retractable vertical float will enable a seaplane, a small ship, or an air cushion vehicle to stay on the ocean surface for long periods while providing the crew with a stable platform.

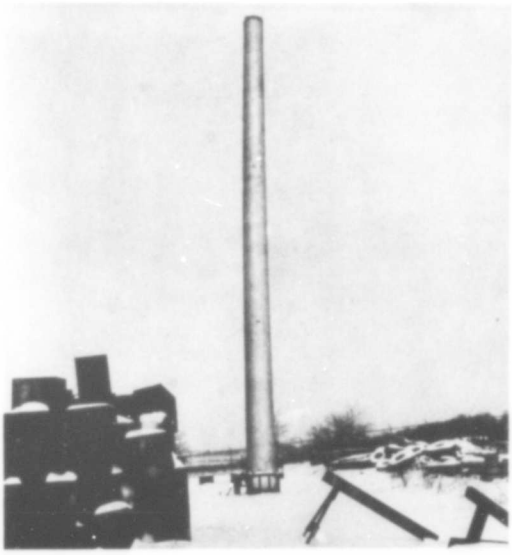

Figure 17 - Environmental Endurance Test (50-Ft Inflatable Mast)

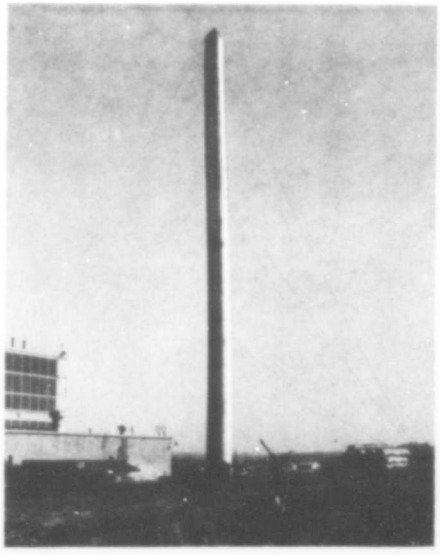

Figure 18 - Environmental Endurance Test (50-Ft Inflatable Mast)

Figure 20 shows a seaplane used for studying the feasibility of vertical floats. For the first time, a practical open ocean-based aircraft was proved to be capable of sustained station keeping on the ocean surface without developing motion sickness that hampers crew performance.

Floating Bridge - Another application of the auto-mast design is an automatically extendable lightweight floating causeway or pontoon bridge. The loss of time in getting men and equipment from ship to shore during an amphibious military operation or across any body of water usually is a severe problem. In addition, space and payload weight are critical factors during landing. Present systems are bulky, heavy, and take too much time to assemble. Even though considerable weight can be saved by reducing the weight of individual components, the auto-mast design concept minimizes not only the weight problem but also the problems of packaging size and assembly time. Overall, Goodyear Aerospace feels that the proposed lightweight quickly erectable causeway design offers a definite advance in the state of the art. It would be designed to carry either tracked or wheeled vehicles. Figure 21 shows the proposed design as well as a cross-section view.

The company's causeway design concept consists of four automatically extendable and retractable pontoon modules connected in parallel. Each pontoon module is packaged in approximately six-foot cubes and can extend up to 200 ft. Sectional lengths of more than 200 ft may be possible and will be considered in future studies.

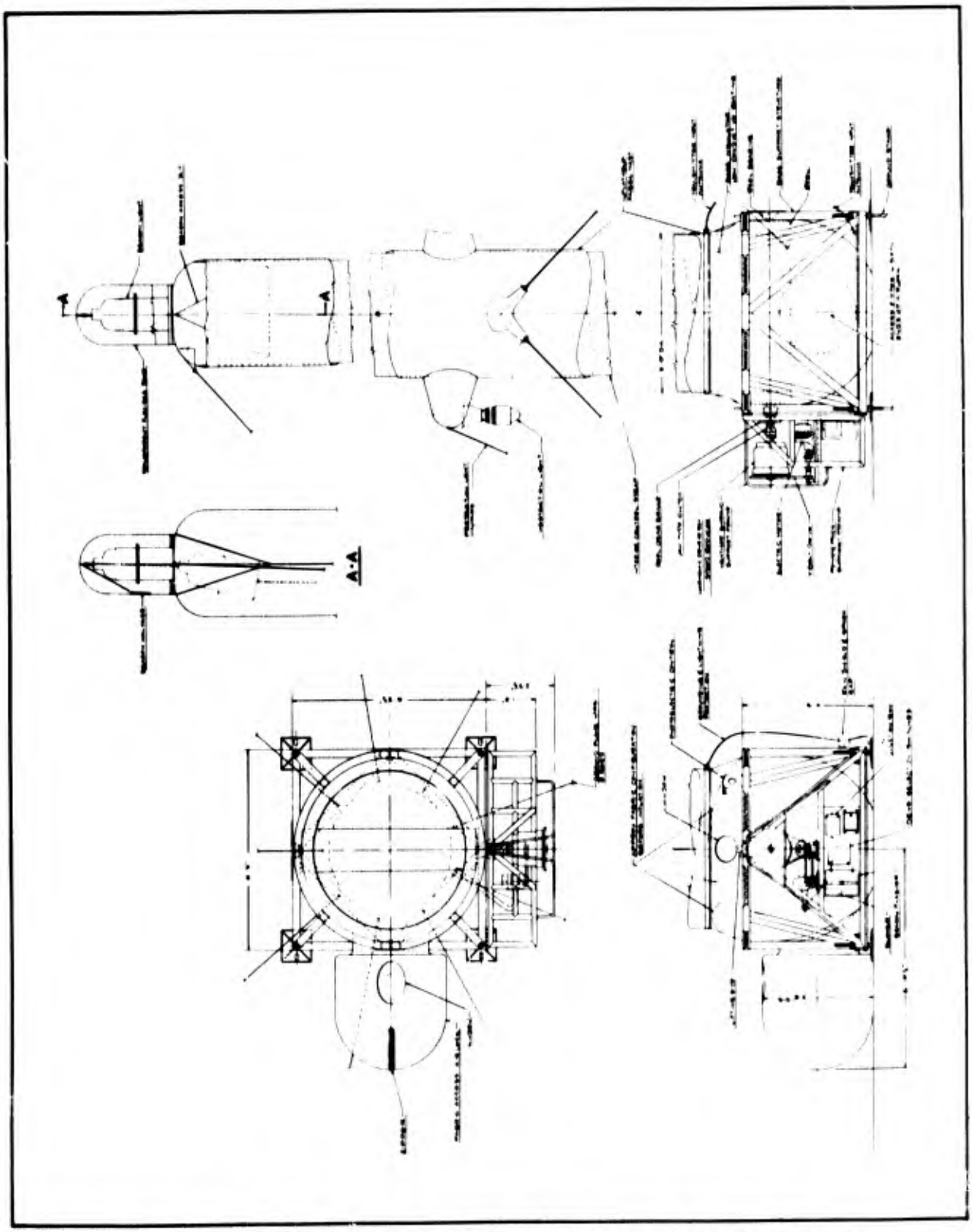

Figure 19 - 300-Ft Automatically Erectable Antenna Mast for LORAN D

Figure 20 - Seaplane Used for Studying Feasibility of Vertical Floats

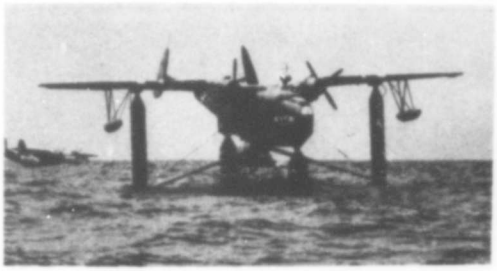

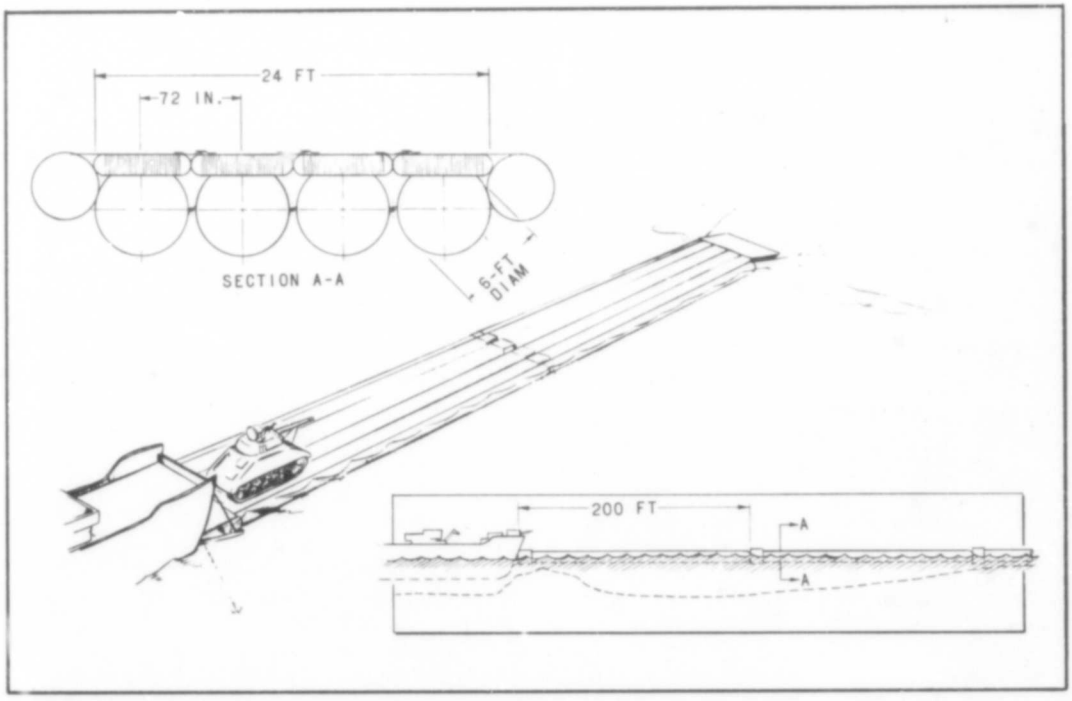

Figure 21 - Automatically Extendable Lightweight Causeway

The causeway design concept is made up of separate pontoon modules that could be grouped together in parallel to make any width of causeway. In some cases, even a single pontoon assembly anchored in position may be adequate if it is needed only for personnel. It would provide a roadway only six feet in width. However, studies have been limited primarily to a design using four pontoons and two stabilizing sponsons for heavy payload applications. A technique of assemblying an expandable causeway is shown in Figure 22.

Space Structures - Space structures provide a number of natural applications for the auto-mast concept. One recently proposed concept was for a lunar

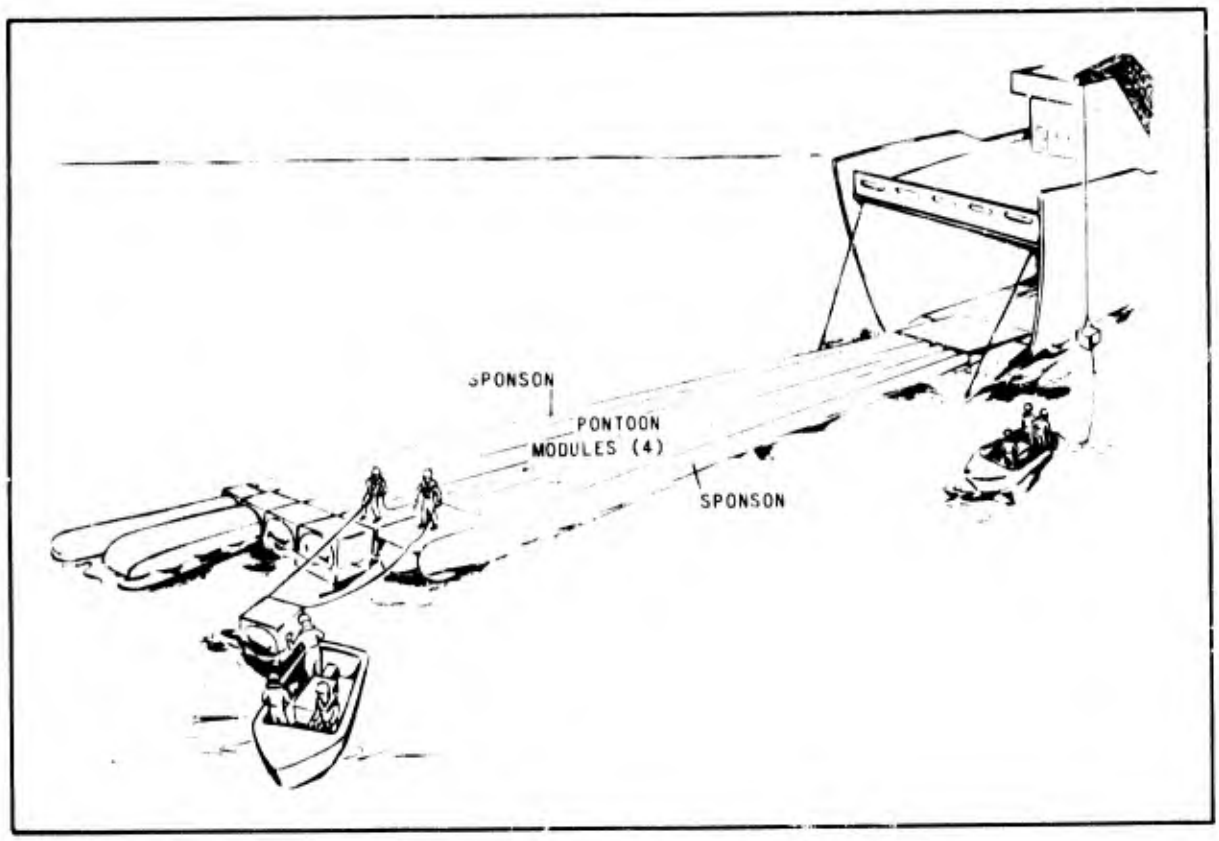

Figure 22 - Causeway Assembly Technique

gravity simulator for the Apollo command and service module and the empty Saturn IV-B (SIVB) stage. In this configuration, the Lunar Excursion Module (LEM) would be replaced by an airlock and boom storage area. The empty hydrogen tank would be inhabited during the test and would provide approximately 1/6 g at a 30-ft radius at 4 rpm.

Figure 23 shows the inertia booms for the SIVB workshop. Preliminary calculations indicate 125-lb weights are needed to support 200-ft booms normal to the longitudinal axis. The experiment is planned for the 209 mission.

The auto-mast design also was used in a contract for a space maintenance hangar study on the Manned Orbital Laboratory (MOL) program. The structure utilized a nine-foot diameter cylindrical structure with an expanded length of 25 ft. This structure attaches to the aft end of the MOL to serve as a pressurized meteoroid protective enclosure for astronauts working on MOL experiments. The expandable hangar construction is a composite wall consisting of an inner triple barrier pressure bladder for gas retention, a web strap structural layer, a two-inch thick polyether foam meteoroid barrier, and a film-cloth laminate outer cover with a thermal coating. The auto-masts are used to deploy and retract the hangar.

An extendable and retractable docking device for facilitating rendezvous in space would be another potential application. This docking mechanism could be mounted

on a ship or space station and would essentially deploy and swing outward to meet an oncoming ship. After attaching itself to the ship, it could draw the two space ships together, thus conserving the fuel it normally would take to maneuver and effect rendezvous. It could then be used for transfer of personnel and supplies.

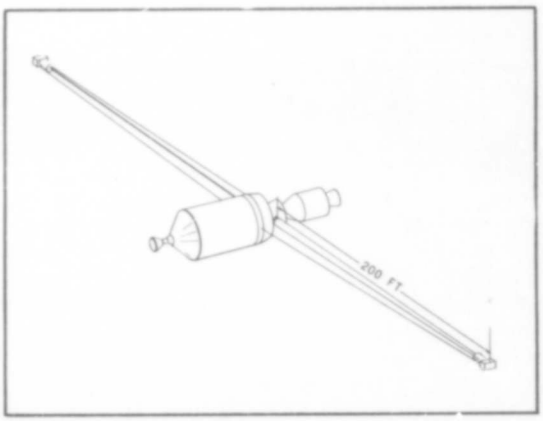

Figure 23 - Inertia Booms for Saturn IV-B Workshop

The auto-mast design could be used in space antennas requiring very large radiating elements. In many cases, where extremely long radiating elements are needed to maintain their shape in space, use of a photolyzable wire-grid film like that used for the 30-ft grid sphere passive satellite experiment may be desirable. Here, the mast would be deployed in the usual manner. After deployment, however, the film would photolyze into the environment, leaving only the wire grid as the radiating element. In this manner, the element would not be affected by hot and cold temperature, the loss of air pressure, or the drag of the antenna in orbit.

Adjustable Scaffolding - Autcmatically adjustable scaffolding for the building industry could significantly reduce the cost of construction in some cases. The amount of scaffolding required, for example, for the 140-ft radome for the BMEWS tracking antenna becomes a large percentage of the fabrication costs (see Figure 24). Figure 25 shows how the auto-mast can be used for automatically adjustable scaffolding. The design also lends itself well to a pneumatic jack application, where a greatly extendable heavy payload jack is required. This unit could be used for in-the-field repair or as part of a transportable maintenance center.

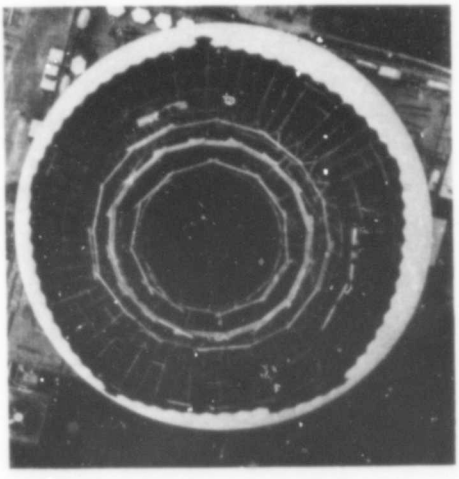

Figure 24 (Left) - Amount of Scaffolding Required; Figure 25 (below) - Pneumatic Scaffolding Used in Radome Erection

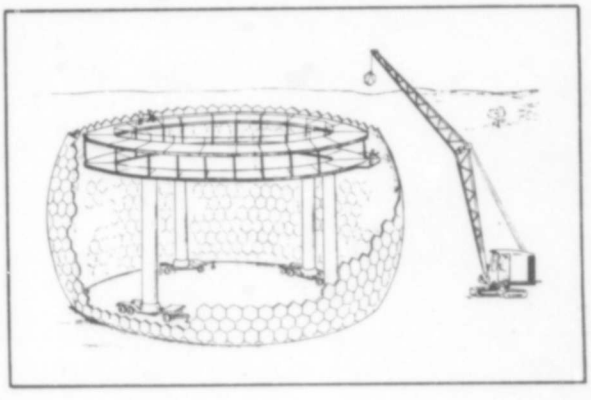

Observation Towers - The masts could be used for portable or transportable observation towers. Figure 26 shows a proposed observation tower mounted in an M-106 vehicle. This tower supports the observer, an optical sight, and a personnel radar unit. If the tower is mounted in a vehicle, heights up to 100 feet or more are possible. The unit would retract down inside the vehicle.

Figure 26 - Observation Tower Mounted in M-106

Mud and Water Legs - A mud and water legs application for an M-113 vehicle also has been studied. In Southeast Asia, considerable mobilizing problems have arisen for the M-113, particularly where the vehicle must cross canals and rice paddies. Figure 27 shows how the addition of the pneumatic mud and water legs not only increases flotation and permits the vehicle to ride higher in the water but also can be used as a pusher device to help lift the vehicle up and over obstacles.

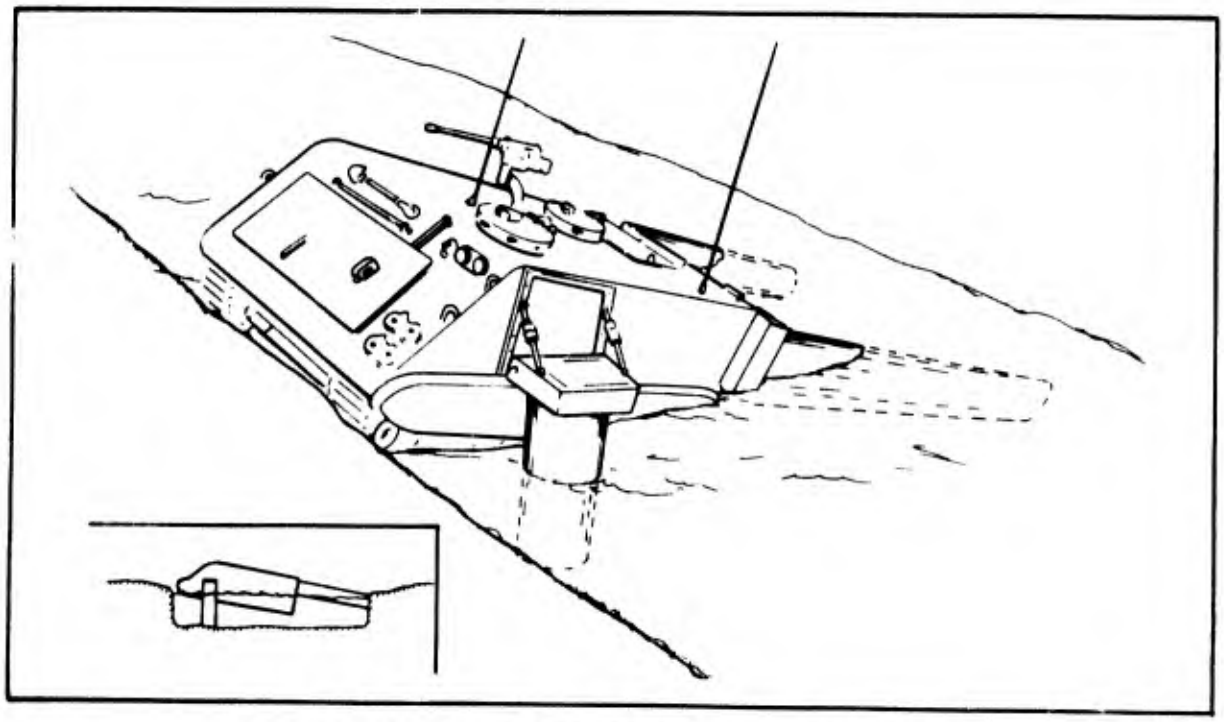

Figure 27 - Mud and Water Legs in Operation

Bumper for Ships - The auto-mast could be used as a bumper to facilitate docking of ships and the transfer of supplies between two ships in mid-ocean (see Figure 28).

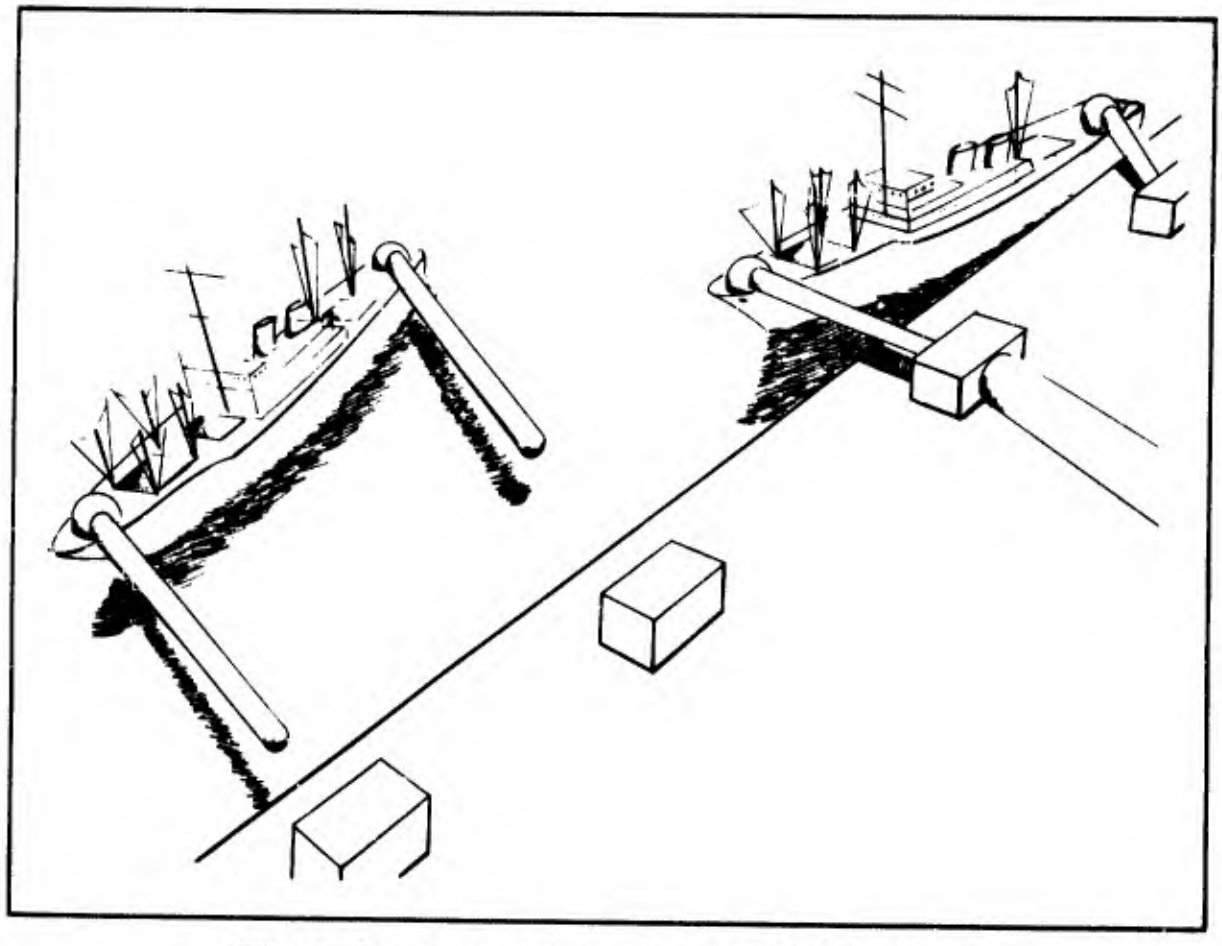

Figure 28 - Impact Bumper and Docking Device

Retractable and Extendable Airfoil - A slight design modification of the mast would permit its use for a streamlined mast or a retractable and extendable airfoil configuration. The mast would utilize diametrically opposite AIRMAT[a] (a structural fabric with top and bottom surfaces connected by drop threads that hold the surfaces a fixed distance apart under internal pressurization) panels to give the mast a contoured shape. The mast itself would be pressurized at one pressure and the AIRMAT at a lower pressure so the air is forced from the AIRMAT when retracted into the mast. When deployed, however, the AIRMAT can be designed to contour the mast into a variety of desired shapes, including an airfoil.

Catapults and Actuators - The auto-mast design also can be used for catapult applications. Actuation speed of the auto-mast depends strictly on the amount

[a]TM, Goodyear Aerospace Corporation, Akron, Ohio.

of pressure supplied to it. If the pressure volume is available, the design can be used as an extremely long stroke catapult.

Many miscellaneous actuator uses also are possible, since the auto-mast design can be built in a great variety of sizes. The mast can be made as small as one-half to one-inch in diameter and, with its packaging ratio of extended length to packaged length as large as 80 to 1, it offers considerable advantage where a greatly extendable actuator is required. The mast also can be used with any actuating medium, including air, steam, water, and hydraulic fluids.

BANQUET SPEECH

BLANK PAGE

SPACE FLIGHT SAFETY

By

Dr. Eugene B. Konecci
Alice G. K. Kleberg Professor
College of Business Administration
The University of Texas at Austin
Austin, Texas 78712

The year 1967 will be marked in history as the first tragic loss of life in the U.S.A. and U.S.S.R. space programs. A flash fire in the Apollo I spacecraft during a simulated launch test on the pad at Cape Kennedy on January 27 claimed the lives of three great American space pioneers: Virgil (Gus) Grissom, Edward H. White, and Roger Chaffee.

This unusual incident at the beginning of the Apollo Lunar Landing program has caused a great deal of discussion, consternation, and focusing of attention on the SAFETY aspects of manned space flight. Questions like, "What happened?" "How could it have happened?" "What can and will WE do about it?" were asked.

The official NASA investigation and the Congressional hearings were professionally and ethically conducted. NASA investigators probed deeply into the manned space program, and their effectiveness can be measured by the large number of program changes already in effect or to be implemented shortly. As an example, the new office of Flight Safety within the Manned Space Flight organization was announced last week by Dr. George E. Mueller, Associate Administrator for NASA's Manned Space Flight. The fine work of Congressman Olin Teague and his subcommittee points up the strength of our democratic system of checks and balances.

The results of the Apollo investigations and hearings are common knowledge, having been covered extensively by the press, radio, TV, and trade journals. Many factors combined made the accident possible. Some critics are disappointed because there is no single scapegoat. Management at several levels in the Apollo government-industry team assumed, as they should, the responsibilities for the accident and other program deficiencies.

Management and Responsibility

Management means responsibility. At this time I would like to quote an appropriate statement, relative to management in general, made by David G. Moore in the October 1960 issue of Nation's Business:

There are no guarantees in any society that those persons who are the most capable and possess the most wisdom and the greatest virtue will inevitably rise to the top. Our system of selecting leadership for the key institutions of our society is crude at best. Indeed, the major achievement of political democracy which has been centuries in the making is not so much in the identification and selection of high-quality leadership but in the safeguards which it provides against continued inept leadership.

We have, in America, the strategic advantage of being able to limit our losses, but we cannot as yet insure ourselves against the rise of mediocrity and even, under some circumstances, gross incompetence.

It takes only a slight twist in the somewhat idealized description of the successful executive to change effective behavior into ineffective. For example, it has been pointed out that executive decision-making must of necessity be highly subjective and somewhat aggressive. If too subjective and too aggressive, it becomes punitive and authoritarian. Successful executives must be conservative with somewhat narrowly focused aims.

If too conservative and too narrow, they can become bottlenecks, impeding progress.

Successful executives must be serious-minded. But if too serious, they can lack introspection, the ability to laugh at themselves, and the ability to be objective. Under such circumstances, work ceases to be fun and becomes a deadly, unhappy pursuit for everyone involved.

Successful executives must be mobile; but, if mobility and the seeking of status and power become the sole objectives, organizational aims are forgotten.

In their respective management roles the government-industry aerospace teams are all concerned about the future of our national aeronautics and space programs. This includes NASA, FAA, A & C, and all the other programs. Many will agree we are not doing everything that could possibly be done in this exciting field. However, our first nine years of space progress has been truly amazing. As Congressman George P. Miller, Chairman of the House Space Committee, stated:

> On October 1, 1958, this nation entered into man's greatest adventure, the exploration of space. Since the National Aeronautics and Space Act was written and enacted by Congress, we have been witnesses to a scientific revolution that has progressed with fantastic rapidity. We

have seen the growth of the aerospace industry into an industrial and economic giant that even now equals or exceeds the automobile industry in numbers of people employed directly and indirectly.

The impact of this revolution has been so broad and so portentous to this and to future generations that it is literally impossible to identify, in historical context, the points of critical decision, or perceive their effect in the course of the NASA programs which have led to the present level of competence and achievement.

Yet there is no doubt that the revolution in science and technology we are presently experiencing has made acceptable to our people the idea that we must go out into space, and has made possible their willingness, expressed through Congress, to appropriate the billions of dollars needed to support our space programs.

Despite the general support of the people we are faced with the problem of convincing many Americans, a few of whom are members of Congress, that there are tremendous benefits, direct and indirect, to come from the national space program--benefits to the nation and to the individual. We are faced in some quarters with an attitude toward the exploration of space that is very closely analagous to that expressed by one of our greatest statesmen, Daniel Webster, with regard to exploring the West. He said:

> What do we want with this vast, worthless area, this region of savages and wild beasts, of shifting sands and whirlpools of dust, of cactus and prairie dogs? Of what use could we ever hope to put these great deserts or those great mountain ranges, impenetrable and covered to their base with eternal snow? Mr. President, I will never vote one cent from the public treasury to place the Pacific Coast one inch nearer Boston than it now is.

It is unnecessary to dwell upon his unfortunate lack of foresight, his myopic view of the future. How fortunate that the American people followed their own instincts.

This nation's achievements in manned and unmanned space flight can make every American proud of our technological advances. We must not stop our achieved momentum but have to proceed on to capitalize on our investments and technology.

Dr. George Kozmetsky, co-founder of Teledyne and now Dean of the College of Business Administration at The University of Texas at Austin, said he went back to-

education to train the needed managers of our technical and intellectual resources for the last third of this century. He gives immeasurable credit to the space program for providing the impetus technology and systems methodology needed to train the new breed of multi-disciplinary managers. Pick a manager at any level in the Apollo or another complex systems program and you will discover he is no longer a specialist in one area. Managers have to be aware of the implications of their activities and decisions on the whole system, and safety becomes of paramount importance.

Safety in R and D

Safety is and must always be a cardinal element in United States civilian and military aeronautics. Similarly, in astronautics the ultimate success of manned scientific exploration, and eventual extensive utilization of the space media for commercial transportation of men and goods, will depend on the over-all attainment of a high degree of safety.

Today few doubt that we will be successful. But success probably has a different meaning to each of us. Every society has certain accepted notions of success and generally defines it in terms of what getting ahead means in that society.

What about the space program?

Well, the manned space flight program has certainly been one of the most outstanding examples of a successful research and development program.

Ah, but here is the rub and key to the riddle: NASA's manned space flight program has been too successful for an R and D program. Research and development in new and advanced technological areas is never smooth or flawless. The R and D road is generally paved with sharp, jagged disappointments, which lead to alternate pathways and even carving of new trails until you are back on the main road leading to your goals.

If the space program is to be scrutinized at this time with a powerful microscope and reappraised with a fine-toothed comb because of the Apollo I tragic accident, so be it. But, it should be done in the light and context of the whole manned space flight program. NASA's manned space flight personnel are competent and dedicated Americans, many having made personal sacrifices to stay with the program because they had the necessary vision and fortitude to try to usher in this new manned space age. No organization composed of humans is or can be expected to be perfect. Mistakes have been made, and others will be made in the future. Critics of the space program are using the Apollo 1 ground test accident to support their thesis that the program is ill conceived, poorly managed, and obviously because of the accident

not successful. The government, industry, and university team that makes up the manned space program may be guilty of not doing a lot of things, like not having a space rescue or escape capability, because of time, resource, and other restrictions; but the team's greatest guilt was that it was too successful in an R and D program--that is, until the Apollo mishap.

Research and development has always been plagued and blessed with failures in programs. Yes, blessed because failure automatically leads to critical self-review of the concepts, methodology, test procedures, and so forth. These periodic reappraisals lead to a better understanding of the fundamentals in the R and D system and guard against complacency and undeserved self-assurance of how well things are going when, in fact, it may just be the calm before the storm. The Apollo tragedy is not being minimized but maximized since its effects are already correcting many program problems that come to light as a result of the accident investigation that do not necessarily bear directly on the Apollo fire.

Reflections on Recent History

Memories of past experiences tend to dull with time. The successful United States Mercury and Gemini programs here and the Vostok and Vokhod in the U.S.S.R. were greeted by excitement and world-wide concern for the safety and well-being of the astronauts.

President Johnson at a White House ceremony honoring Virgil I. Grissom and other NASA personnel on March 26, 1965, stated:

> A sense of history is present strongly here today. All of us are conscious that we have crossed over the threshold of man's first tentative and experimental ventures in space. The question of whether there would be a role for man himself in space is already firmly and finally answered, and answered affirmatively. Man's role in space will be great, it will be vital, and it will be useful.
>
> Equally important, we can comprehend now better than we ever have been able to in the past the role of space in the life of man on earth will also be great and vital and useful.
>
> So in this springtime of 1965 it seems incredible that it was only four springtimes ago when young Americans, including Gus Grissom, first flew into space. We have come very far in a very few short years. Yet the quickening pace of our advance will carry us far beyond this point of achievement even before one more year passes.

> The program we pursue now is a planned and orderly program with but one purpose--the purpose of exploring space for the service of peace and the benefit of all mankind here on this earth. We are not concerned with stunts and spectaculars, but we are concerned with sure and with steady success.
>
> Since we gave our program direction and purpose seven years ago, many such successes have been achieved through the efforts of a great American team, which now numbers 400 thousand men and women in industry, on campuses, and in government. And this team is inspired and stimulated and led by a former Marine and a great public servant--Jim Webb.
>
> We have come here today to honor just four of these 400 thousand men on his team.

As the Gemini program got into high gear and began to register one success after another, the operations appeared to be routine, and the people closest to the program, as well as the public in general, began to exhibit the symptoms of complacency.

Repeated attempts in the last few years by a number of individuals from Executive, Congressional, and industrial groups have been made, alerting the public to the hazards and pending dangers.

Recently Evert Clark of the New York Times reminded me of the words I spoke at the at the Third Annual Meeting of the A.I.A.A. in Boston two months before the Apollo spacecraft fire. In covering the space rescue subject, I stated, "We intuitively know that someday, maybe in the not too distant future, we and/or the Soviets will suffer a manned space catastrophe.

This grim prophecy came true with Apollo I, adding to it the death of cosmonaut Colonel Vladimir N. Komarov in the Soviet Soyuz I crash.

There was not one warning voice. On the contrary, there were many--including President Johnson, Vice President Humphrey, Congressman Olin Teague, and many other individuals in and out of government. The most persistent warnings over the last three years must be attributed to Dr. Edward C. Welsh, Executive Secretary of the President's Space Council. At the time it was an unpopular position in light of such successful flights. However, his foresight, interest, and encouragement lead to numerous studies in and out of government, including the Space Rescue paper presented at the A.I.A.A. meeting. A month earlier I chaired a panel composed of government and industry experts, including Colonel Francis X. Kane of USAF, Alfred Mayo then LTV, Theodore J. Gordon of Douglas, and Harold L. Bloom of

General Electric. The subject was "Space Rescue" at a meeting of aviation and space writers in New York City. The consensus was that a true space rescue system would take several years to develop. In the meantime we need some emergency escape devices.

Escape Technology

Gentlemen, your three aerospace conferences on expandable and modular structures are pointing the way to providing the technology needed to give us an interim space escape/rescue capability. Details of what you and others are doing in this field have been highlighted in Congressman Teague's committee report on "Space Rescue."

NASA has a number of in-house and contract studies, and their proposed Saturn S IV B Orbital Workshop will serve as an ideal laboratory to try out many different development concepts of survival and escape systems. The paper given yesterday by your program chairman, Fred Forbes, from the USAF Aeropropulsion Laboratory and prepared with Goodyear Aerospace Corporation, Air Force 6570th Aerospace Medical Research Laboratory, and NASA Langley Research Center on "Expandable Airlock Experiment for the S IV B Workshop" is an example of an effective and cooperative effort. As you know, the D-21 "Airlock" Expandable Experiment is scheduled for orbital flight testing in the Apollo Applications Program, Flight AAP-2. The S IV B Orbital Workshop itself will add to our capabilities for space escape and survival. The objective of the S IV B Workshop is to evaluate the feasibility of using the empty shell of the spent S IV B to support crew operations for a 30-day orbital mission. The D-21 can be used for emergency survival and crew transfer.

The Air Force Space Systems Division is conducting a space escape study on contract to North American. General Electric is continuing its in-house efforts on MOOSE (Manned Orbital Operations Safety Equipment). Lockheed Missile and Space Systems is doing some basic R and D work on expandable structures for the Aeropropulsion Laboratory. The technology from this program could be applicable to space rescue and escape.

D-22 Experiment technology of a space rigidized-metal truss recovery capsule with heat shield might be scaled up as a manned escape/rescue system from orbit. In addition, a chemical rigidized panel with flexible heat shield will be tested as part of D-23.

There are, of course, many other studies and concepts with which you are more familiar than I.

I believe it is appropriate to commend you, the technologists in aerospace expandable and modular structures area, on your efforts these last several years despite the

odds and lack of recognition and support from many quarters. You are proving your value as unsung heroes in the exciting aerospace adventure.

Your contributions to space flight safety may prove to be the difference between success and failure for our long-range objectives of eventually permitting every man, woman, and child to travel in space. Your technological contributions for our everyday needs are evident by the many shelters and devices you have on exhibit at this conference. You are helping the nation and the space program with your technology to overcome the immediate hurdle caused by the recent U.S.A. and U.S.S.R. accidents. Hopefully your efforts will lead shortly to survival and escape devices and interim rescue systems that will reduce the probability of loss of life. We must now brace ourselves for the true space tragedy in orbit, on the moon, etc. that will come sometime in the future. The Apollo ground test accident has helped point to and clear up many problems. The Apollo program will now be a much better and safer program.

Conclusion

In conclusion, the space program has accomplished much, but it is still in its exploratory, pioneering stages. Manned space flight is still a hazardous business.

The danger is a matter of degree. We kill about 40,000 Americans on our highways each year, but these losses do not have the same impact as the loss of an astronaut.

There is no question that we have conquered space; now we have to take the necessary steps to guarantee a reasonable degree of safety.

I believe it is appropriate to quote the words Dr. Welsh spoke as the Bauer Lecturer at the Aerospace Medical Society meeting April 10, 1967, in Washington, D. C.:

> As you can readily observe, I am optimistic about our leadership in space and in aviation. I am also optimistic about the growing technological competence of this nation and our ability to afford even greater investments in such growth in the near future.
>
> But I warn that we cannot afford to wait or even slow down in this era of technological competition. We cannot afford to do less than employ to the maximum the managerial techniques, the trained personnel, the modern facilities, and the technical knowledge in the solution of the many complex problems which confront us.
>
> Moreover, we have to meet the challenge of keeping our ethical and political standards up to the level reached by the technology of the

aerospace revolution. We must look to the future and get busy. We have no time to waste!

I would like to add this, a final thought: It is a fact that the space program is in its infancy, a pioneering research and development effort. We must accept as the first constraint that regardless of how hard we try and how much technical effort we devote and how much money we spend, we cannot guarantee 100 per cent success of all manned space missions.

A good flight safety program, well managed, will minimize the risks and insure acceptable safety standards and training without impeding our progress in the space program.

SESSION V

DEVELOPMENT AND APPLICATION OF NEW MANUFACTURING TECHNOLOGIES FOR EXPANDABLE STRUCTURES

J. F. Keville*

New materials systems and manufacturing technologies have been developed for high strength and high temperature expandable structures during a four year program recently completed by the Space-General Division of Aerojet-General Corporation for the Manufacturing Technology Division of the Air Force Materials Laboratory. To develop and demonstrate the capability of fabricating an expandable structure for space applications, a re-entry, space rescue paraglider was chosen. The vehicle would be packaged in a small volume aboard an orbiting space station, and when the requirement arose to return a man to earth, the paraglider would be ejected from the space station, inflated, de-orbited by retro-rockets, and it would re-enter the earth's atmosphere using small gas jets for attitude control. Upon obtaining adequate aerodynamic control, the flight attitude could be controlled by wing warping using variable gas pressure to permit bending of the inflated leading edges. An artist's conception of the deployment of the paraglider from a space station is shown in Figure 1.

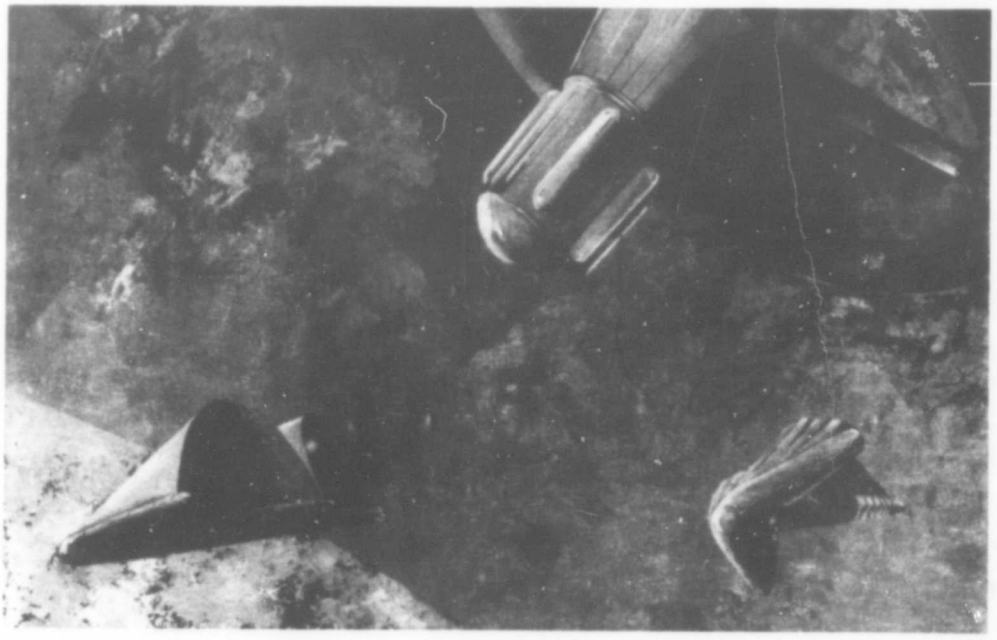

Figure 1. Deployment of Escape Vehicle

* Mr. J. F. Keville is Program Manager at Space-General, a Division of Aerojet-General Corporation.

A model of the vehicle illustrating the re-entry heating effects is shown in Figure 2. The vehicle would be 23 feet long with a wing spread of 28 feet. Three inflated tapered tubes would constitute the leading edges and the keel boom while a light weight wing membrane between the keel boom and each leading edge boom would assume a semi-circular shape during atmospheric flight. The man would be enclosed in an insulated crew capsule in the center keel boom along with the necessary life support and flight control equipment.

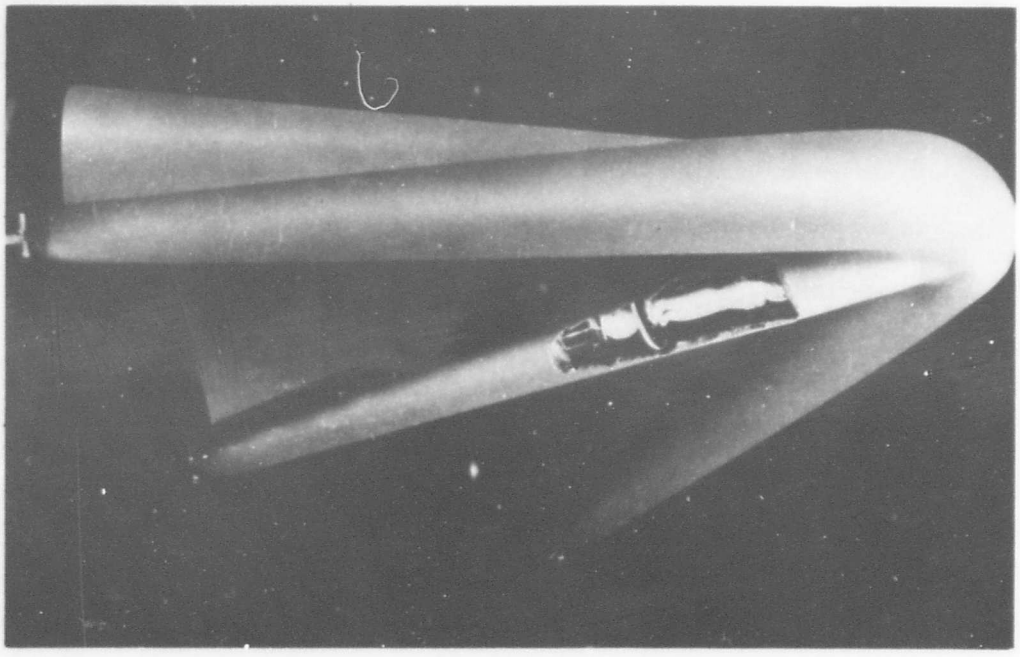

Figure 2. Re-entry Paraglider

Due to its maneuvering capabilities, this lifting vehicle would be capable of landing anywhere within an earth footprint approximately 1,400 miles long and 450 miles wide. Additional details concerning the proposed design of the paraglider, along with its trajectory parameters and aerothermodynamic characteristics, were presented in a paper at the Second Aerospace Expandable Structures Conference in May, 1965. This paper also presented details of the physical construction and properties of the nickel-chromium metal fabric used as a flexible structural material. The impregnation or saturation with high temperature silicone rubber and the coating of the vehicle with a varying thickness of the necessary ablative silicone rubber were also discussed in the previous paper.

One of the most significant developments of this program was the special, semi-automatic, deep throat welder which was designed to make flexible, high strength seams in metal fabrics. The welder makes two rows of closely spaced, small diameter spot welds in the fabric using a 1/2 to 3/4 inch overlap of the fabric layers. At least five layers of fabric can be joined so intersecting seams and multiple plies can be accommodated permitting the construction of surfaces with compound curvature.

The welder has a seven-foot deep throat and is shown in Figure 3. In this view the horizontal arm or center arm is installed. This arm is used for welding longitudinal and circumferential seams in cylindrical shapes. A lower "L"-shaped arm can be substituted for the horizontal arm so that curved shapes such as the toroidal apex of the paraglider, can be welded. The speed of the welder is operated by a foot pedal through a timing circuit in the upper control box at the rear of the machine. The timer controls the synchronized speed of the upper and lower welder head, as well as the pulsing of the weld current from the welder power supply in the lower control unit at the rear of the machine. The machine is equipped to operate at seven different speeds from approximately 2 to 8.5 inches per minute. The heads can be rotated at various angles and indexed with a splined support so that joints may be made at angles to the axis of the machine.

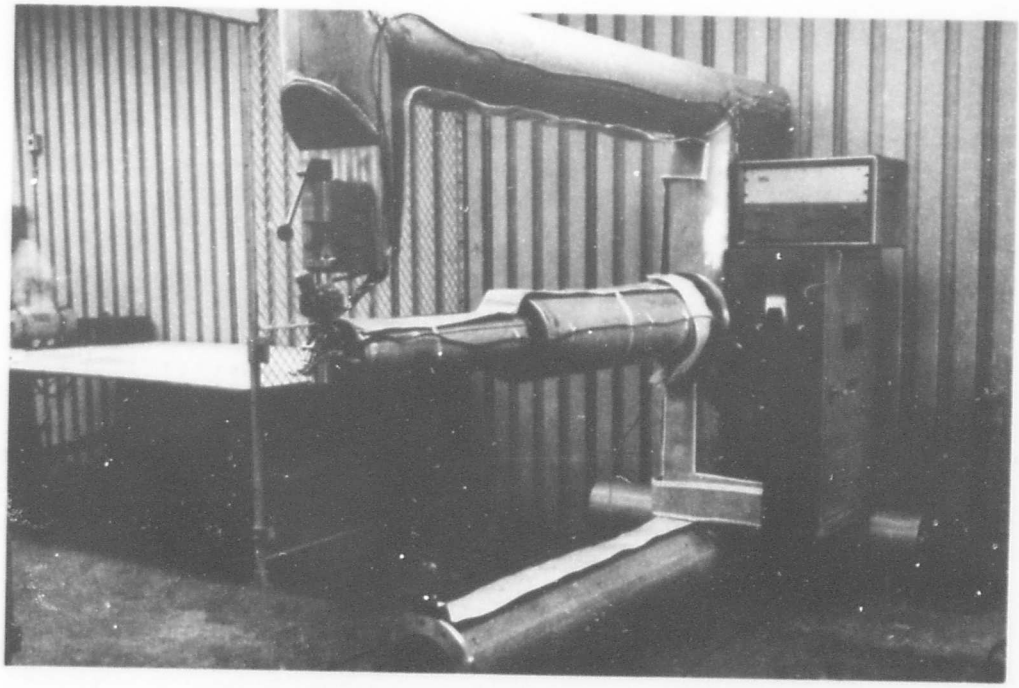

Figure 3. Special Welder for Metal Fabric

The extensive qualification testing on this welding system shows that the weld strength exceeds 89% of the parent fabric strength for a large population of tensile test coupons at the 90% confidence level. The original goal was a weld efficiency of 85% and statistical analysis of the qualification test results indicate that there is more than 99.95% confidence that the average tensile strength of a two-layer weld exceeds this value. In welding the complicated, toroidally shaped apex of the paraglider, the average efficiencies of process control test coupons were 92% for two layer and 87% joint efficiency for five layers.

The entire fabrication technique begins with a very careful cutting, as illustrated in Figure 4, of the metal fabric using templates which have previously been fitted to master forms. The fabric is then layed up on these forms and "basted" in place using a small capacitance discharge power supply and a hand-held copper electrode with the other electrode being a thin copper strip inserted under the proposed joint. After basting, the form is removed from the fabric structure (in the case of the apex it must be disassembled from within the structure), and the unsupported flexible material is taken to the large welder. For a structure with maximum shear strength in the reinforcing skin, permitting torsional loads, two similar structures are assembled with one having the fabric in bias relationship to the other. One of these plies is then inserted within the other and the form again placed within the two ply fabric assembly. This fabric assembly on the form tool is then vacuum impregnated with a liquid silicone rubber. The impregnated fabric may subsequently be overlayed or coated with additional protective or ablative coatings if required. The impregnation process was the subject of considerable developmental effort and the technique which was adopted resulted in complete saturation of the fabric with no voids. This is important for a space structure, since voids would tend to blister and delaminate if the structure were exposed to hard vacuum, and contact of the metal filaments would increase heat transfer and encourage internal fabric abrasion during packaging and in-flight flexing.

Figure 4. Layout and Cutting of Fabric

The objectives of this program included not only the development of material systems and manufacturing techniques, but the testing of a number of components of the paraglider using simulated re-entry loads and temperatures to prove out the design technology as well as the fabrication methods. Fifteen 7 to 10 inch diameter, open ended frustums (tapered cylinders) were fabricated including complete impregnation and ablative coating. These were tested with end closures in place at internal pressures producing the proper reinforcing fabric loading while torsion, shear, and bending loads were applied both at room temperature and temperatures simulating those of the re-entry regime.

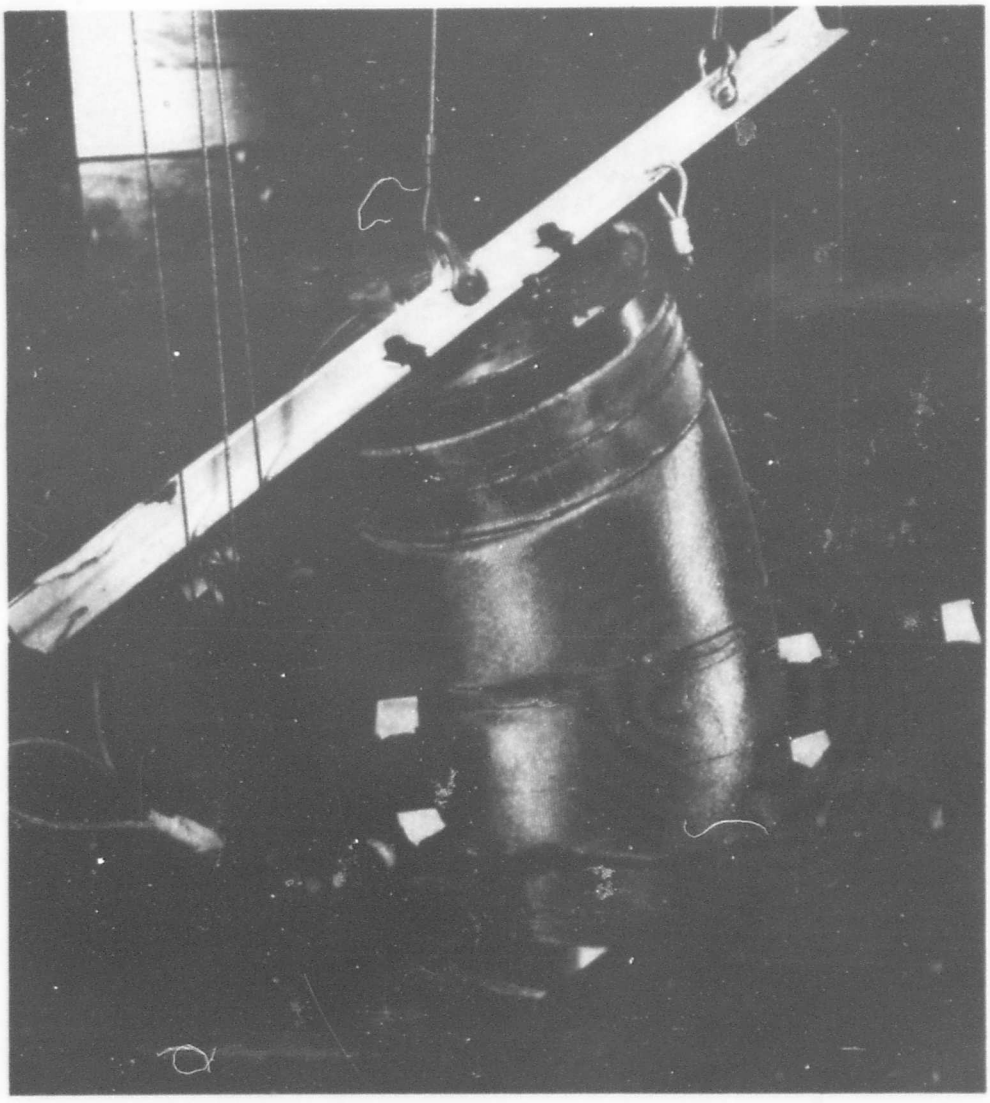

Figure 5. Bending Test on 7-inch Diameter Bias Cylinder

A single ply cylinder which was not coated, but inflated using a thin liner, is shown in Figure 5 during bending test. A typical view of a 10-inch by 30-inch long inflated frustum set up for fatigue loads and pneumatic burst test is shown in Figure 6. Typical results of a burst test are shown in Figure 7. This frustum was exposed to ten 0 to 100% limit load cycles using combined shear, bending and torsion loads while being heated non-uniformly from one side such that external charring of the silicone ablative coating occurred and the metal fabric substrate reached 700 to 800°F. Finally this cylinder has pressurized to final burst at 97 psig while the fabric was at 790°F. All of the frustums and test components were similarly fabricated, but the burst pressure, indicating the uniformity of weld and impregnation processes, increased as fabrication experience was gained. The design calculations on the frustums with two-ply construction for a metal fabric with 340 pound per inch tensile strength indicated we should expect a burst pressure of 61 psig. All of the frustums burst in the range range of 78 to 102 psig, regardless of the effects of previous packaging, creasing, and folding, or high bending, shear, and torsion loads with temperatures to 900°F during the tests. There is no evidence that burst strength was significantly affected by any of these conditions.

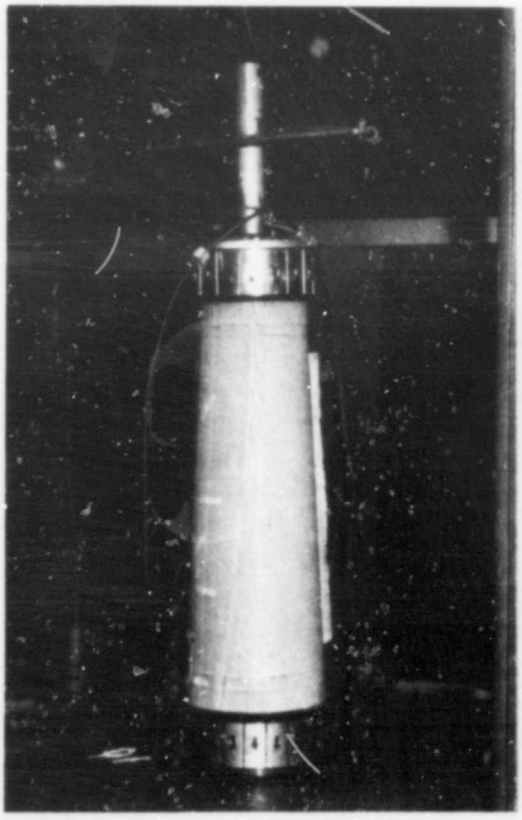

Figure 6. Frustum Set Up for Test - Fatigue Loads and Pneumatic Bursts

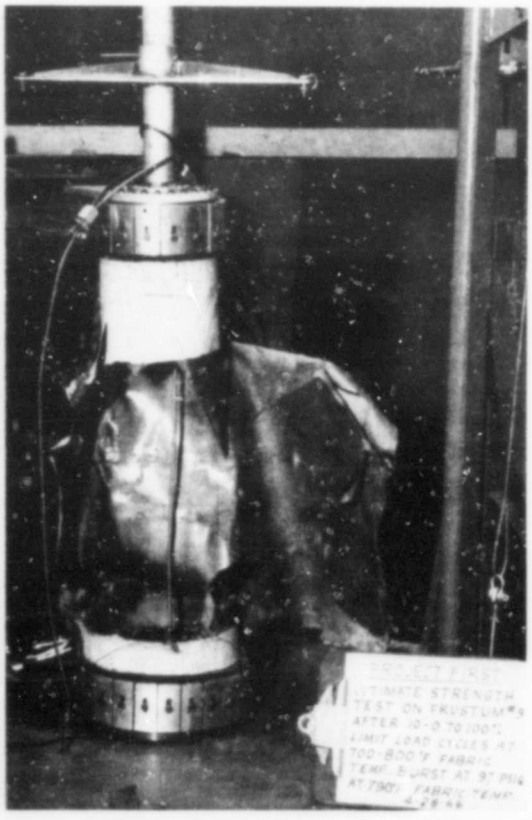

Figure 7. View of Frustum After Bursting

Typical packaging of a frustum is shown in Figure 8 in which the part was folded into a small box resulting in a packaging ratio relative to material of 2.0. The ratio of the volume of the inflated frustum to the package volume was 12.7. This package was subjected to about 80 pounds of preload and exposed to the vibration regime simulating an Apollo launch environment. Subsequently this specimen was burst at 86 psig with failure occurring along the entire longitudinal seam and not in the areas of the folds. This high burst pressure indicated that the preloading, packaging, and vibration while packaged had little, if any, detrimental effect on the ultimate strength of the component.

Based on the experience gained in manufacturing the small cylinders and frustums, a full scale boom tapering from 32 inches to 13 inches diameter and 17 feet long was constructed. The boom is shown in Figure 9,

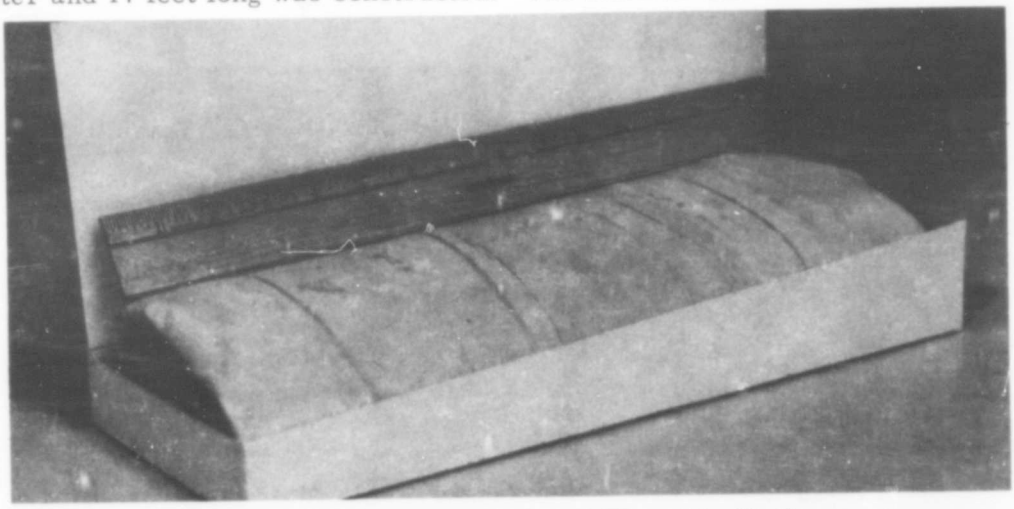

Figure 8. Frustum Folded and Placed in Package

Figure 9. Boom Inflated and Mounted on Supporting Fixture

pressure stabilized at 11 psig and mounted directly under the 100 kw quartz heating lamp bank. Although the smaller test frustums were exposed to separate tests to determine the effects of one type of exposure at a time, the boom was successively exposed to all of the environmental and load conditions anticipated during the re-entry flight of the paraglider. The tests, in order of sequence, included pressure proof and permeability along with accurate recording of the small dimensional changes during pressurization, folding and packaging and packaged vibration, vibration while inflated followed by static limit loads and additional leak and permeability tests.

As part of the packaging test on the boom, it was rolled as shown in Figure 10 and inserted in a metal can for exposure to the Apollo launch vibration test. The volume of the inflated boom was 48.25 cubic feet, while the volume occupied by the rolled boom was 2.35 cubic feet. Therefore, the inflated volume to package ratio was 20.5. The packaging ratio relative to actual material in the boom was 3.1.

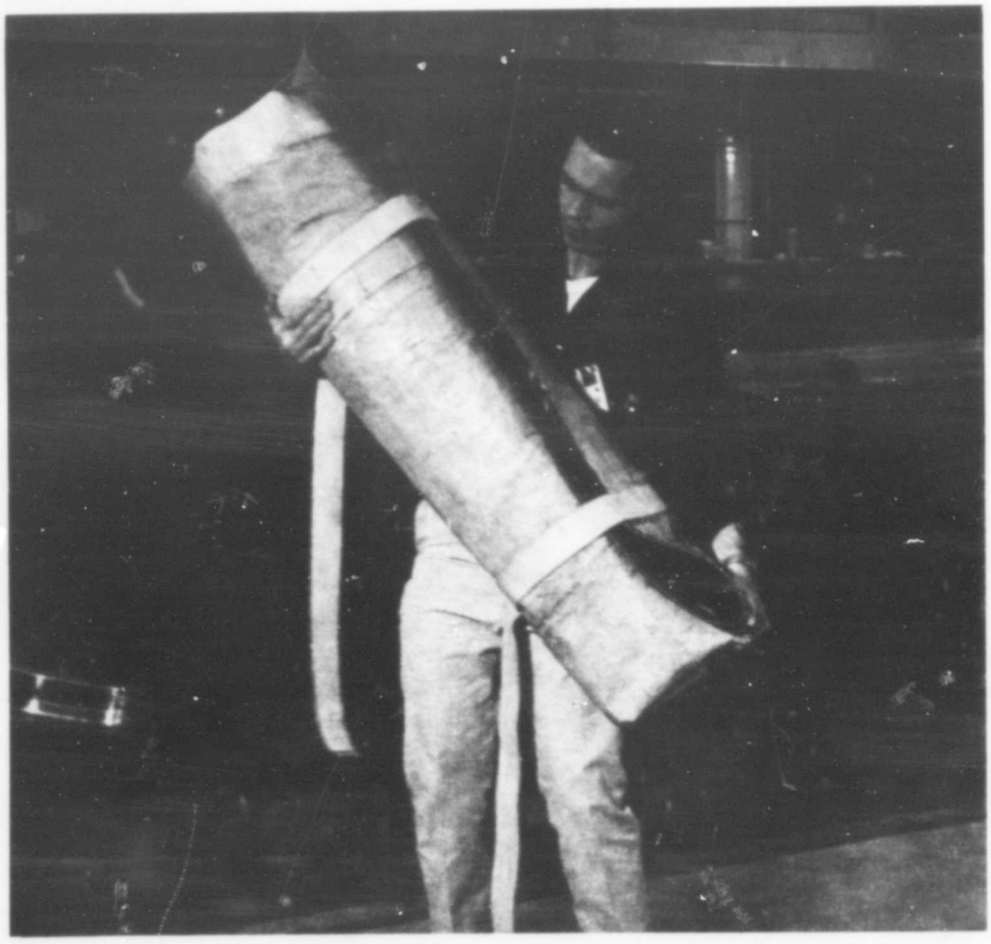

Figure 10. Boom Rolled and Ready to be Packaged in Canister for Vibration Tests

The boom was then remounted on the test support inflated and enclosed in a plastic tent which was purged to about 1% oxygen to simulate the oxygen partial pressure at the re-entry heating altitude. The metal fabric substrate was heated to 800-850°F for ten minutes during which normal charring of the external ablative surface occurred with char reaching approximately 2,000°F. During this heating period the boom was cycled ten times from 0 to 100% of combined limit loads at one cycle per minute. Immediately thereafter, while still being heated, the boom was subjected to a fundamental natural frequency (determined during room temperature testing) of 16 cps at 0.25 g for one minute.

After cooling, the boom was inspected and although severe charring of the ablative material occurred, no significant leakage of pressurizing gas occured as a result of the heating, due to the fact that the impregnated metal fabric substrate showed no damage. The first post-temperature test performed on the boom was another cyclic limit load, fatigue test requiring the combined limit loads of 340 pounds on the tangential wing attachment flap using a whiffletree loading device. The specimen showed no adverse effects from this test. Another vibration test was conducted, and finally combined loads were applied in increments up to a maximum of 300% of design limit load or 1,020 pounds distributed along the wing flap. Incipient buckling was noted at the large supported end of the boom at approximately 240% of limit load.

The large toroidal apex section of the paraglider was constructed using over 200 separate fabric segments welded together in a jigsaw pattern to produce load carrying skin with compound curvature. One ply of this structure is shown in Figure 11. Three-foot long, 32 inch diameter stub

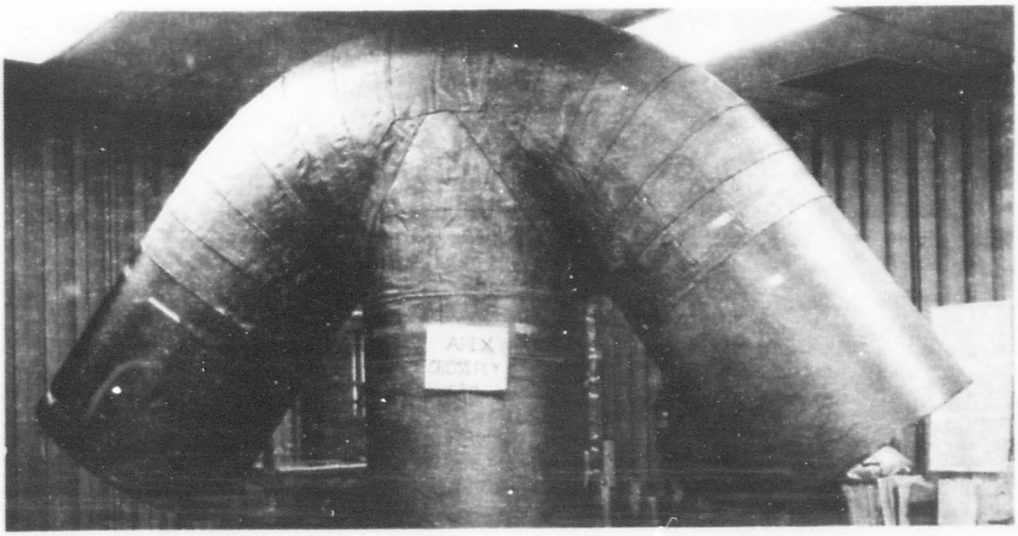

Figure 11. Welded Metal Fabric Outside Ply of Apex Before Applying Metal Tape Wrapping

booms were a part of the apex assembly. After impregnation with silicone rubber the structure appeared as in Figure 12. The outer ply of the apex was "mummy wrapped" with 1.6-inch wide metal fabric tape to carry the circumferential loads through the small radius crotch areas between the keel and leading edge booms. A close-up of the tape wrappings is shown in Figure 13.

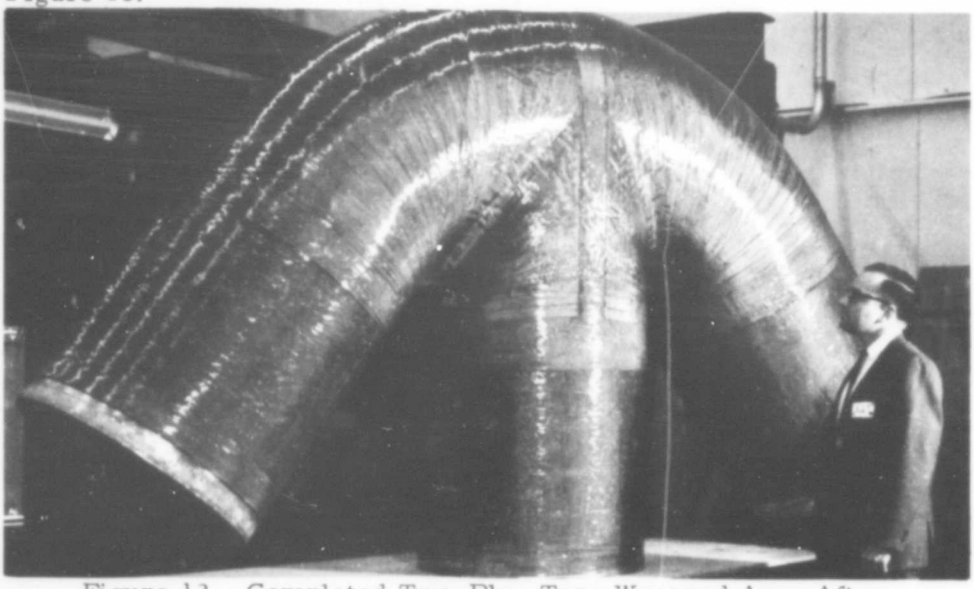

Figure 12. Completed Two-Ply, Tape Wrapped Apex After Impregnation

Figure 13. Close-Up View of Multiple-Layer Tape Wrapping on Apex

Figure 14. Apex Folded in Storage Condition

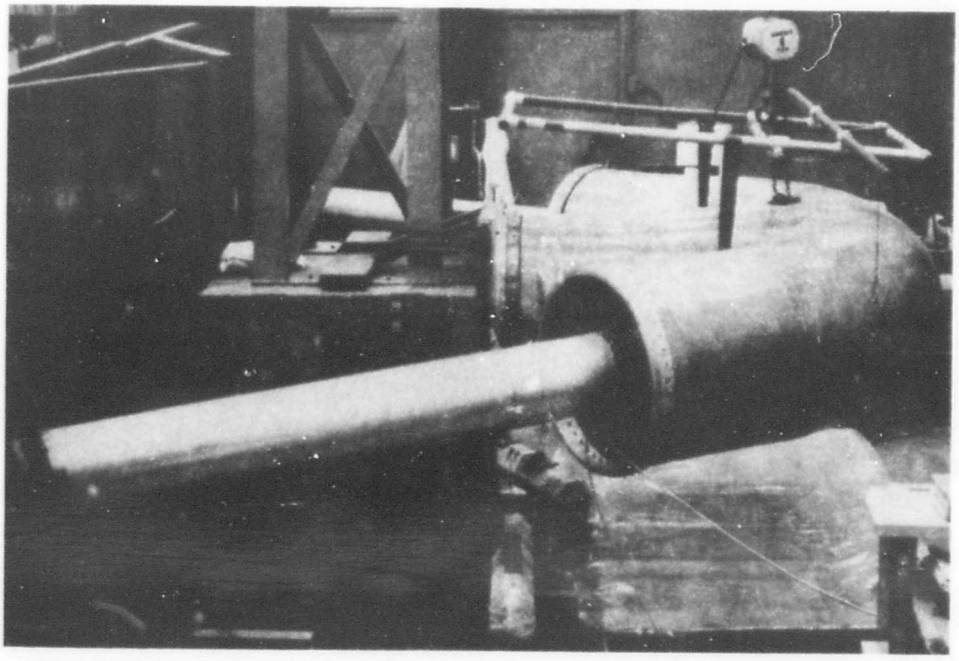

Figure 15. Inflated Apex With Extension Booms for Static Loads Testing

The folded and packaged apex is shown in Figure 14. The corresponding ratio of the inflated volume to the package size was 29.0 while the ratio of the packaged apex to the actual material volume contained was 6.6. It should be noted that the frustums, boom and apex were all equipped with double ply reinforcing cuffs at the closure attachment openings and a steel wire was inserted in this cuff to facilitate clamping of the closures for pressure testing. These wires and cuffs were not removed and this tended to increase the packaged volume somewhat.

The apex mounted for final testing, with boom extension tubes to simulate the proper bending moments which would be created by the wings, is shown in Figure 15.

The results of the tests on these numerous components indicate that both small and large complex metal fabric reinforced, expandable structures can be successfully fabricated by the techniques which have been developed.

Technologies developed in the project are applicable not only to a re-entry vehicle for both manned and other payload return, but to many other space, air, land and sea uses. These include re-entry decelerators, parachutes and other drag devices, inflatable afterbodies, high strength space, land and sea station structures, expandable rocket nozzles, high temperature, high strength protective space suits, blast and radiation resistant enclosures, bullet and shrapnel protection suits and enclosures, inflatable buoys for deep-sea rescue and recovery of large objects such as submarines, inflatable deep-sea buoyant structures, deep-sea vehicle fairings and numerous other less exotic uses such as high temperature tire reinforcement -- and even uses in architecture and interior decorating.

In summary, the technologies which have been developed and which are applicable to these numerous uses include the utilization of ultrafine metal wire and the production of metal yarn for weaving high strength high temperature fabrics to suit the application, capability of producing highly efficient multiple layer seams in these fabrics, and impregnation and coating with not only elastomeric materials, but also with rigid materials such as epoxy and phenolic plastics. It is anticipated that this new materials and fabrication technology will open a vast new realm of applications to make man's life more comfortable and his explorations more successful.

DYNAMIC THERMOELASTIC PROPERTIES OF INFLATABLE DELTA WINGS

*Samuel J. Pollock

SECTION I - INTRODUCTION

The use of inflatable structures for winged entry vehicles is attractive because of the good packaging characteristics during boost and reduced aerodynamic heating provided by low wing loading during re-entry. The highly flexible nature of inflatable materials means that their structural dynamic properties must be given special consideration. Thermoelastic properties of inflatables are required to evaluate their dynamic characteristics at hypersonic speeds.

A process of weaving metal fabric structures, developed by Goodyear Aerospace Corporation, has the trade name "Airmat". Several investigators have studied the stiffness and vibration characteristics of inflatable structures constructed of nylon, dacron, or metal fabric. Analytical and experimental investigations of inflatable fabric plate-like structures were performed by Leonard, et al (Reference 1), McComb (Reference 2) and Stroud (Reference 3). Influence coefficients have been determined for inflatable delta wing models and used to predict vibration characteristics by Seath (Reference 5), Martuccelli, et al (Reference 6) and Mar (Reference 7). Most of the previous investigations were for inflatable structures at room temperature. The prediction and evaluation of dynamic characteristics of inflatables at hypersonic speeds requires a knowledge of the effect of temperature on stiffness characteristics. Since material system properties of this relatively new construction have not been established, this effect must be determined through tests.

The purpose of this investigation was to determine the static and vibration characteristics of inflatable Airmat models at temperatures up to 650 degrees Fahrenheit for various model internal pressures. The 65 degree sweep delta wing models with a root chord length of 51.1 inches chosen for this investigation are geometrically similar to the flutter models of Reference 6, which had a root chord length of 24 inches. Three models were purchased from Goodyear Aerospace Corporation for this investigation. Stiffness and vibration properties of these models were determined by uniform load, influence coefficient, and vibration tests at temperatures up to 650 degrees Fahrenheit in the Structural Test Facility at WPAFB, Ohio. Deflection and vibration predictions using available theories and measured influence coefficients are correlated with experimental results.

*Aerospace engineer at the Air Force Flight Dynamics Laboratory, Wright-Patterson AFB, Ohio

SECTION II - MODEL DESCRIPTION

The Airmat models investigated had a nominal leading edge sweep angle of 65 degrees. The root chord was 51.1 inches and the trailing edge span was 24.5 inches. The models were 3 inches thick and had rounded leading and trailing edges. Figure 1 shows the model assembly.

The model structure consists of two basic materials; woven stainless steel Airmat, and a silicone elastomer coating. The Airmat material is the basic wing structure when inflated and the elastomer coating makes internal pressurization possible.

The Airmat material was woven from Type 304 annealed stainless steel wire .0045 inches in diameter. The Airmat faces have 98 wires per inch in both the warp and fill direction. The drop wires were of the same material and there were 31.2 drop wires per square inch. The warp direction of the Airmat was oriented parallel to the base plate.

Models one and two were coated with S-2077 silicone elastomer while model three was coated with CS-105 silicone-ceramic elastomer. Dow Corning Corporation's S-2077 silicone elastomer is a proprietary composition of a silicone polymer, filler, binder, plasticizer, and vulcanizing agent. The CS-105 elastomer consists of S-2077 loaded with Harshaw Chemical's AW-35 ceramic frit. Reference 4 contains an evaluation of the coatings. The white S-2077 coating is considered adequate for temperatures up to 800 degrees Fahrenheit while the black CS-105 coating is used for higher temperature applications.

The first step in the model fabrication was to cut a triangular shape out of the woven Airmat metal fabric. The drop wires in the leading and trailing edges were then clipped back to allow the top and bottom faces to be brought together, lapped, and resistance spot welded. This provides semi-cylindrical leading and trailing edges when the models are inflated. The drop wires in the base plate area were then clipped back and a one-half inch thick stainless steel base plate inserted. Airmat metal fabric was attached to the base plate by resistance spot welding. A clamping bar around the periphery of the base plate prevented tension loading on the spot welds that attach the Airmat to the base plate. The stainless steel clamping bar was attached to the base plate by stainless steel screws with approximately two inch spacing. Sixteen tapped holes in the base plate were used to attach the model to the test jig. Pipe threaded holes in the base plate provided attachment of air inlet and pressure gage fittings.

A number of stainless steel discs were welded to the upper and lower surfaces of the Airmat models prior to coating. The location of these discs is given in Figure 2. The discs on the upper surface were ¼ inch in diameter and approximately 1/8 inch thick. The discs on the lower surface were ½ inch in diameter and approximately 1/16 inch thick.

The Airmat assembly was next cleaned and coated with elastomer. After the coating was cured the clamping bars were fitted and attached. Further information on model properties and construction is contained in References 8 and 9.

The actual weights of the three models, not including the base plate and clamping bar were:

Model One - 2.83 lbs.
Model Two - 2.86 lbs.
Model Three - 3.65 lbs.

SECTION III - INSTRUMENTATION

A. PRESSURE CONTROL

Model internal pressure was regulated during the tests by the control system shown schematically in Figure 3. Pressure was recorded by a Data Sensors, Inc. model PB536G-1 pressure transducer with a range of 0-15 psig. The transducer inaccuracy is ± .0465 psig.

B. DEFLECTION TRANSDUCERS

Standard deflection potentiometers were modified by removing the spring and adding a pulley and weight system to reduce the load on the model as discussed in Reference 10. The wires from the transducers were attached to the lower surface of the model at locations given in Figure 2 by hooks welded to the ½ inch discs discussed in the previous section. Figure 4 shows twelve transducers attached to model one for measuring static deflections.

C. THERMOCOUPLES

Thermocouples were installed on the models by Goodyear Aerospace Corporation for use in controlling and monitoring the model skin temperature. Additional thermocouples were installed by the Air Force Flight Dynamics Laboratory personnel to obtain better temperature control. Thirty-four thermocouples of the Chromel-Alumel (ISAK) type were used at various locations on the upper and lower surface and along the center line of the leading and trailing edges.

D. ACCELEROMETERS

Endevco Model 2226 accelerometers were attached at six of the loading points given in Figure 2 on the upper surface of model one by Eastman 910 glue. These accelerometers weigh only 0.1 ounce each and should not significantly affect the model vibration characteristics.

Modified accelerometer mounting studs were made interchangeable with the deflection transducer hooks on the lower surface of models two and three. Ten Endevco Model 2245B accelerometers were attached to the lower surface of model two for the room and elevated temperature vibration tests as shown in Figure 6. These accelerometers are capable of operation at temperatures up to 750 degrees Fahrenheit and weigh about one ounce each. Since there are ten of these accelerometers on the model and the model weighs less than three pounds, the accelerometers have a significant effect on vibration characteristics. For the inflatable model considered as a simple spring-mass system, the resonant frequency is reduced by about ten percent due to the added mass of the ten accelerometers. To determine the actual vibration characteristics of model two, the effects of this added mass would have to be evaluated. Since only qualitative information concerning the effects of temperature on mode shapes and frequencies were required, no corrections were made to the measured vibration data. In order to obtain vibration data on model three at temperatures above 750 degrees Fahrenheit, an accelerometer was attached at the bottom of the shaker where it was shielded from the high temperatures.

SECTION IV - TEST PROCEDURES

A. UNIFORM LOAD

Uniform load tests were conducted on models one and two (silicone elastomer coating without ceramic frits) at room temperature with internal pressures of 2, 4, 6, 8, and 10 psi. The uniform loading was accomplished by means of small bags containing lead shot placed over the planform of the wing as shown in Figure 4. The deflections were simultaneously recorded for all of the transducers.

B. INFLUENCE COEFFICIENTS

Influence coefficients were obtained for model one at internal pressures of 2, 4, 6, 8, and 10 psi at room temperature and 2, 6, and 10 psi at 650 degrees Fahrenheit. Twelve load points for influence coefficient tests were located on the top surface of model one as discussed under model description. Figure 7 illustrates the method of loading. Loading plates with diameters of 2.75 inches were placed on the loading points in order to avoid excessive local deformations. The loading plates contained a depression to allow accurate positioning of the loading rod.

Deflection readings were taken at all 12 points on the model for zero load and three other loads applied at each point. Due to large hysteresis effects, only deflections measured for increasing load increments were used to determine influence coefficients. This procedure was repeated until loads had been applied at all 12 points. A total of 1152 plots of deflection versus load were required to establish

12 x 12 flexibility influence coefficient matrices for five different pressures at room temperature and three different pressures at 650 degrees Fahrenheit.

C. VIBRATION TESTS

Vibration tests were conducted on all three of the cantilevered, inflatable models. A five pound force electro-magnetic shaker was attached near the tip of the models as shown in Figure 6. A long rod was attached to the shaker and to the model. The fundamental frequency of the rod was not within the range of excitation frequencies used during the vibration tests. This should prevent any significant influence of rod dynamics on the model vibration characteristics. The output from the accelerometers was observed on a voltmeter or on the oscilloscope and the frequency obtained from an electronic counter. The data were recorded on a tape recorder and/or on an oscillograph for analysis. Vibration tests were conducted at room temperature on all of the models. In addition, model two was tested at 500 and 650 degrees Fahrenheit. Model three (silicone elastomer coating with ceramic frits) was also tested at 300, 500, 650, and 800 degrees Fahrenheit.

Damping was determined by shutting off the excitation of the model at the shaker. The damping coefficient was determined from the logarithm of the ratio between the amplitudes of successive cycles in the decay curve.

Node lines were obtained at room temperature by sprinkling white sand, coffee grounds, or sunflower seeds over the surface of the model and observing the nodal pattern for the various modes. Different materials were required to aid observation on the various models which were either black or white and all materials mentioned were successful for this purpose. At elevated temperatures, mode shapes were obtained from the accelerometer data.

The vibration frequency was found to depend on amplitude of vibration, being higher at lower amplitudes. The amplitude of excitation was kept small during the tests in order to minimize variations in the frequency due to amplitude. This nonlinear behavior was also reported by Martuccelli, et al, for the flutter models of References 6 and 7.

SECTION V - THEORY

A. SHEAR THEORY

A simplified method of computing deflection and frequency characteristics of inflatable plates has been derived by Martuccelli, et al, and is briefly described in Reference 6. This section contains a summary of the method and results of its application to the delta wing models. The coordinate system used is shown in Figure 2. The strain energy expression for an inflatable Airmat plate of uniform thickness, h, undergoing small deformations is:

$$U_s = \frac{h^2}{4} \iint_S \left\{ A_{11} \left(\frac{\partial \alpha}{\partial x} \right)^2 + A_{22} \left(\frac{\partial \beta}{\partial y} \right)^2 + 2A_{12} \frac{\partial \alpha}{\partial x} \frac{\partial \beta}{\partial y} + A_{33} \left(\frac{\partial \alpha}{\partial y} + \frac{\partial \beta}{\partial x} \right) \right\} dx\, dy + \tfrac{1}{2} \iint_S ph \left\{ \left(\alpha + \frac{\partial w}{\partial x} \right)^2 + \left(\beta + \frac{\partial w}{\partial y} \right)^2 \right\} dx\, dy \quad (1)$$

where the internal pressure, p, has been substituted for the shear modulus, G, in the stress-strain relations. The drop chords remain straight and rotate to an angle α from the vertical in the x direction and β from the vertical in the y direction. The deflection, w, is positive down. If the surfaces are treated as orthotropic with the x and y axes aligned with the principal direction then:

$$A_{11} = E_1 t / (1 - \mu_{12} \mu_{21}) \qquad A_{12} = \mu_{21} E_1 t / (1 - \mu_{12} \mu_{21}) \quad (2)$$

$$A_{22} = E_2 t / (1 - \mu_{12} \mu_{21}) \qquad A_{33} = Gt$$

E is Young's modulus, t is the Airmat cover skin thickness and $E_1 t$ and $E_2 t$ are the extensional stiffnesses in the x and y directions, respectively. μ_{12} is the Poisson's ratio associated with a contraction in the y direction caused by a tensile stress in the x direction and μ_{21} is the corresponding ratio for the other direction.

If the bending deflections are considered negligible in comparison with shear deflections, that is, deformations are purely of the shear type, then $\alpha = \beta = 0$ and the strain energy becomes:

$$U_s = \tfrac{1}{2} \iint_S ph \left\{ \left(\frac{\partial w}{\partial x} \right)^2 + \left(\frac{\partial w}{\partial y} \right)^2 \right\} dx\, dy \quad (3)$$

Using the Rayleigh-Ritz method, the deflection, w, is represented by:

$$w(x, y, t) = \sum_{n=1}^{N} q_n(t)\, w_n(x, y) \quad (4)$$

where the quantities $q_n(t)$ are generalized coordinates and $w_n(x,y)$ are assumed displacement functions that satisfy the geometric boundary conditions. The following powers of $\bar{x}$ and $\bar{y}$ are chosen:

$$w_1 = \bar{y}\ ,\ w_2 = \bar{x}\,\bar{y}\ ,\ w_3 = \bar{y}^2\ ,\ w_4 = \bar{x}^2\,\bar{y},\ \ w_5 = \bar{x}\,\bar{y}^2,\ w_6 = \bar{y}^3,\ w_7 = \bar{x}^2\,\bar{y}^2,$$

$$w_8 = \bar{x}\,\bar{y}^3 \ \text{ and } \ w_9 = \bar{y}^4 \qquad (5)$$

where $\bar{x} = x/c$, $\bar{y} = y/c$ and c is the root chord.

1. DEFLECTION PREDICTION

The deflection under a uniform static load was calculated by Martuccelli, et al, from the solution to the non-homogeneous Lagrange's equation. For a 65 degree delta wing the deflection due to a uniform load is given by:

$$w(\bar{x},\bar{y}) = c^2 f/ph\,[.3698\bar{y} - .0622\bar{x}\bar{y} - .5338\bar{y}^2 - .3139\bar{x}^2\bar{y} + .2795\bar{x}\bar{y}^2 + .2084\bar{y}^3$$
$$- .3383\,\bar{x}^2\bar{y}^2 - .3426\bar{x}\bar{y}^3 - .0173\bar{y}^4] \qquad (6)$$

where f is the load intensity in psi.

2. VIBRATION PREDICTION

The expression for kinetic energy can be formed and the homogeneous form of Lagrange's equation applied to give an eigenvalue problem. The eigenvalue can be written:

$$\lambda = \omega^2\,\bar{m}\,c^2/\,ph \qquad (7)$$

where $\bar{m}$ is the mass per unit area. For a 65 degree delta the first three eigenvalues were found by Martuccelli, et al, to be:

$$\lambda^{(1)} = 19.224, \quad \lambda^{(2)} = 77.549, \text{ and } \lambda^{(3)} = 147.32 \qquad (8)$$

with the associated eigenvectors:

$$q^{(1)} = \begin{Bmatrix} -0.012 \\ 0.106 \\ -0.198 \\ 0.053 \\ 1.000 \\ -0.873 \\ -0.906 \\ 0.772 \\ 0.031 \end{Bmatrix},\ q^{(2)} = \begin{Bmatrix} 0.035 \\ -0.313 \\ -0.167 \\ 0.304 \\ 1.000 \\ -0.253 \\ -0.964 \\ 0.746 \\ -0.567 \end{Bmatrix},\ \text{and } q^{(3)} = \begin{Bmatrix} -0.037 \\ -0.533 \\ 0.642 \\ 0.962 \\ 1.000 \\ -2.943 \\ -2.714 \\ -0.808 \\ 4.851 \end{Bmatrix} \qquad (9)$$

B. VIBRATION PREDICTION USING INFLUENCE COEFFICIENTS

The vibration analysis using measured influence coefficients is based on standard procedures described in Reference 11. The equation to be solved is usually written as:

$$\frac{1}{\omega^2}\{w\} = [C][m]\{w\} \qquad (10)$$

where w is the deflection of the wing, C is a matrix of flexibility influence coefficients, and m is a diagonal matrix of lumped section masses. The solutions for $1/\omega^2$ are called eigenvalues and the w's associated with the eigenvalues are called eigenvectors.

Flexibility influence coefficients were obtained from the measured deflection-load data as illustrated in Figure 8. Two sets of influence coefficients were calculated. The first set of influence coefficients represented a straight-line approximation to the measured data, omitting the zero load point. Since the model was vibrated at small amplitudes, the influence coefficients were also calculated by drawing a curve through the measured deflection load points and using a tangent to the curve at the zero load point.

The mass matrices for inflatable model one (coating without ceramic frits) and the influence coefficient matrices calculated from the measured data by the above procedures are presented in Reference 12.

SECTION VI - RESULTS

A. UNIFORM LOAD TESTS AND CORRELATION WITH SHEAR THEORY

Static vertical deflections due to uniformly distributed loads at model internal pressures of 2, 4, 6, 8, and 10 psi are presented in Reference 12 for models one and two which do not have ceramic frits in the coating. The results were essentially the same for both models at the same loading and pressure conditions.

Figure 9 presents the measured vertical deflections due to a uniform load, together with shear theory predictions for an internal pressure of 4 psi. The experimental deflection for point 9N which is located near the leading edge of model two is always lower than predicted. This is caused by the stiffening effect of the rounded edges which is not accounted for by the theory. It should also be noted that the predicted deflection at point 9N is higher than that at 9, since 9N is one inch farther from the root than 9. However, the experimental deflections are always less for point 9N than for point 9. This is a further demonstration of the stiffening effect of the rounded leading edge. Good agreement was obtained between experiment and shear theory predictions for points away from the edges of the models.

Figure 5 shows that the slope at the root for the cantilevered model is not zero. This indicates that shear deformation must be considered in the

static and vibration theories for the inflatable Airmat structure.

B. VIBRATION TESTS AND CORRELATION WITH SHEAR THEORY

Figure 10 presents a comparison between shear theory prediction and experiment for the first vibration mode frequency versus pressure for model three (ceramic frits in coating). These results are for room temperature conditions. The vibration frequency predicted by shear theory is 40 percent lower than experiment at a model internal pressure of 2 psi. As internal pressure is increased, agreement between shear theory and experiment improves and the predicted value for the first mode frequency is 20 percent lower than experiment at 6 psi and 9 percent lower than experiment at 10 psi. Agreement between shear theory predictions and experiment was better for the first vibration mode frequency of model one which had no ceramic frits in the coating; the predicted frequency was 17 percent lower than experiment at 2 psi and only two percent lower at 10 psi. The better agreement at the higher pressures indicates that shear theory provides a better structural representation at the higher internal pressures. Possible reasons for discrepancies between experiment and shear theory predictions can be seen in the mode shapes.

From the measured mode shapes presented in Reference 12, the relative amplitude in the first mode for model two at point 9N is less than that at point 8 at all internal pressures although 9N is five inches farther from the root than 8. Since point 9N is near the leading edge, the lower amplitude is probably due to the stiffening effect of the rounded edges which is not accounted for by shear theory.

The vibration frequencies for model one plotted versus pressure on a log-log scale in Figure 11 are straight lines as noted by Seath in Reference 5. This indicates that the frequency is an exponential function of the model internal pressure. The exponent is about ¼ for the first mode and approaches ½ for the higher modes. Shear theory predicts an exponent of ½.

In Figure 12 the node lines predicted from the vibration analysis using shear theory are compared with the experimental node lines for the second and third modes of models one and two (no ceramic frits in coatings). The predicted node line for the second mode is in good agreement with experiment, but the predicted node line for the third mode deviates somewhat from experiment.

C. VIBRATION TESTS AND CORRELATION WITH PREDICTIONS USING INFLUENCE COEFFICIENTS

The correlation between the measured vibration frequencies at room temperature and the frequencies predicted by analyses using tangent-curve influence coefficients are shown in Figure 11 for the first three vibration modes of model one. Vibration predictions were made using influence coefficients based on both tangent-curve approximation at the zero load point and straight-line approximation omitting the zero load point as described previously. Calculated vibration frequencies for the first two modes using influence coefficients based on tangent-curve approximations, were about five percent higher than the corresponding calculations for straight-line approximations. This five percent

increase in frequency greatly improved the correlation between calculated and experimental frequencies. The predicted first and second vibration mode frequencies using tangent-curve influence coefficients average 6.0 and 4.5 percent, respectively, below experiment. This is believed to be within the accuracy of the experimental techniques. Some uncertainties in the measured influence coefficients used in vibration predictions were caused by nonlinear load-deflection characteristics, large hysteresis effects, and inelastic behavior of the structure. Measured vibration frequency uncertainties result from nonlinear dependence on amplitude of excitation and extreme sensitivity to variations in temperature around 70 degrees Fahrenheit.

In Figure 13, node lines interpolated from vibration calculations using influence coefficients measured at room temperature are compared with the corresponding experimental node lines. Agreement between prediction and experiment is reasonable for the first five modes except for the fourth mode. The node lines for the fourth mode predicted by calculations based on influence coefficients are similar to the experimental node lines observed for the fourth mode of the flutter models by Martuccelli, et al, in References 6 and 7.

By Maxwell's law of reciprocal deflections for an elastic structure, $C_{ij} = C_{ji}$ where C_{ij} is the influence coefficient for the deflection at i due to a load at j (Reference 11). The experimental values for C_{ij} and C_{ji} differed considerably in some instances. Similar behavior was reported in Reference 7 for the inflatable delta wing models of that study. The largest discrepancies were for stations near the root on the forward part of the model. Some of the influence coefficient matrices were made symmetrical by averaging the C_{ij} and C_{ji} terms. When these symmetrical influence coefficients were used in vibration calculations, no appreciable difference was noted in the predicted vibration frequencies or in the eigenvectors as compared to calculations using the unsymmetrical measured coefficients. Measured values of influence coefficients were used in the vibration analyses of this investigation.

D. TEMPERATURE EFFECTS ON VIBRATION

The measured room temperature vibration characteristics for model one (no ceramic frits in coating) are presented in Reference 12. The model was held at 650 degrees Fahrenheit for approximately five hours to obtain influence coefficient data, then cooled to room temperature. When the models are exposed to temperatures of 650 degrees Fahrenheit or higher, crazing occurs after cooling. The coating becomes flaky and tends to crack if flexed. The first mode frequency was about 16 percent higher for an internal pressure of 2 psi after the 650 degree Fahrenheit test. However, at internal pressures of 4, 6, 8 and 10 psi, the first mode frequencies after the 650 degrees Fahrenheit test were essentially the same as before the test. The relative amplitude in the first mode was the same except near the leading edge where it was about ¼ the value prior to the 650 degree Fahrenheit test for all model internal pressures. There was practically no change in the second and third mode frequencies or mode shapes.

The first three vibration mode frequencies calculated for model one based on influence coefficients measured at 650 degrees Fahrenheit are presented in Reference 12. The predicted first mode frequency at 2 psi and 650 degrees Fahrenheit is about 11 percent higher than the predicted room temperature value. At 10 psi and 650 degrees Fahrenheit the predicted first mode frequency is about 1.5 percent higher than the predicted room temperature value. This predicted rise in frequency from room temperature to 650 degrees Fahrenheit was observed during vibration tests of model two which has the same type of coating as model one. For model two the increase in the first vibration mode frequency at 650 degrees Fahrenheit was 32 percent at 2 psi and 9 percent at 10 psi. The predicted and observed increase in second and higher vibration mode frequencies at 650 degrees Fahrenheit was less than for the first mode. An evaluation of the eigenvectors given in Reference 12 indicates that the mode shapes predicted for the first mode of model one at 650 degrees Fahrenheit are not significantly different from the room temperature mode shapes. However, the second and higher vibration mode shapes at 650 degrees Fahrenheit are altered considerably from the comparable values at room temperatures.

Figure 14 shows the effect of temperature on the first vibration mode frequency of models two and three at 10 psi (model two was coated with S-2077 elastomer without ceramic frits and model three was coated with the CS-105 elastomer which contains ceramic frits). Data were obtained at about 70, 300, 500 and 650 degrees Fahrenheit. Vibration frequencies decreased from about 70 degrees Fahrenheit up to about 300 degrees Fahrenheit and then increased from about 300 to 650 degrees Fahrenheit. The vibration equency varies most rapidly at room temperature. The first mode frequency of model three at an internal pressure of 2 psi changed by six percent as the room temperature changed from 68 to 73 degrees Fahrenheit. The trends with temperature were generally found to be similar to those observed by Martuccelli, et al, who determined by tests at small increments of temperature that the minimum frequency occurred at about 300 degrees Fahrenheit. The curves of Figure 14 were drawn to incorporate these previously observed trends. At 650 degrees Fahrenheit, the first vibration mode frequency for model two was as much as 32 percent higher than at room temperature while the corresponding frequency for model three was about ten percent lower than at room temperature. The mode shapes for model two at 500 degrees Fahrenheit and 650 degrees Fahrenheit did not change appreciably from room temperature values.

The measured structural damping coefficients for model two are presented in Reference 12. In the first mode the damping coefficient at room temperature was about 0.15. This is higher than most conventional structures. In higher modes the damping coefficient decreased to as low as 0.02 for the fifth mode. At 650 degrees Fahrenheit the damping coefficient decreased to as low as 0.04 in the first mode and .008 in the fifth mode. the damping coefficient, g, depends on the amplitude of vibration and is higher for higher amplitudes.

Model three (ceramic frits in coating) burst during hot vibration tests. The conditions at failure were an internal pressure of 10 psi and a uniform temperature of approximately 800 degrees Fahrenheit. The temperature distribution prior to failure is given in Reference 10. Smoke was observed before the explosion and the drop cords appeared to have failed in tension. This type failure was unexpected since the calculated internal pressure for average ultimate strength of the stainless steel drop wires was about 32 psi at 800 degrees Fahrenheit.

SECTION VII - CONCLUSIONS

From this analytical and experimental investigation of inflatable Airmat delta wing structures, it is concluded that:

1. Vibration calculations using influence coefficients, based on drawing a tangent to the measured deflection-load curve at the zero load point, gave satisfactory correlation with experiment. The tangent-curve approximation was required because of the nonlinear deflection-load behavior and the small vibration amplitudes. Locating some of the stations for influence coefficients closer to the leading and trailing edges of the models would probably improve correlation of vibration predictions with experiment since these rounded edges act as stiffeners or spar-beams.

2. Shear theory predictions for the first vibration mode frequencies were lower than experiment by as much as 40 percent at 2 psi, but only 9 percent at 10 psi. This indicates that shear theory provides a relatively good structural representation for higher internal pressures, but for low internal pressures, metal fabric bending terms must also be included in the analysis for good vibration prediction.

3. For deflections due to a uniformly distributed load, good agreement was obtained between shear theory predictions and experiment. Some local discrepancies occurred close to the leading edge where the experimental deflections were smaller than predicted. This again demonstrates the stiffening effect of the rounded leading edges, which is not accounted for in this theory.

4. When inflatable structures with silicone elastomer coatings are exposed to temperatures above 500 degrees Fahrenheit, and then cooled to room temperature, the coating becomes flaky and tends to crack if flexed. After cooling to room temperature, the first vibration mode frequency is considerably altered while higher mode frequencies are relatively unaffected. For a model without ceramic frits in the silicone elastomer coating the first vibration mode frequency was about 16 percent higher at 2 psi after the model was heated to 650 degrees Fahrenheit and then cooled.

5. The effects of high temperature on vibration were somewhat different for the two types of coating. For the model with the CS-105 elastomer coating (with ceramic frits), the first mode frequency at 650 degrees Fahrenheit was about 10 percent <u>below</u> the room temperature value,

whereas for the model coated with the S-2077 elastomer, the frequency was as much as 32 percent above the room temperature value. Similar results were obtained for the second and higher vibration mode frequencies although the percentages were less.

6. Additional analytical and experimental work on inflatable structures is needed in the following areas to improve accuracy of prediction methods and increase confidence in the design of inflatable structures for re-entry applications:

a. The free edges of the delta wing models with rounded leading and trailing edges act as stiffeners or spar-beams. These edges should be included in the structural analysis as discrete elements to attempt to improve agreement between theory and experiment.

b. A better knowledge of the stiffness properties of the surface material is required so that bending-type deformations can be included in structural dynamic analyses for low internal pressures where these bending terms may become important. Bending terms were not included in the analyses of this paper.

c. The determination of scaling laws for inflatable structures is required so that these results can be used in preliminary design of full-scale inflatable wings.

SECTION VIII

REFERENCES

1. Leonard, R. W., Brooks, G. W., and McComb, Jr., H. G., Structural Considerations of Inflatable Re-entry Vehicles, NASA TN D-457, Sept 1960

2. McComb, Jr., H. G., A Linear Theory for Inflatable Plates of Arbitrary Shape, NASA TN D-930, Oct 1961

3. Stroud, W. H., Experimental and Theoretical Deflections and Natural Frequencies of an Inflatable Fabric Plate, NASA TN D-931, Oct 1961

4. Cross, W. B., Marco, D. M., and Nass, F., New and Improved Materials for Expandable Structures (Phase III - Re-entry Coatings) ASD-TDR-62-542, Part IV, Oct 1963

5. Seath, D. D., Vibration of an Inflatable Fabric Wing Model, Dissertation for the Degree of Doctor of Philosophy, Iowa State University of Science and Technology, Ames, Iowa, 1963

6. Martuccelli, J.R., Durgin, F. H., and McCallum, R. B., "Construction and Testing Techniques of Inflatable Flutter Models", RTD-TDR-63-4197, Part I, Proceedings of Symposium on Aeroelastic and Dynamic Modeling Technology, March 1964

7. Mar, J. W., Static and Vibration Behavior of Inflated Rectangular and Delta Planform Plates, AFFDL-TR-65-203, January 1966

8. Scoville, R. I., Topping. A. D. and Nordlie, R. W., Model Data, Inflatable Model for Dynamic Thermoelastic Tests, GER-11740, 1964

9. Nordlie, R. W., Model Data, Inflatable Model for Dynamic Thermoelastic Tests, GER-11740, Supplement 1, 1965.

10. Monfort, J. B. Inflatable Structure Test Program, AFFDL-TR-65-181, Dec 1965

11. Bisplinghoff, R. L., Ashley, H., and Halfman, R. L, Aeroelasticity, Addison-Wesley Publishing Company, Inc., Reading, Massachusetts, 2nd Printing, Nov 1957

12. Pollock, S. J., Stiffness and Vibration Characteristics of Inflatable Delta Wing Models at Temperatures up to 650 Degrees Fahrenheit, AFFDL-TR-66-14, June 1966

LIST OF ILLUSTRATIONS

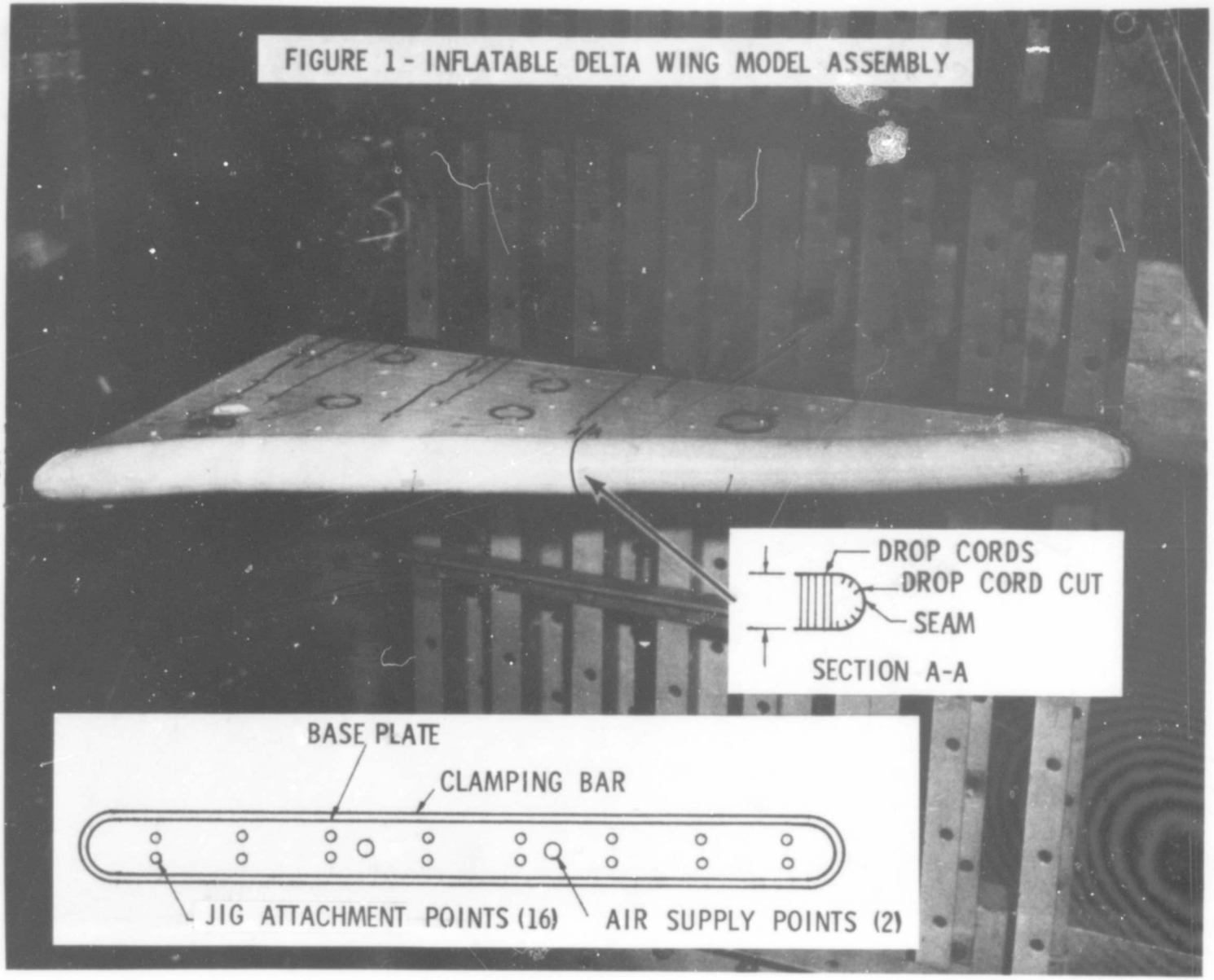
FIGURE 1 - INFLATABLE DELTA WING MODEL ASSEMBLY
DROP CORDS
DROP CORD CUT
SEAM
SECTION A-A
BASE PLATE
CLAMPING BAR
JIG ATTACHMENT POINTS (16)
AIR SUPPLY POINTS (2)

FIGURE 2 - LOCATION OF LOADING, DEFLECTION MEASURING, AND ACCELEROMETER ATTACHMENT POINTS

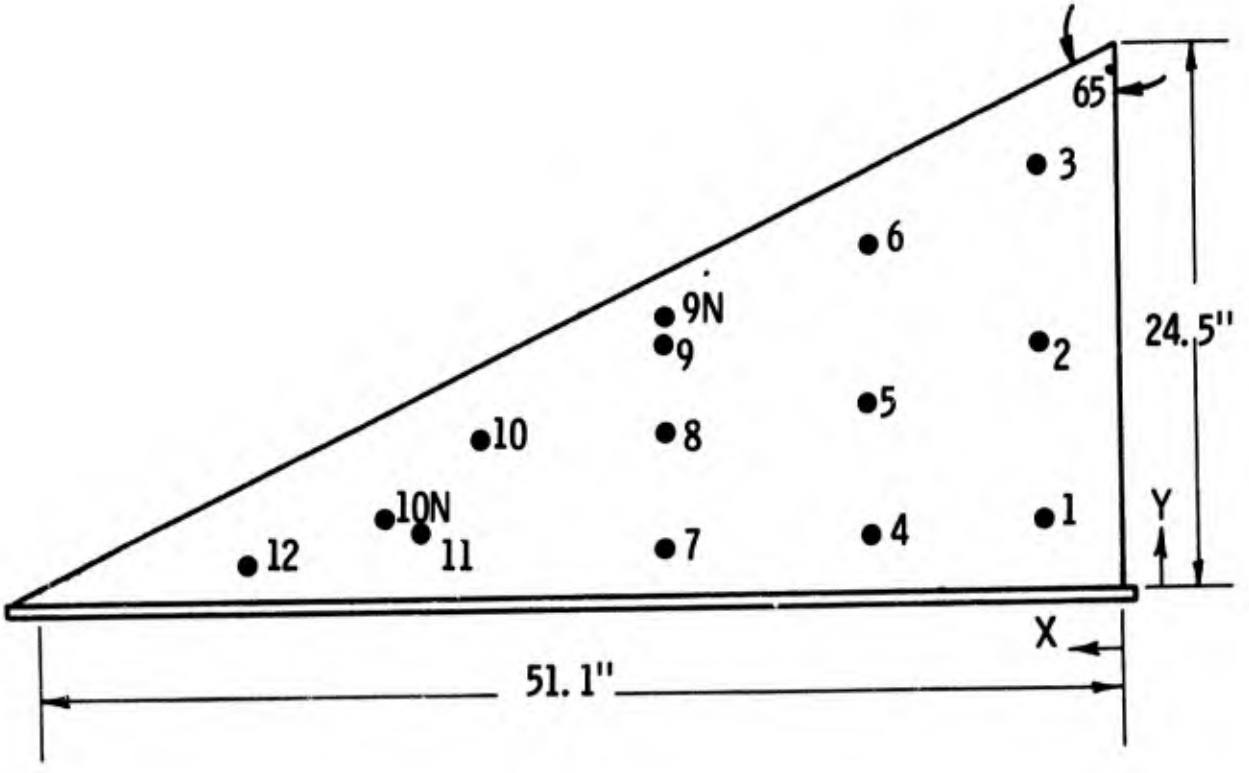

FIGURE 3 - PRESSURIZATION EQUIPMENT SCHEMATIC

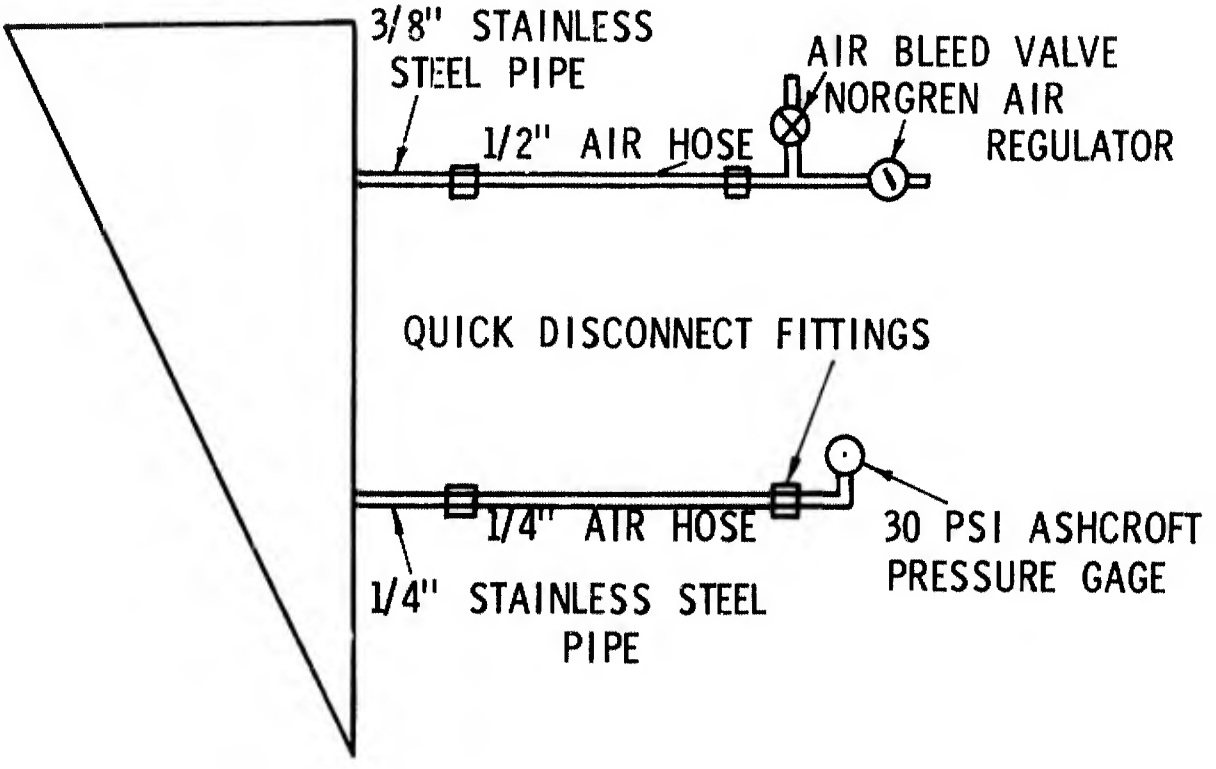

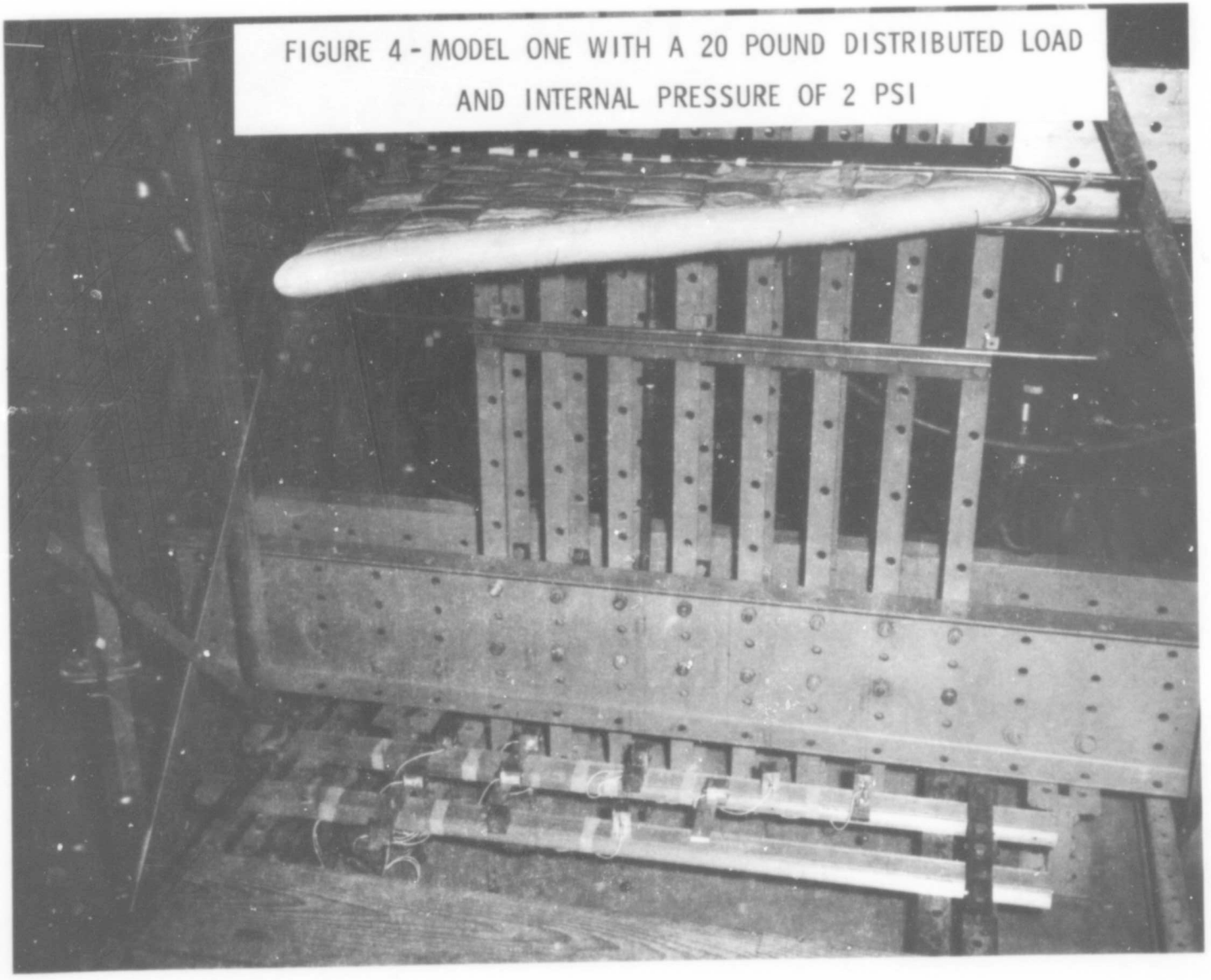

FIGURE 4 - MODEL ONE WITH A 20 POUND DISTRIBUTED LOAD AND INTERNAL PRESSURE OF 2 PSI

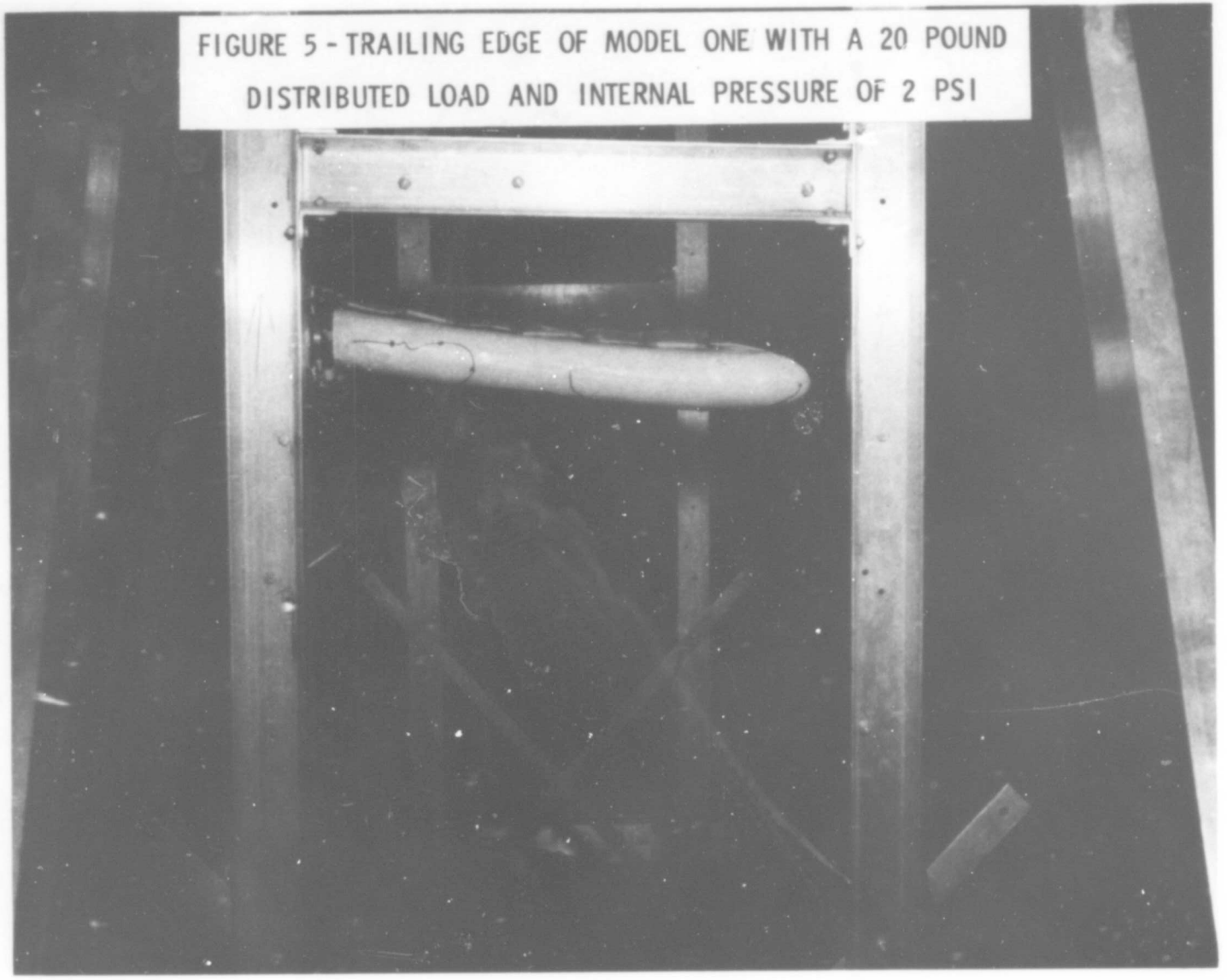

FIGURE 5 - TRAILING EDGE OF MODEL ONE WITH A 20 POUND DISTRIBUTED LOAD AND INTERNAL PRESSURE OF 2 PSI

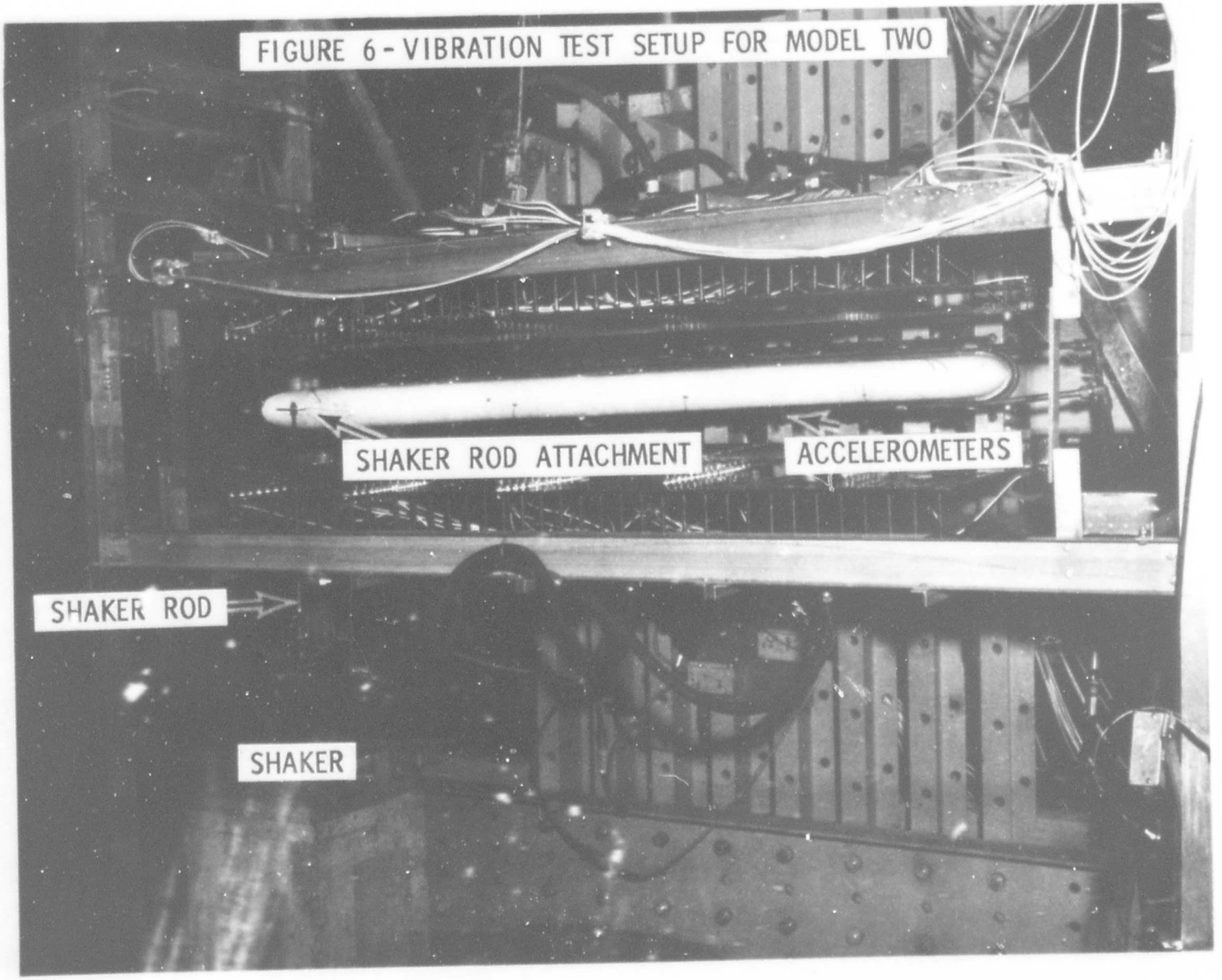

FIGURE 6 - VIBRATION TEST SETUP FOR MODEL TWO

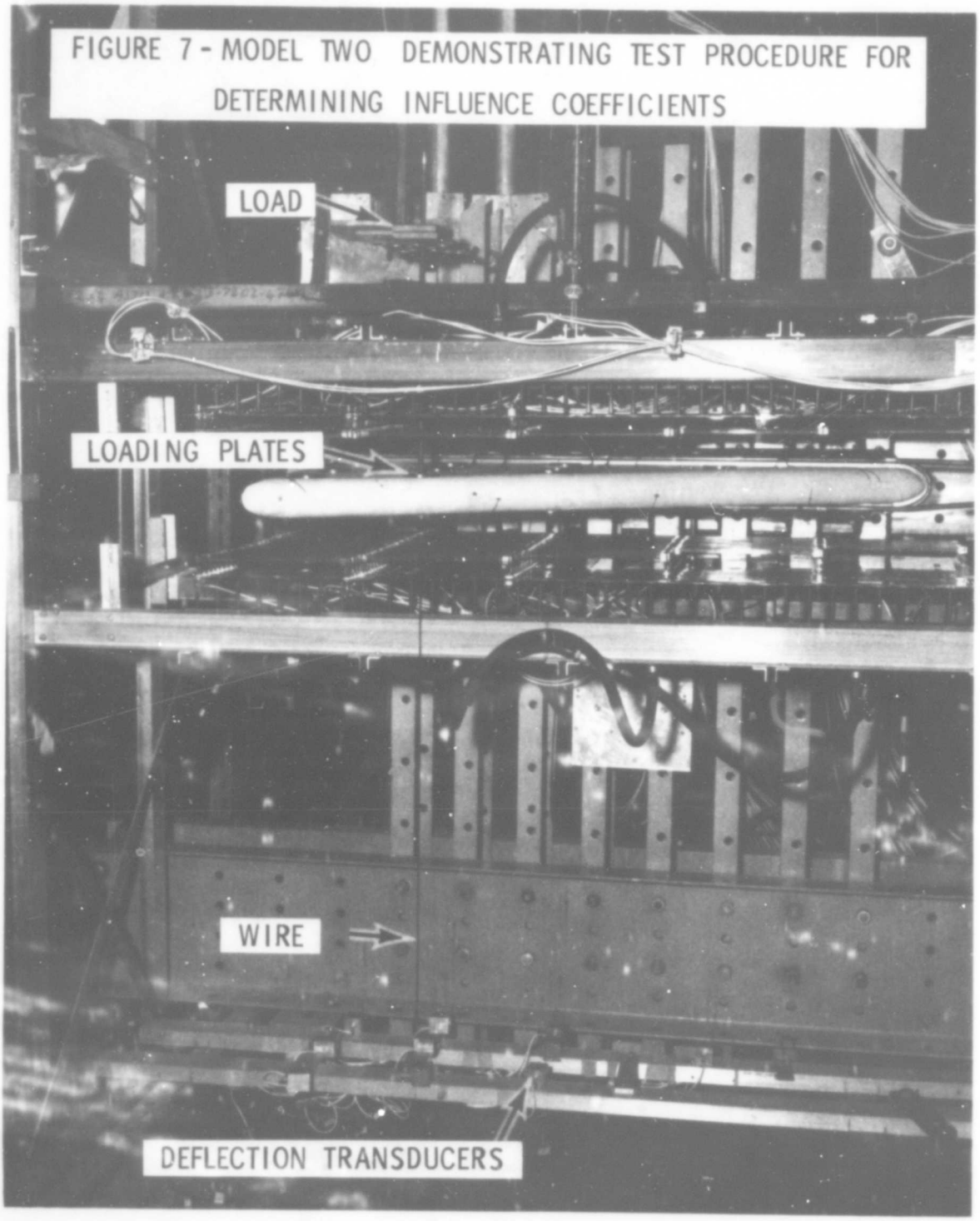

FIGURE 7 - MODEL TWO DEMONSTRATING TEST PROCEDURE FOR DETERMINING INFLUENCE COEFFICIENTS

FIGURE 8 - TYPICAL FLEXIBILITY INFLUENCE COEFFICIENT PLOT

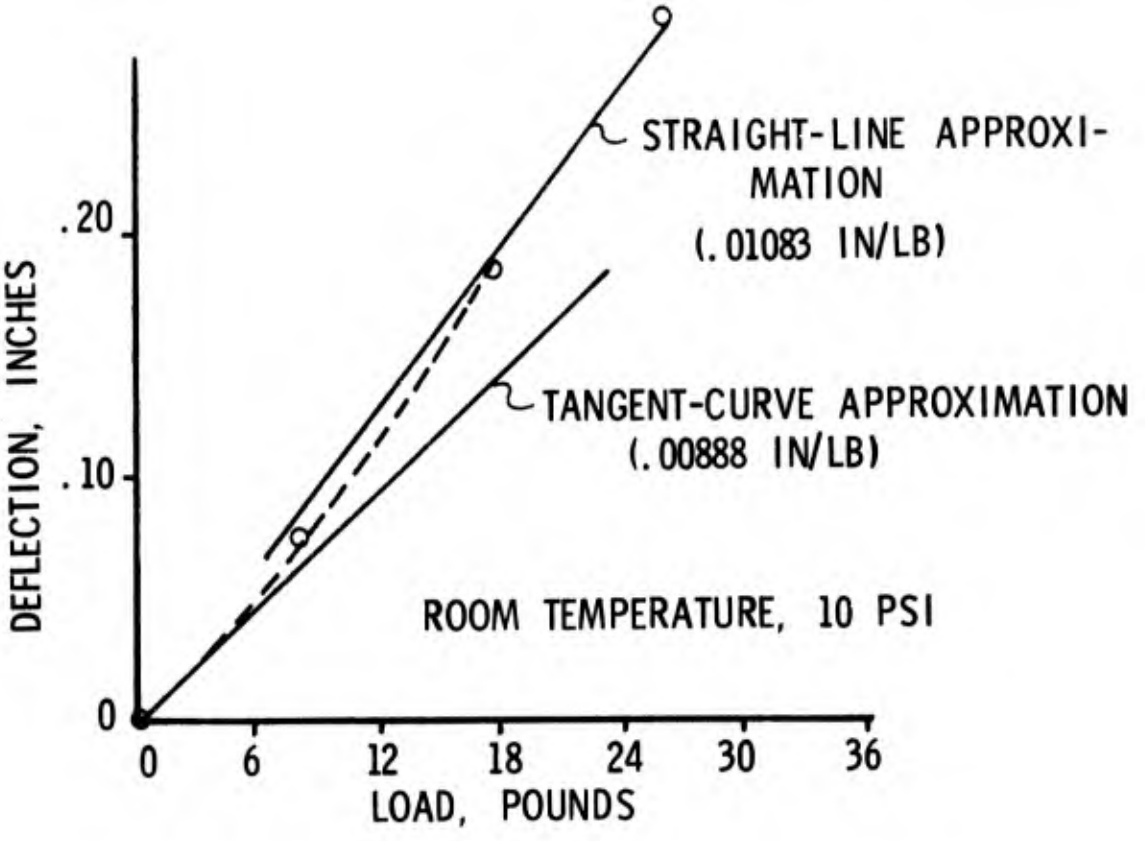

FIGURE 9 - VERTICAL DEFLECTIONS DUE TO A TOTAL LOAD OF 30 POUNDS UNIFORMLY DISTRIBUTED WITH A MODEL INTERNAL PRESSURE OF 4 PSI

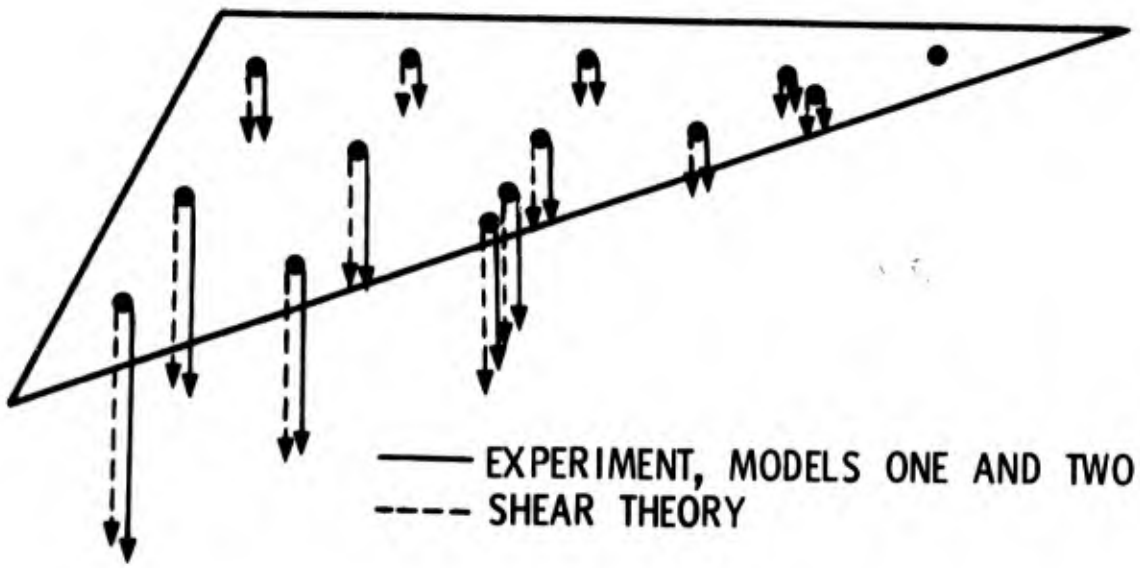

FIGURE 10 - PREDICTED AND MEASURED FIRST VIBRATION MODE FREQUENCY , ROOM TEMPERATURE

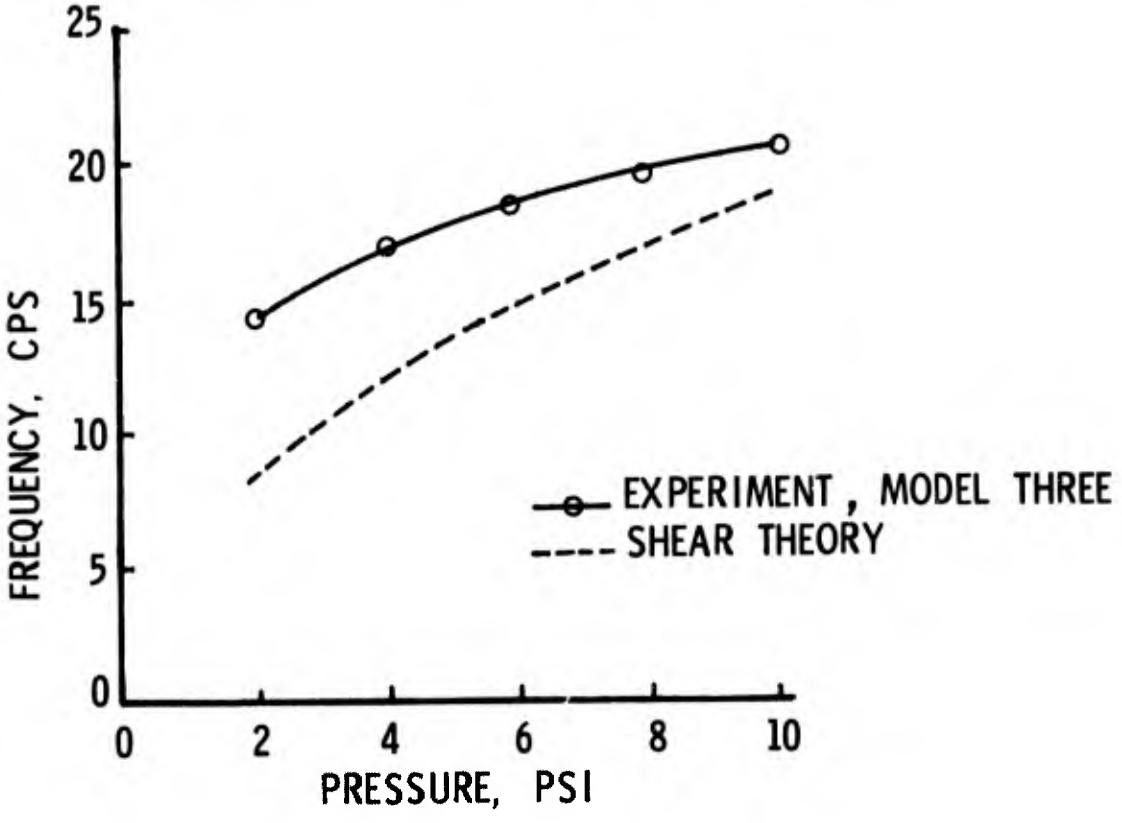

FIGURE 11 - VIBRATION FREQUENCY VS INTERNAL PRESSURE

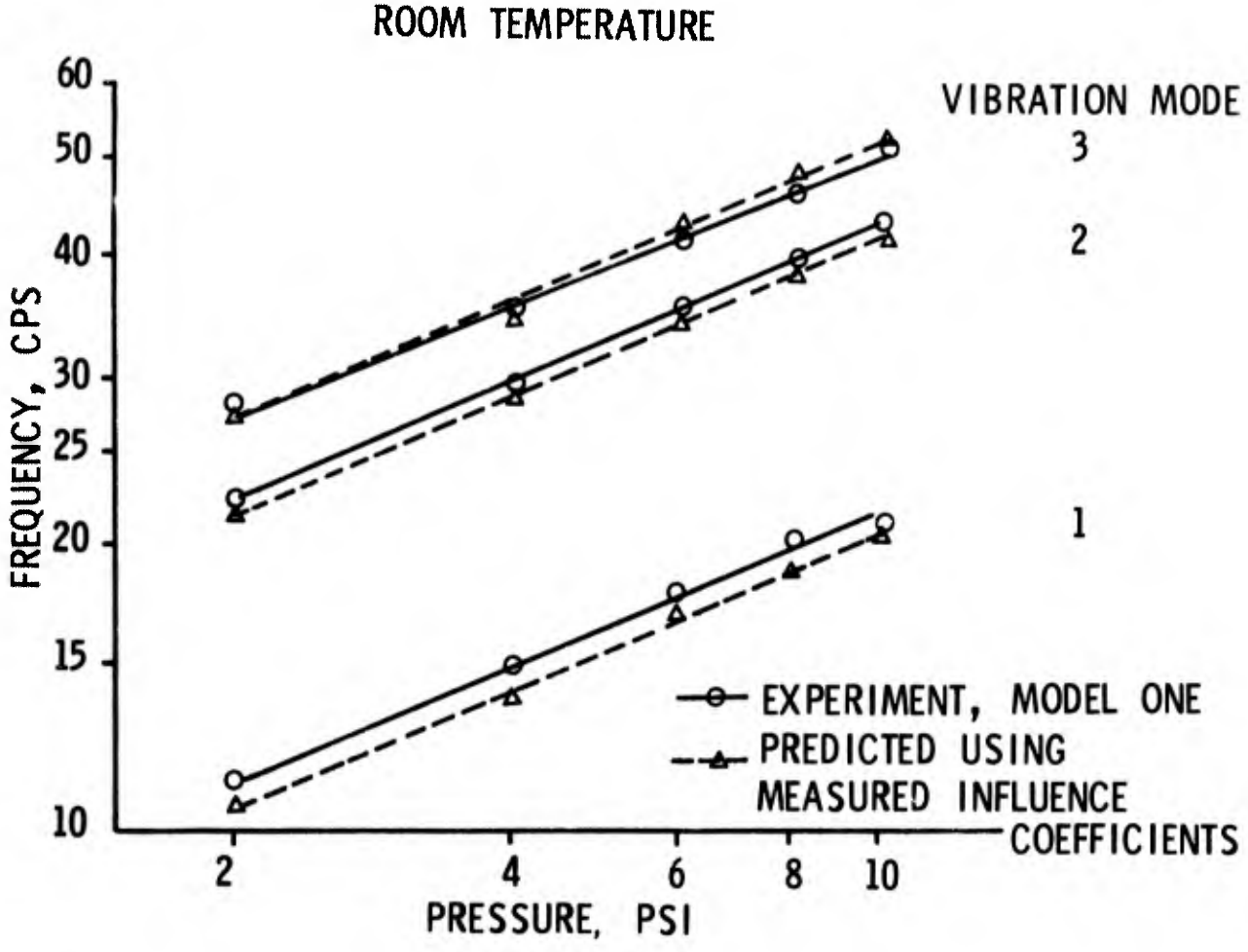

FIGURE 12 - NODE LINES FOR THE SECOND AND THIRD MODES FROM SHEAR THEORY PREDICTION AND EXPERIMENT

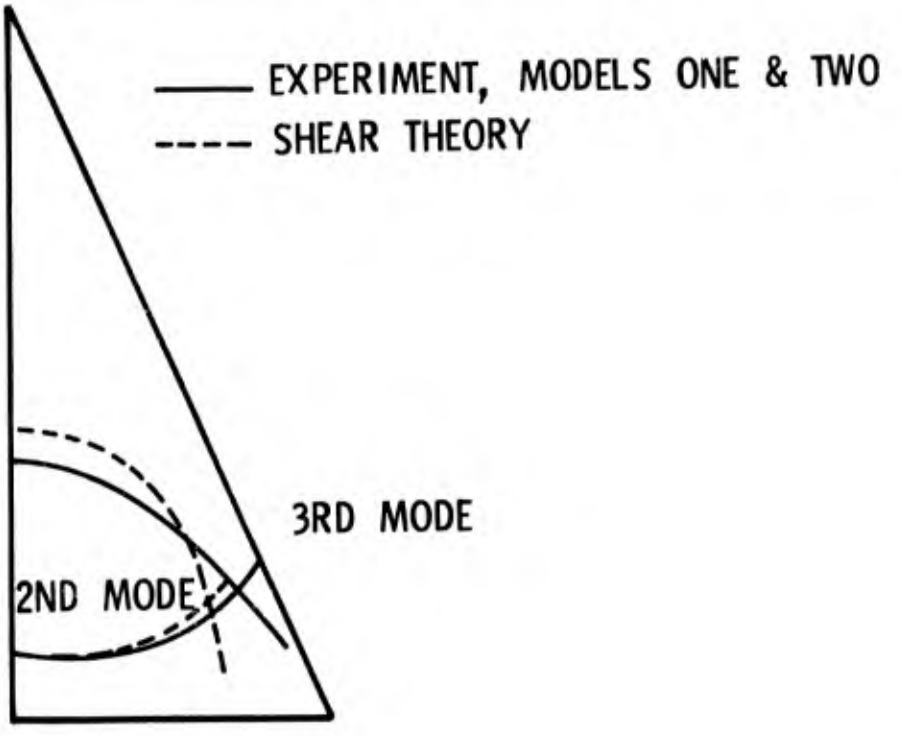

FIGURE 13 - NODE LINES FROM VIBRATION CALCULATIONS USING INFLUENCE COEFFICIENTS AND EXPERIMENT

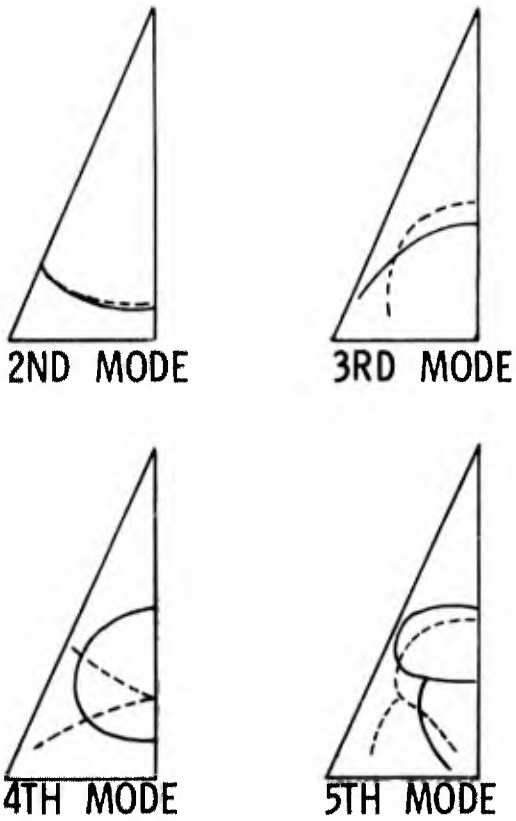

——— EXPERIMENT, MODELS ONE AND TWO

- - - - - INFLUENCE COEFFICIENT CALCULATIONS

FIGURE 14 - EFFECT OF TEMPERATURE ON THE FIRST VIBRATION MODE FREQUENCY AT 10 PSI

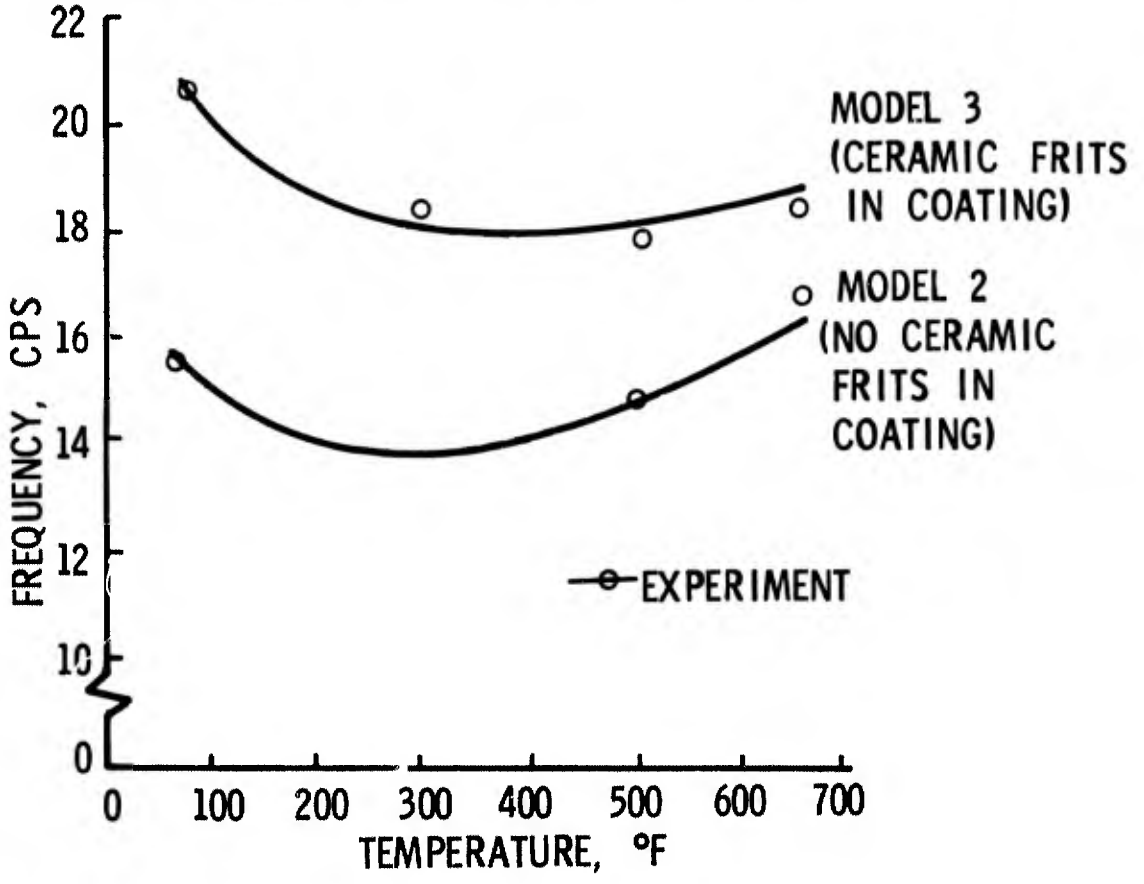

BLANK PAGE

REINFORCED BALLOON FILMS

Thomas W. Kelly*

INTRODUCTION

Within the scheme of things, plastic balloon technology is of comparatively recent vintage--a product of cooperative university, contractor and governmental efforts during the past fifteen years. Prior to World War II, scientific ballooning was confined to an exceedingly small number of projects which were severely limited by the expensive and heavy rubberized fabrics in use at the time. Some of you may recall the flights of the Explorers I and II, and the several flights of Dr. and Mrs. Picard. Each flight was an undertaking of major proportions.

After World War II, the advent of commercially available plastic sheeting of comparatively high quality made the creation of inexpensive balloons for high altitude experimentation a most attractive possibility. Early work by General Mills, New York University, and others was largely successful. Initial success with light payloads created a burgeoning demand for balloon vehicles to carry heavier payloads to higher altitudes for longer durations. Ensuing problems with heavier payload flights forced the balloon using community to develop more detailed materials data, improvements in fabrication techniques, better flight control instrumentation, and a clearer understanding of the dynamics and thermodynamics of flight. The effectiveness of the response by the scientific community and the speed with which this technology developed can be judged from the fact that balloon flights not possible ten years ago are now conducted on a virtually daily basis.

Most recently, there has been another marked increase in the weight and value of balloon-borne experiments associated primarily with the experiments in balloon-astronomy. Once again, problems with the flight of these larger payloads (in the two to five ton weight range) forced a reassessment of the current technology in ballooning and a return to fiber reinforced materials for balloon construction. The relatively high cost of such reinforced materials and of reinforced material balloons has been the driving force behind an AFCRL program to develop lower cost reinforced balloons.

The objective of this paper is to consider some of the contemporary balloon flight problems as related to available and soon

---

* Supervisory Aerospace Engineer, AFCRL (CREB)

to be available materials and to present recently developed techniques for producing inexpensive reinforced materials which may have application beyond the field of balloon design.

ZERO PRESSURE BALLOON

This discussion will center on the conventional zero pressure balloon which has an opening to the atmosphere at the base of the balloon. The flight performance of such balloons (Figure 1) is characterized by an ascent rate which is nearly constant to a preselected ceiling altitude; flight at maximum altitude until noon or shortly thereafter; a protracted, slow descent during the afternoon; a rapid post-sunset descent to a nighttime flight level that is determined by pressure-activated ballast drops; constant level flight during the night; then a rapid ascent following sunrise to a daytime flight level that is slightly higher than that of the previous day. The ballast control level can be altered to provide nearly constant day-night floating levels as needed. Gas valving and ballasting can also be controlled by radio command to make the balloon flight performance conform to special scientific or mission requirements.

In terms of materials and design, such balloons are axially symmetrical when full with stresses longitudinally polarized. The balloons are, of course, only partially full on the ground and assume a variety of assymetrical shapes during ascent. During ascent, the stresses are clearly not uniformly polarized, thereby necessitating that the balloon material have some transverse strength. Additional stresses are imposed by the wind shears associated with the jet stream level which coincides roughly with the level of minimum atmospheric temperature. Such temperatures are frequently below -70°C. A final factor, that of gas permeability, is not critical in balloon design as all candidate plastic materials are sufficiently impermeable to helium lifting gas.

Until recently, nearly all zero pressure balloons were made from polyethylene. Polyethylene has a moderate tensile strength, low cold brittleness temperature (-68°C), moderate extensibility and excellent storage properties. The heat sealability of polyethylene and the inherent low cost of the resin make this an eminently suitable film for the low cost balloons required by the majority of scientific experimenters. Tests of polyethylene balloons in the 4,000 pound payload range, however, were not sufficiently successful to risk using such balloons to carry men or expensive scientific experiments.

In response to the need for heavy payload flight, a new type of laminated balloon material was developed which provided extra strength for very heavy scientific payloads and maximum reliability for the flight of new or very expensive equipment. The most spectacular use of an early "scrim" balloon was the historic manned flight of White and Kittinger to 80,000 feet. The balloon carried a 5200 pound payload to an altitude of 80,000 feet. While thin

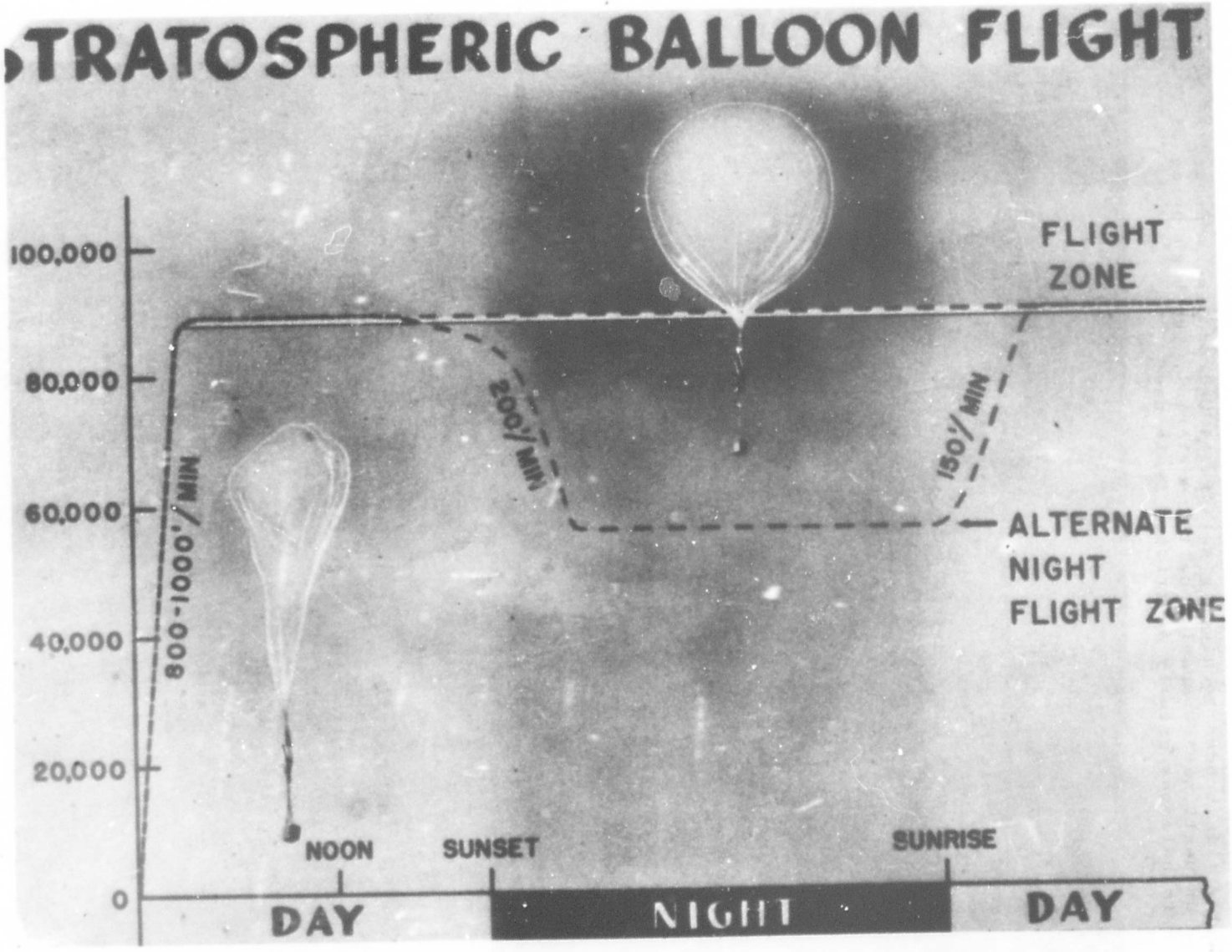

Figure 1 - Stratospheric Balloon Flight

Mylar film bonded to a woven network of Dacron fibers proved to be an unquestionably superior balloon material, the high price of scrim balloons greatly restricted their use.

FLYING THREAD LOOM

In 1963, the Air Force Cambridge Research Laboratories (AFCRL) initiated a program to lower the cost of scrim balloons. Eighteen months later, the goal of a 30 percent cost reduction was realized through value-engineering analyses of designs, materials and production techniques. Apart from the actual economies effected, the most far-reaching result of this program was the introduction of an entirely new family of balloon materials which substitutes a non-woven grid of reinforcing threads for the woven scrim fabric used in the conventional scrim-laminate. A machine, known as the Flying Thread Loom (FTL), developed at AFCRL, is used to produce non-woven scrim.

The principle of operation of the FTL is illustrated in Figure 2. A web of longitudinal threads is fed through the center of a large rotating drum which is fitted with a preselected number of spools of thread. As the web advances (from right to left in the diagram) and the drum rotates, the drum threads overwrap and underwrap the web threads producing a non-woven thread matrix. Virtually any material strength and thread configuration can be obtained by varying the speed of the drum, the movement of the web, the number of spools in the drum and the denier of the fibers.

Figure 3 shows the first model of the machine, fabricated at AFCRL. The web enters the interior of the drum from the right and the grid is shown emerging from the left-hand end of the drum. Although the drum was only 6 inches in diameter, the model satisfactorily demonstrated the principle of operation. Figure 4 shows the full-sized FTL. The drum shown is 9 feet in diameter. The input end of the 64 inch laminator can be seen on the far side of the FTL.

The first material fabricated on the FTL for balloon use, designated GT-99, is illustrated in Figure 5. A medium-payload material, its design mission was to carry 1300 pounds to 98,000 feet. It may be compared in weight to 1.0 mil thickness polyethylene which weighs 0.005 pounds per square foot and has a tensile strength of approximately 3 pounds per inch of width. A balloon fabricated of GT-99 was successfully flown on 21 May 1965.

The next step in the development of the new family of FTL materials was an effort aimed at carrying a 200 pound payload to 150,000 feet. When one tries to fly a balloon above 100,000 feet, the weight of the basic balloon material is critical. For example, at a 120,000 foot altitude a saving of 100 pounds in balloon weight reduces the balloon volume by 300,000ft^3, while at 60,000 feet, the same saving in balloon weight reduces the balloon volume by only 16,000ft^3, Figure 6 shows the composition by weight for

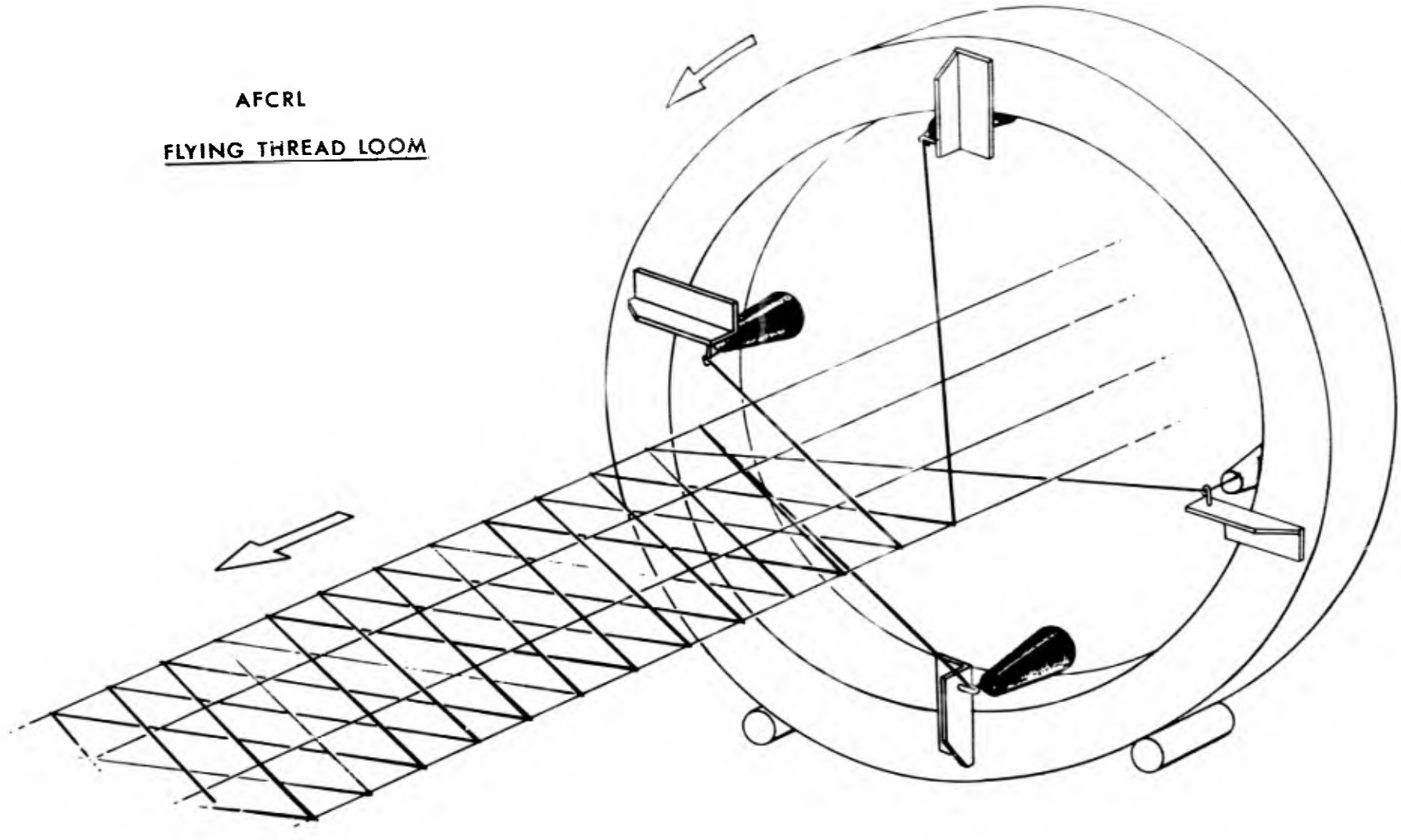

Figure 2 - Principle of Operation for the Flying Thread Loom

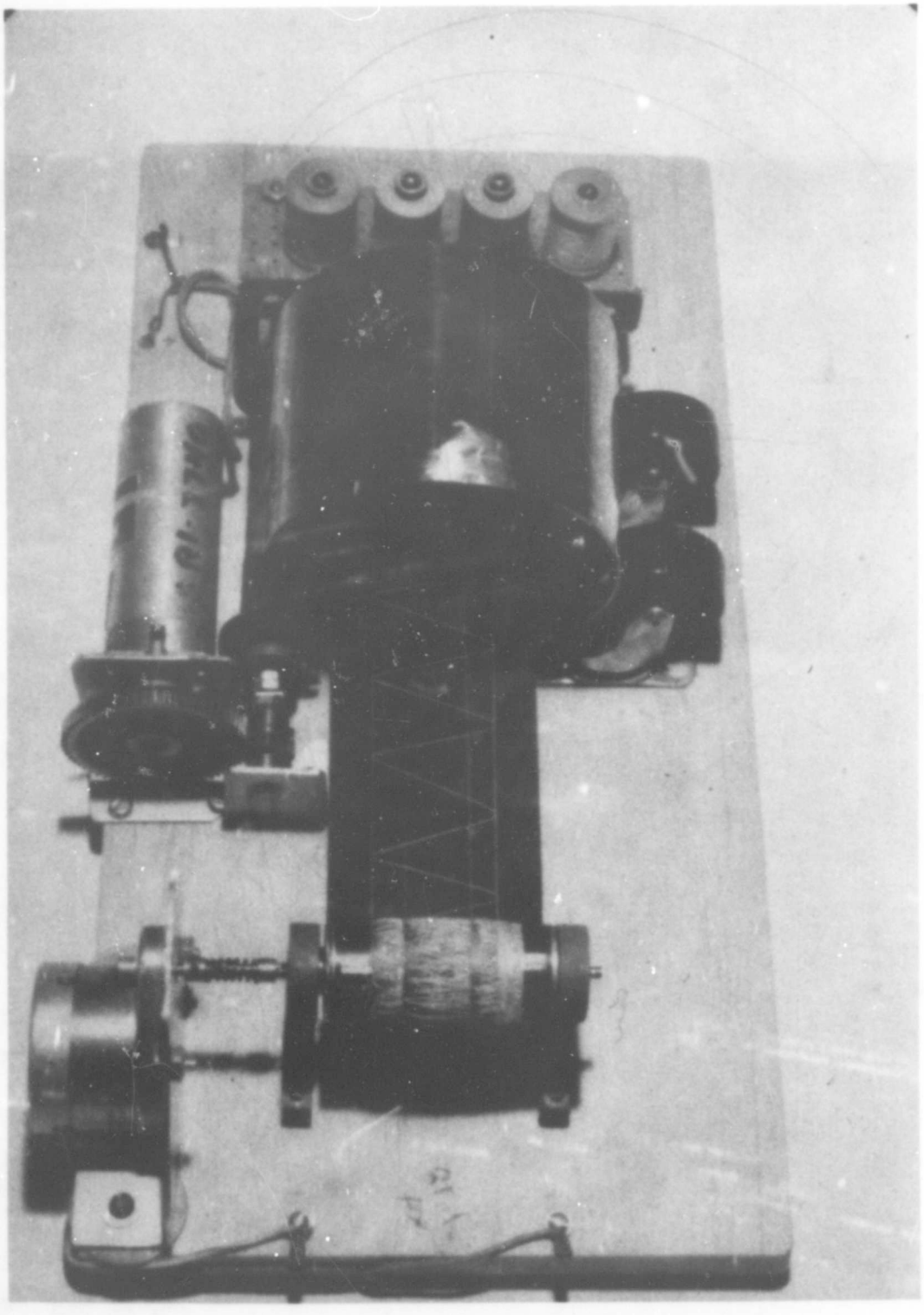

Figure 3 - First Working Model of the Flying Thread Loom

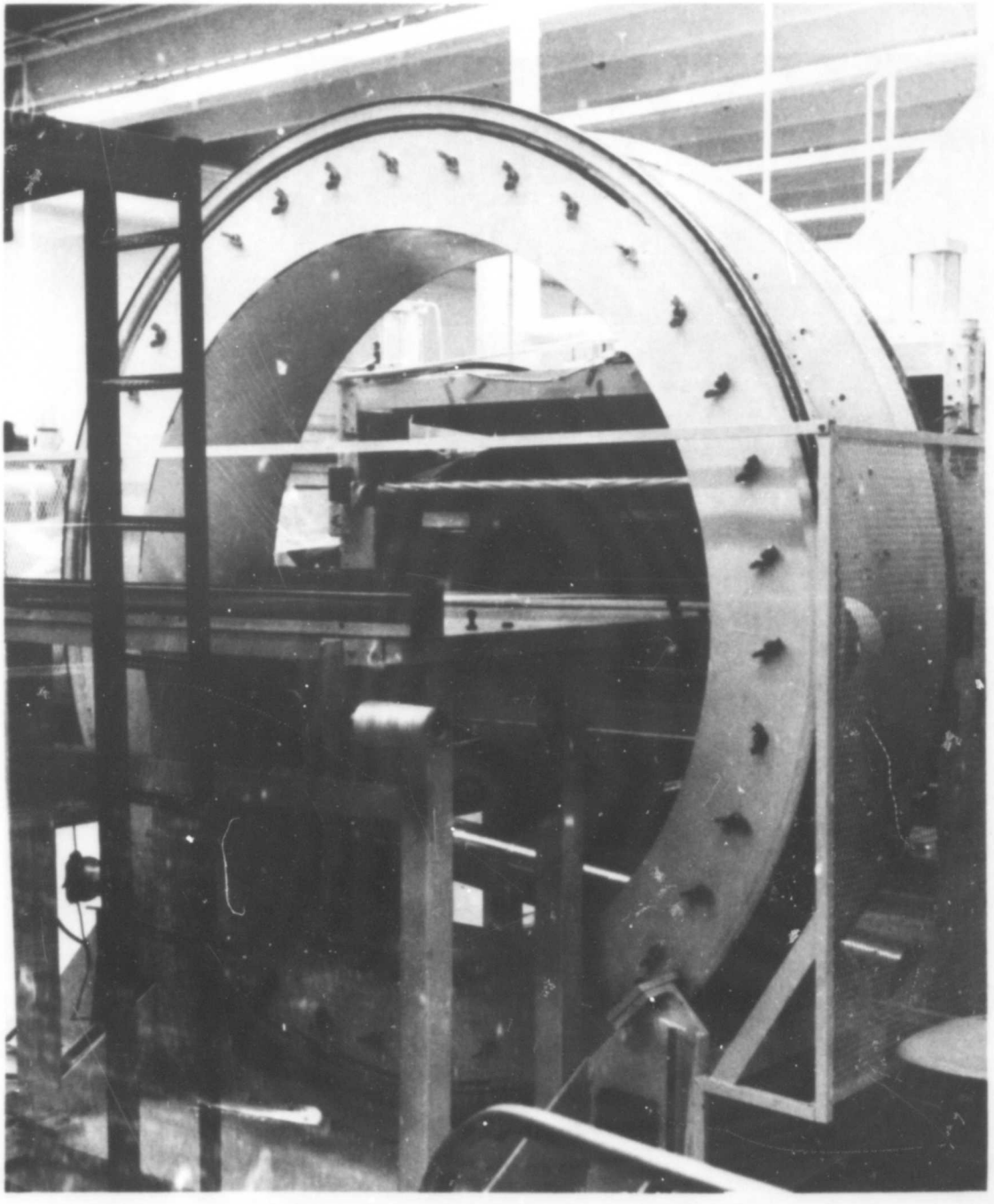

Figure 4 - Full Size Flying Thread Loom

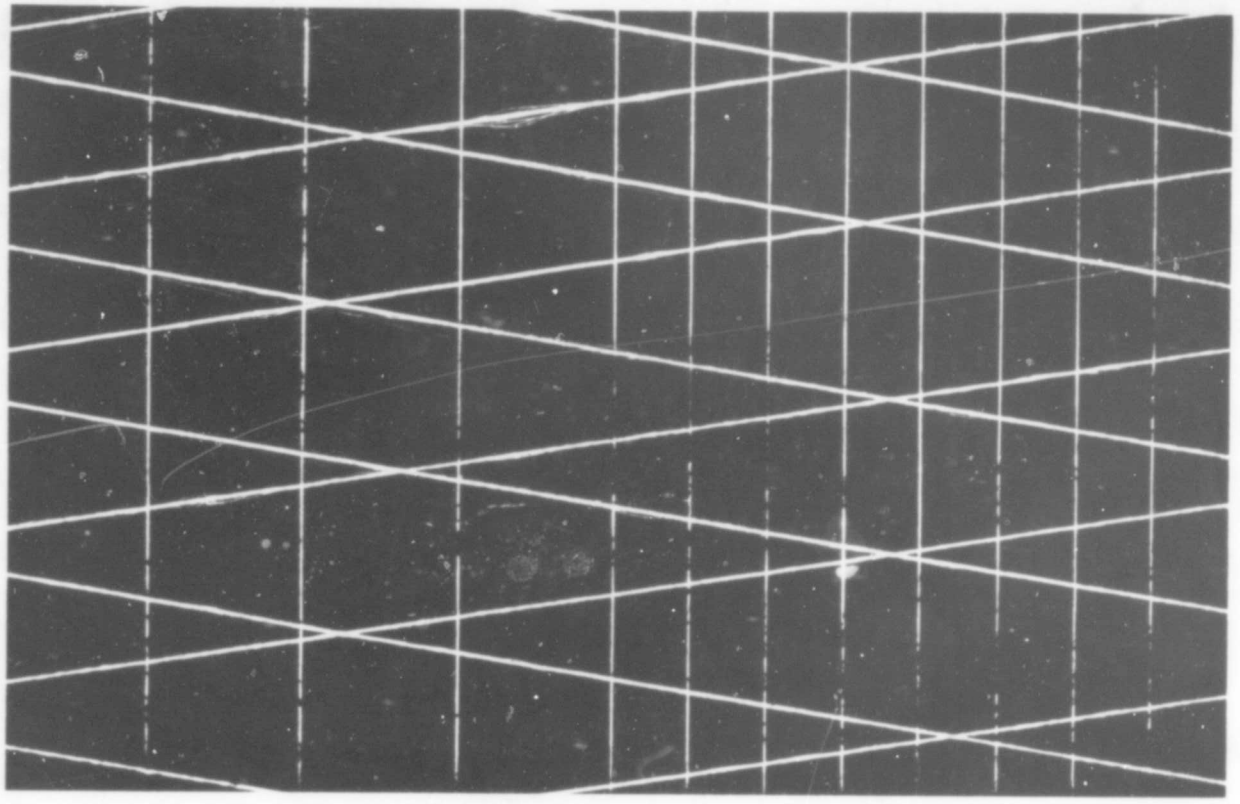

GT-99

WEIGHT: 0.0056 LB/FT^2

TENSILE STRENGTH: M.D. 12 LB/IN
T.D. 12 LB/IN

MYLAR: 0.35 MIL

ADHESIVE: ON THE FILM

REINFORCEMENT: 2/IN-CENTER TO INCHES
1/IN TO EACH EDGE.
2/IN TRANSVERSE @30°
220 DENIER HIGH TENACITY DACRON

Figure 5 - GT-99 Material

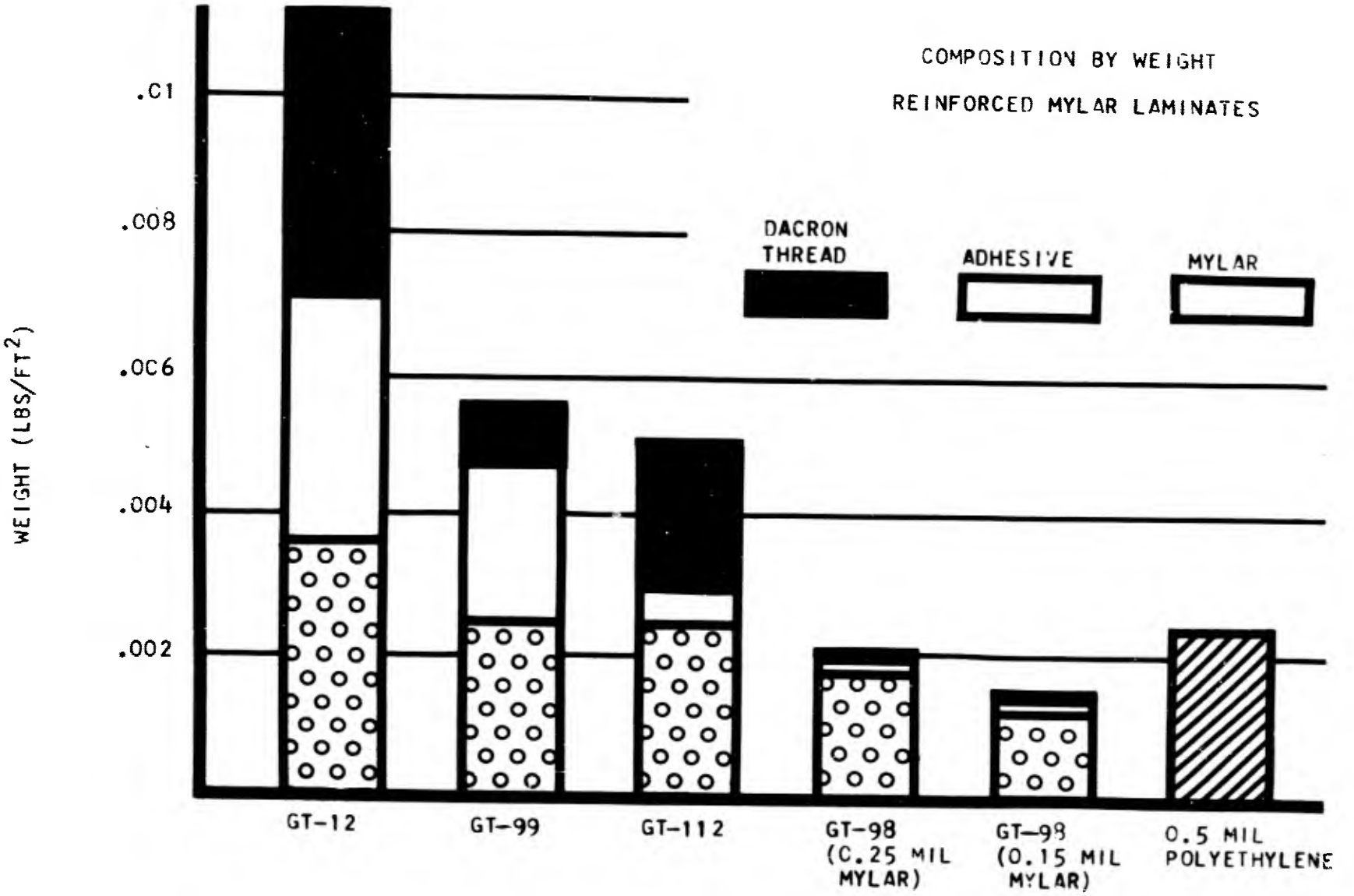

Figure 6 - Composition by Weight, Reinforced Mylar Laminate

several scrim-reinforced Mylar laminates. GT-12 material is made from woven scrim; the other laminates are all non-woven scrim materials. The weight breakdowns for GT-12 and GT-99 shows that the adhesive spread over the entire surface of the gas-barrier material in a conventional lamination accounts for thirty to forty percent of the material weight. It was consequently decided to devise a method to coat the fibers prior to lamination to minimize the adhesive weight. After considerable effort, a workable system was developed which minimizes the adhesive weight in balloon laminates.

The significance of this development is illustrated by Figure 7. The heavy, solid curves represent the actual balloon weight vs. volume for balloons made from the new GT-98 lightweight FTL material and from GT-10 (woven scrim, 1/4 mil Mylar), the lightest weight Mylar-Dacron scrim material available a year ago. The curve labelled "200 pounds to 150,000 feet" is the "mission curve". Each ordinate of this mission curve represents the calculated permissible weight, W, for a balloon carrying a 200 pound payload, where the corresponding balloon volume displaces (W + 200) pounds of air at 150,000 feet. It is clear that GT-10 material is unsuitable for this task because all values of actual balloon weight for GT-10 are higher than the permissible values denoted by the mission line, and beyond the range of these curves the size and cost of a balloon would be unreasonable. The new GT-98 material, however, fulfills the mission with an 8 million ft^3 balloon of reasonable size and cost.

The first balloon fabricated from the lightweight GT-98 film was flown as the primary balloon in a tandem system on 30 August 1965 and failed. An exhaustive study of the recovered balloon was made and it was determined that the problem related primarily to the balloon system configuration, not the material.

The culmination of FTL balloon materials application, from the balloonist's viewpoint, came with the successful flight of a 26,000,000 cubic foot balloon fabricated of a non-woven reinforced film, designated GT-111, consisting of 1/3 mil thickness Mylar and a reinforcing web of fibers patterned as in Figure 8b. Past balloons employed a woven rectangular grid reinforcement, as in Figure 8a, from which a segment, or gore, of the balloon was cut. In contrast, the Voyager balloon material employed a high density of longitudinal fibers in the gore center with a diminishing fiber density to the gore edges.

This preferentially structured material of extremely light weight resulted in a balloon of vastly smaller size and lesser cost than a balloon made of convential GT-12 reinforced material. Tables 1 and 2 illustrate the volume and cost savings to be expected with balloons designed to lift a 3,000 pound payload to the indicated altitudes fabricated of non-woven materials having the laminating adhesive on the thread only.

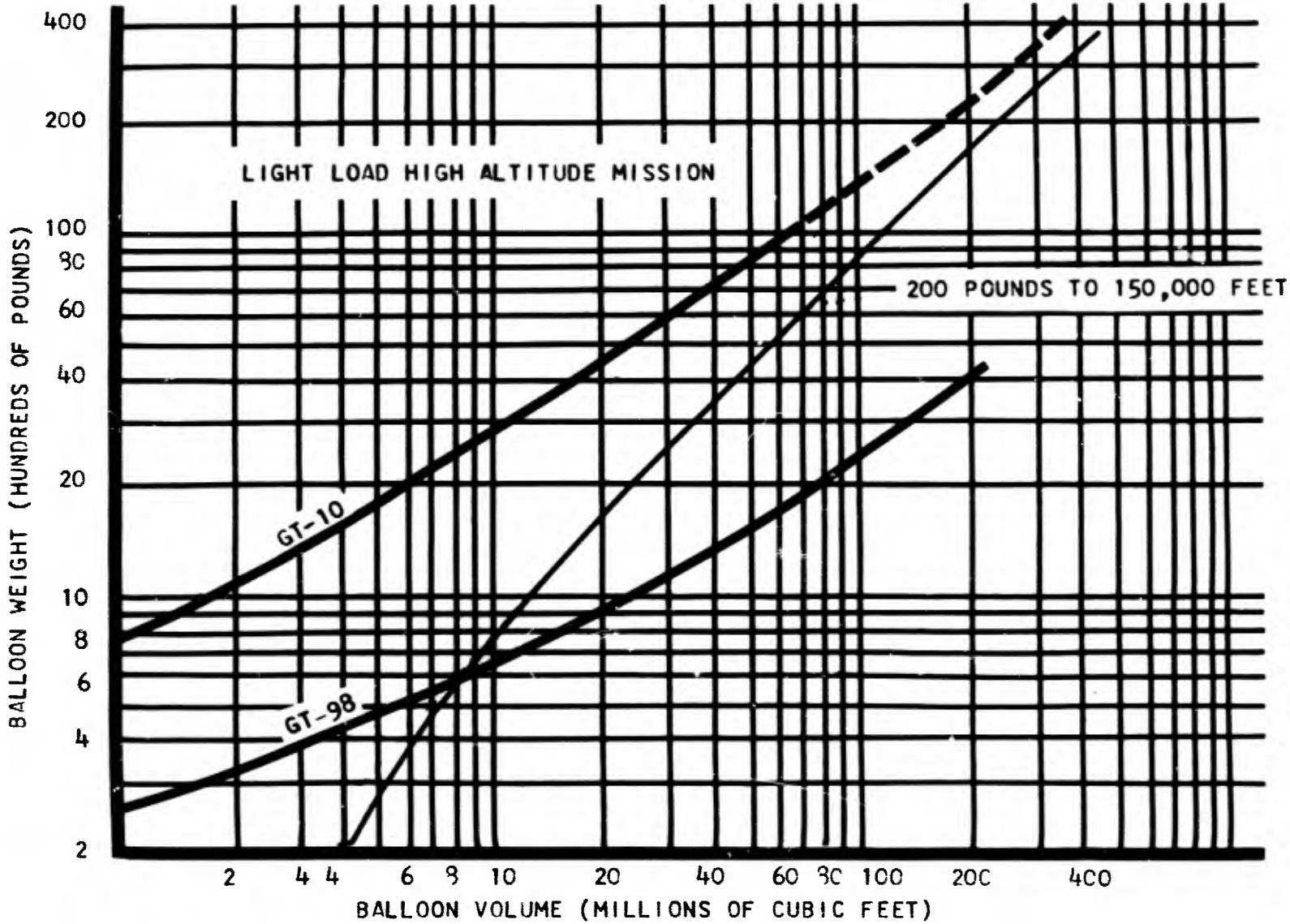

Figure 7 - Light Load High Altitude Mission

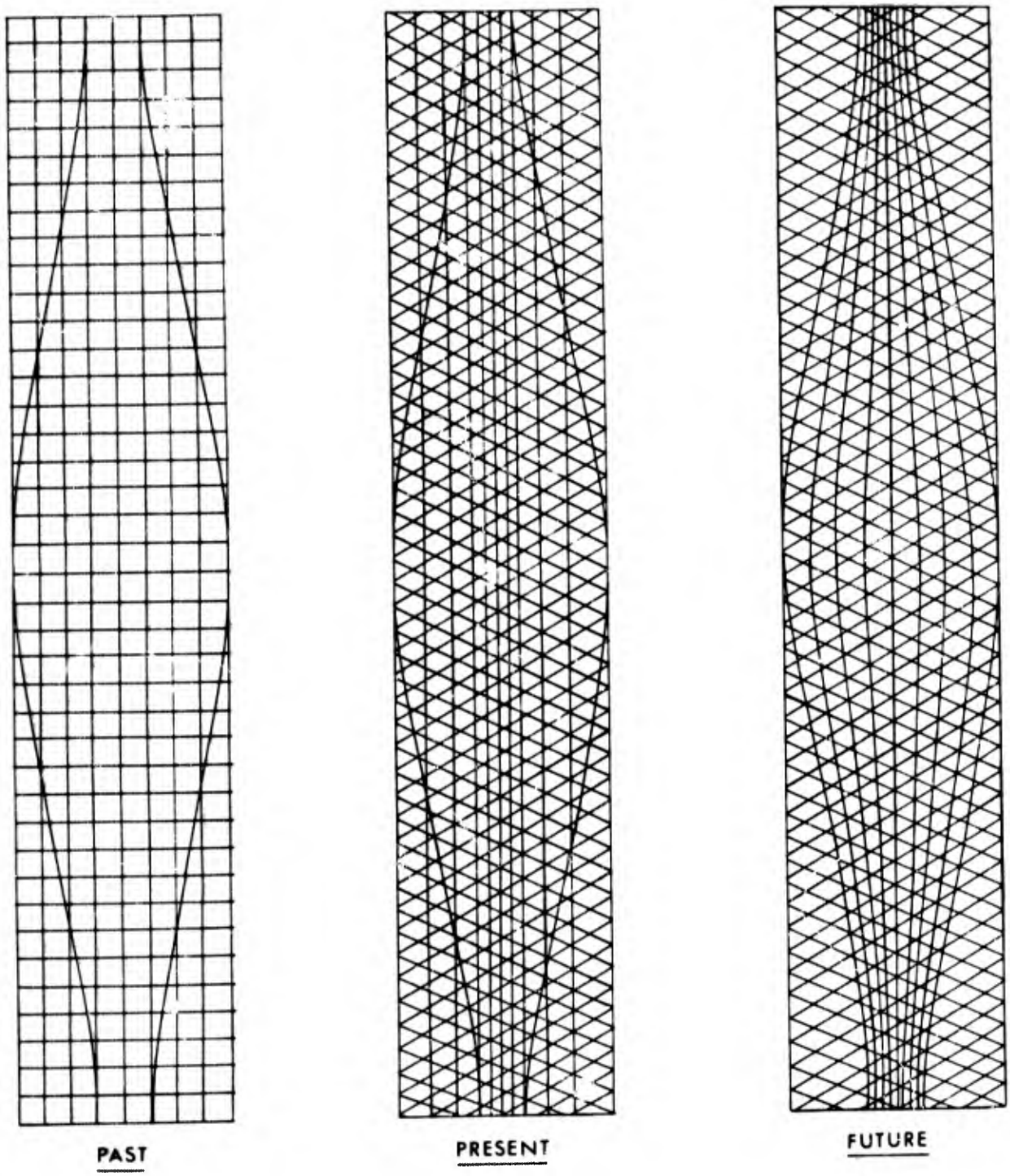

Figure 8 - Balloon Gore Tailoring

3000 Pound Payload

Flight Altitude K ft.	Balloon Volume ($ft^3 \times 10^6$)	
	Woven Scrim	FTL Material
80	1.64	1.44
100	5.44	4.19
120	23.18	13.64
130	54.40	25.93
140	142.54	52.08

Table 1 - 3000 Pound Payload (Balloon Volume Versus Altitude)

3000 Pound Payload

Flight Altitude Kft.	Balloon Cost K$	
	Woven Scrim	FTL Material
80	22.4	14.4
100	50.0	29.0
120	131.5	64.1
130	233.5	98.6
140	445.2	157.0

Table 2 - 3000 Pound Payload (Balloon Cost Versus Altitude)

PRESENT NON-WOVEN MATERIAL TECHNOLOGY

The techniques of producing lightweight non-woven reinforced balloon materials having a wide range of strength and weights have been adequately demonstrated for balloon design purposes. It is true, however, that the exact limits of the FTL technology have not been adequately defined beyond the range of strengths and weights of material used for balloons although it is certain that heavier and stronger materials can be produced. A few examples and comparisons may illustrate some of the merits of FTL materials.

Table 3 provides the strength/weight ratios for a variety of materials having equivalent weights. As can be seen, the strength of the non-woven materials exceeds that of the woven Dacron fabric by an appreciable margin. The non-woven material in this comparison assumes use of .15 mil thickness Mylar as a gas barrier and an adhesive weight equivalent to 15% of the total laminate weight. If we were to add the same film and adhesive weight to that of the woven fabric, the advantage of the non-woven material would be greater. A direct comparison b tween non-woven materials and the best of the conventional woven material balloon films is made in Table 4. The experimental X-975 has approximately 50% more strength per unit weight than the GT-12 in the machine direction and nearly 100% higher strength in the transverse direction. Other physical properties are essentially equivalent.

In the range of ultra-light balloon materials, a comparison of woven materials with GT-98 weighing approximately 0.002 pounds per square foot ($0.3 oz/yd^2$) is not possible as a source for sufficiently lightweight woven materials for producing such laminates is not known.

FURTHER OUTLOOK

Beyond the realm of already prepared and tested materials is the promise of still further material improvements. Figure 8c illustrates the coming generation of FTL materials. This concept permits structuring the gore in conformance with the stress distribution in a balloon. The density of transverse fibers will be controlled by varying the relative speed of the drum and the moving web and the number of fiber spools on the FTL drum. Longitudinal film distribution will be controlled by a pantograph coupled with a gate type mechanism of the type depicted in Figure 9. Further refinement will include an automatic gore cutting device, Figure 10. It would appear that further reductions in adhesive weight holds little promise in achieving light materials and that balloon technology will necessarily seek thinner gauge gas barriers and higher tenacity fibers for further weight reductions.

SUMMARY

The range of capabilities of plastic balloons has been greatly expanded through improvements in balloon materials. The AFCRL

STRENGTH TO WEIGHT COMPARISON

	TENSILE STRENGTH PDS PER INCH	WEIGHT OZ PER YD^2	STRENGTH WEIGHT RATIO
MYLAR 2.0 mils	30	2.0	15
DACRON FABRIC	60	2.0	30
NON-WOVEN * MATERIAL #1	93	2.0	47
NON-WOVEN * MATERIAL #2	140	3.34	42

* 220 DENIER DACRON, 0.15 mil MYLAR

Table 3 - Strength-to-Weight Comparison

COMPARISON OF GT-12 AND X-975

		GT-12	X-975
TENSILE (MD)	POUNDS PER INCH	45	55
TENSILE (TD)		25	40
WEIGHT	OUNCES PER YD^2	1.6	1.3
STRENGTH / WEIGHT (MD)		28	42
STRENGTH / WEIGHT (TD)		16	31
COST	DOLLARS/LINEAR FOOT	.23	.13

TABLE 4. Comparison of GT-12 and X-975

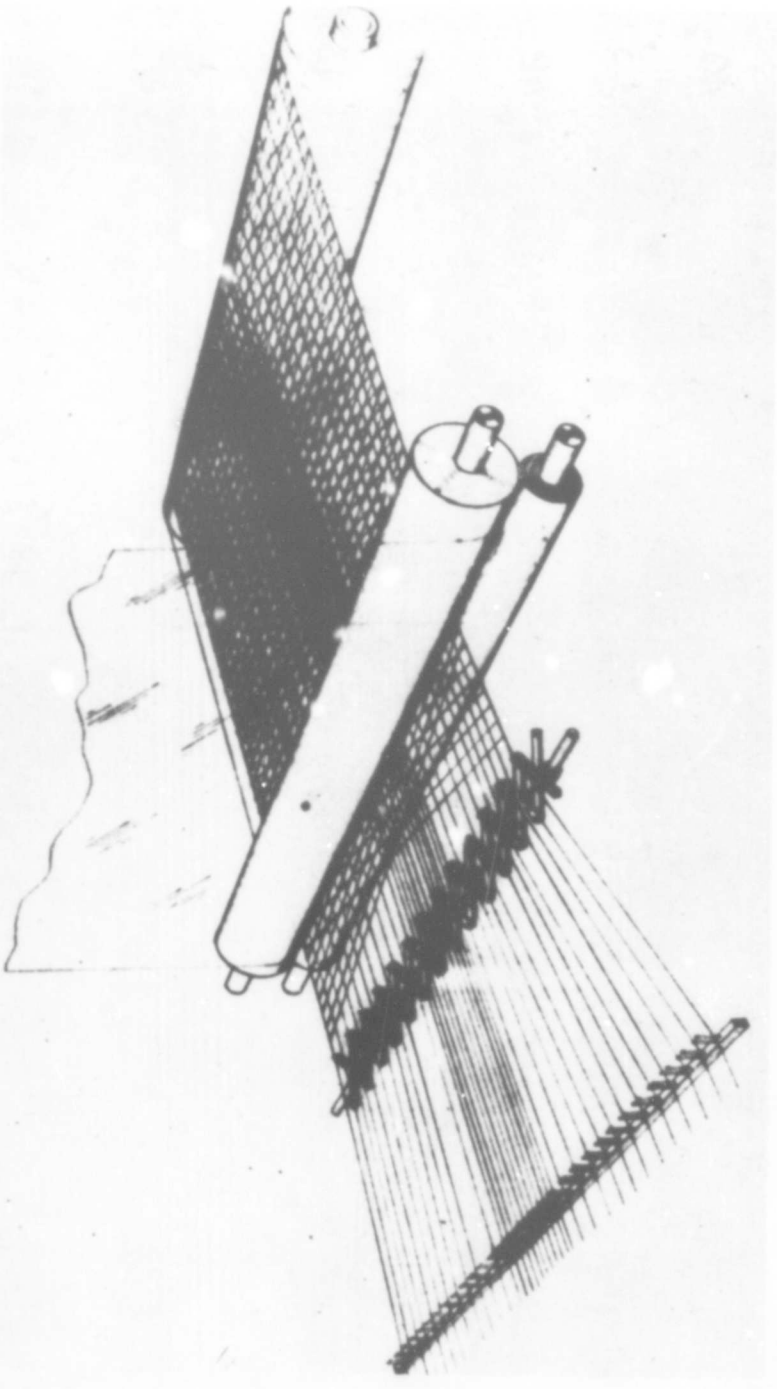

Figure 9 - A Proposed Gore Tailoring Device

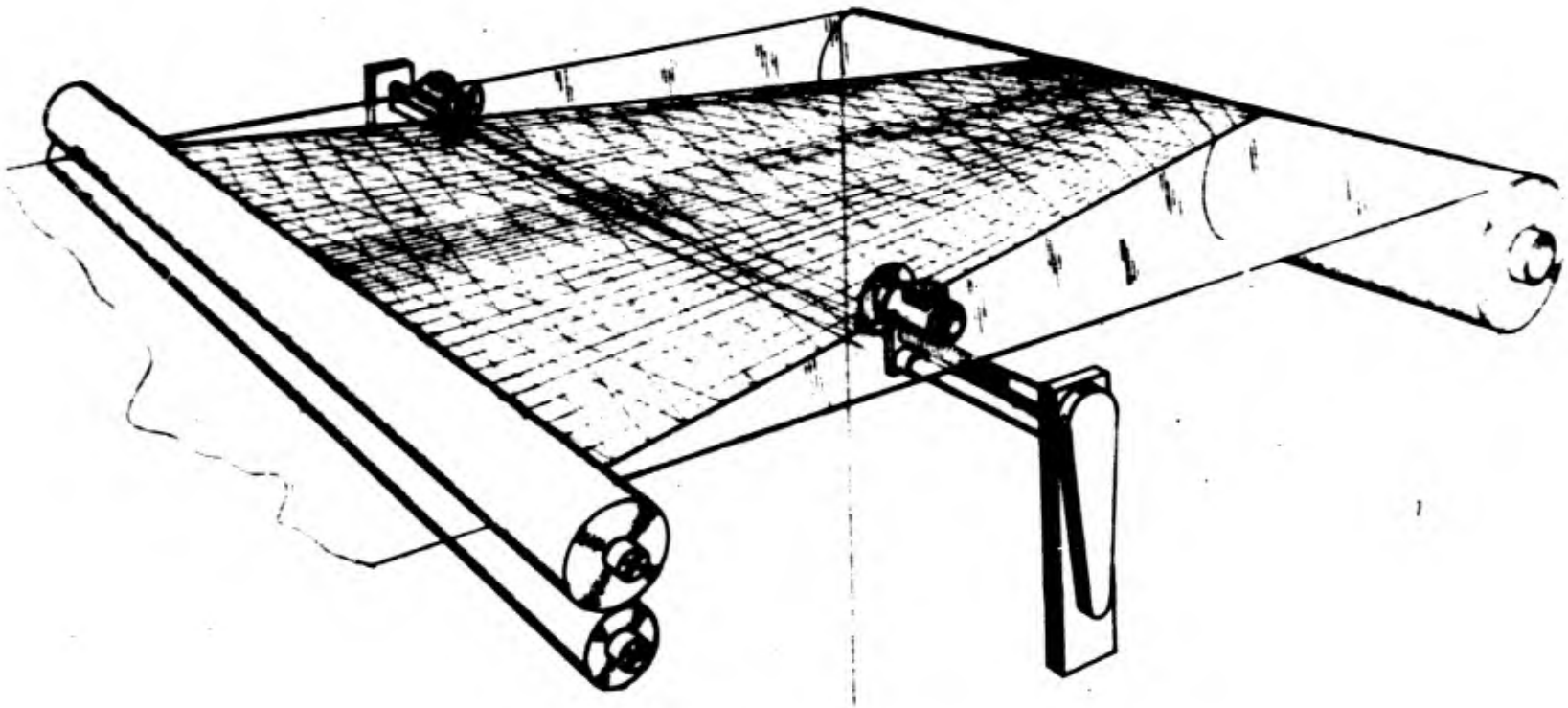

Figure 10 - A Proposed Gore Cutting Device

Flying Thread Loom can now be used to produce non-woven reinforced Mylar-Dacron materials ranging from approximately ten to one hundred and forty pounds per inch tensile strength. The upper limits of material strength which can be produced is not known.

Variations in number of fibers, fiber tenacity and denier, and the relative speed of the drum and web permits an almost infinite variety in strength-weight possibilities for FTL materials.

Non-woven materials are better, on a strength-weight basis, than woven reinforced laminate materials.

The possibility of designing reinforcing materials to meet the structural demands of an inflatable may offer interesting possibilities beyond the field of balloon design.

ACKNOWLEDGEMENTS

The contributions of Arthur O. Korn in the preparation of this paper are hereby acknowledged.

AN UNFOLDING ANTENNA WITH MECHANICAL SCANNING SYSTEM FOR SATELLITE APPLICATIONS

James W. Titus*

This design project was undertaken in order to demonstrate the feasibility of using, in satellite applications, relatively large antennas equipped for mechanical sector scanning. By "relatively large" is meant apertures of about 24 feet. This report will give a description of the particular antenna and pedestal which were built and a detailed discussion of some of the mechanical design problems and their solutions.

Mechanically scanned antenna systems have capabilities which can be highly advantageous in specific system applications. Among these are accurate pointing of the beam, angle coverage of up to 360 degrees for a single axis, convenience of using more than one axis of rotation, adaptability for either a parabolic reflector or one of many other kinds of antenna, and relatively light weight. The most severe limitation is that of maximum angular acceleration. This means that a finite time must be allowed for reversal in the case of a sawtooth scan, and that even a sinusoidal scan will have a maximum safe amplitude for any given scan frequency. A random scan would be impractical. Although this limitation of maximum angular acceleration is real, it is by no means relevant in all systems which require a scanning antenna beam.

SPECIFIC OBJECTIVES

A hypothetical system application required an antenna which would produce a pattern 2 degrees horizontal by 17 degrees vertical with aperture efficiency of close to 50% at L-band frequencies. The beam was to be steerable in azimuth through 360 degrees with a fixed angle of depression 25 degrees below the horizontal, have an azimuth scan adjustable in amplitude up to a maximum of ± 30 degrees at a frequency of 15 cycles per minute. The antenna was to be stowable in a space 3 by 4 by 9 feet and deploy through a hatch 32 by 42 inches.

The torque reaction on the vehicle during scan operation was to be less than 1.0 lb-ft. The total weight of the antenna, pedestal, and supporting structure was not to exceed 100 pounds. The contemplated duration of the mission was to be 30 to 60 days. The power requirement for scanning was to be a minimum consistent with the other requirements.

GENERAL DESCRIPTION

The objectives of antenna pattern and efficiency were met using a reflector in the form of a parabolic cylinder with an aperture of 24 feet by 40 inches and a focal length of 6 feet. A slot array feed was designed by H. P. Coleman of the Microwave Antennas and Components Branch, NRL. This design is based on work described in NRL Memorandum Report 1633.**

*Mechanical Engineer, Radar Division, Naval Research Laboratory, Washington, D. C.

**H. P. Coleman and B. D. Wright, "Gain and Pattern Measurements of Large Aspect Ratio Reflectors," NRL Memorandum Report 1633, July 1965

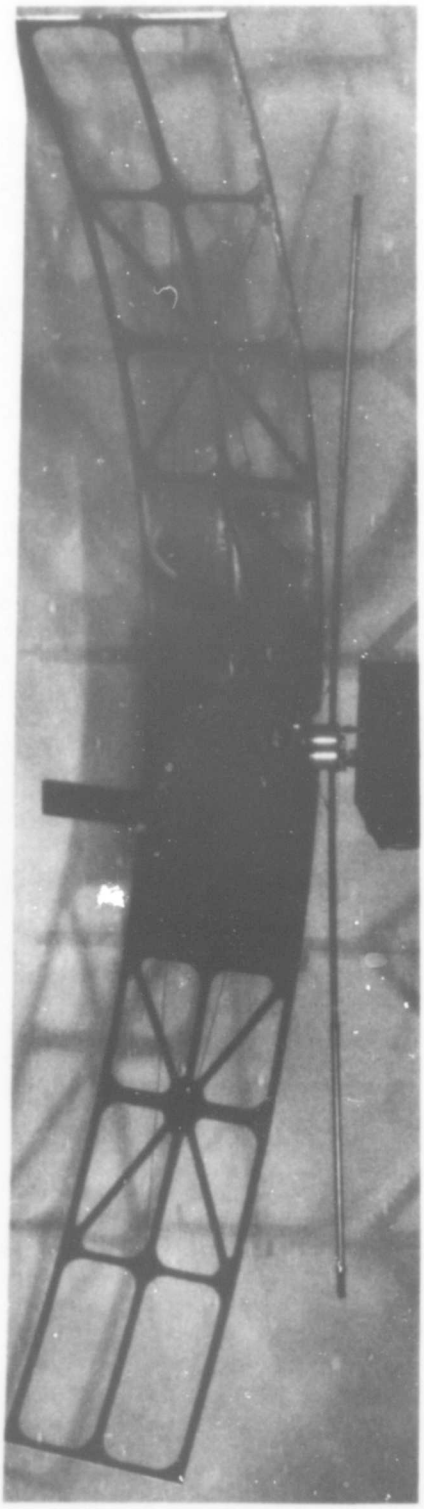

Fig. 1 - Unfolded antenna

The antenna, shown mounted on its pedestal in Fig. 1, is designed to be stowed folded inside an unpressurized vehicle or portion of a vehicle until time for deployment. The reflector consists of three panels hinged on each side of a small central panel, a total of seven parabolic panels. (The central panel was actually made planar to simplify construction. Since it has only a 17-in. chord along the 6-ft focal length parabola, the error is small in comparison with a wavelength at L-band.)

The antenna is shown in Fig. 2 with the reflector folded close up to the feed. Since the six hinges joining the panels are all parallel, the unfolding of the reflector can be conveniently described in terms of a line diagram, Fig. 3. Figure 3a shows the arrangement as folded. Hinge joints are at points 1 through 6. Unfolding is actuated by telescoping struts 0-3 and 0-4, which are gas operated. In Fig. 3b, these struts have extended slightly so that the reflector forms a letter W. Flexible fiberglass stays 9-7 and 10-8 run from the base of the feed to a point near the center of each outer panel. These stays are slack in Fig. 3b.

In Fig. 3c, the struts have extended further. Stays 9-7 and 10-8, acting on the short levers extending from the outer panels at hinges 5 and 6 are swinging the outer panels forward. In Fig. 3d, the reflector has reached its normal parabolic shape. Stays on the back surface, 7-11-2 and 8-12-1 together with struts 3-11 and 4-12 prevent the outer panels from swinging too far forward. (These stays and hinged struts were not shown in Figs. 3a and 3b.)

When the reflector is fully unfolded, the feed support together with the pedestal yoke form a rigid "backbone," 1-2-10-9 for the antenna, providing a stable base line for the two telescoping struts and four stays which resist forces and moments in the plane of the paper, Fig. 3. The antenna feed support, a length of L-band waveguide, is rigidly attached to the rotating part of the pedestal, as is a two-piece yoke, to which is attached the center section of the reflector. The details of the pedestal and of the yoke and its associated linkage will be discussed in the next section.

STOWAGE AND DEPLOYMENT

The antenna stowage and deployment sequence are indicated in Fig. 4. The relative positions of antenna feed, folded reflector, and pedestal, as stowed in a vehicle of 10-foot outside diameter are indicated in Fig. 4a. There are four steps in the deployment. The first of these is the translation of the antenna-pedestal assembly in the z direction, through the hatch, to the position shown in Fig. 4b. The second step is a rotation of the entire antenna-pedestal assembly about an axis normal to th x-z plane to the position shown in Fig. 4c. The axis of rotation of the pedestal is now parallel to the z axis (vertical) and the feed is at the correct angle for a beam with the required angle of depression. This rotation of the pedestal brings the waveguide in the pedestal into register with the waveguide from the transmitter and receiver circuits inside the vehicle. The third step is the unfolding of the reflector (Fig. 3), positioning it correctly with respect to the feed. The fourth step is the deployment of the supplementary inertia arms (Fig. 4d).

In order to reduce the dimensions of the stowed package in the fore-and-aft or x direction in Fig. 5a, the reflector is moved relative to the pedestal yoke by a four-bar linkage. Thus, in Figs. 5a, 5b, and 5c the pedestal is between

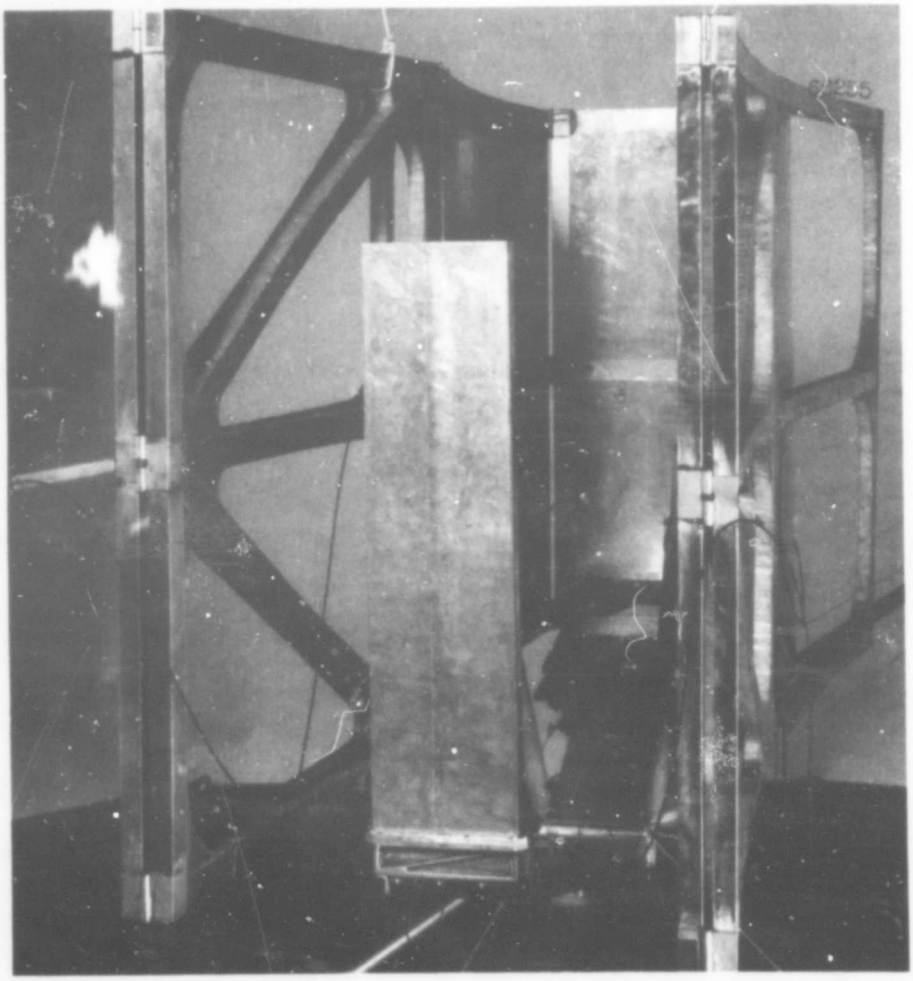

Fig. 2 - Folded antenna

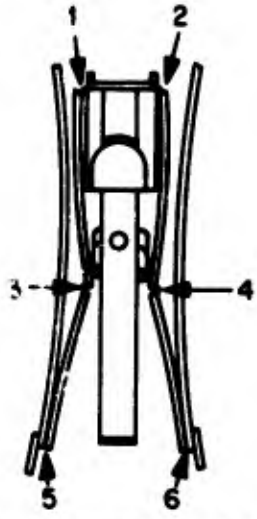

(a) Arrangement as folded

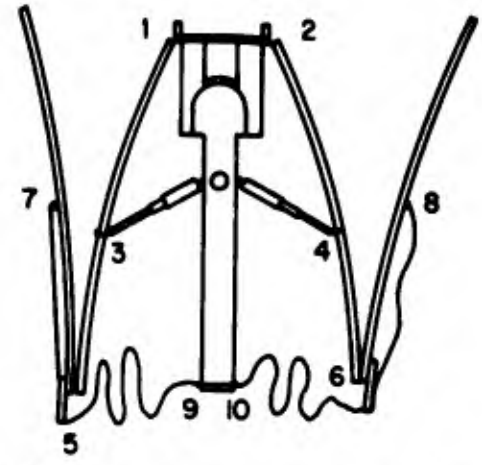

(b) Struts extend; unfolding begins

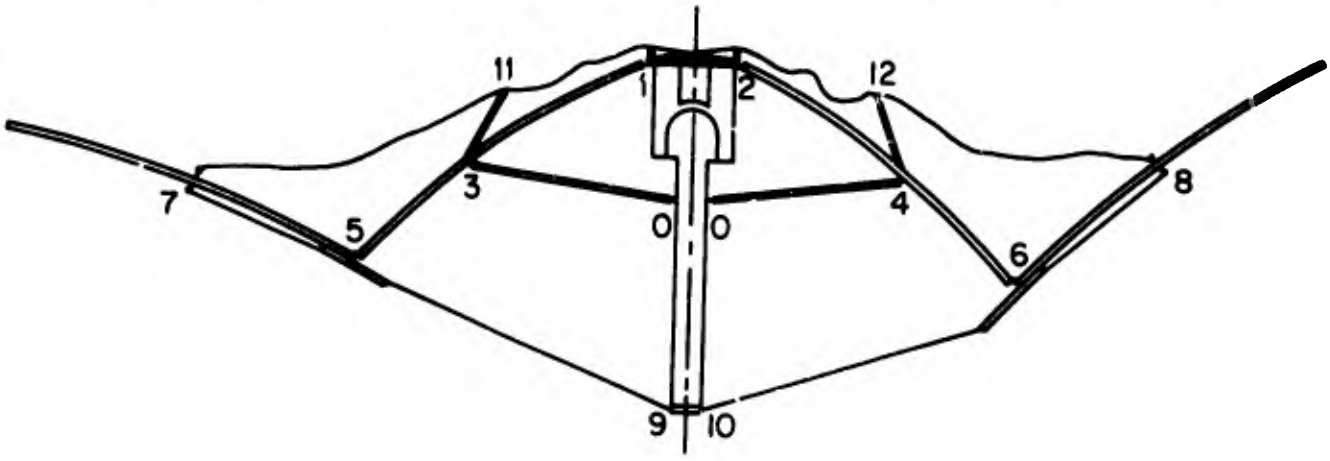

(c) Stays 9-7 and 10-8 pulling the outer panels forward as the struts continue to expand

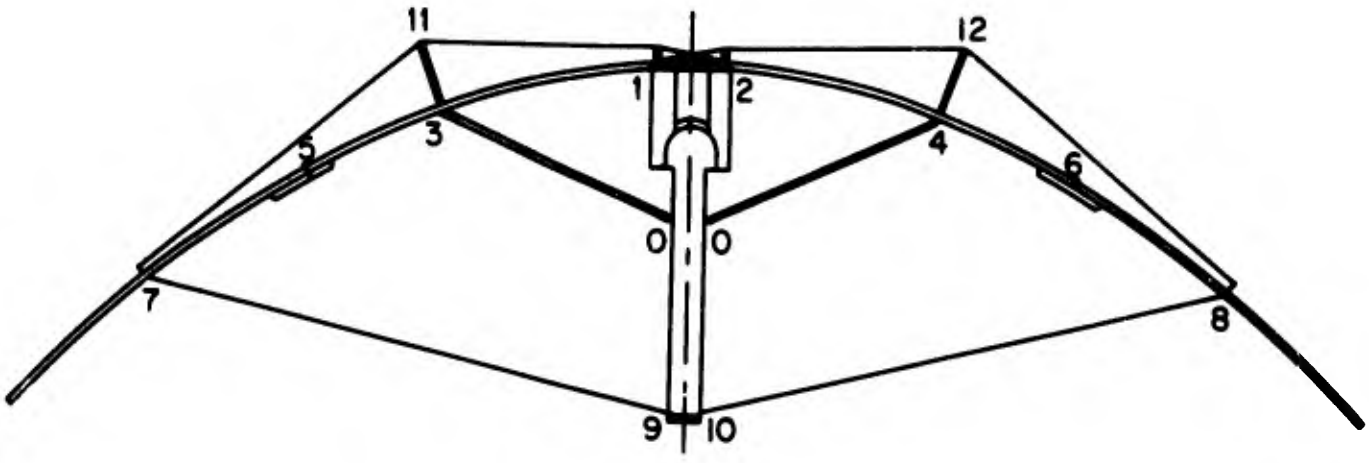

(d) Completion of the unfolding

Fig. 3 - Unfolding of the reflector

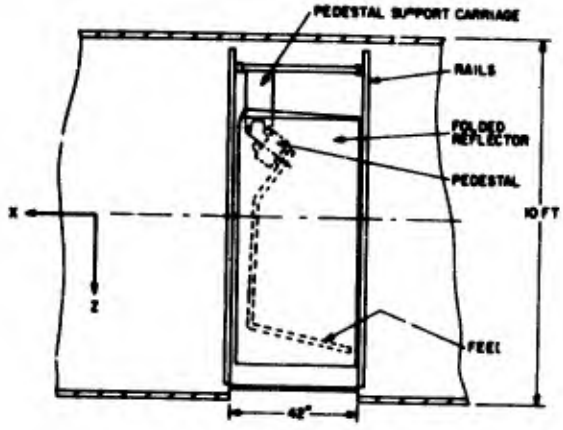

(a) Stowed antenna

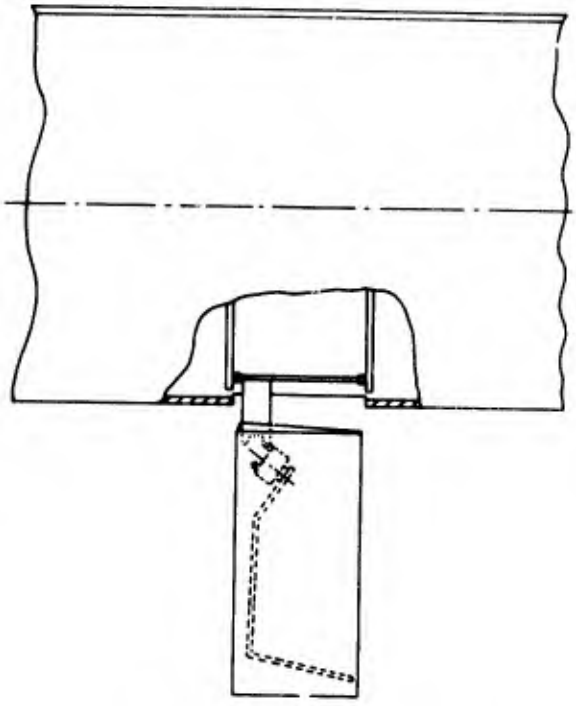

(b) Antenna after translation to outside of vehicle

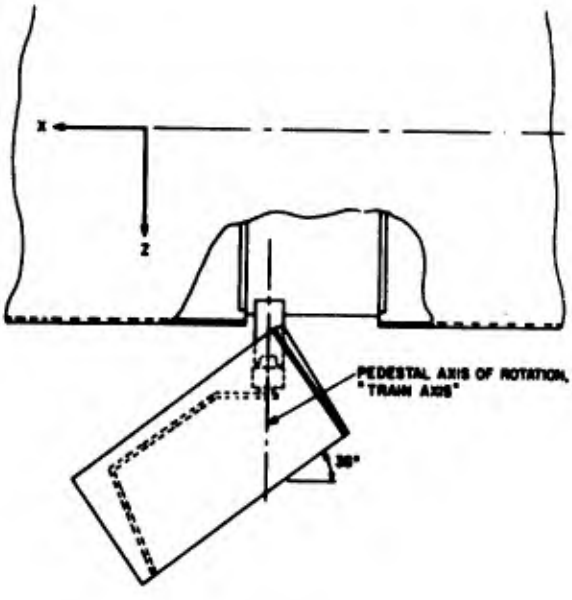

(c) Pedestal axis parallel to azimuth axis

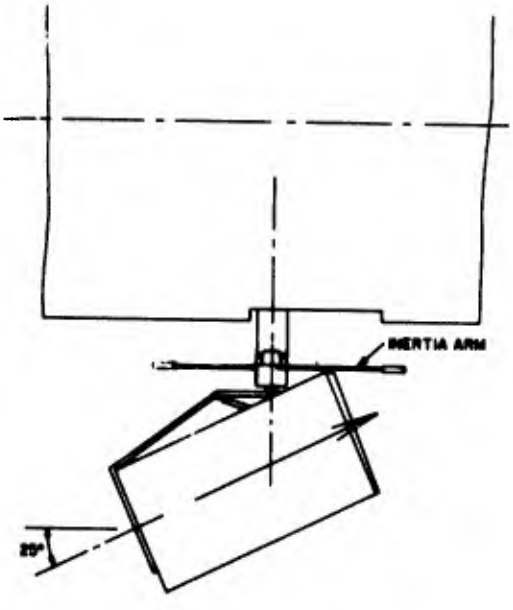

(d) Antenna after full deployment

Fig. 4 Antenna Deployment Sequence

the three center panels of the reflector. The linkage, actuated by the same gas-powered struts which unfold the reflector, swings the moving part of the pedestal yoke and the center panel of the reflector (and hence the whole reflector) into the correct alignment shown in Fig. 5d. A spring snubber is provided to control shock. Latching pins are provided to hold the linkage and telescoping struts in the deployed position after gas pressure has been lost in the struts.

The two supplementary inertia arms (to be discussed later) telescope and hinge so as to stow alongside the feed support. (These arms were omitted from Figs. 5a, 5b, and 5c, for clarity.) Each of these arms has a gas cartridge and release valves at the outer end. At deployment these arms slowly extend to their design length. The extension process tightens shroud lines which swing the arms to alignment in a plane normal to the pedestal axis of rotation as shown in Fig. 5d.

The sequence of the deployment steps described above can be established as follows. The same command which controls the jettison of the hatch cover can initiate the translation of the antenna-pedestal assembly through the hatch. Just before the antenna-pedestal assembly reaches the "locked-down" position, a wire or other mechanism discharges a gas cartridge to operate the actuator which rotates the pedestal to the position shown in Fig. 5c. As the pedestal base reaches its final position, it in turn causes another gas cartridge to discharge and operate the telescoping struts which unfold the reflector panels. As these struts begin to extend, they first activate the release mechanism which restrains the panels as folded. After the panels have extended sufficiently to clear the path of the supplementary inertia arms, the telescoping struts discharge the gas cartridges which extend the supplementary inertia arms.

OTHER MECHANICAL DESIGN PROBLEMS

In the design process, there were a number of mechanical problems in addition to those of stowage and deployment, considered above. Among these are dynamic reactions on the vehicle, conservation of power, construction within dimensional tolerance, maintenance of these tolerances within the expected environment, and the accomplishment of all this with a limited weight.

Dynamic Reactions

A scanning antenna is shown deployed below an orbiting space vehicle in Fig. 6. The x-y plane is taken through the center of gravity (c.g.) of the vehicle, the x axis is directed along the forward tangent to the orbit (assumed circular), and the z axis is directed toward the center of the orbit. Assume that the antenna rotates about the z axis at a constant angular velocity. Neglect gyroscopic torques. If the antenna is dynamically balanced about its z axis, no reaction torques will be developed about any axis, except for the friction drag of the z-axis bearings and slip rings. If the antenna is statically balanced (i.e., its c.g. is on the z axis) but not dynamically balanced, there will be a moment about an axis lying in the x-y plane and rotating with the antenna. The moments about the x and y axes then will be sinusoidal functions respectively displaced 90 degrees in phase. If the antenna is statically unbalanced, these moments about the x and y axes will become larger.

If the antenna is oscillated to provide a sector scan, the peak reaction torques about an axis in the x-y plane will be the same if the peak angular

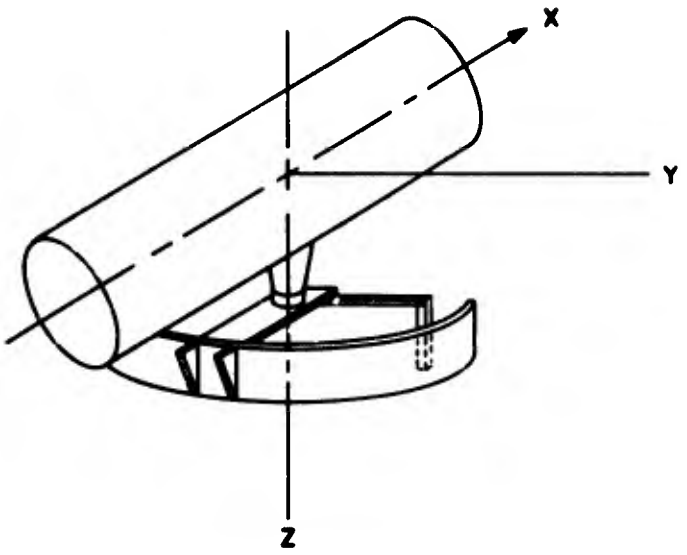

Fig. 5 - Orientation of axes with the antenna deployed below a satellite vehicle.

velocity of the sector scan is the same as that presupposed for the constant angular velocity. However, to obtain a sector scan, z-axis torque must be applied to accelerate the antenna. This requires an equal and opposite reaction torque. Unlike the reaction torques mentioned above, this is a driving torque and cannot be balanced by any arrangement of the antenna mass distribution.

The magnitude of the driving torque requirement is

$$T_z = J_z\ddot{\theta} + f_1(\dot{\theta}) \qquad (1)$$

where

T_z = torque, lb-ft (about z-axis)

J_z = moment of inertia, ft-lb-sec^2 (about z-axis)

θ = angle of antenna, radians

$f_1(\dot{\theta})$ = friction function.

If the friction is viscous and of reasonable magnitude, then for a sinusoidal scan $\theta = A \sin wt$, the maximum torque requirement is

$$T_{max} = JAw^2 \qquad (2)$$

If bearing friction is small, then the magnitude of the disturbance imposed upon the basic vehicle by the torque required for a mechanical scan is given by

$$\theta = \theta_a \frac{J_{za}}{J_{zv}} \qquad (3)$$

Where the subscripts a, and v refer to antenna and vehicle.

For example, an antenna of the size considered might have an inertia of 30 ft-lb-sec^2 about the z axis. Suppose it were used on a 25-foot-long vehicle with gross weight 25,000 pounds, uniformly distributed. Then J_{zv} 40,000 ft-lb-sec^2. For a scan angle of ±30 degrees,

$$\theta_v = 30 \times \frac{30}{4 \times 10^4} = 0.0225 \text{ degree amplitude.}$$

Peak to peak excursion would be 2.7 minutes. This excursion, at the scan frequency, might or might not be harmful, depending upon the requirements of other subsystems mounted on the vehicle. A major purpose of the project was to demonstrate a technique for reducing the reaction torque which causes this disturbance.

The pedestal is designed to isolate the motor reaction torque from the vehicle by means of antifriction bearings. Figure 6 is a simplified cross section of the essential arrangement of the pedestal, shown inverted to correspond to Fig. 1. The inboard section of the antenna feed support waveguide is actually made integral with the shaft, 1, which is mounted on bearings, 2 and 7. The rotor of the scan torque motor, 3, is secured to the shaft, whereas the stator, 4, is secured on the cup-shaped housing, 5. It will be noted that the housing is supported by a single four-point-contact ball bearing, 6, on the base, 8.

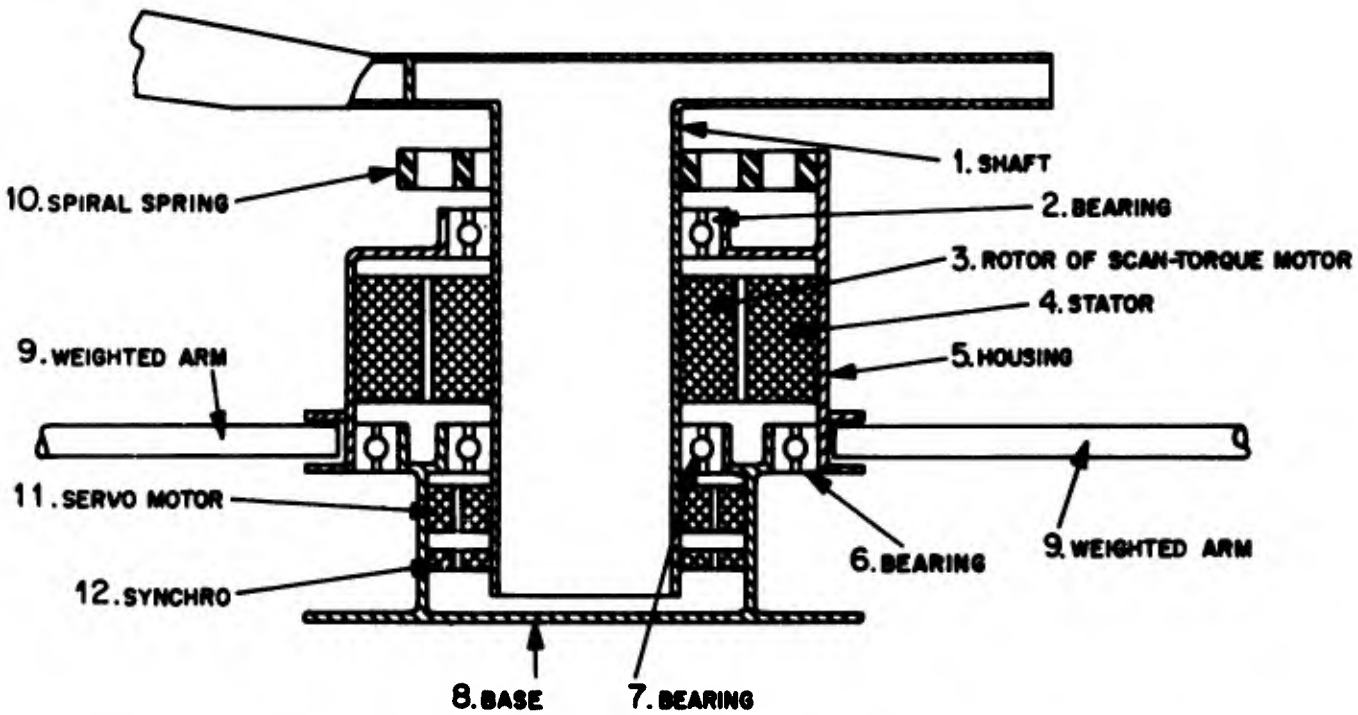

Fig. 6 - Simplified Cross-Section of Pedestal

When torque is developed by the scan motor the rotor with the antenna accelerates in one direction and the stator and housing accelerate in the opposite direction. The rates of acceleration of these two counterrotating assemblies responding to a given torque are, of course, inversely proportional to their respective inertias (assuming that friction is small). The essential point here, though, is that the stator torque does not react against the base (and hence the vehicle) but instead reacts against the inertia of the bearing-mounted housing.

The only z-axis torques acting on the base are the friction torques of the two bearings. Since antenna and housing rotate in opposite directions, even these

friction torques tend to cancel one another. In this design, a four-point contact bearing is used for stability in bearing 6. As this type has relatively higher friction than the standard deep-groove type used for the inner bearing, the cancellation is not very effective in this pedestal. A different arrangement of the components shown in Fig. 6 could provide for further reduction in the z-axis torque transmitted to the base. This objective was not pursued, however, because the present friction torque is already small compared to the reaction torque which would be present without isolation.

The antenna inertia is evidently very large compared to the inertia of the pedestal housing as described. Thus, the acceleration and velocity of the housing would be orders of magnitude higher than those of the antenna, causing problems of stress due to centrifugal force, excessive power losses in bearings, and other problems. Long weighted arms, 9, called "supplementary inertias" have been attached to the housing in order to bring its effective inertia up to the same order of magnitude as the antenna. There is no special value in having the supplementary inertia identical to that of the antenna. Presumably the weight gain advantage in letting the supplementary inertia rotate at relatively high speeds can be traded off against the advantages of lower speed. This was not done, because the adoption of the resonant drive system (using the spiral spring, 10, to be discussed later) put a direct limitation on the allowable relative excursion between antenna and supplementary inertia arms.

The pedestal is also shown in the photograph, Fig. 7. Parts that are visible in the photograph are identified by the same numbers used in Fig. 6. The fixture which supports the pedestal in this photograph contains a ball-bearing turntable. This was used to demonstrate the small value of the reaction torque.

Power Consumption

Because of the high cost of supplying electrical energy in an orbiting vehicle and because of the weight of actuators capable of producing high torque, the power requirement is evidently an important design consideration even if the reaction torque on the vehicle is at an acceptable magnitude. From Equation 2 we find that a sinusoidal torque T of about 40-lb-ft amplitude is needed to oscillate an antenna through a scan angle of ±30 degrees at a frequency of 15 cpm, if the inertia J about the scan axis is 31 lb-ft-sec^2. (Reasonable amounts of viscous friction will not appreciably affect the amplitude of the required torque.)

The required power for scanning an antenna having the stated inertia and a relatively high value of viscous friction, B = 3.0 ft-lb-sec / rad is presented in Fig. 8 on the lines labeled "simple drive". Since these figures depend upon the characteristics of the chosen motor, as well as the load, results are shown for three different motors. Evidently, a tradeoff can be made between motor weight and power consumption, since larger motors tend to have parameters favoring lower power consumption. Motor 1 (Inland T-10004-A) used for the example is undoubtedly too heavy (110 pounds) for the application. Lighter direct-drive motors, however, would be incapable of as large scan angles and, even within their capability, would use more power. Geared motors could improve the efficiency and reduce weight, but they would introduce undesired complexity and also make it difficult to isolate the z-axis reaction torque.

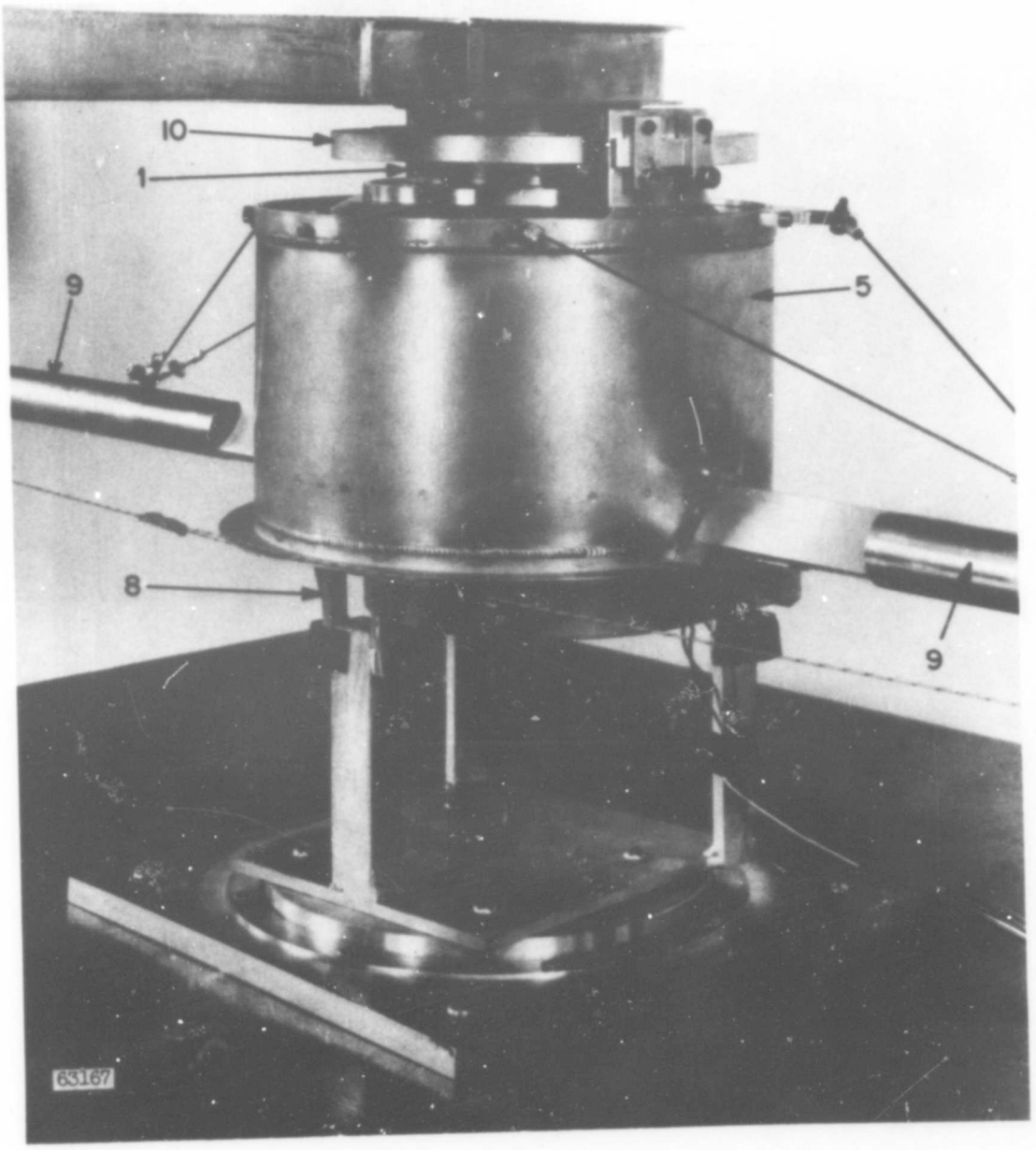

Fig. 7 - Pedestal with parts numbered as in Fig. 6

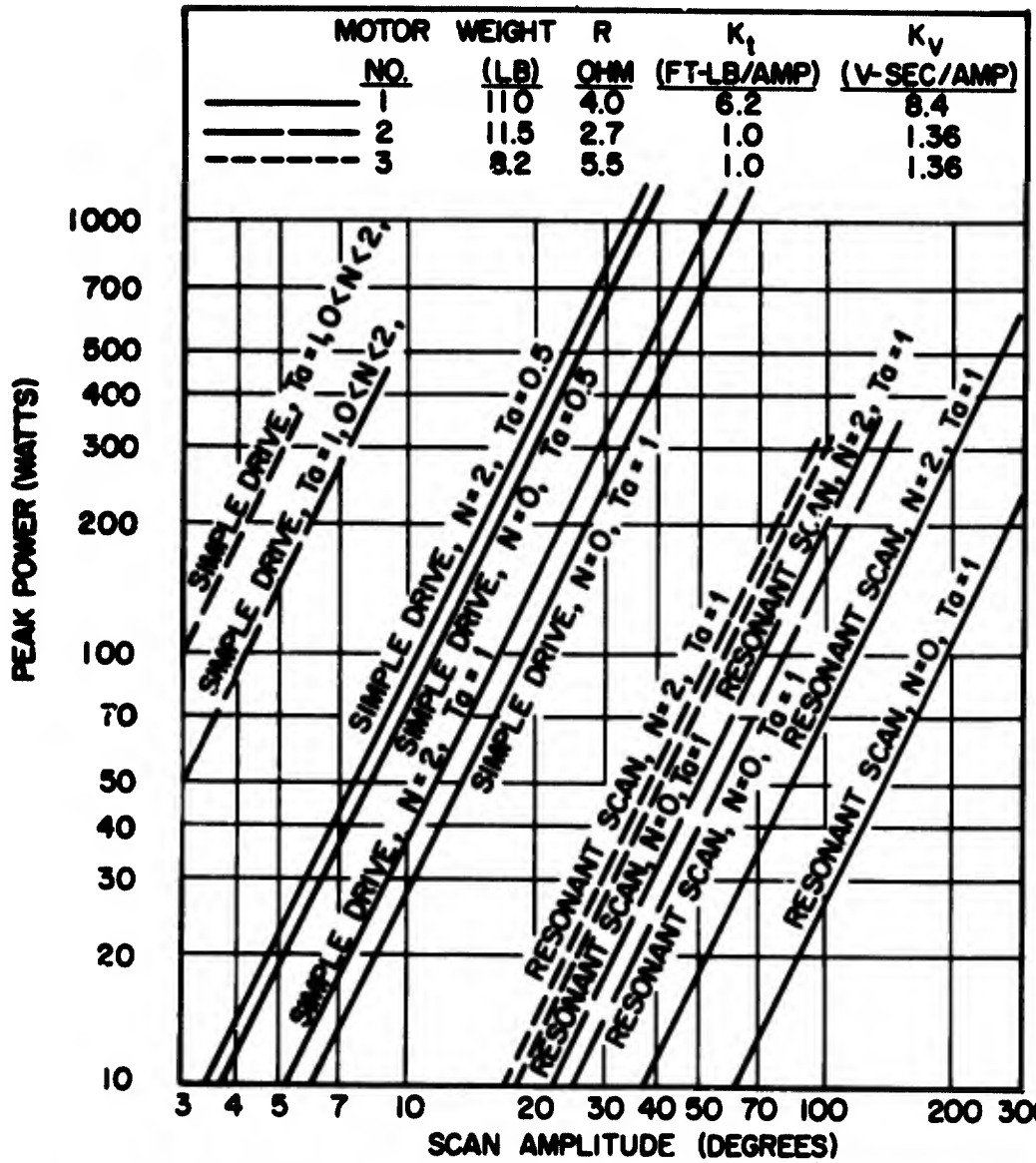

Fig. 8 - Driving Power for a load inertia, J = 31 ft. lb. sec^2, damping B=3.0 ft. lb. sec/rad; Modified sawtooth scan with period 4 seconds.

The scan power requirement for the present antenna is reduced to a reasonable level by designing the antenna-pedestal scan mechanism as a spring-mass system resonant at the desired scan frequency. This is done by connecting shaft 1 and housing 5 by the spiral spring 10 in Figs. 6 and 7.

In this design, the motor is required only to make up the losses due to friciton in the bearings and slip rings and hysteresis in the spring itself. Calculated power for the resonant drive is shown in Fig. 8 for the same three motors used in the hypothetical simple drive.

To measure power requirements, a simple structure was mounted on the pedestal to simulate the inertia of the antenna. This structure had air drag at least an order of magnitude less than the antenna. With this simulated antenna scanning at an amplitude of 27 degrees and a frequency of 15 cpm the peak power supplied was measured as 26 watts. This checks fairly well with the value of 25 watts read from Fig. 8. Values of power calculated for resonant drive systems are necessarily very rough, since the critical factor, the viscous friction B, is usually not accurately known.

Accuracy of the Reflector Surface

The surface of the antenna reflector must be manufactured to tolerances appropriate to the wave length at which the antenna is to be operated. The deviations from the ideal shape must of course remain within tolerance in the operating environment. Particular attention must be paid to the dynamic deflections caused by the thermal environment.

The contour of this reflector as a whole is determined by the contour of the individual, relatively rigid panels, and by the adjustable tension and compression members which set the hinge angles between these panels. In view of the long wavelength contemplated (8-1/4 inches) it was expected that a quickly-built wooden form would give adequate accuracy to sandwich panels laminated thereon. All panels have a 1-inch thick core of a 3/8-inch hexagon-cell honeycomb of 0.001-inch-thick 5052 aluminum alloy. Skins are of 0.0037-inch-thick 6061 aluminum alloy. Heavily loaded areas of the panels are reinforced with 0.010-inch-thick 6061 aluminum alloy strips. In the outer panels, the sandwich structure forms open frames (Figs. 1,2, and 3); these openings are covered with "S-band Sucal Cloth" (not shown).

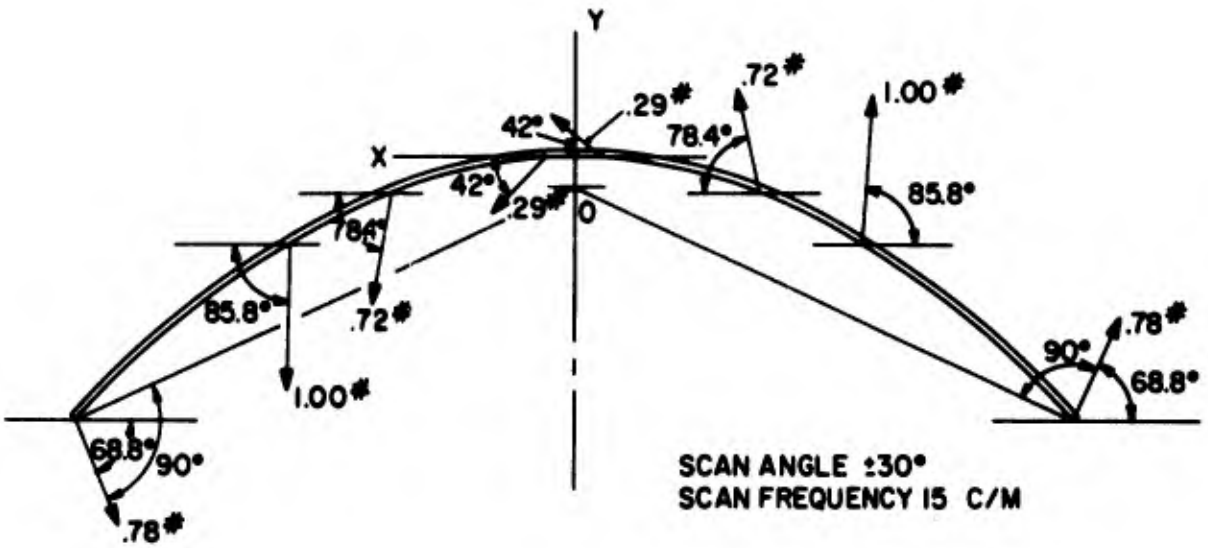

Fig. 9

Static Simulation of the peak angular acceleration forces during a scan of ±30 degrees at a frequency of 15 cpm.

Besides providing strength and stiffness to the reflector, the truss arrangement provides six independent adjustments of the shape of the reflector, thus easing the requirement for precision manufacture of the panels. These adjustments are made as follows (Fig. 3): Adjustment of the length of the fully extended struts, 0-3 and 0-4, controls the angles between the center panel and the inner hinged panels, 1-3 and 2-4. Adjustments of shims at hinges 3 and 4 respectively control the angles between the intermediate hinged panels, 3-5 and 4-6, and the inner hinged panels. Finally, adjustments of fittings at point 7 and point 8 respectively control the angles of the outer panels. Because of the elasticity of the tension members 7-9, 7-11-2, etc., and of the panels themselves, there is some interaction between the last four adjustments mentioned. This interaction, however, is not great enough to cause difficulty in adjustment.

Dynamic Deflections - The dynamic deflections are caused by centrifugal acceleration and angular acceleration. The centrifugal acceleration gives a symmetrical loading which is radial from the scan axis. It reaches a maximum when angular velocity is maximum, which is at the center position of the scan angle. The angular acceleration gives an unsymmetrical loading which is maximum at the extreme positions of the scan. For the particular scan cycle considered, the unsymmetrical dynamic loading at the instant of maximum angular acceleration provides the critical design load for the feed horn support, the tension members such as 9-7, and most of the structure. Members 9-7 and 8-10 are made from 1/8-inch-diameter five-strand cable using fiberglass tire cord bonded with polyurethane.

While dynamic deflection measurements could be made, the several methods considered would have required a rather large effort compared to the static method used. Static forces were applied at eight points in the plan view (Fig. 9), with magnitude and direction calculated to simulate, conservatively, the peak "acceleration forces" acting on the panels during the scan cycle. Each of the forces shown in Fig. 9 was actually divided into two equal parts, one applied at the top chord and one at the bottom chord of the reflector.

The test procedure was as follows: First, the reflector was set up with the hinge axes vertical to minimize the deflections due to gravity. A vertical line was rigged from the outer part of each inner folding panel (near hinges 3 and 4) over pulleys to counterweights to relieve part of the weight from the pedestal yoke and thus further reduce static deflections caused by gravity. A template was set close to the center chord of the reflector. Distances between template and reflector were measured at 28 stations. Each measurement was made parallel to the axis of the parabola (the y axis). Second, the template was moved clear and loads applied as described above. Third, the template was again moved close to the reflector and the deviations again measured at the same stations. The whole procedure was repeated to verify results.

Before application of load, the peak error of the reflector surface was 7/16 inch; rms error was 5/32 inch. Under load, the peak error from the best fit parabola was 9/16 inch; rms error increased to 7/32 inch. The method of test described tends to produce greater deflections in the tip panels than would a true acceleration field. Since the observed rms error is small, corresponding to $\lambda/37$ at 1350 MC, it did not seem necessary to refine the measurement.

Thermal Effects - The contour of the reflector surface could be degraded by differential thermal expansion between the reflector surface and the struts and guys, and also by warping of the individual panels caused by thermal gradients through them. The former effect is small, because the open nature of the reflector surface permits most of the thermal radiation to pass through and illuminate the portions of the truss (struts or guys) on the "shadow side," thus keeping small the thermal gradients in the truss. The geometry of the truss is arranged so that the differential expansion that does occur will not cause severe maladjustment of the surface.

In the environment of space, the thermal equilibrium conditions, in general, require heat flow through exposed panels. The resulting temperature differential between "front" and "back" surfaces causes the panel curvature to change. The greatest deflection will occur at the tip sections of the outer panel which extend as cantilevers beyond the attachment point of the outer guy lines. The maximum deflection between this attachment point and the point controlled by the

strut will be smaller than that of the tip.

Calculated values of these maximum deflections are displayed in Table 1 for several severe environmental conditions. Also listed in Table 1 are values of the deflections of the feed support guide, calculated for several conditions

This waveguide section which supports both the feed and the forward guy lines is subject to fairly severe E-plane distortion due to the temperature differential between the upper and lower surfaces. The deflections of this simple design appear to be tolerable. If necessary, they could be reduced by the geometrical effect of a deeper section, by improving the heat conduction between upper and lower surfaces, or by some more elaborate technique.

Table 1
Summary of Calculated Thermal Deflections

Sunlight	Assumed Temperature (R)		Calculated Temperature (R)		Peak Deflection	
	Ground	Vehicle	Differential Across Item	Mean of Item	Inches	Wavelengths
Tip of Reflector						
None	500	480	2.8	408	0.081*	1/102
None	540	515	4.0	438	0.115*	1/71.8
Normal to panel	520	500	5.0	489	0.144*	1/57.3
Feed Support Guide						
60 degrees from normal	500	460	22	469	0.333	1/24.8
None	540	500	22	440	0.333	1/24.8

Bearings and Slip Rings

Bearings and slip rings can be subject to cold welding and seizure in the hard vacuum environment of space. The relatively short mission (30 to 60 days) specified for this study allows at least two approaches to the bearing lubrication problem, namely, the use of low-vapor-pressure lubricant or bonded coatings of either solid or fluid lubricant.

The present pedestal was designed to be usable with low-vapor-pressure lubricants. Labyrinth seals are provided at three points to impede the escape of the lubricant vapor. With the present design the weight penalty is about 10 ounces for these seals. Two factors, however, make it difficult to maintain the narrow clearance required to make the seals effective over a long time. The first of these is the heat flow variation between standby condition and scanning

operation. (The motors dissipate up to 80 watts.) The elastic deflections, especially those caused by the large spring forces, are a second factor. Since the pedestal has not been tested in vacuum, the efficacy of this aspect of the design has not been demonstrated. Additional weight may be required in order to obtain the rigidity necessary for successful functioning of the seals.

The use of a bonded coating of molybdenum disulfide for lubrication of the ball bearings seems to offer a reliable alternative. At least one manufacturer is offering services for applying such coating. Long operating lives are reported* in tests run at pressures of 10^{-8} mm Hg. It is also reported that successful performance of torque motors similar to those used in this pedestal was obtained in the Orbiting Solar Observatory (OSO) as well as in extensive chamber testing.

Variations of the same process have been used with success for both power slip rings and instrument slip rings. The process is relatively expensive because the coated assemblies must be run in and tested in a high vacuum in order to insure reliability. The high-power slip rings constructed for this pedestal are silver with rhodium plating. Silver graphite button brushes are used.

Table 2
Breakdown of the Measured Weight of the Antenna and Pedestal

Reflector panels		
Center panel	3.125 lb	
Inner panels, two at 4.50 lb	9.000 lb	
Middle panels, two at 2.50 lb	5.000 lb	
Outer panels, two at 4.062 lb	8.125 lb	
Total reflector panels		25.25 lb
Pedestal		24.50 lb
Links		0.55 lb
Telescoping struts		1.12 lb
Feed subassembly		
Feed support guide	0.87 lb	
Feed	0.56 lb	
Miter elbows, flanges	1.50 lb	
Total feed subassembly		2.93 lb
Supplementary inertia struts, two at 4.62 lb		9.24 lb
Fiberglass guy cord		0.26 lb
Miscellaneous hardware		0.50 lb
Screws		0.10 lb
Total weight		64.45 lb

* Technical Memorandum 22.0, Ball Brothers Research Corp., Boulder, Colorado, Feb. 1965.

Weight

The weight of the antenna and pedestal is 64.6 pounds. This figure does not include external electronics, such as for the control system. A breakdown of the measured weight is given in Table 2. All of the reflector panels weighed somewhat more than their design values, because of excessive adhesive used. The structural design is also far from optimum. Nevertheless the total weight obtained is well within the specified goal, leaving more than 35 pounds available for the structure and mechanism required to support the stowed antenna, deploy it, and support it in its deployed position.

POTENTIAL FOR OPERATING AT FREQUENCIES HIGHER THAN L BAND

A reasonable reflector surface tolerance for operation at S band would be 3/16-inch rms error and 1/2-inch peak error. The present reflector, under an unfavorable combination of thermal deflection and dynamic load, would exceed these figures. Similar sandwich reflectors, however, could be fabricated much more precisely, simply by using an accurate mold. Both the thermal and the dynamic deflections of the present tip panel could be reduced by a change in location of the outer support point of this panel. Thus a reflector of this type could be made sufficiently accurate for use at S band with a very slight increase in weight.

A requirement for an S-band antenna of 24-foot aperture would not necessarily imply the same type of feed used in this project. In any case, a structure would be needed to support the waveguide to the feed. This could be made with requisite rigidity and precision, but the resulting feed assembly might be up to 50% heavier than the present feed assembly (Table 2).

ANTENNA POINTING CONTROL

A resonant drive system such as described limits the azimuth scan frequency to the single value provided by the design, in this case 15 cpm. The scan amplitude can be controlled by varying the power supplied to the scan motor at this frequency. The tuning of the mechanical system is not affected significantly by temperature change.

The center of the scan pattern can be rotated through a full 360 degrees. The center is positioned by a feedback control system which is independent of the resonant scan. A block diagram of this system is given in Fig. 10. Transfer functions of each block are also given. A small torquer (part 11, Fig. 6) is the servo motor in this control system. The pancake-type synchro (part 12, Fig. 6) is mounted directly on the pedestal shaft to read out the train angle. A chopper demodulates the 400-cycle error signal from a synchro control transformer manually set to the desired position. The smoothed output of the chopper detector is a sine wave whose amplitude is a measure of the amplitude of the scan and whose average value is proportional to the pointing error of the midpoint of the scan sector. The nonlinear "peak-average circuit" detects this pointing error with a shorter time delay than would be introduced by a simple passive network.

The pedestal transfer function shows the two quadratic factors typical of a motor-inertia-load combination with a second inertia coupled through a spring.

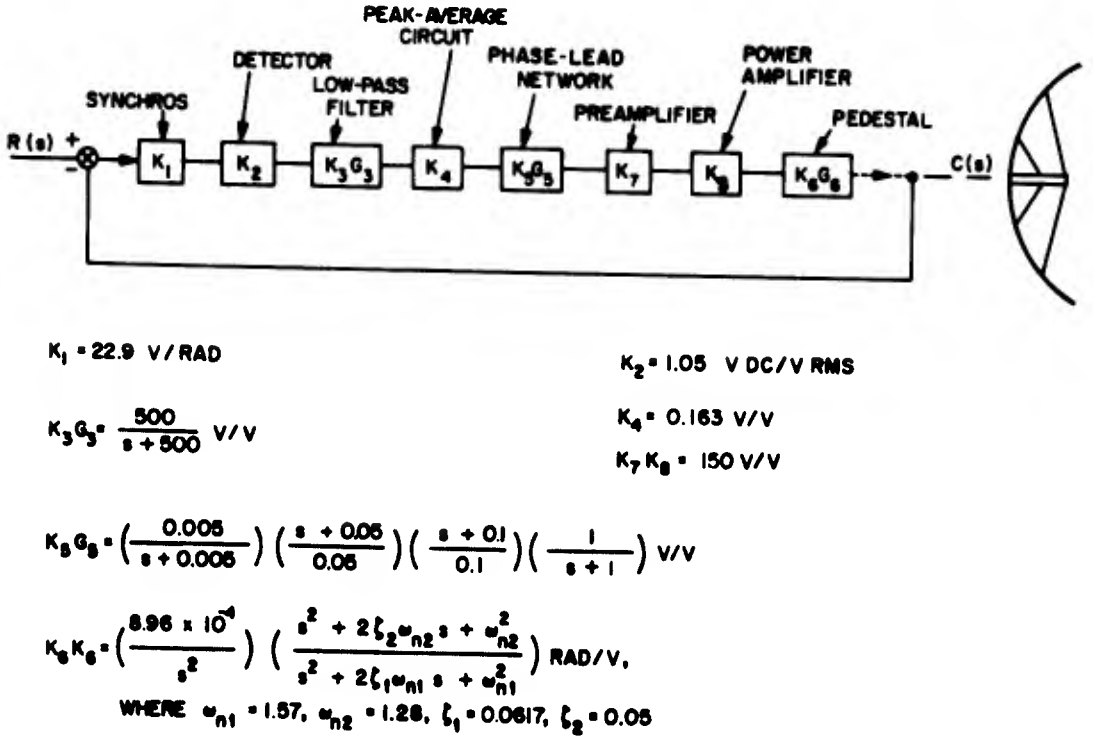

$K_1 = 22.9$ V/RAD

$K_2 = 1.05$ V DC/V RMS

$K_3G_3 = \frac{500}{s+500}$ V/V

$K_4 = 0.163$ V/V

$K_7K_8 = 150$ V/V

$$K_5G_5 = \left(\frac{0.005}{s+0.005}\right)\left(\frac{s+0.05}{0.05}\right)\left(\frac{s+0.1}{0.1}\right)\left(\frac{1}{s+1}\right) \text{ V/V}$$

$$K_6K_6 = \left(\frac{8.96 \times 10^{-4}}{s^2}\right)\left(\frac{s^2 + 2\zeta_2\omega_{n2}s + \omega_{n2}^2}{s^2 + 2\zeta_1\omega_{n1}s + \omega_{n1}^2}\right) \text{ RAD/V,}$$

WHERE $\omega_{n1} = 1.57$, $\omega_{n2} = 1.28$, $\zeta_1 = 0.0617$, $\zeta_2 = 0.05$

Fig. 10 - Antenna pointing control system.

The frequency $w_{n1} = 1.57$ rad/sec is, of course, the design frequency for the resonant scan. The low damping which was required for minimum scan power makes it necessary for the z-axis position control system to have an appreciable gain margin at this frequency. A conventional lag-lead network, K_5G_5, is provided to stabilize this "type-2" system. Calculated control loop gain is plotted versus the logarithm of frequency on Fig. 11, treating the system as a linear one. (Actually the operation of the peak-average detector circuit makes this a sampled data system.) The value chosen for the product K_7K_8 places gain crossover in the neighborhood of 0.5 rad/sec.

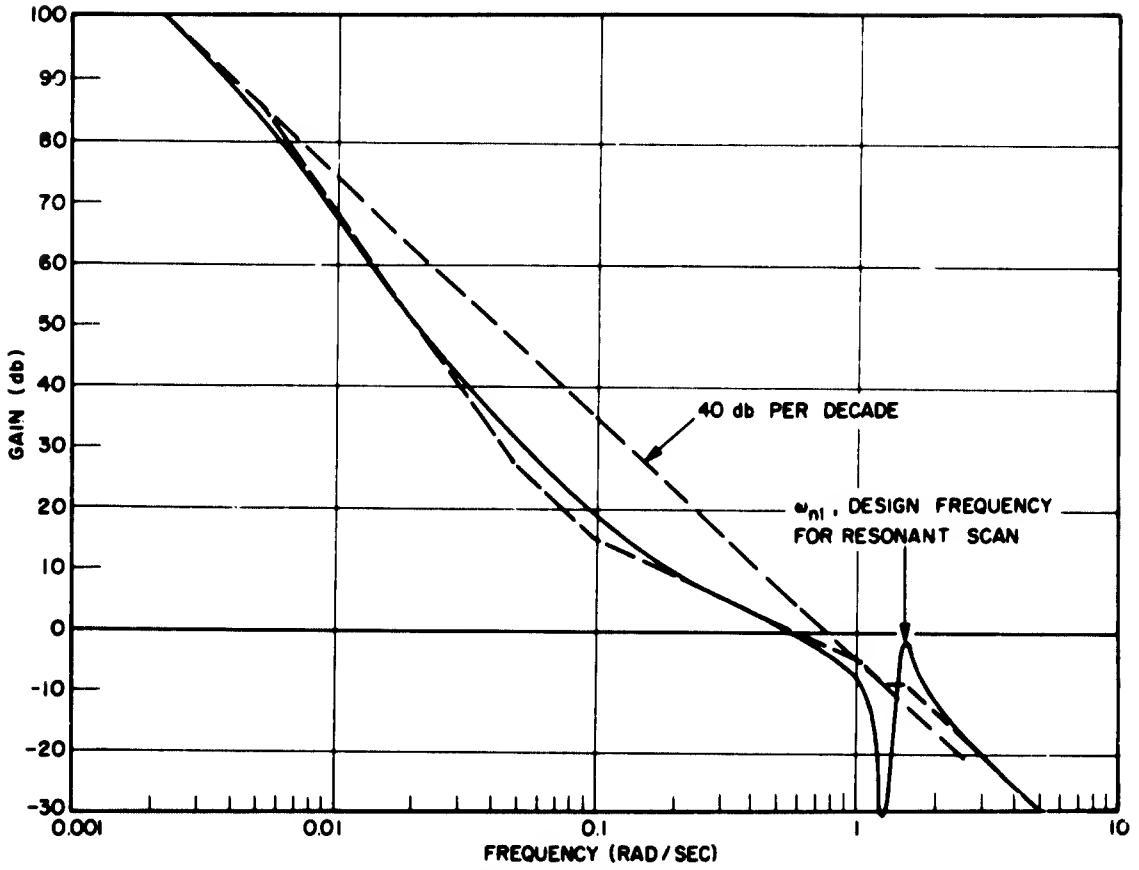

Fig. 11 - Calculated control loop gain.

CONCLUSIONS

The model as constructed has met the design goals for accuracy, weight, performance, stowage, torque reactions, power, etc., established by the requirements of an L-band search radar system. The weight can be further reduced by careful refinement of the design of the parts. Thus feasibility has been demonstrated for the use in a satellite of scanning L-band antennas having apertures of about 24 feet. It is clear that satisfactory S-band antennas can also be made in this range of apertures.

BLANK PAGE

VARIABLE GEOMETRY LIFTING SURFACES FOR LIFT RE-ENTRY

Jerry D. O'Brien*

INTRODUCTION

The typical class of manned spacecraft which has seen operational service during the past six years may be characterized as low L/D, ballistic re-entry vehicles which possessed limited maneuverability or piloted landing capabilities. Vehicle recovery operations relied on the droque chute-parachute methods of deceleration and landing. Therefore, while these vehicles were manned, pilot landing techniques were not utilized by virtue of the limitations which are inherent in the low L/D class of vehicles. Increasing emphasis is now being placed on lifting vehicle concepts which offer the possibilities of glide, maneuver, and horizontal landing. These vehicles enter the atmosphere at shallower re-entry angles which results in lower heating rates than encountered by the non-lifting vehicles. There is a longer re-entry time, with the result that the total heating to which the vehicle is subjected, is greater than that of a drag capsule. An equilibrium temperature is reached in which the incoming aerodynamic convecting heating is equal to the outgoing radiation. By careful design of the vehicle shape and designating flight paths which will avoid critical heating regions, the surface material temperature may be maintained at an acceptable level for radiative structures and ablatives (required for low L/D re-entry) may not be required.

Re-entry vehicle configurations which are aerodynamically efficient in the hypersonic flight regime are often inefficient in the lower speed ranges of the flight profile. This is due to vehicle aerodynamic changes which occur in low speed flight, such as the shift in center-of-pressure location during the transition from high Mach number flight to subsonic flight. Consequently, for a vehicle to have good performance characteristics in the low speed ranges, design compromises which degrade the hypersonic configuration are often required. Numerous aerodynamic investigations sponsored by the Air Force Flight Dynamics Laboratory have shown, however, that variable geometry lifting surfaces which can be deployed from an efficient hypersonic vehicle during the terminal phase of the

* Aerospace Engineer, Structures Division, Air Force Flight Dynamics Laboratory, Wright-Patterson Air Force Base, Ohio.

flight profile provide a solution which improves maneuverability and low speed performance in the landing mode. As a result, the aerodynamic characteristics required for an efficient hypersonic configuration are retained. While there have been structural studies of variable geometry for advanced aircraft application, these investigations, by their very nature, have not considered the problems involved in a re-entry environment. An investigation sponsored by the AF Flight Dynamics Laboratory to determine variable geometry structural concepts for lifting re-entry vehicles has provided basic information regarding the penalties incurred with the addition of deployable lifting surfaces. Combinations of three basic re-entry vehicles, three wing planforms, and three construction methods were investigated (as indicated in Table I) to determine the preliminary feasibility of the variable geometry concept as a function of lifting surface location and construction. A representative variable geometry concept for each of the three vehicles was then chosen for a more detailed structural and weight analysis. The basic requirement to be met by each configuration was that the wing planform area be sufficient to provide a minimum L/D max of 4.5 during the landing phase of terminal re-entry. The trajectory used for each vehicle corresponded to a minimum entry angle.

Although twenty-seven concepts were initially evaluated for preliminary feasibility, we will look at just a few of the concepts derived. These indicate the problems involved with rigid, semi-rigid, and inflatable types of construction and their relation to structural complexity, vehicle internal usable volume, and weight as a function of wing location. The vehicles to which the variable geometry concept was applied are the modified elliptically shaped SORTIE, the slender conical shaped M-22F, and a medium L/D re-entry configuration investigated by the Space and Information System Division of North American Aviation, designated the SID-1 (see Figure 1).

SORTIE VARIABLE GEOMETRY CONCEPTS

The SORTIE vehicle is designed for a superorbital entry with a hypersonic L/D of 0.9. The vehicle has a relatively blunt, elliptical nose to withstand the severe heating environment encountered on re-entry from parabolic speeds. Since we are interested only in the terminal portion of re-entry for concept evaluation, a re-entry velocity of 26,000 fps was chosen. Some of the variable geometry concepts derived during the feasibility investigation are shown in Figures 2 to 6.

Figures 2 and 3 show rigid and semi-rigid rectangular lifting surfaces in the midwing configuration. This location on the vehicle is ideal for surfaces which must be stored internally from the standpoint that it allows the utilization of a wing of maximum planform area, and the surfaces are protected from the thermal environment.

Stowage of wings in this location reduces the available useful internal volume. However, with the semi-rigid concept shown in Figure 3, the volume penalty is reduced when the inflatable trailing edge is packaged within the main structural wing box.

Two delta wing configurations are shown in figures 4 and 5 which eliminate the volume penalty previously discussed and maintain the basic body structure.

The semi-rigid design uses the flat upper surface of the basic body as the storage area and does not rely upon excessive structural modification of the vehicle body. The inflatable structure results in a reduction of the Mach number at which the wing may be deployed because of dynamic problems anticipated during high speed deployment. The concept of Figure 5 utilizes a hinged rigid wing which basically is acceptable for high speed deployment. In this concept, the excessive number of rotatory actuators required for deployment, in addition to the problem of leading edge protection prior to deployment, results in unnecessary complexities.

Figure 6 shows the variable geometry concept which was selected as the most promising from a feasibility standpoint for the SORTIE vehicle. This design was selected because the upper mold line of the basic vehicle may be utilized for stowage of the lifting surface, reducing the amount of internal volume required for basic body modification. The rigid wing construction also has the advantage of reusability. An inverse tapered planform (that is, with the maximum wing chord at the tip) is required to satisfy the area requirement needed to achieve the minimum L/D max of 4.5. The thickness-to-chord ratio must be increased inboard in order to obtain the necessaty structural stiffness and strength needed to carry the maximum load introduced at the tip.

M-22F VARIABLE GEOMETRY CONCEPTS

The M-22F is a conceptual de-coupled high L/D vehicle which has very good hypersonic characteristics but is aerodynamically unstable during the lower portion of the flight trajectory. Because of this, wing deployment must be accomplished in the range of Mach 2 to Mach 4. An orbital re-entry trajectory of 26,000 fps was used for this vehicle in the evaluation of the variable geometry concepts. A few of the concepts are shown in Figures 7 to 10.

Figures 7 and 8 show rigid and expandable delta wing configurations. For achieving maximum wing area from an internal stored wing, the expandable delta offers the greatest potential. The use of this design is limited, however, to cases of low speed deployment because of aeroelastic deformations which may arise at high angles of attack at high speeds. The rotating rigid delta shown in Figure 8 uses the flat surfaces on the sides of the basic body as the storage areas

and the loss of internal volume is negligible. In addition, the long hinge line offers a better load distribution to the vehicle body. The wing planform area obtained with this concept is insufficient however to achieve the minimum L/D max of 4.5.

Two low wing rectangular configurations located to give maximum wing planform area are shown in Figures 9 and 10. The semi-rigid wing can be stowed in a minimum volume but additional actuation units must be incorporated in the structure for outboard leading edge extension. The rigid concept shown in Figure 10 may utilize conventional materials and an internal pivot mechanism for wing deployment. With a rigid wing, control surfaces may be incorporated in the design if necessary. The major disadvantages with this concept are that considerable body volume is required for wing storage and extensive structural modification to the basic body is needed. This variable geometry configuration was selected for further evaluation because the lifting surface provides an area large enough to obtain the desired lift-to-drag ratio and can be stowed in an area which can accommodate it. The deployment system is also stowed internally, thus being protected from the thermal environment.

SID-1 VARIABLE GEOMETRY CONCEPTS

The SID vehicle configuration is typical of other medium L/D configurations which are currently being investigated for manned maneuverable flight. These vehicles aerodynamically are compromised for flight in all speed regimes. Vehicles of this type would use variable geometry primarily as an added assist in the approach and landing modes only, because the basic vehicle already possesses maneuvering flight characteristics in the low speed regime.

Figures 11 and 12 show two mid-wing variable geometry schemes utilizing a rigid structure as the basic lifting surface. By adding an expandable structure to the basic wing, the additional planform area obtained results in an increase of L/D. If this concept were used, the wing would have to be moved forward since the increased planform area given by the inflatable structure would shift the vehicle center-of-pressure aft, thereby leading to an instability problem. Both of these concepts require cutting into the basic structure, therefore structural modifications will be necessary in order to redistribute the loads from the fins to the vehicle body. Another disadvantage of these concepts is the reduction of internal volume needed for stowage of the wings, however, the percentage of usable volume reduction on this vehicle does not present as serious a problem as on the previous two vehicles.

The most promising variable geometry concepts for this vehicle are shown in Figures 13 and 14. Although structural modifications to the body frames are necessary in order to carry the deployment loads during wing rotation, the resultant volume penalties would be negligible. The lowest weight penalty is encountered with the split-fin configuration

since a vertical control surface is required in the full rotating fin concept for directional stability. With the split-fin concept, localized heating is likely to be encountered along the gap caused by the mold line discontinuity where the trailing edge of the rotating surface meets the leading edge of the fixed surface. Hinge line heating is a problem however which would be encountered by both concepts. The full rotating concept was selected for further investigation since it offered minimum volume and heating penalties.

FINAL VARIABLE GEOMETRY DESIGNS

Table 2 summarizes the structural materials chosen for the lifting surfaces as a result of a detailed design analysis which was performed on the selected variable geometry configurations. Only the re-entry environment with maneuver and gust loads was considered in the analysis.

The maximum load-at-temperature condition is the most critical for the SORTIE and sets the design loads for the wing and supporting structure. Full-depth honeycomb sandwich of titanium Ti-13V-11Cr-3Al with core densities varying along the span of the wing (increasing towards the root) results in a minimum weight structure. Wing deployment begins at Mach 2.5 and is accomplished with a single hydraulic cylinder actuator with linkages connecting the actuator to the pivot arms of the wings (Figure 15).

The maximum leading edge temperature selects the wing materials for the M-22F. This temperature occurs at initial wing deployment (Mach 3.68) and is 930 degrees F. The maximum load-at-temperature condition determined the design loads for the wing. The wing structure is constructed with full depth titanium Ti-13V-11Cr-3Al honeycomb sandwich. The main wing box is closed off by two channel edge members. The trailing edge section is also full depth honeycomb consisting of a lighter density core. The wings are deployed by means of a ball-screw and nut actuator system (Figure 16).

The maximum temperature-at-load condition determined the materials for the SID rotating fin concept which is shown in Figure 17. The design conditions for the wing skin panels were obtained from high dynamic pressure-at-temperature conditions. The fin is of two spar, corrugated cover panels. The lower cover panels, caps, and webs are of columbium B-66 to withstand surfaces temperatures of 2200 degrees F. The upper panels and caps are subjected to a maximum temperature of 1400 degrees F and may be constructed from superalloys such as Rene 41. A tantalum T-222 segmented leading edge is attached to an auxiliary leading edge spar. Fin rotation is accomplished by two Curtiss-Wright power hinges which are attached to the main spars and the vehicle body frames.

WEIGHT AND VOLUME PENALTIES

The weight and volume penalties for the three variable geometry concepts selected for detail design are summarized in Table 3. The

weight penalties include not only the wing and deployment weights but also structural modifications to the basic vehicles which are necessary in order to accommodate the variable geometry system. The SID variable geometry concept is the lightest from the standpoint of weight penalty percentage. This is primarily due to the use of the original outboard fins as the variable geometry lifting surfaces. The fins must be modified to carry the increased bending moments which arise when the fins are deployed for approach and landing. The major weight increase is due to the addition of the center fin which is required for directional stability.

The volume requirements associated with the variable geometry systems for the three vehicles are presented in Table 3 in terms of internal stowage volume and basic body mold line volume. Internal payload volume for the three vehicles is not defined accurately enough to arrive at an actual volume penalty.

The SID vehicle has the smallest internal volume requirement since the wings are externally stowed. The volume penalty arises through the addition of the rotation feature to the outboard fins. The volume penalty for the SORTIE is also due primarily to the internal stowage of the deployment system since the wings on this vehicle are externally mounted outside of the basic body mold line. The M-22F requires the most internal volume since the entire variable geometry system is internally housed.

It should be noted that the volume data in Table 3 are given only to show vehicle characteristics and cannot be used to indicate the relative merit of the vehicles from a volume standpoint, i.e., the three vehicles cannot be compared to each other on the basis of internal stowage volume versus basic body mold line. The reasons for this are 1) the outboard fins of the SID vehicle are inherent in the basic body mold line, 2) the lifting surfaces of the SORTIE are outside of the mold line, and 3) the entire variable geometry system of the M-22F is enclosed within the mold line.

A comparison of rigid and inflatable wing weights is shown in Figure 18 for the SORTIE and the M-22F. The inflatable wing weights are basic on elastomer coated type 304 stainless steel two ply AIRMAT*. A constant wing thickness of three inches is used in the estimation of the inflatable wing weights. The AIRMAT concept used in this comparison has a temperature capability of approximately 800 degrees F as compared to a temperature of 930 degrees F as experienced by the M-22F titanium wing. Although there is an allowable temperature difference between the two material systems this factor was not considered in making this preliminary weight comparison. This comparison is made only to show the potential weight savings which are possible with inflatable configurations.

* TM, Goodyear Aerospace Corporation, Akron, Ohio 45315

CONCLUSIONS

The results of this preliminary design study have shown that construction of a rigid type wing appears feasible with present state-of-the-art materials and fabrication techniques, and offers the advantages of high speed deployment and reusability. Disadvantages are the weight and volume penalties, which are related to the wing position on the vehicle. For externally mounted wings, such as the final concepts derived for the SORTIE and the SID vehicles, the rigid wing presents no insurmountable problems. The amount of internal volume needed would be minimal. For configurations with internally stowed wings, usable payload volume is seriously affected. For vehicles of this type, it is advantageous to consider expandable lifting surface structures as a means of reducing weight and volume requirements.

As previously stated, the inflatable lifting surfaces involve lower weight and volume penalties and can be utilized when large planform areas are required. Their use is limited, however, to cases of low speed deployment because of aeroelastic problems which may arise at the higher velocities. These structures would be ideal for internally stored midwing configurations where internal volume is at a premium. Flexible coatings able to withstand packaging and high temperatures are required however for reusability.

The semi-rigid concept for variable geometry surfaces, although a compromise, does combine the advantages of both the rigid and the inflatable concepts. In cases where high speed deployment is necessary, the rigid leading edge or main structural wing box may be deployed. In the lower speed regime, deployment may be completed by the extension of the expandable trailing edge structure in order to obtain additional planform area for lift requirements.

The variable geometry wing-body combinations derived during this investigation fall short of optimum configurations desired for operational flight systems. The objective to demonstrate the initial feasibility of the variable geometry concept has shown however what may be expected or encountered in terms of structural weight, complexity, and volume. The design of operational variable geometry vehicles for the future will depend upon the proper integration of aerodynamics, flight control, and structures in order to achieve the desired goal of manned maneuverable re-entry with reliable minimum weight structures.

REFERENCES

1. Analysis of the Thermostructural Requirements for the Atmospheric Re-entry of Satellites and Space Vehicles, W. S. Pellini, NRL 5655, 15 August 1961.

2. Analytical and Experimental Investigation of Coated Metal Fabric Expandable Structures for Aerospace Applications, ASD-TDR-63-542, November 1963.

3. Structural Design Concepts for Variable-Geometry Lifting Surfaces of Re-entry Vehicles, N. G. Gordy, R. M. Wright, Jr., and M. A. Price, AFFDL-TR-66-175, October 1966.

Table 1

Vehicles	Wing Planforms	Wing Construction
SORTIE	Rectangular	Rigid
M-22F	Swept	Semi-rigid
SID	Delta	Inflatable

TABLE 2

Vehicle	Wing Construction	Wing Material
SORTIE	Full Depth Honeycomb Sandwich	Ti-13V-11Cr-3Al
M-22F	Full Depth Honeycomb Sandwich	Ti-13V-11Cr-3Al
SID	Two-spar Corrugated Rib Stiffened	Rene 41 (Upper Panels) Columbium B66 (Lower Panels) Tantalum T222 (Leading Edge)

TABLE 3

Vehicle	Stowage Volume (cu ft)	Basic Body Mold Line Volume (cu ft)	Weight Penalty	
			(lbs)	(%)
SORTIE	7.2	340	380	7.6
M-22F	38	340	850	11
SID	3	825	800	7

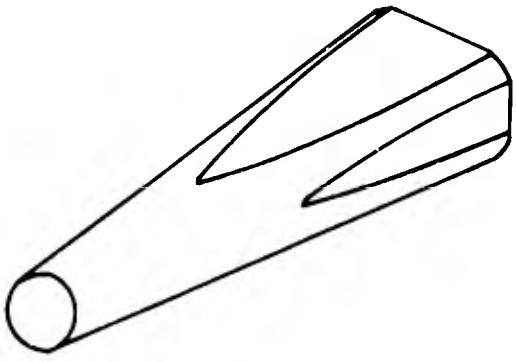

SORTIE

Length - 19.5 ft.
Weight - 5000 lbs.

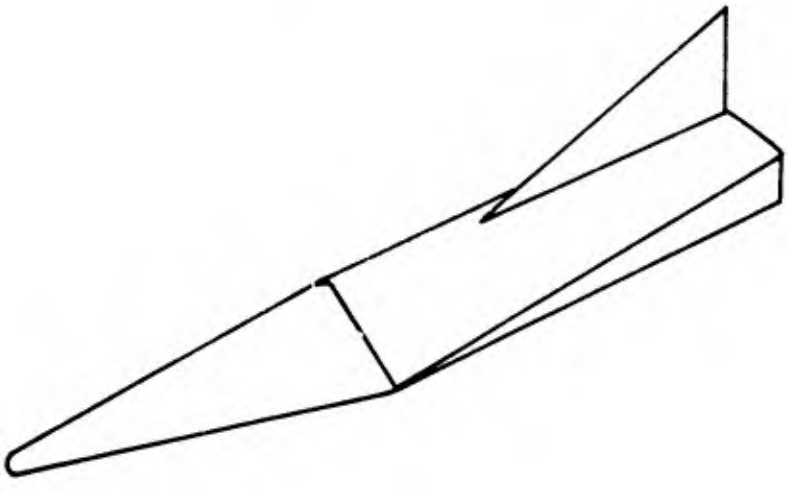

M-22F

Length - 32.5 ft.
Weight - 7700 lbs.

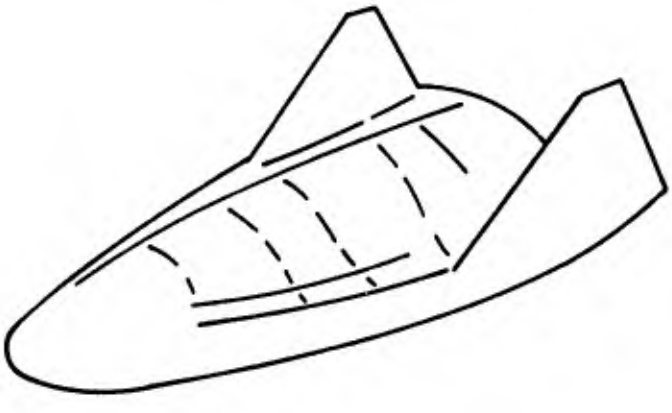

SID

Length - 25.5 ft.
Weight - 11500 lbs.

Figure 1.

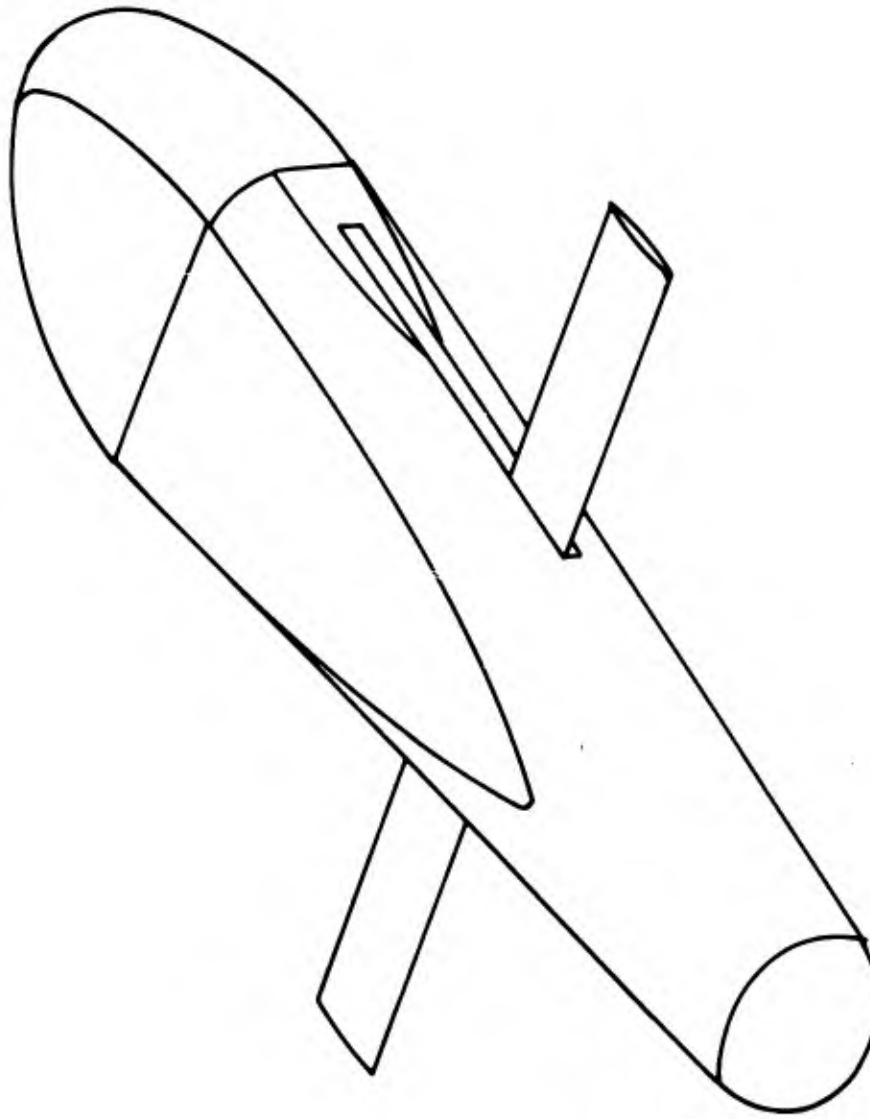

Figure 2. SORTIE Rectangular, Rigid, Midwing Configuration

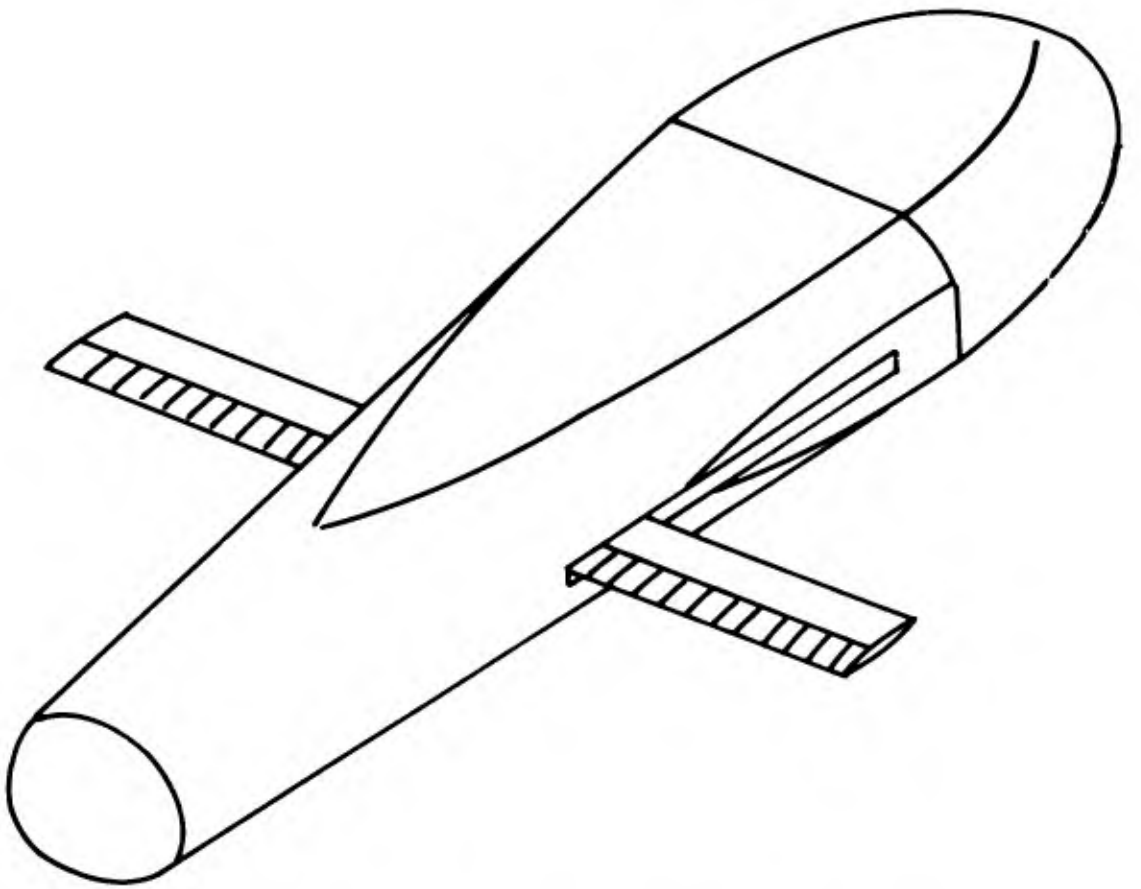

Figure 3. SORTIE Rectangular, Semi-rigid, Midwing Configuration

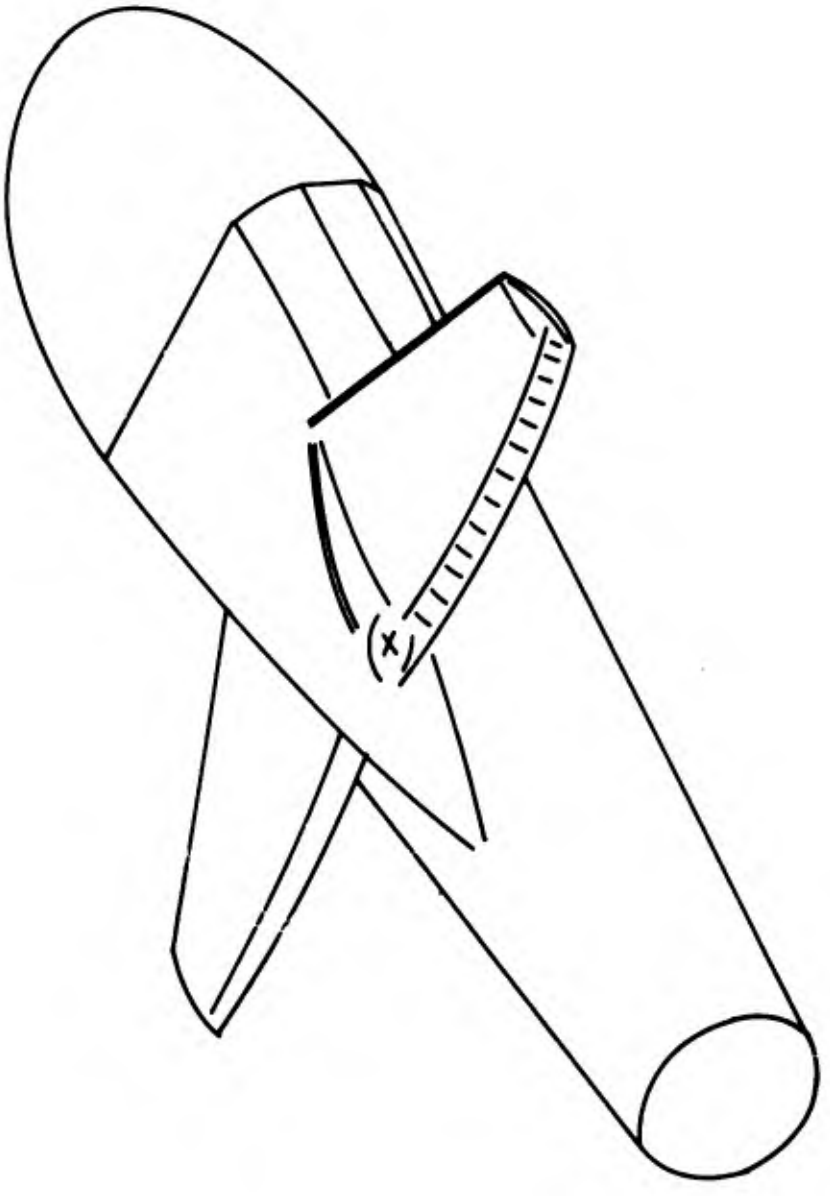

Figure 4. SORTIE Semi-rigid, Upper Wing Configuration

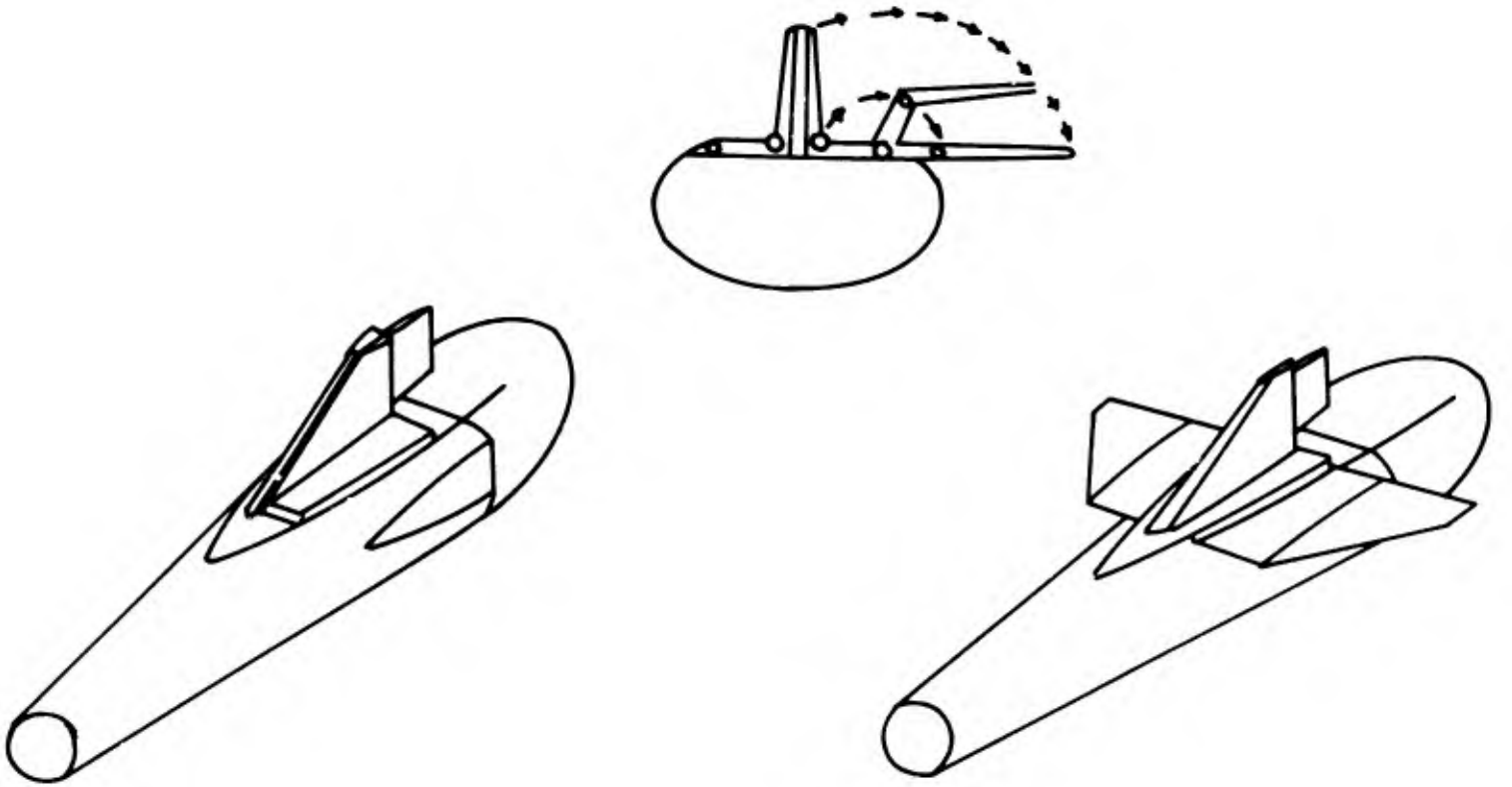

Figure 5. SORTIE Delta, Rigid, Upper Wing Configuration

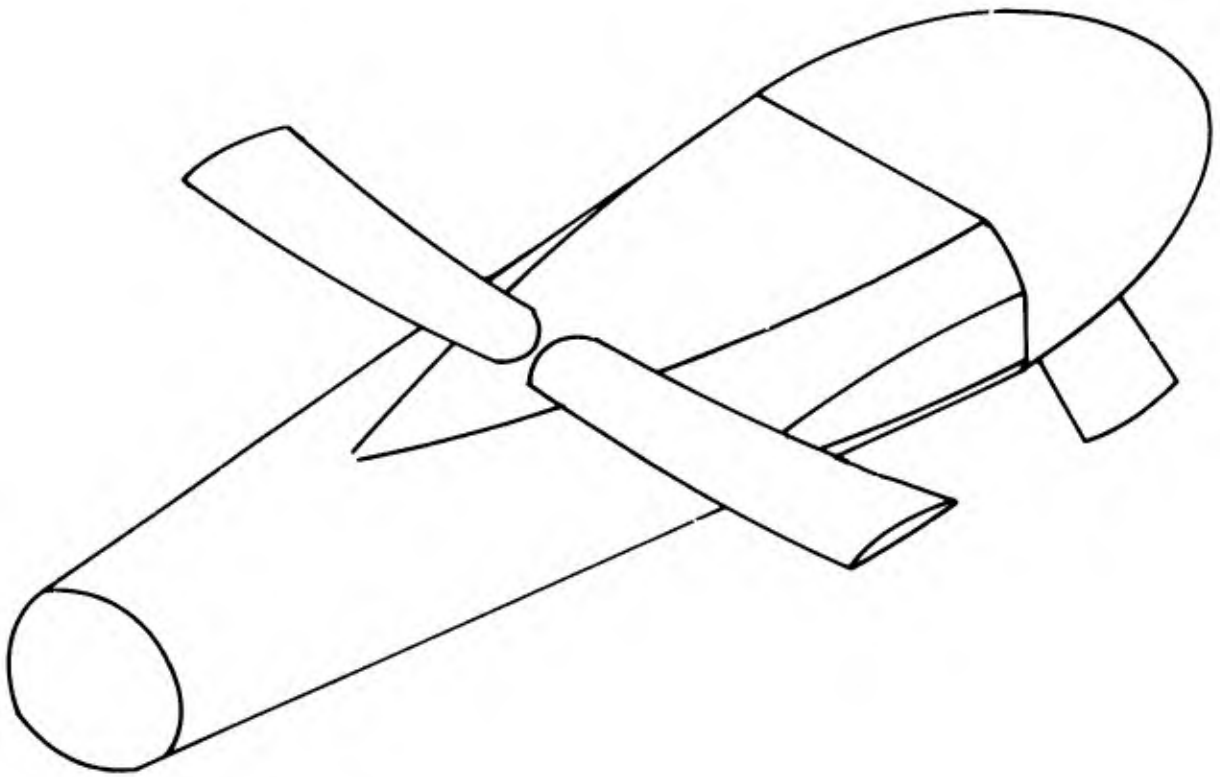

Figure 6. SORTIE Rectangular, Rigid, Upper Wing Configuration

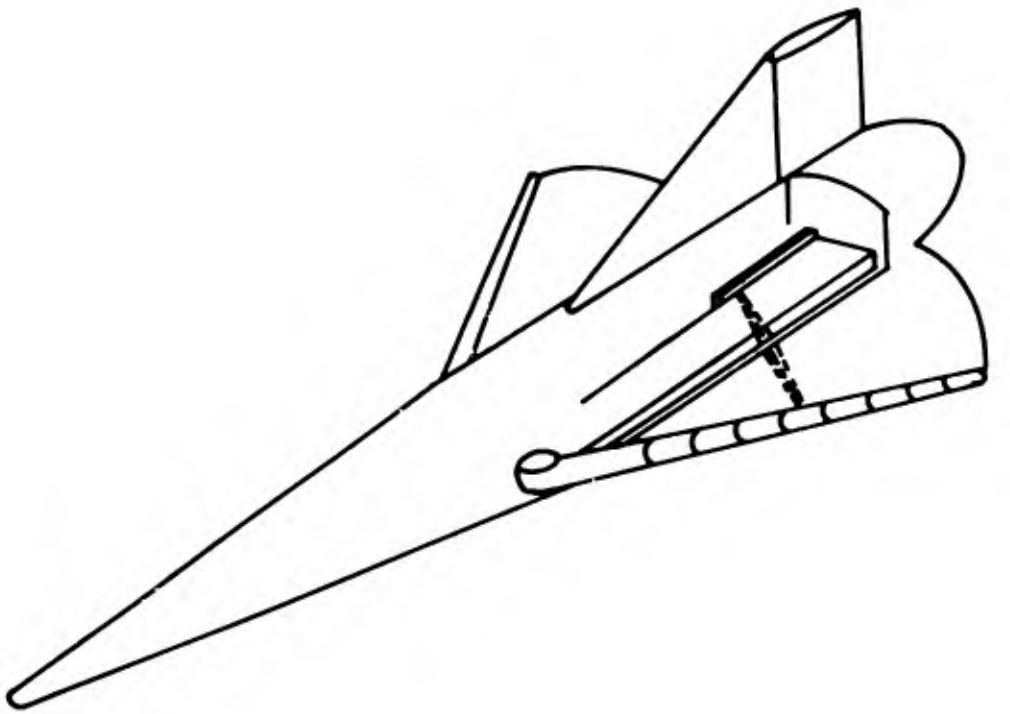

Figure 7. M-22F Delta, Expandable, Low Wing Configuration

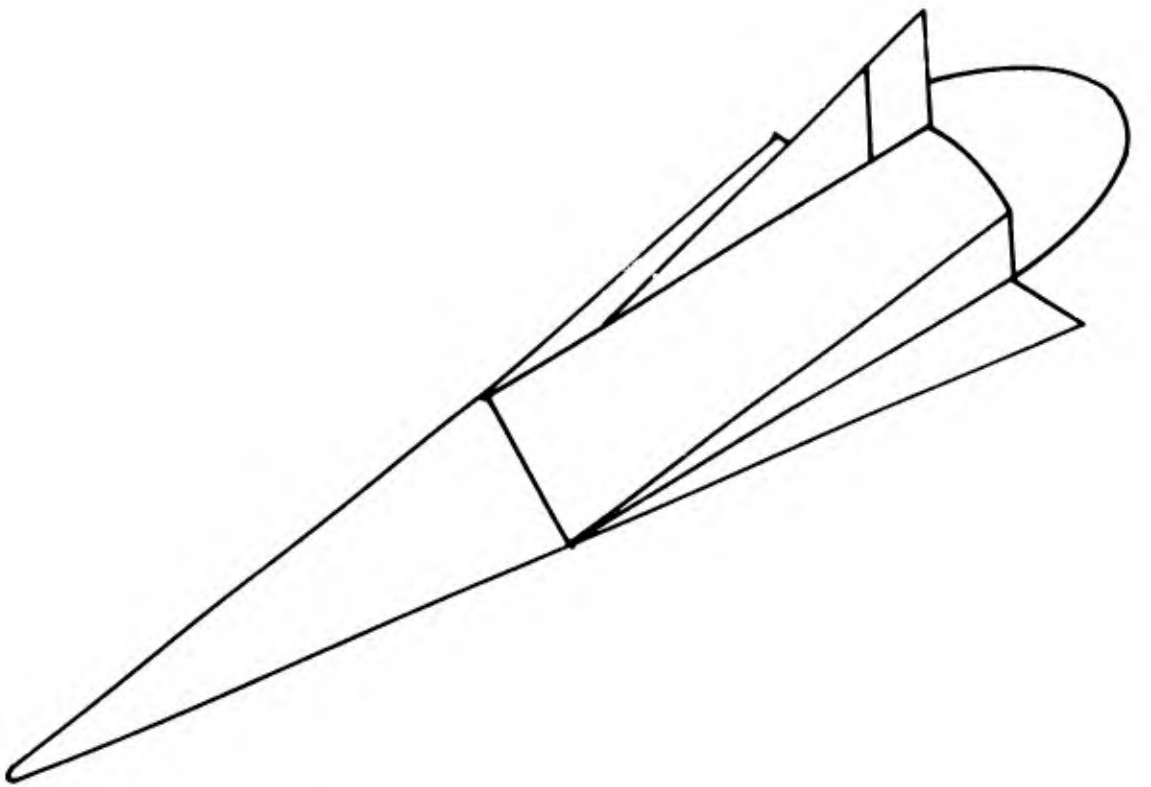

Figure 8. M-22F Delta, Rigid, Low Wing Configuration

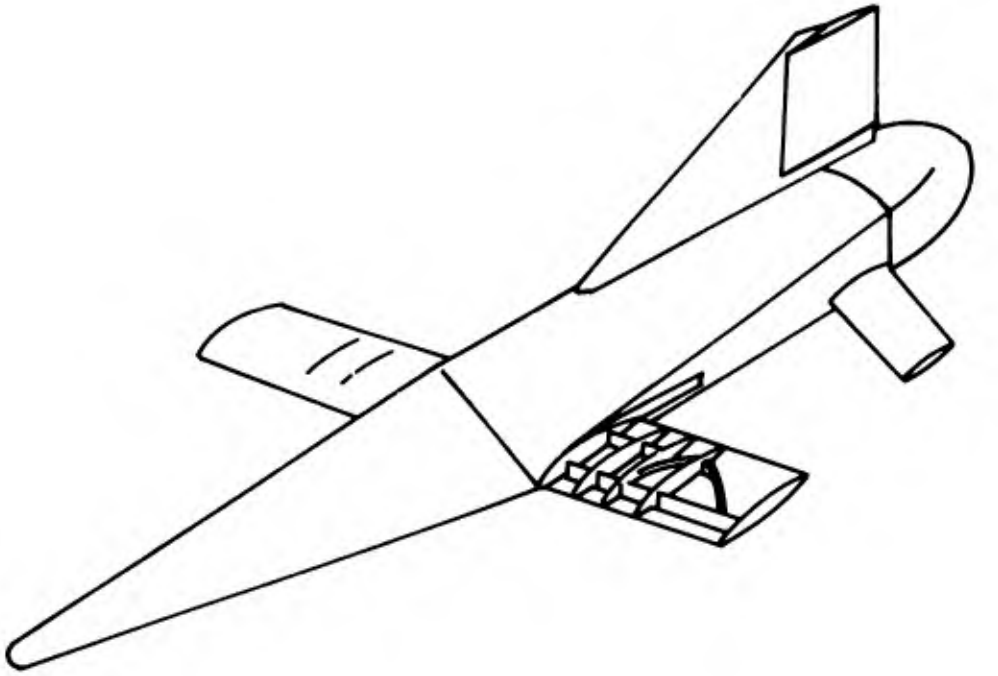

Figure 9. M-22F Rectangular, Semi-rigid, Low Wing Configuration

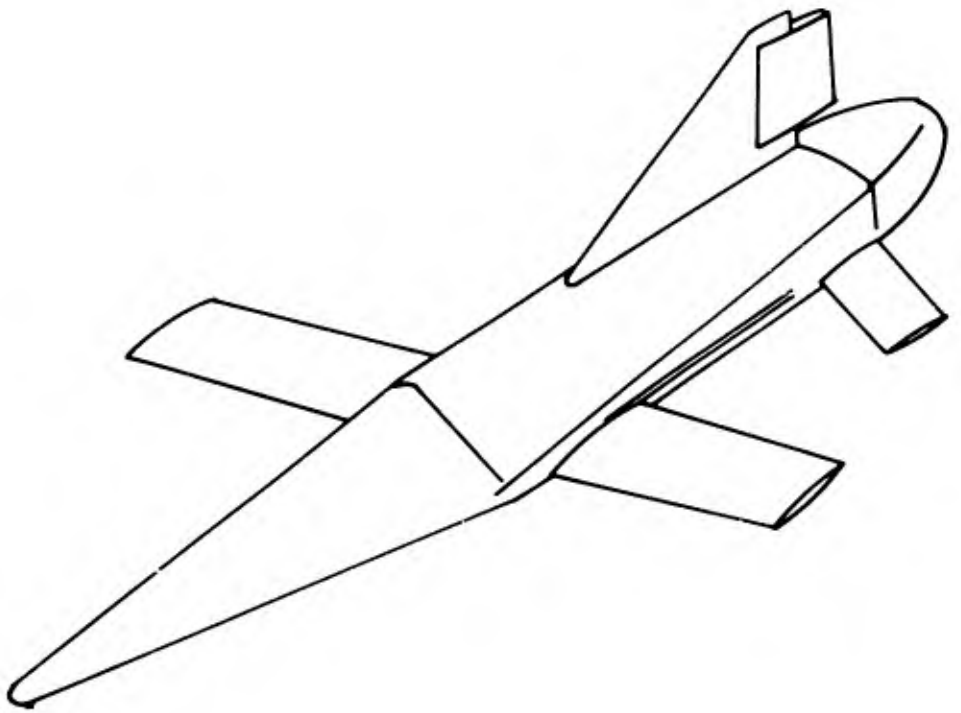

Figure 10. M-22F Rectangular, Rigid, Low Wing Configuration

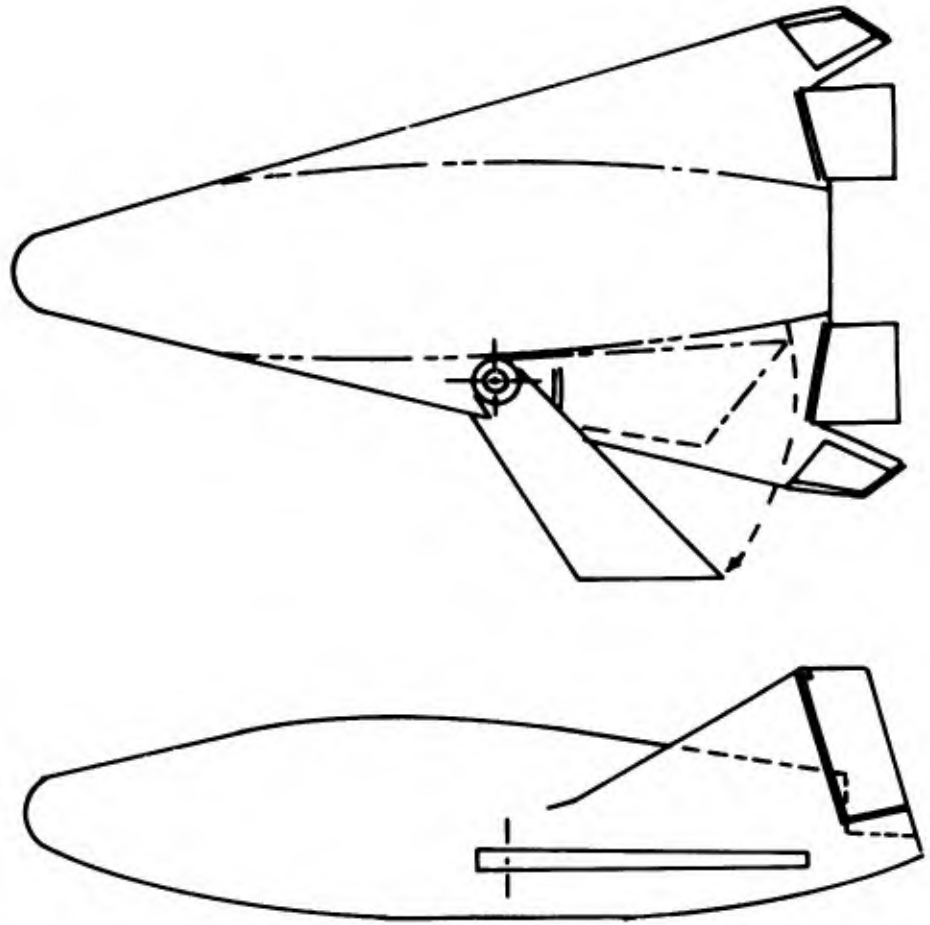

Figure 11. SID Swept, Rigid, Midwing Configuration

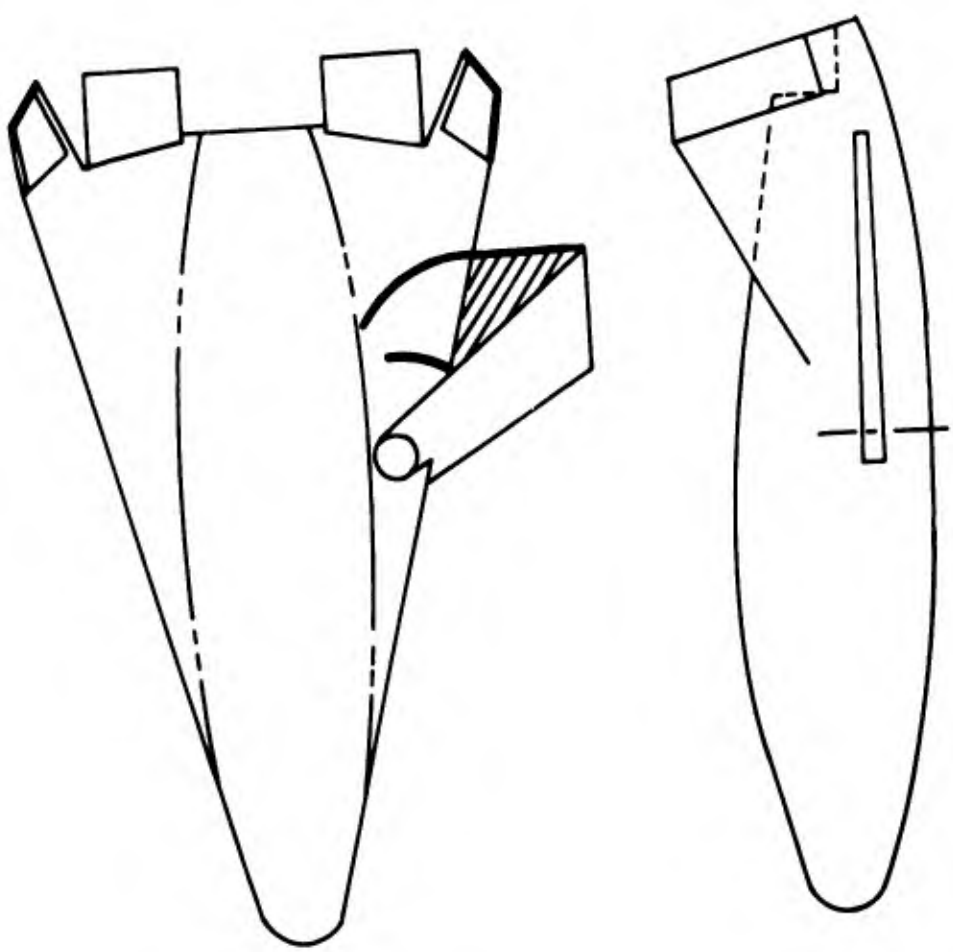

Figure 12. SID Delta, Semi-rigid, Midwing Configuration

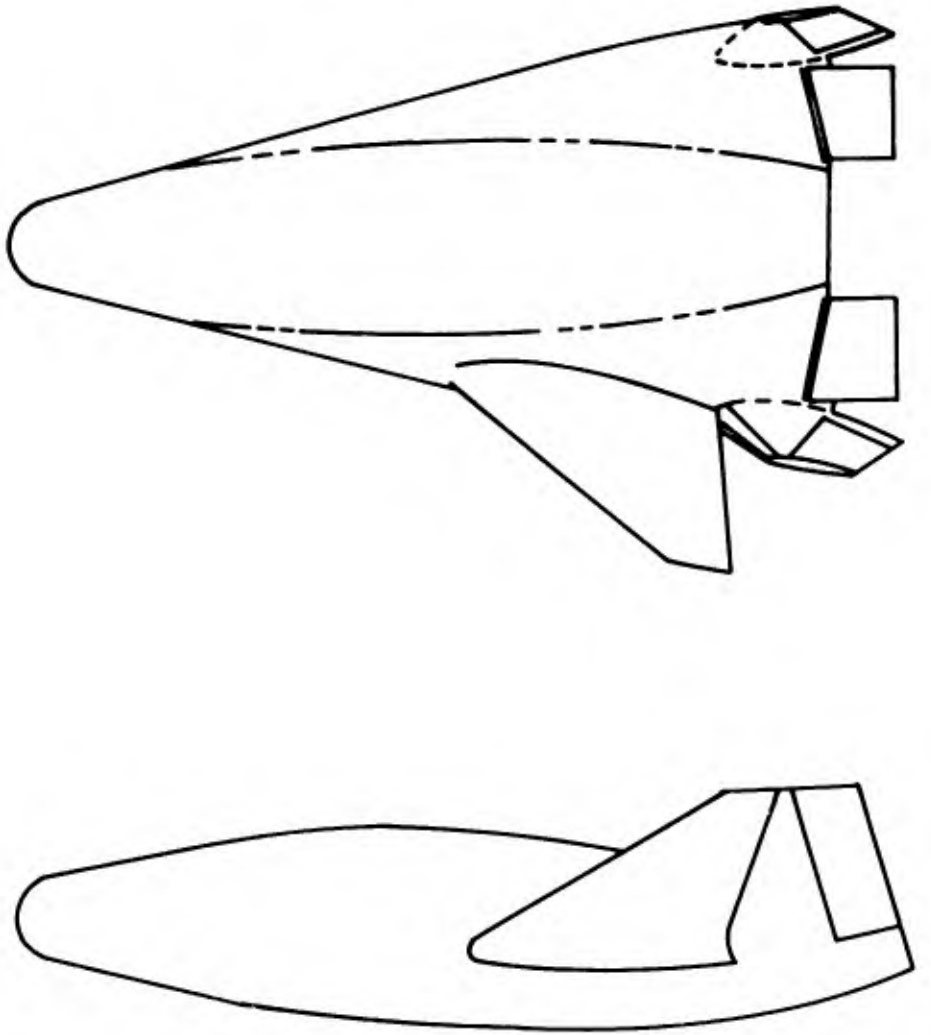

Figure 13. SID Rigid, Split-fin, Rotating Fin

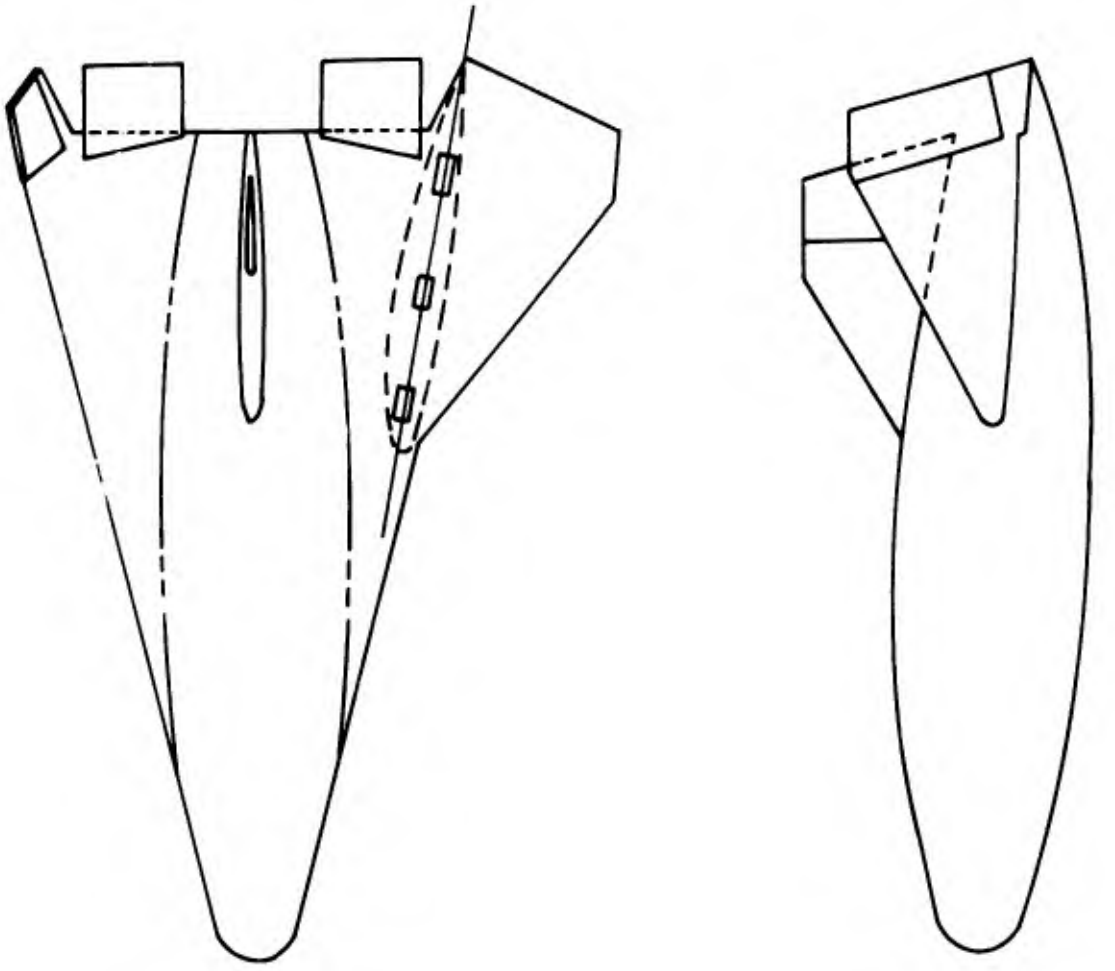

Figure 14. SID Rigid, Full Rotating Fin

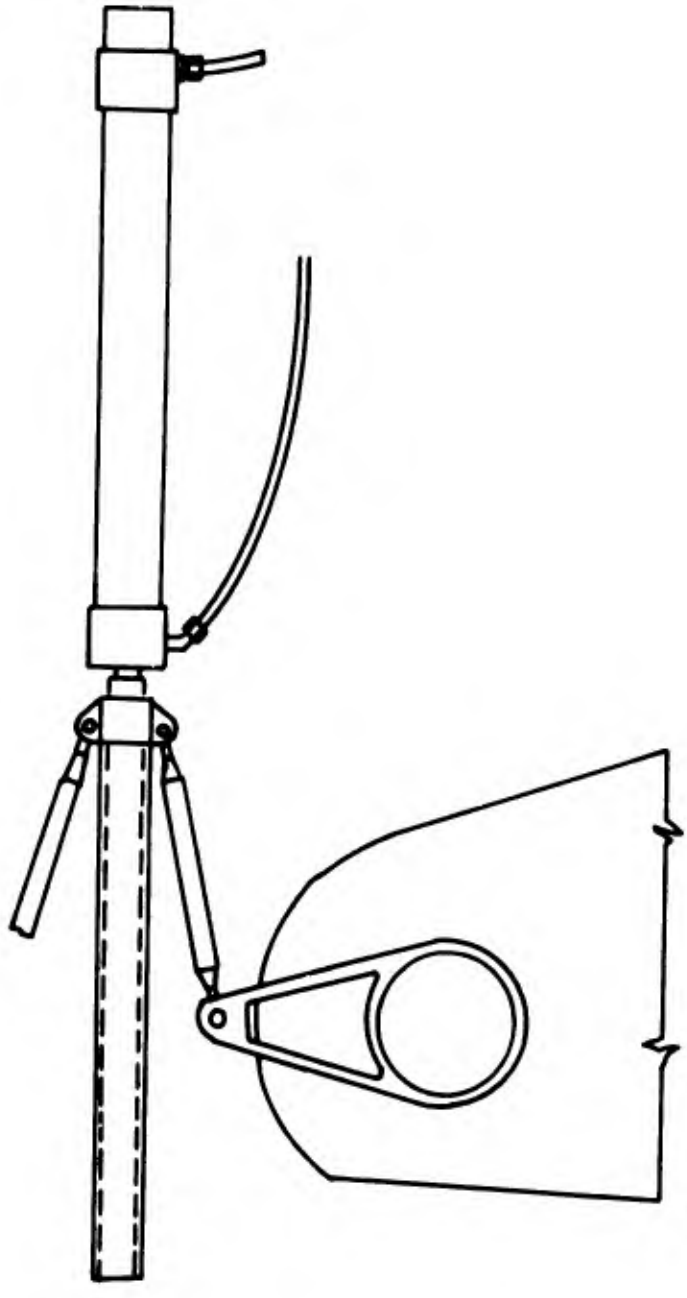

Figure 15. SORTIE Wing-Deployment System

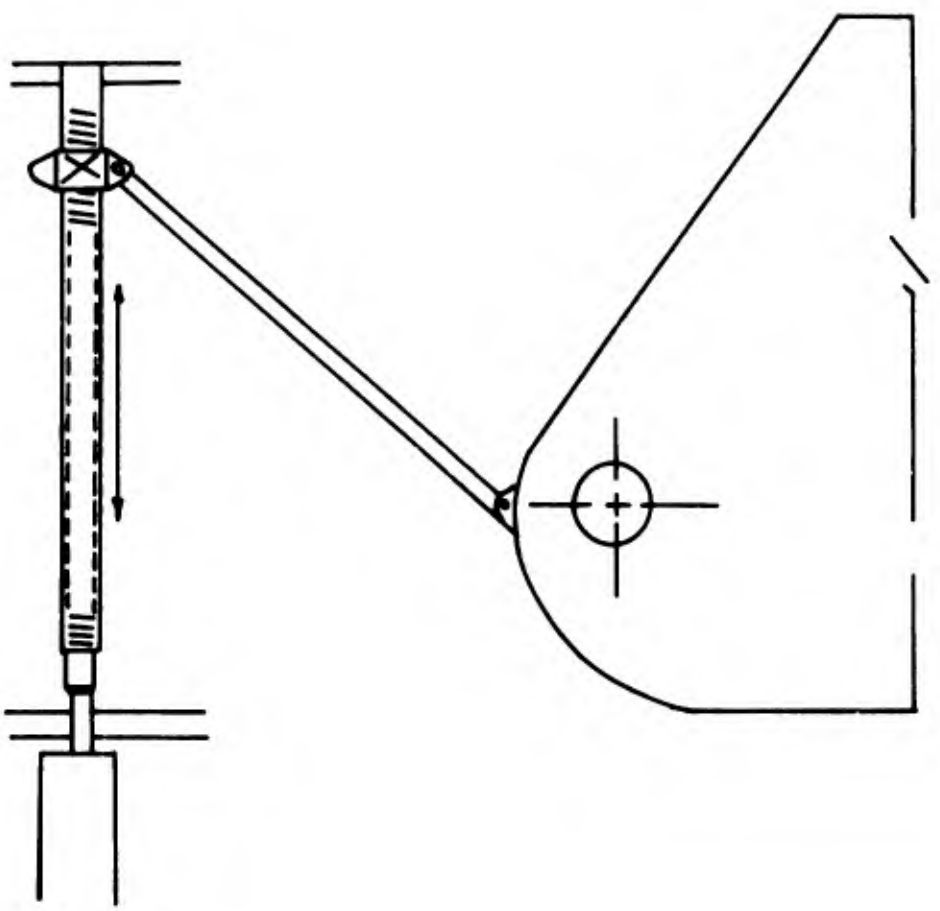

Figure 16. M-22F Wing-Deployment System

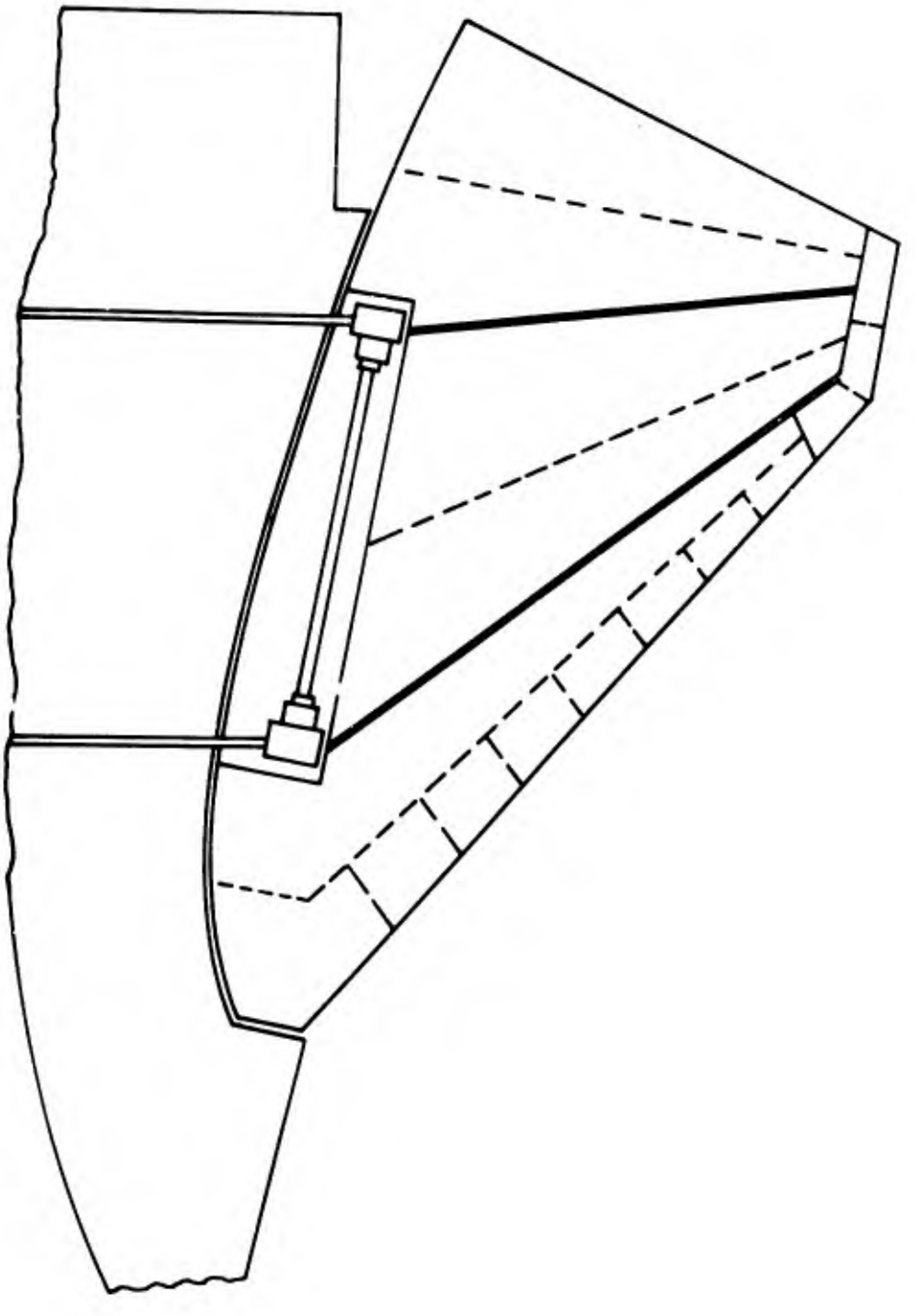

Figure 17. SID Fin-Deployment System

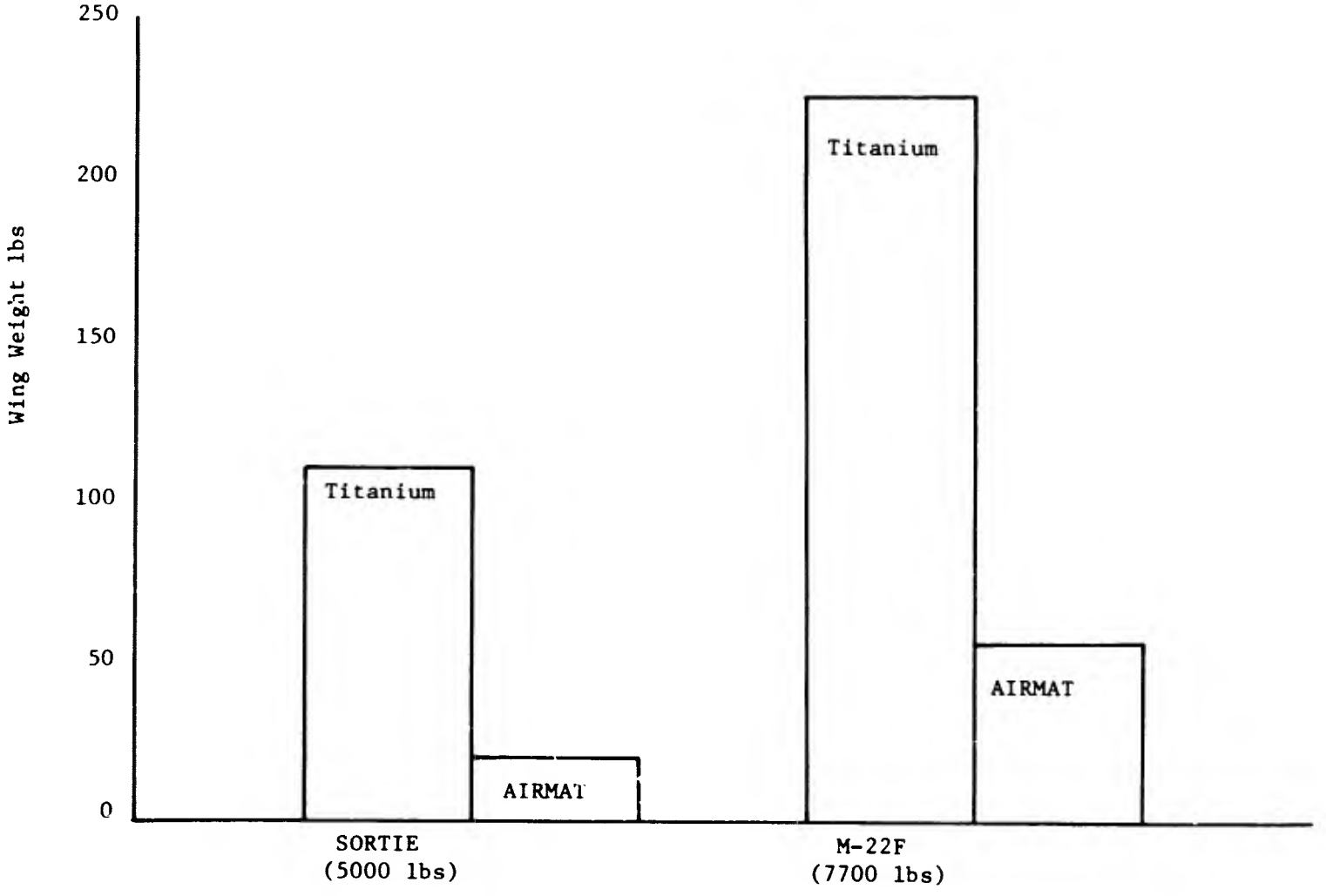
250
200
150
100
50
0
Wing Weight lbs
Titanium
AIRMAT
Titanium
AIRMAT
SORTIE
(5000 lbs)
M-22F
(7700 lbs)

Figure 18.

BLANK PAGE

POSITIVE DEPLOYABLE SOLAR ARRAY

Thomas Berry*

INTRODUCTION

The high reliability of solar cells combined with their capacity to furnish power for a considerable time has led to their use for approximately 95% of current space flights. It is expected that for the foreseeable future they will also provide the bulk of the space power for missions of any extended duration. To date the development of moderate to large solar arrays has focused on the use of fixed, rigid panels and rigid-erectable panels for mounting these cells. A recurring problem with these methods is packaging for flight loads and making the design compatible with the ever diminishing volumes allotted within the payload fairings. Optimization of rigid solar panels is now approaching a state of diminishing returns as relates to packaging efficiency and power-to-weight ratio, therefore new concepts are needed. This paper presents the result of one of the initial effort in this direction.

Specifically, this paper describes the development, fabrication and testing of a deployable solar array for a spin-oriented spacecraft application. This approach employs a flexible substrate erected by a linkage extension system. The motive power for deployment is provided by potential mechanical energy stored in springs. Significant requirements for the design were: (1) a 2π steradian field of view, (2) deployment at spin rates up to 160 RPM, (3) self-supporting horizontally under 1 g conditions, (4) capable of withstanding shock, vibration and acceleration of launch, and (5) the use of non-magnetic state-of-the-art, space-qualified materials.

During this program a 2.16 foot wide by 8.20 foot long flexible array system was developed and tested. Back-to-back substrates using silicon solar cells were used to provide the necessary view angle. The arrays are deployed from a pair of syncronized rollers using spring energy and are supported in the deployed configuration by a mechanical linkage. The total area of both arrays are 35.5 ft^2. The packaged array will fit within a 1.3 cubic foot package and weighs 29 pounds. This is 1.23 square feet per pound for a deployed array and .0318 cubic foot per square foot for a packaged configuration. The weight of the assembly was slightly more than that anticipated, but is due in part to a decision to deploy it vertically under 1 g. The added weight was approximately 3.2 pounds of which 2.1 pounds are springs. Actual flight weight could be reduced to 25.8 pounds increasing the area/weight ratio to 1.37 square feet per pound. The array minus mechanism was fabricated for 2.25 square feet per pound using 6-mil covers on nominal 13-mil cells. The deployed array is shown in Figure 1.

---

* Manager Design
Fairchild Hiller Corporation
Space and Electronics Systems Division

Testing included vibration, humidity and spin deployment of the complete system, and humidity, vibration, tension-fatigue and thermal cycling of a sample array. During testing no malfunction or serious damage occurred to any of the components or to the mechanism itself.

The work was accomplished at the Space and Electronics Systems Division of Fairchild Hiller under Contract NAS 5-9658 with the Goddard Space Flight Center.

ARRAY

The material chosen for the array substrate is a 3-mil "Kapton" film. It exhibits very high radiation resistance and has a zero strength temperature of 800° C. Other properties making this material attractive for substrate use is a tensile strength of 20, 000 psi, a low moisture uptake, good chemcial resistance and a high dielectric strength. The weight of the 3-mil film is .0226 lb/ft^2.

The solar cells applied to the substrate were 13-mil, 1 x 2 cm silicon. They were mechanically functional but no attempt was made to obtain high electrical efficiency. Six-mil microscope slide stock, trimmed to fit the cells were used for simulated filters.

The cell interconnect was expanded silver arranged in a generalized series — parallel circuit with the slots in the material running perpendicular to the flexing axis. A total of 3 sq ft^2 of cells were applied to the arrays. Two sq ft^2 were at the tip and 1 sq ft^2 at the root. These locations were chosen since they represent the most probable areas of cell damage. The remainder of the area is covered by .025 in x 2 cm x 1 cm anodized aluminum chips used for weight and volume simulation.

The cells, both live and simulated, are bonded to the substrate using RTV 102 and RTV 108 silicon rubber adhesive. These were a compromise between adequate bond strength and adhesion low enough to make replacing damaged or broken cells practical. Cover glass was attached to the front of the live cells using RTV 602.

Additional stiffness was added to the substrate by magnesium strips bonded to the aft face of the substrate. These help considerably during handling and fabrication.

To prevent scuffing of the cells and breaking of the cover glass, a backing of .032 polyethalene foam was applied to the aft surface of the array.

The weight of the array excluding any mechanism is .45 lb/ft^2 and is

distributed as shown below. These are actual weights based on 425 cells per ft^2. It can be reduced to .355 lb/ft^2 using 8-mil cells.

Substrate Weight Summary

Cover glass	=	.074
Bond	=	.022
Cells (13-mil)	=	.209
Connection	=	.019
Bond	=	.061
Substrate	=	.023
Stiffeners	=	.018
Bond	=	.019
Foam	=	.004
Toal		.449 lb/ft^2

DRIVE AND EXTENSION MECHANISM DESIGN

The extension mechanism is primarily to deploy the array and support it during and after erection in space. Secondary requirements involving handling and test have considerably increased the structural requirements, however, and the linkage as presently designed will support itself horizontally, and deploy vertically upwards, under 1 g conditions. The links are rectangular aluminum tubes that when fully extended are 103.0 inches long. Lightning holes have been included to reduce weight and improve accessability and an anodic coating was applied for surface protection. Plastic bushings are used throughout to reduce friction. The screwjack is made of titanium for its weight and non-magnetic properties. The torsion springs in the links are .125 square music wire. The design is shown in Figure 2.

RELEASE MECHANISM DESIGN

The release mechanism will support the extension mechanism during vibration, shock, thrust and spin loading and prevent inadvertent deployments. The design is shown in Figure 3. The release sequence is initiated when current is applied to the solenoid. The solenoid is operated only long enough to pull the sliding cam upward to a point where both cam and solenoid armature can be captured by the cam latch. Pulling the cam frees the array gear train allowing the arrays to start deployment, and displaces the push rod to start release of the linkage. The push rod has locking blocks on each end which provide a positive interference lock for the restraint levers mounted on the side plates. The levers, when freed, allow the clamping arms to release the front plate thereby permitting the linkage to deploy.

BRAKE SYSTEM DESIGN

A damper is required to reduce the radial deployment rate of the arrays and extension mechanism to eliminate excessive side loads due to Corolis and deceleration forces. The system used is a centrifugal brake driven by the array rollers. Significant components of the device are shown in Figure 4.

Torque imparted to the rollers by the substrate is transferred to the flyweights through a 21.46 to 1 planetary gear train. The flyweights, under influence of this rotation and the rotation of the spacecraft about its spin axis, cause the friction pads to contact the brake drum, thus restraining deployment.

The gears used in the system are aluminum and bearing mounted where necessary to eliminate frictional forces for low load applications. The flyweights are made from sintered tungsten. Three weights are employed to provide smoother operation. Teflon brake pads are mounted within the flyweight arms and are a trade-off between very low speed deployments where little damping is needed and deployment at high rates where force on the arms compensate for the low frictional characteristics.

STRUCTURE DESIGN

The structure design for the deployable solar array was intended to provide a sound base from which to mount the linkage, array and release mechanism. In addition, the structure also supplies handling and shipping protection and to some extent protection against dirt and humidity.

Weight was an important aspect of the design and much was taken to minimize this through careful selection of materials and processes. The principle load carrying members are the machined magnesium side plates which support the array rollers, the front, top and bottom plates and the release mechanism. They are intended to be bolted directly to the primary structure of the spacecraft. Material for the balance of the structure is magnesium or aluminum sheet. Protective coating for the parts are Dow 9 and black anodize, respectively.

TESTING

The system testing consisted of spin deployments at various rates, three axes vibration, and humidity testing to determine storage capabilities. Tests performed on the substrate were also of an environmental nature and included thermal cycling, humidity, tension-fatigue and vibration tests.

SUBSTRATE TEST

The humidity test indicated no discoloration, deterioration, corrosion or swelling of the materials. Comparison of post-test and pre-test functional check also indicates no electrical performance degradation.

Thermal cycling shock tests were performed on the test array between temperatures of -120° to + 180° F with cycles ranging from 10 to 19 minutes in length. Output voltage was continuously monitored during the 27 cycles and indicated no failures.

The results of the vibration test given in Figure 5 indicate considerable damping is obtained through the foam layers. Visual and electrical checkouts after test indicated no mechanical or electrical degradation.

The tension-fatigue test was conducted to demonstrate the reliability of the solar arrays when exposed to a tension-fatigue environment simulating that experienced during deployment. Electrical continuity was not broken between the cells during the test and the output voltage remained constant throughout the 500 cycles.

SYSTEM TESTING

The humidity test of the system was performed while in an undeployed condition and was intended to evaluate the storage capability of the array. The test was made in a 24-hour period at 86° ± 2° F at a relative humidity of 95% ± 5%. Several deficiencies were noted upon completion of the test. Of perhaps greatest consequence was galvanic corrosions between dissimilar metals. This could have been prevented with proper surface preparation.

The DSA vibration test included a three-axis sinusoidal and random shake. Electrical checks before and after testing indicated no electrical failures. The DSA showed no electrical or mechanical failures and continued to deploy and repackage successfully between axis testing. Figures 6A and 6B compare vibration levels at several points on the structure with the input levels.

The spin deployment test was to simulate as closely as possible the conditions expected on a spacecraft deploying two arrays and spinning at 160 RPM (16.75 radians/sec). A "zero gravity" fixture was used to relieve vertical loads on the linkage to provide a more realistic deployment, and a vacuum chamber produced a test free of aerodynamic forces. The setup is shown in Figure 7.

Due to the large moment of inertia difference of the test fixture

compared to the assumed spacecraft and the fact that one rather than two arrays are being deployed makes exact deployment simulation impossible. Therefore, a test spin rate was selected that would allow matching the pertinent parameters of substrate tension, tangential bending and shear between the test and the calculated design loads expected at 160 RPM. The results of a computer study show that a rate of approximately 10.3 rad/sec (98.5 RPM) will satisfy the requirements. This evolved into a test program which included runs of 40, 60, 80 and 100 RPM. The test results are compared with the analysis in Figure 8. Data taken in addition to the decay rate included continuous voltage monitoring while deploying, functional and visual inspection between deployments and high speed motion picture coverage.

CONCLUSIONS AND RECOMMENDATIONS

The experience gained during development of the Deployable Solar Array has indicated the concept is feasible and represents an improvement in weight and packaged volume over existing photovoltaic systems. Specifically, the concept of a flexible substrate for single crystal silicon solar cells has proven workable. The mechanical system used for deployment although not overly sophisticated has functioned well under the testing as described. The method of attaching the cells to the substrate, and the interconnection for the cells, methods of handling and the necessary data on roll diameter and roll build-up have also been established.

Additional items to be considered for future work are radiation testing, more extensive thermal shock testing and microscopic and metalgraphic inspection. Thermal testing in a vacuum chamber under simulated flight conditions should also be instituted to support the thermal analysis and structural natural frequencies of the deployed array are needed for use in despun operational modes.

Investigation to modify the present array into a semi-universal solar power system is recommended. This would include extension mechanism redesign so that links can easily be added or deleted to change the total length. Along with this change is the consideration of making the substrate in modules such that they can also be deleted or added. A secondary advantage of this would be easier fabrication, handling and inspection.

If the array is to be attached to a vehicle having more than one solar panel it is advisable to look at various means of simultaneously deploying several solar arrays. A more pressing item than any of the foregoing, however, is to obtain a flight for an experimental array. The need is to gain additional information under actual flight conditions and to demonstrate proven flight capability.

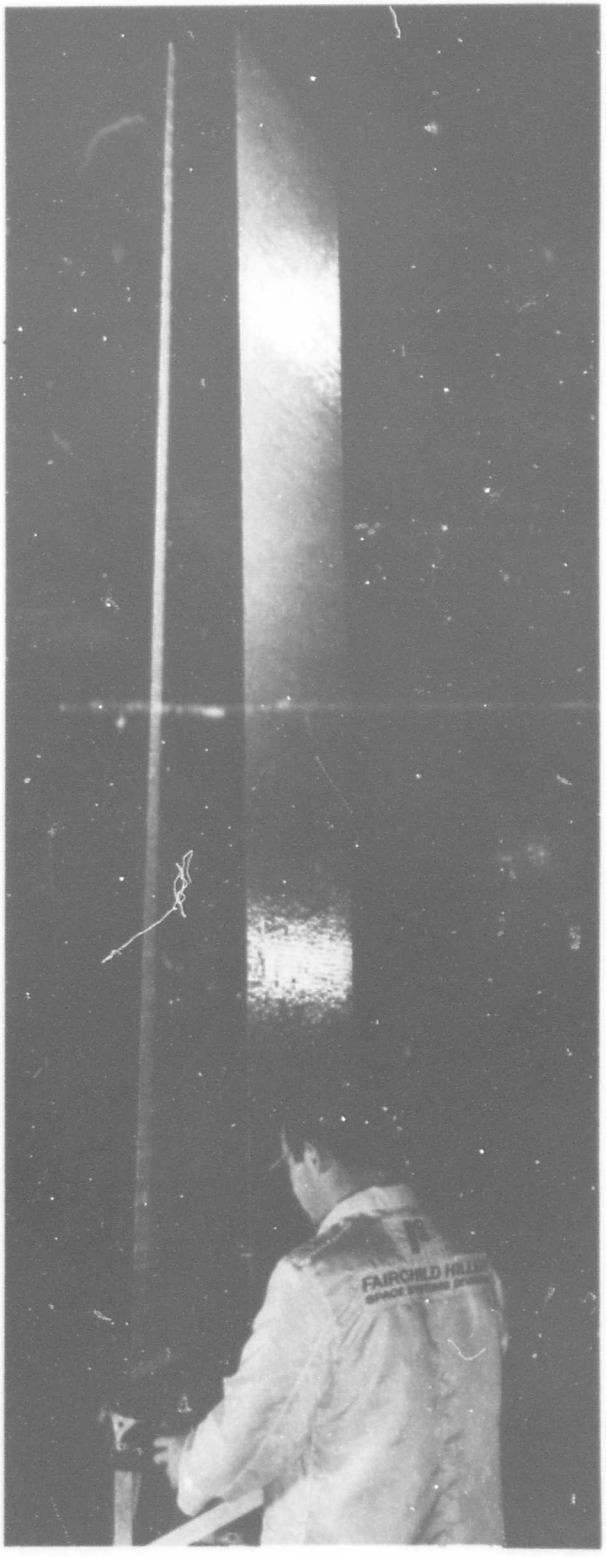

FIGURE 1
DEPLOYABLE
SOLAR ARRAY

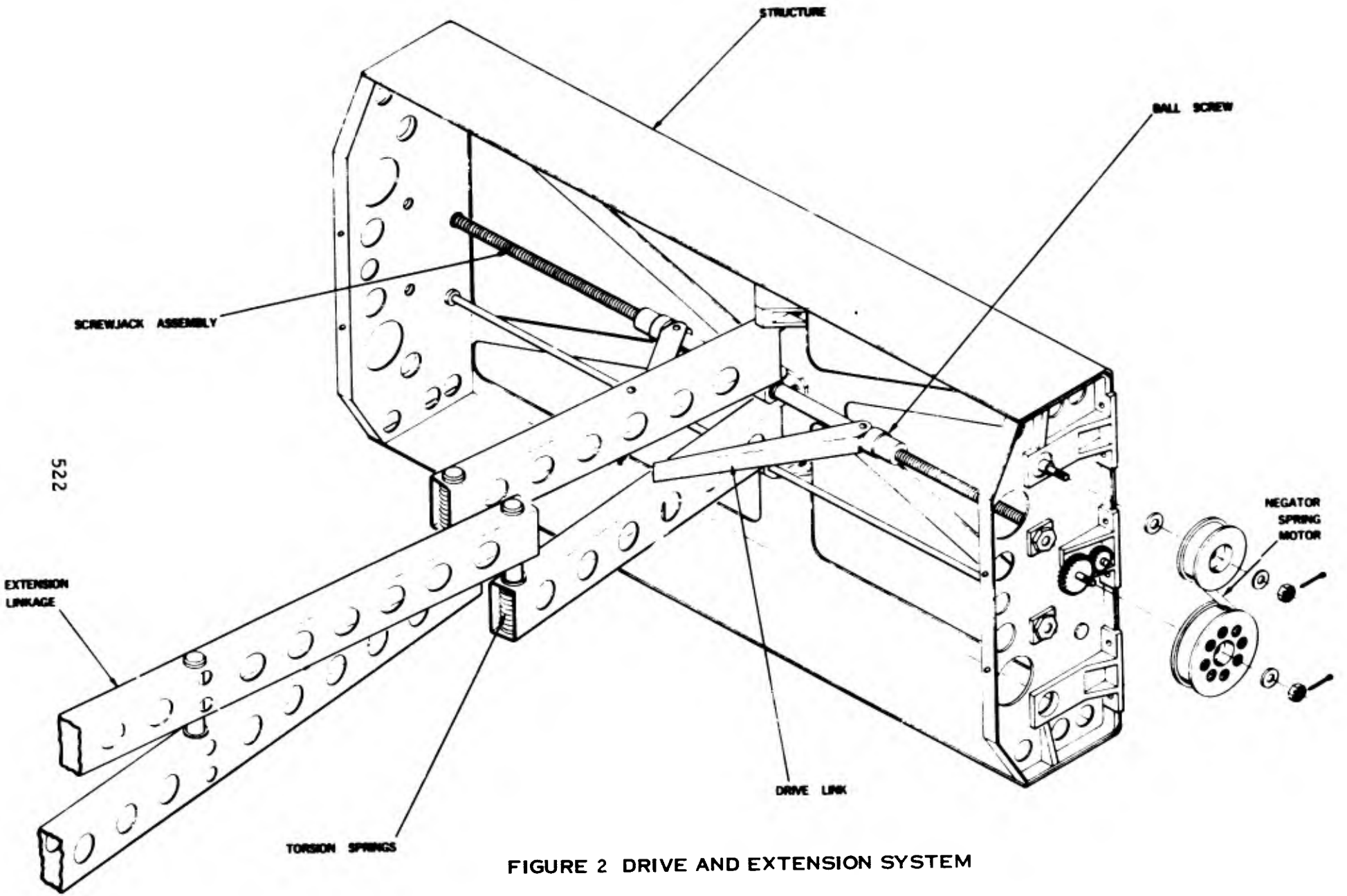

FIGURE 2 DRIVE AND EXTENSION SYSTEM

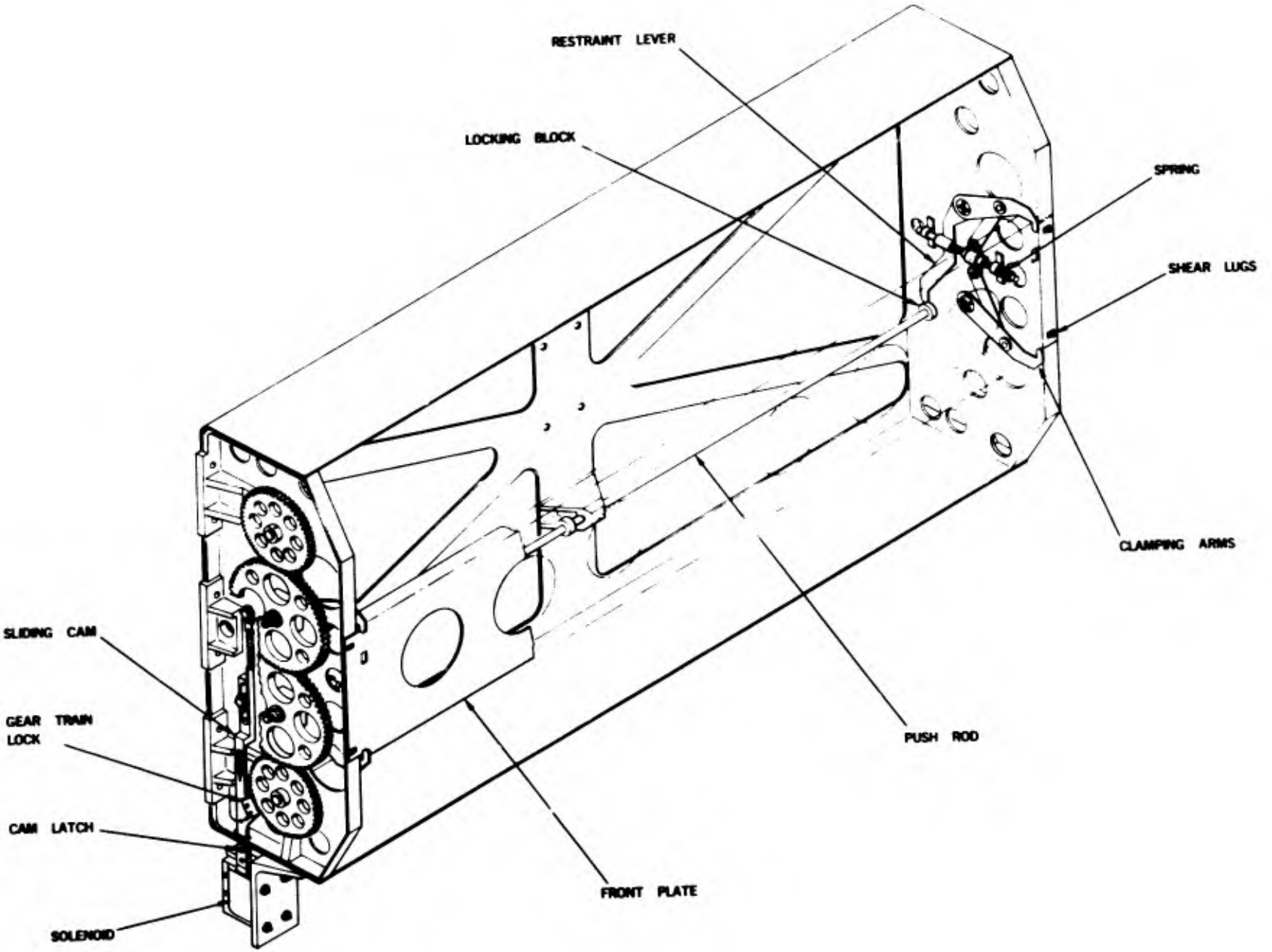

FIGURE 3 RELEASE SYSTEM

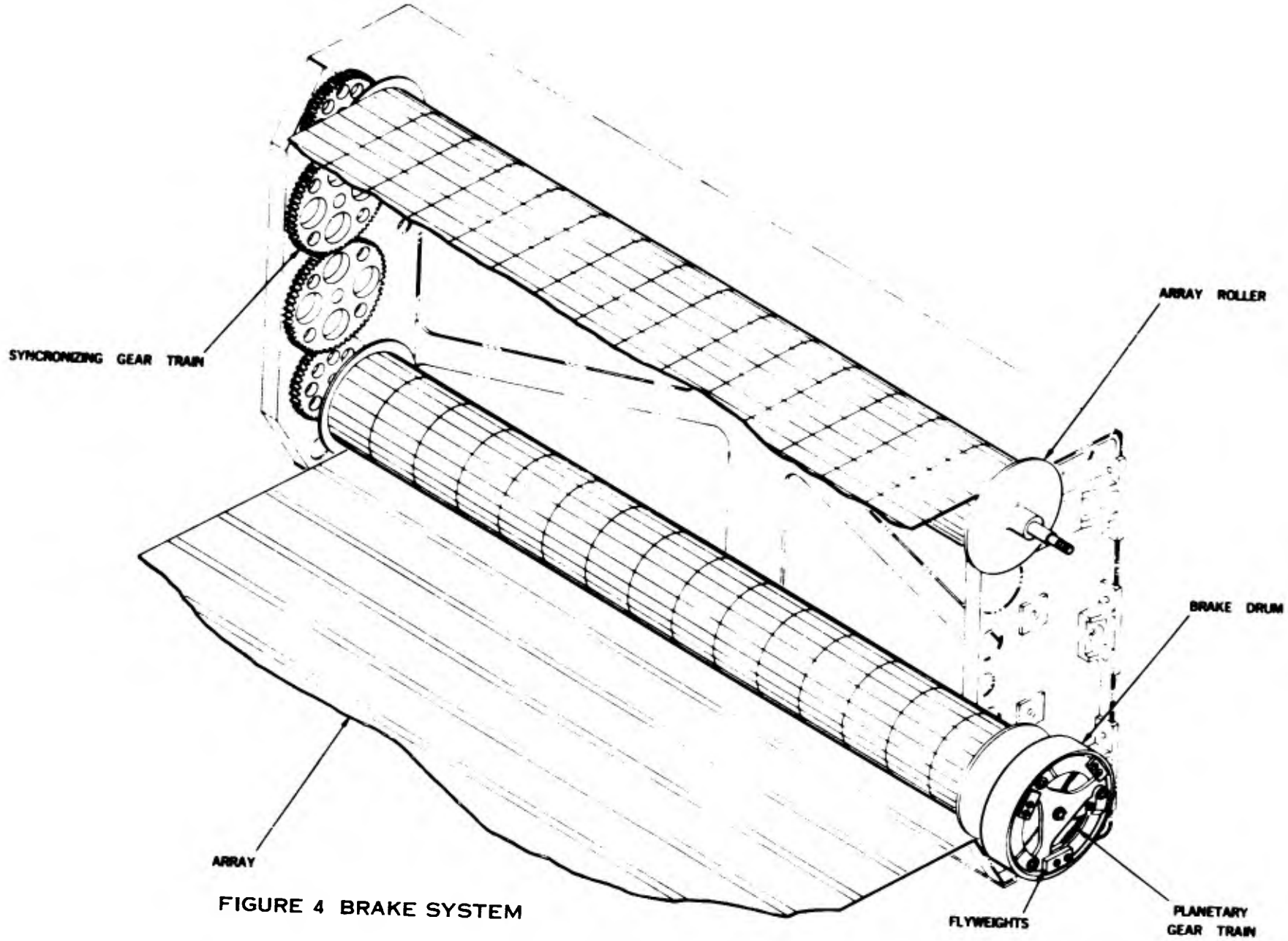

FIGURE 4 BRAKE SYSTEM

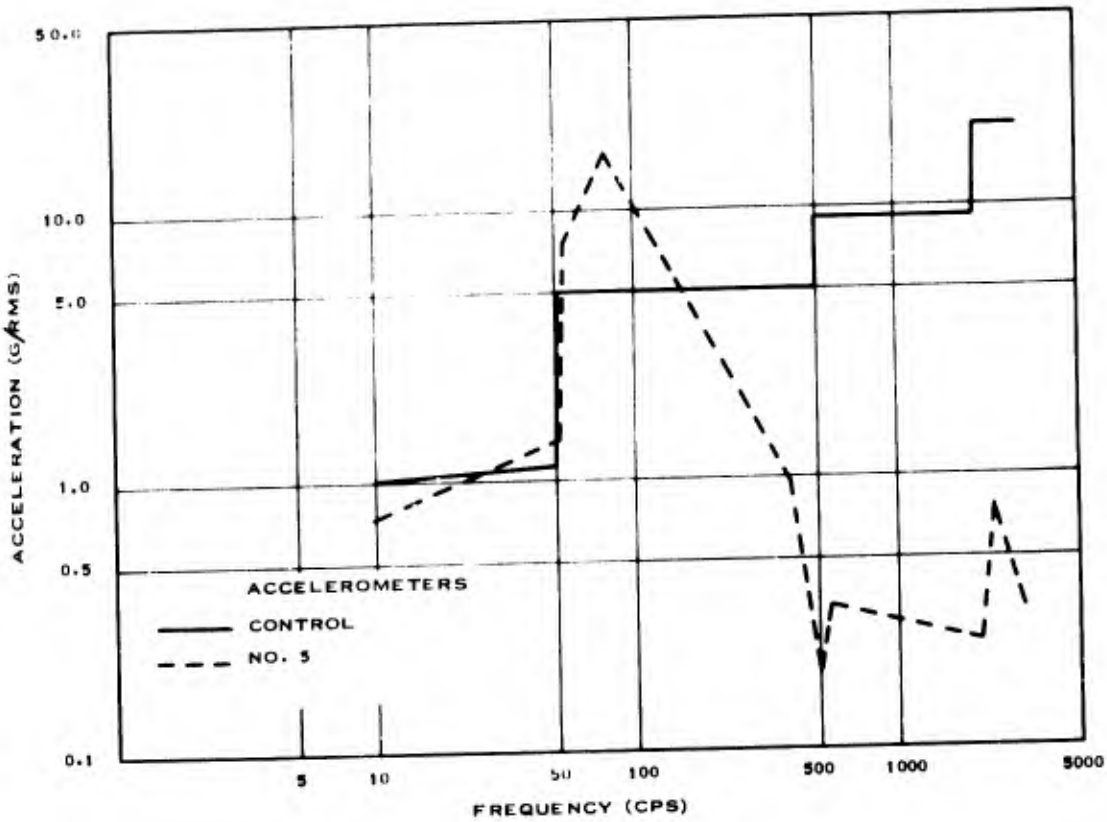

FIGURE 5A SUBSTRATE VIBRATION TEST THRUST AXIS (SINE)

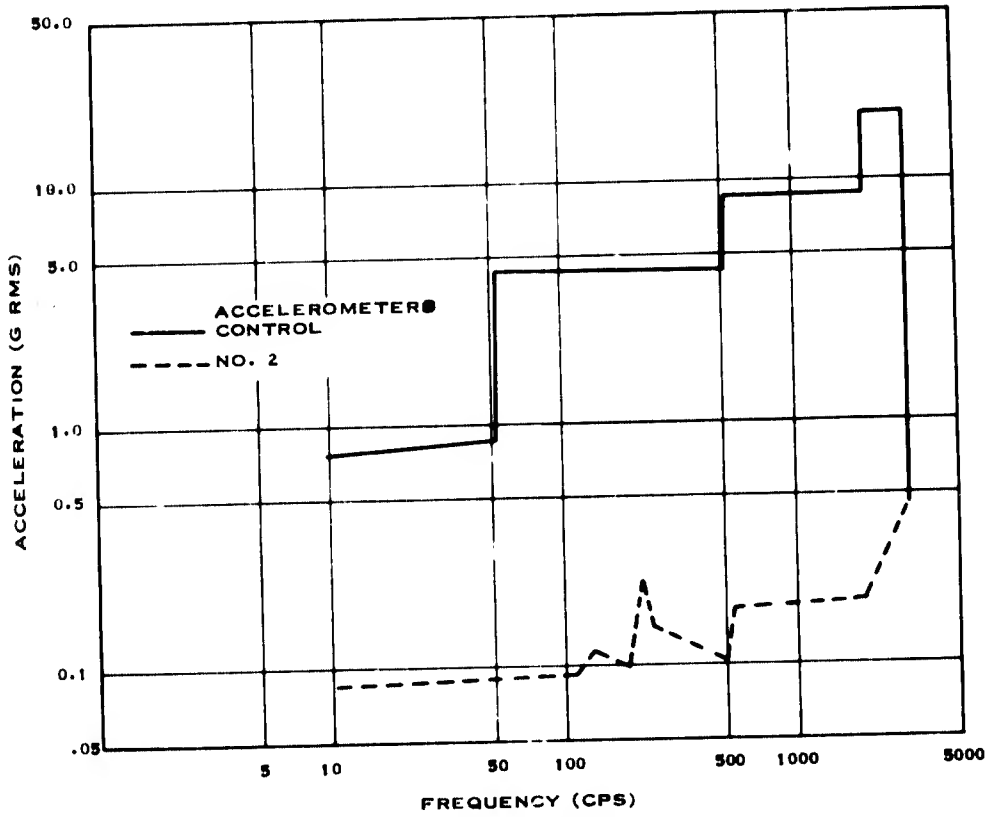

FIGURE 5B SUBSTRATE VIBRATION TEST LATERAL AXIS (SINE)

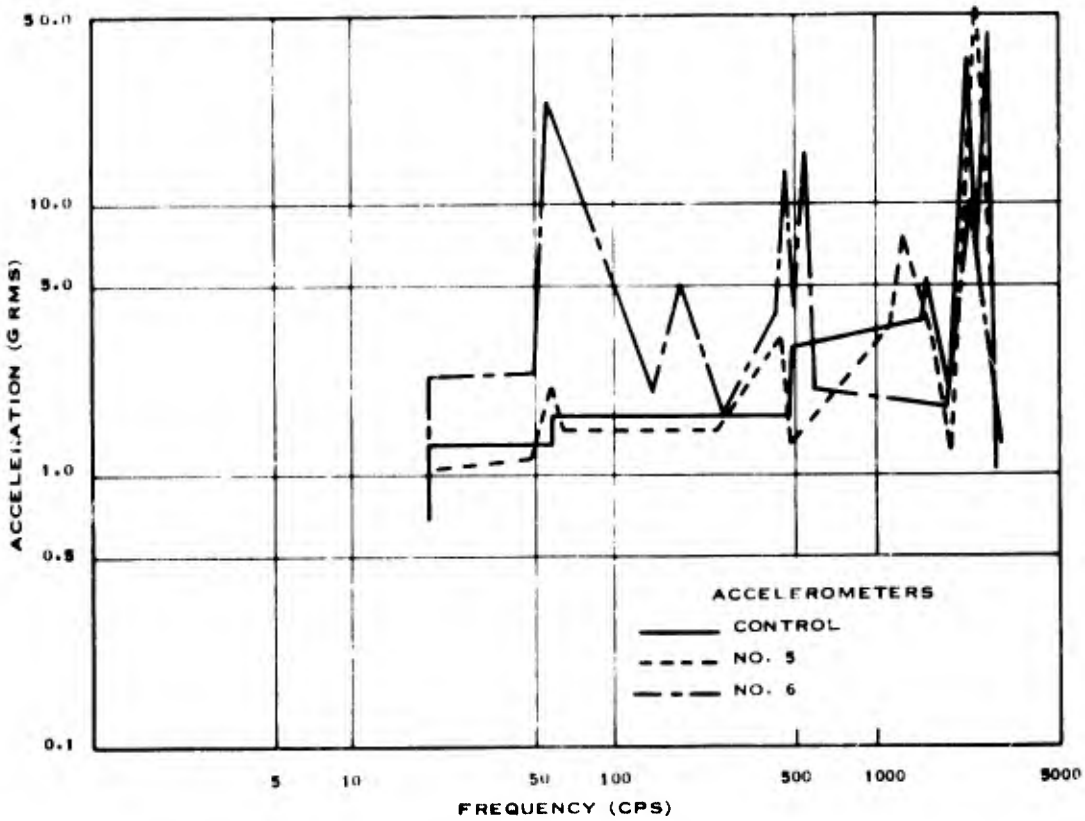

FIGURE 6A SYSTEM VIBRATION TEST X–AXIS (SINE)

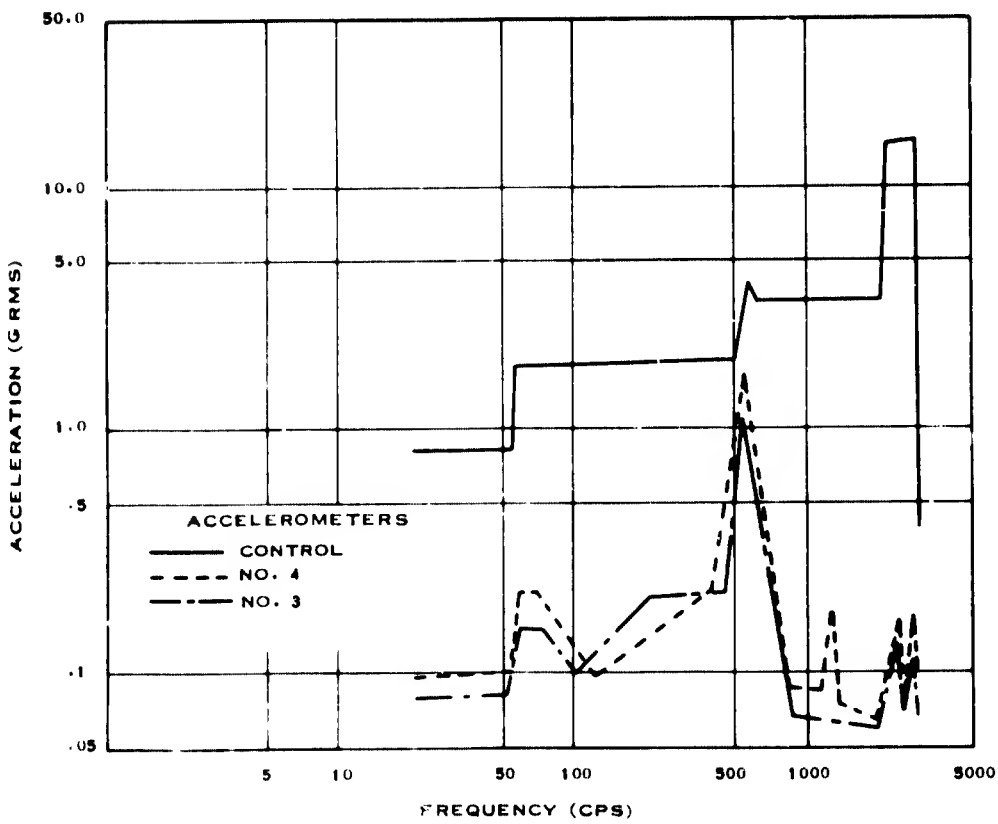

FIGURE 6B SYSTEM VIBRATION TEST Y–AXIS (SINE)

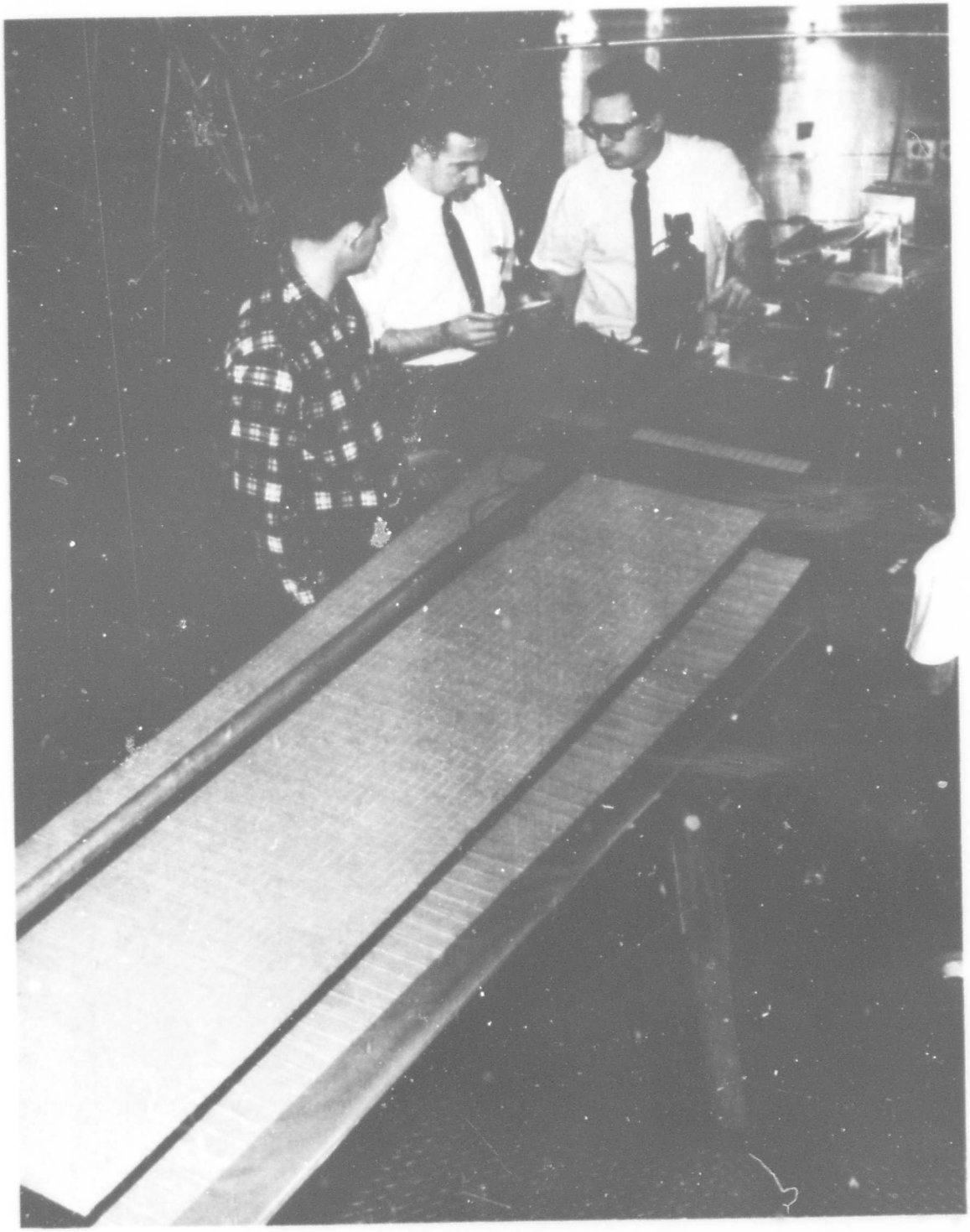

FIGURE 7 SPIN DEPLOYMENT TEST SET–UP

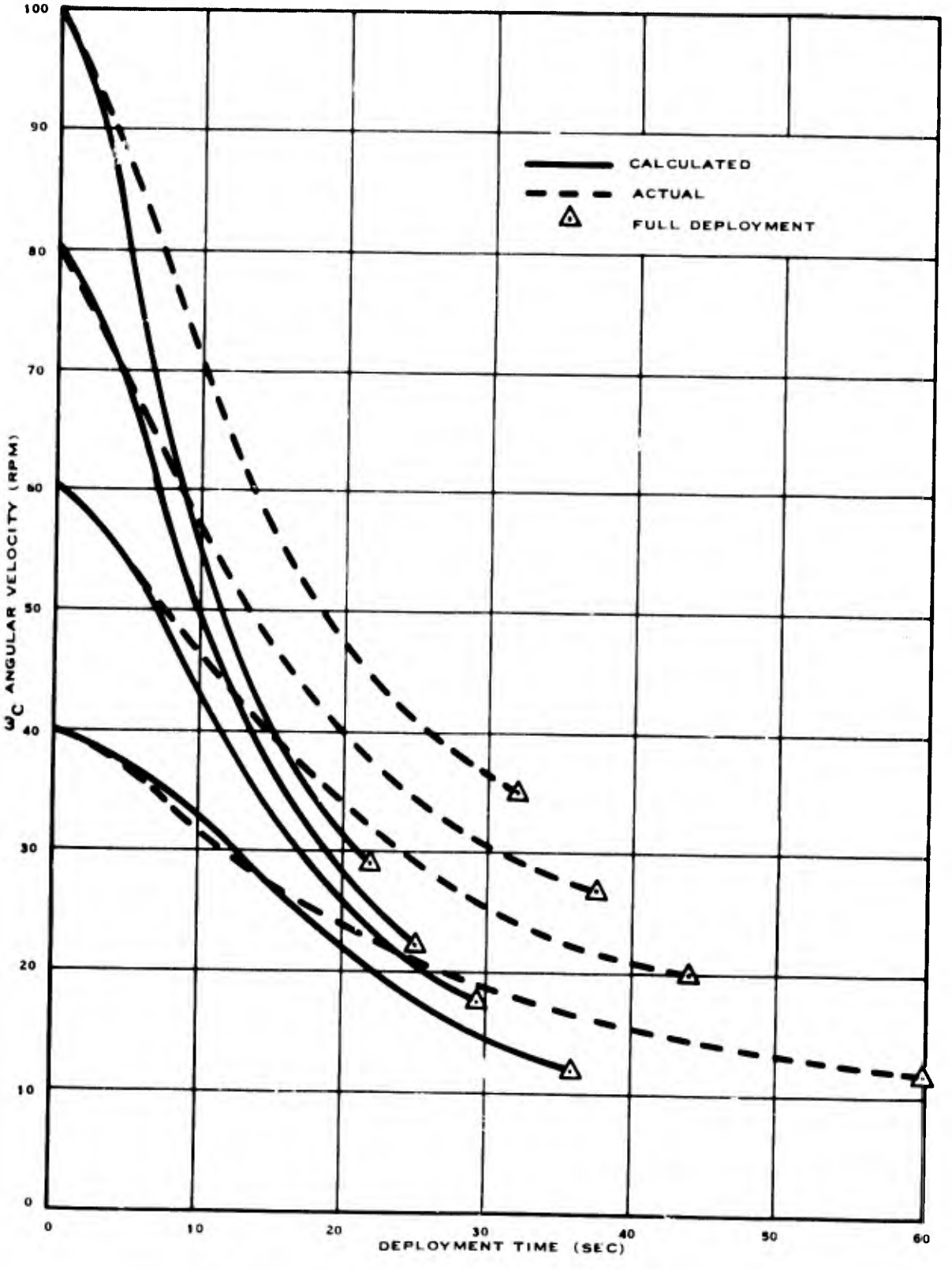

FIGURE 8 CALCULATED AND ACTUAL DEPLOYMENT TIMES

SESSION VI

BLANK PAGE

SESSION VI

LIGHTWEIGHT PORTABLE SHELTERS FOR BARE BASE APPLICATIONS

James M. Alexander*

BACKGROUND

The ability of the Tactical Air Command (TAC) to conduct tactical air combat operations anywhere in the world is dependent on the availability of suitable operating bases. TAC forces have been fashioned into packages designed to include all weapons systems appropriate to meet a particular threat. These forces are capable of conducting limited warfare activities from remote base sites known as bare bases.

In order to respond effectively, tactical units must be provided with a family of air transportable, lightweight, durable shelters which can be erected in minimum time.

INTRODUCTION

Under the sponsorship of the Air Force Aero Propulsion Laboratory at Wright-Patterson Air Force Base, the University of Cincinnati has been conducting work on developing shelter systems for bare base applications.

The research group is composed of faculty, recent graduates and upperclass co-op students from the departments of Architecture and Industrial Design. The faculty members are Professors James M. Alexander, Joseph M. Ballay, Bruce E. Goetzman, Karl H. Merkel, and Richard H. Stevens. Research assistants are Lawrence L. Fabbro and John R. McKnight. Project Engineers from the Aero Propulsion Laboratory are Messrs. Fred W. Forbes, Robert Huie, and Steven Shook.

The work has involved three Air Force contracts. This paper will summarize work completed under one contract (AF 33(615)1285) and report on current activity on the other two (AF33(615)3242) and (F33615-67-C-1259). Certain basic areas of concern are common to shelters studied and/or developed under all three programs. These include: lightness of weight, low package volume, short erection time, compatibility with cargo aircraft and their pallet systems, reuse capability, and meeting

*Professor of Design; Head, Department of Industrial Design, College of Design, Architecture, and Art, University of Cincinnati.

established windload and weathering requirements.

Paralleling in general the tasks as assigned under the three contracts, the following material will be organized under these three headings:

1. Research, Design, Fabrication, and Field Testing of 16' x 32' Lightweight Expandable Shelters.

2. Research, Design, Fabrication, and Field Testing of 50' x 80' Portable Aircraft Maintenance Dock.

3. Design, Fabrication, and Testing of Advance Modular Shelters for Small and Medium Size Shelter Applications.

RESEARCH, DESIGN, FABRICATION, AND FIELD TESTING OF 16' x 32' LIGHTWEIGHT EXPANDABLE SHELTERS

The basic research and design phases of the shelters developed under this effort were presented at the Second Aerospace Expandable Structures Conference 25-27 May 1965 and were published in the conference transactions.*

After a brief review of the two concepts carried to prototype stage, this report will concern itself with production of subsequent shelters, field testing and climatic hangar testing, and design improvements resulting from the test program.

Both of the shelters developed utilized ¼" thick foam sandwich board marketed as FOME-COR. The foam is 2#/cu.ft. density polystyrene and the liners are 42#/1000 sq.ft. Kraft paper. The coating used is a 4 mil coating of epoxy type paint.

SHELTER #1 - "BOW-TIE" CONCEPT

This concept utilized "bow-tie" shaped modules that were shipped flat and folded up into the configuration shown in Figure 1. The shelter was constructed at the University and was, as previously reported, field tested at Indian River III exercise. (Figure 2).

FURTHER TESTING OF SHELTER #1

Shelter #1 was erected at the University of Cincinnati and weather tested from November 1964 thru June 1965. No deterioration of material or finish could be detected during this exposure.

By this time new concepts had been involved, and it was decided that Shelter #1 should in effect, be "retired." It

*Technical Report No. AFAPL-TR-65-108 - March 1966

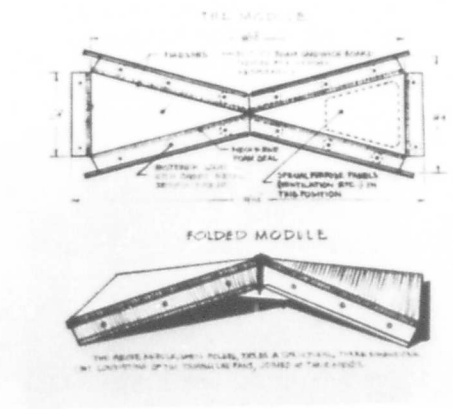

FIGURE #1 - Basic Module- "bow-tie" concept, Shelter #1

FIGURE #2 - Shelter #1 at Indian River III exercise, Eglin AFB, Fla., September, 1964

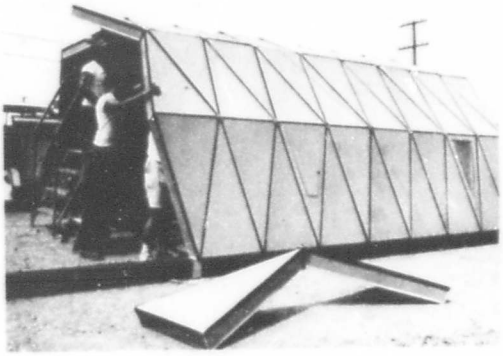

FIGURE #3 - Erection of Shelter #1-El Centro Naval Air Facilities July 1965

FIGURE #4 - Shelter #1 after being struck by twister in aftermath of Hurricane Helga September 1966.

was shipped to the El Centro Naval Air Facility where it was erected (Figure 3) and used by the 6511th Test Group (Parachute) (AFSC) for material storage. Reports on weather conditions encountered revealed temperature ranges from 28° to 130° F and humidity from 10 to 71 percent. The shelter withstood winds of 65 knots. No deterioration of material or finish was evident.

On September 18, 1966 the shelter was lifted from the ground and deposited some 30 ft. from its erected position by a small twister in a wind and rain storm in the aftermath of Hurricane Helga. The structure was damaged beyond repair. (Figure 4).

SHELTER #2 - "FOLDED BEAM" CONCEPT

Following exploration of a "folded diamond" concept, the basic concept to be utilized in all further shelters constructed under this program was evolved. This "folded beam" concept is explained in Figure 5. Central to the design of this concept was the use of Velcro as an attaching device and neoprene-coated nylon as a flashing material.

A prototype "folded beam" shelter was built at the University and demonstrated at Langley Air Force Base and at the 2nd Aerospace Expandable Structures Conference. Erection time was approximately three hours for a four man crew.

TEST PROGRAM FOR "FOLDED BEAM" SHELTERS

An extensive program of testing the "folded beam" shelter was initiated in the summer of 1965 and is still continuing. In that time seventeen more shelters have been built, several improvements have been made and field tests have been conducted at both continental and overseas test sites.

1. Canal Zone

The original prototype "folded beam" shelter was shipped to Howard Air Force Base, Canal Zone on 8 September 1965. It remained until 11 November. During this period the shelter was set up first adjacent to an air strip and, second, in a jungle clearing (Figure 6). Detailed meteorological data was recorded by an Army Meteorological Detachment. Temperature ranges were from 72° to 92° F, relative humidity ranged from 60 to 100 %. Maximum rainfall experienced in a 24 hour period was 2.44 inches. Rain fell on 51 of the 61 days of test exposure. Winds to 28 knots were clocked.

Major deficiency noted in the tropic tests was the heat build up inside the shelter. Inside temperatures ranged from 4° to 9° higher than outside temperatures, though inside humidity was lower by from 3 to 12%. Inadequate air movement made the interior very uncomfortable. This led to a restudy of vent design and an eventual increase in number of vents.

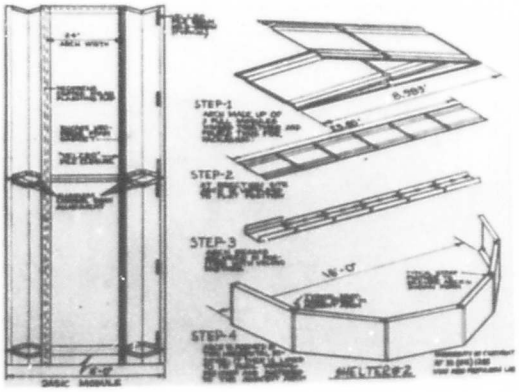

FIGURE #5 - Basic Module and typical arch- "folded beam" concept

FIGURE #6 - Shelter in jungle clearing test site- Howard AFB, Canal Zone, October 1965

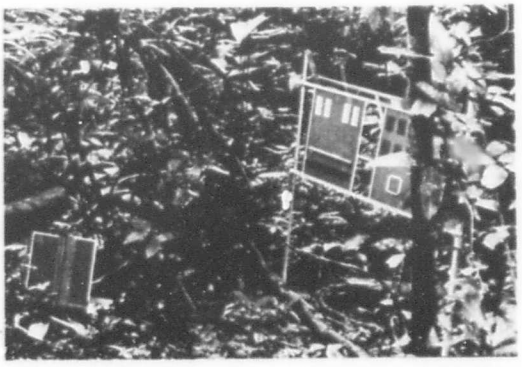

FIGURE #7 - Test panels installed at Tropic Test Site, Fort Sherman Canal Zone

FIGURE #8 - "Folded beam" shelter in Vietnam, 1966.

The shelter did not leak, no deterioration of material was noted (except for two punctures from a falling limb), and extreme heat caused only insignificant dimensional changes.

As a continuing study on the effect of a tropical environment on the materials employed in the shelter, test panels were set up under the jungle canopy at the tropic test site at Fort Sherman, Canal Zone (Figure 7). Epoxy painted Fome-Cor, as well as samples of aluminum grade beam, Velcro nylon fasteners, plastic fabric and tape, and cotton webbing, was left for approximately seventeen months at the test site. At time of writing the samples are en route to the U.S. and will be closely examined and subjected to structural tests when received.

2. Vietnam (Group 1)

The largest single procurement of the "folded beam" shelter was authorized while the Panama test program was being conducted. Ten shelters were ordered and were manufactured by Minnesota Aerospace Corporation of Anoka, Minnesota. The design was the same as that of the first shelter. The shelters were delivered November 5, 1965 and were flown shortly thereafter to Southeast Asia.

The shelters were set up at various air bases in South Vietnam and are still in service. It has been difficult to obtain detailed data on the performance of the shelters. Unlike the tests in Panama, it was impossible to send University personnel to Vietnam to make on the spot observations. Figure 8 shows one of the ten set up in Vietnam.

Comments received ranged from enthusiastic acceptance to criticism of several aspects. The heat build-up inside the shelter first observed in Panama was noted in Vietnam. Some warping of window flaps occured. A return to a wide door and improvement of door hardware were called for. Figure 9 shows the inside of one of the shelters in use as personnel housing.

3. Alaska

An Arctic Test program was programmed next. The original "folded beam" shelter was sent in to the Arctic Aeromedical Laboratory at Ft. Wainwright, Alaska in late December, 1965. University personnel accompanied the shelter and observed its erection by Air Force personnel. This was the eighth erection of this shelter. The contract work statement had called for five erection cycles.

The test period was from 31 December 1965 to 7 April 1966. Temperatures ranged from -52° F to +45° F. Greatest snowfall in 24 hour period was 20.1 inches. Total snowfall: 64.3 inches. Maximum wind: 22 mph. (Figure 10).

Conclusions and recommendations by the Aeromedical Lab stated that "The Fome-Cor portable shelter is an adequate and

FIGURE #9 - Interior of shelter used for personnel housing, Vietnam, 1966.

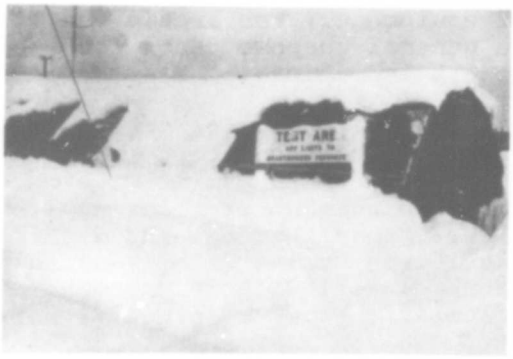

FIGURE #10 - Arctic Test, Ft. Wainwright, Alaska, January 1966.

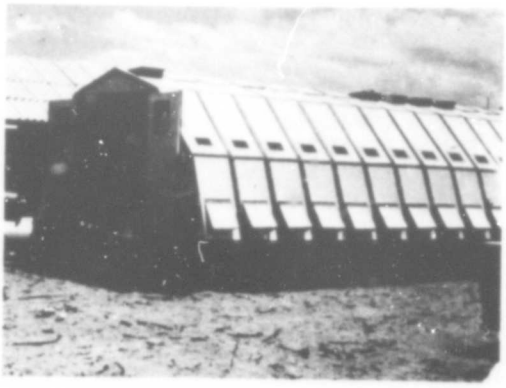

FIGURE #11 - Improved shelter, Vietnam, Summer 1966.

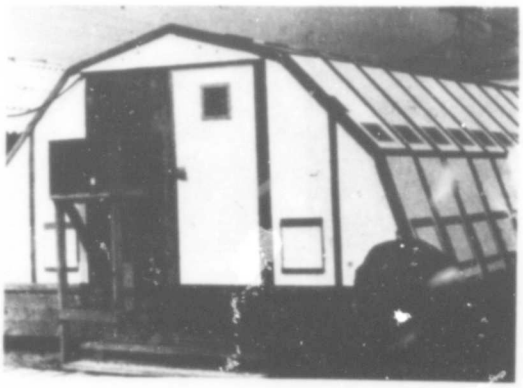

FIGURE #12 - Air Conditioning unit in improved shelter, Vietnam, Summer 1966.

useful item in an arctic environment. The shelter is suitable as a temporary shelter for human occupancy or for long term storage of equipment. For arctic use, the shelter appears to be superior to general purpose tents for applications such as emergency field hospitals, command posts, temporary housing, etc."

Specifically for arctic applications general design modifications were suggested. They included 1). a vestibule or double door arrangement with outside door swinging inward, 2). improvement of flooring system. A structural floor or a fabric one that remains flexible at -40°, 3). an auxiliary insulation system (the 1" urethane panels provided proved extremely brittle in low temperatures) 4). improvement of ventilation system (non existent with all openings closed).

The shelter was heated to 68°F with a 75,000 BTU Kerosene Space Heater. Considerable interior condensation occured resulting in a heavy coating of frost. Erection time was 25½ man hours in temperature of -25°F. without the benefit of any heating. Anchoring was impossible in frozen ground but banked snow assured stable positioning.

4. Sweden

An additional shelter was manufactured by Minnesota Aerospace Corporation in December 1965 and shipped to the Army Motor School, Strangnas, Sweden for winter testing. University of Cincinnati and Aero Propulsion Laboratory representatives accompanied the shelter. The test was conducted from 18 February to 5 March 1966.

Temperatures during the Swedish test ranged from -27°C to +4°C. At these temperatures wet snow caused considerable deflection. Some difficulty was experienced in using the Velcro connectors effectively at low temperatures. Anchoring in frozen ground was difficult and tension straps across the ground restraining the grade beam were recommended. The insulation kit was adequate although the urethane slabs were brittle. A space heater was employed. The shelter was used as a locker room for motor school trainees during the test period.

5. Vietnam (Group 2)

Three improved versions of the "folded beam" shelter were constructed by the G.T. Schjeldahl Company of Northfield, Minnesota in the early summer of 1966. Improvements included a completely redesigned ventilation system. This featured shielded vents at the base and ridge of each arch as well as at both ends of the shelter. Fixed plastic view panels were also included in each arch.

For use in connection with a stabilized earth project being conducted by the Aero Propulsion Laboratory, two shelters were rushed to completion and shipped to Vietnam in July 1966. Figure 11 shows one of the shelters erected in Vietnam. The shelters

were used for the storage of chemicals so the interior had to be kept relatively cool. For this reason the exterior was painted white (as compared with the usual olive drab) and an air conditioning unit was installed in one end of the shelters (Figure 12). The cooling with the air conditioning was very effective. One 30,000 BTU commercial type unit maintained an 84°F interior temperature when outside temperature was 97°F. The use of the air conditioning of the shelter prohibited detailed observation of the new vent design.

Packaging technique and hardware were improved. Some difficulty was encountered in alignment and operation of enlarged double doors (an inherent problem in as flexible structure as one made of foamboard material and capable of being erected on sites that are not perfectly level). Heavier Kraft paper liner (69 #/1000 sq.ft.) was used.

6. Climatic Laboratory Testing

The third of the three shelters manufactured by G.T. Schjeldahl was completed in late August 1966. In order to experiment with a different type foamboard, two 16' x 16' shelters were constructed instead of one 16' x 32' structure. One was constructed of Fome-Core (polystyrene foam) and one of a polyurethane foamboard as manufactured by Allied Chemical Corporation.

The polyurethane foam, while offering greater strength and somewhat better insulation, proved inferior to the polystyrene due to its higher density and resultant difficulty in scoring. A "memory" feature tends to cause the scoring to return to an unscored state when the arches are stored flat.

The Fome-Cor 16' x 16' shelter was shipped to Eglin Air Force Base for field testing and testing in the Climatic Laboratory. Field testing consisted of erection at two sites and use as a classroom and as a storage building. The packaged shelter is shown in Figure 13 and erection for field testing in Figure 14. Functionally the shelter served its assigned purpose in a very satisfactory manner.

Testing in the Climatic Laboratory folled the following sequence:

1). +70°F, rain, wind, no controlled humidity
2). +125°F, rain, wind, air conditioning, no controlled humidity.
3). -45°F, ice, wind, heat, no ice
4). +95°F, relative humidity 65%, 85%, 90%; circulating fan; air condition; wind.
5). -65°F, heat, wind, no ice
6). 0°F, with ice, heat, wind
7). +30°F, with ice, heat, wind

Figure 15 shows the shelter set up in the Climatic Laboratory under the overhead rain frame. Figure 16 is a picture taken during

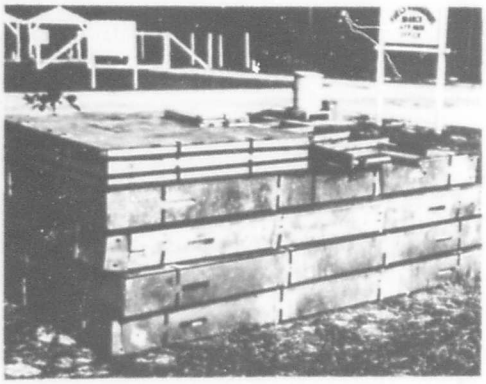

FIGURE #13 - 16'x16' shelter packaged, Eglin AF Base

FIGURE #14 - Field Erection of 16'x16' test shelter

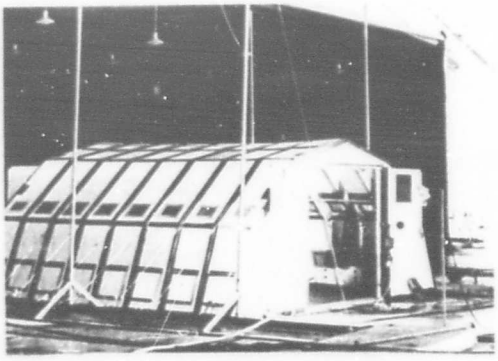

FIGURE#15 - 16'x16' Test shelter installed in Eglin Climatic Laboratory

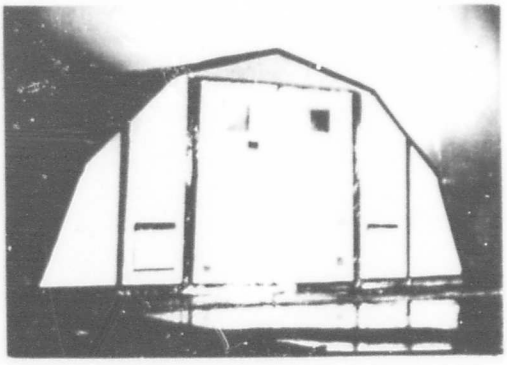

FIGURE #16 - Shelter undergoing Climatic testing, Eglin AF Base

the test when the shelter is being subjected to rain and wind.

A draft copy of the test results comments on the effectiveness of the Velcro fasteners and the good insulating qualities of the Fome-Cor. No adverse effects were evident from the 50 knot wind loadings at test temperatures. Though a great amount of flexibility was noted, the shelter moved as an integral structure not as eight individual arches.

Recommendations for improvement included development of a protective covering capable of being folded around a tight radius without forming surface cracks (in this design all such folds are inside the erected shelter). The only leakage occured at the head of the door. This was also the point of maximum heat loss. The report concludes that "with minor modifications and improvements ... the modified University of Cincinnati shelter could fulfill the forward operating base concept requirements for a general purpose portable shelter."

Two more "folded beam" shelters have just been constructed (by Minnesota Aerospace Corp.). They incorporated a modified commercial self-storing combination screen-storm door design. One of these structures is exhibited at this conference.

RESEARCH, DESIGN, FABRICATION, AND FIELD TESTING OF 50' x 80' PORTABLE AIRCRAFT MAINTENANCE DOCK

This continuing effort has produced several unique concepts with the likelihood that full-sized test sections will be produced this year and a full sized hangar early in 1968.

The structure resulting from this contract will be a candidate for inclusion in the Bare Base package and will serve as a maintenance dock for fighter aircraft. The requirements include low package weight, package cube, and erection time. The hangar must be broken down into components that fit the 463-L pallet system, and one complete hangar must be capable of being transported in a single C-130 cargo aircraft. It should have a minimum erected life of three years and a shelf life of fifteen years in disassembled and packaged state. Wind load requirements, originally set at 90 mph, are currently 65 mph.

In the initial stages of the contract several different concepts were evolved. Four of them are shown in Figures 17 through 20 and are identified as concepts "A" through 'D". A presentation was made to the Air Force in February 1966. At this meeting a decision was made to further develop concept "D"- the double-curvature barrel vault.

This concept envisioned nesting modular panels of sandwich construction that would be connected to each other to form semi-circular arches. The arches then would be tipped up into position, each arch being pivoted upward so it could settle into a position partially overlapping with its lip the previously

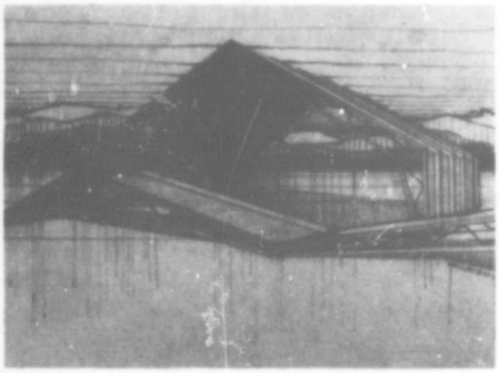

FIGURE #17 - Concept A- three-hinged arch with rigid panels.

FIGURE #18 - Concept B - "Space Frame" with rigid panels.

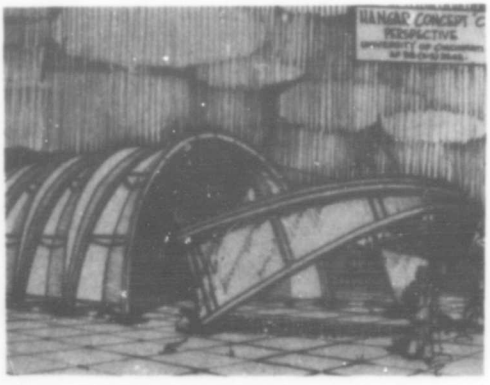

FIGURE #19 - Concept C - sectional arches with fabric cover.

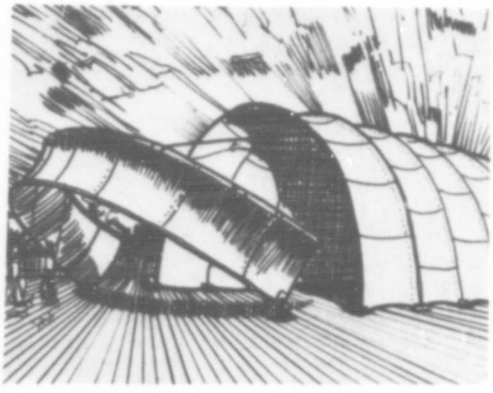

FIGURE #20 - Concept D - Double curvature barrel vault

erected arch.

Material considered for the shell was impregnated paper honeycomb with polyester reinforced fiberglass facings. A fabric door at one end and alternate solutions for the fixed end were proposed, one rigid and one flexible.

A subcontract for the detailed stress analysis and engineering design of this concept was awarded to the Whittaker Corporation of La Mesa, California. As work progessed, it became apparent that to meet the 90 mph wind load requirement, more elaborate hardware than originally anticipated would be required. Interlocking aluminum extrusions were designed into the horizontal edges of the panels and self-engaging vertical joint connectors were engineered. Figures 21 through 24 show the basic information and some details of this concept. Note that the skeletons of the shipping containers double as scaffolding for making attachments along the vertical joints.

The complexities of hardware and the estimated production costs of this concept have dictated some review of requirements on one hand and a further study of some other concepts on the other. As a result of a decision to lower wind load requirements from 90 mph to 65 mph a look has been taken at a single curvature vault. This elimination of the double curvature can result in economics of construction but, as a testimonial to the strength of the double durvature shape, the wall thickness required has increased to the point that it is questionable that a shelter can be stored aboard the C-130 aircraft. Figure 25 shows a single curvature 65 mph variation on the basic barrel vault concept.

Under a redirection to the contract we are examining at least two other approaches. A very direct and rather unsophisticated approach utilizes segmented arches and paneled sheathing. The firm Live Structures, Inc. of Stratford, Connecticut has produced a wood arch, plywood sheathed hangar of this type. Figures 26 and 27). We plan to work with this firm with the goal of reducing weight and erection time in a concept such as this. New materials, end wall improvements, and hardware restudies will be undertaken.

The second new approach to be studied involves the long-span capabilities of scored and folded foamboard. Configurations will be designed, erection procedures and connections evolved, and a test arch made and loaded. This approach is certainly an interesting one. Actual translation of it into a complete hangar may well lead us to a resultant structure that is light in weight but exceeds packaged cubage requirements. One simple approach utilizing a collopsible box section with rigidizing X-splines is illustrated in Figure 28. Working with us as subcontractors on this effort will be International Structures, Inc. of Cornwells Heights, Pennsylvania.

At time of writing the redirect authorizing these new studies

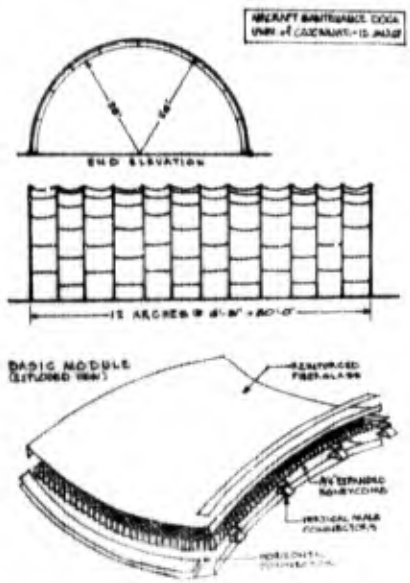

FIGURE #21 - Concept D -
Elevations and Basic Module

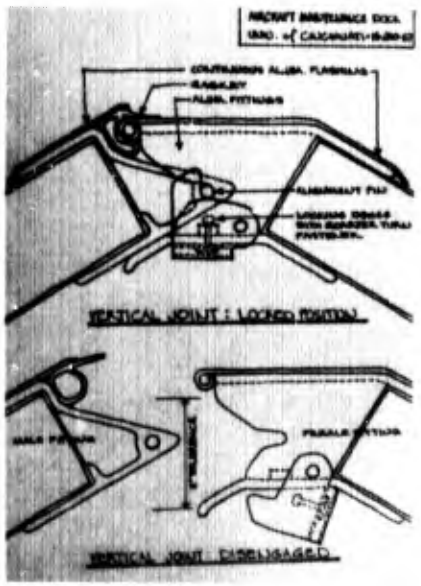

FIGURE #22 - Concept D -
Vertical joint detail

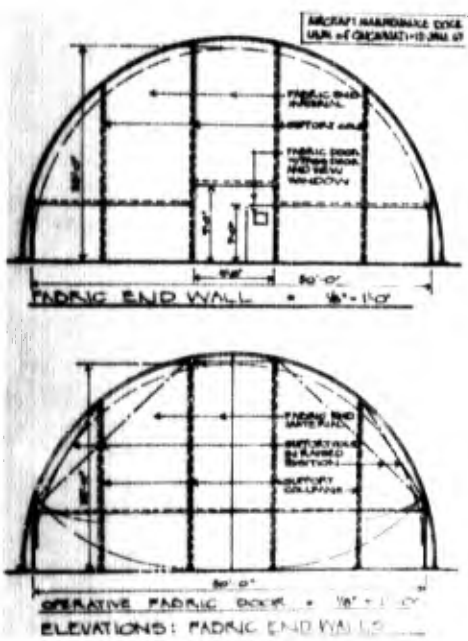

FIGURE #23 - Concept D -
Fabric End walls, operative
and inoperative

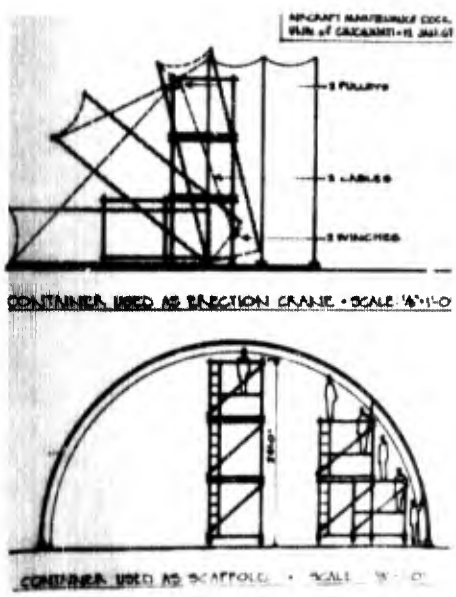

FIGURE #24 - Concept D -
Use of container in erection

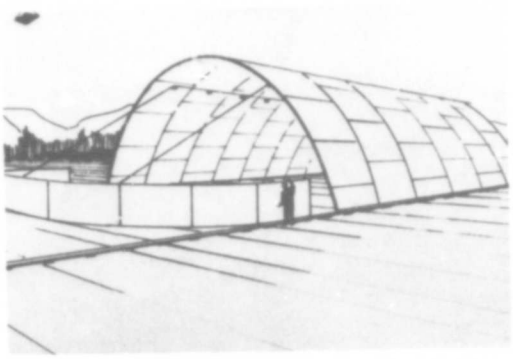

FIGURE #25 - Single curvature barrel vault concept

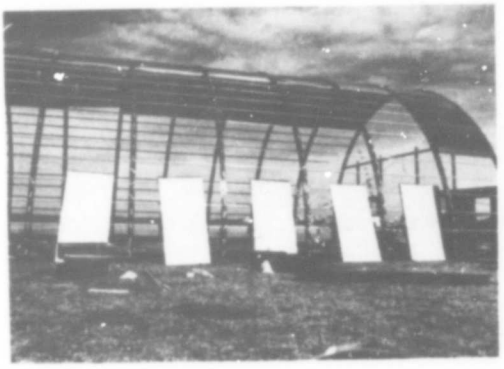

FIGURE #26 - Wood beams and plywood sheathing - Live Structures, Inc.

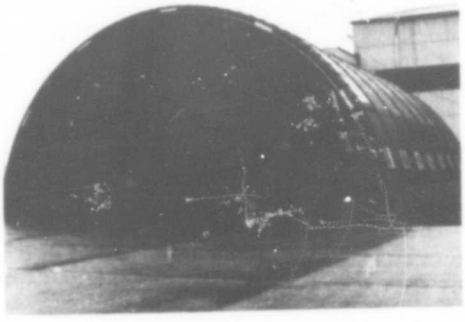

FIGURE # 27 - Live Structures shelter erected

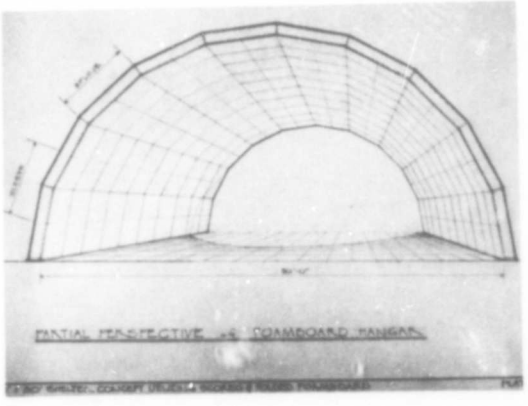

FIGURE #28 - Folded foamboard arch concept 50' span

has just been negotiated and we are working toward presentation of progress along these several lines in the late summer of this year.

DESIGN, FABRICATION, AND TESTING OF ADVANCED MODULAR SHELTERS FOR SMALL AND MEDIUM SIZE SHELTER APPLICATIONS

This formidable title describes the most recently initiated program by the University of Cincinnati in the area of lightweight shelters. In this effort we are working with International Structures, Inc. who, as subcontractor, is to fabricate the prototype shelters to be built. Three shelters of 16' x 32' size and three of 24' x 40' size are to be produced from concepts jointly arrived at.

International Structures, Inc. has developed and marketed a small 17' x 24' accordian type structure known by the name Plydom Model 100. (Figure 29). It has been widely used for migrant workers and has been tested in disaster areas in this country and overseas.

To date the major effort has been directed toward the small rather than the medium size shelter. Two concepts have been developed through preliminary model stage and have been presented to the Limited Warfare Office and Headquarters TAC. Erection of the first concept is demonstrated in the sequence of views shown as Figures 30,31, and 32. Unlike previous shelters developed by the University or International Structures, a vertical seven foot side wall is specified. This design has as its main features:

1). very compact packaged cubage
2). a small number of pieces
3). a minimum number of attachments and pieces of extraneous hardware
4). simple, rapid, and easily comprehended erection procedure

The second approach utilizes a combination shelter and package approach. Currently it is 13 ft. in width so as to efficiently fit the C-130 aircraft although not technically conforming to the 463-L pallet system. This concept packs its own floors as fold-down faces for the container. The accordian fold shelter is then withdrawn from both sides of the rigid package and attached to the flooring. This sequence is illustrated in Figures 33,34, and 35. A large work area in the package provides space for storage of related equipment.

This approach probably surpasses the first one in simplicity of erection. It does represent a departure from previous designs in that it requires one large (13' x 3' x 4') package rather than several small ones.

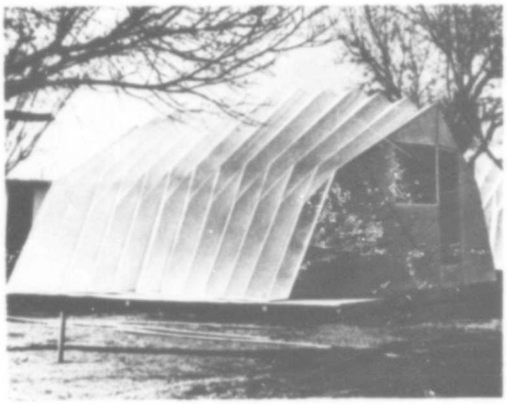

FIGURE #29 - Plydom Model 100, International Structures, Inc.

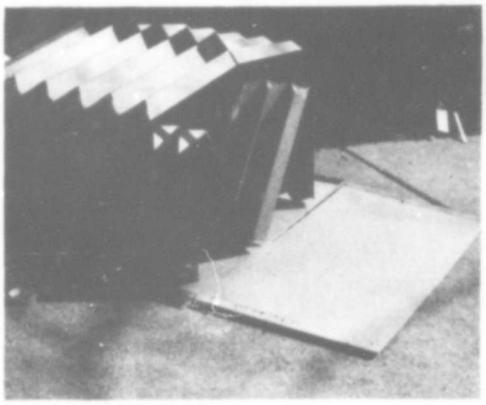

FIGURE #30 - New 16'x32' concept releasing folded arch

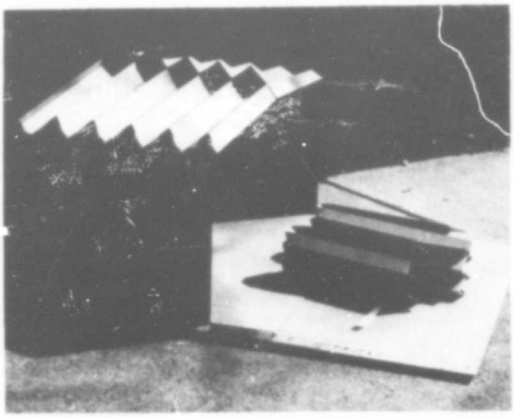

FIGURE #31 - New 16'x32' concept erection of typical arch

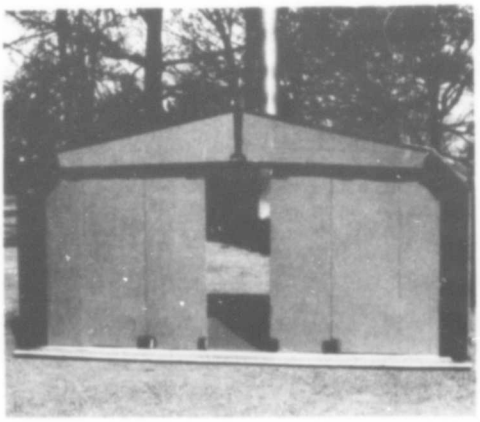

FIGURE #32 - New 16'x32' concept Panelized end wall

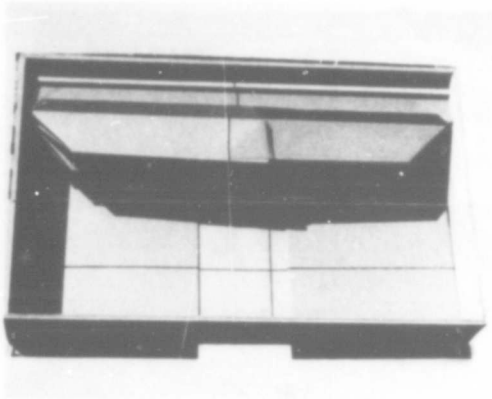

FIGURE #33 - Shelter-container concept- stored position with face removed showing void for equipment storage

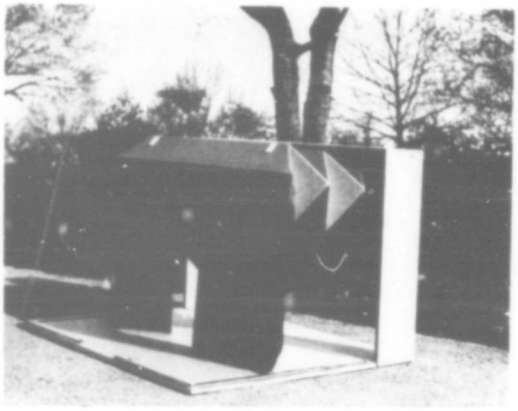

FIGURE #34 - Shelter-container partially expanded

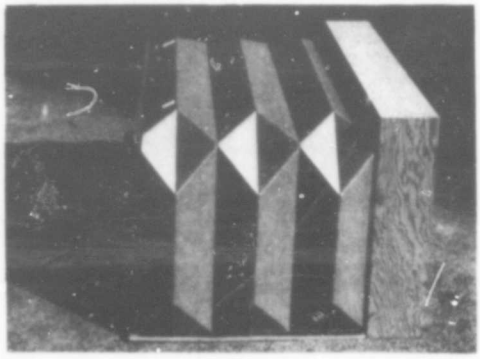

FIGURE #35 - Shelter-container concept - one quarter section fully expanded

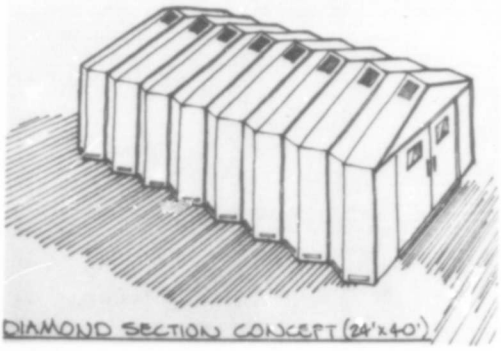

FIGURE #36 - New 24'x40' concept utilizing diamond section double wall construction

Medium Size Shelters

The 24' span structures have been studied only superficially at this point. One possible concept is presented in Figure 36.

Material To Be Employed

The expandable portions of these concepts utilize a foam sandwich board. Because of its superior qualities, polyurethane foam will most likely be employed.

A change in formulation of the foam gives promise of overcoming the "memory" aspect of urethane. These concepts visualize storage in folded rather than flat configuration. Most likely candidate for coating the foam sandwich is a 69# Kraft paper, 1 mil aluminum foil, and a thin outer skin of poly-vinyl chloride (PVC). A trial run of this material has been run. It seems superior to the University's epoxy type coating with its tendency to crack at severe folds and the polyethylene film previously used as an exterior coating by International Structures with its poor long-term resistance to ultra-violet light. This new material (designated ISC 504) is not an optimum one but seems the best available at this time.

SUMMARY

The author and other members of the University research team have concluded that:

1. A valid need exists for a family of shelters for the Bare Base Package and that optimum designs have not yet been developed.

2. One important reason that solutions existing or proposed don't reach this optimum state is the reliance on essentially "off the shelf" light-weight sandwich materials.

3. A major research and development effort should be initiated to develop new materials that are more rugged ("G.I. proof") than existing ones and that have superior weathering qualities and resistance to fracturing when folded repeatedly.

4. In the final analysis the design of a shelter is the design of a process as much as it is the design of items of hardware.

5. Simplicity of erection and fool-proof methods of connections and weather sealings are of paramount importance.

BLANK PAGE

WATER-EXTENDED POLYESTER RESIN (WEP) FOR LIMITED WAR SHELTER CONSTRUCTION

Robert H Leitheiser,* Richard J Hellmer, and Edwin T Clocker

INTRODUCTION

Water-extended polyester resin (WEP) is a new material of construction which should be uniquely suited for those applications where good logistics, rapid cures, flame retardancy and lower densities are desired. WEP can be made to cure rapidly enough to be load bearing in less than ten minutes. The favorable logistics, economics, and flame retardancy result from the ability to use 60, 70 and even higher percentages of water from locally available sources to extend the resin.

WEP is prepared by dispersing water in a polyester resin and rapidly curing the low-viscosity product to a load bearing composite.

$$\text{POLYESTER} + \text{WATER} \xrightarrow{\text{CATALYST}} \text{STRUCTURAL MATERIAL}$$

Major advantages of the cured product--WEP--are:

Good Logistics
Structural Strength
Low Cost
Ease of Use
Fast Cure
Good Chemical Resistance
Excellent Fire Resistance
Versatility

These advantages will be discussed briefly, but not necessarily in this order.

---

* Senior Research Chemist, Archer Daniels Midland Company, Minneapolis, Minnesota.

LOGISTICS

Realizing that transportation is a major factor when considering a material for use in a bare base application, the logistics of WEP are compared with those of concrete and No 2 pine in Table I.

Using pounds of material to be transported per cubic foot of fill as the criteria for comparison, we see that WEP is superior to wood and comparable to concrete if local aggregate is available but vastly superior to concrete if aggregate must also be transported to the site. If ease of handling is considered, WEP is preferred to either concrete or wood because all of the ingredients are easily pumpable liquids.

PHYSICAL STRENGTH PROPERTIES

When physical strengths are compared, WEP appears to be intermediate between concrete and wood. The compressive strength is one-half that of concrete but two to three times that of wood (see Table II).

The tensile strength is one-half that of wood but twice that of concrete. WEP is considerably more resilient or flexible than either wood or concrete as can be seen from the flexural modulus.

Because of the newness of the material, we are confident that the physical strengths of WEP can be significantly increased. We feel that a 50% increase in compressive strength, and a three-fold increase in tensile strength--especially if fibrous reinforcement is used--can be easily realized by continuing formulation studies.

WEP can be best visualized by considering it to be a foam with the cells filled with liquid rather than a gas. To illustrate this point, WEP is compared in Table III at two water levels with polyurethane foam at three densities. For comparative purposes, the weight of resin per cubic foot is used rather than overall density since the liquid water obviously weighs more than the fluorocarbon gas in the cells. As can be seen, the urethane foam at low densities is deficient in load bearing properties. At essentially equal resin weights per cubic foot (16 vs 18), WEP has a significantly higher compressive strength but a lower flexural strength as compared to urethane foam. We believe this data demonstrates the ability of the water in WEP to hydraulically distribute the load when under compression resulting in higher load bearing strengths even though the polymer is inherently weaker as evidenced by the lower flexural strength. Although undoubtedly acceptable for bare-base applications, the urethanes are too expensive to use at the higher densities required for adequate load bearing properties.

Like any foamed material, the properties obtainable with WEP are a function of the formulation. This is dramatically illustrated in Figure I which shows the increase in flexural strength with increase in styrene content and decrease in water content. At excessively high styrene levels the cure is retarded and rubbery composites can result. Even at 70% styrene, the cure rate is retarded, hence 60% styrene with 60% water was selected as the best compromise between strengths, cure rate and economics for the recently completed field trials at Wright-Patterson Air Force Base under Contract No AF33(615)-3519.

FLAME RETARDANCY

Because of the large amount of entrapped water which acts as a heat sink, WEP is flame retardant and a very effective heat barrier. It takes approximately ten minutes to burn through a one-inch thickness of conventional WEP with a propane torch. By using halogenated resin and a flame retardant such as ammonium phosphate in the water, the burn through time can be increased to 30 minutes or longer. WEP does not actually burn, but is carbonized at the surface by the intense heat of the propane torch.

PREPARATION AND TESTING OF WEP

The ease of preparation of WEP is demonstrated in Slide 1. The water is added to the precatalyzed resin in a Hamilton Beach mixer. The mixture is then poured into a suitable void such as a cardboard box. Within a few minutes this low viscosity, milk-like liquid polymerizes to a load-bearing solid.

Hand mix techniques obviously are not suitable for large pours, hence two continuous mixing machines were fabricated under Contract No AF33(615)-3519. The initial machine as shown in Slide 2 had an output of one gallon of dispersion per minute and was used to fill 2' x 2' x 1' voids at the ADM Research Center which were load bearing in 30 minutes or less.

A second larger machine (see Slide 3), with a capacity of greater than five gallons per minute, was constructed for scale-up studies. Voids as large as 30 cubic feet were filled in the ADM Research Center parking lot in less than 45 minutes. The pours were load bearing within 30 minutes after the pours were completed.

This machine was subsequently used to make four test pours at depths of 18, 12, 9 and 6 inches in the 4' x 5' simulated bomb craters at Wright-Patterson Air Force Base. No reinforcing was used in any of the pours. The 18, 12 and 9 inch pours passed the 30,000 pound moving wheel load test.

The 6 inch pour broke when similarly tested, but it is believed the failure resulted from inability to compact the waterlogged back fill to give an adequate sub-base. For the final 6 inch pour, the vibratory packer could not be used because it tended to "bury" itself in the wet sand, being used as back fill material. Based on compressive strength and related test data, 6 inches of WEP on adequately compacted sub-base material should pass this test.

PROPOSED STRUCTURAL APPLICATIONS FOR WEP

The favorable logistics, rapid cure rates and excellent engineering properties suggest the use of WEP for structural applications such as storage shelters, maintenance hangers, and personnel housing in forward area tactical air bases. The simplest approach would be the extrusion of panels, beams or blocks of various sizes and dimensions as shown in Figure II. In this concept, the extrusion head is moved rather than the extruded object so as to eliminate the continuous belt normally used with industrial extrusion processes. Hydraulic pressure generated by the liquid WEP could be used to propel the movable extrusion head.

The walls of various shaped structures could be readily formed as a single operation by slip forming as shown in Figure III. The rate of rise of the mold can be easily timed to coincide with the rate of gelation of the WEP. Hydraulic pressure exerted by the WEP could be used to raise the mold if the top of the mold were enclosed. This concept appears to be especially suitable for construction of storage tanks and bins. Openings such as window and doors, however, could easily be subsequently cut in the structures to permit human occupancy.

A more sophisticated method of preparing cylindrical structures would be spiral generation as shown in Figure IV where only a small section of mold is moved in an ascending spiral to form the structure. The size of the structure can be varied by changing the length of the boom. By decreasing the length of the boom and tilting the mold segment, a domed structure could be generated.

For arched roofs, individual segments could be generated in a horizontal position and then be tipped into place as shown in Figure V. An alternate approach to a domed structure would be spraying WEP over a collapsible mold as shown in Figure VI. Such sprayed-up structures appear feasible based on preliminary laboratory data.

ECONOMICS

The use of WEP obviously must be justifiable economically. Although significantly more expensive than concrete as can be seen in Table IV, it is competitive with wood, especially the better grades of wood.

SUMMARY

Water-extended polyester resin--WEP--has been demonstrated to be a suitable material for rapidly repairing bomb damaged runways.

The favorable logistics, excellent engineering properties, and rapid cure times of WEP suggest its use for fabrication of structures for forward tactical air bases.

Although not as cheap as concrete, WEP promises to be competitive with wood.

ACKNOWLEDGEMENT

Developmental work on the use of water-extended polyester resin (WEP) for the rapid repair of damaged runways was done under Contract Number AF33(615)-3519 with the United States Air Force Aero Propulsion Laboratories at Wright-Patterson Air Force Base, Dayton, Ohio. Lt C R Lieberman was contract monitor.

TABLE I

LOGISTICS

CONSTRUCTION MATERIAL	DENSITY LBS/FT^3	POUNDS MAT'L SHIPPED/CU. FT.	
WEP	60	RESIN	18-24
CONCRETE	150	CEMENT	21
		AGGREGATE*	120
NO 2 PINE	35		35

*MAY NOT BE AVAILABLE LOCALLY

TABLE II

PHYSICAL PROPERTY COMPARISON

PROPERTY	WEP CURRENT	WEP PROJECTED	CONCRETE	NO 2 PINE
COMPRESSIVE, PSI	2,100	3,000	4,500	300 TO 900
TENSILE, PSI	610	1,800	300	1,200
MOD ELASTICITY	100,000	150,000	3,625,000	1,760,000
PUNCH SHEAR, PSI	555	1,000	360	---

TABLE III

COMPARISON WITH URETHANE FOAM

MATERIAL	RESIN LBS/CU. FT.	COMP STR PSI	FLEX STR PSI	COST $/CU. FT.
URETHANE FOAM*	3	40	70	1.50
	8	190	270	4.00
	16	550	750	8.00
WEP (70)	18	900	600	3.85
(60)	24	2,300	1,500	5.16

*CORNELL AERONAUTICAL LABORATORY, INC.

TABLE IV

COMPOSITE COST

	$/LB	$/CU. FT.
WEP		
50% WATER	.108	6.50
60% WATER	.086	5.16
70% WATER	.065	3.85
80% WATER	.043	2.58
CONCRETE	--	0.62
NO 2 PINE	0.053	1.92
NO 1 PINE	0.097	3.50

FIGURE I

STRENGTH VS. FORMULATION

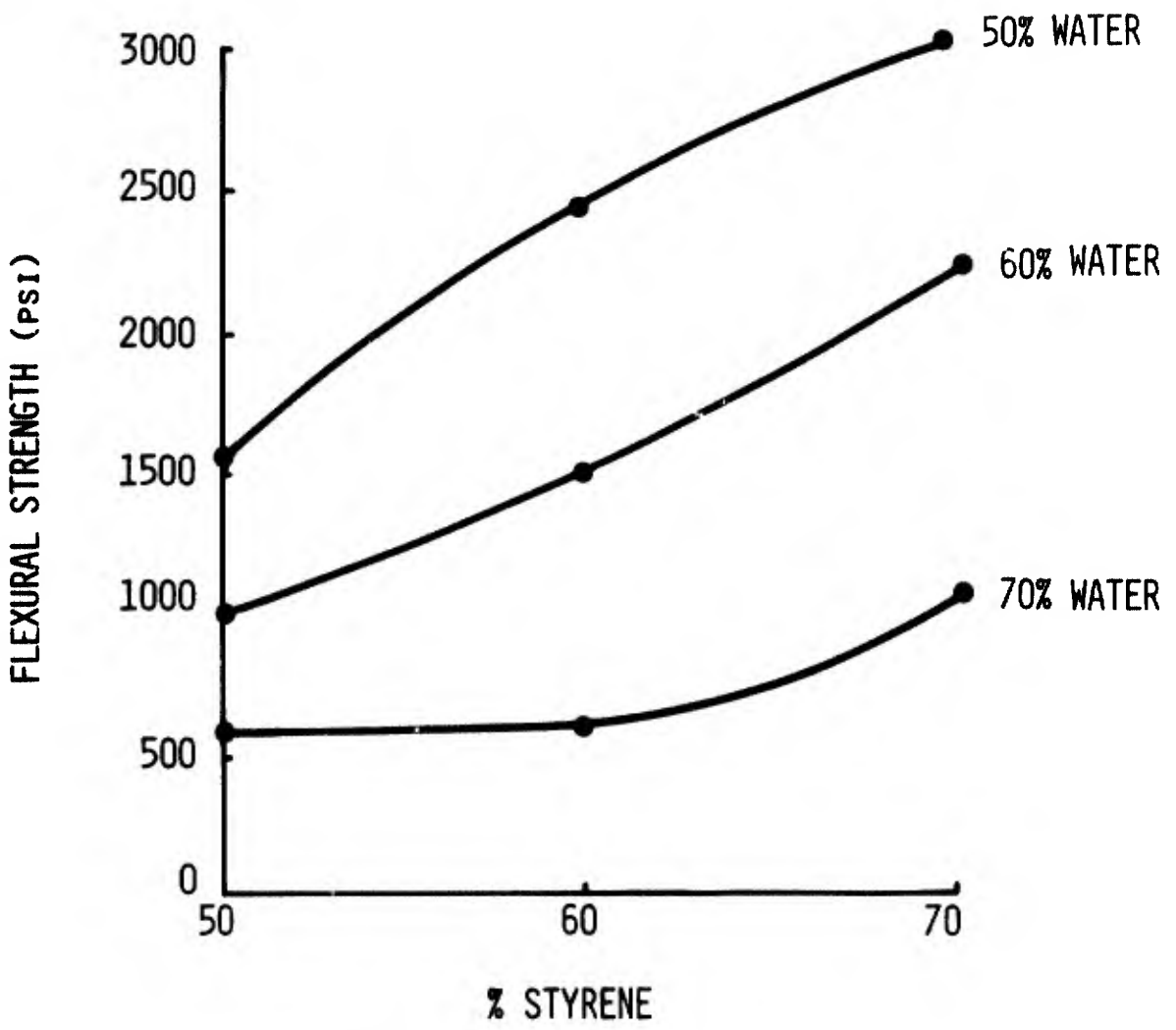

FIGURE II. HAND MIX PREPARATION OF WEP.

FIGURE III. SMALL CONTINUOUS MACHINE.

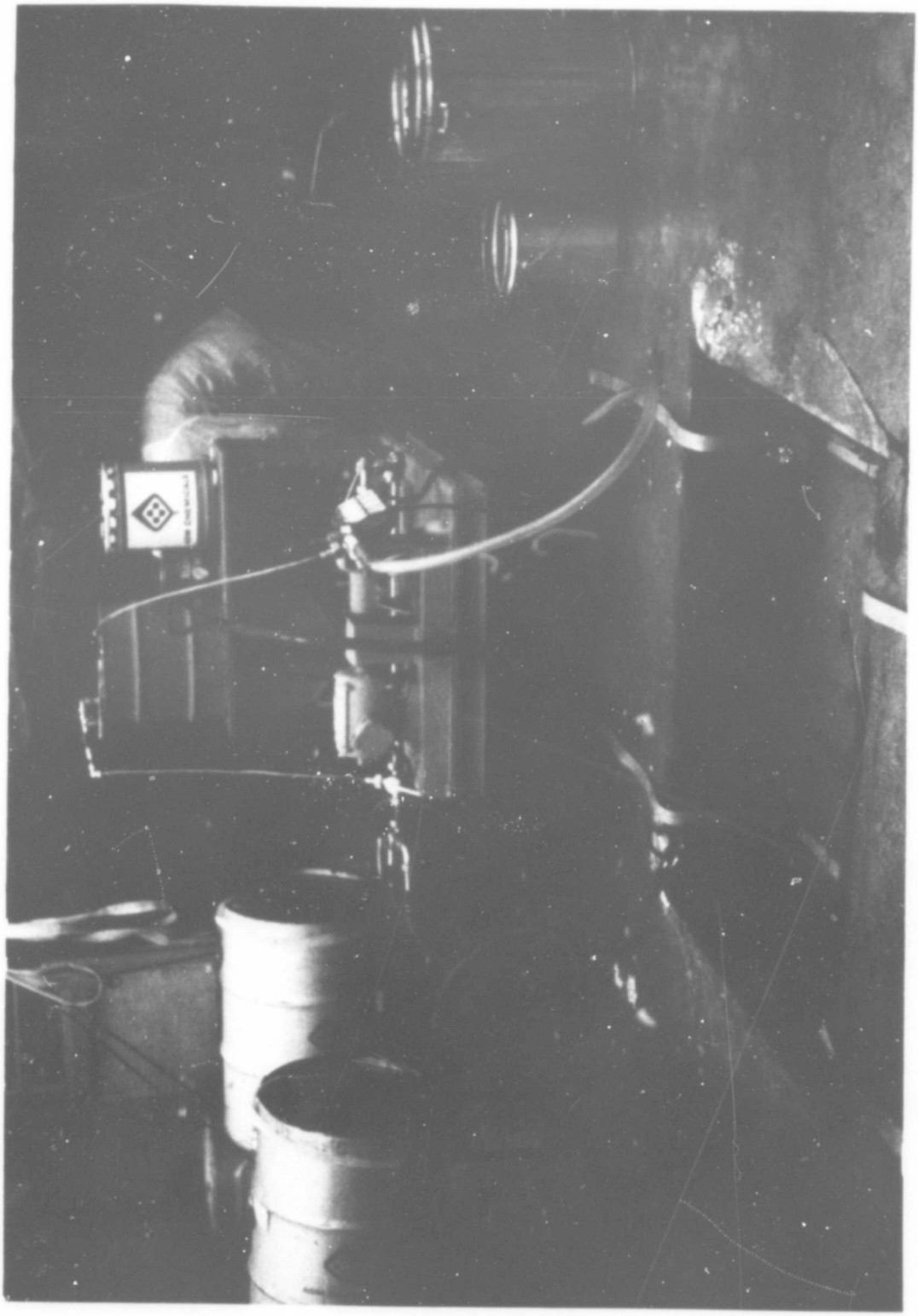

FIGURE IV. LARGE CONTINUOUS MACHINE.

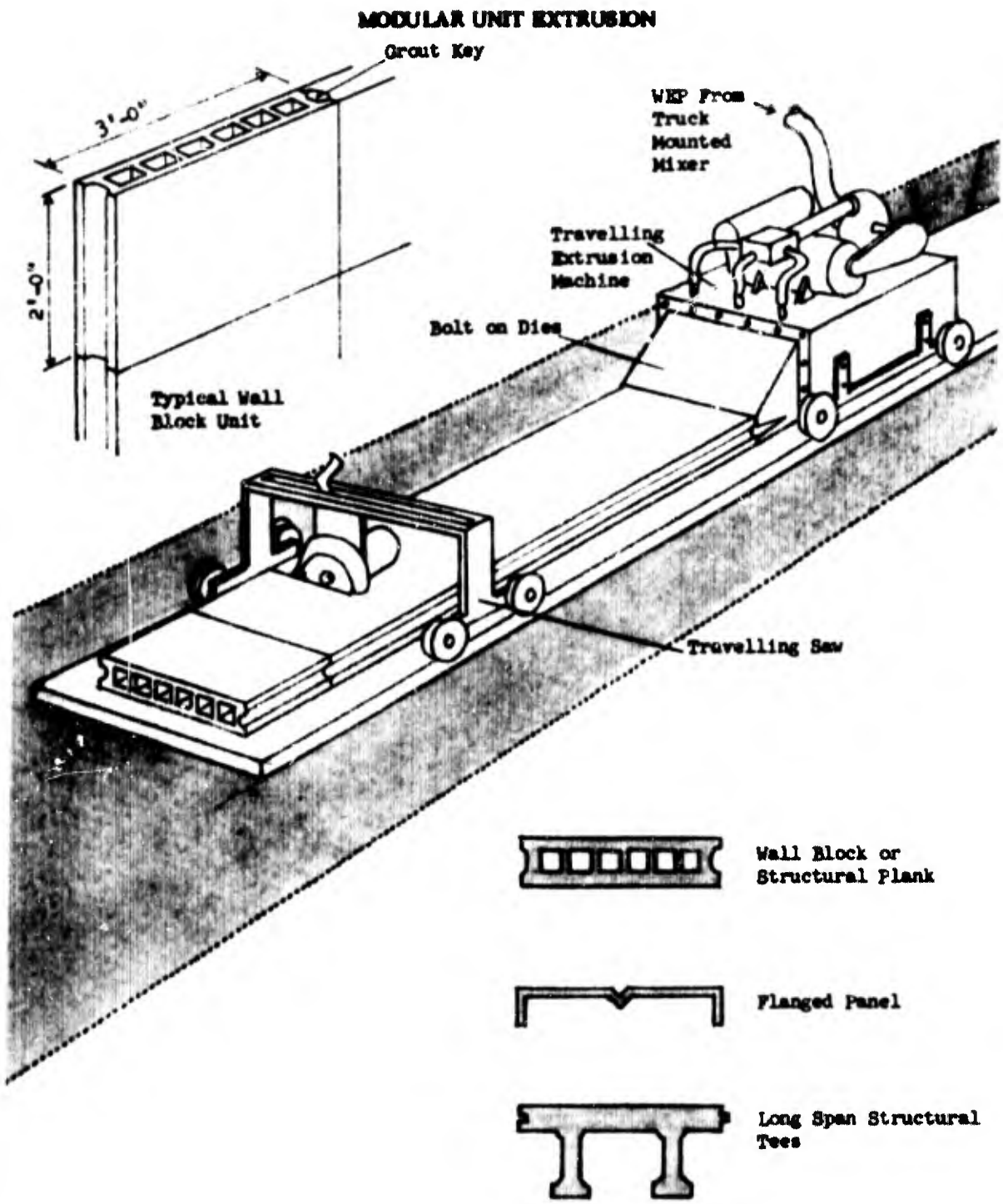

FIGURE V. MODULAR UNIT EXTENSION.

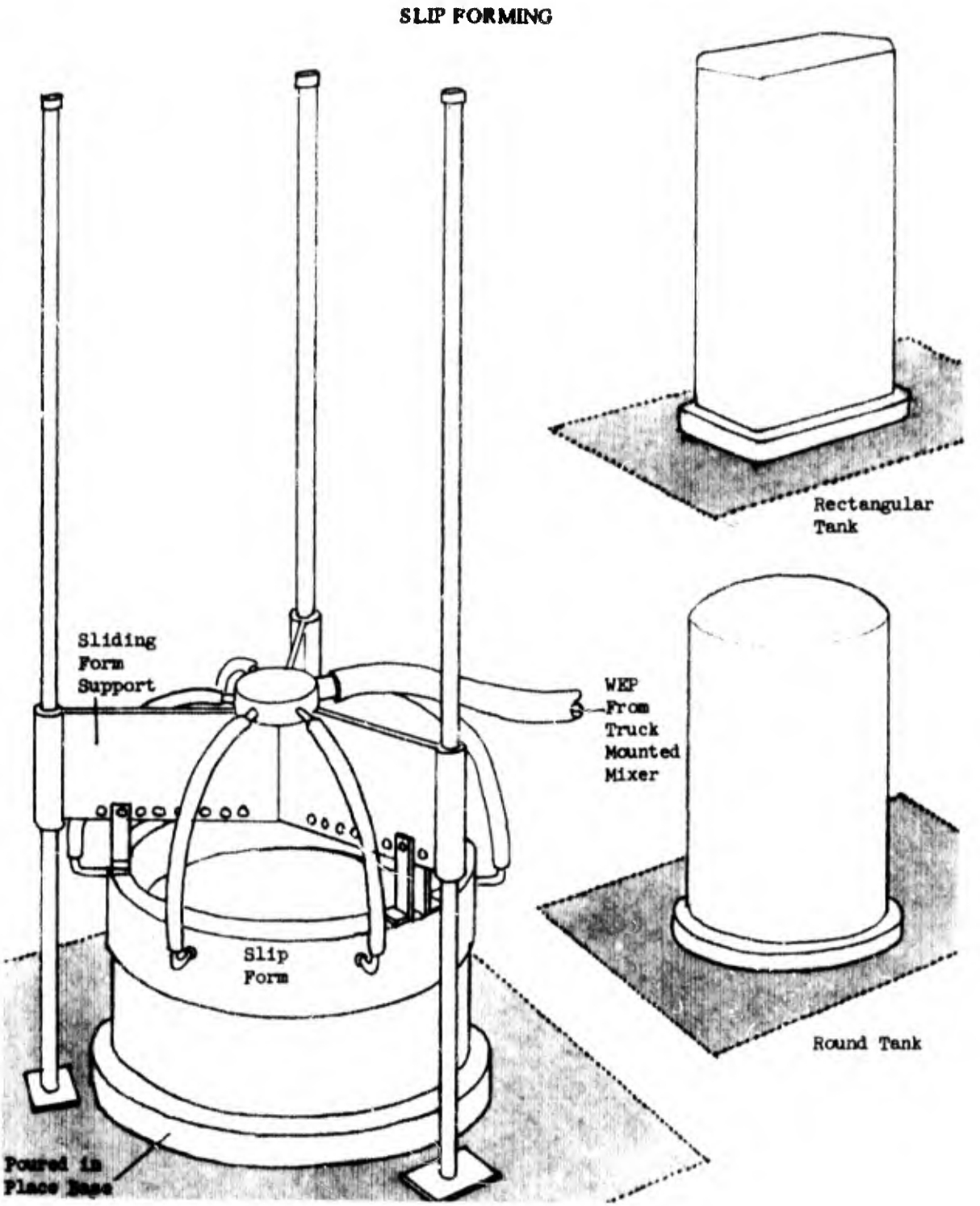

FIGURE VI. SLIP FORMING.

SPIRAL FORMING

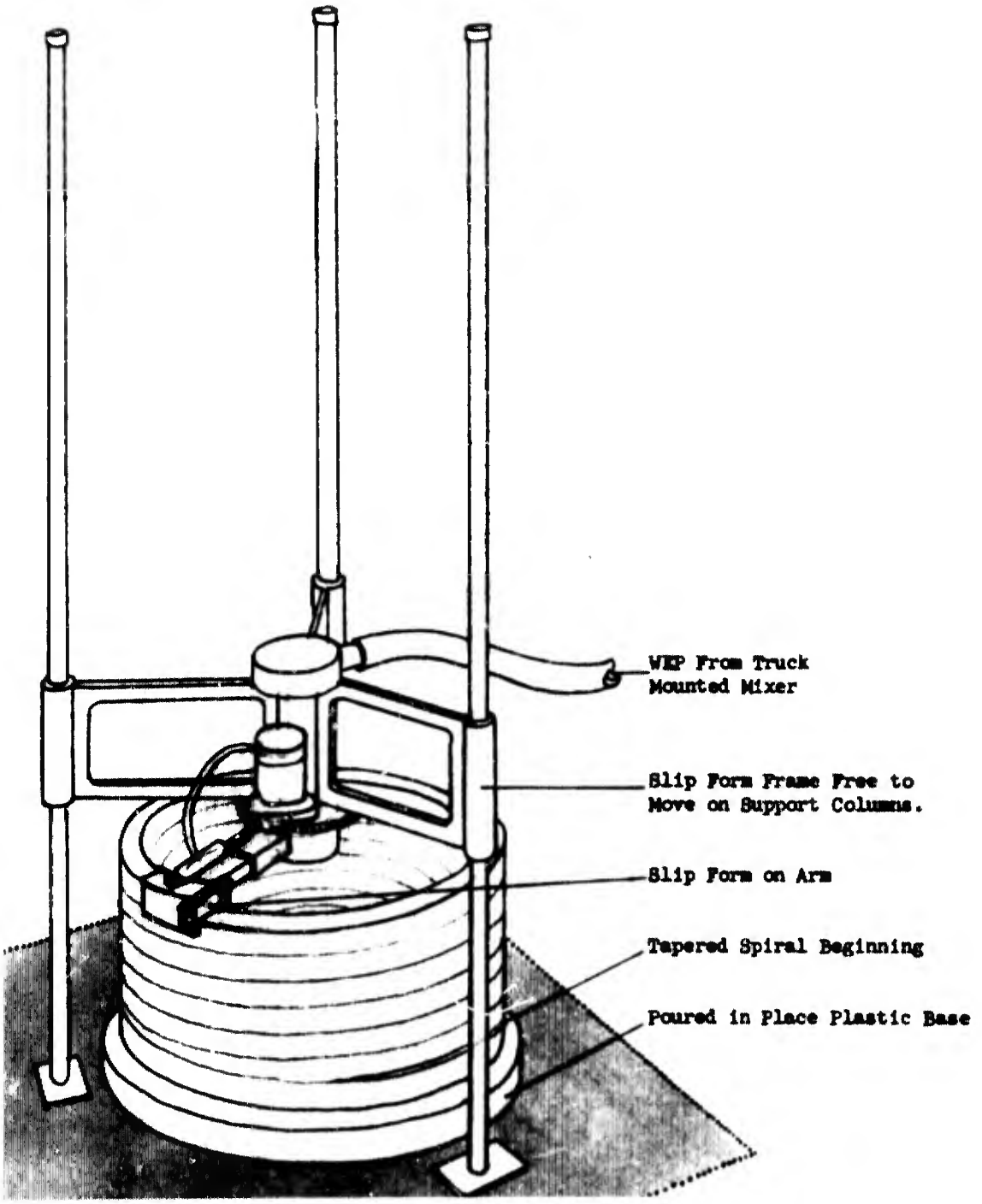

FIGURE VII. SPIRAL FORMING.

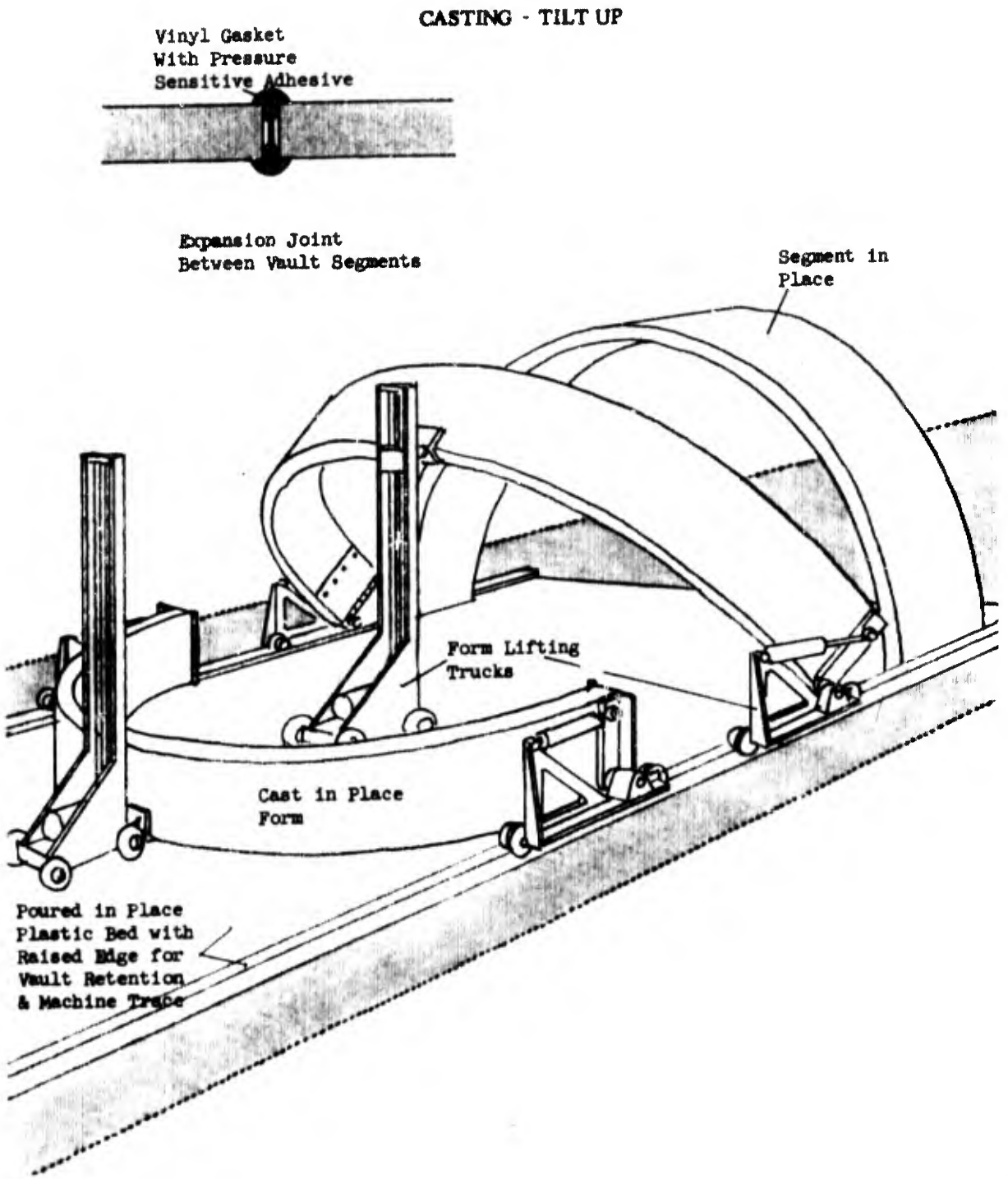

FIGURE VIII. CASTING-TILT UP.

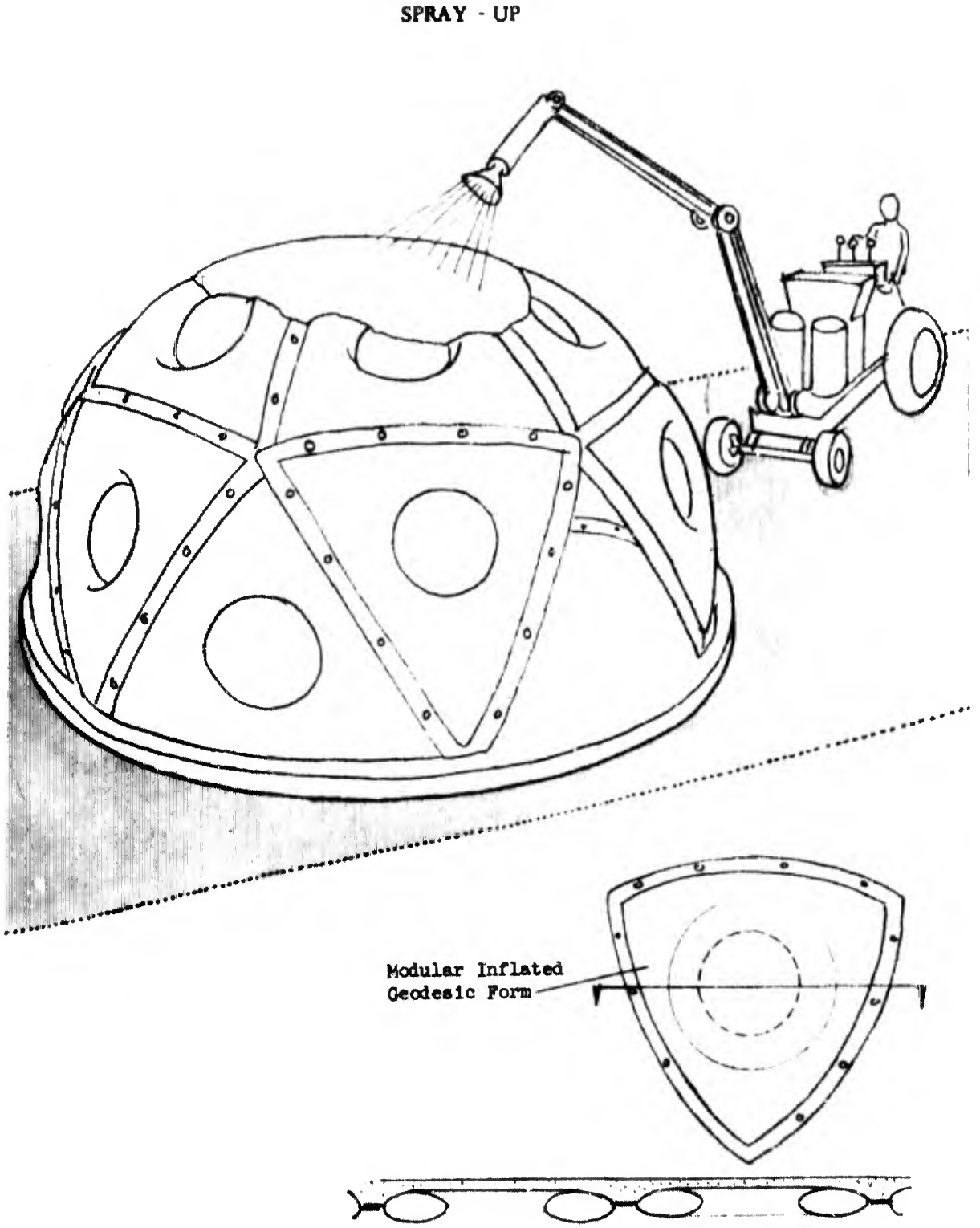

FIGURE IX. SPRAY-UP.

A PORTABLE SHELTER WITH SOLID VERTICAL WALLS AND ROOF

L.J. Boler*

and

J.S. Tandon**

*Senior Project Engineer, Advanced Programs Division, G.T. Schjeldahl Company
**Scientist, Advanced Programs Division, G.T. Schjeldahl Company

1.0 INTRODUCTION

There are several combinations of structural concepts, construction methods and errection techniques which may lead to economical structures. After preliminary structural analysis and considerations to constraints of weight, volume, foldability, errection time and cost, a frame and panel type structure was considered for detailed study.

This structure has vertical up and down rigid walls, a sloping roof for proper drainage and has conventional doors, windows and ventilators. Thus in spite of being a conventional structure, it is readily expandable, collapsible and has very light weight and volume. The weight of the structure is of the order of 1-2 pounds per sq. ft. of the base area and the estimated cost is expected to be $2-$3 per sq. ft. as against $10-$15 for conventional buildings. Furthermore, because of its light weight, it needs no substructure and the structure can be errected on uneven terrain.

2.0 STRUCTURAL ANALYSIS AND DESIGN OF 16- BY 32-FT SHELTER

Structural Concept: Structural Frame and Panel Construction

The configuration of the structural frame and its dimensions are shown below. The frame is assumed hinged or pin connected at the bottom. The panels span the space between the frames and transfer the load to the frames which in turn transmit it to the ground.

The design of this concept is divided into two parts. The first part deals with the analysis and design of panels, and the second part deals with the analysis and design of the gable frame.

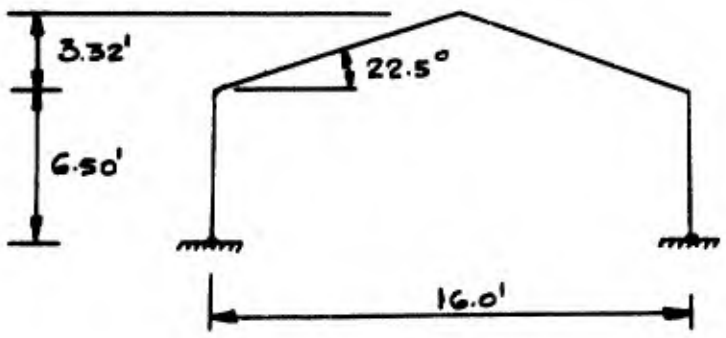

Gable Frame

Figure 1

2.1 PANEL ANALYSIS

Assume frames spaced at 4.0 ft

Use 6 panels each 4.0 ft wide	=	24.0 ft
5 intermediate frames each 1.0 ft wide	=	5.0 ft
2 outside frames each 1.5 ft wide	=	3.0 ft
total length	=	32.0 ft

The wall panels are 6.5 ft by 4.0 ft while roof panels are 8.6 ft by 4.0 ft. The governing design would be for 8.6 ft by 4.0 ft size panels.

The plate is neither entirely simply supported nor entirely fixed ended. In the computations that follow, an end condition that is midway between simply supported and fixed ended case is assumed. Consequently, moments and deflections are computed both for the fixed ended case and the simply supported case, and the mean of the two is taken to obtain conditions that simulate the actual support.

For simply supported plate:*

$$\text{Panel aspect ratio} = \frac{8.6}{4.0} \sim 2.1$$

$$W_{max} = \alpha_1 \frac{qa^4}{D}$$

$$M_{max} = \beta_1 qa^2$$

For aspect ratio = 2.1; $\alpha_1 = 0.01013$

$$\beta_1 = 0.1017$$

For fixed ended plate:

$$W_{max} = \alpha_2 \frac{qa^4}{D}$$

$$M_{max} = \beta_2 qa^2$$

*Timoshenko & Woinowsky-Krieger "Theory of Plates and Shells", McGraw Hill Book Company, 1959.

For aspect ratio = 2.1; $\alpha_2 = 0.0025$

$\beta_2 = 0.0412$

For actual support conditions, we obtain:

$$W_{max} = 0.00633 \quad q \frac{a^4}{D} \tag{1}$$

$$M_{max} = 0.0714 \quad qa^2 \tag{2}$$

$a = 4.0$ ft

$q = 10$ psf

Rearranging equation (1), we get

$$D = \frac{0.00633\ qa^4}{W_{max}}$$

Assume $W_{max} = 1$ in.

and $D = 2{,}340$ in-lbs.

$$M_{max} = 0.0714\ qa^2$$

$= 11.4$ in-lbs/in

$h = 0.4$ in

$$\sigma_{max} = M_{max} \times \frac{6}{h^2} = 415 \text{ psi} \quad \text{O.K.}$$

Since the plate rigidity of the material under consideration is 3000 in-lbs, no reinforcement may be necessary.

2.2 CABLE FRAME ANALYSIS

There are three basic load conditions for which the structure must be safe:

(a) live load
(b) wind load
(c) live load plus wind load

Each of these cases will be analyzed individually. For brevity only, live load analysis has been presented.

2.3 LIVE LOAD ANALYSIS:

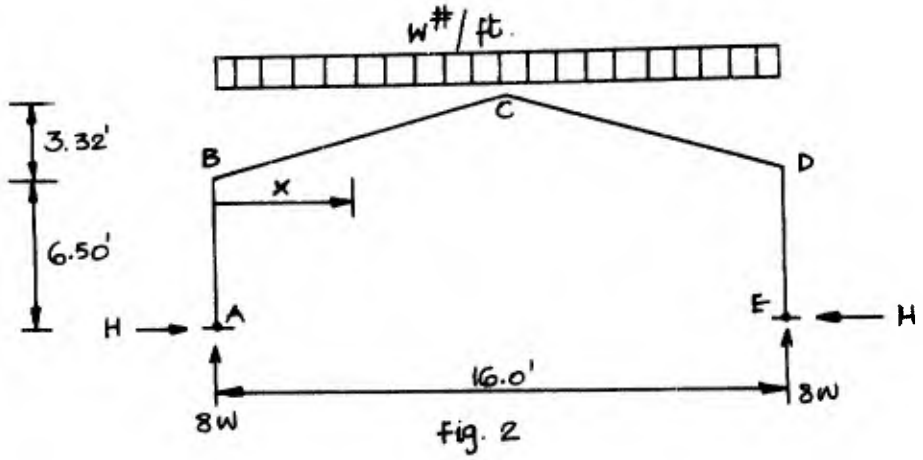

fig. 2

The frame is one times statically indeterminate and if the horizontal component H of the reaction is selected as redundant, then

$$H = \int \frac{Mmds}{EI} \div \int \frac{m^2 ds}{EI}$$

It can be seen that the maximum bending moment will occur at the junction of the column and the girder, it being assumed that the same structural shape will be used throughout the frame.

Since $\int Mmds = \int_0^8 (8\,wx - \frac{wx^2}{2})\,(6.5 + \frac{3.32x}{8})\,1.08\,dx$

$= 1580\,w$

and $\int m^2 ds = \int_0^{6.5} y^2\,dy + \int_{6.5}^{9.8} y^2 .\, 2.61\,dy$

$= 574$

then $H = 2.75\,w$

$Mb = 6.5 \,.\, 2.75\,w = (17.85\,w)$ ft pounds

$Mc = 8\,w \,.\, 8 - 2.75\,w \,.\, 9.8 - \frac{w.8.8}{2}$

$= 5\,w$ ft pounds

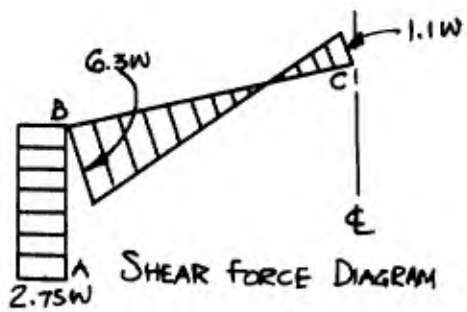

SHEAR FORCE DIAGRAM

The bending moment and shear force diagrams can now be drawn. These diagrams are shown in the adjoining sketches. The analysis for wind loads and the combination of wind and live loads can similarly be made. The members of the frame should be designed to carry shear as well as bending and axial loads.

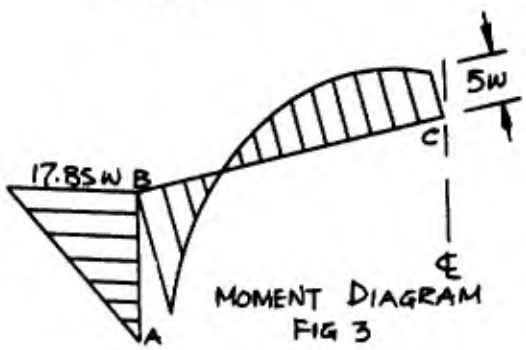

MOMENT DIAGRAM
FIG 3

Since it is generally uneconomical to construct a base fixed against rotation, rigid frames are designed as if hinged at the base. The size of the structure, size of the pallet and the facilities for errection will determine the number and location of field splices. Since splices are a weak point in a structure, their number should be minimum and their location near the points of contraflexure.

A variety of materials may be considered for the frame ranging from metals to sandwich construction material consisting of a laminate of kraft-paper and aluminum as facing and polyurethane foam as core. If aluminum is utilized for the frame, a quick calculation shows that hollow circular tubing will be more economical than a channel section for the present design. Sandwich construction material may be used in the form of closed triangular or rectangular cross section. It can be seen that bending capacity (section modulus) of rectangular section is about 89% larger than that of triangular section, utilizing same amount of material. Furthermore, these sections are lighter than aluminum sections. It is, therefore, recommended that rectangular box beam section made out of sandwich construction material be used for the frame. This section is not only the most economical of those considered, but also helps span the length of the shelter.

3.0 MATERIALS SURVEY AND EVALUATION

The design concepts for expendable shelters considered from a materials viewpoint were divided into those with rigid walls, and those covered by a flexible membrane. A survey was made of properties of materials which fit these categories. An early decision was made to use a rigid wall and roof material because this would yield a significant advance over a tent type structure in that it would be more livable for personnel.

3.1 RIGID MATERIALS

Table I gives physical properties for some homogeneous rigid wall materials which were considered. Table IA shows representative rigid plastic materials. The materials in Table IA were selected on the basis that their tensile and flexural moduli be greater than 30,000 psi (per ASTM D638 and D790). The rigid plastic materials were unattractive because they are heavy. Their densities range from 64 to 82 lb/ft^3. Stiffness considerations indicate that plastic wall plates no less than 1/8-inch thick would be required. This results in a weight per shelter for the walls alone of approximately 560 to 720 lbs. Homogeneous, flat rigid plastic plate walls were not considered after this initial investigation. Corrugated plastic wall panels would be lighter but present packaging difficulties.

Table IB shows the physical properties of some nonplastic rigid plate materials. Aluminum is attractive because of its strength and high modulus. If used as a rigid wall panel to span any distance, thicknesses greater than 0.160 inches must be considered. (The walls of a shelter having 1250 square foot surface area constructed of 160 mil aluminum would weigh about 2800 pounds.) Particle board is too heavy and has poor strength. These materials were not considered after this initial investigation.

Table IA Typical Properties of Rigid Wall Materials (Plastic)

Material	ABS	Acrylic	Polystyrene	Polycarbonate	Polyvinyl Chloride
Type	Medium impact	General purpose	Medium hard impact	Non filled	Rigid
Density lb/ft^3	66	73.5	64	75	82
Fire rating	Flammable	Flammable	Flammable	Self-extinguishing	Self-extinguishing
Tensile strength lb/in^2	7500	8000	2500	9500	5500
Tensile modulus lb/in^2	370 000	400 000	300 000	345 000	350 000
Elongation %	5-20	2-7	5-50	75	5-25
Flexural modulus lb/in^2	400 000	400 000	350 000	340 000	380 000
Flexural strength lb/in^2	11 500	15 000	Did not break per ASTM D790	13 500	11 000
Compressive strength lb/in^2	10 500	14 000		12 500	11 000
Thermal conductivity $BTU/hr/ft^2/^oF/ft$	0.08-0.12	0.12	0.024	0.11	0.07

Table IB Typical Properties of Rigid Wall Materials (Non Plastic)

Material	Aluminum Corrugated Sheet	Balsa	Particle Board
Type	3003	12% moisture content	Medium density
Density lb/ft^3	167.6	11	26
Fire rating	Non-burning	Burns	Burns
Tensile strength lb/in^2	70 000	3000 grain 120 grain	500 to surface 40 to surface
Tensile modulus lb/in^2	10 000 000	500 000	
Elongation %	7		
Flexural modulus lb/in^2		625 000	150 000
Flexural strength			
Compressive strength lb/in^2		1900 grain 100 grain	1400
Thermal conductivity $BTU/hr/ft^2/^oF/ft$	109.2	0.27	0.40
Maximum size available	16 mil thickness 3 ft x 12 ft	6 in x 10 ft	5 ft x 12 ft

3.2 COMPOSITE MATERIALS

The composite materials should consist of an inexpensive, low density core, and inexpensive, lightweight, high rigidity facings.

Composite materials such as honeycomb panels, cardboards, and paper-foam laminates were considered. Cardboard panels were eliminated because no production source of impregnated board could be found.

3.2.1 Core Materials

Paper honeycomb core material is the most inexpensive of the honeycomb types, and is available made from 80-lb and 99-lb kraft paper. When impregnated with a phenolic resin, it should be resistant to fungus and moisture damage. Paper honeycomb was not chosen because it cannot be scored and folded for packaging.

3.2.2 Sandwich Panels

A sandwich-type panel using a lightweight foam for the core material will require facings with a relatively high modulus of elasticity. The combination will provide panel stiffness and must have a certain amount of impact resistance for "GI-proofing".

Monsanto's FOME-COR is a composite panel of polystyrene foam faced with kraft paper. It is available in thicknesses down to 0.140 inches. The 0.25-inch thick material has a compressive strength of 25 psi, a tensile strength of 560 psi, and a thermal conductivity of 0.23 $BTU/ft^2/hr/^oF/ft$. However, the unavailability of a high modulus facing, the low melting temperature of polystyrene, and the strength loss of paper when wet, were disadvantages which resulted in the choice of urethane foam board.

Urethane foam is manufactured by many companies in the United States; however, only a few companies produce a composite of urethane foam with various structural facings. Allied Chemicals Fabrelt Division and Apache Foam Products supplied composite materials which were evaluated under this program.

Table II illustrates comparative weights and costs of several facing materials when combined with the chosen 0.4 inch thick urethane foam core.

Table II

Expendable Shelter Urethane Panels

Thickness, Weight & Cost Factors

Core

	Thickness inches	Weight lbs/ft^2	Cost $\$/ft^2$
Urethane foam	0.4	0.08	.08

Facing

		Thickness inches	Weight lbs/ft^2	Cost $\$/ft^2$	Thickness inches	Weight lbs/ft^2	Cost $\$/ft^2$
1.	a) Aluminum	.002	.03	.03	0.404	0.14	.14
	b) Aluminum	.005	.07	.15	0.410	0.22	.38
	c) Aluminum	.010	.14	.19	0.420	0.36	.46
2.	Particle Bd.	1/8	.67	.086	.650	1.41	.452
3.	Plywood	1/8	.49	.09	.650	1.06	0.46
4.	Polyester	.032	.157	.045	.464	.394	.37
5.	Steel	.002	.083	.026	.404	.246	.132
6.	Kraft paper	.020	.069	.02	.440	0.218	.120
7.	Laminate of 1 mil aluminum 0.069 lb kraft paper and 1 mil aluminum	.022	.1	.10	.444	0.278	0.28

Item 1 Aluminum Foil

The 2 mil, 5 mil and 10 mil aluminum is not available in a production foamboard. The production foamboard requires a paper carrier and is then limited to 2 mils of aluminum. The 2 mil aluminum by itself is too puncture sensitive and marginal on structure. The 5 mil and 10 mil aluminum become expensive because of the hand lamination required.

Item 2 Particle Board

This material cannot be scored and folded for packaging and has a high price because it must be hand laminated.

Item 3 Plywood

This material is heavy, must be painted and requires hand lamination which results in a high price.

Item 4 Polyester

This material is very strong and puncture resistant but is not flexible. This results in a packaging problem because a scored and folded corner is necessary. This material must be hand laminated.

Item 5 Steel

This is a low priced high modulus material which has good possibilities. The problem at this time is that it is available only in 2 ft widths and the production foamboard companies are not interested in it for that reason.

Item 6 Kraft Paper

It requires painting and is not fire resistant.

Item 7 Aluminum Kraft Paper Aluminum Laminate

This material was chosen as the best compromise because it is strong, fire resistant and is obtainable in a painted condition.

4.0 SHELTER DESCRIPTION

4.1 SIZE

The inside floor dimensions are 16 by 30.5 feet. The side walls are 6.5-ft high and the roof peak is 9.75-ft high. The enclosed volume is 3910 ft^3 and the floor area is 488 ft^2.

4.2 MATERIALS

The walls and roof are 0.4-in thick sandwich construction material consisting of 2.25-lbs/ft^3 urethane foam faced on both sides with a triple laminate of 1-mil aluminum foil, 69-lb/1000 ft^2 kraft paper and 1-mil aluminum foil. This laminate is lacquered for color and additional weather protection. Colors can be chosen depending upon end use. Inside and outside can be different colors. This material is fire resistant in that it cannot be ignited with a small flame.

The flexible joints which connect the panels utilize neoprene-coated nylon. The windows are urethane foamboard with transparent Mylar panes. The screening is fiberglass.

4.3 DOORS

A single 3 ft by 7 ft door with a standard screen door type door knob that locks from the inside is provided on one end. At the opposite end double doors make an opening 8-ft wide by 7.5-ft high. All the doors include a standard window.

4.4 WINDOWS & VENTILATORS

The four windows in each end are screened, and have a total open area of 18 square feet. The windows can be designed to open either in or out.

Each end of the shelter has a ventilator normally covered by foamboard flaps which can be opened by loosening two straps. The open area of each ventilator is 7.5 square feet. The total screened area per shelter is 33 square feet.

Windows can be added to the sides of the shelter with increased cost.

4.5 PACKAGE SIZE

The entire structure can be packaged into a box 8-ft 10-in long by 4-ft 4-in wide by 3-ft 4-in high. The packaged volume of shelter is 127 cubic feet.

4.6 WEIGHT

The entire shelter weighs about 650 pounds.

4.7 COST ESTIMATES

15 units	$1,500.00 each
100 units	$1,250.00 each
1,000 units	$1,200.00 each

4.8 Figure 4 shows a cross section detail of the frame and panel interface. Photographs of the shelter as it was being set up and taken down at the G.T. Schjeldahl plant are included as Figures 5 through 7 .

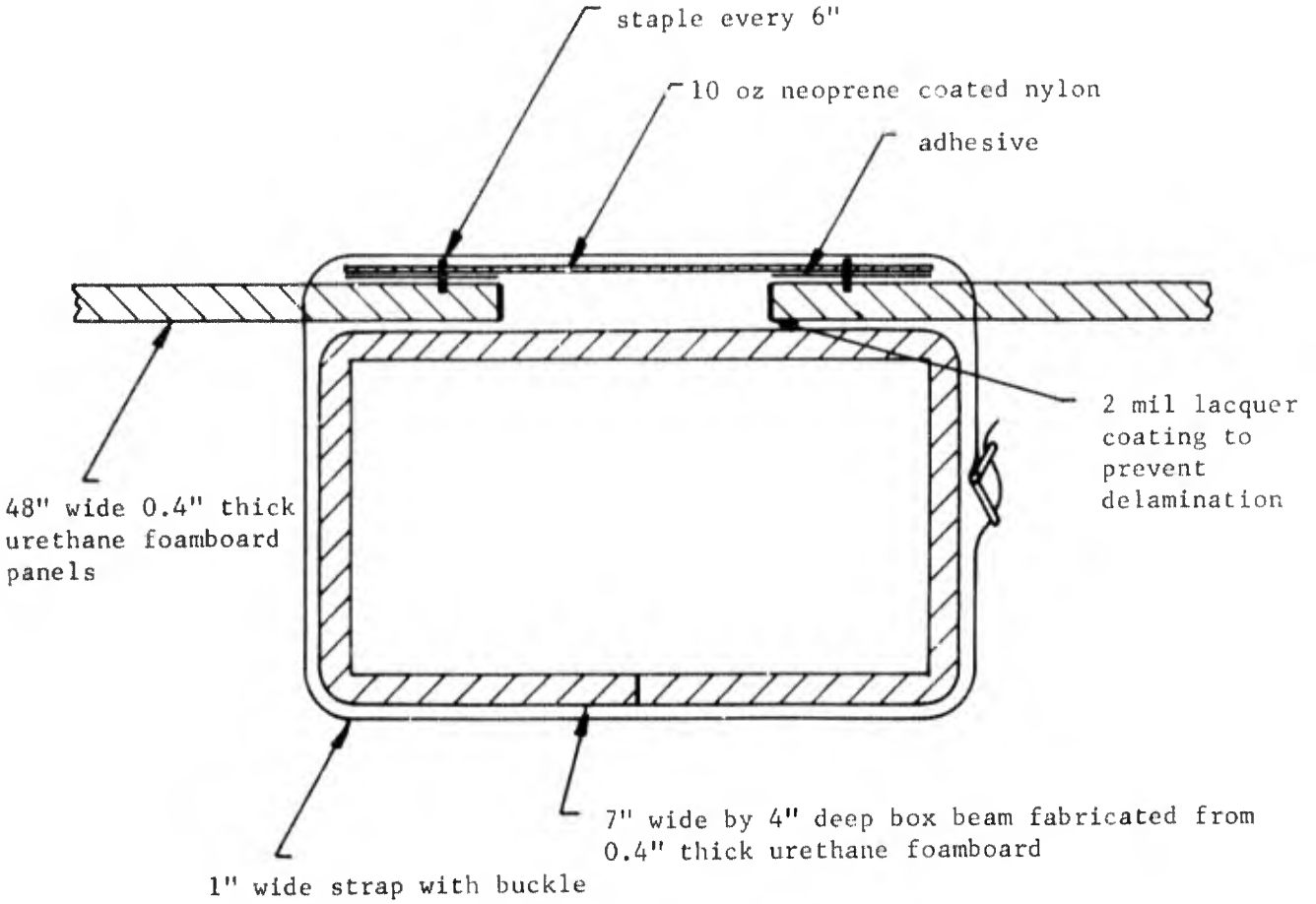

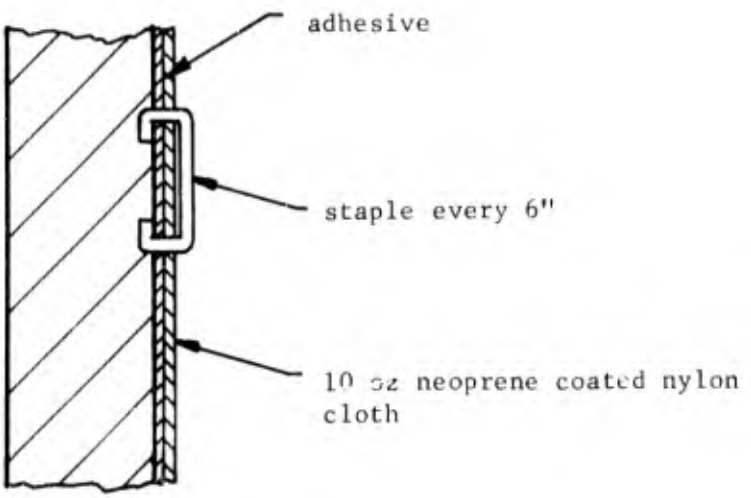

Frame and Panel Connection

Figure 4

Interior Views Toward End With Double Doors
Figure 5

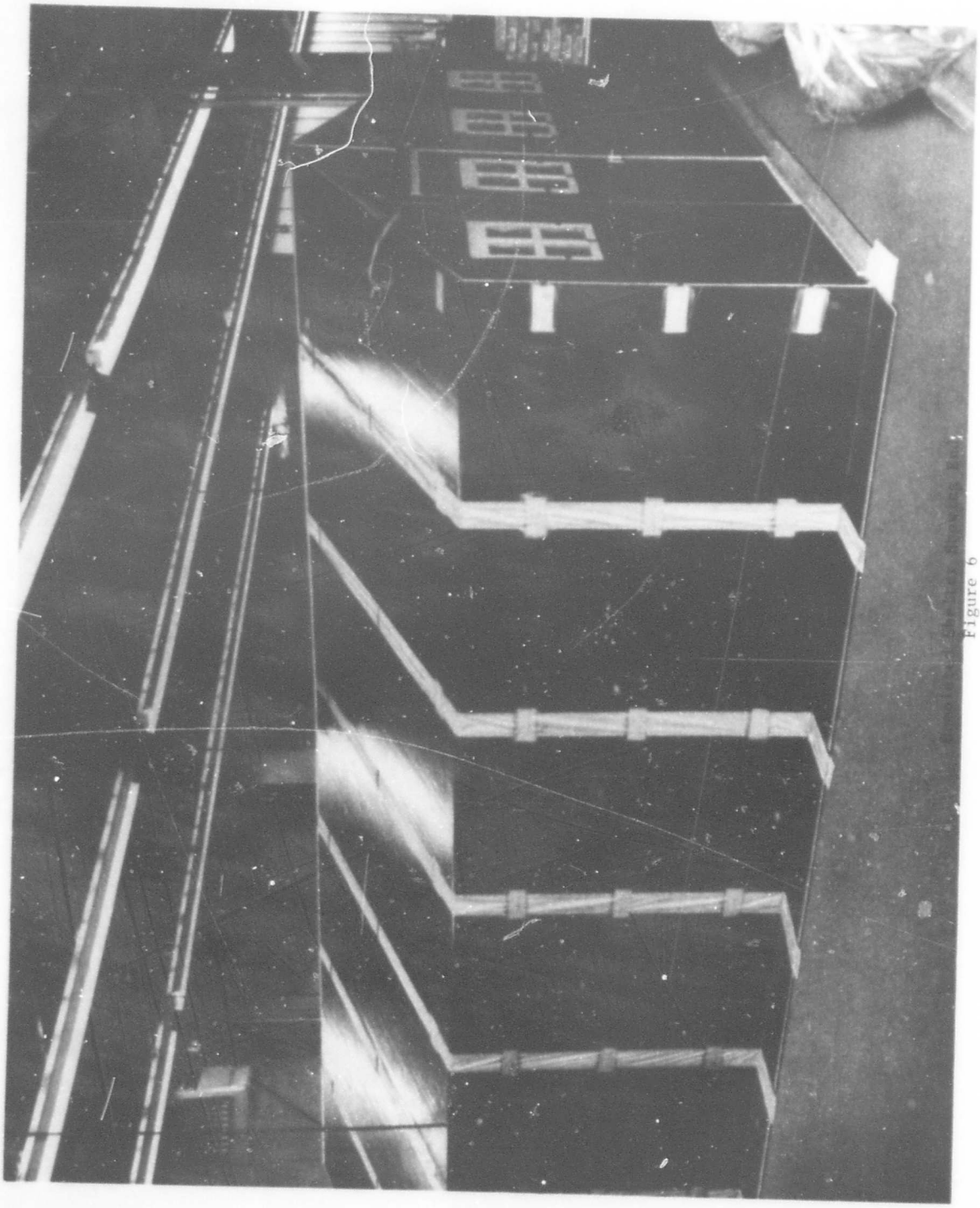

Figure 6

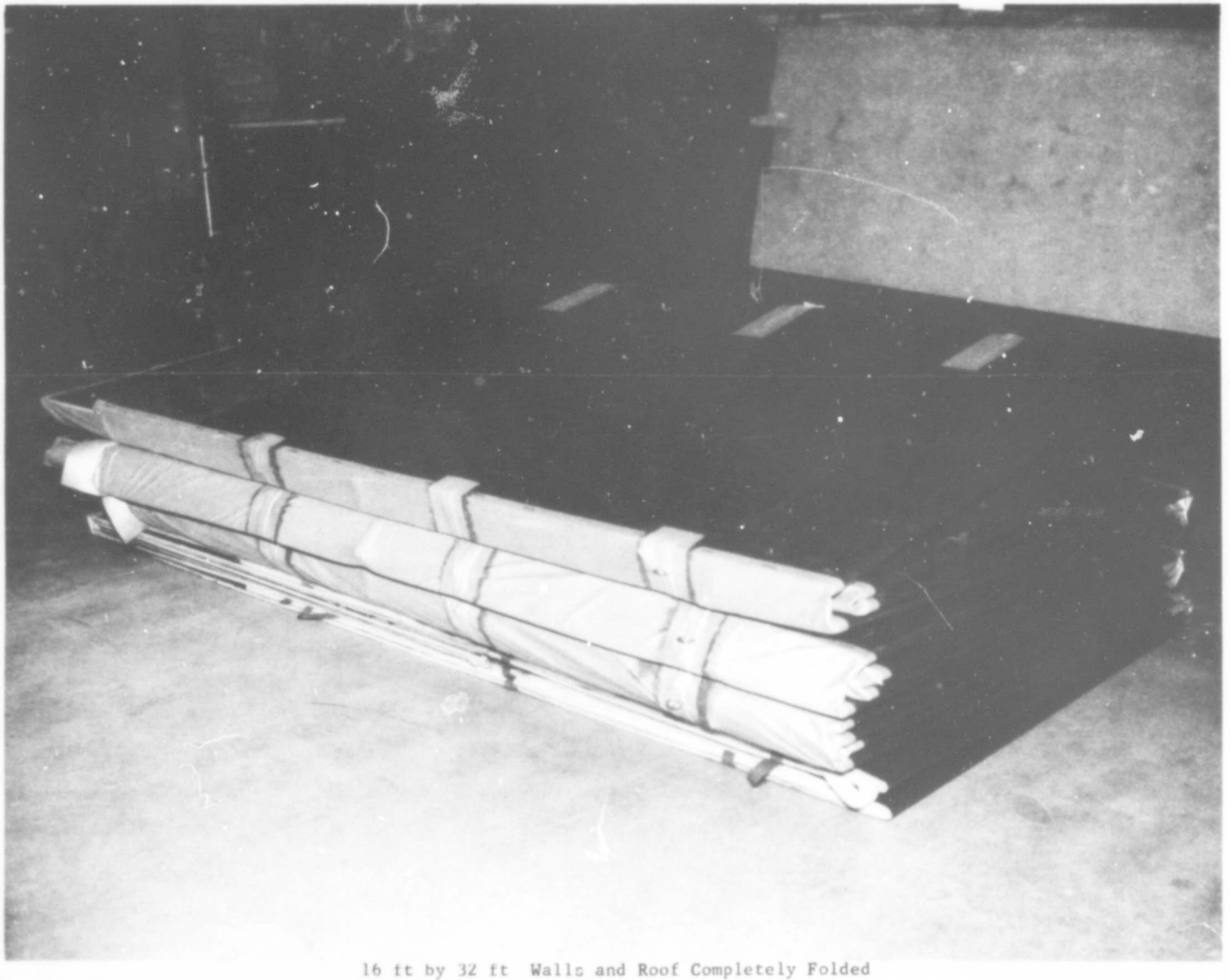

16 ft by 32 ft Walls and Roof Completely Folded
Figure 7

LIST OF SYMBOLS

a = length of the smaller side of the panel

b = length of the larger side of the panel

D = flexural plate rigidity

E = modulus of elasticity of the material

H = horizontal reaction at the bottom of the frame

h = thickness of the plate

I = moment of inertia of the section about the axis of bending

M = bending moment

m = bending moment caused by redundant load

q = intensity of superimposed load

V = vertical reaction at the bottom of the frame

W = deflection in the panel

w = load intensity on the frame

α = a constant that depends on aspect ratio of the plate

β = a constant that depends on aspect ratio of the plate

σ = bending stress

ds = infinitesimal length along the frame

dx = infinitesimal length along X-axis

dy = infinitesimal length along Y-axis

References

1. Expandable Space Structures by L.J. Boler and J.S. Tandon
   International Conference on Space Structures 1966, London, England

2. Statically Indeterminate Structures by Paul Andersen
   The Ronald Press Company, New York 1953

3. Theory of Plates and Shells by Timoshenko & Woinowsky-Krieger
   McGraw Hill Book Company, 1959

BLANK PAGE

EXPANDABLE WING TANKS FOR AIRCRAFT

Presented

by

I. O. Salyer,

J. L. Schwendeman,

C. J. North of

Monsanto Research Corporation

A. Zappanti, Capt. USAF,

Aero Propulsion Laboratory

A. Olevitch of

Air Force Materials Laboratory

R. S. Ross of

Goodyear Aerospace Corporation

I. INTRODUCTION

The importance of expandable structures is well known to workers in the aerospace industry. Many types of expandable structures are now being developed by the Air Force, NASA, the Army, and the Navy. The majority of the expandable systems have been primarily aimed at attaining structures for space applications, where the essential requirement is that the material be light in weight and flexible, so that it can be folded into a very small space and then deployed and rigidized in the vacuum of space. However, many expandable structures are used in earth environments such as balloons, life rafts, and shelters.

A review of the work done in expandable, rigidizable structures reveals that the approaches usually involve either (a) telescoping mechanically unfolding devices, (b) physical chemical or, (c) chemical rigidization systems.

In the case of physical chemical and chemical rigidization systems, research has centered on using a plasticizer or solvent to flexibilize a normally stiff resin, and then allow the resin to become rigid again through evaporation of the plasticizer. The rigidization by plasticizer boil-off is probably best illustrated by the water-plasticized gelatin system in which the plasticizer can also supply the pressure needed to deploy the structure in a space environment. However, for space applications,

the plasticizer evaporation mechanism carries with it the penalty of the extra weight of the volatile plasticizer, which must be boosted into orbit but is lost during rigidization and contributes nothing to the strength of the final structure. To overcome this limitation of plasticized resins, Monsanto Research Corporation is also investigating a polymerizable plasticizer rigidization system.

Other approaches have used a chemical reaction to accomplish rigidization by polymerization. The polymers employed in the polymerization-rigidization approach normally have been of the thermosetting type and include urethanes, epoxies, and polyfunctional vinyls. Vapor phase catalysts, heat, and ultraviolet radiation have been used to activate the chemical reaction to convert the monomer, or prepolymer, into a rigid resin. The chemically reacting, thermosetting rigidization systems are usually irreversible, so that once the structure has been deployed it cannot be folded and subsequently redeployed at another site. The chemical reaction rigidization process may also be adapted to simultaneously generate a foam for applications where the insulation or other special properties of foams are required.

This discussion presents a new concept for making expandable, self-rigidizable structures which differs in several ways from those cited above. It was originated by Monsanto Research

Corporation and developed under Air Force contract; patent applications on both the process and product have been filed. The process makes use of the reversible change of state from a rigid glass to a rubber which occurs when amorphous, lightly crosslinked, thermosetting polymers are heated to above their second order transition and subsequently cooled to below it.

In this process the structure is heated to the point of flexibility, deployed by a low pressure, inflating gas, and rigidized automatically by cooling - in any environment where the temperature is below the glass transition temperature of the polymer. Furthermore, by suitable "tailoring" of the components which make up the polymer chain, the glass transition can be shifted to any desired temperature range which is below the temperature at which the polymer begins to undergo spontaneous thermal decomposition. For greater strength the resins used in this second order transition system can be advantageously disposed on reinforcing substrate materials, such as glass cloth, and fabricated into laminate composites by conventional processing techniques.

To describe the phenomenon of recoverable elasticity which occurs when lightly crosslinked, rigid, thermosetting polymers are heated to above their glass transition, we have selected the term "thermoelasticity." This term distinguishes the process

from the more familiar thermoplastic deformation where melt flow occurs and the deformation is not recoverable. The term thermoelasticity also differentiates this process from the true rubbers, which are already above the glass transition and elastic at use temperatures. We have named the products which are capable of reversible, rigid, and rubbery behavior by temperature cycling alone (and which are rigid at ordinary use temperatures), 'thermoelastomers' or thermorubbers.' Either of these terms is descriptive of the behavior of this new class of materials.

The feasibility of the thermoelastic system for making aircraft prototype wing tanks was investigated under Air Force contract AF 33(615)-1484. To our knowledge this is the first time that flexible, self-rigidizable structures have been proposed for aircraft wing tanks. The results obtained in this feasibility study, which are being reported here today, are to continue through a follow-on contract to make full-scale, expandable wing tanks for the F-5A and F-5B aircraft. The results obtained in the feasibility study and some of the design concepts for the full-size wing tanks are reported herein.

The question arises, 'Why turn to a relatively exotic approach for a rather prosaic piece of hardware?" To answer this question we must examine in some detail how the present metal fuel tanks are make, as illustrated schematically in Figure 1.

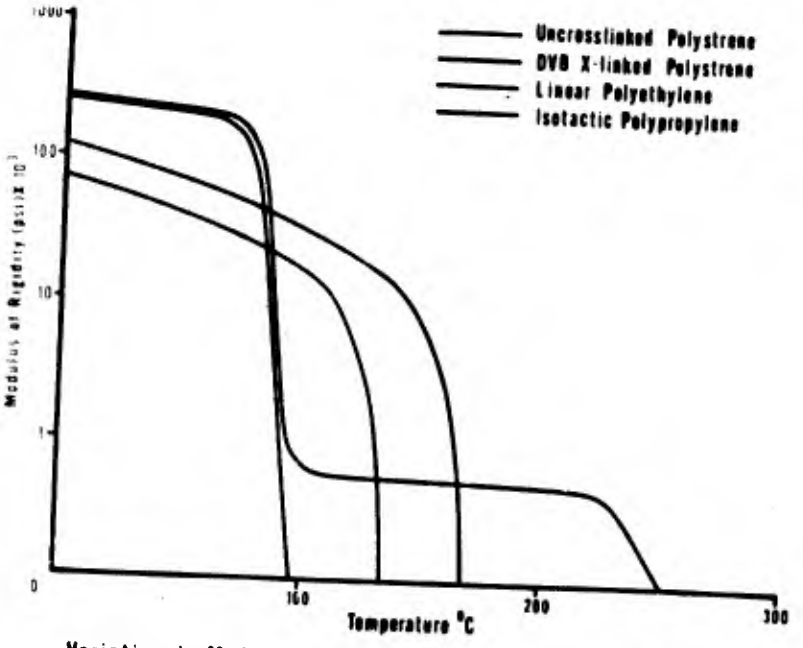

Variation in Modulus of Polymers with Temperature

Presently such tanks are made of aluminum and designed to be shipped and stored disassembled.

These component parts are nested, that is. nose and tail sections are stacked one-in-another. The center section pieces are similarly stacked, one section in the other. Numerous small parts and the beam and sway brace unit are assembled into a separate, so-called small parts pack. In this way one can achieve nestability as shown in Figure 2. In the package volume occupied by one assembled tank one can ship and store up to 10 disassembled tanks, or, in other words, achieve a nesting ratio of 10 to 1. Nestability thus offers advantages in reduced shipping costs and reduced storage space.

Significant disadvantages for the metal tank exist, however. Labor is required to assemble the tanks and often it is difficult to do this properly with relatively unskilled personnel. Because of the disassembly feature more seals are required and these have a limited shelf life (5 years) and must be replaced. This is especially costly in the case of assembled tanks stored in reserve. These tanks have to be disassembled, the seals replaced, and the tanks reassembled. For the F-100 series aircraft tanks, the total materials and maintenance costs for five years of seal replacement is $37,300,000. Any concept which reduces the number of seals will result in substantial reduction of these costs. Assembly times for these nested tanks vary with the size but can be as

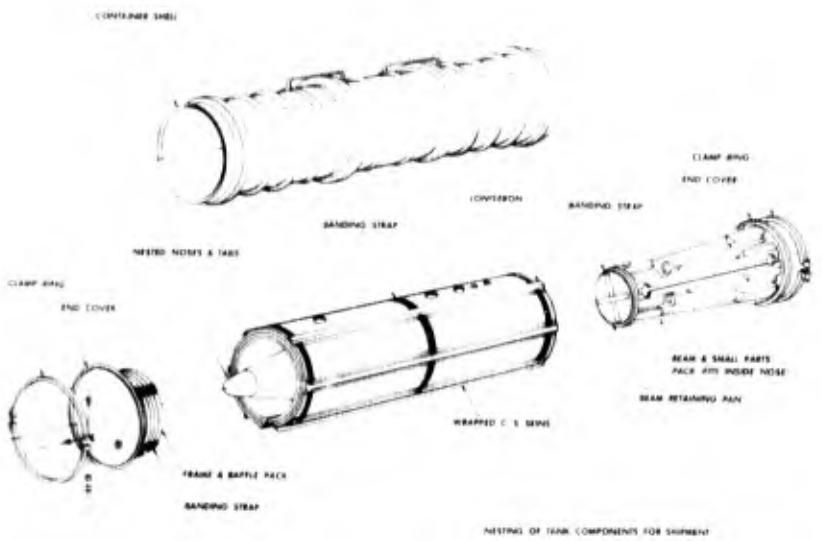

NESTING OF TANK COMPONENTS FOR SHIPMENT

little as 1 manhour per tank, provided that all necessary tools are available and experienced personnel are used. However , 1 manhour assembly is not usually attained, and usual assembly times are on the order of 5 to 20 manhours per tank. When unskilled personnel are used in field assembly, leakage is also encountered in an objectionable number of tanks. Since the total number of tanks for the F-100 series of fighter aircraft is in the many tens of thousands, the total labor figure per year is quite high.

Therefore, another approach is being investigated, one which achieves nestability and at the same time reduces or eliminates assembly time and costs and maintenance. The concept to be discussed herein, a reinforced, expandable thermoelastic tank, has the potential of achieving these goals. The following discussion describes work demonstrating the feasibility of this approach, the possible materials, fabrication techniques, design concepts, and a scheduled program to further exploit this system in full-scale wing tanks.

II. EXPERIMENTAL APPROACH

A. RESIN SELECTION AND DEVELOPMENT

The resin system for making flexible, deployable, self-rigidizing structures using the phenomenon of thermoelasticity should have several properties in addition to the ability to become flexible when heated. Ideally, the physical properties should be fully and completely comparable to those of other polymers used for making high-performance laminates. The principal resin requirements are summarized in Figure 3.

The prime requirement is that the resin should be in the glassy state over the range of temperature wherein it is desired that the structure be rigid, form stable, and strong. In the rigid state, the base resin should have physical strength properties which approach or equal those of the best binder resins now used in other composite laminates.

The transition from the rigid to the rubbery state must occur at a temperature which is (a) above the use temperature and (b) below the decomposition temperature of the polymer.

The transition from the rigid to the rubbery state should be reasonably sharp and take place over a relatively narrow range of temperature, e.g., 20°C. Thus, by heating a few degrees above

RESIN SYSTEM REQUIREMENTS

1. GLASSY STATE AT USE TEMPERATURE
2. TRANSITION ABOVE USE AND BELOW DECOMPOSITION TEMPERATURE
3. TRANSITION ZONE MUST BE NARROW – eg. 20°C
4. NON-TACKY RUBBER STATE
5. ADAPTABLE TO FIBROUS CLOTH REINFORCEMENT
6. CONVENTIONAL PROCESSING TECHNIQUES
7. ENVIRONMENTAL RESISTANCE

the glass transition temperature the material will become very rubbery and can be folded or deployed upon cooling a few degrees below the transition, it will immediately set up and become rigid.

In the rubbery state the resin must not become tacky, must be foldable without cracking, and must have sufficient strength so that it can be handled and deployed.

The resin system should be suitable for application to reinforcing substrate materials such as glass or organic fiber cloth.

The processing of the resin and reinforcing substrate system should be adaptable to ordinary vacuum bagging or other established fabricating techniques.

The rigidized resin system should have satisfactory resistance to chemicals, fuels, and other environmental factors to which the structures will be exposed.

The resins examined in this study fell into one of two broad, general classifications - thermoplastic and thermosetting.

Until recently, it was very simple to distinguish between a thermoplastic and thermosetting polymer. Thermoplastic resins were limited largely to plasticized cellulose esters, polystyrene, and polyvinyl chloride. Thermosets consisted principally of phenol formaldehyde, urea formaldehyde, and melamines.

However, there are now available on the market in this country more than 2,000 commercial resins and at least 200 major chemical types. Furthermore, the classification of any particular chemical type of resin as belonging to the thermoset or thermoplastic category has almost entirely lost its meaning. Several of the thermoplastic types can be modified or tailored to be thermoset, and many of the thermosetting resins can be modified or tailored to be thermoplastic. Accordingly, for purposes of this discussion, we shall classify as thermoplastic the polymers which are soluble, remoldable, and exhibit irreversible melt flow at temperatures above the second and first order transition under low pressure.

The thermosetting materials are those which are insoluble and do not exhibit melt flow under relatively low pressure at any temperature below the thermal decomposition point. By this definition, thermoplastic and thermosetting materials represent two different extremes in degree of crosslinking.

Thermoelastic rubbers fall between these extremes. Although insoluble, they may swell highly in specific solvents but still do not exhibit viscous flow under low shear stress at temperatures below the thermal decomposition temperature. Those new materials differ from conventional vulcanized rubbers in that they are rigid at use temperatures whereas the conventional rubbers by definition are elastic at use temperature.

1. INVESTIGATION OF THERMOPLASTIC RESINS

The thermoplastic resins examined in our study included, among others, the following types, as shown in Figure 4.

The modulus characteristics of these thermoplastic resins were determined using the method of Clash-Berg as described in ASTM D 1043-61T. Characteristic curves of modulus vs. temperature for some of these polymers are shown in Figure 5. From the Clash-Berg modulus curves, it was observed that the temperature modulus characteristics of these thermoplastic polymers fall into two distinct categories.

The crystalline materials such as polypropylene and polyethylene have very broad transition regions with gradual and progressive decreases in modulus up to just below the 1° transition or crystalline melting point. These crystalline polymers (and other highly crystalline ones not included here) were deemed unsuitable for our expandable structure application since they did not meet two of the specified prime requirements: (1) conversion from a highly rigid to a very rubbery material over a narrow temperature range, and (2) high strength and high modulus over the anticipated military use range (-65 to +165°F).

The broad, gradual transition of the crystalline materials is clearly evident as are the generally higher modulus and melting point of crystalline polypropylene compared to high-density polyethylene.

Polystyrene
(Lustrex HH101)

Styrene acrylonitrile Copolymers
(Lustran A-11)

Acrylonitrile butadiene styrene
graft copolymers
(Lustran I)

Polyvinyl chloride
(Opalon 300)

Polypropylene
(HiFax)

High density polyethylene
(Marlex 6001)

Polymethyl methacrylate
(Lucite 140)

Polycarbonate
(Merlon M-60)

Polyphenylene oxide
(GE – PPO)

Thermoplastic Aromatic
Polyether
(Phenoxy PRDA 8060)

THERMOPLASTIC RESINS EVALUATED

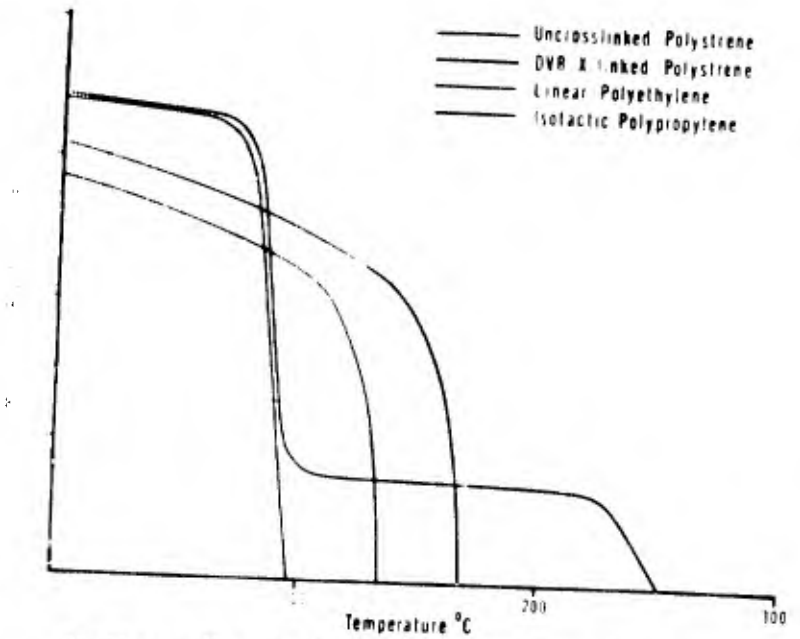

Variation in Modulus of Polymers with Temperature

The amorphous thermoplastics such as polystyrene, polymethyl methacrylate, and the styrene/acrylonitrile copolymers have a relatively high glass transition temperature and also soften abruptly over a very narrow range of temperature (20°C). Since they contain no crystalline phase, the modulus of these thermoplastic polymers is very low at temperatures above the 2° or glass transition.

Above the glass transition temperature the thermoplastic materials simply soften progressively until they become very low viscosity materials at temperatures of 50 - 100°C above the second order transition. Vulcanization of these resins would, of course, eliminate the extensive softening and decrease in viscosity above the glass transition, as indicated by the curve for divinyl benzene-crosslinked polystyrene.

Some of the temperature modulus data on thermoplastics obtained from the Clash-Berg tests are shown numerically in Figure 6.

A composite model tank of 181E-A1100 glass cloth, impregnated with Phenoxy PRDA 8060 thermoplastic resin, is shown in Figure 7.

A second model structure using integral electrical resistant heating wires is shown in the deployed configuration, Figure 8.

N.B.P	Materials	Type of Sample	Clash-Berg Data			
			T_F °C	$T_{675\ psi}$ °C	SR[a] °C	25° Mod psi
346-1	Lustran I (761)	Solid Molding	87	112	25	110,000
346-2	Lustran I (710)	Solid Molding	82.5	107.5	25	100,000
346-3	Lustran AII (2020)	Solid Molding	96.0	108	12	170,000
346-4	Lucite 140	Solid Molding	87	113	26	165,000
346-5	Phenoxy PRDA (8060)	Solid Molding	88	101	13	130,000
346-6	Hercules Polypropylene (6523)	Solid Molding	67	166	99	140,000
346-7	Monsanto Polyethylene (935)	Solid Molding	-22.5	96	115.5	115,000
346-8	Marlex (6015)	Solid Molding	36	132	92	160,000

CLASH-BERG MODULUS DATA OF SELECTED THERMOPLASTIC RESINS

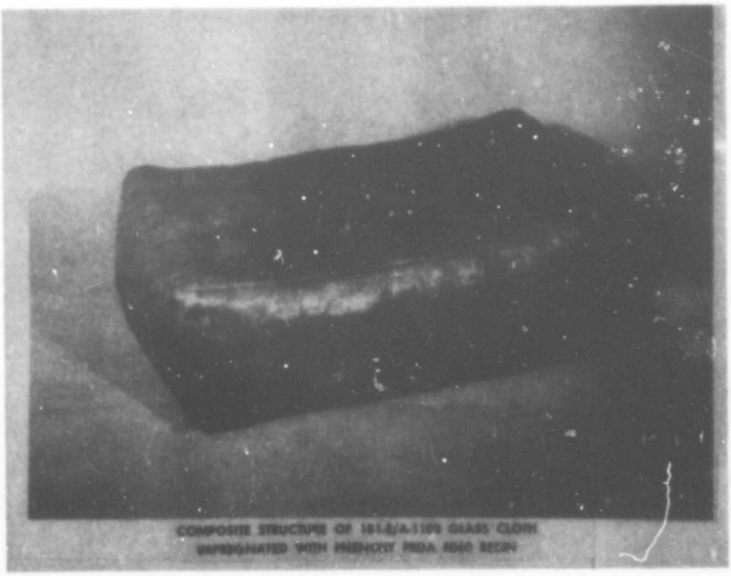

COMPOSITE STRUCTURE OF 181-E/A-1109 GLASS CLOTH
IMPREGNATED WITH FIBERITE PRDA 8060 RESIN

STRUCTURES WITH INTEGRAL HEATING WIRES (DEPLOYED)

However, after preliminary evaluation, including building model structures, the investigation of the truly thermoplastic polymers was discontinued for two reasons. They were difficult to process, and the stickiness of the resins (even without solvents) suggested that if in actual application the product should be substantially overheated, welding of the thermoplastic components into a fused mass could occur.

For these reasons we abandoned the investigation of true thermoplastic materials at an early stage and turned to thermosetting resins to avoid these difficulties.

2. THERMOSETTING RESINS

The work on thermosetting resins for the expandable wing tank prototype was limited to a study of epoxies with various types and amounts of curing agents. In the case of epoxies, the use of the term curing agent is probably a misnomer since the curing agents used (polyfunctional amines, anhydrides, phenols, etc.) are in reality comonomers used in stoichiometric amounts equal to that of the starting epoxy resin.

The choice of epoxies was dictated by the excellent established properties of this resin system in laminate and composite applications, good adhesion to the probable reinforcing substrate materials which we were considering (glass and/or nylon cloth),

and our own experience which had indicated that it was quite possible to make thermosetting epoxies which will show a very pronounced thermoelastic transition. The Clash-Berg modulus curve of Epon 828 cures with bis(hexamethylene triamine) (BHTA) illustrating this point in shown in Figure 9.

It is not surprising that epoxies as well as other thermosetting polymers show a more or less pronounced heat distortion or second order transition below the thermal decomposition temperature. It is a well-known limitation of several commercial epoxy systems that the heat distortion temperature is too low for some applications.

After evaluating several combinations of amines, anhydrides, diphenols, polyphenols, and amide curing agents with various epoxy resins (especially Epon 828 and Epon 1031), it was found that a resins meeting most of the requirements for the wing tank structures could be made from Epon 828 cured with less than the stoichiometric amount of Curing Agent Z (a mixture of isomers of phenylene diamine). It was learned that Curing Agent Z produced flexible castings or laminates at temperatures above 100°C when about 2/3 of the stoichiometric quantity of this curing agent was used. At 50% of the stoichiometric amount of amine, the castings were tacky at 100°C. With 100% of the theoretical amount, a definite heat distortion was still obtained at about 100°C but the modulus was much too high to permit ready folding.

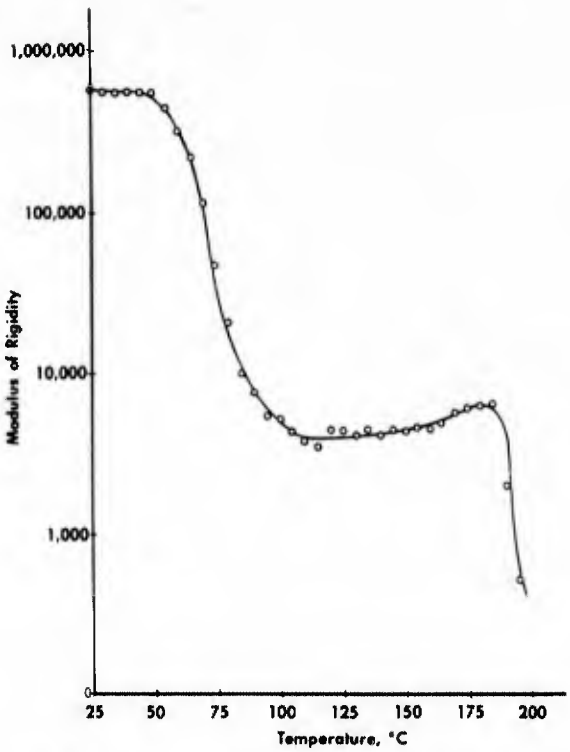

CLASH-BERG MODULUS VERSUS TEMPERATURE, EPON 828 CURED WITH BIS (HEXAMETHYLENE) TRIAMINE

Resins made with Epon 828 and 62.5% of the stoichiometric amount of Curing Agent Z are quite rigid and strong at room temperature and retained considerable strength when heated to flexibilize. Qualitatively, these resins and laminates made from them appear to be superior to the other systems tested.

It was decided to concentrate on this resin system for building subscale prototype tanks.

B. SUBSTRATE SELECTION

1. Type of Reinforcing Substrate

Our work on the selection of a suitable reinforcing substrate for building a prototype wing tank was concentrated almost entirely on various types, weights, and weaves of glass cloth for an obvious reason. It is one of the strongest, high modulus reinforcing materials commercially available at reasonable cost, and has proven performance in composite applications. Coast Manufacturing Company's 2P122 glass cloth was picked as the primary substrate material for early work based on its acceptable flexural strength and its good drapability (draped over a 2-inch square ended bar). The various substrates investigated and their properties are given in Table 1.

Nylon cloth and combinations of nylon cloth with glass cloth were also given preliminary evaluation. On the basis solely of

Table 1

SUBSTRATE PROPERTIES

Manufacturer of Fabric	Fabric Identification	Properties in Tension (1) Elongation - inch	Strength lbs/ply	Flexural Strength (2) (psi) Parallel to Fill	Parallel to Warp
Coast Mfg. Co.	2B104 38 F16	1.256	124	5[illegible],300	59,700
" " "	2S133 38 F39	1.445	22	54,500	58,400
" " "	2P122 60 16M	1.197	16	56,800	61,700
" " "	2S181 44 F15	1.18	68	74,000	66,500
" " "	2P128 38	1.21	47	5[illegible],500	54,900
" " "	1P28 F16	1.37	46	52,800	51,200
Stevens	27520 S 920	1.74	32	126,000	22,000
"	Polyglass(Dacron & Glass)	1.54	7	19,400	42,800
"	27184 1557-38 S 920	0.55	6	127,800	31,800
"	112-38-6 4639 27329	1.91	44	59,200	59,300
"	1674/38 4654	1.66	26	46,100	50,900
"	181-38-17(501)3326 Volan 2319	1.25	101	70,900	72,700
Uniglass	192/38 Volan	1.80	20	64,700	60,000
"	3528/38 Volan M M 619	1.35	45	69,000	61,800
Lamports	Nylon 1067 SHS(2 oz/yd)	2.95	144	11,500	10,800

(1) Run on 2"x 6" strips of cloth cut on the bias (single ply of cloth supported by single ply of masking tape).

(2) Run using Epon 828 resin cured with Tetraethylenepentamine (stoichiometric amount)

tensile strength and elongation of the cloth, nylon is a promising material. However, the relatively low flexural strength of nylon laminates mitigates heavily against its use in the wing tank prototypes. The lower modulus of nylon may be a definite asset in a foldable structure and, accordingly, combinations of nylon with glass cloth were tested. As indicated previously, the glass cloth was Coast Manufacturing Company 2P122 glass. The nylon was Lamports 1067 HS cloth.

Room and elevated (100°C) temperature flexural strength of glass and glass/nylon laminates of Epon 828 cured with 62.5% of Curing Agent Z are shown in Figure 10. The lower modulus of glass/nylon composites is noteworthy.

2. Glass Finish

In the case of the glass cloth to be used with an epoxy binder, it was considered that any of the standard glass finishes such as A-1100 or Volan A should provide adequate resin-to-glass bonding and wet strength.

3. Ply Orientation

Four types of ply or layer orientation are possible:

(a) parallel to center line

(b) angle to center line

(c) 90° to center line

(d) at random

Curing Agent	Stoichiometry	Substrate	Temperature °C	Flexural Strength (psi)	Flexural Modulus (psi)
Epon Curing Agent Z	1.0/0.625	2P122 Glass	RT	52,300	2.5×10^6
			50		1.6×10^6
			75		1.3×10^6
			100		1×10^6
Epon Curing Agent Z	1.0/0.625	Alternate plies 2P122 glass and Nylon	RT	37,500	1.4×10^6
			50		1.6×10^6
			75		0.6×10^6
			100		0.5×10^6

MECHANICAL PROPERTIES OF THERMOELASTIC EPON 828 RESINS

Of these four, only tank sections with ply orientation parallel to the center line folded well. For this type of structure tape wrapping was considered to be the type of ply orientation most likely to succeed. Regular Helical (figure eight) filament winding was tried but appeared unpromising from the standpoint of foldability.

4. Fiber Orientation

Of the three types of fiber orientation (warp and fill, bias, and random), bias orientation appeared to offer a high probability for successful folding. In bias tape the fibers can reorientate themselves under stress as shown in Figure 11. In a rubbery matrix such as is obtained in thermoelastomers at elevated temperature, fiber reorientation of the type illustrated should occur.

C. PROBLEMS IN FOLDING A THERMOELASTIC WING TANK

Even when using resins that are flexible at elevated temperature (100-120°C) it doesn't necessarily follow that glass cloth laminates made from them will also be flexible. This is especially true in laminates made with relatively low resin content. The inflexibility in the low resin content laminates is accordingly attributed entirely to the high modulus of the substrate.

Two factors, either alone or in combination, may contribute to the rigidity of thermoelastic laminates made with glass cloth or other high-modulus fibrous reinforcing material.

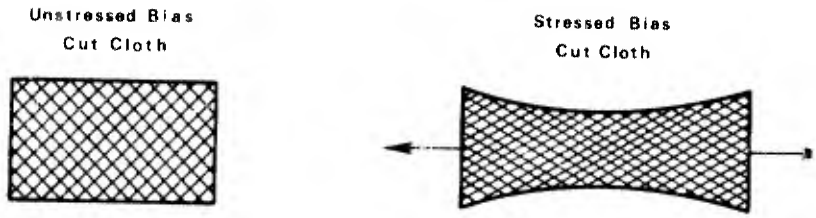

Fiber Reorientation Under Longitudinal Stress

The first of these is the high modulus of the glass (or of the fiber itself) which restricts bending. Additionally, in a highly compact, dense laminate the plies of glass cloth are interlocked, so that movement of one ply over another is prevented.

Second, the geometry of the wing tank contributes to difficulties in folding. As shown earlier, the tank is in essence a cylindrical section enclosed at each end with elongated, conical end pieces. Neither the cylindrical nor the conical sections, when separated from each other, present problems in folding. However, when joined together as in the completed tank, folding presents real problems in that a two-dimensional change in the geometry of the section is involved.

Figure 12 shows a plan view of a deployed tank ("a") and what happens to the three geometric sections of the tank when it is flattened ("b"). It will be noted that the cylindrical section flattens to a rectangular shape, whereas the two conical end sections become sector shaped pieces. In folding the corners, the sectors are displaced a considerable distance from the corners of the flattened cylindrical portions in the model. However, this displacement is prevented in the actual tank, as the conical ends are integral with the central cylinder. Thus in folding the tank, high stresses are generated which could cause the tank to tear itself apart at the juncture of the conical and central cylinder sections, unless the stresses can be relieved by wrinkling or dimpling of the tank walls.

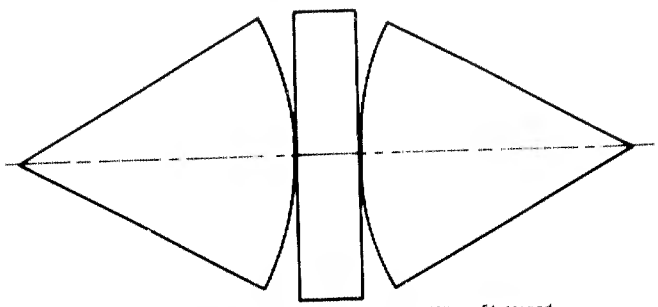

Configuration Sections of Structure When Flattened

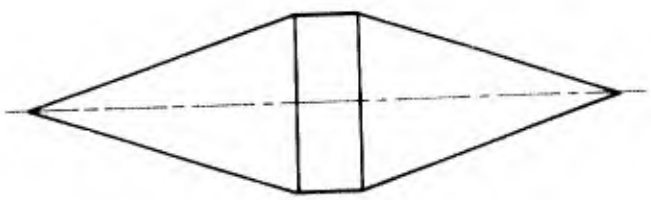

Deployed Structure

Strains Caused by Folding In a Conical End Model Wing Tank

From the above it can be seen that any design for a foldable, self-rigidizable wing tank must be a compromise between a composite which produces laminates of good strength, and the design factors which will enable the tank in its finished form to be folded. The considerations of strength, foldability, and geometry indicated certain methods of construction, type, and orientation of substrate.

D. FABRICATION OF SUBSCALE MODEL TANKS

Several different types of mandrels were tried including plaster mandrels, polystyrene foam mandrels, metal male mandrels, and wooden male mandrels. Of these mandrels the one most extensively investigated was the cast plaster male mandrel, which was subsequently removed by break-out or wash-out.

Three methods of fabrication were evaluated: tape wrapping, filament winding, and hand lay-up of gores on a male mandrel. Compression molding in matched metal molds and blow molding were considered but no actual work was done on these methods.

Most of the work on subscale model tanks was on 1/4 scale configurations which were either (a) filament wound or hand laid-up tanks on metal mandrels, or (b) gore lay-ups on wash-out plaster type mandrels. Although some work was also done on the models built on a male metal mandrel, this approach was subsequently abandoned. It was felt that sealing or otherwise joining together

the separate sections of the tank, necessitated by the use of a male metal mandrel, would tend to defeat the foldability. Accordingly, all later work concentrated on gore lay-ups of resin-impregnated glass cloth on plaster wash-out male mandrels.

Bias cut tape wrapping still appears to be a desirable method of fabricating the tank. However, it was only briefly examined because of the lack of suitable tape wrapping equipment.

One filament-wound tank was built and tested but found not to fold readily. The bulk of the work was concentrated on gore lay-up of glass and/or nylon cloth on washout-removable plaster mandrels.

A finished plaster mandrel is shown in Figure 13. In addition, in order to further simplify the fabrication, a half-male mandrel was constructed from which gore lay-ups could be made to produce half-tank sections which could then be assembled. This method was not as satisfactory as the removable plaster mandrel since tank assembly and sealing problems were still involved.

Several model tanks were then build with the removable plaster mandrels, cured, then heated, folded, and redeployed several times. Some of these model tanks in both the folded and redeployed state are shown in Figure 14.

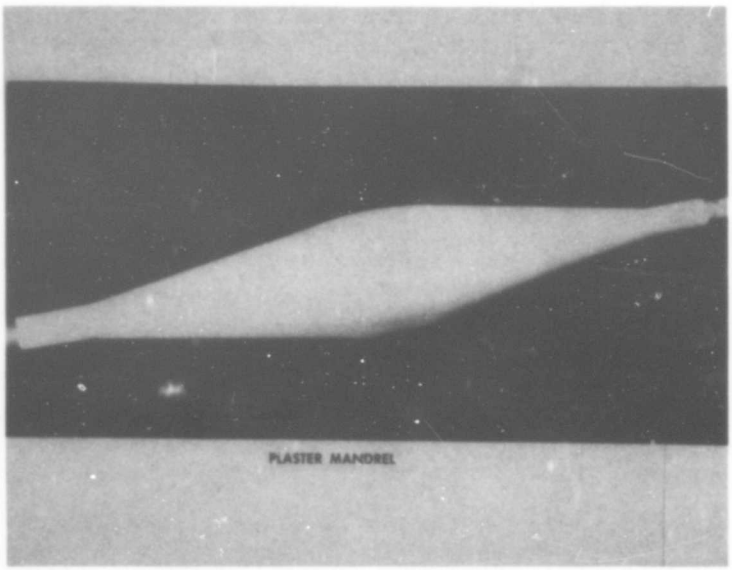
PLASTER MANDREL

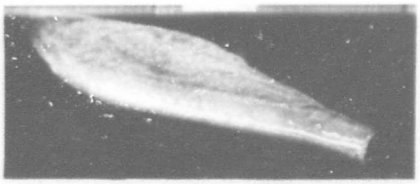

FOLDED IN PRESS

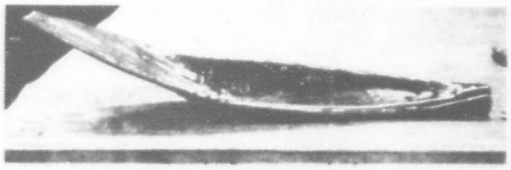

FOLDED UNDER VACUUM

REDEPLOYED AFTER VACUUM COLLAPSE

TANK NO. 2

A partial vacuum (Figure 14) was also used in some cases to aid folding, while in others simple hand pressure or a compression molding press was used. The collapsing of a tank under hand pressure is shown in Figure 15. Figure 16 shows the tanks after collapse, and Figure 17 shows the tank after it was redeployed.

III. CONCLUSIONS

The Air Force-sponsored research presented here today has shown feasibility for the use of the phenomenon of thermoelasticity to fabricate flexible, self-rigidizable structures which are reversibly rigid or flexible, depending upon temperature alone, and can be tailored to be rigid within specified temperature ranges.

Specifically, this phase of the program, as detailed in the reference (Final Report, AF 33(615)-1384), demonstrated that a reversible, flexible, self-rigidizable, quarter-scale wing tank prototype could be made from lightly crosslinked thermoelastomers.

It was shown that a wide variety of reinforcing substrates could be used but the final choice of substrate would have to be a compromise between that which would allow optimum foldability and maximum strength. It was also demonstrated that the internal strain of a folding wing tank prototype could be relieved by dimpling or forming of recessions in the midsection of the tank.

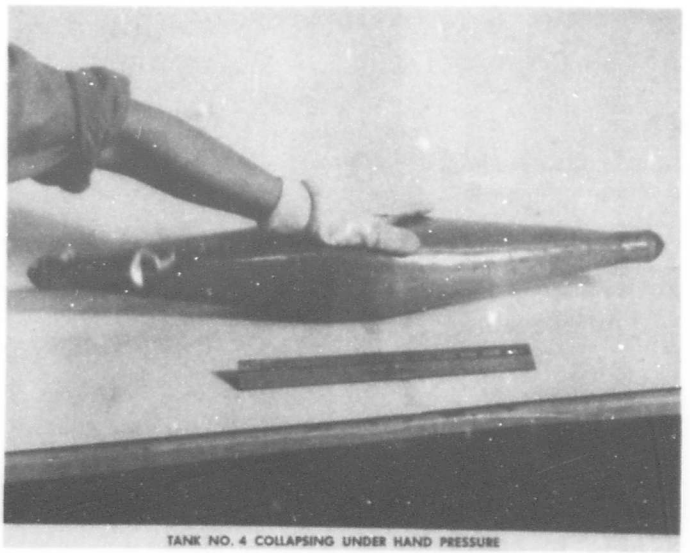

TANK NO. 4 COLLAPSING UNDER HAND PRESSURE

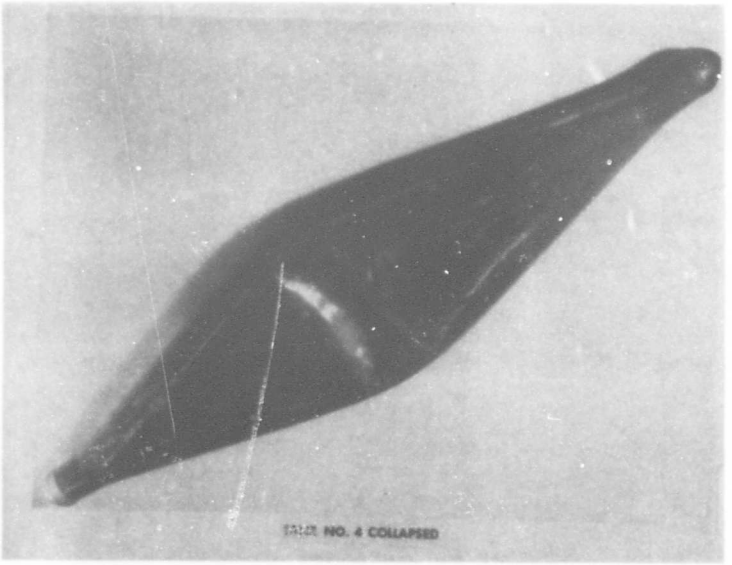

TAIL NO. 4 COLLAPSED

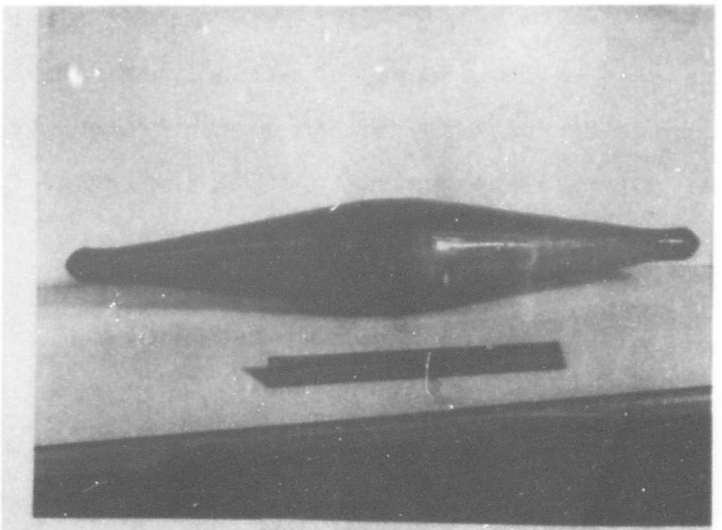

TANK NO. 4 REDEPLOYED

A follow-on program to design, construct and deliver to the Air Force two full-size wing tanks for the F-5A and F-5B aircraft is scheduled. Although the follow-on work has not yet gotten under way, it was felt that a review of the concepts for this type of thermoelastic wing tank would be of interest at this conference.

The thermoelastic process offers the following advantages:

Inherent Simplicity The flexibilizing and rigidizing process makes use of a basic property of all polymeric materials - the reversible change of state from glass to rubber (and back) which occurs when polymers are heated to above the second order transition and subsequently cooled.

High Reliability Since no complicated mechanical unfolding or chemical reaction is required, the thermoelastomer system should be highly reliable in flexibilizing, deploying, and rigidizing.

Storage Stability Storate stability of more than 1 year at ambient temperature has been demonstrated, and theoretically should be much longer.

Adaptability to Environment The second order transition thermoelastic system can be operated in a wide variety of earth and space environments, including arctic and tropic regions, humid and dry climates, and the vacuum of space.

Reversibility for Redeployment As noted earlier, the reaction is a completely reversible physical transformation and requires only that a heat source be available whenever it is desired to flexibilize the structure.

Reasonable and Predictable Power Requirement This system requires only the sensible heat to raise the temperature of the structure from ambient to above its second order transition temperature to render it flexible. For organic polymers, the amount of heat is about 1/2 calorie per gram or cc of material. Depending upon the specific application, the power required may be supplied by several different means. For example, electrical resistance heating wires may be used and can be made an integral part of the final structure and also contribute to the strength of the structure. A pyrotechnic heating device may also be used. In earth applications, ovens or heat from the exhaust of vehicles could be used for heating. For space applications, where available power may be minimal, most or all of the preheating could be accomplished on the ground immediately prior to launch.

Versatility of System Many uses for these thermoelastic products are foreseen as distinct possibilities, most of which would present less difficulties than does the wing tank. These include self-erecting shelters for remote stations of field military use; pipe (especially large pipe) which can be transported to the site in the compact folded form, deployed and rigidized; self-erecting antenna; individually formable casts for broken limbs, and expandable boats and emergy rescue aircraft for both military and civilian use. The boats and aircrafts would have the advantage of being able to withstand considerable damage (bullet holes) without collapsing.

I am sure your imagination can add many others.

BLANK PAGE

EXPANDABLE SHELTER/CONTAINER FOR BARE BASE

Adam W. Cormier *
&
David F. Ferree **

INTRODUCTION

The Air Force must be capable of deploying to trouble spots or areas of conflict anywhere in the world and initiating operations in support of interests and objectives of the United States. With the advent of in-flight refueling and higher performance aircraft, the operational capability of deployed fighters has been greatly increased. However, the full potential of this capability can only be realized if a suitable operational base is available where needed and is manned, equipped and supplied with the support needs of the deployed aircraft.

In recent years, there has been a tendency for tactical air power needs to arise in remote places, often in underdeveloped areas where suitable airfield and support capabilities do not exist. Further, fast developing events frequently make the time factor all important. Often the most effective application of this power is to arrive promptly enough to prevent a threaten conflict from breaking out. These requirements have emphasized the need for an air transportable, fast reacting support capability. To date this capability is lacking.

A clear need exists for new deployment packages greatly reduced in weight and volume with increased utility and operational capability to permit rapid activation of a bare base, facilitate its early build-up to full operational capability and support sustained operations thereafter. A program called the Bar Base Support System was initiated to achieve this capability.

A Bare Base is defined as a base having a runway of minimum length and width, constructed of matting or otherwise stabilized taxiways, parking areas, and having a source of water (see Figures 1 and 2).

There are two important requirements of the Bare Base concept; high efficiency of logistical support and temporary, mobile, hard wall maintenance and support facilities. This dual requirement is satisfied to some extent by the Expandable Shelter/Container (ES/C). The ES/C will be utilized as an aircraft/engine maintenance area and for other workshop and support functions.

* Project Engineer; Wright-Patterson AFB, Ohio
** Major, USAF; Langley AFB, Virginia

DESCRIPTION, CONTAINER MODE

The ES/C is a multi-purpose structure featuring two modes of operation with each mode satisfying a specific requirement of the Bare Base. In the container mode of operation, the ES/C will function as a transporter of cargo (see Figure 3). It will be compatible with the 463L Cargo Handling System wherein its base will be designed identical to the 463L pallet. This will allow the ES/C to be used with the automated loading system presently installed on the C-130 and C-141 aircraft. The ES/C will also be compatible with the M-689 ground transporter system, which is a four wheeled, pneumatic tired, two wheel towing transporter system. The ES/C will feature built-in attachments that will permit utilization with the M-689. In the container mode of operation, the structure will be approximately 13' long, 8'4" nigh and 8'4" wide (see Figure 4). A 13 foot long structure will allow shipment of three ES/C's in the C-130 or five ES/C's in the C-141. The maximum empty weight will be approximately 2000 lbs and will be designed to transport a maximum of 13,000 lbs of cargo. Maximum over-all design weight in the fully loaded condition will not exceed 15,000 lbs.

In the container mode the ES/C will be designed to accept Type II mobility requirements attached to the M-689 transporter. Type II mobility implies the structure will be towed over semi-prepared terrain with moderate slopes and small protrusions similar to what is considered as an unpaved country road. Although the M-689 transporter, as presently configured, has a maximum payload of 10,000 lbs, a growth potential to 15,000 lbs for Type II mobility is anticipated.

The ES/C will be designed to function operationally over a ten year period and provide service for five years. That is, its shelf life will be ten years in climatic zones with temperature regions from -25°F to 125°F and humidity from 0% to 100% relative humidity. It will have a service or use life of at least five years in similar environments with an average of six relocation cycles per year.

The container will have a minimum of 150 lbs/sq ft floor load capacity and will be equipped with internal, integral tie-down rings for securing the cargo. It is not intended that the cargo be restrained by the walls of the ES/C. The tie-downs will be secured in the floor/pallet section of the ES/C utilizing through-bolts or epoxy cement. When not in use, the tie-down eyes will be flush with the floor. They will be located around the inside perimeter of the container and will transmit load to the edge structure of the pallet floor.

The ES/C will utilize a double door to facilitate loading and unloading of cargo. It will be approximately 6'8" high and 7 feet wide, permitting a forklift to insert cargo into the structure. It will be located in one end wall, with both doors opening outward. The front door will also permit entry and exit of small hand carried items.

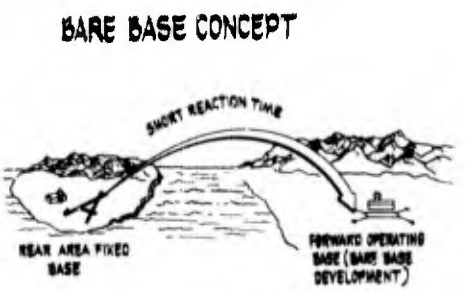

Figure 1

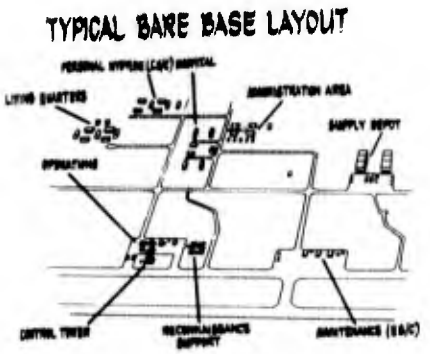

Figure 2

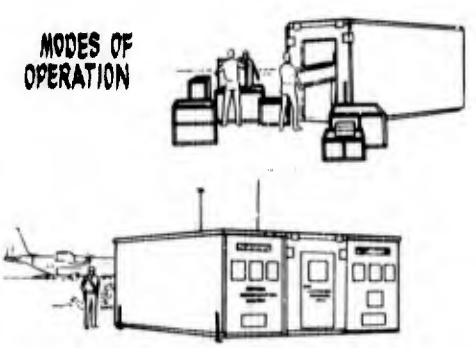

Figure 3

Although the ES/C will not be designed to conform to helicopter airlift requirements, it will have a capability of overhead lift by a crane. Because of the high payload capacity, the lifting eyes will be installed in the base of the structure. The base or pallet will also have the capability of accepting the 5 ton 463L forklift system.

It is expected a ground mobility system of some type, either M-689 forklift or crane will be available at the deployment site, but under wartime conditions this may not always be so. For this reason, the ES/C will be equipped with skids and towing attachment to permit relocation of the structure over short distances in either the forward or aft direction. The skids will not interfere with the 463L cargo system and will place the ES/C above ground to facilitate use of a forklift or M-689 mobility system. The skids will be designed to reduce shock transmitted to the structure in transport. Various modes of transportability are depicted in Figure 5.

The structure will be capable of being physically locked in all modes of operation and will be capable of deployment to the shelter mode of operation without removal of contents packaged in the container mode.

DESCRIPTION, SHELTER MODE

The shelter mode of operation of the ES/C satisfies the second basic requirement of the Bare Base concept, that is, providing hard wall housing to support various personnel functions. Personnel functions include workshop, hygiene, kitchen, and maintenance shop.

In the shelter configuration, the structure will be approximately 24 feet wide, 13 feet long and 8 feet 4 inches high (see Figure 6). An expansion ratio of roughly 3 to 1 is achieved. An expansion ratio of greater than this can be obtained but at a sacrifice in reduced container volume, increased weight and reduction in structural integrity in the shelter mode. The maximum expansion time will not exceed two manhours; refolding time will also require less than two manhours.

The ES/C in the shelter mode will be capable of withstanding 60 knots steady winds or 90 knots gust with guy wires. The roof system will support a minimum of 20 lbs/sq ft. The expandable floor will have a capacity of supporting no less than 80 lbs/sq ft.

The over-all coefficient of heat transfer for the shelter with all doors and windows closed will not exceed 0.35 BTU/hour ft^2F^o. The ES/C will be designed so that standard government stocked heating and air-conditioning equipment may be integrated into the structure.

Available window and vent areas are vital to shelters being utilized for human occupancy. Windows will be capable of being blacked out and vents will have screens and reusable dust filters and will provide rain protection when opened. Screens and filters will have an integral storage capability when not in use. The vents will provide enough ventilation to assure a minimum of eight air changes per hour in 3 to 5 mile per hour winds. The windows will provide a minimum light level of twenty foot cables on an overcast day.

Figure 4

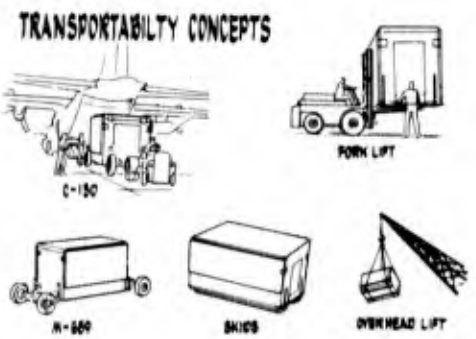

Figure 5

Figure 6

At least two personnel doors will be provided. These are the same doors described previously in the Container Mode section of this paper. The doors will have windows installed and will be capable of being locked from within or from the outside.

The shelter will be equipped with integral wiring and lighting. All wiring and switches are to be concealed in or imbedded into the wall. Sufficient lighting will be available to provide at least 100 foot candles at working levels. Exterior lights will be provided at each doorway. The electrical circuitry will have a minimum of eight outlets with four outlets having a 220 volt 3 phase capability with a total capacity of 40 amps. An exterior quick disconnect capability for grounded three phase 110/220 volt service also will be provided.

The walls of the shelter will be capable of supporting roof loads, and equipment loads suspended from the walls. The walls will support a shelf load of 100 lbs per linear foot. Shelf attachment will be similar to tiedown lugs and will be either through-the-wall bolt type or bolt insert attachment embedded in epoxy. The system used will depend upon the material and fabrication technique employed.

The shelter will be provided with telephone and intercom communications capability and will be capable of being erected level over a 10% grade. The leveling system will probably be a system of four integral leveling jacks preinstalled on the structure. The ES/C will also be capable of grouping with other ES/C's to provide larger shelters.

The most critical structural considerations are seals and panel construction. The seals to be employed on this structure will be of the latest design and of maximum reliability and weather tightness. An extensive study of seals is intended prior to selection of a final design. The ES/C will be designed to preclude delamination or buckling when the structure is subjected to thermal shock in the shelter mode. The ES/C will be capable of sustaining, without damage, a temperature rise of $4^{\circ}F$/min through the wall panels. Extensive materials and fabrication tests will be performed prior to acceptance of a final design to establish this capability.

MATERIAL AND STRUCTURAL CONCEPTS

The prime structural requirement of the ES/C is a high strength-to-weight ratio as maximum strength with minimum weight is a critical requirement for air transportable structures. This will be achieved by employing a laminated sandwich composite structure incorporating thin skins and a lightweight core. The over-all thickness of the panel is approximately two inches with varying skin thickness depending upon floor or wall loading requirements.

A considerable number of materials are available which have applications to this type of structure and meet the strength-to-weight requirement. Potential candidates for the skin panels are aluminum, fiberglass, steel and magnesium. Magnesium is not desirable because of its corrosion characteristics. Core materials to be considered are resin impregnated paper honeycomb, polyurethane foam, polystyrene foam, foam filled paper honeycomb, and aluminum honeycomb.

A considerable number of adhesives are available from various suppliers which are suitable for use on this structure. Non rigid skeletal supported walls were considered but its application to this program is questionable from a structural and facility use standpoint. Some candidate material concepts are presented in Table 1.

A preliminary trade-off study was performed considering all parameters such as cost, weight, panel function and design, environment, permeability, structural requirements, thermal requirements, and fire, fungus, rot and mildew resistance. The material candidates have been reduced to fiberglass or aluminum facings, and polyurethane foam or resin impregnated paper honeycomb cores. Foam filled paper honeycomb will be further investigated, the primary concern being cost of fabrication. Its main advantage is lower thermal "U" factor. It is believed to achieve a .35 BTU/hr ft^2F^o overall "U" factor for a two inch thick panel, it is necessary the "U" factor per panel be approximately .2 BTU/hr ft^2F^o or less. The "U" factor for a two inch foam filled core panel is 0.12 BTU/hr ft^2F^o.

The choice of adhesives are limited to available resinous organic and inorganic types. The primary function of the adhesive is to attach the facings to the core, therein providing rigidity to the panel. There are three important properties to consider when the adhesive is selected: tensil strength, creep resistance and peel strength. The tensile strength is required to restrict the facings from buckling and to transmit shear loads from the paper honeycomb to the facings. Creep resistance is needed to prevent slippage in the core-to-face bond and to prevent failure or permanent set of the panel while loaded in flexure. A high peel strength is necessary because it provides resistance of an adhesive bond to propagation of a damaged area.

The primary function of the facing material is to carry axial tensile and compressive loads. Facings must be of sufficient strength to resist compressive or tensile stresses from axial loading conditions.

The panel thickness is a function of the structural use and design criteria proposed for the ES/C. The panel as a whole will perform two functions: as a beam when used as roof and floor, and as a column when used to support the roof. Wall panels are load-bearing and subjected to simultaneous wind pressures and edgewise compression due to the roof loadings. It is anticipated panel thickness will be approximately 2 inches with facings approximately 0.35 to 0.45 inches thick. The ES/C can be divided into four structural areas, each requiring different load bearing criteria: walls, roof, container floor, and shelter floor.

The greatest difficulty to be encountered in this program will be the design and fabrication of seals, panel joints and fasteners. The structure's ability to eliminate leakage, heat transfer and other environmental effects is a function of seal and joint design. The structural integrity of the ES/C is dependent upon design of the fastener in both modes of ES/C operation. The specific technique to be employed in joining panels and in selecting fasteners will depend upon the final material and design configuration to be employed. Joint design and fastening technique will vary with use of a honeycomb or foam filled core panel.

TABLE 1

CANDIDATE STRUCTURAL MATERIAL CONFIGURATIONS

FACING	CORE	PANEL THICKNESS (INCHES)	PANEL WEIGHT (LB/FT^2)	"U" FACTOR PANEL $BTU/HR/FT^2/F^o$
ALUMINUM	PAPER HONEYCOMB	2	1.6	.21
FIBER GLASS	PAPER HONEYCOMB	2	1.3	.18
STEEL	PAPER HONEYCOMB	2	1.4	.20
ALUMINUM	POLYURETHANE	2	1.92	.14
FIBER GLASS	POLYURETHANE	2	1.87	.10
STEEL	POLYURETHANE	2	1.98	.13
ALUMINUM	POLYSTYRENE	2	1.25	.12
STEEL	POLYSTYRENE	2	1.31	.11

Fastening techniques to be selected will not degrade panel strength, result in bond delamination or provide a thermal path between the inner and outer skins. Joints will be protected against weather effects by employing a seal which does not require air pressure to operate and will be either of flexible plastic or neoprene.

TECHNICAL APPROACH

A ten month effort is planned for the development of the ES/C. The first 6 weeks of the program will be utilized to perform a detailed engineering analysis on the material and fabrication concept selected by the successful bidder. It is intended the contractor will justify his selection by analytical and experimental methods. Extensive tests on materials following ASTM test requirements will be required to establish satisfactory compliance with requirements.

Two prototypes will be designed and built; the first deliverable in about 4 months after completion of the test phase and the second four months after delivery of the first prototype. Each prototype will be extensively tested in the field for operational use capability and in the Eglin Climatic Hangar. The ES/C will be evaluated in all modes of operation including Type II mobility capability in unison with the M689 transporter. At the conclusion of this test the results will be evaluated, changes recommended and studied. The second prototype will be fabricated incorporating all changes and subjected to a similar test program emphasizing the weak points discovered in the first prototype. Results of this second test will be evaluated and changes recommended. A final design will be submitted from which volume production can be initiated.

CONCLUSION

1. It is believed the structure will be a major factor in the implementation of the Air Force Bare Base concept. Utilization of the ES/C will reduce shipping volume and weight, and deployment time. In addition, transportation efficiency of the Bare Base system will increase significantly.

2. The ES/C will provide a rigid wall enclosure for maintenance work. It is anticipated that efficiency of aircraft/engine maintenance crews will improve with resulting increase in aircraft reliability and safety.

BLANK PAGE

NEW RAPID SITE CONSTRUCTION TECHNIQUES FOR SUPPORT FACILITIES

by

A. VASILOFF

INTRODUCTION:

The use of expandable structures in a limited war environment has proven successful because of their ease of erection, low packaged volume, and their consequent lowering of the logistic burden in utilizing this concept for remote or forward area use.

The use of expandable structures designed from lightweight foam board has been proven successful in various tropical and arctic tests, ranging from the Panama Canal Zone to Alaska and Southeast Asia. The use of tents and inflatable structures are also being utilized in current military operations. Panalized buildings made from aluminum, sheet steel or wood are also familiar sights on most remote base operations. As a more permanent structure, the standard sheet metal covered steel frame buildings, such as the industry "Butler" building, are used for various purposes, on military bases. In some cases, shelters are built from any existing material available, as shown in Figure 1, which is a shelter used in an early build up phase under war time conditions.

Each of these shelters have one common problem; that is each shelter requires a load bearing floor to fully utilize the overhead or covered protection. This problem has been solved in many varied and ingenious ways. Troops in the field usually try to find logs or parts of packing crates to make floors for their tents or shelters. Some shelter designers realizing this fact, have designed the packing crate to be utilized as the floor, as in the 16' x 32' foam board shelter built by the Air Force Aero Propulsion Laboratory. Other shelter systems have solved this problem by constructing shelters on existing and/or old taxiways to provide a load bearing surface. This is particularly true for those shelters being constructed to accomplish maintenance work on aircraft. The heavy wheel loads require that a good load bearing surface be available.

This paper deals with new methods to quickly, within hours, fabricate a rigid, load bearing surface that can be utilized with the particular shelter mission. Presented are the results of three areas of research which are directed to the objective of providing rapid load bearing surfaces.

SPRAYABLE REINFORCED PLASTIC PAD FABRICATION

The Air Force Aero Propulsion Laboratory has sponsored research in the past several years to achieve a goal of spraying a fast curing plastic resin on the ground surface to fabricate a load bearing surface. Originally, this research was conducted to solve the problems associated with operating Vertical Take-off and Landing (VTOL) aircraft in remote areas. A remote area VTOL site

---

* Technical Area Manager
Limited War Support
Ground Support Branch
AF Aero Propulsion Laboratory
Wright Patterson AFB, Ohio

Expediently built shelter fabricated from scrap materials.

Figure 1.

requires some type preparation as the heat and blast generated by the downward impingement of the vertical jet engines causes natural terrains to rapidly deteriorate. The flying dust and debris resulting from the unprotected terrain causes foreign object damage to the aircraft engines and fuselage. Even basic construction materials as asphalt and concrete degrade under this hot (1200-3000°F) environment, as the heat causes the surface area to melt or spal.

To combat this problem, the AFAPL initiated a research program for a quick cure sprayable plastic material that could stabilize the ground and resist the temperature and blast environment of a VTOL aircraft. As a result of this research, a polyester resin material modified with certain ablative materials and strengthened with fiber glass was developed. The material was sprayable, cured to the required hardness in about 15 minutes, and withstood the vertical afterburner blast of a J-85-5 engine. Figure 2 gives a cure time graph of a representative polyester resin, cured using methyl ethyl ketone peroxide catalyst and cobalt napthenate promoter. A polyester resin fiber glass reinforced mat with a glass content of 32% sprayed upon the ground, would have the approximate following characteristics:

Flexural strength, psi	30,000
Flexural modulus, psi	1.2×10^6
Tensile strength, psi	20,000
Tensile modulus, psi	1.5×10^6
Compressive strength, psi	40,000
Barcol Hardness	50-60

However, the type and percentage of fiber glass, plus the specific polyester resin all have an effect on these characteristics. Figure 3 shows the results of testing with one polyester resin but varying the types and percent of fiber glass reinforcement.

Through a series of optimization programs, a field operational application system was fabricated for full scale field evaluation of this new rapid site material. A spray pump system and resin tank trailers were fabricated for field tests in England and Germany with the English P.1127 and German VJ-101 VTOL aircraft. The completed equipment consists of a pumping system mounted on a 3/4 ton four wheel drive pick-up truck and four 400 gallon tank trailers. See Figure 4. The pumping systems is operated by a power takeoff from the drive of the truck. It pumps resin from the tank trailer, through the pumping and metering system and forces it through hoses to the spray nozzle. The resin is catalyzed at the head of the spray nozzle, and the resin is ready for cure as it is sprayed onto the site. See Figure 5. Fiber glass is applied to the ground site either by continuous roving sprayed by compressed air, or laid out on site in the form of woven fiber glass blankets. See Figure 6. These fiber glass blankets are standard in the industry, some commercial names being "fabmat" and "rovecloth". The application of the blanket fiber glass allows a uniform percentage of glass to be applied, and hence establishes a good strength control, as the high strength of the reinforced plastic pad is dependent upon the glass content.

The resin and fiber glass reinforced site is sprayed to any thickness desired, with a 1/2" thick site being sufficient to withstand the loads of most modern type aircraft, provided the original ground site possesses some strength.

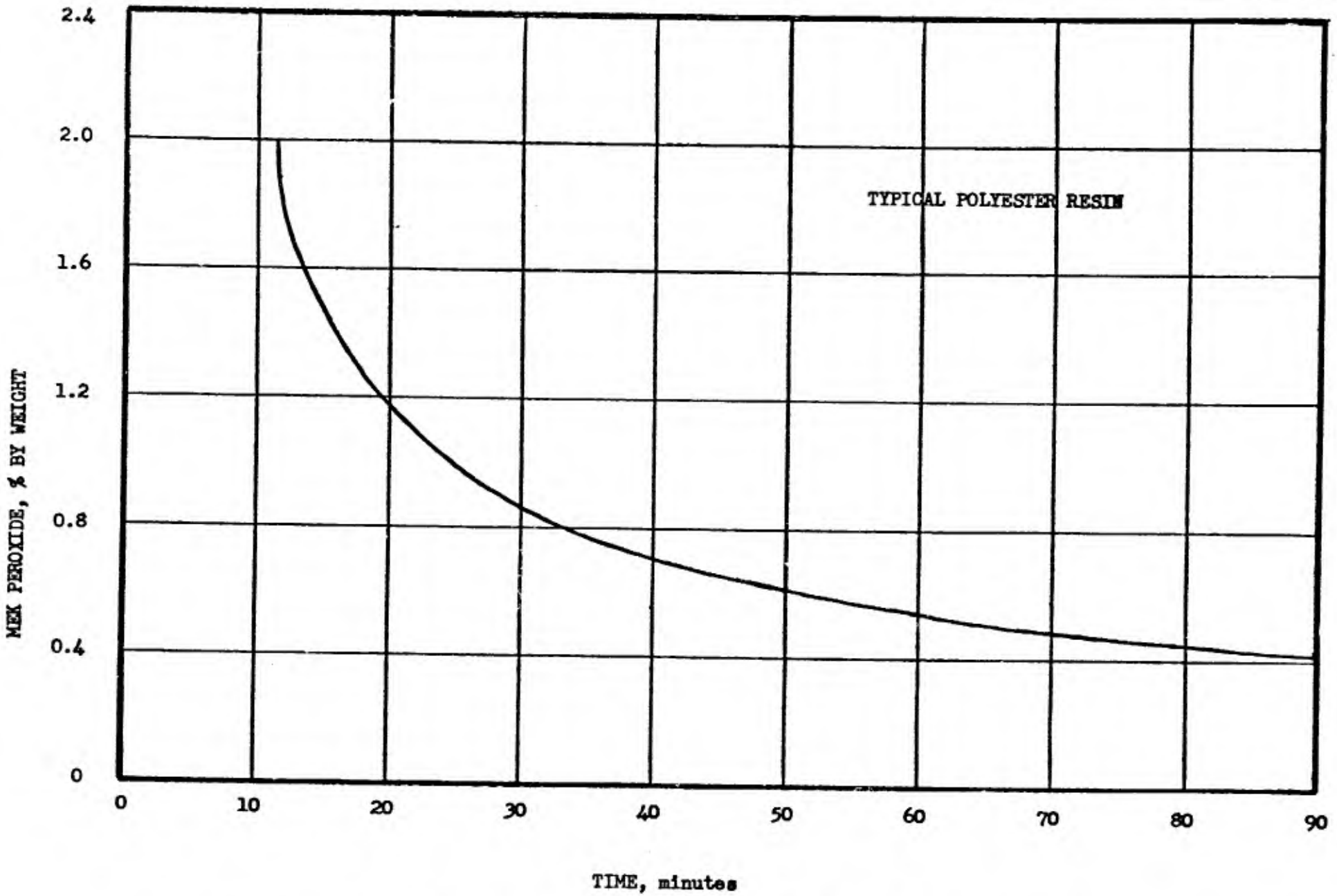

EFFECT OF MEK PEROXIDE CONCENTRATION ON GEL TIME AT 24°C (75°F) USING 0.2% COB. NAPH. PROMOTER

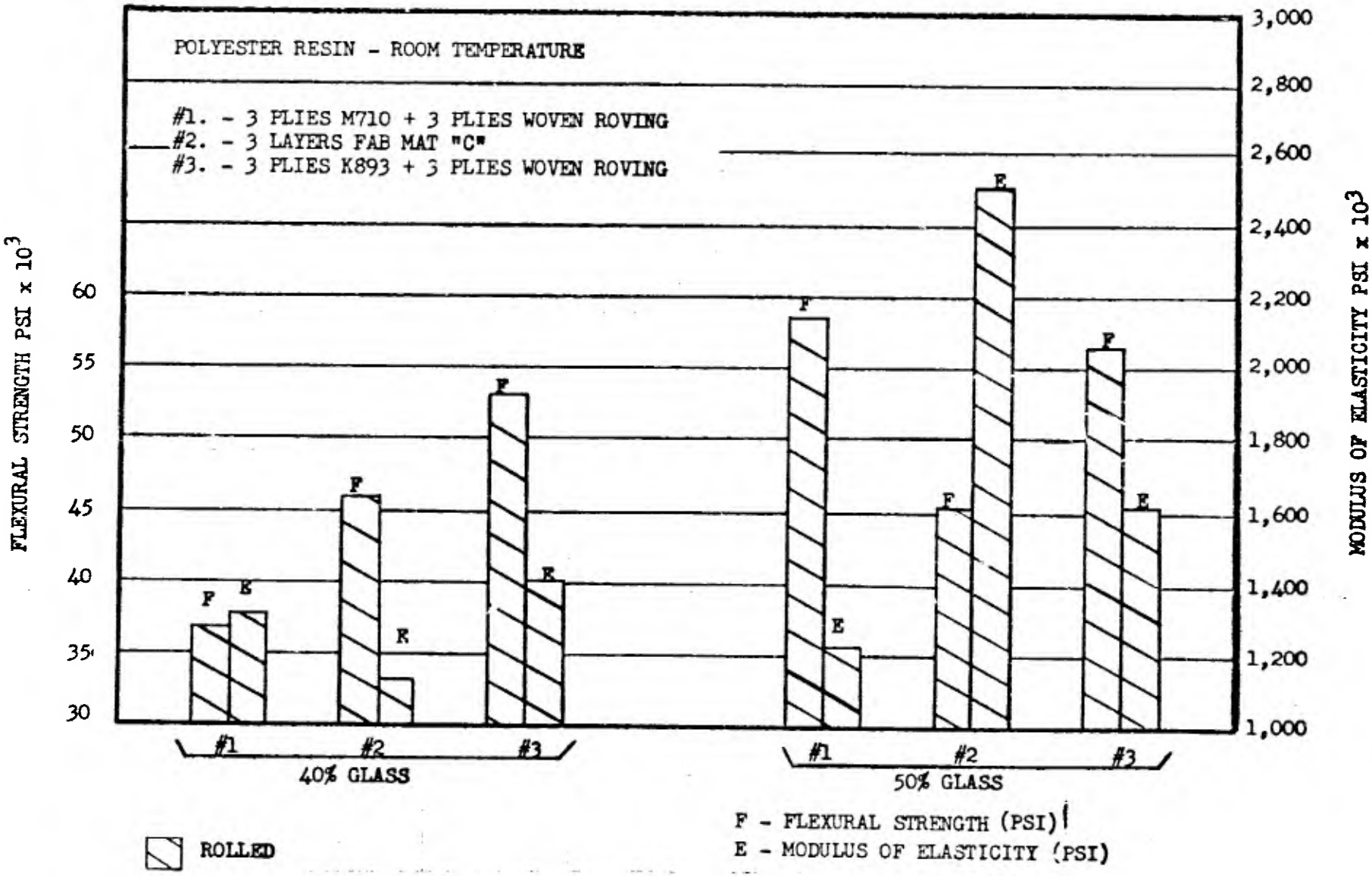

COMPARISON OF THREE GLASS SYSTEMS - 40% and 50% REINFORCEMENT

Figure 3.

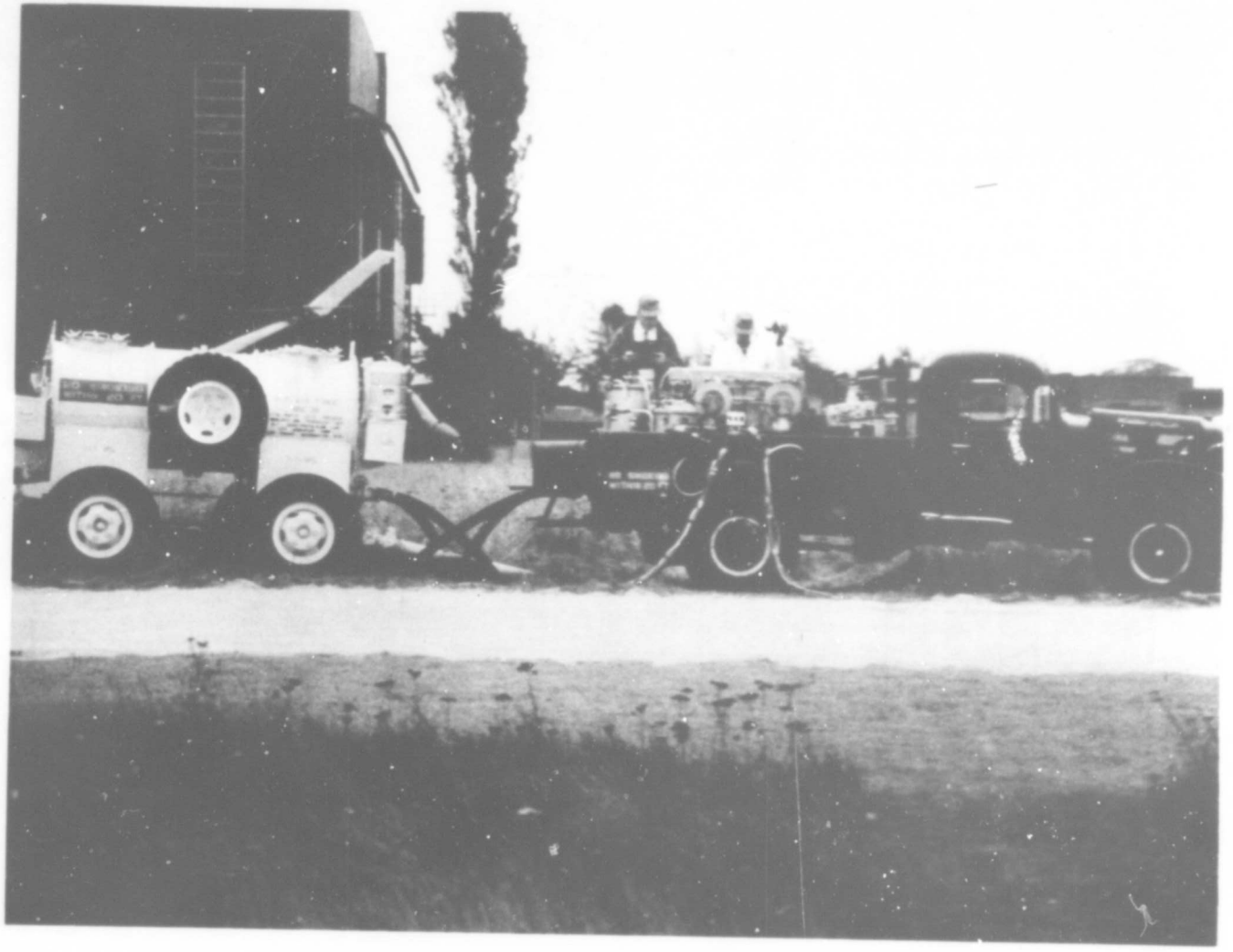

Rapid Site application equipment

Figure 4.

Rapid site material being sprayed onto field site.

Figure 5.

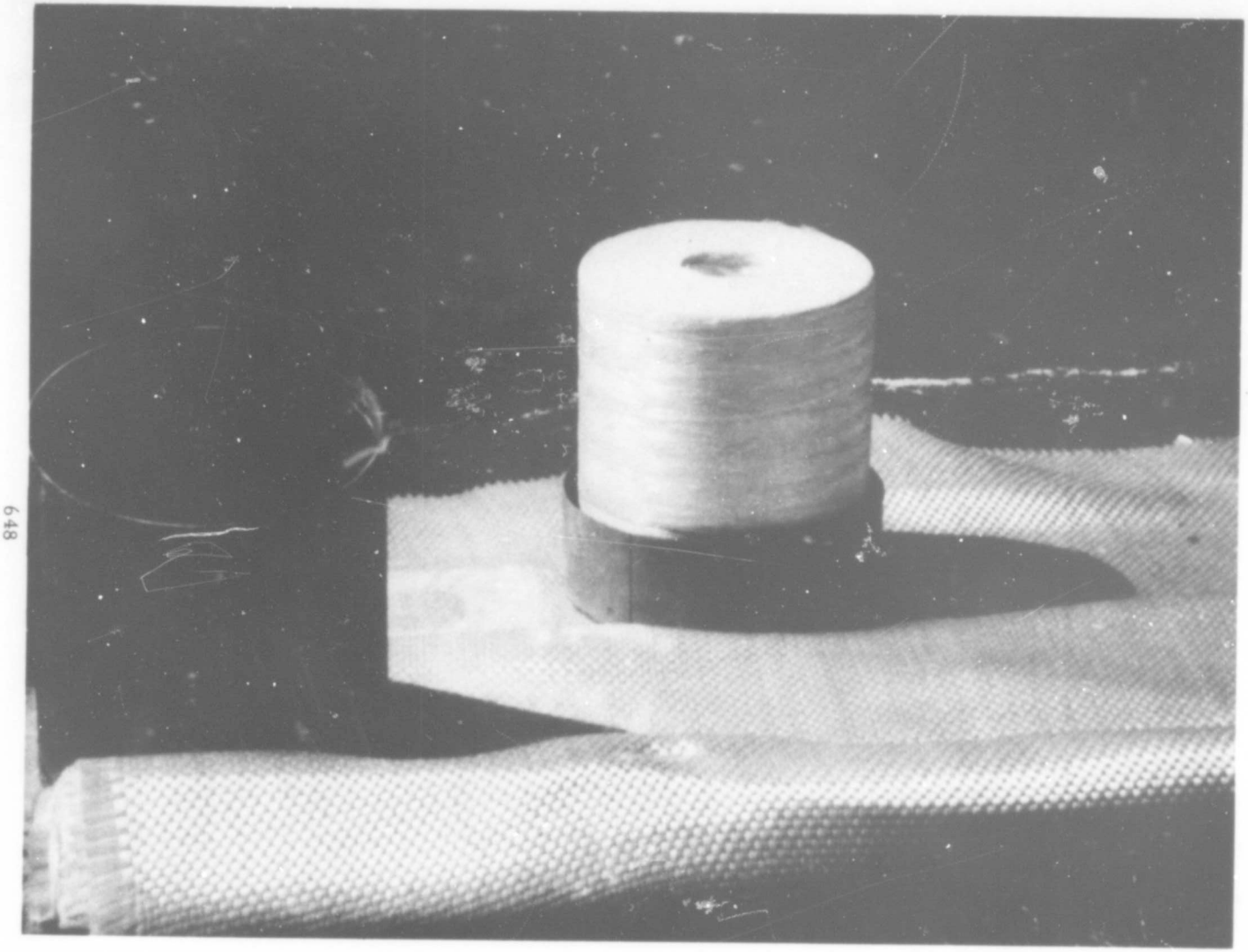

Types of fiber glass used in site preparation.

Figure 6.

Using the above described technique, several sites were prepared in England, Germany, and in the U.S. Site sizes ranged from 55' to 100' in diameter. Figure 7 shows the P.1127 operating from a 100' diameter site at Eglin AFB, Florida.

The polyester resin/fiber glass material was also investigated for application for providing rapid shelter floors and other load bearing sites, such as helicopter pads and hangar floors. For this application, the high temperature additives were removed from the resin system and just the base resin with the fiber glass was utilized. This provided an excellent method for rapidly constructing high load bearing surfaces. Using this technique, a 1/4 inch thick, 120 foot diameter helicopter site was fabricated, along with a 50' x 100' aircraft hangar floor, and several 16' x 32' shelter floors. All these were tested with varying wheel loads, including auto sedans up to 3,000 lbs., a 17,000 lb. fire truck, a 30,000 lb. helicopter, a 32,000 lb. XC-142 VSTOL transport aircraft and an F8U jet fighter aircraft. In each case, a thin 1/4 inch thick to 1/2 inch thick pad was sufficient to support these heavy wheel loads.

To aid in references to this material, the relationship of pad thickness to area density of the resin/fiber glass material is given in the table below. The current cost of this resin material is approximately $0.35 per pound. Fiber glass price varies according to type, but is in the range of $0.40 to $0.50 per pound.

Area Density (#/sq.ft.)	Thickness (inches)
1.0	.125
2.0	.25
3.0	.375
4.0	.50
5.0	.625

The thickness of the site can be varied by the number of spray passes and fiber glass mat layers over a given area. The spray mixture is set up in approximately 15 minutes, dependent upon the temperature conditions, and the catalyst proportions. Strength build-up is rapid, and 90% of the total strength is attained within one hour.

The operational feasibility of utilizing this process in the field for providing fast load bearing surfaces was also demonstrated in Southeast Asia (SEA), South Vietnam, in September-October 1966. During this time period, a technical team from the Aero Propulsion Laboratory, and one from the contractor, Ling Temco Vought, stabilized various sand surfaces utilizing the polyester material.

The following types of areas were successfully stabilized.

a) Sand Revetment Site - See Figure 8.

A 45° sloped sand dike revetment approximately 60 feet wide at the base, and 20 feet high was stabilized for a length of 860 feet. This was accomplished because severe wind conditions near the beach area would erode unstabilized sand revetments, and other techniques such as sprayed asphalt had proven unsuccessful.

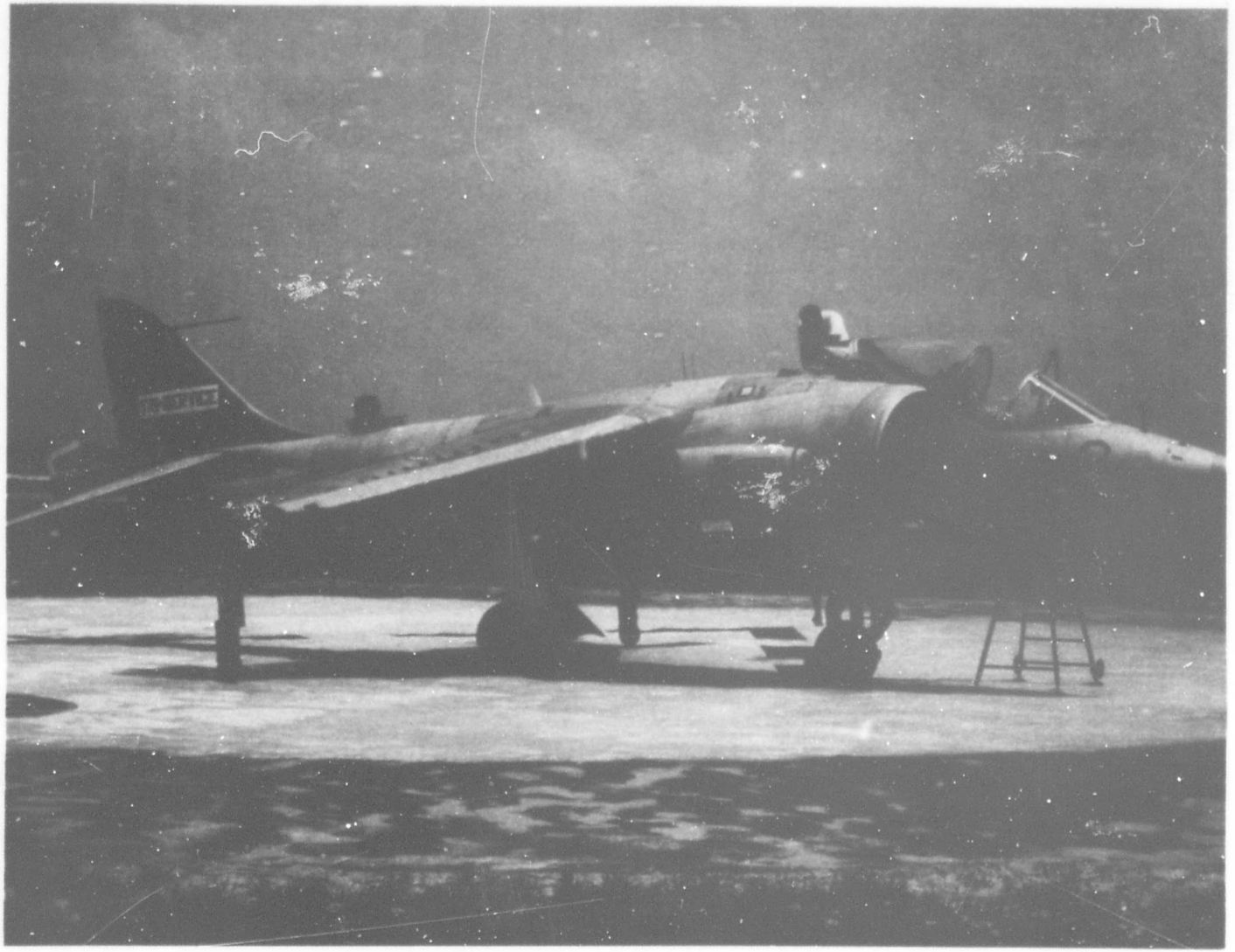

P.1127 VTOL aircraft on 100 foot diameter, 1/2 inch thick site fabricated from resin and fiber glass.

Figure 7.

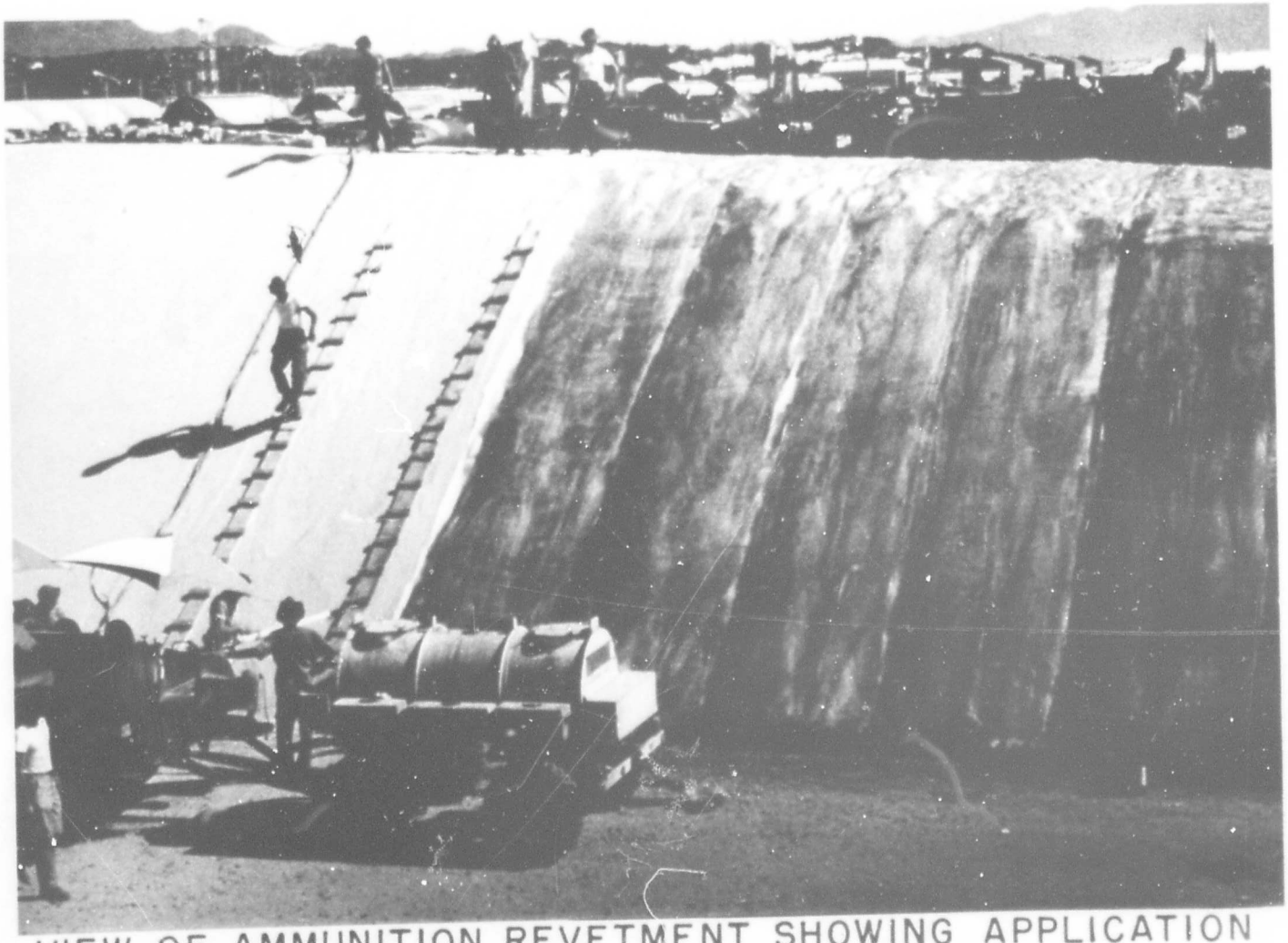

VIEW OF AMMUNITION REVETMENT SHOWING APPLICATION TECHNIQUE USED IN STABILIZING WITH RAPID SITE MATERIAL

Figure 8.

b) Cargo Storage Area - See Figure 9. A 50' wide by 360' long cargo storage area was fabricated over a sand base. The thickness was varied from 1/4" to 5/8" for test evaluation purposes. The area was being used on one end while the fabrication was being completed on the other end. Moving wheel loads of fork lifts and trucks did no damage to the pad.

c) Test Engine Run-Up Test Station Site - This area was sprayed to accomplish sand stabilization to prevent erosion caused by the wake of the jet engine. Sand bags and ground were stabilized around this area, and no damage occurred after testing with current jet fighter aircraft.

d) Helicopter Landing Site - See Figure 10. A 120' x 120' 1/4" thick helicopter landing site was fabricated over a sand base. Over three hundred landings by helicopters in a three month time period has not damaged the pad.

e) Maintenance Sites - A maintenance hardstand area was fabricated to allow work on mechanical equipment. This provided an excellent work area.

f) Miscellaneous Sites - Other sites were also fabricated that included patching of metal mats and revetments, overspraying of pierced steel planking (PSP) and fabrication of a short aircraft taxiway entrance area.

The results of the VTOL site test programs, and the results of the SEA test program proved the operational feasibility of providing load bearing surfaces by means of a sprayed reinforced plastic technique.

Figure 9.

View of 120 foot square, 1/4 inch thick resin/fiber glass helicopter site fabricated over a sand base.

Figure 10.

MOLTEN SULPHUR TECHNIQUES

Another fast preparation method of providing a load bearing surface is the use of molten sulphur. The cost of sulphur is slightly over $0.01 per pound, and can offer a major cost savings over other building concepts. In addition, sulphur, in the solid state, can be found in great quantity around the world, and can be stored simply by piling the material as one would store aggregate. The melting point of sulphur is rather low, that being approximately 245°F. To change the molten sulphur to solid form requires no chemical reaction, as in the case of resins, but only involves changing from liquid to solid by the cooling process. Thus, to fabricate a site, the molten sulphur is simply sprayed from an insulated trailer truck containing the molten sulphur. Upon cooling to the solid form the site is ready for use. Figure 11 shows the flexural strength for sulphur as a function of time and curing temperature.

The Air Force Aero Propulsion Laboratory has sponsored exploratory development to establish the use of the sprayed molten sulphur techniques for fabricating load bearing surfaces. Of particular interest was the use of fiber glass as a reinforcing agent to allow a thin load bearing surface to be fabricated. Large scale aggregate was also utilized as a filler to form a sulphur concrete type mixture. These rapid fabricated sites were prepared for such uses as a helicopter site, shelter floors, and aircraft parking hardstands. These sites were fabricated over varying soil conditions and strengths, and tested with moving wheel loads to ascertain their usefulness.

One 120 foot diameter, 3/8" thick helicopter site, three 16 x 32 ft. x 1/2" thick shelter floors, and three 20 x 30 foot aircraft hardstands of varying thicknesses were fabricated. Figure 12 shows the start of the helicopter site fabricated and Figure 13 shows the fabrication of a shelter floor over soft desert sand. The molten sulphur was sprayed up to a rate of 30 gallons per minute at a temperature of 230°F. Cool down time to change to the solid form was dependent on the mass applied at a certain point, but in general was very short, in the order of minutes.

The test areas were subjected to various wheel load tests. The shelter floors and hardstands were tested with a 4,000 lb. automobile, and a 30,000 lb. (fully loaded weight) forklift. A water filled, 55 gallon barrel was also dropped from a 14 foot height for an impact test. A UH-1 helicopter operated from the helicopter site, and a 36 ton crane made thirty wheel load tests passes on the helicopter pad. The results of the moving wheel load tests revealed that with a normal strength subgrade, (i.e., CBR 8 or over), a sulphur/fiber glass mixture could be utilized to quickly fabricate a load bearing surface. In addition, when molten sulphur was poured over large aggregate fill, a solidification occurred which resulted in a sulphur concrete composition, and was very successful in carrying heavy wheel loads similar to those in an aircraft hardstand area. This sulphur/aggregate method presented a very economical method of fabricating load bearing surfaces.

Several problem areas were encountered in the exploratory development program that should be solved before molten sulphur can be used to full advantage. These are:

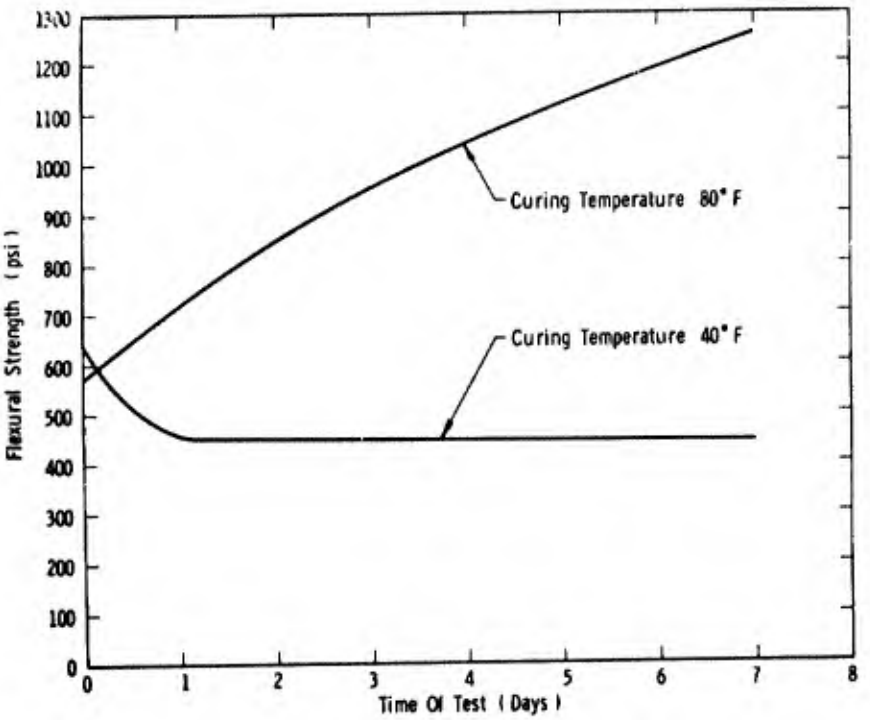

Flexural strength of sulphur as a function of time and curing temperature.

Figure 11.

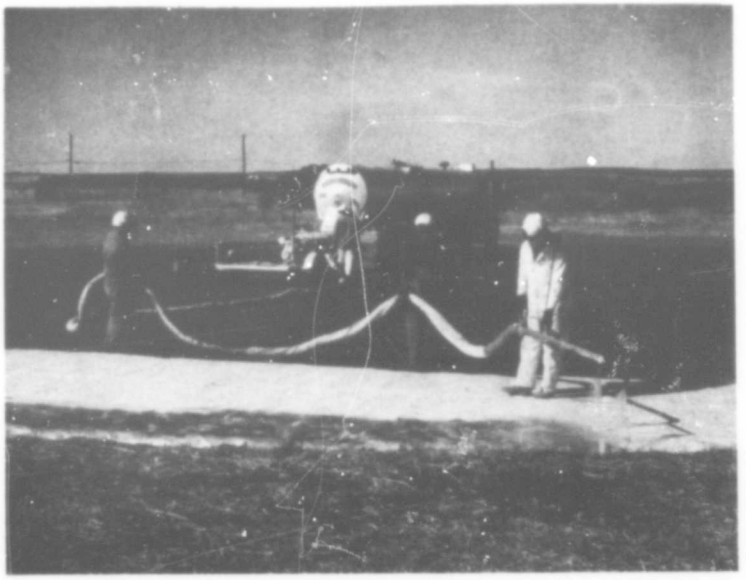

Molten sulphur sprayed on fiber glass for construction of 120 ft diameter helicopter site.

Figure 12.

Preparing a shelter floor over desert sand with molten sulphur and fiberglass.

Figure 13.

a) A fire retardant additive or technique for use with sulphur construction must be found, as sulphur does support combustion.

b) A fiber glass sizing compatible to sulphur should be developed. This is required, as most standard fiber glass sizings are manufactured for compatibility to plastic resins and not sulphur. Hence, wet out of the fiber glass by the sulphur is difficult.

c) A method to improve the weathering and wearing characteristics of the solidified sulphur must be established. The softness of the sulphur causes a "dusting" to occur during use, which should be eliminated.

The Air Force Aero Propulsion Laboratory is continuing its investigation in these areas to solve these problems.

In summary, it has been proven that the molten sulphur technique can be utilized as an economical fast construction technique for fabrication of load bearing structures.

ULTRA FAST CURE CEMENTS

The use of portland cement in the form of concrete is a standard construction method in the building industry. However, normal concrete takes 28 days for full strength cure, and normally cannot be used as a fast method of fabricating a load bearing surface. Some fast setting cements as "Speedcrete" or "INCOR" (Long Star Cement) have cut the working time down to a few days. The logistics aspect of placing and working a huge volume of concrete has also kept this method from being considered as a rapid construction technique. Methods such as "gunite" have also been used to place concrete in thin shells to resolve some of these problems.

The Air Force Aero Propulsion Laboratory has investigated the use of ultra fast cure cements to rapidly repair bomb damaged runways. The goals of the repair program were to quickly patch the runway in a short time period (hours if possible), and allow this repaired section to support up to 30,000 lbs. on a single moving wheel load, with a tire pressure of 275 psi.

A series of tests were conducted with many of the standard and fast setting materials and cements; however, under testing with this large moving wheel load, most proved too long curing to provide a fast construction and repair concept. Upon further research, a cement type material dubbed "Fast Fix" was recently formulated that will give a 3000 psi compressive strength in 30 minutes. This is equal to a strength equivalent to 28 day concrete in just 30 minutes. Figure 14 shows this comparison. Further refinement of this formulation has allowed a neat slurry mixture of this Fast Fix cement to be pumped at a rate over 1000 gallons per minute. Figure 15 shows an artist's concept of the equipment being designed to accomplish this feat. In this manner, the slurry mixture will be aimed at the repair section and pumped into the cavity area. Aggregate may be added before hand to the cavity for the slurry to percolate through if desired. Being in a slurry form, the mixture is self leveling, and no finish work is required. In 30 minutes the area is ready for load carrying duties.

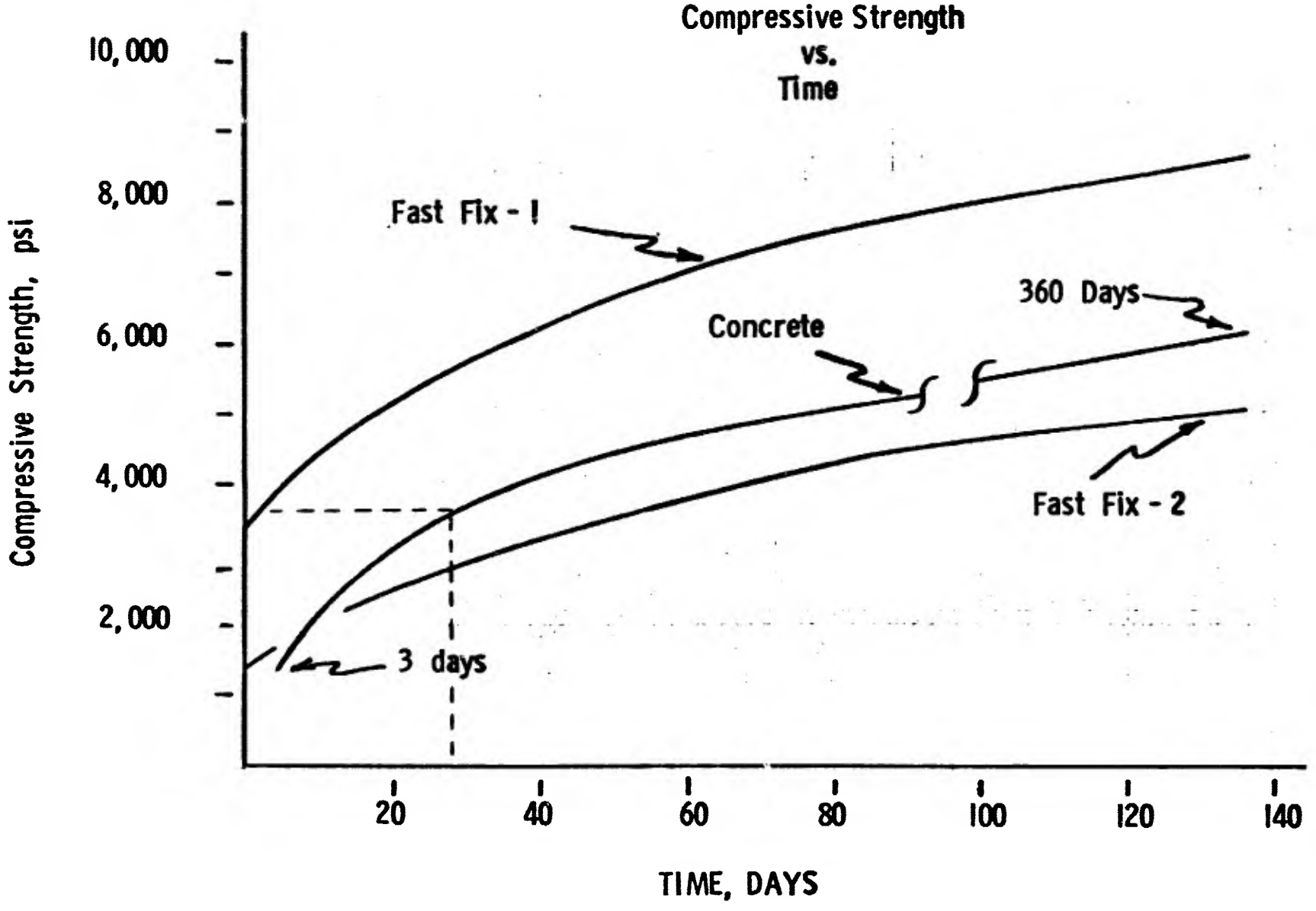

A comparison of the strengths of two new Fast Fix cements and regular concrete.

Figure 14.

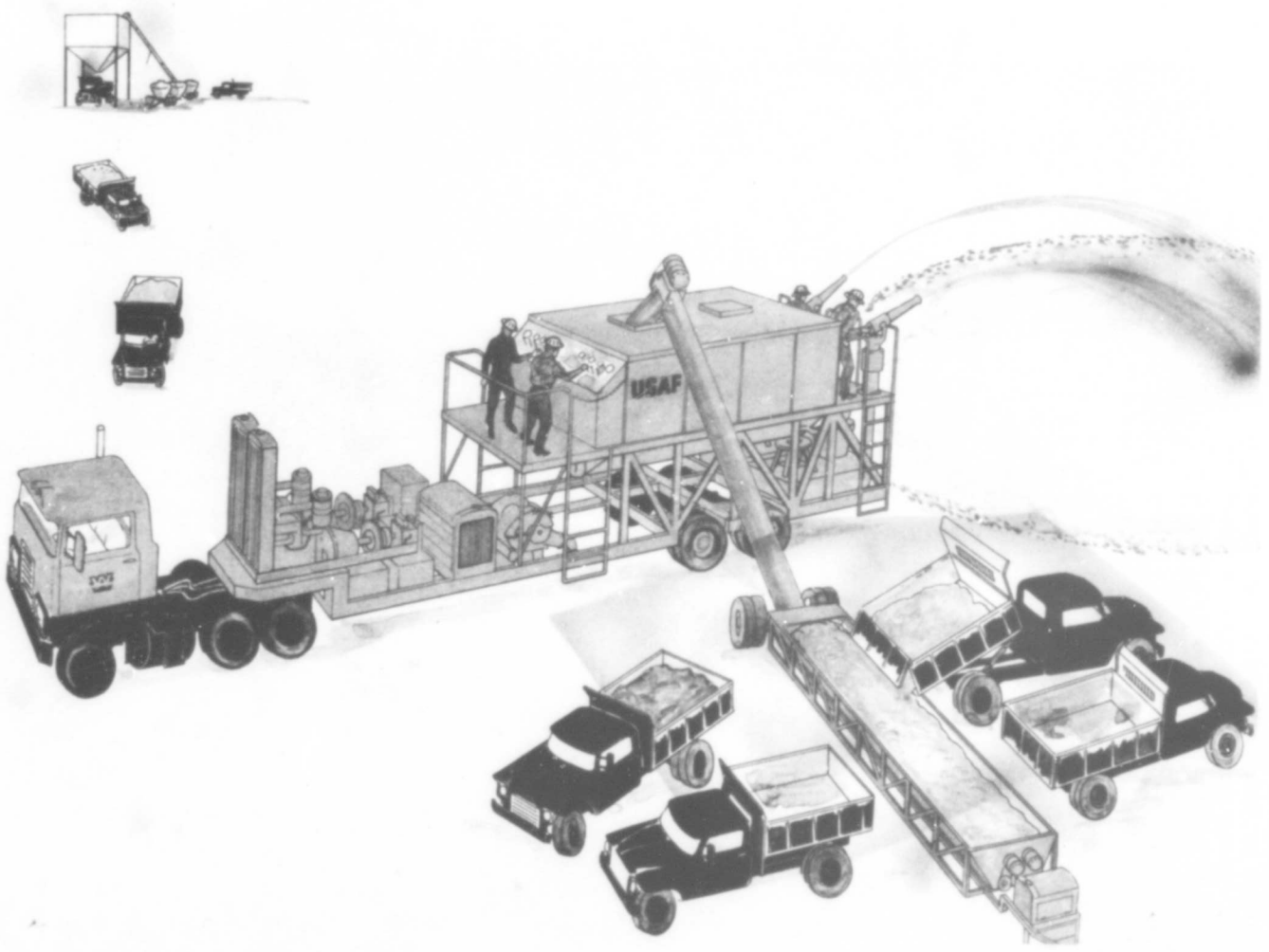

An artist's concept drawing showing 2000 gpm fast fix cement slurry mixing unit being supplied fast fix cement from a 13,000 lb./min. feed hopper.

Figure 15.

The advancement reported here is relatively new, and no large scale tests have been conducted to date, although some are currently scheduled. The Fast Fix formulation is undergoing many varied tests to ascertain all of its properties under freeze-thaw, strength time relationships, water cement ratios, etc., and its full range of use has not been determined. However, the concept is very intriguing, and if all the data on the Fast Fix characteristics turn out as anticipated, it could represent a significant advancement in the state-of-the-art in cement construction and rapid construction and repair technology.

CONCLUSIONS:

From the research test programs conducted on the three areas given above, it can be concluded that:

a) The fabrication of load bearing sites for shelter and hangar floors by the plastic/fiber glass application method is feasible.

b) The use of molten sulphur as a rapid preparation material has application for certain missions, and further research is needed to extend its usefulness.

c) The use of a new ultra fast cure cement, pumped at a high rate, appears to hold promise for rapid fabricating of load bearing surfaces that will equal standard concrete performance.

REFERENCES

1. Blakely, Clarence, et al, "Rapid Preparation of Quick Cure Resin Test Sites in Southeast Asia, Part I", LTV Aerospace Corporation, Dallas, Texas, Technical Report AFAPL-TR-66-148, dtd 28 February 1967.

2. Bankhead, H.R., et al, "Tests of Rapidly Prepared Remote Sites with P.1127 VTOL Aircraft", Air Force Aero Propulsion Laboratory, Technical Report AFAPL-TR-66-46, dtd June 1966.

3. Gifford, F., et al, "Rapid Shelter Flooring and Helicopter Landing Sites", LTV Aerospace Corporation, Dallas, Texas, Technical Report AFAPL-TR-67-43, March 1967.

4. Dale, J.M., "Demonstration of Sulphur as a Load Bearing Material", Southwest Research Institute, San Antonio, Texas, Technical Report AFAPL-TR-66-151, dtd February 1967.

5. Western Company, "Rapid Runway Repair Program, Final Report, Volume I", Prepared for Air Force Aero Propulsion Laboratory, contract AF33 (615)-3747, unpublished to date.

ADDITIONAL PAPERS

BUILDINGS IN BARRELS, PART IV *

S. B. Swenson **

INTRODUCTION

At the Aerospace Conference of 1965, we had the honor of presenting a paper describing the Army's program in the development of fabrication processes for plastics structures and the concentration of this research toward systems of on-site fabrication of structures through the utilization of low bulk field expandable materials such as polyurethane foam. The logistic advantage of this approach has been the major attraction from the military standpoint; however, the possibility that a modified concept along the same lines could be adaptable to the aims and requirements of future space applications is offered as justification for discussion of the subject before this group.

Details of the background of the so-called "Buildings in Barrels" program are covered in the 1965 report. We shall briefly review the processes involved for the benefit of new participants and attendees of the present conference.

The Army's first disclosure of the "Buildings in Barrels" concept at the 1962 Society of the Plastics Industry exhibit, and again in 1964 before the same body, served to establish the Industry's interest in our activity. The USAERDL has been steadily pushing its research ahead as much as modest budgeting would allow and has now arrived at a point of limited implementation aimed at endorsement for large scale field application.

The "Buildings in Barrels" concept makes a system available for field fabrication of aluminum- or plastics-clad polyurethane core buildings, 16 feet or 20 feet wide and any required length, expandable in 4-foot increments. Modules and end walls are fabricated by pouring expandable

---

* The paper presented before this body in the 1965 conference proceedings was titled "Buildings in Barrels, Part III." Parts I and II on the same subject are identifications of papers presented before the Society of Plastics Industries, Reinforced Plastics Division Conferences in 1962 and 1963.

** Plastics Engineer, U. S. Army Mobility Equipment Command, U. S. Army Engineer Research and Development Laboratories, Fort Belvoir, Virginia.

polyurethane foam materials into mold cavities lined with appropriate facing material and allowing the foam to expand to fill the mold cavity. After a curing cycle ranging from 15 minutes to an hour, the casting can be removed from the mold as a finished structural panel. Two of these panels are connected at the ridge to form a 4-foot module, any number of which, when assembled with the end walls, result in a very efficient structure.

PROGRESS 1965-1967

At the time of the 1965 conference, the project was at a stage where several satisfactory structures had already been erected at various localities. (Two in Greenland, and two in the vicinity of Fort Belvoir, Virginia.) In the two years since the last report, the laboratories and shops at USAERDL have had an opportunity to improve and modify the techniques involved. Perhaps the greatest improvement was in the adoption of a mechanical froth foaming technique for mold cavity filling, rather than the hand pouring previously employed. The complexity of mixing machines is fast disappearing. The present froth foaming system in use at USAERDL utilizes nitrogen pressurized supply tanks piped to metering valves which introduce the two components into a labyrinth mixing chamber. The material is dispensed directly into the mold cavity as a partially expanded foam. The apparatus is self contained and utilizes no operating power other than nitrogen pressure. Despite symplicity of design, results using this equipment are very satisfactory--foam quality is consistently good, capacity is relatively high (19 lb/min), and molds can be charged without excessive pressure buildup.

THE VIETNAM OPERATION

In the latter part of 1965, the project was considerably accelerated by the receipt of a military requirement for a 16- by 60-ft plastics-faced structure to be erected in Vietnam. This assignment was pursued with vigor and a confidence born through experience gained in producing hundreds of feet of typical modules using the molds procured in 1964 and the techniques and equipment previously described. Ordinarily, the Vietnam operation would have called for the molds, equipment, and material to be shipped to Southeast Asia for on-site application in conformity with the concept; however, in this instance, the existence of a lone gang mold dictated that a preliminary on-site evaluation of the utility of the structure should be made so as to obviate the expense of mold shipment and personnel training, which would be unjustifiable in the case of a single unit requirement. To this end, a 16- by 60-ft FRP (Fiberglass Reinforced Plastic) faced foam core building was fabricated and test erected at Fort Belvoir, then dismantled and shipped to Vietnam where it was re-erected on a prepared concrete slab. The structure was installed by local troop labor, none of whom had any prior knowledge of the erection procedures involved. On the first day (6 hours), the

assigned detail of six men, with technical supervision, had installed the base angles on the slab and assembled eight modules. This 6-hour period included the time required to repair the many panels damaged in shipment. On the second day (9 hours), the erection of all panels, including the end walls, was completed. The finished length was 60 feet. Two panels, which were considered spares were beyond repair. (Two of the original four spares did not arrive at the destination.) On the third day, the building was secured to the base angles, joints were caulked and taped, and the building was completed except for air conditioners and power hookup.

On completion of the construction phase, a conference was held which, among other things, resulted in an agreement between the Military Command representatives and the USAERDL representative stipulating that reports of performance would be forwarded to the developing agency from time to time, especially during and after the rainy season. These reports would be useful in determining necessary modifications and improvements if deficiencies should present themselves. This decision proved to be of great value in perfecting adequate weatherproofing techniques.

DEVELOPMENT OF 20-FOOT SPAN

Back in 1961, polyurethane applications in USAERDL building design were predicated on two factors: (1) The width of the trenches and tunnels on the Greenland Ice Cap dictated that the building width should not exceed 16 feet, and (2) since no roof loads were encountered in this application, adequate structural strengths were easily attained, even with unfaced polyurethane foam modules. When the research venture emerged to be considered for possible surface application, design modifications were in order. Effort in this respect evolved semi-elliptical modular arch designs demonstrating more than adequate strength to resist arctic snow loads. One shortcoming remaining in the structure was the 16-foot span hangover from the Greenland days. Since military structures, especially barracks, do not lend themselves efficiently to the 16-foot width, a concentrated effort toward the development of a 20-foot span became the next order of business.

Because, as mentioned before, the 16-foot module demonstrated adequate strength to resist arctic snow loads, it is reasonable to assume that a 4-foot increase in span would still allow sufficient strength for tropic application where roof loads encountered are practically zero.

The anticipated hazards of wind lift are counteracted by over-the-roof holddowns. At the same time, there was some thought that a modular shape might be devised which would be more conservative of material or that would render gang molds simpler to fabricate and, therefore, be less costly. After thorough investigation it was determined that, with an accepted design load of 15 psf for tropic application, there was not sufficient justification to abandon the original semi-elliptical arch roof design.

TABLE I

LOAD-STRAIN-DEFLECTION RESULTS
SNOW LOAD TEST
20' GAMBREL CASE I

NOTES:

1. HORIZONTAL DEFLECTIONS OF FULL ARCH MEASURED 60" FROM FLOOR LEVEL.
2. VERTICAL DEFLECTIONS MEASURED FROM APEX OF ARCH.
3. ALL STRAINS ARE COMPRESSIVE UNLESS MARKED "T".

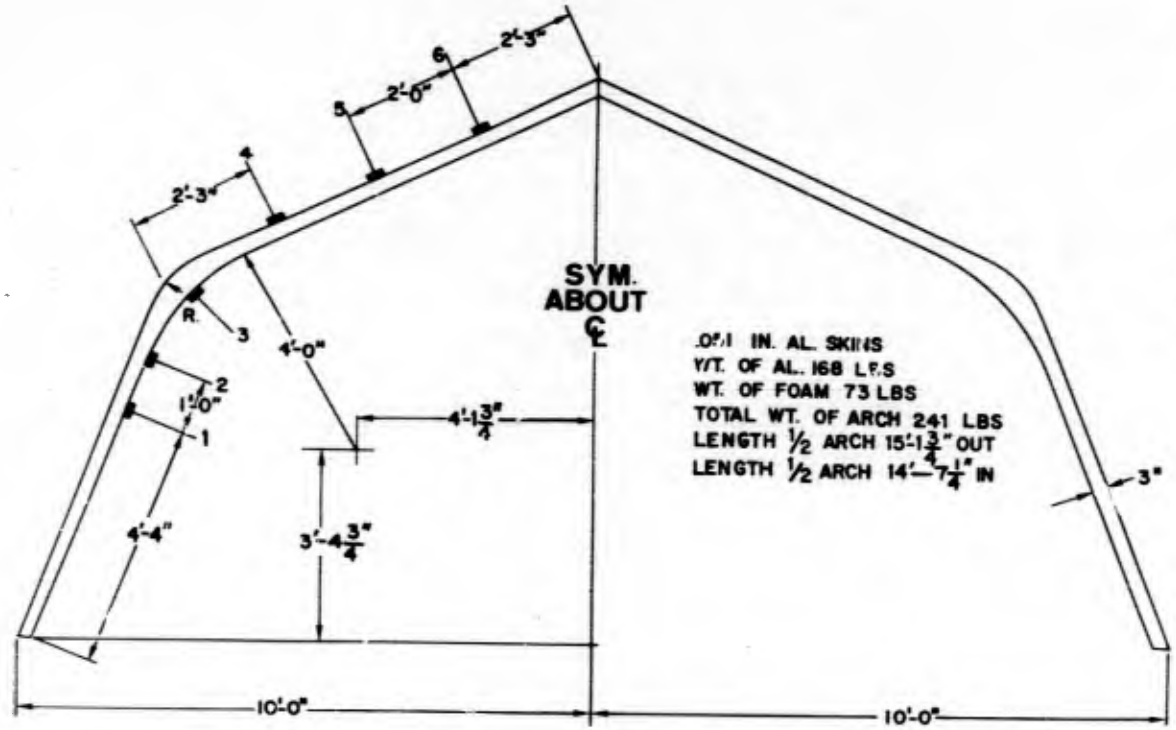

LOCATION OF STRAIN GAGES
SNOW LOAD TEST
20 FOOT GAMBREL

APPLIED LOAD LBS	APPLIED LOAD LBS PER SQ. FT.	STRAIN, MICRO-INCHES PER INCH						DEFLECTION-INCHES	
		GAGE I	GAGE II	GAGE III	GAGE IV	GAGE V	GAGE VI	VERTICAL	HORIZONTAL
0	0	0	0	0	0	0	0	0	0
294.0	5	30	40	10	10	30	20	-	-
586.5	10	50	70	20	30	80	70	3/8"	1/4"
877.0	15	70	100	30	40	80	50	-	-
1162.0	20	100	130	40	60	50	30	5/8"	5/8"
1452.0	25	120	170	50	50	70	20	-	-
1740.5	30	140	200	70	30	70	40	15/16"	1.0
2038.0	35	160	240	80	20	90	50	-	-

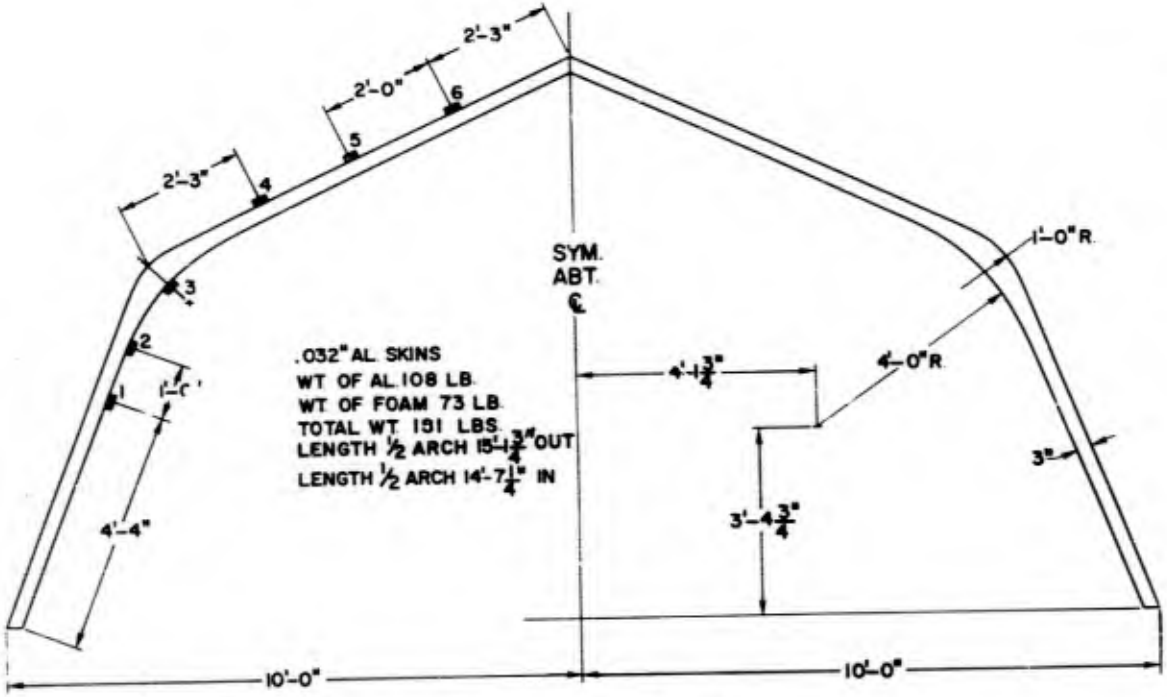

LOCATION OF STRAIN GAGES
SNOW LOAD TEST
20 FOOT GAMBREL

TABLE II

LOAD-STRAIN-DEFLECTION RESULTS
SNOW LOAD TESTS
20' GAMBREL CASE II

NOTES:

1. HORIZONTAL DEFLECTIONS OF FULL ARCH MEASURED 60" FROM FLOOR LEVEL.
2. VERTICAL DEFLECTIONS MEASURED FROM APEX OF ARCH.
3. ALL STRAINS ARE COMPRESSIVE UNLESS MARKED "T".

APPLIED LOAD LBS	APPLIED LOAD LBS PER SQ. FT.	STRAIN, MICRO-INCHES PER INCH						DEFLECTION-INCHES	
		GAGE I	GAGE II	GAGE III	GAGE IV	GAGE V	GAGE VI	VERTICAL	HORIZONTAL
0	0	0	0	0	0	0	0	0	0
289.0	5	30	30	20	50	70	30	0	-
572.0	10	90	80	40	80	110	120	-	1/4"
860.5	15	150	160	60	90	180	190	17/32"	5/8"
1150.0	20	170	180	80	70	80	180	5/8"	3/4"
1429.0	25	220	250	110	10	80	130	13/16"	1.0
1706.0	30	260	300	130	0	80	150	1.0	1-1/4"

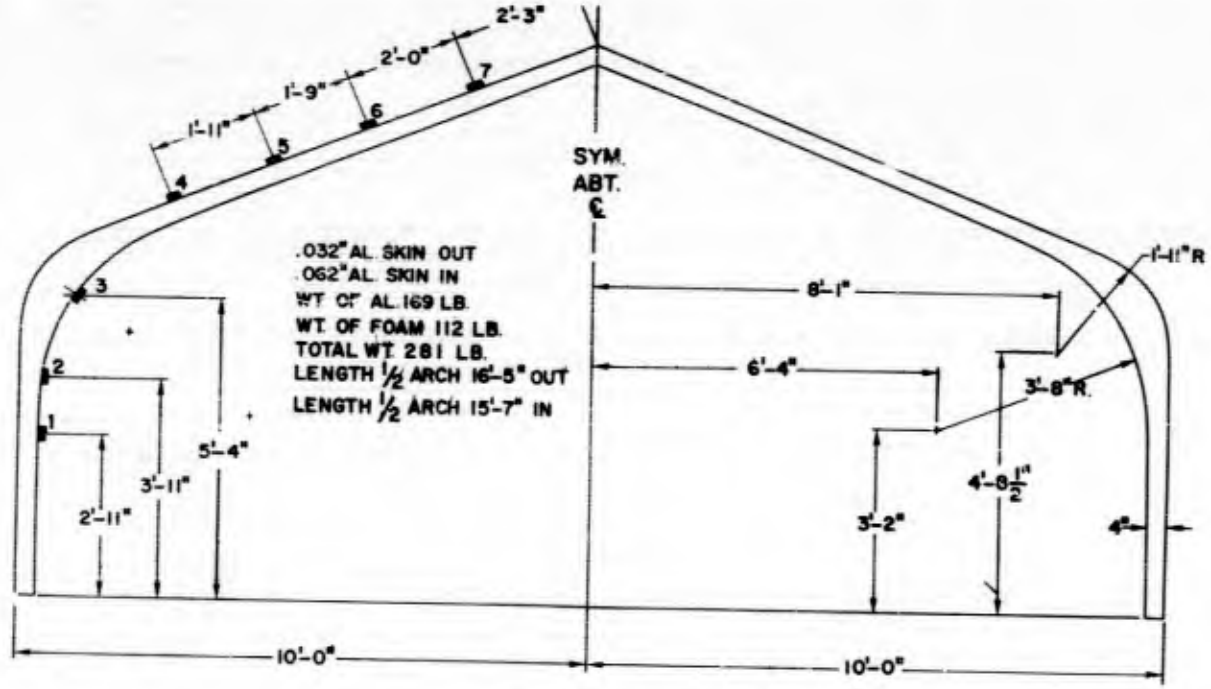

LOCATION OF STRAIN GAGES
SNOW LOAD TEST
20 FOOT STR. WALL

TABLE III

LOAD-STRAIN-DEFLECTION RESULTS
SNOW LOAD TESTS
20' STRAIGHT WALL CASE I

NOTES:

1. HORIZONTAL DEFLECTIONS OF FULL ARCH MEASURED 58" FROM FLOOR.
2. VERTICAL DEFLECTIONS MEASURED FROM APEX OF ARCH.
3. ALL STRAINS ARE COMPRESSIVE UNLESS MARKED "T".

APPLIED LOAD LBS.	APPLIED LOAD LBS. PER SQ.FT.	STRAIN, MICRO - INCHES PER INCH							DEFLECTION - INCHES	
		GAGE I	GAGE II	GAGE III	GAGE IV	GAGE V	GAGE VI	GAGE VII	VERTICAL	HORIZONTAL
0	0	0	0	0	0	0	0	0	0	0
350.0	5	25	40	10	30	50	50	40	—	—
706.0	10	50	90	30	20	30	50	100	1-1/4"	13/16"
1052.0	15	80	160	40	60 T	10	50	140	—	—
1397.5	20	100	200	50	20 T	120	90	180	—	1-9/16"
1758.5	25	120	260	60	110 T	70	130	200	—	—
2104.5	30	150	330	70	140 T	110	150	250	2-1/4	2-3/4"

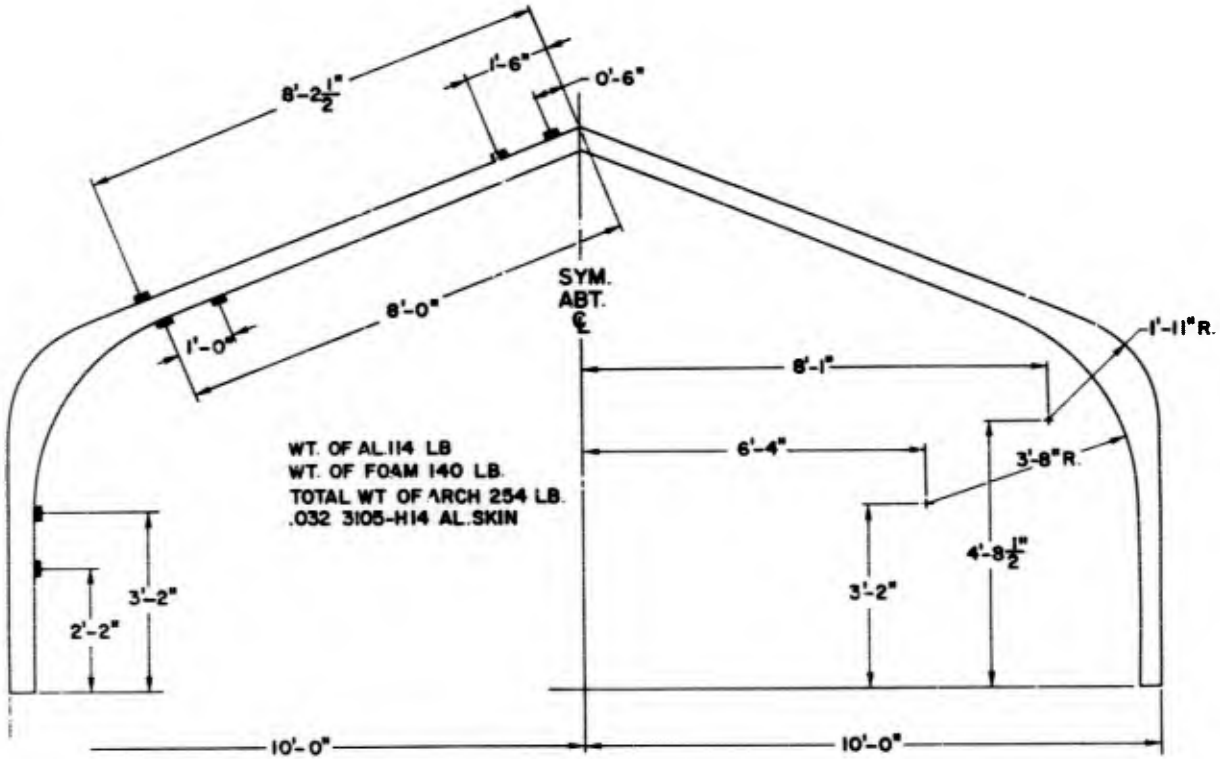

LOCATION OF STRAIN GAGES
SNOW LOAD TEST
20 FOOT STR. WALL

TABLE IV
LOAD-STRAIN-DEFLECTION RESULTS
SNOW LOAD TESTS
20' STRAIGHT WALL CASE II

NOTES:
1. HORIZONTAL DEFLECTIONS OF FULL ARCH MEASURED 58" FROM FLOOR.
2. VERTICAL DEFLECTIONS MEASURED FROM APEX OF ARCH.
3. ALL STRAINS ARE COMPRESSIVE UNLESS MARKED "T".

APPLIED LOAD LBS.	APPLIED LOAD LBS. PER SQ.FT.	STRAIN, MICRO - INCHES PER INCH							DEFLECTION--INCHES	
		GAGE I	GAGE II	GAGE III	GAGE IV	GAGE V	GAGE VI	GAGE VII	VERTICAL	HORIZONTAL
0	0	0	0	0	0	0	0	0	0	0
344	5	40	50	10	10	50	10	10	3/16"	1/8"
692	10	100	140	60	50	15	90	60	3/8"	3/8"
1046	15	150	220	80	60	20	165	180	11/16"	5/8"
1403.5	20	200	290	110	85	10	150	145	3/4"	5/8"
1748.5	25	255	390	160	130	60 T	160	175	1-1/16"	1-1/8"
2107.5	30	300	480	190	150	120 T	260	100	1-1/2"	1-3/8"

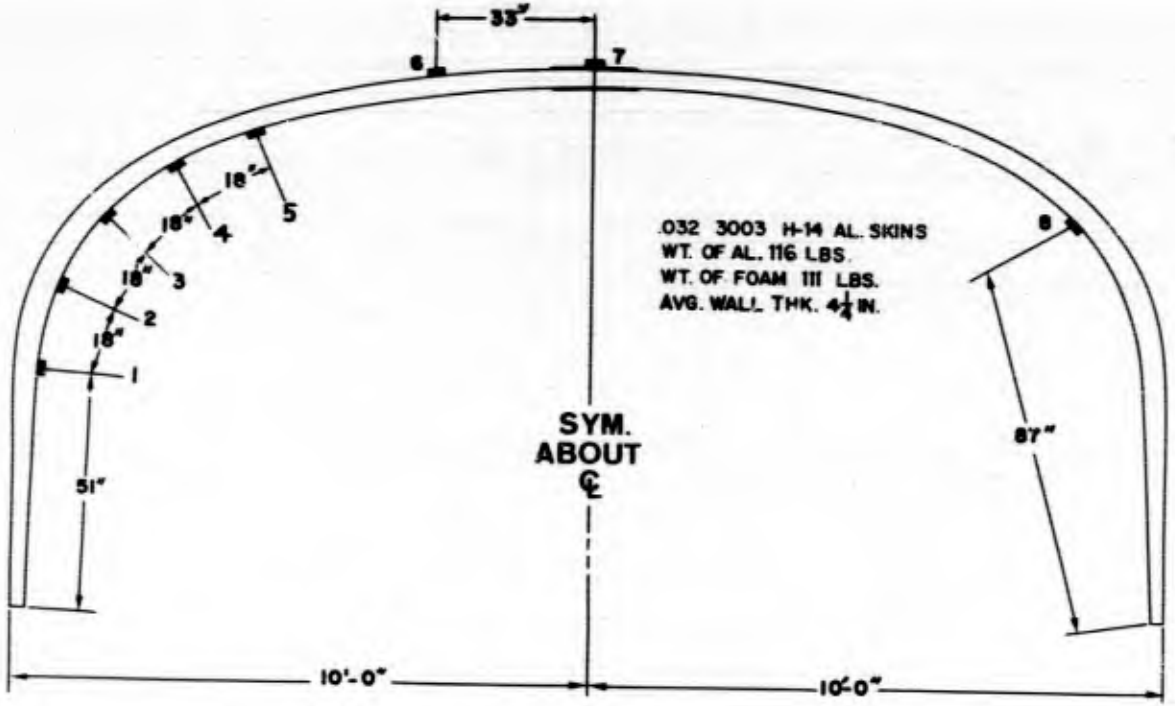

LOCATION OF STRAIN GAGES
SNOW LOAD TESTS
20 FOOT ARCH

TABLE V

LOAD-STRAIN-DEFLECTION RESULTS
SNOW LOAD TESTS
20' SEMI-ELLIPTICAL ARCH CASE II

NOTES:

1. HORIZONTAL DEFLECTIONS OF FULL ARCH MEASURED 51" ABOVE FLOOR.
2. VERTICAL DEFLECTIONS MEASURED FROM APEX OF ARCH.
3. ALL STRAINS ARE COMPRESSIVE UNLESS MARKED "T".

APPLIED LOAD LBS	APPLIED LOAD LBS. PER SQ. FT.	STRAIN, MICRO INCHES PER INCH								DEFLECTION-INCHES	
		GAGE I	GAGE II	GAGE III	GAGE IV	GAGE V	GAGE VI	GAGE VII	GAGE VIII	VERTICAL	HORIZONTAL
Not Recorded	0	0	0	0	0	0	0	0	0	0	0
Not Recorded	5	60	50	80	70	60	10	10	80	1/4"	1/8"
Not Recorded	10	110	100	150	130	80	30	20	120	15/32"	3/8"
Not Recorded	15	170	140	240	260	150	40	30	200	3/4"	5/8"
Not Recorded	20	220	170	300	335	170	120	50	270	1-3/16"	13/16"
Not Recorded	25	260	190	350	430	220	120	70	310	1-7/16"	15/16"

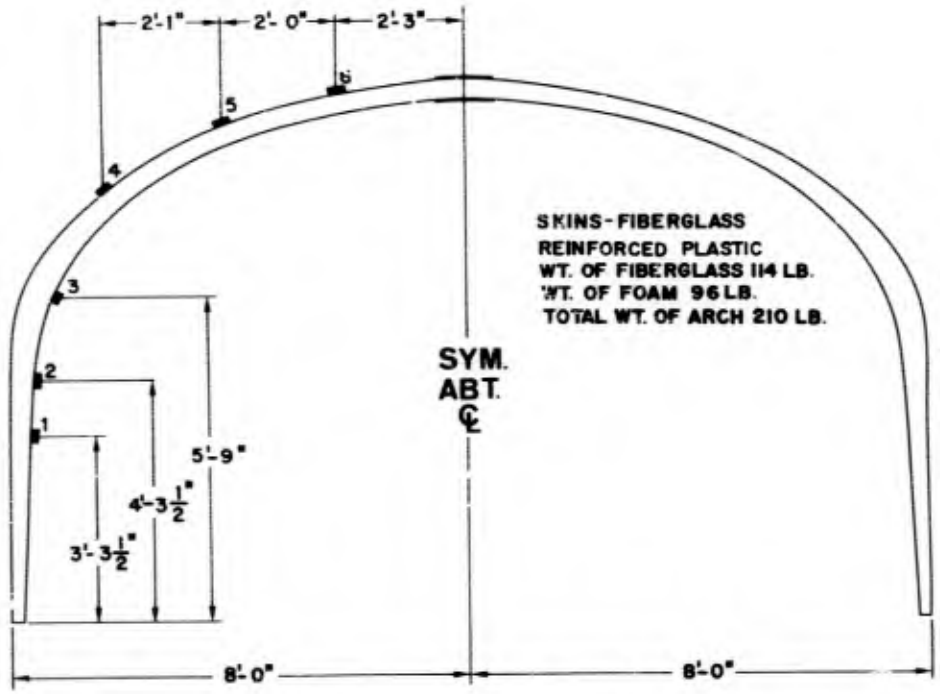

LOCATION OF STRAIN GAGES
SNOW LOAD TEST
16 FOOT ARCH

TABLE VI

LOAD STRAIN DEFLECTION RESULTS
SNOW LOAD TESTS
16' SEMI-ELLIPTICAL ARCH

NOTES:

1. HORIZONTAL DEFLECTIONS OF FULL ARCH MEASURED $50\frac{1}{2}$" ABOVE FLOOR.
2. VERTICAL DEFLECTIONS MEASURED FROM APEX OF ARCH.
3. ALL STRAINS ARE COMPRESSIVE UNLESS MARKED "T"

APPLIED LOAD LBS	APPLIED LOAD LBS. PER SQ. FT.	STRAIN, MICRO - INCHES PER INCH						DEFLECTION-INCHES	
		GAGE I	GAGE II	GAGE III	GAGE IV	GAGE V	GAGE VI	VERTICAL	HORIZONTAL
0	0	0	0	0	0	0	0	0	0
265	5	200	270	300	140 T	120 T	90	1/2"	1/4"
536	10	360	460	520	190 T	200 T	180	3/4"	1/4"
779	15	580	760	870	400 T	280 T	300	1-3/8"	1.0
1040	20	820	1060	1210	640 T	300 T	460	1-15/16"	1-1/2"
1300	25	1020	1360	1580	900 T	280 T	470	2-11/16"	1-3/4"

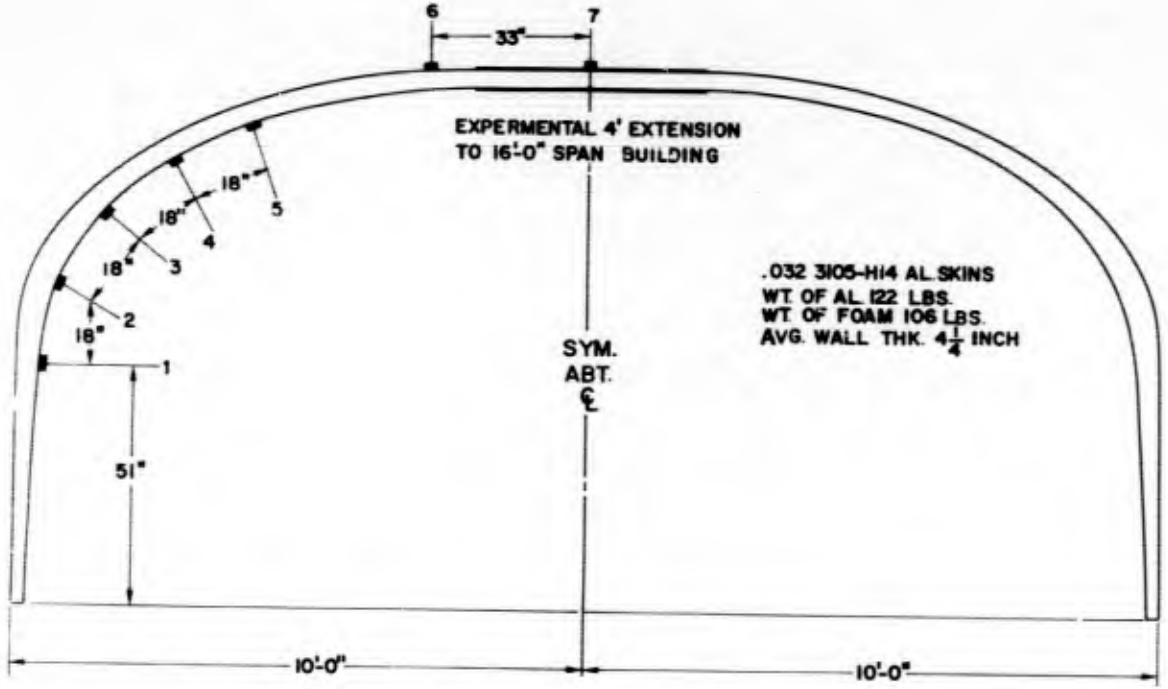

LOCATION OF STRAIN GAGES
SNOW LOAD TESTS
20 FOOT ARCH CASE I

TABLE VII
LOAD-STRAIN-DEFLECTION RESULTS
SNOW LOAD TESTS
MODIFIED SEMI-ELLIPTICAL ARCH

NOTES:
1. HORIZONTAL DEFLECTIONS OF FULL ARCH MEASURED 51" ABOVE FLOOR.
2. VERTICAL DEFLECTIONS MEASURED FROM APEX OF ARCH.
3. ALL STRAINS ARE COMPRESSIVE UNLESS MARKED "T".

APPLIED LOAD LBS	APPLIED LOAD LBS PER SQ. FT.	STRAIN, MICRO INCHES PER INCH							DEFLECTION - INCHES	
		GAGE I	GAGE II	GAGE III	GAGE IV	GAGE V	GAGE VI	GAGE VII	VERTICAL	HORIZONTAL
0	0	0	0	0	0	0	0	0	0	0
338.5	5	50	50	50	30	20	15	60	1/4"	1/8"
681.5	10	125	130	150	100	60	60	110	11/16"	3/8"
1024.0	15	180	180	210	130	90	80	170	15/16"	1/2"
1361.5	20	255	260	320	200	140	140	200	1-11/32"	3/4"
1698.5	25	310	320	390	220	170	170	260	1-3/4"	1.0

Following the deductions from the results of these studies, an expedient, shop-built, single-cavity mold was used to fabricate 30 panels of modified arch shape, sufficient to make fifteen 4-foot modules which were erected and fitted with end walls. The resultant 20- by 60-foot structure is now undergoing test at the USAERDL, Fort Belvoir, and modifications are being incorporated to eliminate or overcome any shortcomings or deficiencies as they are being reported relative to the Vietnam prototype. Initial observations and results of rather severe tests during the 1966-67 fall and winter season indicate full adequacy of design for tropic applications. With minor modifications, the design load could be increased to fulfill requirements for use in temperate zones.

A new six-cavity gang mold to accommodate the new 20-foot span module design is now under construction and is scheduled for completion in March of 1967. Prototype panels or structures from this mold could conceivably be in existence as early as May 1967.

SUMMARY

The USAERDL, after 6 years of concentrated research, has arrived at a point that it can state without too much risk of contradiction that a system or method of on-site building fabrication is a reality and can be implemented in a reasonably short lead time after receipt of a valid requirement.

Sufficient background, experience, and know-how has been built up to back up these remarks. Nine structures, comprising a total of 460 feet of buildings, have been fabricated as of this writing. Of these, all but one are still in use. Two of them were dismantled and re-erected in new locations, in both instances by inexperienced personnel. The 70-foot structure installed at Camp Century, Greenland, was abandoned under the ice cap, with the closing of that installation in 1965. The Vietnam structure, in spite of some leakage problems in its early tenancy, is now performing excellently.

We have submitted this report and commentary as a continuation of our discussion at the conference proceedings of 1965 with the hope that, as stated in that presentation, some methods, processes, equipment, or materials described in our research effort may stimulate thinking or in some way aid the vast research and endeavor toward human existence in the extraordinary environments of space or interplanetary movement.

For the present, we have arrived at our immediate goal. Future plans call for even more challenging projects such as hangar-type buildings and multi-purpose structures. Whether more exotic methods or materials will be evolved to achieve this end, only the future can reveal. We may well look to future aerospace developments to solve some of these problems.

PREFABRICATED BUILDINGS BRANCH
Project M643303D55004

Subject: Prefab.Bldgs.Comparison Data

BUILDING CHARACTERISTICS	A RIGID FOAM PLASTICS (ALUMINUM SKIN)	B RIGID FOAM PLASTICS (GLASS FIBER SKIN)	C RIGID FOAM PLASTICS (ALUMINUM SKIN)	D STRAIGHT WALL QUONSET (STEEL)	E T-5 (PLYWOOD)
	16' x 48' (768 Sq Ft)	16' x 48' (768 Sq Ft)	20' x 48' (960 Sq Ft)	20' x 48' (960 Sq Ft)	16' x 48' (768 Sq Ft)
Net Weight (pounds)	2900#	2650#	3200#	7100#	8800#
Shipping Weight (pounds)	3325#	3075#	3500#	8510#	11800#
Shipping Cube	53 cu ft	59 cu ft	67 cu ft	272 cu ft	1300 cu ft
Fabrication Time (M.H.)	90 M.H.	90 M.H.	90 M.H.	*	*
Erection Time (M.H.)	65 M.H.	65 M.H.	65 M.H.	182 M.H.	54 M.H.
Fabrication & Erection Time	155 M.H.	155 M.H.	155 M.H.	*	*
Shipping Wt/100 Sq Ft Floor Area	430#	400#	365#	890#	1530#
Shipping Vol/100 Sq Ft Floor Area	7.3 cu ft	8.1 cu ft	7 cu ft	28 cu ft	170 cu ft
Site Labor Cost @ $5.00/M.H.	$ 775.00	$ 775.00	$ 775.00	$ 910.00	$ 270.00
Total Material Cost	2000.00	2375.00	2200.00	**2700.00	**12,200.00
Packing Cost/Building	39.00	39.00	41.00	*	*
Shipping Cost - New York to SEA ($29.00/Ship-Ton)	38.00	43.00	49.00	197.00	940.00
1/100 Mold Cost	250.00	250.00	250.00	NA	NA
1/100 Mold Packaging Cost	4.00	4.00	4.00	NA	NA
Cost of Building - Erected	$3106.00	$3486.00	$3319.00	$3807.00	$13,410.00
Building Cost/Sq Ft-Without Floor	$ 4.05	$ 4.55	$ 3.46	$ 3.97	$ 17.40

Notes: Bldgs. A, B & C - Fabricated on site with 1 door and 1 window per each end wall.
Bldgs. D & E - Fabricated in vendor's plant. Cost based on present production price less estimated cost, weight and cube of floor.

* - Fabrication and packing done at vendor's plant.
** - Completed building.

Basis of Estimate: Aluminum .032" thick, $0.22/Sq Ft (Coated).
Glass Fiber Skin .045" thick, $0.37/Sq Ft.
Rigid Foam $0.60/lb.
Bldgs. A, B & C - (1) Mold amortized for 100 Buildings.
(2) Shipping cube based on material plus 1/100 mold cube.

26 October 1966

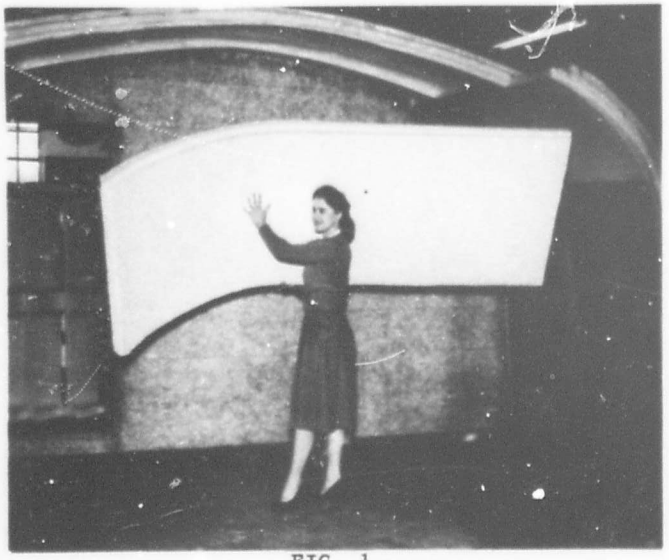

FIG. 1

FIG. 2

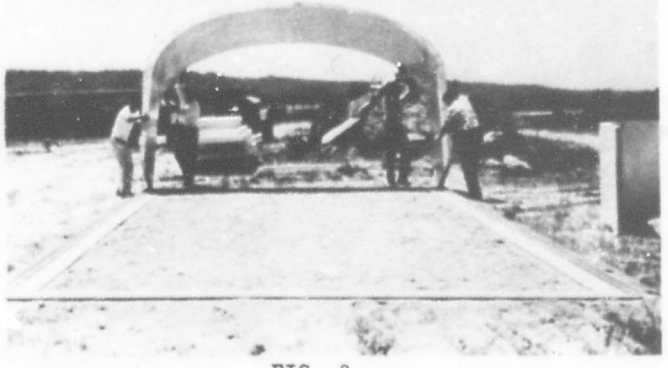

FIG. 3

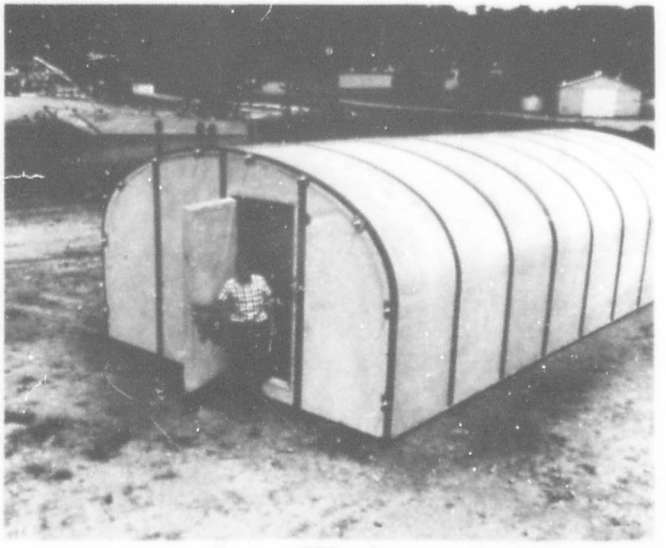

FIG. 4

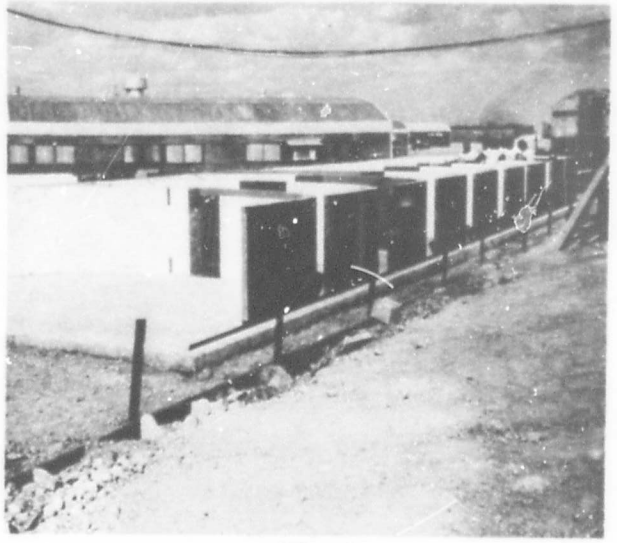

FIG. 5

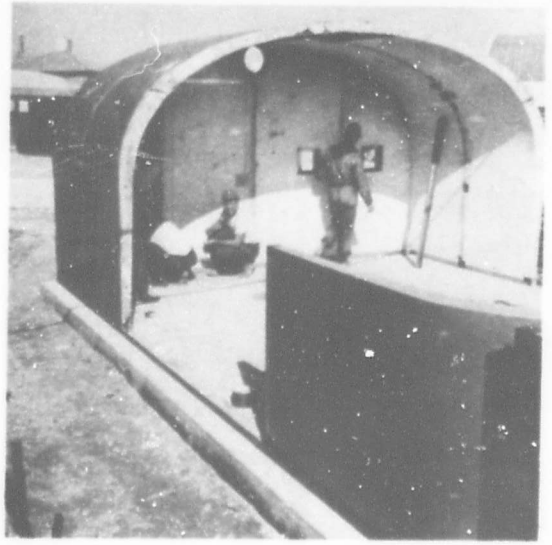

FIG. 6

FIG. 7

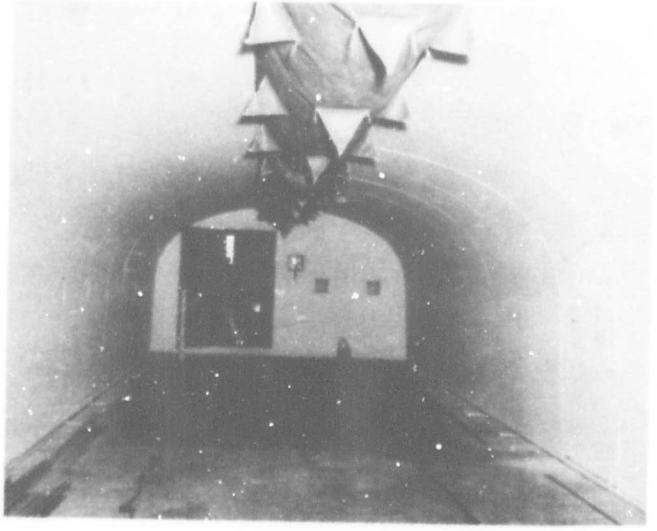

FIG. 8

FIG. 9

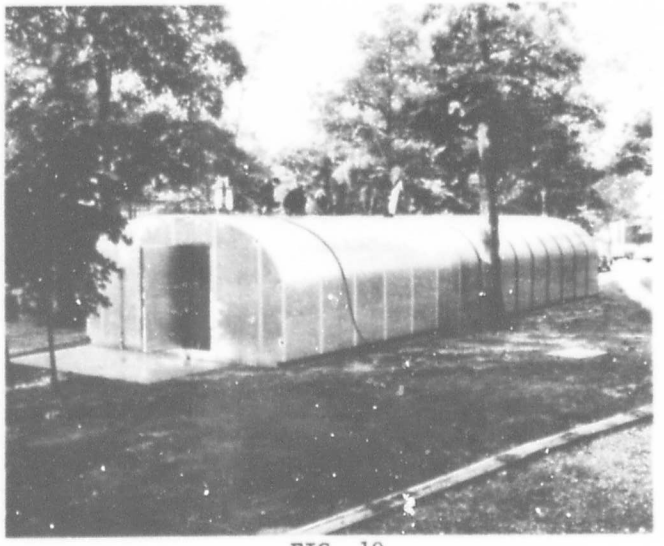

FIG. 10

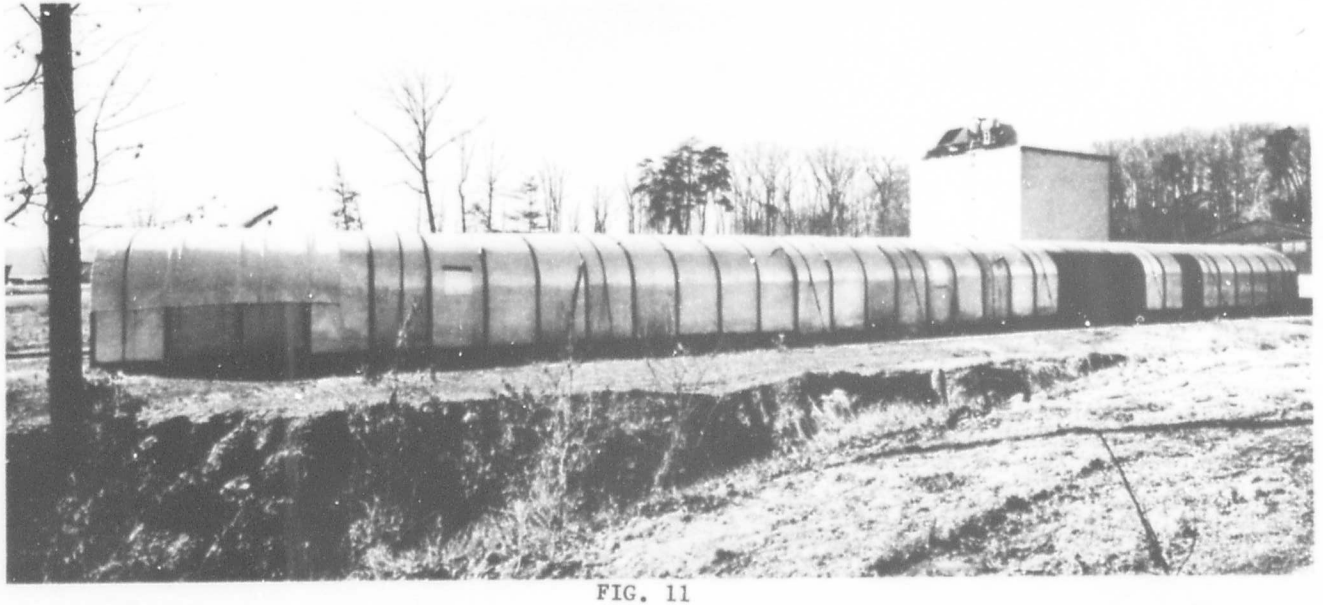

FIG. 11

ILLUSTRATIVE NOTES

Fig. 1 - The young lady easily handles a typical module section of the type originally designed for no-load applications in the Greenland Ice Cap installation. The weight of these uncoated polyurethane panels averaged approximately 25 pounds each. It was soon realized, however, that a tougher surfacing material would have to be added because the friability of the unprotected foam was not compatible with troop tenancy.

Fig. 2 - At the termination of the second testing season in the Arctic ice tunnel, this experimental structure was dismantled by troops and stored at the Polar Research surface camp. The photo illustrates the above ground installation in progress, again by troop labor, during the succeeding summer season.

Fig. 3 - This is one of several Fort Belvoir installations and shows the start of the assembly of the arches on the prepared base. Four men easily handle and erect the 4-foot modules.

Fig. 4 - The same installation shown in the preceding illustration, as it appears completed. This structure was designed as a special purpose, non-metallic structure, and as such was constructed using plastics materials throughout, including the longitudinal draw bars, which were fabricated of plastics impregnated fiberglass strands.

Fig. 5 thru 8 - These illustrations represent the phases of erection of the plastics structure installed in the hospital complex at Bien Hoa, Vietnam. In Fig. 5, the 4-foot modules are shown assembled, ready for erection on the slab. Fig. 6 shows the start of the second day's work, with the end wall and the first two modules assembled. Fig. 7 shows the completed building ready for occupancy. (To the right of the picture and in the background may be seen the corrugated steel "Straight Wall Quonset" structures presently considered more or less standard.) The interior of the plastics structure is illustrated in Fig. 8. The apparatus shown suspended from the ceiling is a fabric duct designed to distribute the cooling air from the two 36,000 BTU air conditioning units originally supplied with the building.

Fig. 9 and 10 - Subsequent to the Vietnam operation, a stated requirement to increase the building design span from 16 feet to 20 feet resulted in a design study inclined toward achieving necessary strengths compatible with economy of material and production at the wider span. Illustrated in Fig. 9 are the various experimental shapes evolved, the end result of which is represented in Fig. 10. This structure, 20- by 60-feet, is presently undergoing test at Fort Belvoir. It is interesting to note the number of men working simultaneously on the roof with no apparent ill effects or weakness in the structure.

Fig. 11 - This illustration is presented for two purposes: First, because of the unusual requirement for a temporary special purpose building 140 feet long, and secondly, but of equal interest, was the low procurement cost experienced due to the fact that it was constructed entirely of experimental and reject panels accumulated during the course of our research procedures and were otherwise scheduled for consignment to the dump.

REFERENCES

1. Ray H. Anderson, USAERDL, Fort Belvoir, Virginia, Memorandum Report, "Rigid Foam Plastics Shelters, Arctic Field Tests," 16 April 1962.

2. Robert K. Hedrick and Abraham Perez, USAERDL, Fort Belvoir, Virginia, Memorandum Report, "Rigid Foam Plastics Shelters, Structural Tests of Reinforced Plastics Beams, Honeycomb Panels, and Experimental Arctic Building," 15 October 1962.

3. Abraham Perez and S. B. Swenson, USAERDL, Fort Belvoir, Virginia, Memorandum Report, "Rigid Foam Plastics Shelter by Spray Application to an Air Supported Mold," 30 July 1963.

4. S. B. Swenson, USAERDL, Fort Belvoir, Virginia, "Buildings in Barrels, Part II," Paper to the Society of the Plastics Industry, Reinforced Plastics Division, 6 February 1964.

5. S. B. Swenson, USAERDL, Fort Belvoir, Virginia, "Buildings in Barrels, Part III," Paper to Second Aerospace Conference, 27 May 1965.

SELECTION AND DEVELOPMENT OF AN EXTENDIBLE, FLAT, CAVITY-BACKED SPIRAL ANTENNA

R. A. Farran* and G. Yee**

SECTION I. INTRODUCTION

An investigation of several methods of deploying flat, cavity-backed spiral antennas in space was completed in late 1965 in conjunction with a space vehicle study performed at Aerospace Corporation. A storage volume constraint within the spacecraft necessitated the use of expandable antennas having expanded diameters of five to ten feet. During the study, thirteen designs were considered, including various mechanical, elastic recovery foam, and inflatable structures. The designs were compared on the basis of factors such as reliability of deployment, ease of handling and testing prior to launch, simplicity of fabrication, surface contour accuracy, deployment time, storage volume, pattern testing, and state-of-the-art of materials and fabrication. For the size of antenna required, and for the particular conditions and packaging volume available on the space vehicle, the design selected as the most promising was an extendible arm concept. This paper briefly describes the various designs and shows how they were evaluated to isolate the most desirable concept. A more detailed description is then given of how a working model of the selected antenna was fabricated, tested in the shop, and further improved prior to a full-scale development effort currently being conducted by a contractor.

SECTION II. DESCRIPTION

A flat, cavity-backed spiral antenna is often desirable when communication is required over a wide range of frequencies. This type of antenna consists basically of two flat, parallel surfaces, one of which is used as a structural support for one or more pairs of individual spirals. The spirals emanate from the center of the surface on which they are mounted, and a coaxial cable is used to feed each spiral at this central point. This surface which supports the spirals is transparent to RF radiation. The other surface serves as a reflector to amplify the signals emitted and received by the spirals.

Ideally, an antenna of this type can be made by fabricating the antenna to specification on a thin, rigid shell structure which can then be deployed simply by swinging the shell into the desired position at the appropriate deployment time. However, this would entail utilization of a relatively large packaging volume within the space vehicle where space is at a premium. Therefore, for maximum available space utilization, an expandable type of structure is desirable.

*Staff Engineer, Aerospace Corp., El Segundo, Calif.

**Member of Technical Staff, Aerospace Corp., El Segundo, Calif.

SECTION III. GENERAL REQUIREMENTS FOR THE EXPANDABLE ANTENNA

Mission constraints and antenna design objectives pertinent to this study were:

1. One-year mission duration
2. Negligible solar pressure and aerodynamic drag effects
3. Capability of ground deployment and testing without auxiliary support
4. Extended storage period without degradation
5. High ratio of expanded volume to packaged volume
6. Dimensions and tolerances:

Antenna diameters	5 to 10 ft
Diameter-to-depth ratio	3 to 4
Flatness tolerance (D = diameter of spiral antenna)	
0 - 1/2 D	±0.01D
1/2 D - D	±0.02D
Depth tolerance (between surfaces)	±0.02D
Spiral tolerance (radial)	±0.01D

SECTION IV. DESIGN CONCEPTS

The design concepts investigated can be classified into three categories: mechanical, elastic recovery foam, and inflatables. Most of these techniques require the unfurling of two fabric surfaces: a top fabric surface to which the metallic foil spiral antenna is attached and a lower fabric surface which contains a conducting material which acts as a signal reflector. These two surfaces and a central support tube form the desired antenna. All of these concepts present problems which are associated with the various ways in which a structure can be expanded, rigidized, and maintained in a space environment for a period of up to one year.

The mechanical concept utilizes unfolding arms to deploy the antenna; in the foam concept, deployment is effected by elastic recovery of the foam.

The inflatable concepts use a system of inflating a ring or a circular toroid structure to unfurl and support the antenna surfaces. The structure is then rigidized by any of several methods, including polymerization of an organic resin by either catalysis or thermal activation, or hardening of a gelatin solution by evaporation of water. Rigidization may also be accomplished by a strain-hardening process in which an aluminum foil or the metal in a wire grid mesh-film laminate is strained slightly beyond the yield point by internal pressurization of the structure.

Brief descriptions follow of the expandable concepts investigated; these concepts are shown in Figs. 1 through 12. Design features of these antennas, including the ideal, thin rigid-shell design, are compared in Table 1. These are typical designs which were utilized to aid in determining the advantages and disadvantages of each design. It was neither practical nor necessary to consider all possible combinations of materials and techniques to achieve a suitable design for this application.

Table 1. Design Features

Feature / Design	Ground storage	Contour accuracy	State of art	Capable of full ground deployment test	Deployment time (rigidized)	Deployment restrictions
Thin rigid shell	Unrestricted	Excellent	Developed	Yes	Already erected	None
Flexible disk (Fig. 1)	Unrestricted	Excellent	Developed	Yes	< 1 minute	None
Folded sides (Fig. 2)	Unrestricted	Good	Developed	Yes	< 1 minute	None
Flex ribs (Fig. 3)	Unrestricted	Good	Developed	Yes	< 1 minute	None
Extendible arms (Fig. 4)	Unrestricted	Good	Developed	Yes	< 1 minute	None
Elastic recovery foam (Fig. 5)	Prolonged storage reduces foam resiliency	Poor	Developed	Yes	< 1 minute	Recovery force depends upon maximum number of folds during packaging
Expandable sandwich-rigidized core (Fig. 6)	Controlled environment required	Fair	In development	Yes	< 1 hour	Water vapor will freeze at low temperature
Expandable sandwich-rigidized foam (Fig. 7)	Controlled environment required	Fair	In development	Inflate - but not rigidized	< 1 hour	Reaction slow at low temperature
Expandable sandwich-rigidized (Fig. 8)	Controlled environment required	Fair	In development	Inflate - but not rigidized	< 1 hour	Reaction slow at low temperature
Circular toroid-rigidized core (Fig. 9)	Controlled environment required	Fair	In development	Yes	< 1 hour	Water vapor will freeze at low temperature
Circular toroid-rigidized foam (Fig. 10)	Controlled environment required	Fair	In development	Inflate - but not rigidized	< 1 hour	Reaction slow at low temperature
Yielded aluminum foil (Fig. 11)	Unrestricted	Poor	Developed	Inflate - but number of rigidizing yields limited	< 1 minute	None
Yielded wire grid (Fig. 12)	Unrestricted	Poor	In development	Inflate - but number of rigidizing yields limited	< 1 minute	None

The simplest, most straightforward mechanical design is the thin rigid shell. This design could be made from any of a large number of materials. Such a structure, however, could not be used in the present application because of its relatively large packaging volume. In all other respects, it is a highly desirable design and was therefore used as a baseline with which all the other designs could be compared.

A. MECHANICAL

Of many mechanical design concepts possible, four generally representative types were investigated (Figs. 1-4).

FIG. 1 MECHANICAL - FLEXIBLE DISK

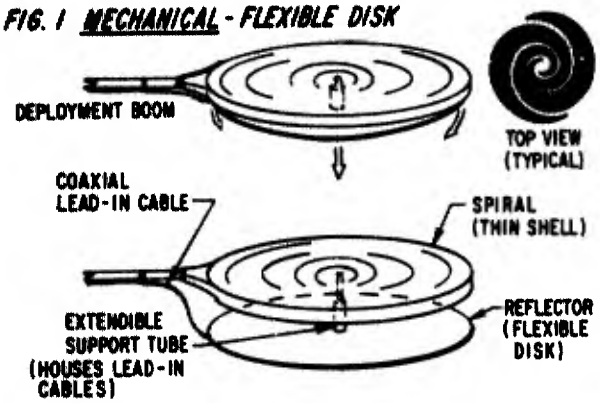

FLEXIBLE REFLECTOR FOLDS UNDER SPIRAL SHELL. EXTENDING BOOM RELEASES REFLECTOR AT DEPLOYMENT

FIG. 2 MECHANICAL - FOLDED SIDES

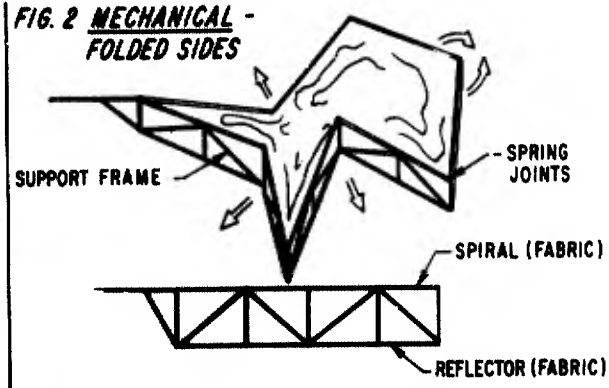

UNFOLDING OF SUPPORT FRAME SIDES BY SPRING LOADED JOINTS STRETCHES ANTENNA SURFACES

FIG. 3 MECHANICAL - FLEX RIBS

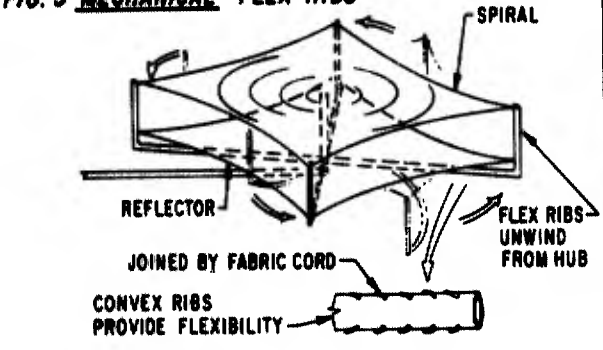

UNWINDING FLEX RIBS FROM CENTER HUB DEPLOY ANTENNA SURFACES

FIG. 4 MECHANICAL-EXTENDIBLE ARMS

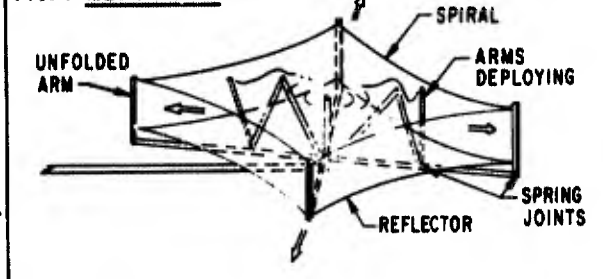

UNFOLDING SPRING LOADED ARMS STRETCH ANTENNA SURFACES AT CORNERS AND HOLD ANTENNA

1. FLEXIBLE DISK

In the flexible disk design (Fig. 1) the spiral surface is attached to a rigid thin-shell structure. The reflector surface consists of a thin flexible disk. For packaging, the reflector is folded, or bent, to meet the rigid spiral surface. This concept permits the antenna height to be reduced for packaging without disturbing the spirals. Compact storage is further facilitated by retracting the central tube that supports the antenna and the coaxial lead-in cables. Deployment is accomplished by releasing a spring mechanism within the central cable support tube which extends into its full deployed position, at which time the lower reflector sheet springs back into a flat disk shape. Since the spirals are built on a rigid structure, they can be fabricated to very close tolerances. The disadvantage is that for large antenna diameters the packaging within a restricted spacecraft volume will be difficult, if not impossible.

2. FOLDED SIDES

The mechanical folded side concept (Fig. 2) consists of a box-shape support frame with a series of spring-loaded joints located along the sides of the box. These joints are designed such that the support frame can be folded into a semi-star shape for packaging. Spiral and reflector surface fabrics are attached to the upper and lower frames of the support structure. As the structure unfolds into a square shape, the fabrics are stretched across the square to form the antenna. Support lines to the corners of the frame provide support for the central coaxial support tube.

3. FLEX RIBS

The flex rib concept (Fig. 3) utilizes the spring action of ribs, wound around a center hub, to deploy the antenna. As shown in the figure, the rib is comprised of two thin convex metallic strips, joined together at the edges with fabric lacing, thereby providing a lenticular cross-section when in the extended position. The rib is designed to withstand bending loads but also has good resistance to torsion. When folded about the central hub, the sides of the rib are flattened together. Upon release of a band, or similar restraining device, the ribs are free to spring into their preferred (extended) position. The antenna surfaces are supported at the corners and at the center by the lead-in cable support tube which, in turn, is attached to the deployment boom.

4. EXTENDIBLE ARMS

The extendible arm design (Fig. 4) utilizes a concept* of four (or more) spring-loaded arms for deploying and supporting the antenna surfaces. The arms are constructed to resist torsion as well as bending. The arms are folded against each other about a center post and are deployed by releasing a band or similar restraining device. The antenna surfaces are supported at the corners and at the central support tube. Sections VI, VII, and VIII describe the laboratory model, test results, prototype antenna development, and materials and fabrication considerations.

*This concept, which is the one eventually selected for additional analysis and development in this study, was proposed by Mr. John E. R. Bennett of Aerospace Corporation.

B. ELASTIC RECOVERY FOAM CONCEPT

The elastic recovery foam concept (Fig. 5) uses an elastic recovery foam or sponge-like material to deploy the two antenna surfaces. The foam has a spoked-wheel shape over which the antenna surfaces are stretched. The antenna is compressed into a number of folds during packaging and, upon release, the foam assumes its original shape thereby deploying the antenna. In this design, the antenna surfaces are fully supported by the foam. There is some question as to the ability of the foam to deploy the antenna to the contour accuracy required. This will be particularly noticeable for an antenna which has been packaged for any length of time because the foam tends to lose some of its resiliency under prolonged compression. This type of structure also needs auxiliary support for antenna pattern testing in a 1-g environment.

C. INFLATABLE CONCEPTS

1. EXPANDABLE SANDWICH - RIGIDIZED FLUTED CORE

The expandable sandwich antenna (Fig. 6) is formed by inflating a ring sandwich structure (using drop cords) to stretch the antenna surfaces. (The drop cords maintain the shape of the ring during inflation.) The external ring consists of a gelatin-impregnated fluted core structure. Rigidization takes place after deployment by evaporation of water from the gelatin. Since the gelatin solution will freeze at low temperatures, it is important that inflation take place immediately upon deployment of the antenna to permit it to acquire the desired shape before freezing. At some point on orbit, the antenna, by virtue of properly selected values of emissivity and solar absorptivity, will achieve a sufficiently high temperature to melt the ice in the gelatin (if the water has frozen) and to evaporate the water to rigidize the structure permanently. Since the structural strength depends upon expanding the fluted cores into shape, air sacs are located intermittently throughout the fluted cores and are inflated at the time of deployment to help the structure attain its desired shape.

This concept is reversible because, after rigidization, the structure may be softened again by exposure to water vapor. This feature may be desirable for ground testing. After the antenna is rigidized, air is released from the inflated ring to avoid adverse effects should the ring be punctured in space. This step is recommended for all inflatable antennas which do not require maintenance of pressure for structural purposes.

2. EXPANDABLE SANDWICH - RIGIDIZED FOAM

This antenna configuration (Fig. 7) utilizes the same inflating, expandable sandwich structure as the previous concept, except that a foam or a sponge-type material is bonded to the external surface of the ring. The foam is impregnated with a resin, and the rigidization process is initiated by electrical heating elements which are spaced within the foam. This rigidizing reaction can be initiated over a wide range of initial temperatures from -100° to +350°F. At low temperatures, the reaction progresses at a slower rate. The rigidization process is irreversible.

3. EXPANDABLE SANDWICH - RIGIDIZED

This concept (Fig. 8) requires the impregnation of the expandable sandwich internal drop cords with a resin. To rigidize the structure, the resin is exposed to a catalyst, water vapor in this case, which is circulated through the inflated ring. This rigidization process is also irreversible.

FIG. 5 ELASTIC RECOVERY FOAM

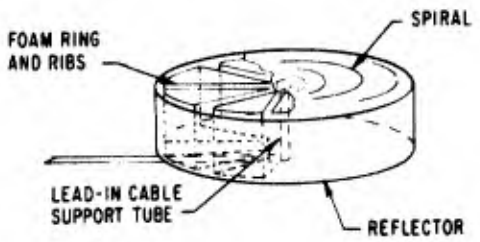

ELASTIC RECOVERY OF COMPRESSED FOAM STRETCHES ANTENNA SURFACES

FIG. 6 INFLATABLE-EXPANDABLE SANDWICH-RIGIDIZED FLUTED CORE

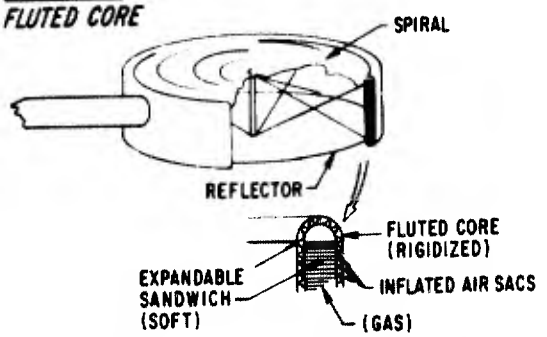

INFLATING RING STRETCHES ANTENNA SURFACES. EVAPORATION OF WATER FROM GELATIN IMPREGNATED FABRIC RIGIDIZES RING PRIOR TO RELEASE OF GAS

FIG. 7 INFLATABLE-EXPANDABLE SANDWICH-RIGIDIZED FOAM

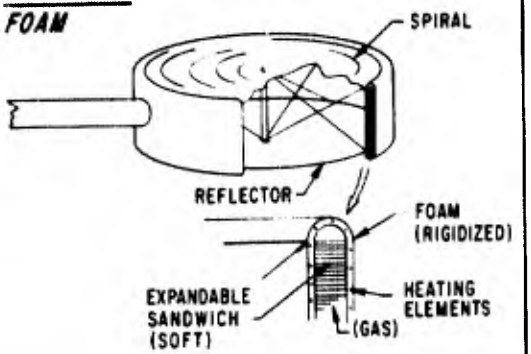

INFLATING RING STRETCHES ANTENNA SURFACES. FOAM ON RING RIGIDIZED BY INITIATING ELECTRICAL HEATING ELEMENTS PRIOR TO RELEASE OF GAS

FIG. 8 INFLATABLE-EXPANDABLE SANDWICH-RIGIDIZED

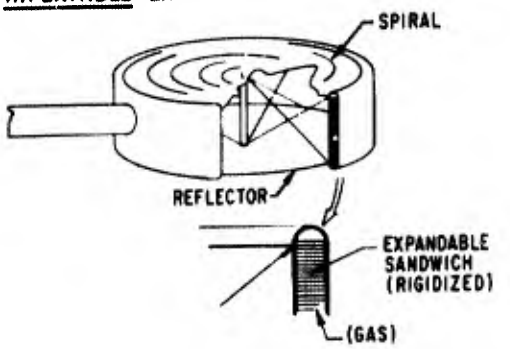

INFLATING RING STRETCHES ANTENNA. RESIN IMPREGNATED EXPANDABLE SANDWICH RIGIDIZED BY WATER VAPOR PRIOR TO RELEASE OF GAS

4. CIRCULAR TOROID - RIGIDIZED

This inflatable structure uses a circular toroid for supporting the antenna surfaces. The difference between this concept and the previous inflatable concept is that an expandable sandwich type structure is not required to maintain the structural shape. Either a rigidized fluted core structure (Fig. 9) or a rigidized foam (Fig. 10) can be used for this purpose. The circular toroid concept requires a series of drop lines between the spiral and reflector surfaces (at their periphery) to control the tolerance on the spacing between them.

FIG. 9 INFLATABLE-CIRCULAR TOROID-RIGIDIZED FLUTED CORE

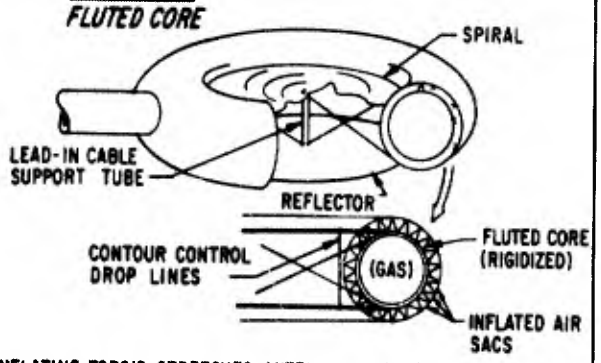

INFLATING TOROID STRETCHES ANTENNA SURFACES. EVAPORATION OF WATER FROM GELATIN IMPREGNATED FABRIC RIGIDIZES TOROID PRIOR TO RELEASE OF GAS

FIG. 10 INFLATABLE-CIRCULAR TOROID-RIGIDIZED FOAM

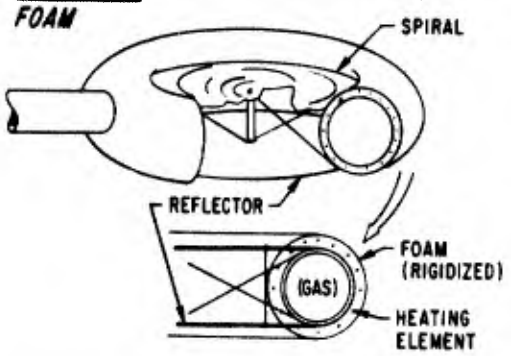

INFLATING TOROID STRETCHES ANTENNA SURFACES. FOAM ON TOROID RIGIDIZED BY INITIATING ELECTRICAL HEATING ELEMENTS PRIOR TO RELEASE OF GAS

FIG. 11 INFLATABLE-YIELDED ALUMINUM FOIL

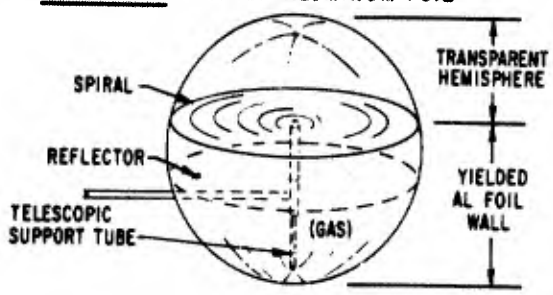

INFLATING SPHERE DEPLOYS ANTENNA. SHAPE RETAINED BY YIELDING AL FOIL PRIOR TO RELEASE OF GAS

FIG. 12 INFLATABLE-YIELDED WIRE GRID

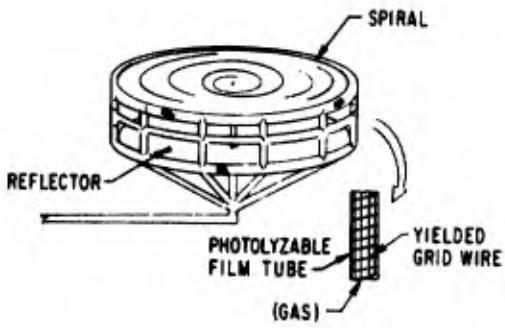

GRID WIRE/FILM TUBE INFLATED TO STRETCH ANTENNA SURFACES AND YIELD WIRE FOR RIGIDIZATION PRIOR TO RELEASE OF GAS. DRAG FORCE REDUCES WHEN FILM PHOTOLYZES

5. YIELDED ALUMINUM FOIL

This concept (Fig. 11) is similar to that used in the "Echo II" balloon. Rigidization is accomplished by inflating with sufficient pressure to yield the aluminum foil walls. The antenna surfaces are stretched across the interior of the balloon and are deployed by the expanding balloon. The upper hemispherical surface covering the spiral surface is made of an RF-transparent material. A telescopic tube extends from the center support tube to the bottom of the balloon to improve antenna structural stability.

6. YIELDED WIRE GRID

This last concept (Fig. 12) consists of a tubular structure made of grid wire laminated with a photolyzable film. The antenna surfaces are stretched across the structure and are deployed by the expanding structure. Rigidization is accomplished by inflating with sufficient pressure to yield the grid wire. Any on-orbit drag forces are reduced appreciably when the film photolyzes.

D. WEIGHT AND PACKAGING VOLUME ESTIMATES

Preliminary weight estimates were made for each design for various antenna diameters. For a typical diameter of 5 ft, for example, the weights ranged from roughly 8 lb for the yielded-wire grid concept to 40 lb for the expandable toroid concept using rigidized foam. A weight of 12 lb was estimated for the extendible arm concept. Since the crude weight estimates were well below the allowable weight for the required application, and since weights did not vary appreciably between concepts, it was decided in this case that weight was not critical, and no extensive weight effort was conducted. In larger designs, or under different circumstances, weight considerations could be very important in concept selection.

In addition, estimates were made of the ratio of antenna expanded volume to packaged volume for the above concepts. The results, tabulated in Table 2, show that this ratio varies from approximately 2:1 for the flexible disk to about 40:1 for the yielded-wire grid structure. The packaging ratio for the extendible arm concept is less than 20:1. These approximations may be expected to vary somewhat, not only with design concept but with antenna diameter. They may also change as design details are more firmly established.

Table 2. Packaging Ratio of Various Antenna Concepts

Packaging ratio*	Concept
1:1	Thin rigid shell
< 2:1	Flexible disk
<10:1	Circular toroid - rigidized fluted core Circular toroid - rigidized foam Elastic recovery foam
<20:1	Folded sides Expandable sandwich - rigidized fluted core Expandable sandwich - rigidized foam Expandable sandwich - rigidized Extendible arms
<30:1	Flex ribs Yielded aluminum foil
<40:1	Yielded wire grid

*Packaging ratio = expanded antenna cavity volume/gross packaged antenna volume (including all support structure required)

SECTION V. COMPARATIVE RELIABILITY ANALYSIS AND CONCEPT SELECTION

A comparative reliability analysis was made of the thirteen typical concepts to determine which types were more feasible for this particular application. Many of the factors listed in Table 3 were evaluated and related quantitatively in a comprehensive reliability study.* The results of this study and other factors were then jointly considered in selecting the desired concept.

Since failure rate data were not available in sufficient quantity for this type of equipment, an absolute reliability number for each antenna design concept could not be determined. Therefore, antenna reliability was evaluated by employing a relative comparison study. This was accomplished by devising a reliability criteria model which would determine the relative "excellence" of each antenna design. In this respect, relative antenna reliability is indicated by numerically ranking the thirteen antenna designs in order of merit based on the sum of the values for each criterion in the reliability model.

The reliability criteria model incorporated those parameters which were believed essential for assuring the successful accomplishment of the mission of the antenna. The two major categories incorporated into the model were antenna criticality (C) and degradation factor (D). Antenna criticality values were selected, on a scale of 0 to 100, to indicate the relative complexities of the equipment being evaluated. Degradation factors were selected between 0 and 1.0 to indicate the relative importance of a particular antenna mechanism functioning correctly. The more complex the equipment item or its importance to perform, the higher the values assigned to each parameter and the lower its reliability. (The combination of degradation and criticality factors is thus analogous to failure probability.) The summation of the product CD is an indication of the relative reliability weighting of the antennas under review, thereby allowing a comparison of antennas in order of merit. The individual values of C and D for various aspects considered for each antenna are summarized in Table 3.

The antennas in Table 3 are listed in order of decreasing reliability, as indicated by the values of ΣCD, and show a distinctive separation into

*W. F. McGrath, Aerospace Corporation, personal communication

Table 3. Reliability Model, Expandable Antennas

Mechanism or function	Degradation factor (D)	Antenna criticality number (C)												
		Thin rigid shell	Flexible disk (Fig. 1)	Extendible arms (Fig. 4)	Folded sides (Fig. 2)	Flex ribs (Fig. 3)	Elastic recovery foam (Fig. 5)	Cir. toroid rigidized foam (Fig. 10)	Yielded wire grid (Fig. 12)	Cir. toroid rigidized core (Fig. 9)	Expandable sandwich			Yielded aluminum foil (Fig. 11)
											Rigidized foam (Fig. 7)	Rigidized (Fig. 8)	Rigidized core (Fig. 6)	
Antenna release mechanism	1.0	10	10	20	20	20	30	30	30	30	30	30	30	30
Antenna positioning	0.9	20	20	20	30	30	20	30	40	30	30	30	30	40
Antenna erection	0.9	20	30	30	30	40	30	40	40	40	40	40	40	40
Spring joints	0.9	10	10	30	30	10	10	-	10	-	-	-	-	10
Locking devices	0.4	-	-	30	30	30	-	-	-	-	-	-	-	-
Gas evacuation	0.4	-	-	-	-	-	-	20	20	20	20	20	20	20
Antenna surface contour	0.8	0	0	20	20	20	50	40	50	40	40	40	40	50
Antenna surface spacing	0.8	0	20	20	20	30	20	30	30	30	40	40	40	30
Antenna support tube	0.4	-	-	-	-	-	-	-	-	-	-	-	-	30
Lead-in cable support	1.0	10	20	10	10	10	10	30	20	30	30	30	30	20
Storage environment	0.4	0	0	0	0	0	20	30	0	30	30	30	30	0
Ground electrical testing	0.2	0	10	0	10	20	30	20	30	30	30	30	30	30
Ground deployment	0.4	0	0	0	0	0	40	10	0	20	10	10	20	0
	ΣCD	65	102	146	157	158	180	207	209	213	217	217	221	221

three main reliability "groups." One antenna, the thin rigid shell, scores at the extreme high reliability end of the scale, while the remaining antennas cluster into two other groups. Closely ranked antennas differ little in their over-all reliability rating. Table 3 shows, as might be expected, that from a reliability standpoint the thin rigid shell ranks appreciably above the other antennas, because it has no moving parts and needs only to be deployed and oriented. The second best group includes the remaining mechanical concepts and the recovery foam concept. The inflatable concepts fall in the third reliability grouping.

The highest ranked concepts, i. e., the thin rigid shell and the flexible disk, were eliminated because of inadequate storage volume on the proposed spacecraft. The extendible arm concept ranked next in reliability, had an adequately small packaging volume, and had a satisfactory weight. For these reasons, the extendible arm concept was selected for more detailed investigation.

SECTION VI. MODEL DEVELOPMENT AND TESTING

Two main problems had to be solved in the case of the extendible arm concept. One was associated with the dynamics and kinematics of the antenna unfurling process. The other was the capability of maintaining the contour of the surfaces within acceptable limits after the antenna had been deployed. Because of the compact configuration of these antennas in the folded position, launch loads did not present a problem. In order to establish the concept feasibility, and to solve these two problems, it was decided to fabricate and test a simplified, but mechanically representative, model.

A nominal 3-ft-diameter × 1-ft-depth antenna was selected. The arms were made of 0. 03-in. thick × 0. 5-in. OD aluminum tubing with torsion springs at the joints for unfolding the arms. A tension spring was also attached to each arm at the central support tube to pull the arms into the fully deployed position. For simulation of the antenna surfaces, a lightweight 2-oz/yd^2 Dacron fabric was used with an elastic cord attachment between the corners of the sheet and the arm members to provide a positive tension on the fabric surface.

While fabrication of the antenna proceeded, improvements in the design were made frequently as various shortcomings became evident. Improvements were made in stiffening the extendible arms in the vicinity of the spring joints (to prevent permanent bending), stops were used at the joints, and spring forces were adjusted to improve both antenna deployment and surface contour flatness with the antenna oriented in various positions.

The final working model is shown in the deployed position in Fig. 13a. Figures 13b and 13c show the antenna as it is being folded, and Fig. 13d shows it in the fully-stored position. Figures 13e and 13f show the top and bottom views, respectively, in the fully-stored position. For experimenting in the shop, a lanyard was used to release the antenna which would then deploy by

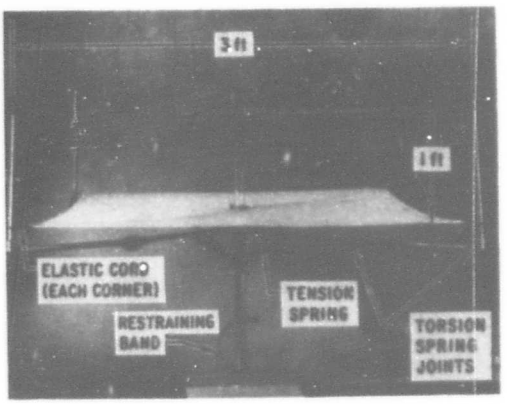

(a)

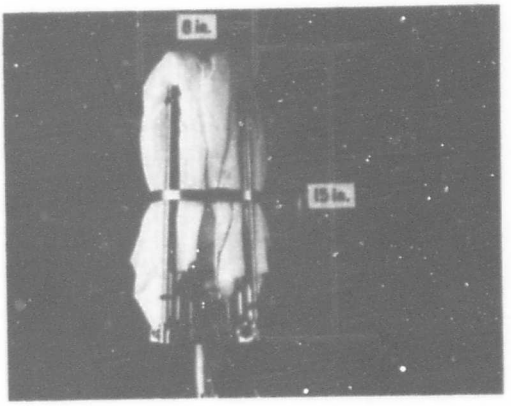

(d)

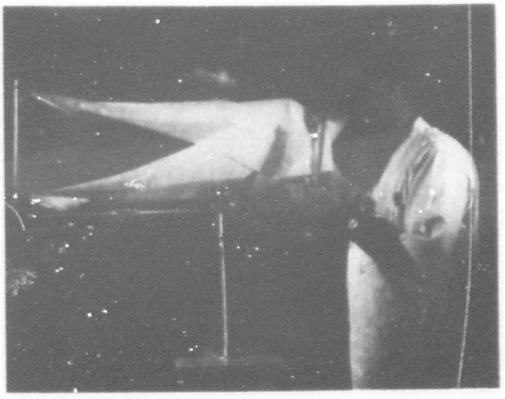

(b)

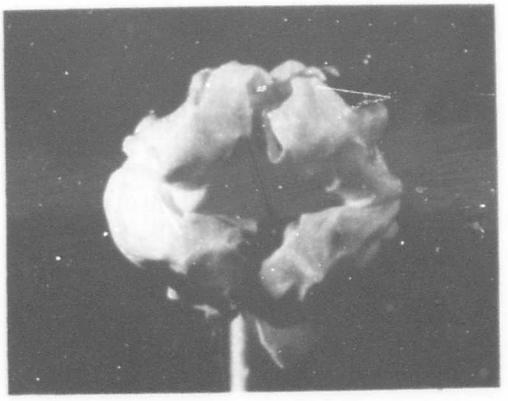

(e)

(c)

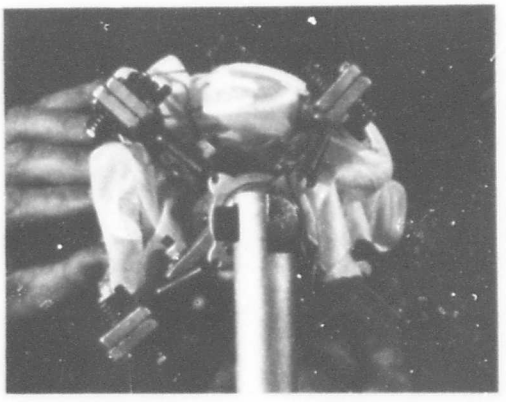

(f)

FIG. 13 ANTENNA PACKAGING

itself because of its spring-loaded members. In the final design, this lanyard would be replaced by a standard remote control device such as a shielded pyrotechnic cable-cutter.

In addition, it was desired to observe in detail the behavior of the various members of the antenna during its deployment in order to anticipate and obviate problems before the full-scale antenna went into development. This was accomplished by taking high-speed films of the opening sequence with the antenna oriented in different positions to develop its deployment capability without relying on the effects of gravity.

A selected sequence of twelve frames taken during a horizontal deployment is shown in Fig. 14. The times shown on the frames were measured starting at the instant when the clip on the antenna restraining band was released. Frame (k) shows that the extendible arms have achieved their final deployed positions after approximately 0.58 sec. In frame (l) the antenna has essentially completed its entire deployment sequence, including flattening of the two surfaces, in a period of 0.89 sec. A complete description of the deployment sequence follows:

1. In frames (a) and (b), the restraining band already has been released and the end members can be seen opening into the locked position, ejecting the restraining band in the process. The fabric antenna surfaces initiate their unfurling process in this phase and exhibit a similarity to the initial phase of an opening parachute as it emerges from its container.

2. The extension arms start moving away from the central support post and the fabric surfaces are beginning to be placed in tension. In frame (c) the upper surface is placed in tension first because it is attached to the upper end of the extension arms. Both surfaces can be seen being stretched across the middle joints of the extension arms [sharp point on upper surface in frames (c) and (d)].

3. The antenna surfaces next start to rise while, simultaneously, the middle joints lower. Contact between these joints and the antenna surfaces is diminished (frame e) and complete separation occurs (frame f).

4. The extension arms reach a straight, but not quite horizontal, position (frame g) and then bend as the stops, placed at the middle joints, are contacted [frame (h)]. One more cycle of straightening, folding, and bending of the extension members can be seen [frames (i), (j), and (k)] as the arms approach a horizontal position.

5. Finally, the antenna is fully deployed while residual, small amplitude vibrations damp out (frame l).

These films show that the extreme end arm members, which are perpendicular to the antenna surfaces when fully deployed, reach their erected position almost immediately after the restraining band is released (frame b). However, the spring force required to maintain these end members in a

(a) 0.031 sec

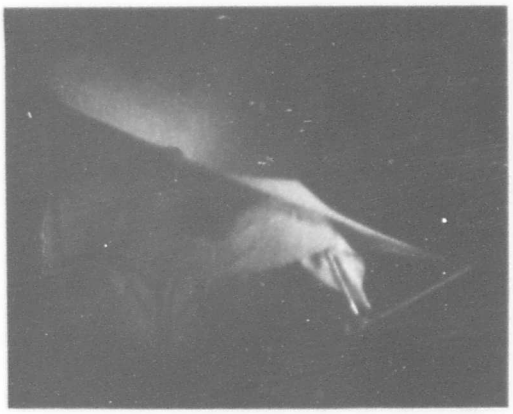

(d) 0.27 sec

(b) 0.063 sec

(e) 0.41 sec

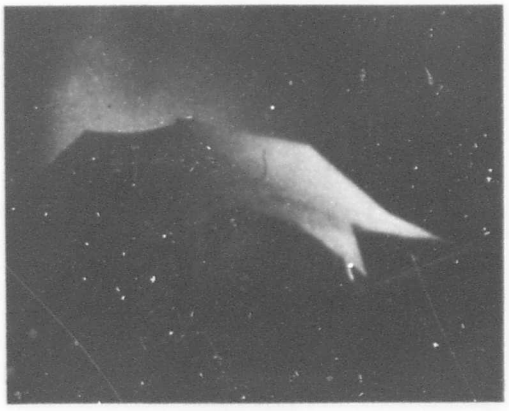

(c) 0.18 sec

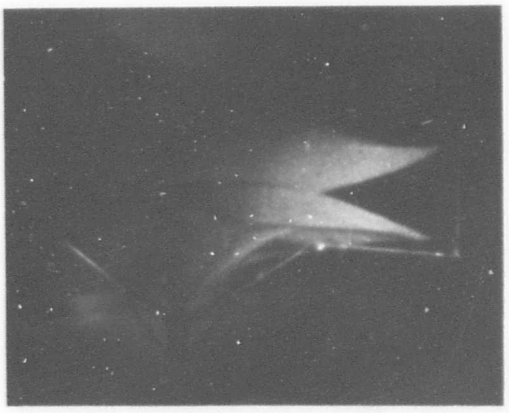

(f) 0.47 sec

FIG. 14 ANTENNA DEPLOYMENT SEQUENCE

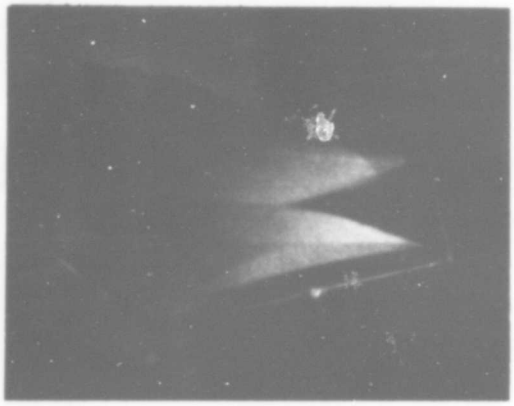

(g) 0.49 sec

(j) 0.54 sec

(h) 0.50 sec

(k) 0.58 sec

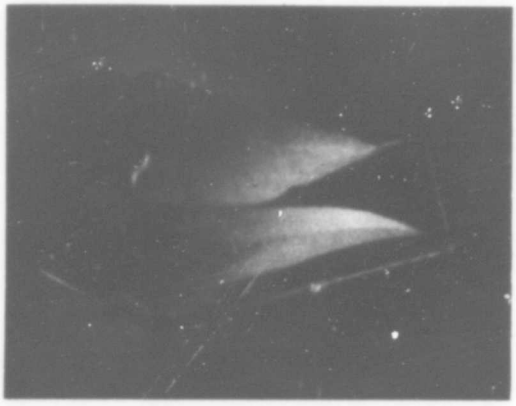

(i) 0.51 sec

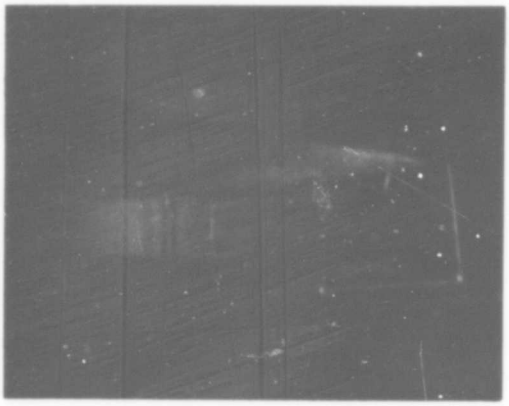

(l) 0.89 sec

FIG. 14 ANTENNA DEPLOYMENT SEQUENCE (CONCLUDED)

vertical position after the antenna was deployed exceeded the force that could be exerted by any spring of reasonable size at these joints. Since these members reach a fully open position early in the erection process, it was possible to install locks at these joints which thereby permitted the use of relatively small springs. The middle joints of the extension arms exert an appreciable force on the antenna surfaces, as mentioned above (see frames c and d). Therefore, a plastic covering was taped to each of the four joints on the model to reduce friction between the antenna fabric and joint and to prevent snagging of the surface in the joint. These photographs also indicate that large forces are exerted on the horizontal members, as indicated by bending of the members, after they have fully opened and encountered their stops while moving at a relatively high velocity.

In addition, it was found during the course of the high-speed photographic studies that certain methods of folding the antenna surfaces were superior to others, and a preferred method was evolved after the antenna hung up during one of the earlier deployments. The folding principle employed in the preferred method was merely to insure that all folds were made over each support member (rather than between adjacent members) and that no fabric wrinkles occurred at the joints. No additional unfolding problems were encountered after this method was employed.

SECTION VII. FULL SCALE ANTENNA

In addition to the improvements made on the 3-ft working model, other improvements were made when the full-scale antenna was developed by a contractor. A drawing of this antenna is shown in Fig. 15. Some of the improvements incorporated in this antenna are described below. Most of these improvements were recognized from observations of the high-speed films and from handling experience gained with the working model:

1. Two additional extendible arms were added for a total of six. This provided more support points to the antenna surface and also reduced the length of the catenary contour used between the supporting extendible arms to more evenly distribute the loads across the fabric surfaces.

2. A tension spring actuator was designed to replace the elastic cord used in the model to stretch the antenna surfaces. This provided a more reliable tension adjustment to the surface from each arm and also provided a positive means of maintaining tension in the fabric under a variety of environmental conditions, such as thermal effects, while on orbit.

3. The individual tension springs at the arm joints, at the point where the joints are attached to the center lead-in cable support tube, were replaced with a single compression spring on the tube and a sliding collar arrangement to which all the erecting arms are attached. This is a simpler arrangement and resulted in a more uniform antenna unfurling.

4. The arms were designed from square tubular sections instead of round sections to increase their moment of inertia in order to more effectively resist bending.

5. The problem of the bending arm members, caused by the relatively high velocity erection of the arms, was further corrected by adding a hydraulic damper inside the central lead-in cable support tube and attaching the damper to the sliding collar. The damper rate is adjustable to insure the optimum antenna unfurling rate. The addition of this damper will be especially helpful in a space environment where the lack of air resistance against the antenna surfaces would otherwise tend to permit the antenna to snap open with undesirable rapidity. (The damper also indirectly reduces the forces exerted on the antenna surfaces by the middle arm joints, as mentioned in Section VI.)

FIG. 15 PROTOTYPE EXTENDIBLE ARM ANTENNA

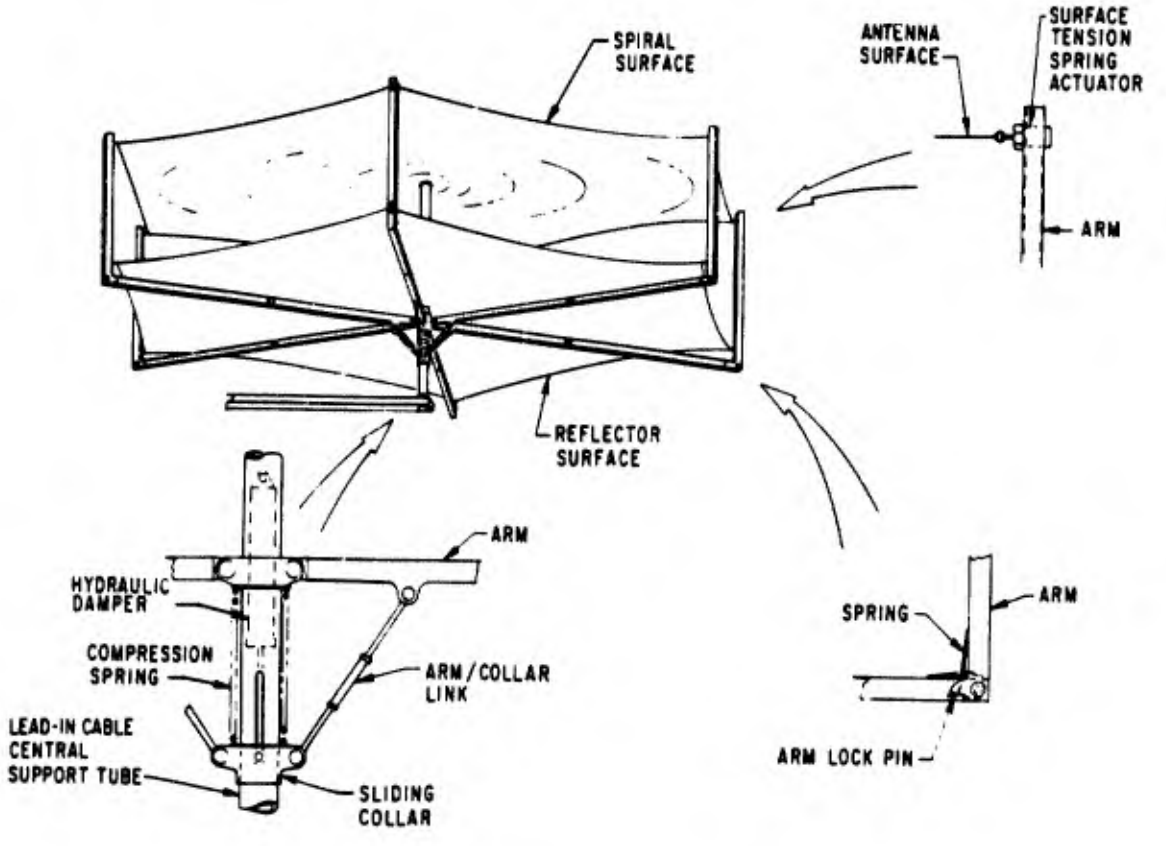

SECTION VIII. MATERIALS AND FABRICATION

There are a number of materials of which the antenna surfaces can be fabricated.* The recommended material for the spiral surface is a film laminate of Kapton/aluminum/Nomex fabric. The aluminum would be etched or vapor-deposited to form the antenna spiral. The thickness of the spiral surface must be at least one electrical skin depth at the lowest frequency of operation. Kapton (DuPonts' trade name for H-film) was selected in preference to Tedlar, Mylar, or polypropylene as a structural film because of its superior resistance to the space environment. Its strength properties are approximately the same as those of the other films but the degradation of Kapton to radiation appears to be less than for the other types of films mentioned. For the antenna fabric back, Nomex (a high-temperature-resistant nylon) was selected because its resistance to the space radiation environment is greater than that of Dacron. By laminating the aluminum spiral between Kapton film and Nomex fabric, the resulting material has an extremely high strength-to-weight ratio and excellent flexibility and abrasion resistance. The various layers comprising this laminate would have the following typical sizes: Kapton, 0.5 to 1.0 mil - aluminum, 0.18 to 0.25 mil - and Nomex fabric, 0.5 to 1.0 oz/yd^2.

The reflective surface also is made of a laminate of Kapton/aluminum/Nomex, with the aluminum foil serving as the signal reflector.

The basic arm structure of the antenna is made of aluminum tubes except for the central support tube between the spiral and reflector surface. This section is made from an epoxy fiberglass material to minimize signal interference between the surfaces.

SECTION IX. SUMMARY

A number of methods were investigated for fabricating flat, expandable, cavity-backed spiral antennas having expanded diameters of five to ten feet. The three general types considered were mechanical, expandable foam, and inflatables. Thirteen individual designs were evaluated for a particular space application, and a mechanical antenna having extendible arms was selected as best suited for this case. A simplified model having four radial arms was fabricated and tested, improvements were made, and the completed model was delivered to a contractor where a prototype flight model was fabricated.

---

*H. Smallen and V. F. Hribar, Aerospace Corporation, personal communication

BIBLIOGRAPHY

Bair, H. Q., and W. H. Fischer, "Dual Wall Inflatible Structures for Space Oriented Applications," Second Aerospace Expandable Structures Conference, AFAPL-TR-65-108, Air Force Aero Propulsion Laboratory in cooperation with Archer Daniels Midland Co., Minneapolis (February 1966), pp. 785-802.

Brink, N. O., "Research on an Expandable Airlock Utilizing the Elastic Recovery Principle," Final Report, Whittaker Corp., San Diego, Calif. (February 1965).

Brink, N. O., et al, "Development and Evaluation of the Elastic Recovery Concept for Expandable Space Structures," NASA CR-121, Whittaker Corp., San Diego, Calif. (December 1964).

Damusis, A., and A. Sanger, "Impregnants for Expandable Rigidizable Aerospace Structures," ML-TDR-64-18, Wyandotte Chemicals Corp., Wyandotte, Mich. (December 1963).

Dyson, J. D., "The Equiangular Spiral Antenna," Tech. Report No. 21, Antenna Lab., Univ. of Illinois (15 September 1957) (Contract AF 33(616)-3220).

Forbes, F. W. "Expandable Structures for Space Applications," AD-607 541, Air Force Aero-Propulsion Lab., Wright-Patterson AFB, Ohio (30 July 1964).

Forbes, F. W., "Expandable Structures," Air Force Aero-Propulsion Lab., also, Space/Aeronautics 42 (7) (December 1964).

Forbes, F. W., et al, "Expandable Structure Concept of Crew Transfer Tunnel for Space Vehicles," Second Aerospace Expandable Structures Conference, AFAPL-TR-65-108, Air Force Aero Propulsion Laboratory in cooperation with Archer Daniels Midland Co., Minneapolis (February 1966), pp 1-18.

Gibson, K. F., and G. M. Peace, "Development and Evaluation of a Rigidized Inflatable Microwave Reflector," Second Aerospace Expandable Structures Conference, AFAPL-TR-65-108, Air Force Aero Propulsion Laboratory in cooperation with Archer Daniels Midland Co., Minneapolis (February 1966), pp. 265-287.

Hanny, J. F., et al, "Chemical Rigidization of Preformed Flexible Foams," Second Aerospace Expandable Structures Conference, AFAPL-TR-65-108, Air Force Aero Propulsion Laboratory in coorporation with Archer Daniels Midland Co., Minneapolis (February 1966), pp. 165-178.

Hawthorn, A. T., et al, "Development of Fabric Base Materials for Space Applications," ML Tech. Doc. Report No. 64-20, Westinghouse Defense and Space Center, Baltimore, Maryland (January 1964).

Humble, J. L., Structural Considerations for an Expandable Lenticular Satellite," Second Aerospace Expandable Structures Conference, AFAPL-TR-65-108, Air Force Aero Propulsion Laboratory in cooperation with Archer Daniels Midland Co., Minneapolis (February 1966), pp. 199-213.

Jouriles, N., "A Predistributed Foam for Rigidizing Membrane Structures in Space," Second Aerospace Expandable Structures Conference, AFAPL-TR-65-108, Air Force Aero Propulsion Laboratory in cooperation with Archer Daniels Midland Co., Minneapolis (February 1966), pp. 339-361.

Keller, L. B., "Rigidization Time of Gelatin/Fiberglass Structures in Vacuum," P65-65, Hughes Aircraft Co., Culver City, Calif. (9 June 1965).

Keller, L. B., and S. S. Schwartz, "Rigidization Techniques for Integrally Woven Composite Constructions," ML-TDR-64-299, Hughes Aircraft Co., Culver City, Calif. (September 1964).

Korbin, W., and R. B. Jackson, "Antennas for Space Vehicles," Goddard Space Flight Center, NASA, Greenbelt, Maryland.

Latture, N. C., "Vacuum Testing of Expandable Self-Rigidizing Structures," AEDC-TR-65-264, ARO, Inc. (December 1965).

Mair, A. D., et al, "High Temperature Polymers: H-Film and SP-Polymer", ONR Technical Report RLT-83, Princeton University, Princeton, New Jersey (August 1964).

McKillip, W. J., et al, "Development and Optimization of Resin Systems for Expandable Honeycomb," Second Aerospace Expandable Structures Conference, AFAPL-TR-65-108, Air Force Aero Propulsion Laboratory in cooperation with Archer Daniels Midland Co., Minneapolis (February 1966), pp. 19-49.

Motta, S., "Aluminum Foil Expandable Structure, "Second Aerospace Expandable Structures Conference, AFAPL-TR-65-108, Air Force Aero Propulsion Laboratory in cooperation with Archer Daniels Midland Co., Minneapolis (February 1966), pp. 572-602.

Rottmayer, E., "Compression Tests of Wire-Film Cylinders," Second Aerospace Expandable Structures Conference, AFAPL-TR-65-108, Air Force Aero Propulsion Laboratory in cooperation with Archer Daniels Midland Co., Minneapolis (February 1966), pp. 519-535.

Russel, I. W., "The Application of Expandable Honeycomb to the Fabrication of Space Structures," Second Aerospace Expandable Structures Conference, AFAPL-TR-65-108, Air Force Aero Propulsion Laboratory in cooperation with Archer Daniels Midland Co., Minneapolis (February 1966), pp. 51-73.

Schwartz, S., "Development of Space Expanded and Rigidized Solar Energy Collectors," Second Aerospace Expandable Structures Conference, AFAPL-TR-65-108, Air Force Aero Propulsion Laboratory in cooperation with Archer Daniels Midland Co., Minneapolis (February 1966), pp. 555-571.

Smith, R. E., "Space Environment Criteria Guidelines for Use in Space Vehicle Development," NASA TM X 53273, Aero-Astrodynamics Lab., George C. Marshall Space Flight Center, Huntsville, Alabama (27 May 1965).

Williams, J. G., "Development of an Expandable Airlock Utilizing the Elastic Recovery Principle," Second Aerospace Expandable Structures Conference, AFAPL-TR-65-108, Air Force Aero Propulsion Laboratory in cooperation with Archer Daniels Midland Co., Minneapolis (February 1966), pp. 467-496.

"Polypropylene Balloon Study" Annual Report, G. T. Schjeldahl Co., Northfield, Minn. (29 October 1964).

"Development of an Adhesive System for Fastening Mylar (Polyester) and H-Film (Polyimide) Flat Conductor Cables to Surfaces of Space Vehicles," NASA CR-69634, Thiokol Chemical Corp., Huntsville, Alabama (4 January 1966).

AUTOMATIC CURING OF REINFORCED PLASTICS IN SPACE

S. Schwartz *
L. B. Keller **
Hughes Aircraft Company, Culver City, California

A review is made of a number of systems for automatically rigidizing expandable, fabric impregnated space structures. Space environment conditions are shown as usable for activation of polyester, polyurethane, epoxy and a new gelatin reversible system particularly well suited for space work. The gelatin system is described in detail, including impregnation and fabrication techniques and physical properties in comparison with conventional resin systems.

INTRODUCTION

With the increasing requirements for different types of structures in space there is now a need for large volume or area structures, which are initially small, compact packages on earth. There are a number of methods by which such structures could be fabricated. These include pre-fabricated, rigid unfolding, unfurling or telescoping devices, and rigid sections to be assembled by men in space. A more promising approach, however, is the use of resin impregnated, fiber reinforced expandable structures. These structures can be fabricated, preimpregnated, and "B" staged on earth. They can then be compactly packaged, and in space, will expand. Cure or rigidization will take place in space, preferably automatically, and using conditions in the space environment to actuate the cure process. This paper presents a review of the most

* Member of the Technical Staff, Materials Technology Department, R & D Dividion

** Head, Plastics Section, Materials Technology Department, R & D Division

promising of these plastics processes and in particular describes a new material and technique which appears to have a number of advantages compared to the other materials

The type of structures now being proposed include the following:

- o Manned or instrumented modules of various types. (Fig. 1)
- o Large paraboloids for rf antennas or solar energy collection. (Fig. 2)
- o Large area flat assemblies for use as solar cell support panels, or meteorite detection.
- o Optical/or radar lunar markers and structures.

In each case the structures have common requirements of large size, lightweight, and rigidity in space. On the other hand, prior to launch, the structures should be capable of being compactly packaged and then later being easily expanded to full size.

Most of the resin systems now in common use lend themselves readily to preimpregnation and "B" staging, so that structures can be made which meet the initial requirements. Conditions existing in space may be utilized to activate the rigidization of most of these resin systems. The use of the space environment to aid in the reaction, rather than considering it a hostile element, is a new concept, and it is one which will help considerably in insuring the reliability of these chemical rigidization schemes.

SPACE ENVIRONMENTAL CONDITIONS

The factors in space which might be used to cause cure of a plastic resin are: (Fig. 3)

- o Vacuum - The omnipresent vacuum of space can be used to remove solvents, or inhibiting agents. Also because of differential pressure, a vapor catalyst will be forced through an impregnated fabric, while at the same time serving as an inflation agent.
- o Ultraviolet light - Ultraviolet radiation can be used to activate several types of free radical cure mechanisms. A familiar example is the use of "sunlight" catalyst in the cure of certain polyester resins.
- o Infrared energy - The infrared radiation from the sun can be used, as on earth, to activate several types of latent catalyst reactions.
- o Cold - The cold encountered in the shadow of the earth, or moon, could also be used in a similar manner to that currently employed, i.e., as a reaction inhibitor or as a means of freezing a structure solid which might later be permanently rigidized by one of the other techniques.

Possibilities therefore exist that automatic cure of plastic structures can be done using the space environment. However, in order to fully utilize these possibilities the resin systems, in addition to capability of actuation by space conditions, must meet other requirements in order to result in a practical process.

SYSTEM REQUIREMENTS

The first requirement is a reasonably high mechanical strength after rigidization, others include fast rigidization time, and long storage life

at room temperature, while catalyzed. Another requirement is that the impregnated material, while in the "B" stage be soft, flexible, and relatively easy to expand to full size. A fifth, important requirement is that the rigidized structure have good resistance to the deteriorating effects of the space environment, i.e., mainly to the vacuum and ultraviolet radiation. Another extremely desirable requirement is that the rigidization reaction be a reversible one. With such a reaction structures can be fabricated and packaged on earth, then expanded and rigidized, and tested for performance, dimensional tolerances, etc. After ground testing the structure can then be reflexibilized and repackaged for space launching. Unfortunately none of the current thermosetting resin systems allow this flexibility. There are, however, a number of systems which meet almost all the above requirements and one which appears to meet them all.

SYSTEMS INVESTIGATED

UV and Infrared Activated Systems

One of the first space structures in which rigidization was desired was the Echo II balloon, the successor to the Echo I. Prior to launch of Echo I, it was anticipated by NASA that the one-half mil inflated Mylar structure would quickly become distorted, after initial pressurization, due to micrometerite punctures, residual air pressure and thermal stresses. It was therefore desired that the Echo II balloon incorporate a rigidizable structure which, it was felt, would have a longer life than the Echo I balloon.

In work done at Hughes Aircraft in 1960 and 1961 three very lightweight systems, incorporating reinforced plastic techniques, were developed

for rigidization of the proposed Echo II balloon. All the structures consisted of a sandwich utilizing one face of one-quarter mil, clear Mylar and one face of aluminized Mylar. In the center of the laminate was an extremely lightweight Dacron marquisette fabric impregnated either with an ultraviolet activated polyester resin or a heat curing epoxy resin. In the case of the polyester resin the clear Mylar face was exposed, so UV radiation would be absorbed causing rigidization to take place within 10 to 30 minutes. The sandwich incorporating the epoxy resin had the aluminized Mylar as its outer face, thus absorbing enough heat after inflation to raise the temperature to approximately 270° F, the initiation temperature for cure of the resin. Rigidization with this system takes approximately 2 hours. The third system utilized the UV activated polyester resin, and in addition a UV decomposable organic salt was added to the resin. This salt, when exposed to ultraviolet radiation, would decompose and liberate nitrogen gas, thus foaming the resin, which would then cure in 20 to 45 minutes, before collapse of the foam. The stiffness of the rigidized sandwich structures ranged from 40 to 150 times as stiff as the original Mylar, with weight increases of from three to five times the original weight. Figure 4 illustrates the varying stiffnesses of samples rigidized by the three systems as compared to the original one-half mil Mylar. (Ref. 1 & 2). These systems, while effective in space and fully automatic, do have the serious limitation that they must be sun oriented, in order to fully cure. Thus normally the structure would have to be rotated slowly so that all surfaces were exposed to the sun's rays. Any parts of the structure not directly exposed or shaded by other sections would then fail to harden.

Another heat activated system was developed for rigidization of various type structures. This utilized a special, one component, polyurethane foam powder which was predistributed on the outer surface of a balloon. On exposure to solar heat, and in a vacuum the material absorbs enough heat to reach a temperature of approximately 275° F, after which foaming takes place. A rigid foam, approximately 1 1/2 inch thick, results after 15 to 30 minutes at the elevated temperature. Fig. 5 illustrates the appearance of a completed balloon-like structure along with a foam chair made in a vacuum chamber at an altitude corresponding to 160,000 feet with simulated solar heat.(Ref. 3.)

Along with the necessity of sun orientation for this system, and the previous heat curing system, another disadvantage of the heat curing systems is that the surface characteristics of the structure must be such that an appreciably high temperature must be reached before the resin is cured. Then, if the structure remains exposed to the sun, it is maintained at this temperature, thus causing a loss of strength. Currently no simple techniques are known which can be used to vary the optical characteristics of a surface to first produce an elevated temperature and then later a low surface temperature. Until such a technique is developed the use of infrared for surface activation then remains very doubtful.

Vapor Curing System

Several vapor curing systems which use the vacuum in space, have also been developed. These systems are activated by the use of catalyst vapors, and thus are not dependent on sun orientation as are the previous

systems. In one method an amine curing agent, triethylamine, has a high enough vapor pressure, (70 mm Hg at room temperature) to act as both the inflating media for the structure and as a catalyst for an epoxy resin. After 48 hours of exposure the catalyst permeates a silicone rubber coated fabric barrier sufficiently to produce laminates of approximately 29,000 psi flexural strength. Ref. 4.

In another system, Refs. 5,6, & 7, a water-amine mixture is used to cure urethane impregnated fabric. Flexural strengths of approximately 14,000 to 38,000 psi were obtained after 2 to 24 hours of exposure. In still another system, reported in Ref. 7, vapor catalysis is used to cure polyesters. In this technique the resin is accelerated by means of a mixture of aromatic amines and a cobalt salt, and a volatile methyl ethyl ketone peroxide is used as the initiator. The resin used could not be the normal styrenated type, because of the high vapor pressure of the monomer. The resin found best with this type of initiation contained special acrylic esters as the reactive monomer.

In the use of any of the vapor catalyst activation systems the main advantage is that there are no limitations with regard to sun orientation to receive UV or infrared radiation. Another feature of these systems is that the structure can be rigidized on command, rather than automatically, just after inflation. On the other hand the automatic feature can be built in; however, with some increase in weight and system complexity. The additional weight of the catalyst storage and valving system and a possible manifolding or distribution system all add to the weight and complexity and possibly lower reliability. Another aspect of the vapor catalyst systems is that it is doubtful if the catalyst would work effectively, at normal ambient temperatures if the resin were "B" staged to a fairly dry condition.

(This type of "B" staging is not yet known to have been accomplished with polyurethane resins).

Cold Utilization

One unique method proposed utilizes the cold of space as an inhibiting agent for delayed action foams. Ref. 8 & 9. In this technique polyurethane foam components are mixed, and prior to foaming, the materials are immediately poured into a bath of liquid nitrogen agitated by a power mixer. The material settles to the botton of the bath as a hard, frozen powder. The powder can then be placed between two layers of cloth, and stored indefinitely, at the low temperature. When allowed to heat above -50° F foaming commences. While this method presents a number of practical difficulties in the way of fabrication, transport, etc., it does offer one method of utilizing the "cold" present in space.

Gelatin (Solvent Loss) System

Perhaps the best system so far developed for space structure rigidization is one which utilizes the vacuum to cause rigidization by simple solvent plasticizer loss. In such a system a volatile plasticizer leaves the impregnated fabric as soon as the structure is expanded in the vacuum. This then results in the utmost in simplicity, combined with the highest reliability. In addition this technique can offer the considerable advantage of a reversible reaction, since the impregnant does not involve a catalyst.

The first solvent loss system reported was by Westinghouse in 1964. (Ref. 10). This consisted of loss of plasticizer from fabrics coated with either polyurethanes, polyvinyl chloride or polyvinyl alcohol. The most successful results were obtained from polyvinyl chloride plastisol coated fabrics, using toluene as the volatile plasticizer. Fairly long

drying times to obtain high strengths were the disadvantages of this system.

An extremely promising solvent loss system utilizing a water-gelatin solution has recently been investigated by Hughes Aircraft Company. This system, which was suggested by the Materials Application Division of the Air Force Materials Laboratory, shows promise of being the best system of all. Refs. 11 & 12.

In the use of gelatin as an impregnant it was found that commercial gelatin can be dissolved in warm water to make a viscous solution of 30 to 40% resin content. This solution at 115° F is similar in appearance, but considerably higher in viscosity, than conventional epoxy or polyester laminating resins. Also the material will gel almost immediately if brushed or squeezed onto room temperature fabric. By the use of peptizing additives, however, a solution can be obtained with a viscosity similar to hand laminating epoxy or polyester resins. More important, such a modified solution has a working life of from 20 minutes to a half hour after cooling to room temperature. With this peptized solution, which also includes wetting agents and fungicides, then the fabric can be dipped into the impregnant, or the impregnant can be brushed into the fabric, similar to conventional laminating techniques. The impregnated fabric, however, can not, at this point be stored as are conventional impregnated fabrics, or have some of the solvent removed to form a "B" staged prepreg.

After impregnation of the fabric if the material is folded or rolled up, and then gelation takes place the material will be hopelessly adhered to itself. If, on the other hand, the material is allowed to gel, but not dry completely, on folding or rolling such a material adhesion also takes place. The use of parting films such as Mylar, cellophene or polyethylene was not found practical. While such films do prevent fabric-to-fabric

adhesion, at the same time the film also seriously inhibits the rate of solvent loss, thus causing later rigidization to take place at an extremely slow rate. Removal of the parting film was also found to be near impossible because of the high adhesion shown by the partly dried gelatin.

The technique which was finally developed to produce a flexible, non-tacky, "B" staged material consists of treating the impregnated fabric with a formaldehyde solution or a similar tanning agent. After treatment with the formaldehyde solution, or vapors, the impregnated material becomes flexible, leathery, and non-tacky, so that it may safely be folded or rolled up with no danger of fabric-to-fabric adhesion.

A formaldehyde treated fabric, or complete part, may be stored in a sealed container, with no shelf life limitation, since the material contains no catalyst. The degree of flexibility in the material depends on the fabric, or laminate thickness and the amount of water absorbed. Normally the minimum water content is approximately 15 to 20% of the total weight, if good flexibility is desired.

Rigidization of the gelatin impregnated material takes place by simply exposing the part to the atmosphere. Naturally exposure to a high humidity environment results in considerably less rigidization than exposure to a dry environment. Exposure to the space environment then results in the maximum rigidity in the shortest time: (1) because of the complete absence of moisture and (2) because of the high vacuum which thus has a maximum effect in causing removal of the water. In actual practice it has been found that rigidization takes place, at room temperature in from 45 minutes to two hours depending on the thickness of the laminate.

With the development of the peptized gelatin solutions and the "B" staging treatments it then becomes possible to use the gelatin in the same manner as conventional hand layup resins, with some minor differences. Structures may be hand impregnated by brushing or by dipping followed by "rubbing out" to cause even resin distribution. The structure is then dried, in the expanded condition. It is treated with the formaldehyde either as a bath, or if the structure is large, to formaldehyde-water vapors. In the latter case simple polyethylene tents are used to completely enclose the part and the solution is heated to 150-180° F to obtain a saturated atmosphere. The time of either treatment varies with the thickness of the part, but ranges from 15 minutes to several hours for the solution treatments and from 24 to 48 hours for the formaldehyde vapor treatments. After the treatment the part is ready for packaging and storage. The flexibilization treatment may be repeated any number of times and it is this feature which gives the process its reversibility and which makes it unique.

PHYSICAL PROPERTIES

Laminates

Laminates, rigidized in a vacuum show strengths comparable to those made using polyester or epoxy resins. Table I shows a comparison of the physical properties of laminates made using the various cure systems.

Sandwich Structures

The fabrics mainly utilized in these studies were glass fiber, three dimensionally woven sandwich materials. One was a 12 oz/yd^2 material with (60°) triangular flutes and another was a 14 oz/yd^2 material with (90°) rectangular flutes. Fig. 6 shows the type of fabric used. For maximum

Table I - Flexural and Tensile Strengths of 181 Glass Fabric Laminates, psi

Test Sample		Cure Technique			Flexural		Tensile		Source
No. Plies	Resin	Pressure	Temp	Exposure Time	Str x 10^3	Mod x 10^6	Str x 10^3	Mod x 10^6	
3	urethane	65 psi	R.T.	48 hr exposure to H_2O & amine catalyst	25-40	1.6-2.8	-	-	13
3	urethane	contact	R.T.	50% R.H. 72 hrs	7-12	.6-1.3	16-25	-	6
2	urethane	contact	R.T.	50% R.H. 13 days + 75% R.H. 7 days	50-65	3.0-3.2	-	-	5
8	gelatin	1000 psi	275°F	1 hr	40-65	3.0-3.2	-	-	14
8 & 13	gelatin	contact	R.T.	38 hr flexibilization plus 48 in vacuum	45-54	2.3-2.4	48-50	2.6-2.8	11
Conventional polyester and epoxy laminates (tested in the dry condition)									
13	polyester	vacuum bag	heated	-	45	2.5	38	2.6	15
13	epoxy	Vacuum bag	heated	-	6[illegible]	3.2	45	3.3	15

physical properties it was found that resin contents should be in the range of 55 to 65%, rather than the conventional 30 to 40%. Tables 2 and 3 show the actual strengths obtained on samples of these fabrics, made in a vacuum chamber with automatic expansion and rigidization.

Table 2 - Edgewise compressive properties, psi (55-65% resin content)

	Ultimate strength	Modulus
12-oz triangular fabric		
Polyester	60	10,000
Polyurethane	125	16,000
Gelatin	60	16,000
Polyurethane foam	120	...
14-oz rectangular fabric		
Polyester	100	29,000
Polyurethane	152	17,000
Gelatin	100	20,000

Table 3 - Flexural properties, psi (55-65% resin content)

	Ultimate strength	Modulus
12-oz triangular fabric		
Polyester	900	40,000
Polyurethane	1100	110,000
Gelatin	1700	320,000
14-oz rectangular fabric		
Polyester	1000	40,000
Polyurethane	1000	40,000
Gelatin	3900	1,000,000

The strengths shown above do not appear impressive, when compared to conventional laminates, of the same weight. However, it should be borne in mind that the actual sandwich materials were relatively very lightweight, and were many times as stiff as normal laminates of the same weight.

FABRICATION TECHNIQUES FOR GELATIN STRUCTURES

In the use of rigidized materials for spacecraft, because of weightlessness, the major emphasis is not on production of materials with the highest strengths, but rather on production of materials showing the highest stiffness-to-weight ratio. For this reason a great deal of effort was devoted to development of techniques for the use of the three dimensional sandwich materials. The materials mainly worked with were three dimensionally woven materials made by the Raypan Company, but also included a small amount of sewn three dimensional fabrics. The general method of working with this material was to saturate the fabric with resin, then to insert polyethylene tubes in the flutes of the fabric as shown in Fig. 7. The polyethylene tubes served two purposes: (1) To act as a parting film, preventing flute-to-flute adhesion and (2) to act as an expansion media. This latter was done by placing a few drops of water, alcohol or acetone in the polyethylene tube and then sealing both ends. At normal room pressures the tubes can easily be folded or rolled up with the fabric assembly. However, when the structure is placed in a vacuum chamber the vapor pressure of the small amount of contained liquid acts to expand the tube and thus automatically erect the structure. In the case of the polyurethane system the water also acted as a catalyst to cause rigidization. Fig. 8 shows some of the parts utilizing gelatin and the vacuum auto-erection and rigidization system.

SUMMARY

The investigation has shown that there are a number of systems which can be used to produce expandable, rigidizable plastic structures. These

structures can be deployed automatically in space from a flexible, compactly packaged assembly. The light structures, either as laminates or as sandwich materials have physical properties comparable to materials of similar density produced on earth. The various chemical systems and fabrication techniques allow great versatility in design to meet varying requirements. These requirements might range from a very fast cure (UV activated polyester), to a flat sandwich structure with varying strength (accomplished by adding additional layers of fabric at specific areas). A summary of the various systems is given in Figure 9.

A summary of the relative advantages of the three systems considered the most promising is as follows:

Gelatin

This is the simplest and most automatic system, and perhaps the strongest. Rigidization occurs by exposure to vacuum only. From 10-15% excess weight (water) must be used. Rigidization time to achieve 80% of full strength is less than 2 hours. Gelatin is the only material that is reversible. The rigid material may be reflexibilized by exposure to humidity, thereby permitting complete ground test of a structure prior to deployment in space.

Polyester

This is a simple system that rigidizes by exposure to ultraviolet light in 20 minutes to 1 hour. It must be oriented or maneuvered to expose all surfaces. There are some limitations on thickness since the ultraviolet must penetrate the material. The system will not rigidize in the earth's shadow.

Polyurethane Resin

This system requires interconnecting tubes or mainfolding to distribute catalyst (water). The weight of water and auxiliary equipment may be over 20% of the weight of the sandwich structure; however, the system will rigidize on command by release of catalyst. Problems remain with excessive stickiness and the necessity of producing and storing the structure in a moisture-free environment. Rigidization time runs from 1 to 16 hours, depending on the formulation.

SUMMARY

Because of the need for large area or volume structures in space, the use of expandable-rigidizable structures becomes very attractive. These structures include manned modules, paraboloids used for communication or solar energy collection, micrometeorite detection, etc.

One of the fabrication techniques suggested is to use preimpregnated fabric structures, which would be expanded and rigidized automatically in space. The simplest and most reliable method of ensuring automatic activation of the resin system would be to use the space environment as the activating agent.

Some of the chemical systems which can utilize the space environment include the following:

1. UV activated polyesters
2. Infrared activated epoxies
3. Vapor catalyzed polyurethanes and polyesters
4. Cold inhibited urethane foamants
5. Solvent loss systems

The best of the solvent loss systems is a gelatin-water system. Using specially prepared solutions fabric reinforced structures can be made in a manner similar to normal laminating. The gelatin impregnated fabrics can be "B" staged and stored indefinitely, and then rigidized on the ground or in space by simple exposure to the environment. Such a system is also unique in that it allows a reversible reaction. Therefore the part can be expanded and rigidized on the ground, tested, and then repackaged and later deployed in space.

Techniques for automatic deployment of expandable structures are discussed. Special emphasis is given to methods of fabrication of double walled

structures utilizing three dimensionally woven fabrics. The physical properties of the gelatin structures were found to be similar to those made with conventional laminating resins.

QUESTIONS

1. What happens if the gelatin systems becomes cold?

2. How precisely can these structures be made?

3. What type of surface is required in order to use the heat activated epoxies?

4. What is meant by a peptizing agent?

5. How can one make joints in the gelatin impregnated material?

REFERENCES

1. Space Structure Rigidization, Hughes Aircraft Company Report P61-13, Sept 1961

2. Schwartz, S., and Zelman, I., "Automatic Rigidization for Inflatable Satellites," Space-Aeronautics Magazine, June 1962

3. Schwartz, S., "Development of a One-Part Foam-In-Space Polyurethane," National Academy of Sciences Conference on Foamed Plastics," Boston, Mass., April 1963

4. Graham, T. L. and Spain, R. G., "Rigidizable Expandable Aerospace Structures," SAE National Aerospace Engineering and Manufacturing Meeting, Los Angeles, Oct 1962

5. Damusis, A., Sanger, A. and Grazulis, V., "Impregnants for Rigidizable Aerospace Structures," Air Force Materials Laboratory Report ML-TDR-64-18, Dec 1963

6. Russel, I. W., Hansaen, N. S., and McKillip, W. J., "Development of an Inflatable Self-Rigidizing Space Shelter and Solar Collector from Honeycomb Sandwich Material," Air Force Aero Propulsion Laboratory Report APL TDR-64-29, May 1964

7. McKillup, W. J., Nordstrom, J. D. and Dunning, E. B., "The Development and Optimization of a Resin System for Rigidization of Expandable Honeycomb Structures," SPI 20th Annual Reinforced Plastics Meeting, Feb 1965

8. Moore, H. R., "Urethane Foams for Aerospace Application," Modern Plastics, June 1962

9. Hefty, R. W.,Hersh, H. R. and Shenker, L. G., "The Rigidization of Inflatable Structures in Space," American Rocket Society, Space Flight Report to the Nation, New York City, Oct 1961

10. Hawthorn, A., Simon, A. B., Brock, C. L. and Sigel, L. A., "Development of Fabric Base Materials for Space Applications,"Air Force Materials Laboratory Report ML-TDR 64-20, Jan 1964

11. Keller, L. B., and Schwartz, S., "Rigidization Techniques for Integrally Woven Composite Constructions," Air Force Materials Laboratory Report AFML-TR 65-402

12. Keller, L. B.,Schwartz, S., Olevitch, A. and Allinikov, S., "Space Rigidized Resin Fiberglas Sandwich Materials," Journal of Spacecraft, April 1966

13. "Expandable, Self Rigidizing Honeycomb Aerospace Shelters and Solar Collectors," Progress Report #1 Contract AF 33(615)-2435, Archer Daniels Midland Company, May 1965

14. Schwendeman, J. L., Robertson, J. L., and Salyr, I. O., "Gelatin as a Possible Structural Material for Space Use," Aeronautical System Division Report ASD-TDR 63-444, May 1963

15. "Plastics for Flight Vehicles," Part I, Reinforced Plastics, MIL Handbook 17 (Dept. of Defense, Washington, D. C., Nov 1959)

FIGURES

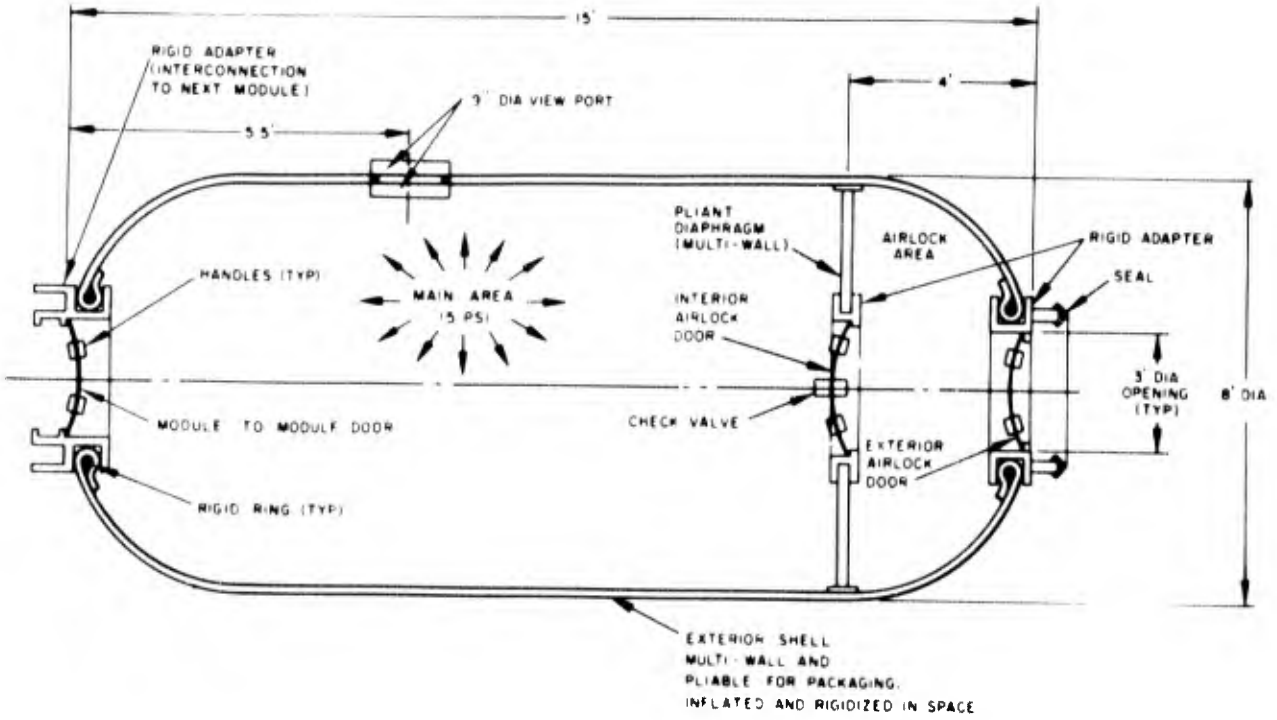

PROPOSED EXPANDABLE, RIGIDIZED, MANNED MODULE

PROPOSED INFLATED AND RIGIDIZED SOLAR ENERGY COLLECTOR

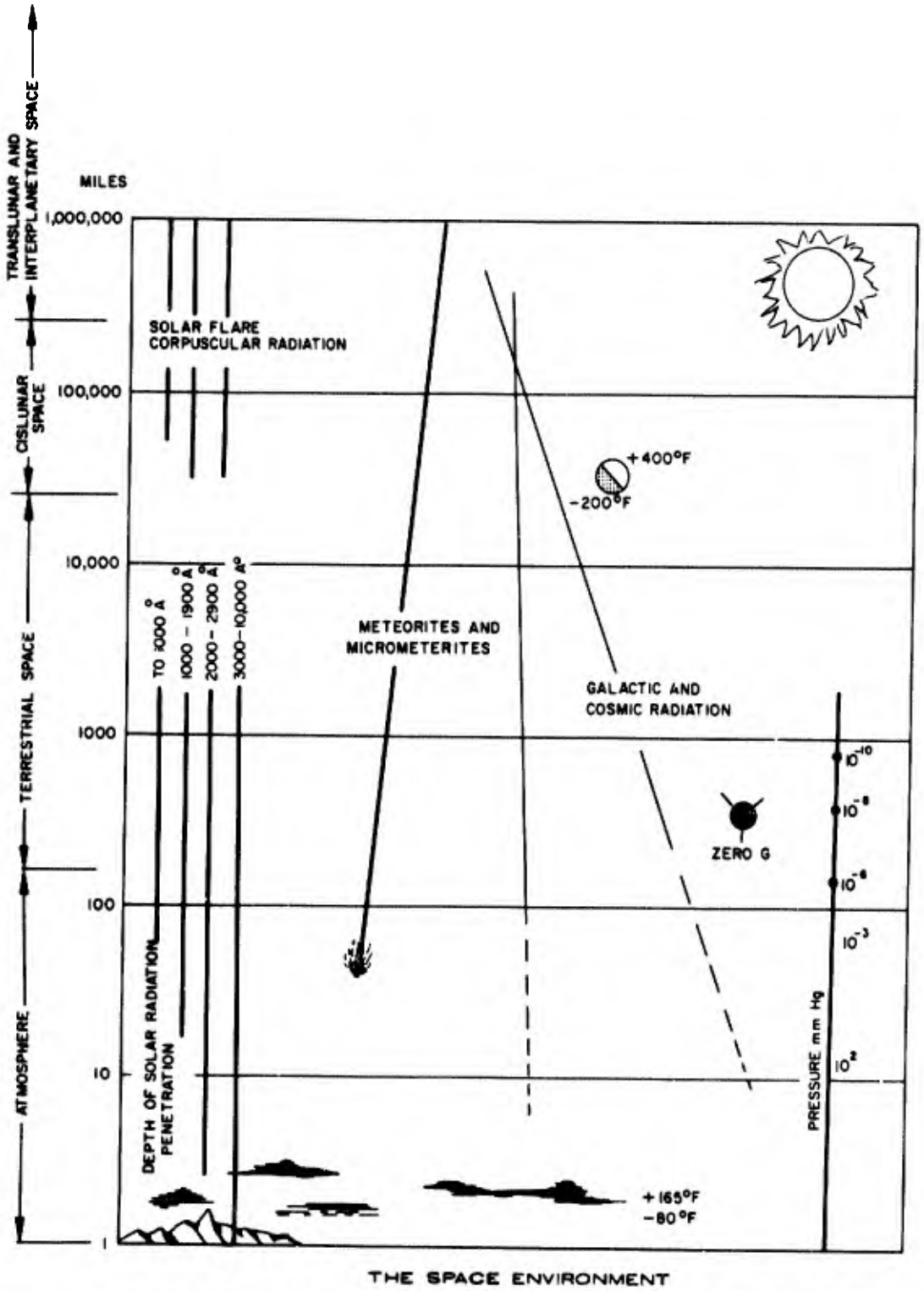

THE SPACE ENVIRONMENT

(REF-T.M McCOY "HYPERENVIRONMENT SIMULATION-ETC-" WADD TECH. REPORT 60-785 JAN 1961)

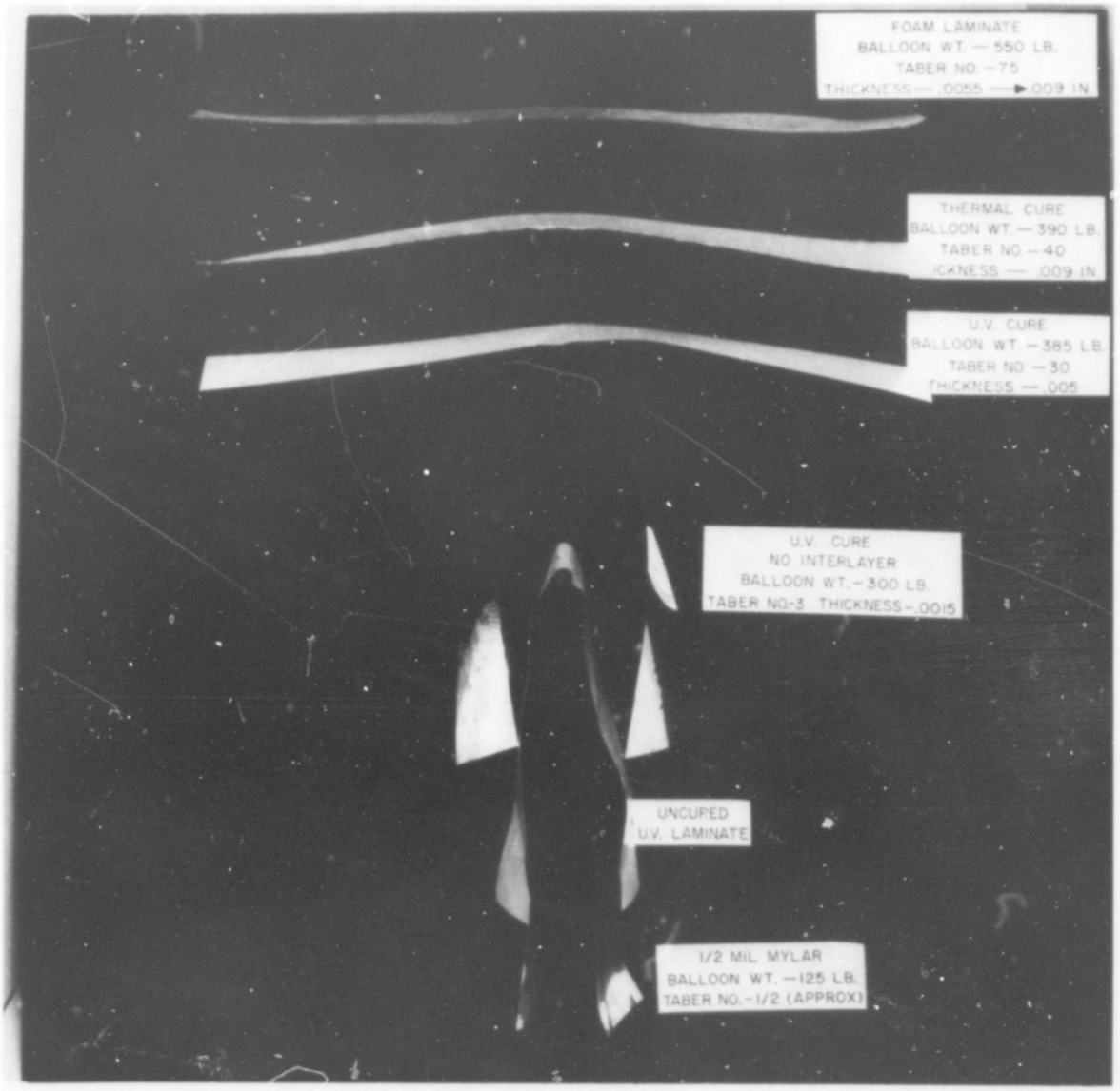
FOAM LAMINATE
BALLOON WT. — 550 LB.
TABER NO. — 75
THICKNESS — .0055 —▶ .009 IN.
THERMAL CURE
BALLOON WT. — 390 LB.
TABER NO. — 40
ICKNESS — .009 IN.
U.V. CURE
BALLOON WT. — 385 LB.
TABER NO. — 30
THICKNESS — .005
U.V. CURE
NO INTERLAYER
BALLOON WT. — 300 LB.
TABER NO-3 THICKNESS-.0015
UNCURED
U.V. LAMINATE
1/2 MIL MYLAR
BALLOON WT. — 125 LB.
TABER NO. - 1/2 (APPROX)

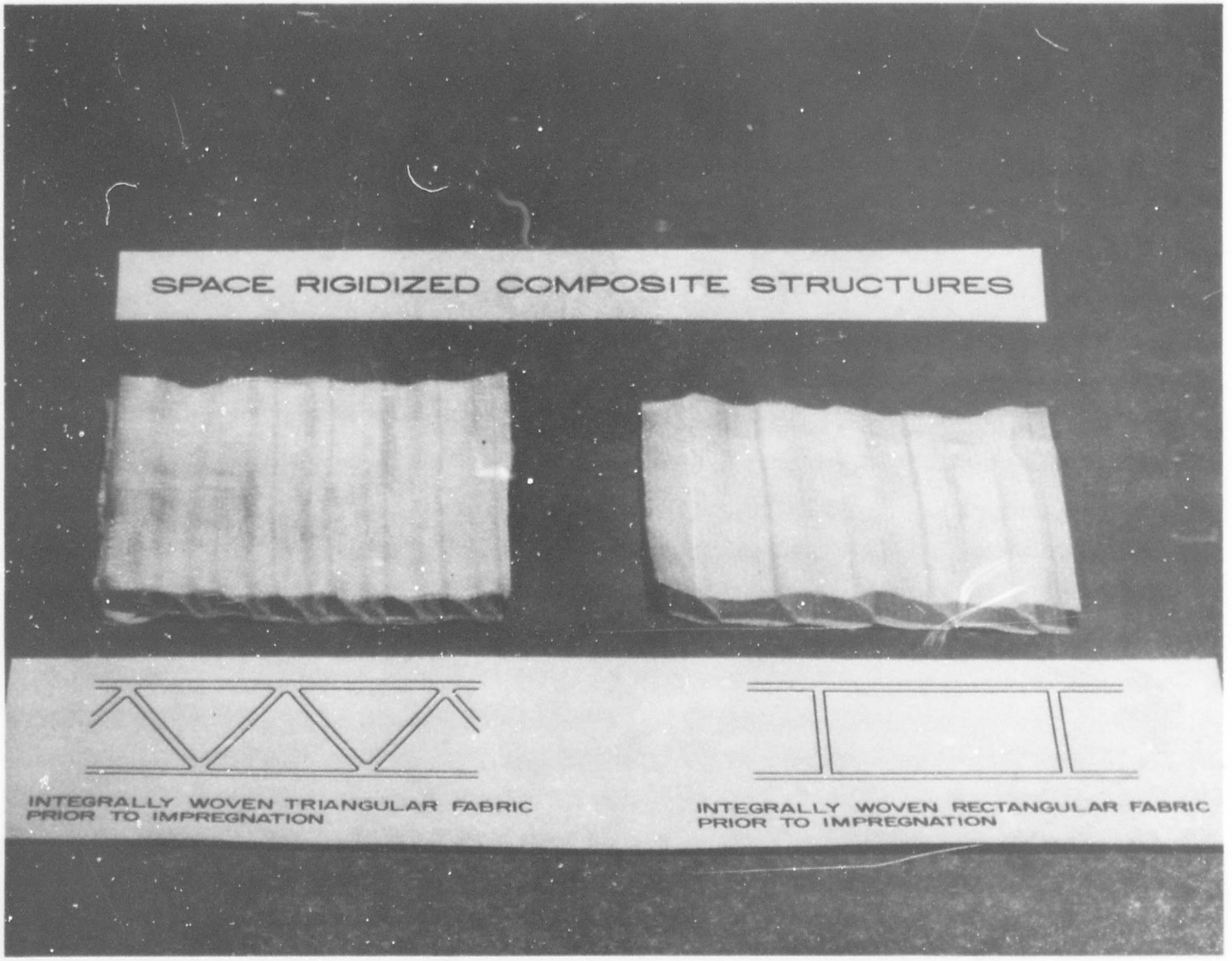
SPACE RIGIDIZED COMPOSITE STRUCTURES
INTEGRALLY WOVEN TRIANGULAR FABRIC
PRIOR TO IMPREGNATION
INTEGRALLY WOVEN RECTANGULAR FABRIC
PRIOR TO IMPREGNATION

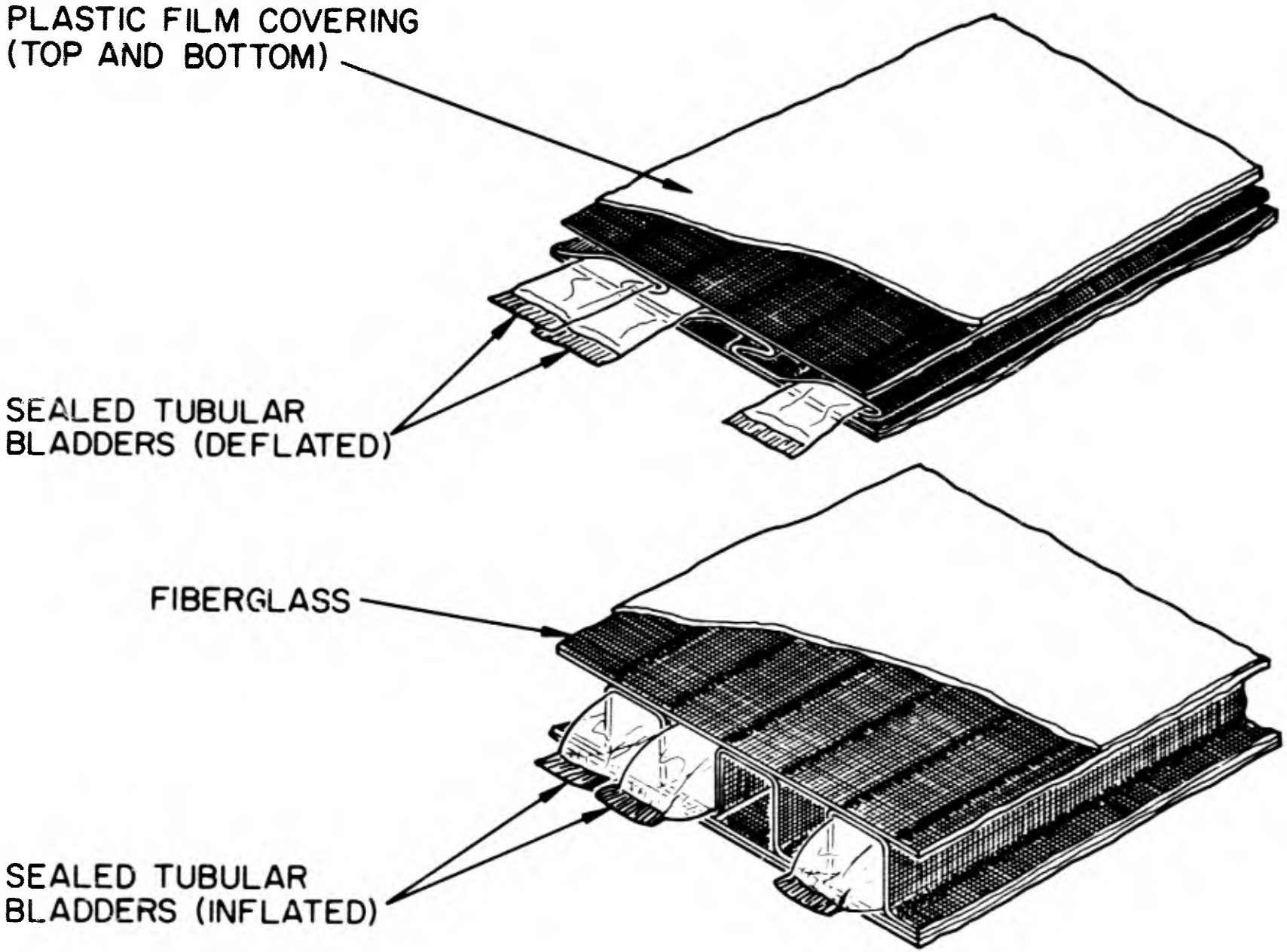
PLASTIC FILM COVERING
(TOP AND BOTTOM)
SEALED TUBULAR
BLADDERS (DEFLATED)
FIBERGLASS
SEALED TUBULAR
BLADDERS (INFLATED)

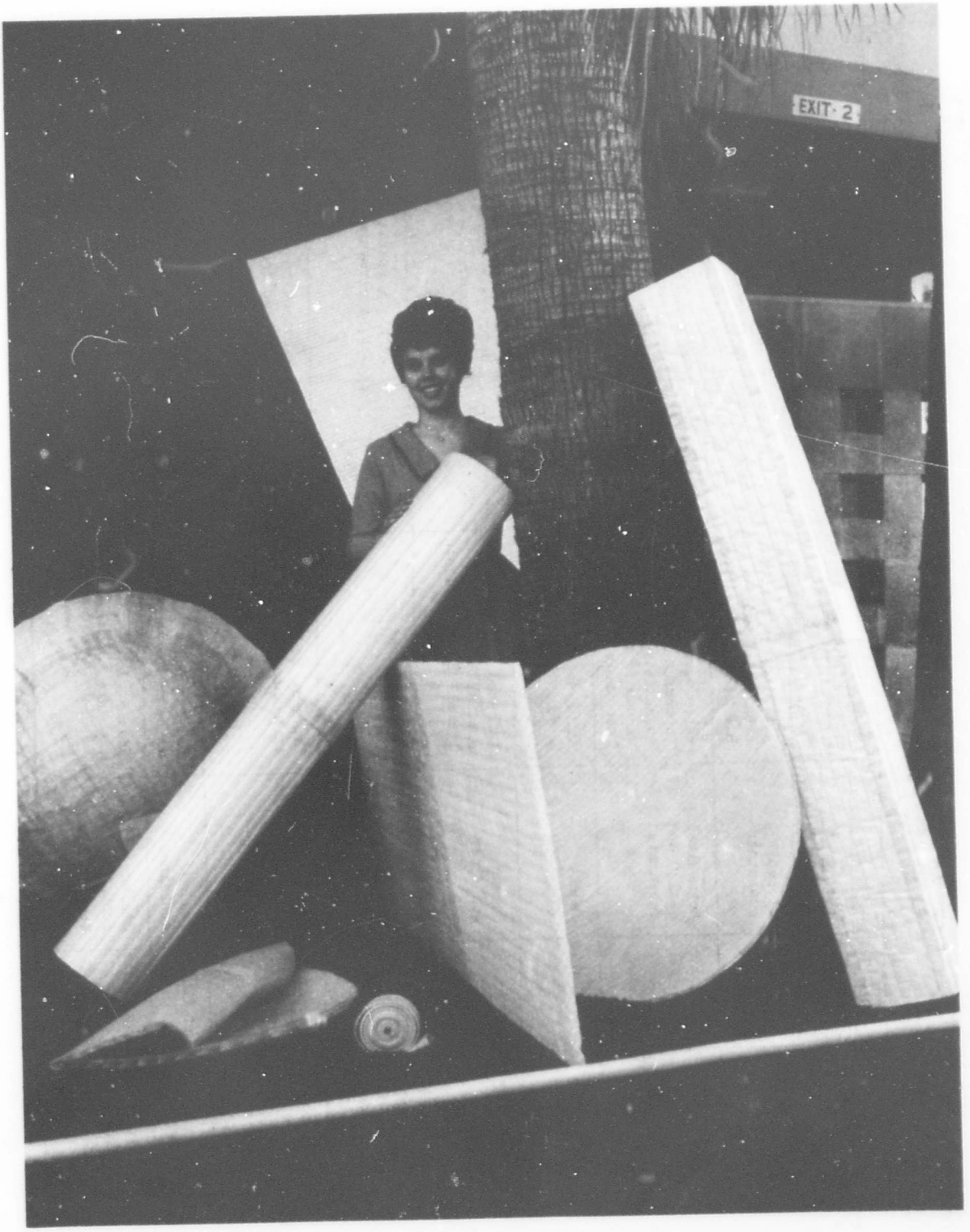
EXIT· 2

Figure 9 - Automatic Expandable Structures Space Rigidization Systems

System	Unrigidized State		Rigidized State		Remarks
	Storage Conditions				
	Room Temp.	Container Req.	Activation Means	Time	
Polyester DAP Resin	1-3 Mo.	Closed container	U.V. light + sunlight catalysts, benzoin and B.P.O.	1-4 hrs at ambient temps.	Very simple to use - requires exposure of all surfaces to sun
Polyurethane Resin	1-2 Mo.	Hermetically sealed and dehydrated	Water vapor alone and in combination with volatile amines - uses vacuum to cause catalyst impregnation	2-24 hrs at ambient temps.	No special orientation - catalyst storage and distribution system required. Moisture free processing
Vapor cured epoxy	Indefinite	Sealed container	Amine vapors - uses vacuum to cause impregnation	8-24 hrs at ambient temps.	No special orientation - catalyst storage and distribution system required
Heat curing epoxy	1-3 Mo.	Sealed container	Infrared heat plus special latent catalysts - BF_3, DiCy, etc.	4-24 hrs at 250-350° F	Requires special surface finish for temperature controls
One component polyurethane foam powder	indefinite	Sealed container	Infrared heat	20 min. to 1/2 hr at 275-350°F	Requires special surface finish for temperature controls
Frozen polyurethane foam	Indefinite	Cryogenically cooled container	Exposure to temperatures above -50° F	Dependent on temperature 5 min to 15 min.	Fabrication and transportation problems are yet to be solved
Vinyl-solvent	Indefinite	Sealed container	Solvent loss - exposure to vacuum	3-24 hrs	Not perfected
Gelatin-water	Indefinite	Sealed container or keep in humid atmosphere	Solvent loss - exposure to vacuum	15 min - 2 hrs depending on thickness and temperature	High reliability - no special orientation - high U.V. resistance. Rigidization is reversible

UNCLASSIFIED

Security Classification

DOCUMENT CONTROL DATA - R & D

(Security classification of title, body of abstract and indexing annotation must be entered when the overall report is classified)

1. ORIGINATING ACTIVITY (Corporate author) AIR FORCE AERO PROPULSION LABORATORY GOODYEAR AEROSPACE CORPORATION G. T. SCHJELDAHL CO. LOCKHEED MISSILES & SPACE COMPANY	2a. REPORT SECURITY CLASSIFICATION UNCLASSIFIED 2b. GROUP

3. REPORT TITLE
TRANSACTIONS, THIRD AEROSPACE EXPANDABLE AND MODULAR STRUCTURES CONFERENCE

4. DESCRIPTIVE NOTES (Type of report and inclusive dates)

5. AUTHOR(S) (First name, middle initial, last name)

6. REPORT DATE FEBRUARY 1968	7a. TOTAL NO. OF PAGES 736	7b. NO. OF REFS
8a. CONTRACT OR GRANT NO b. PROJECT NO c. d.	9a. ORIGINATOR'S REPORT NUMBER(S) AFAPL-TR 68-17 9b. OTHER REPORT NO(S) (Any other numbers that may be assigned this report)	

10. DISTRIBUTION STATEMENT
DISTRIBUTION OF THIS DOCUMENT IS UNLIMITLD

11. SUPPLEMENTARY NOTES	12. SPONSORING MILITARY ACTIVITY AIR FORCE AERO PROPULSION LABORATORY WRIGHT-PATTERSON AFB OHIO 45433

13. ABSTRACT

This report contains a presentation of technical contributions summarizing the status of current and significant research in the fields of expandable and modular structures. The report is based upon the discussions at the Third Aerospace and Modular Structures Conference held 16-18 May 1967 at the Carillon Hotel, Miami Beach, Florida. The conference transactions have been arranged in the order of presentation during the six sessions of the conference

DD FORM 1 NOV 65 1473

UNCLASSIFIED

Security Classification

14 KEY WORDS	LINK A		LINK B		LINK C	
	ROLE	WT	ROLE	WT	ROLE	WT
EXPANDABLE STRUCTURES						
MODULAR STRUCTURES						
AIRLOCKS						
STRUCTURES FOR REENTRY						
SOLAR COLLECTORS						
SPACE STATIONS						
EXPANDABLE ANTENNAS						
CHEMICAL RIGIDIZED STRUCTURES						
PLASTIC RECOVERY STRUCTURES						